ISCOWA

THE HONG KONG POLYTECHNIC UNIVERSITY
香港理工大學

RESEARCH CENTRE FOR
RESOURCES ENGINEERING TOWARDS CARBON NEUTRALITY
±RCRE 碳中和資源工程研究中心

DEPARTMENT OF
CIVIL AND ENVIRONMENTAL ENGINEERING
土木及環境工程學系

rilem

Joint Laboratory on
Solid Waste Science
固體廢棄物科學聯合實驗室

WASCON2023 - HONG KONG
INNOVATIVE VALORIZATION OF ALTERNATIVE MATERIALS AND WASTE TOWARDS CIRCULAR CONSTRUCTION

11TH INTERNATIONAL CONFERENCE ON THE ENVIRONMENTAL AND TECHNICAL IMPLICATIONS OF CONSTRUCTION WITH ALTERNATIVE MATERIALS

13-16 DECEMBER 2023

Conference Proceedings

CONTENTS

Appreciation to Gold Sponsorship

新輝(建築管理)有限公司
Sanfield (Management) Ltd.

Sanfield (Management) Limited is the construction arm and wholly-owned subsidiary of Sun Hung Kai Properties Limited, committed to build with hearts to serve Hong Kong and Mainland China, and inspire the construction industry with advanced and innovative engineering technologies and building materials.

Appreciation to Silver Sponsorships

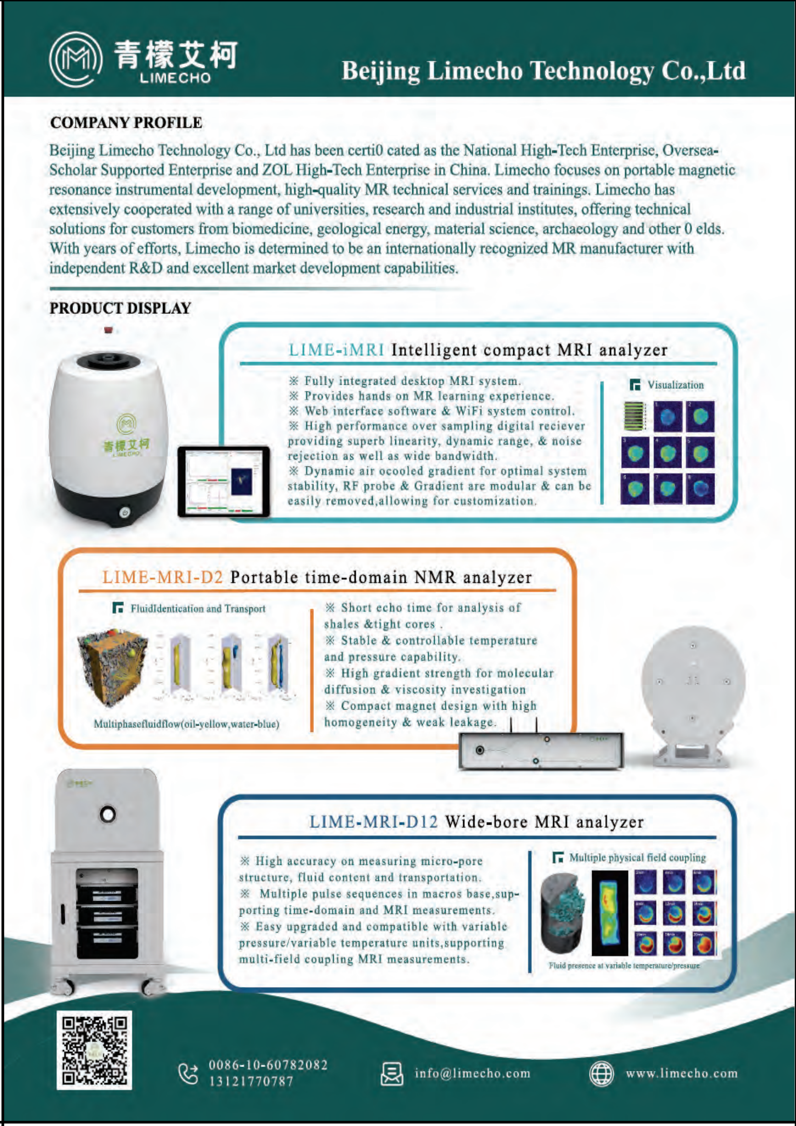

青檬艾柯 LIMECHO

Beijing Limecho Technology Co.,Ltd

COMPANY PROFILE

Beijing Limecho Technology Co., Ltd has been certificated as the National High-Tech Enterprise, Oversea-Scholar Supported Enterprise and ZOL High-Tech Enterprise in China. Limecho focuses on portable magnetic resonance instrumental development, high-quality MR technical services and trainings. Limecho has extensively cooperated with a range of universities, research and industrial institutes, offering technical solutions for customers from biomedicine, geological energy, material science, archaeology and other fields. With years of efforts, Limecho is determined to be an internationally recognized MR manufacturer with independent R&D and excellent market development capabilities.

PRODUCT DISPLAY

LIME-iMRI Intelligent compact MRI analyzer

※ Fully integrated desktop MRI system.
※ Provides hands on MR learning experience.
※ Web interface software & WiFi system control.
※ High performance over sampling digital reciever providing superb linearity, dynamic range, & noise rejection as well as wide bandwidth.
※ Dynamic air ocooled gradient for optimal system stability, RF probe & Gradient are modular & can be easily removed,allowing for customization.

Visualization

LIME-MRI-D2 Portable time-domain NMR analyzer

FluidIdentication and Transport

Multiphasefluidflow(oil-yellow,water-blue)

※ Short echo time for analysis of shales &tight cores .
※ Stable & controllable temperature and pressure capability.
※ High gradient strength for molecular diffusion & viscosity investigation
※ Compact magnet design with high homogeneity & weak leakage.

LIME-MRI-D12 Wide-bore MRI analyzer

※ High accuracy on measuring micro-pore structure, fluid content and transportation.
※ Multiple pulse sequences in macros base,supporting time-domain and MRI measurements.
※ Easy upgraded and compatible with variable pressure/variable temperature units,supporting multi-field coupling MRI measurements.

Multiple physical field coupling

Fluid presence at variable temperature/pressure

☎ 0086-10-60782082
13121770787

info@limecho.com

www.limecho.com

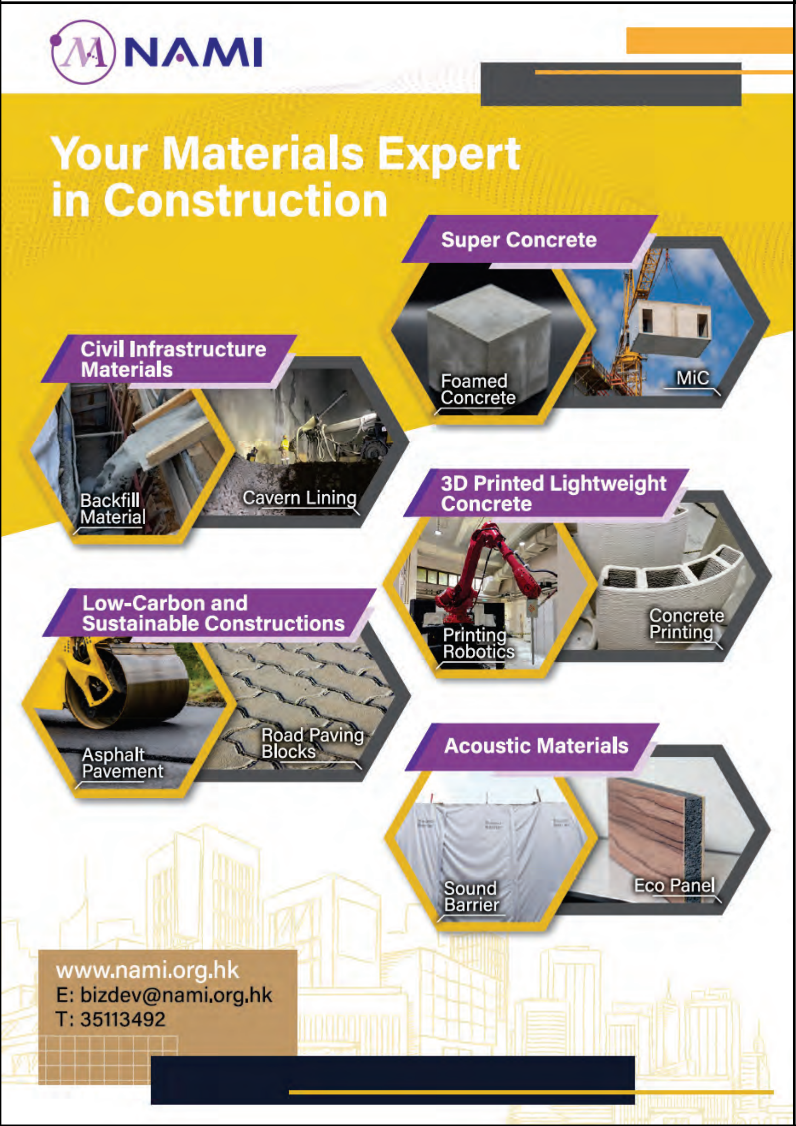

Your Materials Expert in Construction

www.nami.org.hk
E: bizdev@nami.org.hk
T: 35113492

SCORETECH

MASTERING TECHNOLOGY AND PRACTICALITY

The leading dry mortar product manufacturer in Hong Kong utilizing green technologies

Plenary Sessions

Prof. Christopher Cheeseman

Professor of Materials Resources Engineering

Department of Civil and Environmental Engineering

Imperial College London

UK

Review of Industrially Relevant Options for Producing Low-carbon Cement and Concrete using Waste and Alternative Materials

The enormous volumes of concrete used globally mean that it offers major opportunities for the beneficial reuse of waste, either as aggregate, filler or as a supplementary cementitious material. The carbon emissions associated with Portland cement, the main binder in concrete, are also a major issue. There are various ways these can be reduced, and the technologies currently aiming to improve cement sustainability will be reviewed. Many of these use waste and alternative materials. The cement industry is expecting that carbon capture and storage at cement plants will have a major contribution to reducing future carbon emissions. However, technologies using engineered supplementary cementitious materials (SCMs), and the carbonation of wastes, either to form aggregates or SCMs are also expected to have a key role. These include the use of lime calcined clay (LC3) cements, particularly in developing countries, and SCM production from concrete extracted from construction and demolition waste. This technology also has potential to allow the development of circular concrete. Recent research using magnesium silicate minerals as an alternative feedstock, to manufacture low-carbon amorphous precipitated silica and magnesium carbonate construction products, will also be reviewed. The potential impacts of these technologies on achieving low-carbon cement and concrete and opportunities for increased beneficial reuse of waste materials will be discussed.

Biography

Christopher Cheeseman is Professor of Materials Resources Engineering in the Department of Civil and Environmental Engineering at Imperial College London. He is Head of the Materials Section and Director of the Centre for Infrastructure Materials at Imperial, a unique facility specifically dedicated to fundamental and applied research focused on infrastructure materials. Following a period working in industry he joined Imperial in 1990, initially based in the Environmental Engineering Section of the Civil and Environmental Engineering Department. Chris has had a unique opportunity to be involved in a wide range of materials related research associated with waste management, resource efficiency, industrial symbiosis, the circular economy, low carbon cements and greenhouse gas removal technologies. He has supervised over 140 MSc and PhD projects to completion and has published over 240 papers in international journals and conference proceedings. Innovation has formed an important driver for his research and has led to spin-out companies, including Novacem (low-carbon MgO cements), Aeropowder (beneficial reuse applications for waste feathers), Permea (non-clogging permeable pavements) and Seratech (carbon negative concrete).

Prof. Dongmin Wang

Professor

School of Chemical and Environmental Engineering

China University of Mining and Technology (Beijing)

Beijing, China

Research on Resource Characteristics of Red Mud and Preparation and Applications of Waste-based Binder Materials

Ordinary Portland cement (OPC), the main cementitious material in building materials such as mortar and concrete, is responsible for 7% of the world's anthropogenic carbon dioxide emissions. Energy conservation and carbon reduction in the cement industry play a pivotal role in the achievement of Chinese carbon peaking and carbon neutrality goals. For the cement industry with an annual output of nearly 2.4 billion tons of cement clinker in China, the routes of substituting raw resources and flue for the manufacture of clinkers is very limited in popularity and degree of substitution are obviously only a drop in the bucket. Therefore, there is an urgent need to find new low-carbon cementitious material systems comparable to OPC. Waste-based binder materials have significant low carbon advantage and good performances comparable to OPC and especially excellent performances such as sulfate attack and low hydration heat release, which make it a promising alternative to cementitious materials. The red mud produced in the production of alumina oxide by the Bayer process is high-alkalinity and extremely low-utility due to large difficulties to application. Here, the waste-based binders comprising red mud were prepared and developed for several applications in concretes and precast units, road engineering materials, and artificial aggregates et al. The binders present broad and wonderful application prospects. And lastly, the industrialization practices and application progress currently being carried out in Jiaozuo (Henan province) will also be introduced to provide a reference for the development and application of low-carbon cementitious materials.

Biography

Wang Dongmin is a Professor and Ph.D. Supervisor in the School of Chemistry and Environmental Engineering at China University of Mining and Technology (Beijing). Additionally, he serves as an Executive Council Member of the Chinese Ceramic Society and Chairman of the Sub-Committee on Solid Waste and Ecological Materials of the Chinese Ceramic Society. He has been dedicated to research on the fine chemical synthesis and application of modern high-performance cement concrete materials and chemical additives, as well as the treatment of industrial/mining solid waste and the preparation and application of eco-environmental construction materials. His research and patented technologies have been widely applied in major national engineering projects. He has led more than ten key research and development projects of the Ministry of Science and Technology, national natural science funds, regional joint projects of the national natural science funds, and numerous joint research and development projects with industry.

Wang Dongmin has been recognized with multiple provincial and ministerial-level science and technology awards, including the Science and Technology Award of the China Building Materials Federation/Chinese Ceramic Society and the Beijing Science and Technology Award. He has published over 100 papers in journals such as Cement & Concrete Research, Cement & Concrete Composites, Construction and Building Materials, Journal of the Chinese Ceramic Society, and Journal of Building Materials. Additionally, he holds more than 20 authorized invention patents and has authored six academic monographs.

Prof. Zhichao Liu

Professor

School of Materials Science and Engineering

Wuhan University of Technology

Wuhan, China

Industrial Solid Wastes as Carbonatable Binder for CO_2 Utilization

Biography

Prof. Zhichao Liu is currently a Professor at the School of Materials Science and Engineering, Wuhan University of Technology. His research interests include low carbon cement, ultra-high-performance concrete (UHPC), durability and viscoelastic deformation behavior in cementitious materials.

Prof. Julia Stegemann

Professor of Environmental Engineering

Department of Civil, Environmental & Geomatic Engineering

University College London

UK

Construction & Demolition Waste Recovery and the United Nations Framework Classification for Resources

Julia Stegemann[a], Chunbo Zhang[a], Iman Dorri[b] and Soraya Heuss-Assbichler[b]
[a]UKRI Interdisciplinary Circular Economy Centre for Mineral-based Construction Materials, Department of Civil, Environmental & Geomatic Engineering, University College London, UK
[b]Mineralogy, Petrology & Geochemistry, Department of Earth & Environmental Sciences, Ludwig Maximilians Universitaet Muenchen, Germany

The Circular Economy offers a vision of sustainable resource use whereby products, components and materials are maintained at their highest utility and value at all times and scales, with continual interlinked cycling of man-made materials, and cascading cycling of biological materials to ultimately nourish the earth. Its goals are greater economic stability, with more equitable sharing of resources, and maintenance of consumption and environmental impacts within planetary boundaries. The materials and components that comprise construction and demolition waste (CDW) are increasingly recognised as valuable resources in a Circular Economy, but their potential for recovery depends on initiation and operation of sustainable, commercially viable, recovery projects.

In this context, the United Nations Framework Classification for Resources (UNFC) [1,2] provides specifications for classification of anthropogenic resources, as part of the United Nations Resource Management System (UNRMS)[3] . The UNFC is intended to provide transparent information to support developers and investors, including companies, governments and other stakeholders, in decision-making about resource recovery projects. It aims to classify the commercial viability of recovery projects based on: 1) confidence in (understanding of) the quantity of resource to be recovered, 2) the technical feasibility of resource recovery, and 2) environmental-socio-economic viability.

Whereas resource classification has traditionally focussed on technical issues and financial returns (e.g., cost-benefit analysis), there is now an imperative to consider the impacts of recovery projects on wider aspects of environmental and social sustainability. This keynote will present work on-going as part of the Horizon Europe FutuRaM project (https://futuram.eu/) to develop a detailed methodology for classification of anthropogenic resource recovery projects according to the UNFC, which addresses all three pillars of sustainability. Development of a case study for classification of a project to recover resources from a UK demolition site will also be discussed.

---

[1] UNECE (2019) United Nations Framework Classification for Resources, https://unece.org/fileadmin/DAM/energy/se/pdfs/UNFC/publ/UNFC_ES61_Update_2019.pdf

[2] UNECE (2018) Specifications for the application of the United Nations Framework Classification for Resources to Anthropogenic Resources, https://unece.org/fileadmin/DAM/energy/se/pdfs/UNFC/Anthropogenic_Resources/UNFC_Antropogenic_Resource_Specifications.pdf

[3] UNECE (2022) United Nations Resource Management System - Principles and Requirements, https://unece.org/sites/default/files/2023-02/2229237_E_ECE_ENERGY_144_WEB.pdf

Biography

Professor Julia Stegemann is Director of the UKRI Interdisciplinary Circular Economy Centre for Mineral-based Construction Materials, leading a diverse team of 25 co-investigators and more than 50 industrial collaborators to develop the scientific and socio-economic understanding and the technological basis for design and implementation of systems, processes and policy that will support the transition to a resource efficient built environment. Her research and consultancy includes technology and systems development, implementation and evaluation; data mining; computer modelling; and support for waste regulation. She is a co-investigator on the Horizon Europe FutuRaM project, to investigate future availability of raw materials from secondary sources in Europe. Other recent research includes an EPSRC/NSFC project on fate of toxic metals in co-processing of wastes in cement kilns and EPSRC doctoral projects on innovation in construction, materials quantification in building stock, and reuse of building components. JS is also a founding Co-Director of UCL CircEL, a UCL-wide hub for research and education in the Circular Economy and she is an active participant in the UN Framework Classification for Anthropogenic Resources Working Group. She has been funded EPSRC, Innovate UK, European Commission, Leverhulme Trust, Environment Canada, US EPA and industry. JS has published with >100 multidisciplinary and diverse co-authors from >30 excellent institutions in 10 countries.

Mr. Simo Hakkarainen

Business Director

Peikko Group Corporation

Finland

Optimizing Building Life Cycle Carbon Footprint and Operational Emissions with Frame

This abstract explores the importance of optimizing building life cycle carbon footprint and operational emissions through the implementation of a frame system in the construction industry. With the increasing recognition of the building industry's responsibility in climate change mitigation, it becomes crucial to explore strategies that effectively reduce total emissions and encourage sustainable practices. One of the key focuses in this research is the conservation of materials. The concept of "all materials need to be saved" underlines the need to prioritize resource efficiency and minimize waste. The use of adaptable spaces is another key aspect to consider, as it allows for more efficient utilization of buildings throughout their lifespan.

Operational carbon is a significant contributor to the overall carbon footprint of a building. This research will address ways to optimize operational carbon by evaluating the end-of-frame lifecycle and identifying opportunities for reduction and optimization. Additionally, the study will explore the benefits of prefabrication and the use of dismountable connections, which allow for easier deconstruction and reuse of building materials at the end of their life. The cradle to cradle approach will serve as a guiding principle throughout this research. It emphasizes the importance of designing buildings with materials that can be continuously cycled back into the system, minimizing waste and promoting circularity.

The study will focus on three primary construction materials - concrete, steel, and timber - and examine the methods through which their environmental impact can be mitigated. Promising strategies and techniques for optimizing the life cycle carbon footprint and operational emissions will be analyzed, offering practical insights for the industry. By presenting these methods, this research aims to contribute to the ongoing efforts in the building industry to address climate change, enhance sustainability, and foster a more responsible approach to construction.

Biography

Simo Hakkarainen has over 20 years of experience in the construction industry with a diverse background holding different positions. Currently serving as the Business Director in Peikko, in a role overseeing the strategic direction and growth of the organization in the frame business. Simo's educational background is comprehensive, with an MBA, an architecture and an engineering degree. This diverse foundation allows him to bring a unique perspective to his work, combining technical knowledge with business acumen. In addition to his professional accomplishments, Simo is also an experienced lecturer. He has been invited to speak at numerous international events, sharing his insights and expertise with professionals in the construction industry. Sustainability is a key area of interest for Simo. He is particularly passionate about the total impact of carbon on construction projects. Simo strongly believes in the importance of reducing the environmental footprint of the industry through innovative and sustainable practices. Furthermore, Simo is enthusiastic about the effects of digitalization in construction and the power of collaboration. He recognizes the potential for technology to revolutionize the way projects are planned, designed, and executed. Simo also emphasizes the significance of creating spaces that prioritize the well-being and needs of people.

Dr Hirofumi Sakanakura

Head of Material Cycles Assessment Research Section
Division of Material Cycles
National Institute for Environmental Studies
Japan

New Horizon in Interpreting Leaching Mechanisms of Recyclable Materials for Construction

Environmental safety needs to be properly judged for recyclable materials. Among methods for evaluating the environmental safety, leachability of potentially toxic substances are standardized by many national- and international level organizations as leaching tests. However, it is well known that the actual leaching behaviour in field conditions are different from the results of leaching tests conducted indoor. Therefore, establishment of a basic theory that links field condition and indoor leaching test condition is anticipated. This Keynote Presentation highlights new horizons in leaching tests to ensure the theory advances. First, the aspect of adsorption-desorption phenomenon will be introduced in interpreting leaching test results. The key parameter of distribution coefficient, K_d, will be discussed, and the determining method of K_d from a series of batch leaching test with different liquid-solid ratios will be explained. Next, intra-solid diffusion will be introduced. By simultaneously applying the mechanisms of adsorption-desorption equilibrium and intra-solid diffusion, the leaching behaviour that has been observed in Semi-dynamic leach test and Up-flow percolation test but could not have been explained by other theories will be clarified. Besides, the dissolution-precipitation equilibrium that works after leaching from a solid material has been explained by geochemical models. By combining these mechanisms and models, leaching tests in laboratory will become a more robust tool for evaluating the on-site environmental safety of recyclable materials for construction.

Biography

Dr Hirofumi Sakanakura is the Section Head of the Material Cycles Assessment Research Section, Material Cycles Division, National Institute for Environmental Studies (NIES). Before joining NIES in 2006, he worked at Akita National College of Technology. He received his doctoral degree from Hokkaido University in 2000. He is developing environmental safety evaluation system of recyclable materials for construction, in particular, modelling the leaching mechanism from the materials and determining the model parameters by leaching tests. His another focusing research is recovering precious metals and potentially toxic metals from municipal solid waste incineration bottom ash resulting improvement of environmental safety when using them in construction.

Prof. Baoshan Huang

Professor

Department of Civil and Environmental Engineering

University of Tennessee – Knoxville

USA

Recycling in Asphalt Pavements

Asphalt pavement has been attracting various recycling applications. The biggest recycling application in asphalt pavements is the recycling of asphalt pavement itself - reclaimed asphalt pavement (RAP). This presentation reviews the progress during the last twenty years, through the presenter's own research experiences, of the pavement community's understanding of the blending mechanism between the recycled and refresh asphalt binder when RAP is applied during the construction of asphalt pavements; as well as the improvements of technologies on utilizing RAP during the design and construction of asphalt pavements. Another big interest of recycling application in asphalt pavements in the US is the incorporation of recycled plastics in asphalt pavements. The presenter will be showing an on-going research on an innovative procedure to produce quality modified asphalt binder by incorporating the co-stabilized waste plastics and lightly pyrolyzed crumb rubber compound, covering several aspects from the fundamental reaction mechanisms, to engineering properties, and to scaled-up production for field deployable plastic-asphalt binder system.

Biography

Dr. Baoshan Huang is a scholar in civil infrastructure engineering and a civil engineering practitioner in pavement and geotechnical engineering. He received his Ph.D. degree in civil engineering from Louisiana State University, his M.S. and B.S. degrees from Tongji University in Shanghai, China. His professional career includes over 30 years of experience in transportation and geotechnical engineering with academia, industry, and government agencies. Dr. Huang has published over 290 peer-reviewed journal papers that have received over 10,644 Web of Science citations. He has been awarded six US patents as the primary inventor and has one additional pending patent.

Dr Harn-wei Kua

Vice Dean & Associate Professor
College of Design and Engineering
National University of Singapore
Singapore

Toward Net Zero Carbon – Advances in using Biochar for Sustainable Infrastructure and Urban Landscape

In the past 11 years, applications of biochar in construction materials and different functions in urban settings have seen considerable advancement. As a solid by-product of pyrolysis or gasification, biochar used to be discarded as waste. Shown to be a potentially carbon negative material from the life cycle perspective, biochar has been studied and shown, time and again, that it can enhance various hygromechanical properties of concrete and asphalt. Coupled with its potential to reduce net carbon emission from soil in the urban environment, biochar's value-added to the sustainability of existing and new-built infrastructures is beginning to gain popularity in numerous countries around the world, including Singapore.

Focusing on concrete, the benefits afforded by biochar will be highlighted – which include the "lock-in" of carbon (in the char), avoided carbon dioxide (CO2) emissions due to replacement of equivalent amount of fossil fuels with synthetic gas (generated from pyrolysis or gasification), potential reduction in dimensions of structural members containing biochar, and the use of biochar to augment accelerated carbonation of concrete.

Different CO2-dosing methods on biochar concrete and their effects on the carbon sequestration and mechanical properties of concrete will be discussed. On that note, deployment of biochar in different types of concrete will also be summarized. Finally, the use of biochar in specialised functions in the built environment, such as in water-resistant wall coating and even coloured paint, will be presented to illustrate possible future applications of this material that is only beginning to capture our imagination!

Biography

Associate Professor Harn Wei Kua is the leader of the Smart Materials Laboratory of the Department of the Built Environment and the construction 3D printing Thrust Lead in National University of Singapore (NUS). He is also one of the Vice Deans of the College of Design and Engineering. His current research interest is in upcycling and valorisation of biological waste into high performance smart building materials and novel life cycle sustainability assessment methodologies. He is recognized as one of the main drivers of biochar concrete research and global development. Dr Kua has authored more than 130 articles and book chapters. He has been invited to deliver about 100 speeches on various topics related to his research, and he has more than 80 awards and honours for his academic and community service works, including the MIT Carrol Wilson Fellowship, Rockefeller Foundation Academic Writing Residency Fellowship, Fellow of the International Association of Advanced Materials (IAAM), IAAM Scientist Award. In November 2022, he was awarded the *von Klitzing International Engineering Award* (which was established in honour of the 1985 Nobel laureate in physics Klaus von Klitzing).

Prof. Chi-sun Poon

Michael Anson Professor in Civil Engineering, Chair Professor of Sustainable Construction Materials, Head of Department of Civil and Environmental Engineering and Director of Research Centre for Resources Engineering towards Carbon Neutrality

The Hong Kong Polytechnic University

Hong Kong

Turning Wastes into Construction Resources – Hong Kong Perspectives

Biography

Prof. Chi-sun Poon is currently the Michael Anson Professor in Civil Engineering, Chair Professor of Sustainable Construction Materials, Head of Department of Civil and Environmental Engineering (CEE) and Director of Research Centre for Resources Engineering towards Carbon Neutrality (RCRE) of The Hong Kong Polytechnic University (PolyU). He is also one of the Directors of PolyU-NAMI 3D Concrete Robotic Printing Research Centre (RCC3D). He has been awarded the title of Changjiang Chair Professor by the Ministry of Education in 2017. Prof. Chi-sun Poon specializes in the research and development of environmental-friendly construction materials, waste management, waste recycling technologies, concrete technologies and sustainable construction. He is an Editor of Construction and Building Materials since 2014. He is also an Editorial Board Member of Cement and Concrete Composites since 2017. Prof. Poon has published over 700 papers in international journals and conferences (including 580 international journal papers, 160 referred conference papers, and 6 book chapters). His current h-index is 108 with the total number of over 42,000 citations in Scopus. He has obtained more than 10 patents related to concrete and waste recycling technologies. He has been listed among the World's Top 2% Scientists released by Stanford University. He was awarded the State Technological Innovation Award 2017 (2nd Class).

Session A1

Low Carbon Cements and Binders

POTENTIAL OF USING CALCINED CLAY AS A SUPPLEMENTARY CEMENTITIOUS MATERIAL FOR THE PRODUCTION OF LOW-CARBON CEMENT

Chenyuan Ji, **Zengfeng Zhao***, Lei Yao, Can Lin and Jianzhuang Xiao

Tongji University, Department of Structural Engineering, College of Civil Engineering, Shanghai, China
*E-mail: zengfengzhao@tongji.edu.cn

This study investigates the performance of oven-dried clay and calcined clay used as supplementary cementitious martial (SCM) to produce a blended low-carbon cement. Calcined clay was treated under 800°C while the oven-dried clay was dried at 105°C, and then those kinds of clay was ground into powder with ball mining time of 15min, 20min and 25min. Three mixtures, including a reference mixture with Portland cement and two mixtures with oven-dried or calcined clay, were tested and compared to study the feasibility of using treated clay as SCMs in the production of low-carbon cement. Also, a new method of using wet clay was also adopted to assess its possibility used as low-carbon cement. The results indicated that the substitution of 30% cement with either oven-dried or calcined clay can both meet the requirements of mortar with the help of a superplasticizer, but the fluidity property of mortar will be decreased. Meanwhile, the incorporation of oven-dried clay slightly reduced the compressive and flexural strengths, while the calcined clay formed a more amorphous phase compared with the system of oven-dried one, which further improved the mechanical performance of mortar. Using wet clay to prepare mortar is feasible, but it slightly decreased the strength of mortar. Therefore, both oven-dried and calcined clay can be used as SCM to produce low-carbon blended cement.

Keywords: calcined clay; supplementary cementitious material; low carbon cement; mechanical properties

VALORIZATION OF WASTE GLASS FOR LOW-CARBON CONCRETE PRODUCTION IN SINGAPORE

Bong Shin Hau, **Luo Zhiyu**, and Du Hongjian*

Department of Civil and Environmental Engineering, National University of Singapore, 117576
Singapore, Singapore
*Email: ceedhj@nus.edu.sg

1. INTRODUCTION

Waste glass is one of the most common wastes. After end of service, glass products are generally discarded to landfills. The global waste glass recycling rate is reported to be only around 22% (Westbroek, Bitting, Craglia, Azevedo, & Cullen, 2021) and the rate is especially low in Asian countries such as around 14% in Singapore (NEA, 2022) and 13% in Mainland China (Tang, Li, Tam, & Xue, 2020). Waste glass containing mainly amorphous silica can react with $Ca(OH)_2$ crystals to form calcium silicate hydrate (C-S-H), contributing to the durability and later-age mechanical properties of concrete. Besides, replacing cement with glass powder can reduce the carbon footprint of concrete. It is of great significance to recycle waste glass as a supplemental cementitious material (SCM). Although relevant research can be found in as early as the 1970s (Pattengil & Shutt, 1973), the practical application of glass powder in concrete is still at an early stage. To date, there are still challenges restricting the prevalence of glass powder as a component in commercial cement products, and glass in many countries is still treated as troublesome waste rather than valuable resources. This study reports the results from lab and trial production for applying waste glass powder as SCM in Singapore. The performance, environmental impacts, and production-related issues of glass powder concrete are presented and discussed.

2. MATERIALS AND METHODS

Waste glass bottles were collected from the National University of Singapore's campus. The bottles were soaked in water to remove the residues and labels and then subjected to crushing and milling processes. The medium size of the glass powder obtained is 9.68 μm. The X-ray fluorescence (XRF) results in **Table 1** show that the waste glass belongs to soda-lime glass, containing around 70% of SiO_2. The glass powder was used to replace 0, 10%, 20% or 30% of cement. The mix design is shown in **Table 2**, where all samples achieved a slump of 100-150 mm.

Table 1. Chemical compositions of glass powder (% by weight).

Oxide	SiO_2	Al_2O_3	CaO	Fe_2O_3	MgO	Na_2O	TiO_2	SO_3	K_2O	Cr_2O_3	Others
Glass	70.5	1.79	11.34	0.4	1.97	13.26	0.06	0.19	0.26	0.08	0.15

Table 2. Mix proportion of concrete.

Group	Coarse aggregate (kg/m^3)	Sand (kg/m^3)	Water (kg/m^3)	Cement (kg/m^3)	Glass powder (kg/m^3)	Initial SP (l/m^3)	Additional SP (l/m^3)
C	1010	772	171	385	0	2.3	0
G1-10	1010	772	171	346.5	38.5	2.3	0.2
G1-20	1010	772	171	308	77	2.3	0.2
G1-30	1010	772	171	269.5	115.5	2.3	0.4

3. RESULTS AND DISCUSSION

3.1 Mechanical properties

Figure 1 (a) presents the compressive strength of concrete samples tested following EN 12390-3. As can be seen in the figure, replacing glass powder with cement has significant impact on the early-age compressive strength of the concrete. The 2-day compressive strengths of concrete with 10%, 20% and 30% glass powder were 20%, 20% and 43%, respectively, lower as compared to that of the control concrete. The concrete with 10% and 20% glass powder exhibited comparable 7-day and 28-day compressive strengths to the control concrete. However, the 7-day and 28-day compressive strengths of the concrete with 30% glass powder were 36% and 31%, respectively, lower than those of the control concrete. The flexural strength of hardened concrete was measured in four-point bending test setup in accordance with EN 12390-5. As shown in **Figure 1 (b)**, glass powder content has insignificant impact on the flexural strength of the concrete. Overall, the optimum cement replacement rate in terms of mechanical properties is 20%.

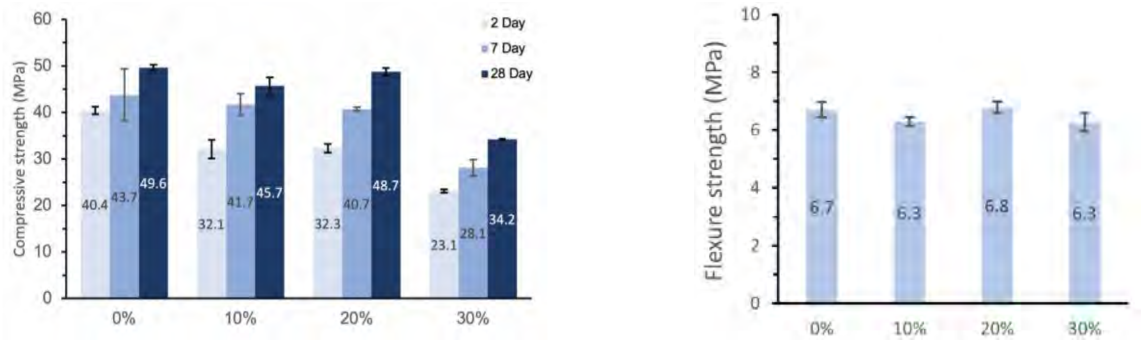

(a) Compessive strength at different ages (b) Flexural strength at 28 days

Figure 1. Mechanical performance glass concrete.

3.2 Durability

A high amount of amorphous SiO_2 in glass powder has been concerned about alkali-silica reaction (ASR) when used in concrete. **Figure. 2** reports the length change of samples over time. ASTM C1260 specifies that the expansions of less than 0.10 % at 16 days after casting are indicative of innocuous behaviour. Obviously, all samples investigated had expansions of less than 0.10 % at 14 days after being stored in NaOH solution (corresponding to 16 days after casting). Besides, the result shows that all glass concrete samples experienced lower expansion than control concrete and the expansion of concrete decreased with the increase of the glass powder content. Thus, the result evidenced that using glass powder does not cause deleterious expansion and cracking of concrete. Instead, glass powder contributed to mitigate the potential risk of ASR.

The water permeability of glass concrete was evaluated by the depth of water penetration under high pressure in hardened concrete in accordance with BS EN 12390-8. As shown in **Figure. 3 (a)**, glass powder positively decreased the water penetration depth, and the effect is especially significant when high glass powder percentage of 30% is used. Similarly, the rapid chloride migration (RCM) results (NT BUILD 492) shown in **Figure. 3 (b)** also reveal the beneficial effects of glass powder. The migration coefficient values of concrete sample with 20% and 30% glass powder were 44% and 58%, respectively, lower than that of the control concrete sample.

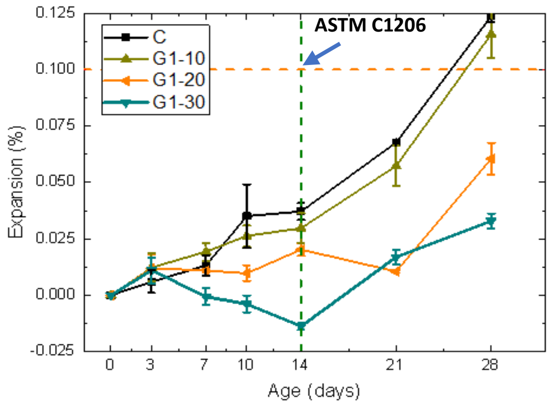

Figure 2. ASR expansion of glass concrete over time.

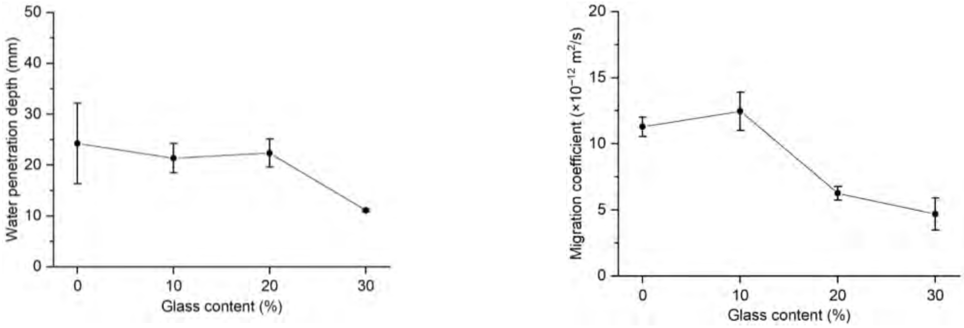

(a) Water penetration depth (b) Chloride migration coefficient

Figure 3. Water penetration and RCM results of glass concrete.

3.3 Trial production of glass concrete

Trial production of glass concrete was conducted as shown in **Figure. 4 (a)**. The glass concrete kerbs were produced by a ready-mix concrete company in Singapore. The bending strength of the kerbs are presented in **Figure. 4 (b)**. Singapore standard SS 214 (SSC, 2022) requires that the bending strength of concrete kerbs shall not be less than 5 MPa. The bending strength of samples all meet the standard and the glass concrete kerbs even have higher bending strength than the control sample. Besides, the water absorption of control, G1-10, G1-20 is 4.12%, 4.55% and 4.87%, respectively, all lower than the limit of 6% specified by SS 214. Therefore, the results indicate the satisfactory performance of glass concrete products produced by industry.

(a) Kerbs (980 mm×125 mm×250 mm) (b) Bending strength of kerbs

Figure 4. Trial production of glass concrete kerbs.

4. CONCLUSION

The investigations and analysis from this study have validated the feasibility of developing low-carbon concrete from waste glass powder in Singapore. The main conclusions can be drawn as follows:

(1) Increasing glass powder content up to 20% has no significant negative effect on the 7-day and 28-day compressive strengths of the concrete.

(2) Glass concrete has superior durability such as ASR resistance, water penetration resistance and chloride ion corrosion resistance to control concrete. The durability improves with increasing amounts of glass powder.
(3) The performance of glass powder concrete kerbs in trial-production meets the requirements of Singapore standard.

5. ACKNOWLEDGMENT

The authors would like to express appreciation for the support from JTC Singapore [A-0009546-01-00].

6. REFERENCES

NEA. (2022). Waste Statistics and Overall Recycling. *National Environment Agency*.

Pattengil, M., & Shutt, T. (1973). *Use of ground glass as a pozzolan.* Paper presented at the Proc., Int. Symp. on Utilization of Waste Glass in Secondary Products, ASCE, Albuquerque, NM.

SSC. (2022). SS214: Specification for concrete kerbs. In. Singapore: Enterprise Singapore.

Tang, Z., Li, W., Tam, V. W. Y., & Xue, C. (2020). Advanced progress in recycling municipal and construction solid wastes for manufacturing sustainable construction materials. *Resources, Conservation & Recycling: X, 6*.

Westbroek, C. D., Bitting, J., Craglia, M., Azevedo, J. M. C., & Cullen, J. M. (2021). Global material flow analysis of glass: From raw materials to end of life. *Journal of Industrial Ecology*.

ENHANCING PERFORMANCE OF SUPERSULFATED CEMENT (SSC) USING WASTE ALKALINE ACTIVATORS: RED MUD AND CARBIDE SLAG

Jixiang WANG, Dongmin WANG*, and Ze LIU

China University of Mining and Technology (Beijing), Beijing, China
*E-mail: wangdongmin@cumtb.edu.cn

1. INTRODUCTION

Supersulfated cement (SSC) is one of the most promising low-carbon binders, consisting of 60-85% blast furnace slag mixed with 10-20% calcium sulfate, along with a few alkaline activators such as clinker (**Z. Sun et al., 2022**). Due to being free of primary resources and non-sintered, SSC produces significantly lower CO2 emissions (**Wu, Xue, & Yu, 2021**), making it the subject of considerable attention from academia and industry as an alternative to OPC. However, the relatively slow development of mechanical properties of sulfate-activated slag cement in the early stage has limited its practical application. To address this, the present study proposes the use of red mud, a byproduct of alumina oxide production through the sintering process (**Wang & Liu, 2012**) and the residue of acetylene produced by calcium carbide hydrolysis (**H. Sun et al., 2015**) as alkaline activators to adjust and improve the performance of traditional SSC. Through a systematic investigation of the phases' assemblage evolution, microstructure, and hydration performances, this study aims to discuss the improvements and adjusting mechanisms in detail, providing new insights and a deeper understanding of the reaction mechanism of SSC.

2. MATERIALS AND METHODS

2.1 Materials

Except for the main raw materials, blast furnace slag, and gypsum, which are used in the production of SSC, two industrial solid wastes, sintering red mud, and carbide residue, are employed as alkaline activators to enhance the performance of SSC. **Figure 1** displays the mineralogical compositions of sintering red mud, along with its main elemental compositions. Carbide residue is generated during the production of acetylene through calcium carbide hydrolysis, and it mainly consists of $Ca(OH)_2$, as indicated in **Figure 2**. The content of $Ca(OH)_2$ in carbide residue is determined to be 70.13% (calculated from the weight loss observed between 341 and 520◦C) using TGA).

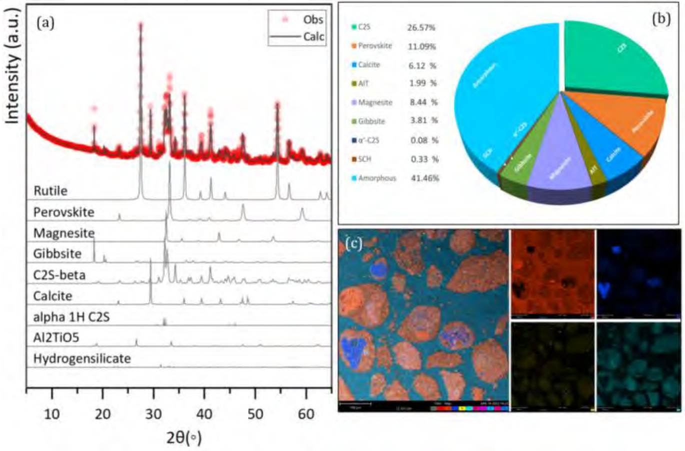

Figure 1. Bauxite residual that discharged from sintering process, (a) XRD patterns and phase assemblages in red mud; (b) quantitative results by Rietveld refinement; (c) elements compositions of red mud partcles.

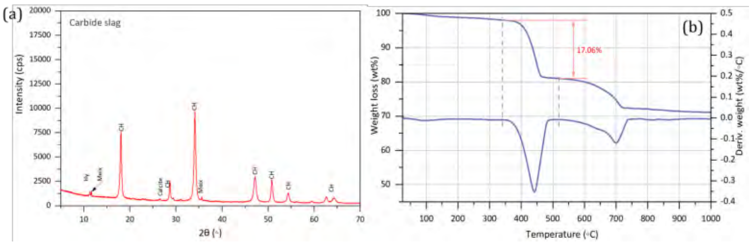

Figure 2 (a) XRD patterns and (b) TG curve of carnide residue.

2.2 Method

In the studied SSC systems, 20 wt% of gypsum was fixed based on previous research, while the alkaline activator, carbide residue, was used in amounts of 0.5 wt%, 1.5 wt%, and 3 wt%, respectively. Sintering red mud-bearing SSCs were prepared by substituting blast furnace slag with ratios of 10 wt%, 20 wt%, and 30 wt%, respectively. The remaining component was blast furnace slag. SSC paste was prepared with a water-to-binder mass ratio of 0.4. After demolding, specimens with dimensions of 40 mm × 40 mm × 40 mm were used for compressive strength tests, and 2 mm thick slices were cut for characterization. Isothermal calorimetry (IC) measurements were conducted using TAM Air calorimetry. The reaction products were analyzed by XRD (Smartlab SE (Rigaku) diffractometer equipped with a D/teX Ultra 250 1D detector) and SEM (Phenom Pure G6 Desktop SEM), respectively.

3. RESULTS AND DISCUSSION

3.1 Optimal carbide residue content and its effectes on SSC hydration

Figure 3 shows the compressive strength of SSC paste at different curing ages. It is observed that the specimen's strength decreased with increasing carbide content at all ages. The SSC system with 0.5 wt% carbide residue exhibited the best strength development. Based on the hydration mechanism of SSC, this trend can be explained. (**Gruskovnjak et al., 2008; Harashima & Ito, 2016; Matschei, Bellmann, & Stark, 2005**), The hydration process of SSC involves two distinct processes: C-S-H deposition and ettringite formation. These two processes appear to be independent, with C-S-H deposition occurring initially. Once the liquid composition reaches the critical supersaturation state, ettringite forms rapidly and densely. As ettringite predominantly forms, the hydration reaction of SSC decreases significantly, reaching a very low level due to the coverage of slag particles. Alkaline activator-calcium hydroxides play a crucial role in adjusting the two main reaction processes: C-S-H deposition and ettringite formation, not only during the initial reaction time but also throughout the duration of the reaction. From the calorimetry response in **Figure 4**, it is evident that the ettringite formation reaction is delayed with an increase in carbide slag content. However, an optimal content exists at a 1.5 wt% dosage.

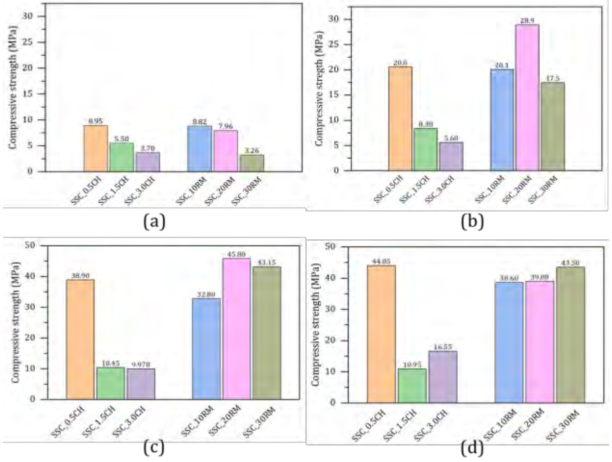

Figure 3 the compressive strength of SSC with different dosage of carbide residue and red mud, (a) 1d, (b) 3d, (c) 7d, and (d) 28d.

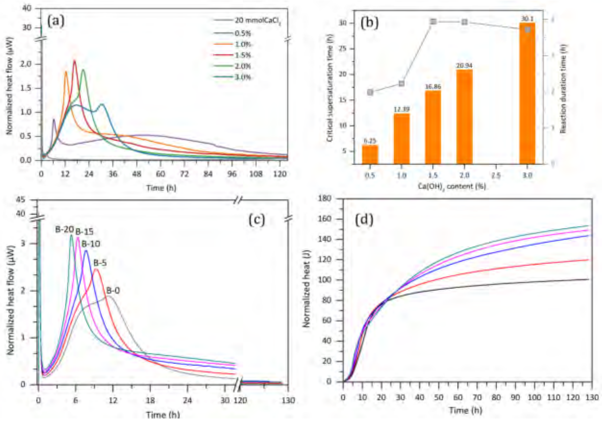

Figure 4 Effects of carbide residue and red mud on the isothermal calorimetry responses of SSC, (a) effects of carbide residue on the normalized heat flow of SSC, (b) carbide residual on the hydration process, effects of red mud on the the normalized heat flow (c) and (d) normalized heat of SSC.

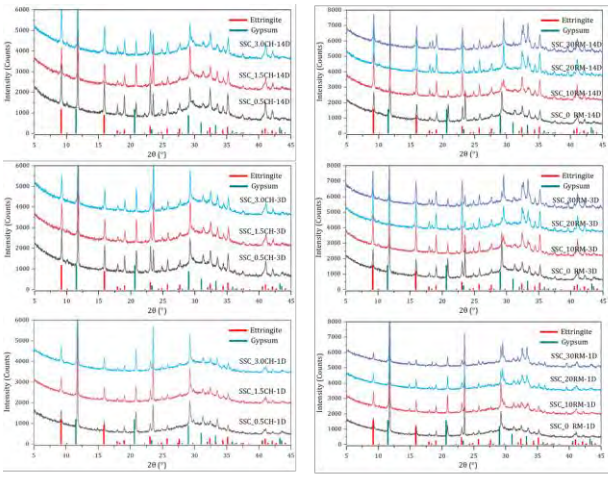

(a) (b)

Figure 5 Phase assemblage of SSC influenced by (a) carbide residue and (b) sintering red mud.

3.2 Optimal red mud content and its effects on SSC hydration

The calorimetry responses in **Figure 4** clearly show that red mud accelerates the SSC reaction. When the red mud content reached 20 wt%, a slight increase has been observed. The compressive results in **Figure 3** also provide evidence of the optimal red mud content being 20 wt%. From the XRD patterns in **Figure 5**, it is evident that the addition of red mud did not change the types of hydration products; however, it significantly increased the ettringite content. There are two possible effects of red mud in the system. One is that the porous red mud particles accelerate SSC hydration (see **Figure 1c**). The other is that the residue of Al-bearing phases in red mud may facilitate the SSC reaction. Due to the limited results currently available, these assumptions require further evidence, which will be investigated in the next set of experiments.

4. CONCLUSION

In this study, industrial solid waste alkaline activators (carbide residue and sintering red mud) have been used to enhance the performances of SSC. The effect mechanism of these activators on the SSC hydration reaction has been investigated and discussed. The following conclusions can be drawn, which would facilitate insight into the reaction mechanism of SSC and the broader application of SSC:

1) Alkaline activator-calcium hydroxides play a very important role in adjusting the two main reaction processes - C-S-H deposition and ettringite formation. Not only the initial reaction time but also the duration time are dependent on the content of calcium hydroxide. Additionally, there is an optimal alkaline activator content.

2) Sintering red mud accelerated the SSC reaction within the 20 wt% substitution of blast furnace slag and improved the performance of SSC. The possible reasons are that porous red mud particles facilitate SSC hydration reaction or Al-bearing components in red mud facilitate the reaction products in SSC.

5. ACKNOWLEDGMENT

The financial support from the National Key Research and Development Program of China under contract No.2022YFC3803102 and Chinese National Natural Science Foundation- Regional Innovation and Development Joint Fund Nos.U20A20313 are gratefully acknowledged.

6. REFERENCES

Gruskovnjak, A., Lothenbach, B., Winnefeld, F., Figi, R., Ko, S. C., Adler, M., & Mäder, U. (2008). Hydration mechanisms of super sulphated slag cement. *Cement and Concrete Research, 38*(7), 983-992. doi:https://doi.org/10.1016/j.cemconres.2008.03.004

Harashima, A., & Ito, K. (2016). The Conditions of Ettringite Formation by the Reaction of a Blast Furnace Slag with Aqueous Alkaline Solutions. *ISIJ International, 56*(10), 1738-1745. doi:10.2355/isijinternational.ISIJINT-2016-347

Matschei, T., Bellmann, F., & Stark, J. (2005). Hydration behaviour of sulphate-activated slag cements. *Advances in Cement Research, 17*(4), 167-178. doi:10.1680/adcr.2005.17.4.167

Sun, H., Li, Z., Bai, J., Memon, S. A., Dong, B., Fang, Y., . . . Xing, F. (2015). Properties of Chemically Combusted Calcium Carbide Residue and Its Influence on Cement Properties. *Materials, 8*(2), 638-651. Retrieved from doi:10.3390/ma8020638

Sun, Z., Nie, S., Zhou, J., Li, H., Chen, Z., Xu, M., . . . Wang, Y. (2022). Hydration mechanism of calcium sulfoaluminate-activated supersulfated cement. *Journal of Cleaner Production, 333*, 130094. doi:https://doi.org/10.1016/j.jclepro.2021.130094

Wang, P., & Liu, D.-Y. (2012). Physical and Chemical Properties of Sintering Red Mud and Bayer Red Mud and the Implications for Beneficial Utilization. *Materials, 5*(10), 1800-1810. Retrieved from doi:10.3390/ma5101800

Wu, Q., Xue, Q., & Yu, Z. (2021). Research status of super sulfate cement. *Journal of Cleaner Production, 294*, 126228. doi:https://doi.org/10.1016/j.jclepro.2021.126228

UTILIZATION OF HIGH TITANIUM SLAG TO IMPROVE THE FIRE-RESISTIVE PROPERTIES OF LOW CARBON CEMENTITIOUS COMPOSITES

Ma, Xiaomeng, Pan, Jinlong

Key Laboratory of Concrete and Prestressed Concrete Structures of Ministry of Education, School of Civil Engineering, Southeast University, Nanjing 211189, P R China

The dumpling of high titanium slags (HTS) occupies abundant land resources and aggravates air, soil as well as water pollution. The meso-regulatory function of the lightweight and thermally stable porous HTS can improve the fire resistive properties of cementitious composites. This paper prepares fire resistive cementitious composites with favorable high temperature resistance by using HTS and studies the residual mechanical properties and microstructure variations after exposure to elevated temperatures. The results reveal that the moderate HTS addition contributes to increasing the residual mechanical strength due to support of interface transition zone microstructure skeleton, modified internal pore structure and high temperature reaction overwhelms the strength loss after high temperature heating. Meanwhile, the addition of HTS does not lead to the change of mineral phase transition trend after high temperature. Instead, the improvement on thermal insulation performance increases the initial temperature of internal mineral phase decomposition, which effectively weakens the mechanical property deterioration caused by thermal decomposition. Finally, based on the CT results, the variation of internal pore structures including pore distribution, porosity and fractal dimensions are systematically analyzed.

Keywords: Fire resistive, solid waste, high temperature, pore structures, residual mechanical properties

RECYCLING CO-COMBUSTION ASH OF SEWAGE SLUDGE AND RICE HUSK FOR LOW-CARBON CONSTRUCTION MATERIAL PRODUCTION

Yan Xia, Lei Wang*

State Key Laboratory of Clean Energy Utilization, Zhejiang University, Hangzhou, 310027, China
*E-mail: wanglei.leo@zju.edu.cn

Incineration is considered as a safe and efficient sewage sludge treatment method. In this study, rice husk was blended with sewage sludge to increase the total calorific value of the mixture. Experimental results revealed that the blending of sewage sludge with rice husk increased the burnout profiles of the fuel and enhanced the stability of the combustion process. The co-combustion of sewage sludge and rice husk bring abundant amorphous SiO_2 in the co-combustion ash (CCA). CCA exhibited a much higher pozzolanic activity than ordinary sewage sludge ash (SSA), which could be recycled in mortars or concretes as a supplementary cementitious materials. The 72-day compressive strength of blended cement with 30 wt% CCA was comparable to that of pure cement. The pozzolanic reaction of CCA was reflected on the second peak of heat flow curves of the deceleration period. Secondary hydration products are generated from the pozzolanic reaction of CCA, which refines the pore structure and promotes the strength development of CCA-based blended composites. CCA-based composites exhibited greater environmental benefits than SSA-based blended composites, owing to that fossil consumption and toxic substance emissions during the co-combustion of rice husk and sewage sludge were lower than that during the mono-combustion of sewage sludge.

Keywords: Sewage sludge, Co-combustion ash, Low-carbon cementitious material, Hydration kinetics, Sustainable waste management

EFFECT OF FLY ASH, SILICA FUME AND COARSE GRADATION IN OPTIMIZING THE MECHANICAL PROPERTIES OF HIGH-PERFORMANCE CONCRETE

Cuevas, D, Bero, B, Cabangangan, T, Hilario A, Samudio L, Santos C, Uson T

Technological Institute of the Philippines – Manila
dgcuevas.ce@tip.edu.ph, mkcbero@tip.edu.ph, mtjgcabangangan@tip.edu.ph,
madhilario@tip.edu.ph, lmsamudio.ce@tip.edu.ph, mcdsantos@tip.edu.ph, mtmsuson@tip.edu.ph

The Philippines' construction industry was expected to grow, particularly in infrastructure construction. This growth would lead to an increased demand for cement, which can have detrimental effects on the environment. As a solution, related studies use supplementary cementitious materials as a partial replacement for cement. This study used the Modified Andreasen and Andersen Particle Packing Model (MAA PPM) to create high-performance concrete (HPC), demonstrating that optimizing the curve for concrete mixtures improved the packing density of the concrete.

This study used different ASTM standards tests to assess the effect of the MAA PPM and the parameter on the properties of concrete. The results indicated that increasing the fly ash binder (FA/B) ratio and silica fume binder (SF/B) ratio enhanced workability for fresh properties. However, the results for hardened properties varied. It achieved the highest compressive, tensile, and flexural strength at the median level of 25% FA/B ratio. Conversely, SF showed a direct relationship with hardened properties wherein as it reaches its highest level of 12.5%, the concrete strength also reaches its peak values. A finer gradation between 4.75mm and 12.5mm improves workability and hardened properties. This study predicts values of fresh and hardened properties through an Artificial Neural Network (ANN) model and equation-derived values. Compared to experimental data, the ANN model yielded a lower average error of 5.11% for slump and 1.52% to 5.94% for 28-day compressive, split tensile, and flexural strength results compared to equation-derived results. These findings suggest that the ANN model predicts concrete qualities with a minimal error by capturing complex data linkages. Incorporating the MAA PPM in concrete mixtures with fly ash (FA) and silica fume (SF) as partial replacements for cement enhanced the mechanical performance and properties of the concrete, consistently demonstrating the potential to achieve a high-performance concrete mix.

Keywords: Supplementary Cementitious Materials, Modified Andreasen and Andersen, Artificial Neural Network

INVESTIGATION OF MECHANICAL PROPERTIES AND MICROSTRUCTURAL EVOLUTION OF CEMENTITIOUS MATERIALS CONTAINING WASTE CLAY BRICK POWDER AT LOW WATER-CEMENT RATIO

Shujun Li, Xu Luo, Yasong Zhao, Cheng Liu, and Jianming Gao*

School of Materials Science and Engineering, Southeast University
*E-mail: jmgao@seu.edu.cn

1. INTRODUCTION

Due to pozzolanic activity, waste clay brick powder (WBP) has received extensive attention in the reuse of waste clay brick in recent years. However, the pozzolanic activity of WBP is not significant compared to traditional supplement cementitious materials such as fly ash, granulated blast furnace slag and silica fume, leading to a poor potential in the conventional water-binder ratio of the specimen. Therefore, this paper investigates the potential of WBP in low-water-to-cement ratio specimens with higher "tolerance" in order to further broaden the use of WBP.

2. MATERIALS AND METHODS

2.1. Materials

Portland cement (PC) P•I 42.5 (Chinese Standard GB175-2007) was used in this study. Waste clay bricks (WCBs) were collected from a construction waste disposal site in Nanjing. These WCBs were screened, crushed, sieved, and ground to produce WBP. The main mineral composition and particle size distribution of PC and WBP are shown in Figures 1 and 2, respectively.

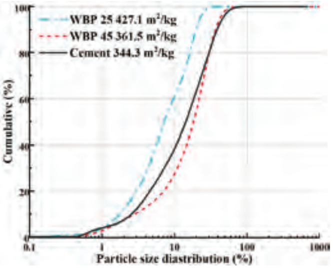

Figure 1. Particle size distribution and Blaine specific surface.

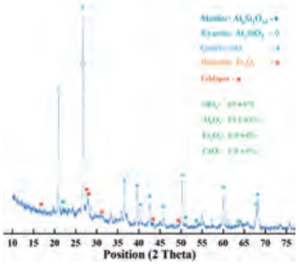

Figure 2. X-ray diffraction pattern of RBP.

2.2. Sample preparation

The moulding process for mortar specimens followed the standard GB/T 17617-2021 (equivalent to EU 196-2005). The moulding process of paste samples complied with the standard GB/T 1346-2011, and the water-to-binder ratio was 0.25. The pure cement slurry is named CP, and the paste containing fine WBP and coarse WBP is named BP25 and BP45, respectively.

Table 1 Mixing proportions of mortar samples (g).

Sample codes	W/B	Cement	RBP	Water	Sand
CP	0.5	450	-	225	1350
BP25/BP45	0.5	315	135	225	1350

2.3. Thermogravimetric analysis (TGA)

TGA was performed using a Simultaneous Thermogravimetry-Differential Scanning Calorimetry instrument (STA 449 F5 Jupiter). The method for semi-quantification of portlandite was adapted from the method proposed by Taehwan et al. [2].

2.4. Mercury intrusion porosimetry (MIP)

The intrusion pressure was performed progressively from 0.10 psi to 61,000 psi. The pore range tested is from 3.0 to 320 μm. The contact angle between the mercury and pore surface is 130°.

2.5. Depth-sensing indentation (DSI)

This nanoindentation instrument is equipped with a Berkovich indenter for nanoindentation testing and has a loading range of 0 to 500 mN. A loading rate of 0.2 mN/s was used. After reaching 2 mN/s, it was held for 5 seconds before unloading at the same rate of 0.2 mN/s.

3. RESULTS AND DISCUSSION

3.1 Compressive and flexural strength

When the W/B was 0.25, mortars containing WBP exhibited compressive and flexural strengths similar to those of pure cement mortars. Moreover, an observable increase in strength was observed with increasing age of WBP-containing mortars.

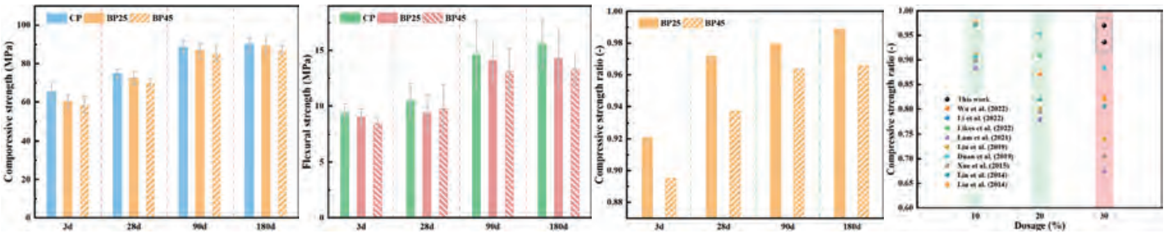

Figure 3. Results of compressive and flexural strengths of mortar containing WBP [3-11].

3.2 TGA

Blended pastes containing WBP exhibited a significant additional decrease in the content of calcium hydroxide (CH) and an increase in the content of chemically bound water (CBW), indicating the contribution of pozzolanic activity of WBP to the formation of reaction products in the system.

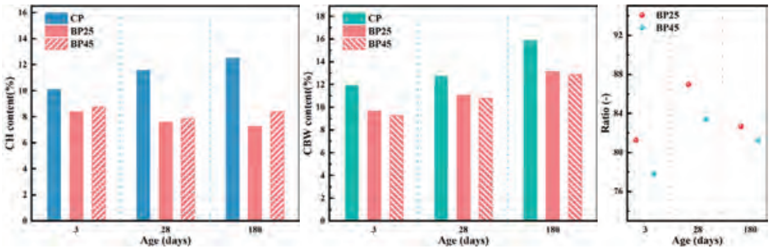

Figure 4 Content of CH and CBW in paste samples at different ages.

3.3 MIP

Blended pastes containing WBP show a pore volume similar to that of cement pastes up to 180 days. Furthermore, Blended pastes containing WBP possess a refined pore structure that becomes increasingly apparent with age.

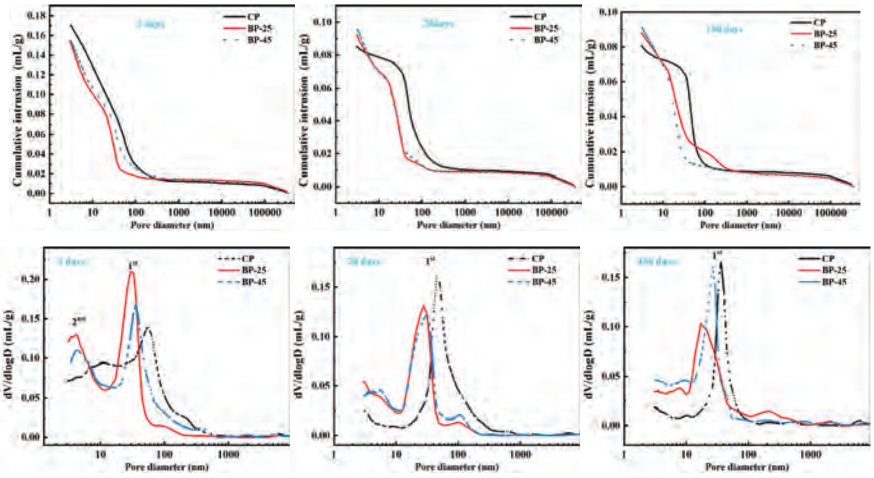

Figure 4. Pore structure of paste samples at different ages.

3.4 Backscattered electron image analysis (BSE-IA) and DSI

BSE-IA analysis shows that RBP particles participated in the reaction, further verifying its pozzolanic reaction.

The results of the DSI test indicate that C-(A)-S-H gel products in 180-day blended pastes containing WBP exhibited slightly decreased hardness and elastic modulus compared to those of the C-(A)-S-H gel product in cement pastes. However, the decreased hardness and elastic modulus of the gel product suggest an increased degree of hydration in the WBP-containing cement paste.

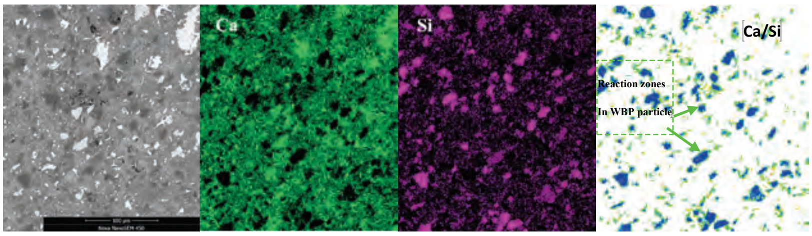

Figure 5. Example for result analysis of reaction of BP25 particle at 180 days using BSE-IA.

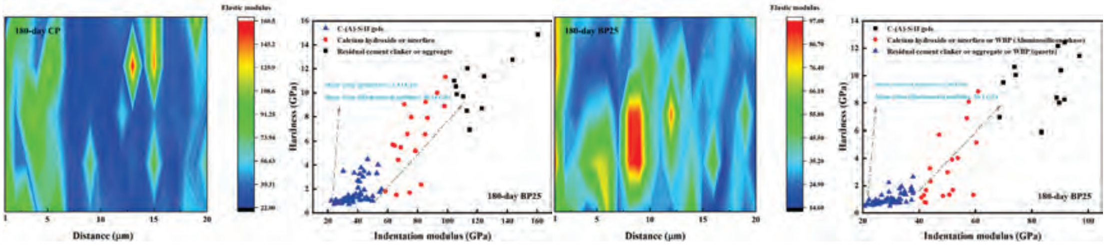

Figure 6. Example for result analysis of hardness and indentation modulus of cement pastes without and with BP25 at 180 days.

.

4. CONCLUSION

This work investigated the potential of RBP as a supplementary cementitious material under low water-to-binder ratios, based on its mechanical performance and microstructure evolution. The following conclusions were drawn:

(1) Addition of RBP did not significantly decrease the compressive and flexural strength of the mortar when the water-to-binder ratio was 0.25. Moreover, the contribution of RBP to the strength of the mortar increased with age.

(2) Addition of RBP resulted in a gradual decrease in the amount of CH and a corresponding increase in the amount of CBW in the cement paste with increasing age. This indicates that the volcanic ash activity of RBP contributed to the strength development of the mortar.

(3) Pore structure of the cement paste was not significantly reduced by the addition of RBP. However, the presence of RBP led to a gradually refined pore structure with increasing age.

(4) Bse-IA analysis showed that RBP particles participated in the reaction, further verifying its pozzolanic reaction.

(5) Addition of RBP caused a slight decrease in the hardness and elastic modulus of the gel products. This decrease, however, suggests an increased degree of hydration in the cement paste containing RBP.

6. ACKNOWLEDGMENT

The authors deeply appreciate the financial support provided by the National Natural Science Foundation of China (No. 52130210 and No. 52171254) and the Jiangsu Key Laboratory of Construction Materials for technical support.

7. REFERENCES

[1] Li, P., Sui, L., Xing, F., & Zhou, Y. (2019). Static and cyclic response of low-strength recycled aggregate concrete strengthened using fiber-reinforced polymer. Compos. B. Eng., 160, 37-49.

[2] Lam, M. N.-T., Nguyen, D.-T., & Nguyen, D.-L. (2021). Potential use of clay brick waste powder and ceramic waste aggregate in mortar. Constr. Build. Mater., 313, 125516.

[3] Taehwan Kim, & Olek, J. (2012). Effects of Sample Preparation and Interpretation of Thermogravimetric Curves on Calcium Hydroxide in Hydrated Pastes and Mortars, J. Transp. Res., 2290.1(2012):10-18.

[4] Lang, L., Duan, H., & Chen, B. (2019). Properties of pervious concrete made from steel slag and magnesium phosphate cement. Constr. Build. Mater., 209(JUN.10), 95-104.

[5] Li, S., Chen, G., Xu, Z., Luo, X., & Gao, J. (2022). Particle-size effect of recycled clay brick powder on the pore structure of blended cement paste. Constr. Build. Mater., 344, 128288.

[6] Likes, L., Markandeya, A., Haider, M. M., Bollinger, D., McCloy, J. S., & Nassiri, S. (2022). Recycled concrete and brick powders as supplements to Portland cement for more sustainable concrete. J. Cleaner Prod., 364, 132651.

[7] Liu, F., Sun, N., Li, W., & He, J. (2014). Feasibility study on recycled brick powder used as admixture. Block-Brick-Tile(8), 11-14.

[8] Liu, Q., Li, B., Xiao, J., & Singh, A. (2019). Utilization potential of aerated concrete block powder and clay brick powder from C&D waste. Constr. Build. Mater., 238, 117721.

[9] Liu, Q., Tong, T., Liu, S. H., Yang, D. Z., & Yu, Q. (2014). Investigation of using hybrid recycled powder from demolished concrete solids and clay bricks as a pozzolanic supplement for cement. Constr. Build. Mater., 73, 754-763.

[10] Wu, H., Liang, C., Wang, C., & Ma, Z. (2022). Properties of green mortar blended with waste concrete-brick powder at various components, replacement ratios and particle sizes. Constr. Build. Mater., 342, 128050.

[11] Xue, C. Z., Shen, A. Q., Chang, Y. T., & Liang, D. (2015). The study of the construction waste brick powder’s activity. Adv. Mater. J., 1079-1080(2015):309-311.

RECYCLING OF MUNICIPAL SOLID WASTES FOR THE PREPARATION, MICROSTRUCTURAL EVOLUTION AND MECHANICAL PROPERTIES OF BELITE-RICH LOW-CARBON ECO-CEMENTS

Lu Zhu, Shipeng Zhang*, and Chi Sun Poon

Department of Civil and Environmental Engineering, The Hong Kong Polytechnic University,
Hung Hom, Kowloon, Hong Kong, China
*E-mail: shipeng.zhang@polyu.edu.hk

For the recycling of solid wastes, incinerated sewage sludge ash (ISSA) and recycled concrete fine (RCF) were used as raw materials to prepare a novel kind of belite-rich low-carbon eco-cements. The results showed that eco-clinkers were successfully sintered with a 95 % utilization rate of the wastes. Due to the formation of the highest belite content, the eco-cement that sintered for 60 min obtained the highest compressive strength. All eco-clinkers that sintered for 60 min at 1000–1200 °C produced belite phases. 1200ARS clinker demonstrated the highest belite concentration and CO_2 uptake value after one-day carbonation curing, which helped to produce the maximum compressive strength of all the cements. A high proportion of $CaCO_3$ phases were produced in 1200ARS cement, and the eco-cement had low porosity (18.1 %) and denser fracture morphologies. As the carbonation curing time increased, the content of $CaCO_3$ phases in OPC and 1200ARS cements both increased by the reaction of belite with CO_2. The compressive strength of OPC and 1200ARS cements was also increased while the increase rate was decreased with increasing curing time. Compared with OPC paste, carbonated 1200ARS eco-cement possessed higher increase coefficients of compressive strength and CO_2 uptake with high reaction coefficients of $CaCO_3$ and belite phases, thus showing optimum carbonation activity.

Keywords: Incinerated sewage sludge ash; Recycled concrete fine; Recycling; Low-carbon eco-cement; Mechanical properties

THE INFLUENCE OF BIOCHAR ON THE IMMOBILIZATION OF HEAVY METALS IN ASPHALT RUBBER

Fuliao, Zou[1], Zhen, Leng[1], Danning Li[1], and Guoyang Lu[2]

[1] Department of Civil and Environmental Engineering, The Hong Kong Polytechnic University, Hung Hom, Kowloon, Hong Kong
[2] Department of Architecture and Civil Engineering, City University of Hong Kong, Kowloon Tong, Kowloon, Hong Kong
E-mail: zhen.leng@polyu.edu.hk (Z. Leng)

Asphalt rubber (AR), a waste-based paving binder prepared with waste tyre rubber and asphalt cement, may contain hazardous components that pose environmental risks when applied to the road surface. This study aims to address the issue of potential metal leaching from AR by introducing an eco-friendly material, low-carbon biochar, into asphalt modifications. A commercial biochar produced via the pyrolysis of fruit pits was utilized in this study. Its surface functional groups were characterized through Fourier-transform infrared spectroscopy (FTIR) testing to verify its efficacy in adsorbing metal ions. Subsequently, the microstructure of the biochar-modified asphalt rubber (BMAR) was assessed via scanning electron microscopy (SEM) testing to reveal any alterations in matrix size as compared to the unmodified AR. The study revealed that the physicochemical attributes of BMAR, including its porous structure and surface functional groups, facilitate the adsorption of heavy metals through both physical and chemical interactions. Results from accelerated and long-term leaching tests confirm that BMAR effectively immobilizes heavy metals and reduces their leaching capacities, with reductions of up to 31% in asphalt mortar samples and up to 44% in open-graded asphalt mixture samples. Findings suggest that the effectiveness of immobilization varies based on the original metal concentrations and pavement gradation. Notably, biochar modification exhibits superior performance in AR samples with higher metal concentrations and porosities. Furthermore, the competitive adsorption of heavy metals onto biochar also impacts the immobilization effectiveness, with more favorable outcomes observed in AR with elevated concentrations of preferred metals, such as Cu and Zn. In conclusion, the overall results suggest that the utilization of BMAR has the potential to effectively mitigate heavy metal leaching to levels deemed environmentally acceptable, specifically achieving a heavy metal pollution index (HPI) of less than 100.

Keywords: Biochar modification, Metal leachability, Asphalt rubber, Adsorption mechanisms, Environmental impact

Session A2

Recycled Concrete Aggregates

INDUSTRIAL PRODUCTION OF WATER-WASHED RECYCLED AGGREGATES USED FOR REAL-SCALE NON-STRUCTURAL AND STRUCTURAL CONCRETES IN BARCELONA

Etxeberria, M[1], Vintimilla C[1]., Pérez, M.A.[2]

[1]Department of Civil and Environmental Engineering, Universitat Politécnica de Catalunya.BarcelonaTECH
[2]Hercal diggers S.L
E-mail: miren.etxeberria@upc.edu

1. INTRODUCTION

The benefits of using recycled coarse and fine aggregates to replace natural aggregate partially lie not only in CO_2 emissions reduction in concrete manufacture but also in the significant mitigation of the environmental impacts induced by stockpiling the respective waste (Plaza et al. 2021).

Several research works show that alternative aggregate, such as recycled aggregate, could be effectively used for concrete pavements (Nassar and Soroushian 2016; Selvam et al. 2022). In addition, highly durable structural concrete production is also possible if limited percentages of cleaned coarse and fine RCA and MRA are used in its production (Cantero et al. 2018; Vintimilla and Etxeberria 2023). However, the use of fine RA in concrete structures requires stricter quality control than NA (Kirthika, Singh, and Chourasia 2020; Zhang et al. 2020) to guarantee a high structural application.

This study presents an innovative recycling plant (HZERO) built in Barcelona by an important demolition company, Hercal Diggers. In this plant, the construction and demolition waste (CDW) is washed in an industrial process to achieve clean concrete (RCA) and mixed (RMA), fine (F) and coarse (C) recycled aggregates usable in non-structural and structural concrete. In addition, clay and silt materials are also recovered. The main objective of this study is to describe the industrial treatment process carried out, the property values of recycled aggregates produced and their applicability in concrete production in real cases.

2. RECYCLING PLANT PROPERTIES OF RECYCLED AGGREGATES

Figure 1 shows the recycling plant. The concrete waste (more than 95% is concrete) and mixed waste (with approximately 40-30% ceramic material) are treated separately. After crushing to the desired aggregate size (usually 0/20 mm) and passing through a magnetic separator, it is sieved in fine (Dmax <4mm) and coarse (4mm < Dmax< 20mm) fractions using water. The coarse fraction is followed by the scrubbing & attrition stage of the washing process, followed by sieving in three fractions (14/20 mm, 8/14 mm and 4/10 mm). In addition, the fine fraction goes to the hydro-cyclone separators, where it is divided into three recycled fraction sizes, 0/4 mm, 0/2 mm and a fraction finer than 63 µm (filler, clay and silk). Although the cleaning procedure is carried out through a water system, the entire volume of water employed in the treatment process is reused satisfactorily. In addition, rainwater is also harvested through storage tanks.

Figure 1. CDW recycling plant to water washed recycled aggregate (Anon 2021)

Five fractions (0/2 mm, 0/4 mm, 4/10, 8/14 and 12/20) of recycled concrete (RCA) and mixed (RMA) aggregates are produced in the plant. While the RCA aggregates composed of more than 95% of concrete is categorised as Tipo A (Rc90, Rcu95, Rb10, Ra1, FL2 and XRg1), the RMA aggregates are categorized as Type B with Rcu50, Rb50, Ra5 and XRg0.5 components, with a maximum of 30% of ceramic recycled aggregates. In this study, fractions FRCA and FRMA (0/4mm in Table 1) employed for concrete production were created by combining the 0/2 and 0/4 mm in 15% and 85% (by weight), respectively. In addition, the CRCA-2 and CRMA-2 (8/20mm in Table 1) were produced by mixing the 8/14 and 12/20 fractions in 40% and 60%, respectively. All the fractions were characterized following the EN 12620 specification. In recycled aggregates (RCA and RMA), sulphate soluble in acid and chloride soluble were lower than 0.8 and 0.05%, respectively. These are the limits established by SC (Spain's code on structural concrete). Following the EN 12620 specification, the shape factor and Los Angeles abrasion coefficient were classified as Fl_{15} and LA_{40}, respectively, for the RCA and RMA aggregates. Table 1 shows the physical properties obtained by the RCA and RMA aggregates. As mentioned above, the recycled aggregates were cleaned with water. Consequently, the RCA and RMA aggregates were stored and used for concrete production with a high moisture content.

Table 1. Properties of all aggregates

	FNA (0/4)	CNA1 (2/10)	CNA2 (8/20)	FRCA (0/4)	CRCA-1 (4/10)	CRCA-2 (8/20)	FRMA (0/4)	CRMA-1 (4/10)	CRMA-2 (8/20)
Dry density (kg/dm3)	2.67	2.65	2.68	2.31	2.22	2.36	2.28	2.15	2.08
Absorption (%)	0.96	0.77	0.73	6.1	6.63	5.15	6.67	8.75	9

3. CONCRETE PRODUCTION AND THEIR PROPERTIES

CEM II A-L 42.5 R cement, a superplasticizer and a plasticizer admixture were used in all concrete production. The plasticiser was necessary to maintain the workability over time.

For the non-structural concretes (C-RCA), after the validation of concrete produced with 100% of fine and coarse recycled aggregates in the laboratory (Etxeberria et al. 2022; Etxeberria and Vintimilla 2021), a recycled concrete pavement base with 100% fine and coarse RCA, achieving 20 MPa compressive strength, was built in the city centre of Barcelona (Etxeberria et al. 2022). The recycled concrete pavement was produced with 300 kg of cement and 0.52 effective water-cement ratio. The hardened state properties of the concrete were determined following EN 12390 specifications. Table 2 describes the mix proportion as well as the average values of the properties of concrete produced. The humidity of the 0/2mm, 0/4mm, 5/12mm and 8/20mm fractions was 22.4%, 10%, 6.5% and 4.5%, respectively.

For structural applications, all the concretes were manufactured using 300kg /m^3 cement and an effective water/cement (effect w/c) ratio of 0.48. In addition, conventional concrete (NAC_2) with an effect. w/c of 0.52 was also produced (see Table 3). All concrete mixtures were designed to have a characteristic strength (fck) of 30 MPa. The dry density and absorption (UNE-EN 12390-7:2020), compressive strength (UNE-EN 12390-3), elastic modulus (UNE-EN 12390-13), sorptivity ISO

15148:2002(E), the water penetration under pressure (UNE-EN 12390-9) and the drying shrinkage (EN 12390-16) properties were determined.

Table 2. Mix proportion of C-RCA, dry mass of each material to produced 1 m^3 of concrete. Properties of concrete (the describe values are the average three different batches)

	RCA fractions					
Cem	**0/2**	**0/4**	**4/10**	**8/20**	**S/P** (%)**	**Total water***
300	196.5	636.6	263.5	652.9	1.2/1	272.8
Concrete properties						
Compressive strength (MPa) (cylindrical specimen 150x300)			**Flexural Strength (MPa)**	**Dry density (kg/dm3)**	**Absorption (%)**	**Water penetration (mm)**
7 d	**14 d**	**28 d**	**28 d**	**28 d**	**28 d**	**Medium/Maximum*****
21.2	24.5	25.7	3.6	2.04	7.7	15.5/ 21 (30/50)

*water including the humidity of aggregates; **S/P: Superplasticizer/Plasticizer in % of cement weight; *** maximum required values into brackets

Table 3. Mix proportions. NAC: conventional concrete; RAC-CX-FY: recycled concrete produced with X% coarse and Y% fine RCA; MRAC-CX-FY: recycled concrete produced with X% coarse and Y% fine RMA

Mix	Cem (Kg)	Total Water (Kg)	FNA (Kg)	FRCA (Kg)	CNA1 (Kg)	CRCA1 (Kg)	CNA 2 (Kg)	CRCA2 (Kg)	S (%)	P (%)	Slump (mm)
NAC$_1$	300	157.5	994	-	247	-	831	-	1.5	-	100
NAC$_2$	300	165	981	-	243	-	815	-	1.0	1.2	160
RAC-C50-F20$_1$	300	190.0	762	163	144	121	416	358	1.2	1.5	180
RAC-C60-F20$_1$	300	194.8	762	163	115	145	333	429	1.2	1.5	200
RAC-C60-F30$_1$	300	199.3	667	244	115	145	333	429	1.2	1.5	160
MRAC-C20-F5$_1$	300	172.1	944	43	198	40	665	130	1,2	1.7	200
MRAC-C30-F10$_1$	300	180.5	894	85	173	60	582	195	1.2	1.7	180
MRAC-C40-F15$_1$	300	189.4	809	122	173	94	499	260	1.2	17	180

Table 4 shows that recycled concrete had lower density (ρa) and higher absorption capacity (Abs) than NAC concrete (see Table 4). Additionally, concrete with recycled aggregates exhibited significantly lower compressive (Fcm) and elastic modulus (Ecm) than NAC$_1$. However, all concrete mixtures met the minimum requirements according to the Spanish structural concrete code (SC-BOE) and the properties achieved by NAC$_2$. The study found that all the mixes met the water penetration requirements set by the (SC-BOE), regardless of the type and percentage of RCA or MRA used. The influence of MRA was found to increase the sorptivity property of the concrete to a greater extent than RCA. The values obtained for the recycled concretes were generally higher than those obtained for NAC$_1$ and similar to NAC$_2$. The use of fine RA has an even more significant effect on shrinkage. However, all concrete made with recycled aggregates complied with the limits established by the American Concrete Institute (ACI), where drying shrinkage ranges between 200-800 με.

Table 4. Mechanical properties of produced concretes

MIX	Fcm		Ecm	ρa (kg/dm3)	Abs (%)	S (mm/min0.5)	Dry Shrinkage	Dmax ≤ 50mm
	28d	56d						
NAC$_1$	53,09	53,44	40,45	2.38	2,8	0,0242	-494,8	12,5
NAC$_2$	44,52	47,74	38,79	2.31	4,18	0,0388	-254,4	12,75
RAC-C50-F20$_1$	45,17	46,32	32.84	2.27	3,88	0,0466	-562,7	12,75
RAC-C60-F20$_1$	44,17	46,59	31.9	2.3	3,85	0,047	-576,7	12
RAC-C60-F30$_1$	42,88	46,93	31.72	2.27	4,14	0,0593	-688,2	12,5
MRAC-C20-F5$_1$	48,16	48,32	34,97	2.32	4,15	0,0324	-531,4	13
MRAC-C30-F10$_1$	47,25	47,74	33,66	2.28	4,21	0,0383	-536,6	16
MRAC-C40-F15$_1$	45,51	45,76	31,94	2.26	4,3	0,0388	-611,7	19,25

4. CONCLUSION

The following conclusions can be drawn from the results of this study: 1) After the cleaning treatment process, the RCA and RMA aggregates achieved adequate properties for concrete production; 2) Non-structural recycled concrete pavement produced (pilot test) with 100% fine and coarse RCA was built successfully, achieving adequate mechanical, physical and durability properties; 3) Structural concrete with up to 60% of coarse and 30% of fine RCA (type A) can be produced without affecting its durability, mechanical strength, or physical characteristics; 4) the use of RMA (type B) is also possible for structural concrete production, with replacement levels up to 40% for coarse and 15% for fine RMA concrete.

5. ACKNOWLEDGMENT

The authors would like to express appreciation for the support of the sponsors L'Agència de Gestió d'Ajuts Universitaris i de Recerca (AGAUR) for the scholarship FI SDUR 2020 (Ref: 2020 FISDU 00576) and LATEM Laboratory of the UPC for their support.

6. REFERENCES

Anon. 2021. “H-ZERO.” Retrieved (https://www.hercalzero.es/h-zero-planta-rcd/).

Cantero, B., I. F. Sáez del Bosque, A. Matías, and C. Medina. 2018. “Statistically Significant Effects of Mixed Recycled Aggregate on the Physical-Mechanical Properties of Structural Concretes.” *Construction and Building Materials* 185:93–101.

Etxeberria, Miren, Mikhail Konoiko, Carles Garcia, and Miguel Á. Perez. 2022. “Water-Washed Fine and Coarse Recycled Aggregates for Real Scale Concretes Production in Barcelona.”

Etxeberria, Miren and Carla Vintimilla. 2021. “Influence of Treated Mixed Recycled Aggregates in Concrete Properties.” in *75th RILEM annul week and he International Conference on Advances in Sustainable Construction Materials and Structures*, edited by J. I. ESCALANTE - GARCÍA, P. CASTRO- BORGES, and P. DURÁN-HERRERA. Mérida.

European Statistics-Eurostat. 2020. *Energy, Transport and Environment Statistics 2020 Edition*. Luxembourg.

Kirthika, S. K., S. K. Singh, and Ajay Chourasia. 2020. “Alternative Fine Aggregates in Production of Sustainable Concrete- A Review.” *Journal of Cleaner Production* 268:122089.

Nassar, R. and P. Soroushian. 2016. “Use of Recycled Aggregate Concrete in Pavement Construction.” *J. Solid Waste Technol. Manage* 42:137–44.

Plaza, P., I. F. Sáez del Bosque, M. Frías, M. I. Sánchez de Rojas, and C. Medina. 2021. “Use of Recycled Coarse and Fine Aggregates in Structural Eco-Concretes. Physical and Mechanical Properties and CO2 Emissions.” *Construction and Building Materials* 285:122926.

Selvam, M., Solomon Debbarma, Surender Singh, and Xijun Shi. 2022. “Utilization of Alternative Aggregates for Roller Compacted Concrete Pavements – A State-of-the-Art Review.” *Construction and Building Materials* 317(June 2021):125838.

Tam, Vivian W. Y., Mahfooz Soomro, and Ana Catarina Jorge Evangelista. 2018. “A Review of Recycled Aggregate in Concrete Applications (2000–2017).” *Construction and Building Materials* 172:272–92.

Vintimilla, Carla and Miren Etxeberria. 2023. “Limiting the Maximum Fine and Coarse Recycled Aggregates-Type a Used in Structural Concrete.” *Construction and Building Materials* 380(December 2022):131273.

Zhang, Huan, Yuyin Wang, Dawn E. Lehman, Yue Geng, and Katherine Kuder. 2020. “Time-Dependent Drying Shrinkage Model for Concrete with Coarse and Fine Recycled Aggregate.” *Cement and Concrete Composites* 105(May 2019):103426.

THE INFLUENCE OF CEMENTITIOUS MATERIAL PROPORTION ON THE SULFATE RESISTANCE OF RECYCLED AGGREGATE CONCRETE

Ting Du[1], Jinghao Chen[1], Qian Chen[1], Xianguo Wu[1], Benyi Xie[2]

[1]School of Civil & Hydraulic Engineering, Huazhong University of Science and Technology, Wuhan 430074, China
[2]Central and Southern China Municipal Engineering Design & Research Institute Co., Ltd, Wuhan 430010, China
E-mail: duting@hust.edu.cn

Fly ash is a kind of industrial waste produced by the power plants, it can be used as a cementitious material to replace cement in equal or excessive quantities and to improve simultaneously the workability and durability of recycled aggregate concrete (RAC). In this study, RAC with four different fly ash contents (r_f) and three kinds of water-binder ratio (r_w) was respectively suffered from a sulfate attack, and the mass loss rate (K_m) and corrosion resistance coefficient of compressive strength (K_f) of RAC under different sulfate wet-dry cycles was tested and calculated. The experimental results revealed that the mass of specimen increased after the RAC was suffered from a sulfate attack, so the compressive strength degradation rate (D_n) of RAC was introduced to take the place of K_f and K_m to evaluate the sulfate resistance of RAC. The results also indicated that D_n of RAC decreased with the growth of r_f, but it increased with the growth of r_w and sulfate wet-dry cycles. Obviously, the sulfate resistance of RAC was improved when the fly ash content was within 20%, and it is reduced with the increase of water-binder ratio and sulfate wet-dry cycles. Finally, based on the experimental results and the numerical fitting method, the dimensionless influence coefficient of the fly ash content η_f and water-binder ratio η_w was introduced to reflect the effect of fly ash content and water-binder ratio on the sulfate resistance of RAC, and a sulfate resistance model of D_n considering η_f and η_w was built. It can be used to precisely evaluate the sulfate durability damage of RAC with different cementitious material proportions.

Keywords: RAC; Fly ash; Water-binder ratio; Compressive strength degradation rate; Sulfate resistance.

CONCRETE MIX DESIGN USING RECYCLED AGGREGATES: UMBRELLA REVIEW

Lapyote Prasittisopin

Architectural Technology Research Unit, Faculty of Architecture, Chulalongkorn University,
Bangkok, 10330, Thailand
E-mail lapyote.p@chula.ac.th

1. INTRODUCTION

A systematic review paper of review publications can be also referred to as umbrella review is a type of systematic review that summarizes and evaluates existing systematic reviews and meta-analyses on a certain research area (Aromataris et al., 2015). Papatheodorou (2019) asserted that this type of review had the potential to offer the superior quality of evidence. In comparison to individual studies or narrative reviews, the umbrella review offers a more in-depth degree of synthesis and analysis and serves as a thorough summary of the data that is currently available on the concrete mix design containing RCA topic. The significance of this work is to summarize and synthesize current evidence on RCA concrete mix design themes that have been obtained from trustworthy and certified sources. The information gaps and contradictions were investigated as a thorough blueprint for future research. It aids in making educated judgments and guiding future research efforts for academics, policymakers, designers, and technical professionals. In recent times, there has been a growing trend in technical and review literature towards the integration of RCA in cementitious materials. The technical publications underscored the utilization of RCA as a substitute, either in part or in entirety, for conventional normal-weight coarse and fine aggregates. Unfortunately, a systemic (umbrella) review publication summarizing / overall aspects of review publication is neither fully presented nor discussed for difficulties and constraints in various aspects, including their mix design. Hence, this systemic review paper aims to accumulate, summarise and brief the pertinent 181 review publications of RCA material technology in construction.

The scope of this review consists of concrete and mortar mixtures containing RCA that were designed using ordinary Portland cement (OPC) and geopolymer, and other mix proportions entail fRCA, chemical and mineral by-products, silica fume (SF), rubber, polymer, and fiber. Concrete mixtures containing these discussed additives and admixtures aim to develop special concretes such as self-consolidating concrete (SCC), 3D concrete printing (3DCP), pervious concrete, and ultra-high-performance concrete (UHPC). The performance, workability, mechanical properties, microstructure, and durability have been analyzed and discussed. The processes of quality improvement of RCA in concrete are elaborated. Moreover, up-to-date environmental studies focusing on life cycle assessment and the circular economy have been reported. This systemic review article can offer knowledge that has already been understood in the field and what research should be assessed for future technical issues.

2. MATERIALS AND METHODS

To determine the state of the art on this subject, systematic quantitative literature reviews were conducted and reported. A systematic review and meta-analysis of all relevant publications on concrete mix design containing recycled aggregate were conducted. Google Scholar, Scopus, and Emerald database searches were investigated. This search for systematic reviews was conducted in publications that included the term "review" in their titles, abstracts, and/or keywords, with no constraints on date or language The terms searched herein were "recycled concrete aggregate" and "mix design," as given in Table 1. The PRISMA model is also shown in Figure 2

Table 1 Search strategy for electronic databases.

Study type	TITLE-ABS-KEY (review)
	AND
Recycled concrete aggregate	TITLE-ABS-KEY (recycl* AND aggregate)
	OR TITLE-ABS-KEY (recycl* AND aggregate AND concrete)
	OR TITLE-ABS-KEY (recycl* AND concrete)
	OR TITLE-ABS-KEY (reclaime* AND aggregate)
	AND
Mix design	TITLE-ABS-KEY (mix* AND design)
	OR TITLE-ABS-KEY (mix* AND proportion*)

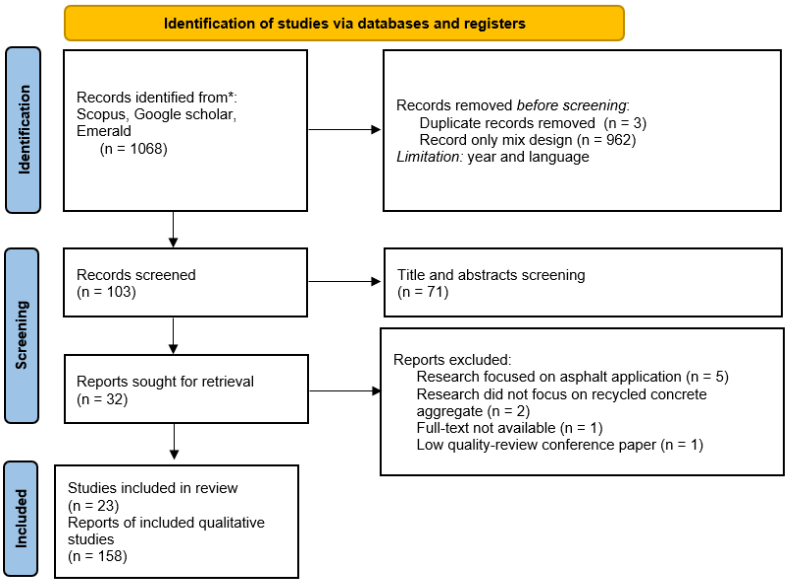

Figure 2. Flowcharts for the studies were identified, displayed, and included in the study (Adapted from the PRISMA Statement; Moher et al. (2009))

3. RESULTS AND DISCUSSION

The narrative review methodology lacks a pre-defined prototype and provides a broader overview of concrete mix design incorporating the topic of recycled concrete aggregate. On the other hand, the systematic review methodology adheres to a pre-defined protocol such as PICO and utilizes data synthesis methods to minimize bias, following formal guidelines such as PRISMA (Pae, 2015). In contrast, the meta-analysis adheres to a structured protocol for synthesizing data and employs statistical techniques to evaluate information gathered from a variety of empirical studies (Field & Gillett, 2010). The number of papers scrutinized for each review article varies between 30 and 253 papers. The mean value is 135.5 documents. In the realm of review classification, this narrative review paper has been the subject of the majority of studies, accounting for 56.5% of the total. This is followed by meta-analysis at 34.8%, and systematic review at 8.7%. The overview of published timeline and review classification is exhibited in Figure 2.

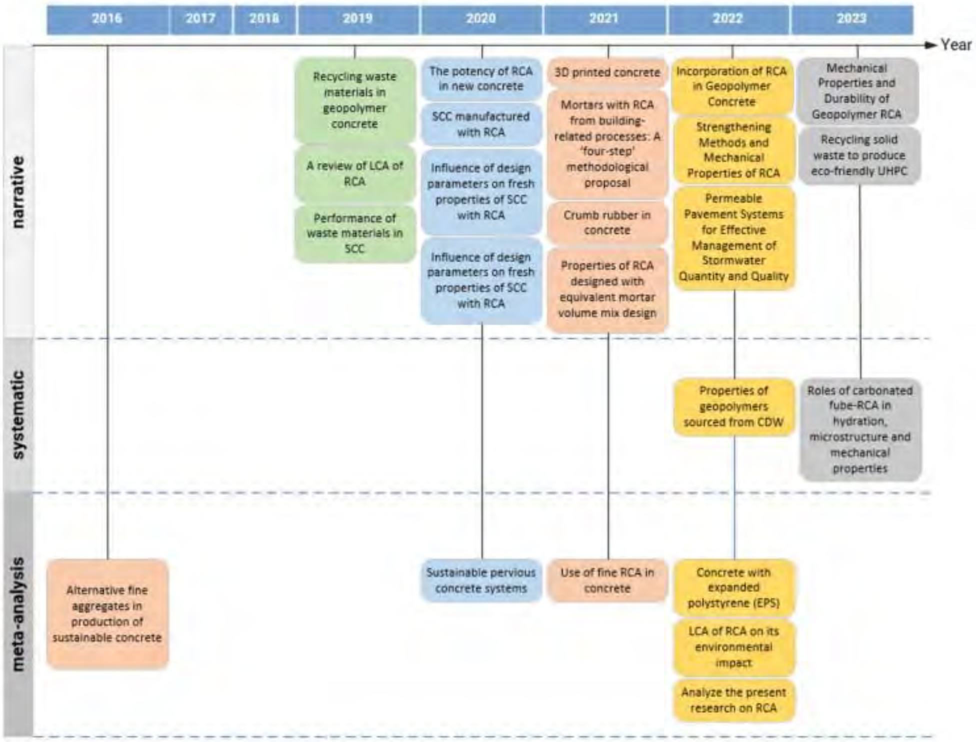

Figure 2. Timeline and review classification of the review papers.

After all considerations of such review articles, it is suggested as shown in Figure 3 that numerous research on RCA performance focuses on fresh and mechanical qualities. The material's endurance is equivocal for practical implementations and experimental measurement of microstructural properties like the ITZ. The quality method of CO2 mineralization needs refining and deployment in production and commerce.

The circular economy and LCA validate RCA's sustainability. The current method for evaluating carbon dioxide emissions from product life cycle phases is unsatisfactory. The construction EPD launch is heavily influenced by stakeholders. Thus, LCA prognostic instruments must be enhanced. Once implemented, the Digital Twin and BIM can help evaluate carbon credit, carbon trade, and carbon taxation at national and global levels. Machine learning algorithms and blockchain technology may help RCA's digitization and sustainability.

Studies have shown that directly replacing RCA into concrete mixtures does not satisfy the typical computation of the concrete mix design. Instead, the revised mix design calculation based on the equivalent mortar volume approach, which includes adherent mortar, should be used to assess RCA mix proportions. SCC, geopolymer, and normal RCA concrete are known study areas. 3D concrete printing, pervious concrete, and UHPC should be considered for future research.

Finally, particular admixtures and additives have received little attention, although fRCA has been extensively studied. This emphasizes the need to maximize RCA's potential in any situation. Future studies could examine the usefulness of adding MK to improve RCA product quality. The research gap should focus on adding steel, glass, and cellulose to natural and synthetic fibers to improve product quality.

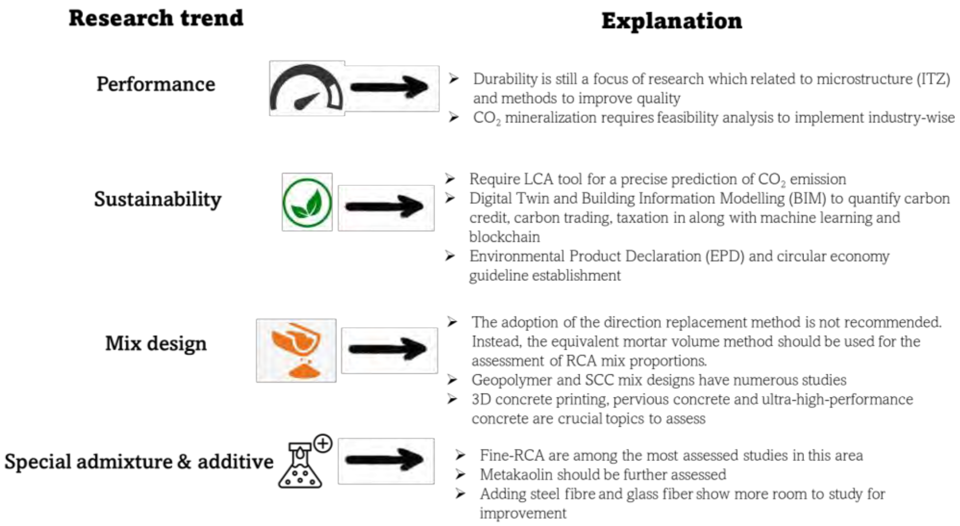

Figure 3. Outline of the research trend and the explaian relating to RCA.

4. CONCLUSION

This umbrella review examines the advantages and drawbacks of incorporating RCA into concrete mix designs. The significance of environmental concerns was deliberated in relation to LCA and the circular economy. The present discourse pertains to a comprehensive analysis of the primary annotations derived from a state-of-the-art review publication.

As per the review, the utilization of RCA from CDW in cement blends presents a distinct function in civil engineering and construction management practices for the promotion of sustainable development. The technical comprehension concerning the fresh and mechanical performance appears to be adequately comprehended. The utilization of RCA is aimed at sustainability. Numerous waste materials and by-products were incorporated with the aim of enhancing either performance or sustainability. Despite certain advancements in the field, the complete adoption of measuring instruments and policy execution for the circular economy is yet to be realized in the realm of production.

5. ACKNOWLEDGMENT

This research project was financially supported by by National Research Council of Thailand (NRCT) and Chulalongkorn University (Grant No. N42A660629).

6. REFERENCES

Aromataris, E., Fernandez, R., Godfrey, C. M., Holly, C., Khalil, H., & Tungpunkom, P. (2015). Summarizing systematic reviews: methodological development, conduct and reporting of an umbrella review approach. *JBI Evidence Implementation*, *13*(3), 132-140.

Field, A. P., & Gillett, R. (2010). How to do a meta-analysis. *British Journal of Mathematical and Statistical Psychology*, *63*(3), 665-694.

Moher, D., Liberati, A., Tetzlaff, J., Altman, D. G., & PRISMA Group*, t. (2009). Preferred reporting items for systematic reviews and meta-analyses: the PRISMA statement. *Annals of internal medicine*, *151*(4), 264-269.

Pae, C.-U. (2015). Why systematic review rather than narrative review? *Psychiatry investigation*, *12*(3), 417.

Papatheodorou, S. (2019). Umbrella reviews: what they are and why we need them. *European journal of epidemiology*, *34*, 543-546.

UTILIZING TUNNEL BORING MACHINE WASTE AS A SUSTAINABLE ALTERNATIVE FOR NATURAL AGGREGATES IN CONCRETE

Chao Qun Lye, Hong Jian Du and Sze Dai Pang*

National University of Singapore
*E-mail: ceepsd@nus.edu.sg

1. INTRODUCTION

Sustainable construction has always been the Singapore government's top priority in promoting economic growth, while protecting the environment for future generations. Currently, the annual local consumption of aggregates in concrete production exceeds 20 million tonnes, emphasizing the need for ongoing efforts and innovative solutions to reduce environmental impact. The local rock excavated waste generated by Tunnel Boring Machine (TBM) presents a promising opportunity to be used as an aggregate component in concrete.

Presently, the only known local example of the use of TBM waste was in pavement construction. Its research for use as concrete aggregates is limited. In this study, the as-received TBM waste was crushed into aggregate with a nominal maximum size of 10mm, and compared with locally commonly used granite aggregates, which served as reference materials. The properties of TBM were evaluated. The potential of TBM waste to replace granite aggregates in concrete was studied for up to 100%, with important engineering properties and durability being tested.

2. MATERIALS AND METHODS

TBM waste was locally sourced from sites and then processed in the laboratory to achieve a desirable size (in this case less than 10mm) suitable for use as concrete aggregates, as shown in **Figure 1**. Crushed granite, having a similar nominal maximum size, was as reference natural aggregates. The physical and chemical properties of TBM waste and granite, characterised in accordance with BS EN 12620 (2008), are given in **Table 1**. In general, the characteristics of TBM waste was comparable to those of granite, except for flakiness index, where TBM waste was found to be flakier than granite. Additionally, x-ray diffraction analysis revealed significant quartz and mica components in the TBM sample.

TBM waste was also evaluated for their potential risk of alkali-silica reaction expansion, using the accelerated mortar bar tests according to ASTM C1260 (2021). According to the classification of aggregate reactivity given in ASTM C1778 (2022), TBM waste was considered moderately reactive (R1) as the 14-day expansion was nearly 0.2%. However, when 50% ground granulated blast furnace slag (GGBS) was used as a replacement for Portland cement (PC), the expansion of TBM waste mortar bars was significantly reduced, falling into R0 category as non-reactive, even up to 28 days.

Figure 1. TBM waste after laboratory jaw-crushing and sieving through a 12.5mm sieve.

Table 1. Physical and chemical properties of TBM waste and granite used in this study.

Property	Granite	TBM
OD particle density, Mg/m^3	2.61	2.67
SSD particle density, Mg/m^3	2.65	2.69
Apparent particle density, Mg/m^3	2.63	2.72
Water absorption, %	0.20	0.70
Flakiness index	FI_{20}	FI_{50}
Water soluble chloride content (as Cl^-), % m/m	< 0.01	< 0.01
Acid-soluble sulphate content (as SO_3), % m/m	0.02	0.02
Sulphate content (as SO_4), % m/m	< 0.1	0.09

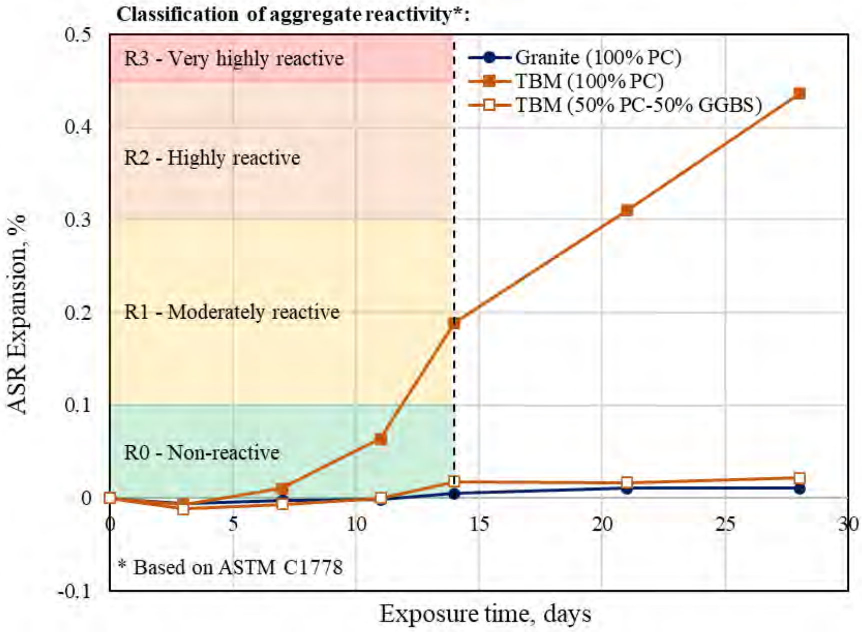

Figure 2 ASR expansion of mortar bars in 1 N NaOH solution at 80 °C

Table 2 shows the mix proportions used for reference concrete and TBM waste concrete, with replacement of granite at 10%, 30%, 50% and 100%. CEM I 52.5N PC was used, and GGBS was introduced at 50% of the total cement content. The water/cement ratio of the concrete was maintained at 0.50, and the consistence of the concrete was controlled at S2 slump class (based on BS EN 206, 2021) with the use of a superplasticiser. For each concrete mix, 100 mm cubes and 100 mm Ø x 200 mm cylinders were cast. The concrete was tested for their compressive strength, modulus of elasticity and drying shrinkage. After demoulding, the concrete specimens were cured in a fog room until the day of testing.

Table 2. Mix proportions for concrete.

Material (kg/m^3)	T0 (Ref.)	T10	T30	T50	T100
PC	175	175	175	175	175
GGBS	175	175	175	175	175
Sand	910	910	910	910	910
Granite aggregate	900	810	630	450	0
TBM waste	0	90	270	450	900

3. RESULTS AND DISCUSSION

The results of the hardened properties of concrete made granite and TBM waste are given in **Table 3**. At 10% replacement, the compressive strength of TBM waste concrete was comparable to that of granite concrete. However, a gradual reduction in strength was observed as the content of TBM waste increased from 30% to 100%, resulting in nearly a 15% strength reduction at full replacement. The findings are coherent with other studies (Huang et al. 2019; Deng et al., 2023), which showed that the flaky/elongated aggregates tend to fracture under external loading.

Table 3. Comparison of hardened properties of concrete made with granite and TBM waste.

Property	Age	T0	T10	T30	T50	T100
Compressive strength, MPa	7	51.9	52.1	48.8	44.5	41.7
Compressive strength, MPa	28	58.5	60.2	55.6	54.1	49.9
Modulus of elasticity, GPa	28	39.4	42.3	39.1	37.3	38.6
(a) Drying shrinkage, µm/m	56	115.8	122.7	130.6	133.9	141.2
(b) Water absorption rate, x10^{-4} mm/s$^{0.5}$	28	4.82	5.08	4.91	5.16	5.58

(a) exposed to 28 °C, 60% RH; (b) based on ASTM C 1585 (2020)

The effect of TBM waste on the modulus of elasticity of concrete was not significant, although the modulus of elasticity of concrete containing up to 30% TBM waste was comparatively similar to that of granite concrete, and the reduction at 50% and 100% TBM waste was not noticeable. On the other hand, it was found that the use of TBM increased the drying shrinkage of concrete. While the increase was negligible at lower replacement levels, the effect became more pronounced as the percentage of TBM waste in the concrete increased.

Similarly, it was found that the water absorption of concrete showed some degree of increment as the content of TBM waste increased, although this effect was again negligible at lower replacement levels. The increase in the water absorption of concrete could be attributed to the higher water absorption nature of TBM waste, as well as its elongated shape which might lead to poorer aggregate packing and, thus, higher voids content.

Overall, TBM waste is a suitable alternative to granite in concrete production, but some precautions should be taken when using it in structural concrete. The process of handling the waste, especially crushing and sieving, is particularly important as its shape tends to be elongated and flaky. Thus, the material is not advisable to use as coarse aggregate having nominal maximum size of 20mm. Introducing a washing process can help remove excess fines content in TBM waste, thus reducing its influence on the drying shrinkage and water absorption of concrete.

The characteristics of TBM waste are generally not too dissimilar to those of granite aggregates, except that TBM waste has the potential risk for ASR expansion. However, this risk can be controlled with the use of GGBS (or any other suitable supplementary cementitious materials) as a partial replacement of PC. Thus, it is necessary to specify the use of TBM waste in conjunction with GGBS in concrete production to address the ASR concern.

Based on the current findings, TBM waste can be used for up to 30% replacement for granite aggregate without compromising the hardened properties of concrete. The use of higher content of TBM waste is possible, but it requires some adjustment in concrete mix design, such as reducing the water/cement ratio by lowering the water content with the help of water-reducing admixtures in maintaining the consistence of concrete (Dhir et al., 1999)

4. CONCLUSION

This study evaluated the feasibility of using locally sourced TBM waste as aggregates in concrete production by comparing its performance with commonly used granite aggregates. The following conclusions can be drawn:

- The physical and chemical characteristics of TBM waste and granite aggregates are mostly the same, but the former has slightly higher water absorption and fines content.
- TBM waste is considered moderately reactive for ASR, but it can be controlled with the use of 50% GGBS.
- In general, the use of TBM waste for up to a 30% replacement level did not show a detrimental effect on the hardened properties of concrete, however, the performance of concrete reduced as the content of TBM waste increased up to 100%.

Although further study is needed, especially on chemical analysis and petrographic analysis of TBM waste, the procedures for processing TBM waste into aggregates require further refinement to enhance its quality.

5. ACKNOWLEDGMENT

The authors would like to express appreciation for the support of the sponsors [A-8001135-00-00].

6. REFERENCES

ASTM C1260 (2021). Standard Test Method for Potential Alkali Reactivity of Aggregates (Mortar-Bar Method). ASTM Internationals, West Conshohocken, PA, USA.

ASTM C1585 (2020). Standard Test Method for Measurement of Rate of Absorption of Water by Hydraulic-Cement Concretes. ASTM Internationals, West Conshohocken, PA, USA.

ASTM C1778 (2022). Standard Guide for Reducing the Risk of Deleterious Alkali-Aggregate Reaction in Concrete. ASTM Internationals, West Conshohocken, PA, USA.

BS EN 12620 (2008). Aggregates for Concrete. British Standards Institution, London, UK.

BS EN 206 (2021). Concrete. Specification, Performance, Production and Conformity. British Standards Institution, London, UK

Deng P, Xu K, and Guo S (2023). Effects of coarse aggregate morphology on concrete mechanical properties. Journal of Building Engineering, 63, 1-13.

Dhir R K, Limbachiya M C and Leelawat T (1999). Suitability of recycled concrete aggregate for use in BS 5328designated mixes. Structures and Buildings, 134(3), 257-274.

Huang Y, Ding Y, Xie T and Fei D (2021). Effect of coarse-aggregate shape on strength of hydraulic concrete. Structural Concrete, 22(Supplement 1), E710-E719.

USE OF RECYCLED AND SIDERURGIC AGGREGATES IN THE URBAN DEVELOPMENT OF THE ISLAND OF ZORROTZAURRE (BILBAO)

Baraibar, J.M

Viuda de Sainz, S.L.
E-mail: jmbaraibar@viudadesainz.com

The city of Bilbao has undergone a model urban transformation in recent years. It has risen from the ashes, shifting from a grey, industrial city to a cosmopolitan capital The island of Zorrotzaurre project is the latest major urban renewal operation in Bilbao (Spain). From the early stages of urban planning, it has been conceived by using sustainability as the main driving force. This directive has influenced the detailed design project of the urban development on the right bank of the Deusto Canal (Figure 1).

Figure 1. Urban development on the right bank of the Deusto Canal

This project is a large-scale example of using recycled aggregates from C&DW and siderurgic aggregates from electric arc furnace steel slag for conforming different construction units, especially concrete slab pavements. This solution avoids the extraction of natural aggregates and the consumption of space in authorized landfills.

The construction unit “Recycled concrete pavement”, with a quantity of 22,300 m^2, used at least 75% of the weight of its aggregates from a recycled origin. Besides, all the granular filling material, with a quantity of 13.000 m^3, came from concrete recycling or from mixed recycled aggregates, according to regional regulations.

The performance of these aggregates was enough to guarantee the structural resistance of concrete for pedestrian pavements, even improving its surface roughness compared to traditional solutions. The use of recycled materials can also provide aesthetic properties, which can be appreciated from an architectonical point of view.

Keywords: recycled aggregate, siderurgic aggregate, C&DW, steel slag, sustainable construction

EVOLUTION OF SERVICE PERFORMANCE OF FERROCHROME SLAG AGGREGATE CONCRETE IN DEEP-UNDERGROUND ENVIRONMENT

Maopeng Jiao [1], Zhidan Rong [2]

[1]Doctor, School of Materials Science and Engineering, Southeast University
[2]Associate professor, School of Materials Science and Engineering, Southeast University
zdrong@seu.edu.cn

1. INTRODUCTION

Traffic construction plays a vital role in improving the development of Western China. In the engineering construction represented by the Sichuan–Tibet railway, complex environments [1, 2] such as high temperature, complex stress and hydrothermal corrosion have emerged, posing higher challenges to the service performance of concrete. Meanwhile, high carbon ferrochromium slag (FS) is a typical solid waste with great application value for its good physical and heat resistance properties [3, 4], and its production capacity is mainly concentrated in the southwest region. Therefore, it can be used as aggregate to prepare concrete to meet the requirements of deep environment for concrete. This study uses FS as the aggregate to prepare concrete, and then uses methods such as XRD, SEM, NMR, and hydration heat to explore the evolution law and degradation mechanism of concrete's deep environmental service performance.

2. MATERIALS AND METHODS

2.1 Raw materials and mix proportions

The cementitious materials were 42.5R ordinary Portland cement and II-grade fly ash (FA). The chemical compositions of them are shown in Table 1, and the distribution of particle size is shown in Fig. 1(a). Local river sand with a fineness modulus of 2.9 was used as the fine aggregate. FS produced in the Sichuan province of China are shown in Fig. 1(b), and Table 1 summarizes that SiO_2, Al_2O_3, and MgO are the main chemical compositions of FS. FS was used to replace the natural aggregate (NA) in the range of 5-25 mm with a continuous grading as the coarse aggregate. A polycarboxylate superplasticizer with a water reduction of 29% was employed to keep the slump of concrete within the range of 150-180 mm.

Table 1 Chemical compositions of raw materials (%)

Contents/%	CaO	Al_2O_3	Fe_2O_3	SiO_2	MgO	SO_3	K_2O	TiO_2	Cr_2O_3
Cement	66.46	4.28	3.49	19.83	0.11	4.18	0.76	0.44	-
Fly ash	10.93	22.89	5.98	53.39	0.44	0.47	2.77	1.96	-
FS	1.18	25.07	3.12	35.01	26.49	0.52	-	-	7.37

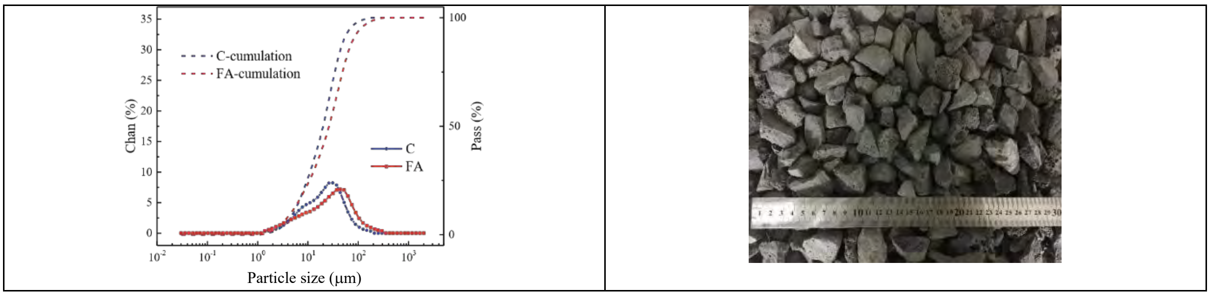

(a) The particle size distribution (b)Morphology of FS

Fig. 1 Raw materials

Concrete was prepared with the different mix proportions as shown in Table 2. After mixed thoroughly in two stages, the freshly mixed concrete was poured into molds with various sizes, covered with plastic, and cured at room temperature for 24 h. Then the concrete specimens were demolded and placed in a standard curing room until curing for the age of experiments.

Table 2 Mix proportion of concrete(kg/m^3)

	w/b	water	Cement	Fly ash	Sand	NA	FS	Water reducer
42NA	0.42	160	266	114	740	1065		1.52
34NA	0.34	156	322	138	731	1053		1.84
42FS	0.42	160	266	114	740		1065	1.52
34FS	0.34	156	322	138	731		1053	1.84

2.2 Methods

Cubic concrete with dimensions of 100 mm×100 mm×100 mm was used for compressive strength tests with a loading rate of 0.6 MPa/s. The durability of the concrete was evaluated by the resistance of chloride ion penetration and sulfate attack, which are mainly in accordance with GB 50082-2009. Furthermore, samples were observed using a TM 4000 scanning electron microscope (SEM). Moreover, the micro-structure of concrete was characterized using low-field nuclear magnetic resonance (LF-NMR) with the MesoMR12-060V-I instrument.

Cement pastes with a same mix proportion were prepared. The hydration heat was conducted using TAM air isothermal calorimeter, the experimental data was collected during the first 3 days. X-ray diffraction (XRD) was conducted using D8-Discover to characterize the mineral composition of FS, the step size and scanning range were 0.02° (2θ) and 5°-70°, respectively.

FS was ground and passed 200 mesh sieves, X-ray photoelectron spectroscopy (XPS) was carried out using the AXIS UltraDLD system to investigate the distribution of chromium element (Cr). In addition, inductively coupled plasma emission spectrometer (ICP-AES) Thermo iCAP6500 was employed to evaluate the leaching of Cr. Samples were crushed and sieved to 3 mm and 0.3 mm, respectively, then blended with deionized water in a 1:10 proportion. After stirring for 8 h and standing for 16 h, 10 mL of the mixture was tested and the leaching of Cr in FS could be calculated.

3. RESULTS AND DISCUSSION

3.1 Mechanical properties

Fig. 2 presents that the water absorption rate of 42FS and 34FS decreases by 11.55% and 20.31% compared to 42NA and 34NA, respectively. Additionally, the permeable porosity of 42NA and 34NA is 8.31% and 6.12%, respectively, while 42FS and 34FS decreases to 7.57% and 5.01%, indicating that the replacement of FS for NA can effectively improve the capillary pore structure of concrete. Furthermore, the replacement of FS for NA has a significant impact on the compressive strength of concrete. Concrete with FS achieves a compressive strength of 73.5 MPa at 28 d as a water-binder ratio of 0.34, which represents a 11.4% increase compared to the reference concrete with NA. Moreover, at the age of 28 d, the compressive strength of 42FS is increased by 15.4% compared to that of 42NA. The increase in compressive strength for concrete with FS can be attributed to the gradation of FS and the improvement of pore structure.

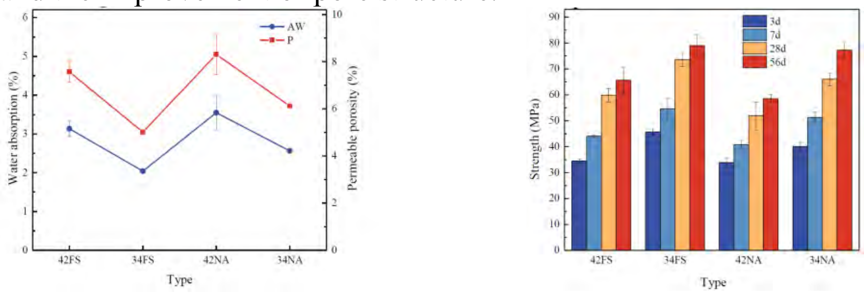

(a)Water absorption rate and permeable porosity (b)Compressive strength

Fig. 2 Mechanical properties of concrete prepared with FS

3.2 Durability

Fig. 3 summarizes that the replacement of FS for NA further reduces the chloride diffusion coefficient, there is a 34.7% decrease in the chloride diffusion coefficient of 42FS compared to that of 42NA at 56 d. Furthermore, the replacement of FS for NA reduces the chloride diffusion coefficient of 42FS to 6.2□10^{-12} m^2/s at 56 d, which satisfies the requirements for concrete materials in railway tunnels with a service life of 100 years (L1 environment) as stipulated in TB 10005-2010. Additionally, Fig. 4 reveals that the relative compressive strength of 42FS is increased by 16.6%, while that of 42NA is only 2.8% after 120 dry-wet cycles. Moreover, the compressive strength of 42NA shows a downward trend after 60 cycles, but it is still slightly higher than that of the initial value at 28 d. Therefore, concrete prepared with the replacement of FS for NA exhibits better service performance [3].

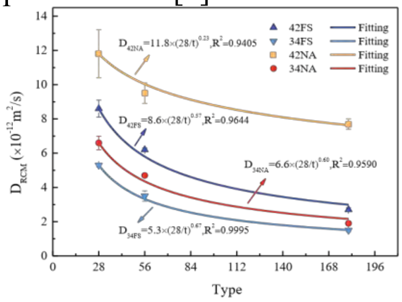

Fig. 3 The chloride diffusion coefficient of concrete

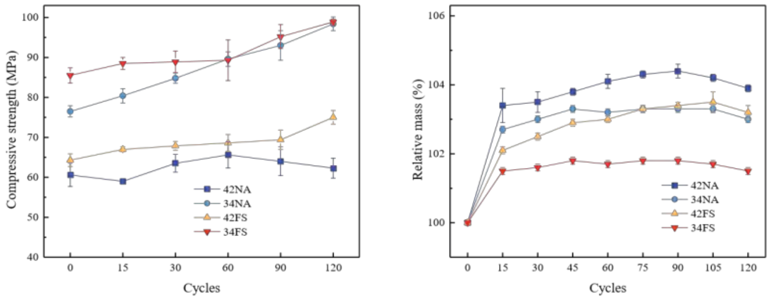

(a)relative strength (b)relative mass

Fig. 4 The resistance on the sulfate attack of concrete

3.3 Characterization of FS

The results of XRD shown in Fig. 5(a) verify that the mineral compositions of FS are forsterite, spinel, enstatite, and un-reacted chromite [5, 6], indicating that there is a potential and beneficial for FS to resist the adverse effects of deep- underground environment. Furthermore, the morphology of FS was observed through SEM, Fig. 5(b) shows that the forsterite is in the shape of plate, surrounded by the polyhedral-like spinel crystal. And the crystal is surrounded by glassy phase of silicon, while cracks and pores also exist around the crystals.

Additionally, Fig. 6 reveals that the relative ratio of Cr^{3+} and Cr^{6+} in FS is 43.2% and 56.8% respectively. And the leaching values of chromium measured by ICP is 0.142 mg/L when the crushed particle size is 3 mm, while the leaching values of chromium is 0.439 mg/L when the particle size is reduced to 0.3 mm, which is still below the minimum limit of Cr^{6+} (0.5 mg/L specified in GB 8978-1996). Therefore, the utilization of FS satisfies the requirements for its leaching performance [4].

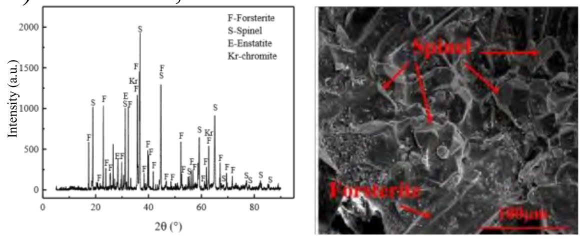

(a)XRD patterns (b)Morphology of FS

Fig. 5 Chemical compositions and morphology of FS

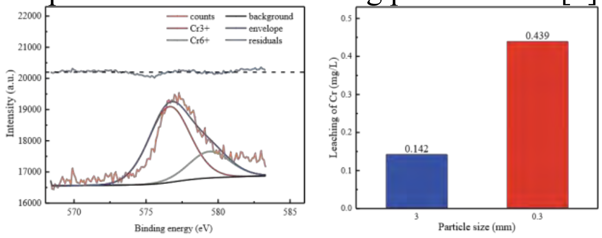

(a)XPS results (b)Leaching value of Cr

Fig. 6 The relative content and leachability of Cr

3.4 Effect of FS on microstructure of concrete

Fig. 7 indicates that the most probable pore size decreases with the replacement of FS for NA, the utilization of FS as aggregate leads to a reduction in the most probable pore size of concrete, with the values of 1.97 nm and 1.87 nm for 34FS and 42FS, respectively, and that of 2.68 nm for 34NA and 42NA.Therefore, the pore structure is improved when FS is used to replace NA. Meanwhile, the porosity of 34FS and 42FS are 5.51% and 6.84%, while this value of 34NA and 42NA are 11.68% and 11.39%, respectively. This reduction in porosity indicates that the continuous gradation of FS is better than that of NA, leading to improved compactness of the concrete. Additionally, the porous and rough surfaces of FS facilitate its combination with cement-based materials, which improves the optimization of ITZ and reduces the number of pores in the concrete.

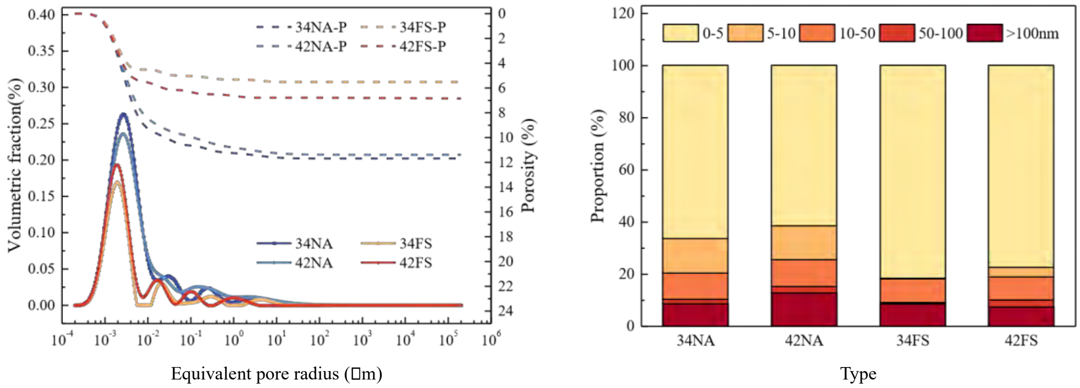

(a)Differential pore distribution and porosity (b) Content of pores in different ranges

Fig. 7 Micro-structure of concrete prepared with FS

4. CONCLUSION

This paper investigates the effect of using high-carbon ferrochrome slag (FS) as a replacement for natural aggregates (NA) in concrete, the mix proportion and performance of concrete are evaluated for mechanical properties and durability. The main findings are as follows:

(1) The permeable porosity of 42NA and 34NA is 8.31% and 6.12%, respectively, while that of 42FS and 34FS decreases to 7.57% and 5.01%, indicating that the replacement of FS for NA improves the pore structure of concrete, thus resulting in better compressive strength with a 11.4% increase for 34FS compared to the reference concrete.

(2) The resistance of concrete to chloride ion penetration and sulfate attack is significantly improved by the replacement of FS for NA.

(3) The improvements in the performance after replacing NA with FS comes from the gradation and the well combination of cementitious materials, thus improving the pore structure of concrete. The porosity decreases from 11.39% and 11.68% to 6.84% and 5.51% when the water-binder ratio is 0.42 and 0.34, respectively.

5. ACKNOWLEDGMENT

The authors would like to express appreciation for the support from the National Key Research and Development Program of China (2019YFC1904902 and 2018YFC0705400), National Natural Science Foundation of China (no. 52178254, no. 51678142).

6. REFERENCES

[1] C. Lu, C. Cai, Challenges and Countermeasures for Construction Safety during the SichuanTibet Railway Project, Engineering 5(5) (2019) 833-838.
[2] D. Zhang, Z. Sun, Q. Fang, Scientific problems and research proposals for Sichuan-Tibet railway tunnel construction, Underground Space 7(3) (2022) 419-439.
[3] J. Zelic, Properties of concrete pavements prepared with ferrochromium slag as concrete aggregate, Cem. Concr. Res. 35(12) (2005) 2340-2349.
[4] S.C. Yaragal, B.C. Kumar, C. Jitin, Durability studies on ferrochrome slag as coarse aggregate in sustainable alkali activated slag/fly ash based concretes, Sustain. Mater. Technol. 23 (2020).
[5] C.B. Liu, L.B. Liu, K.F. Tan, L.H. Zhang, K.J. Tang, X.P. Shi, Fabrication and characterization of porous cordierite ceramics prepared from ferrochromium slag, Ceram. Int. 42(1) (2016) 734-742.
[6] L.H. Zhang, Y.S. Zhang, C.B. Liu, L.B. Liu, K.J. Tang, Study on microstructure and bond strength of interfacial transition zone between cement paste and high-performance lightweight aggregates prepared from ferrochromium slag, Constr. Build. Mater. 142 (2017) 31-41.

COMPRESSIVE BEHAVIOR AND WATER PERMEABILITY OF RECYCLED LUMP-AGGREGATE CONCRETE WITH RECYCLED SAND FROM WRSG

Tao Zhang, Bo Wu

State Key Laboratory of Subtropical Building and Urban Science, South China University of Technology, Guangzhou, 510641, China
E-mail: bowu@scut.edu.cn (Bo Wu)

1. INTRODUCTION

China has an extensive need for cement, natural sand (NS), and natural coarse aggregates (NCAs), which are utilized in the production of approximately 3.29 billion cubic meters of concrete every year. Moreover, an abundance of construction and demolition (C&D) waste is generated, which mainly consists of excavated soil and demolished concrete (Fig. 1). Recycled aggregate concrete (RAC) and recycled lump concrete (RLC), as two effective ways of recycling waste concrete, have led to many research findings. The concept of recycled lump-aggregate concrete (RLAC) has been proposed based on this (Fig. 2) (Lin & Wu, 2022). Furthermore, RLAC completely or partially replacements the NS and NCAs in the fresh concrete of RLC with recycled sand (RS) from excavated soil and recycled coarse aggregates (RCAs), respectively. The simultaneous use of recycled lumps (RLs), RCAs, and RS in concrete can significantly improve the recycling of C&D waste. However, the impact of the three types of waste on the compressive and water permeability performance of concrete is currently not well understood. In this study, compressive and water permeability tests were conducted on RLAC containing the aforementioned three types of waste. In addition, the MIP, XRD, and SEM tests were performed to explain the macroscopic test results. The filling, nucleation, and internal curing effects of RS in RLAC were discussed.

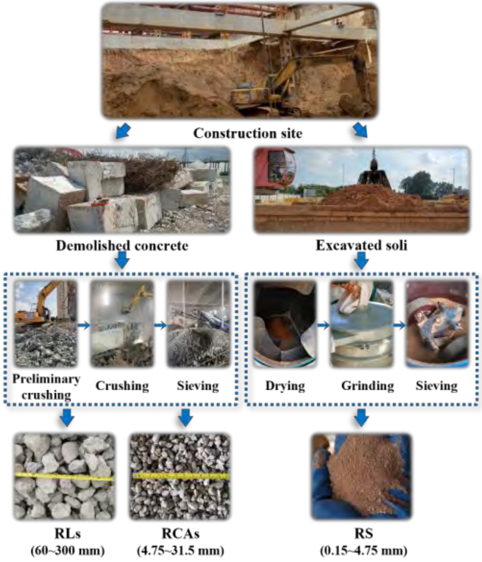

Fig. 1. Construction and demolition (C&D) waste and recycling products.

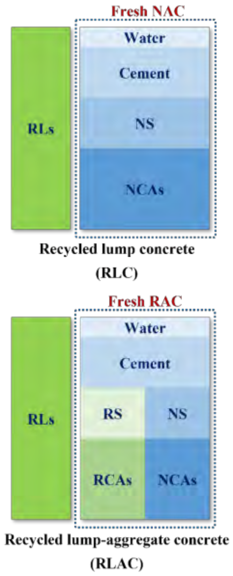

Fig. 2. The composition of RLC and RLAC.

2. MATERIALS AND METHODS

2.1. Materials

Weathered residual soil of granite (WRSG) is a type of excavated soil that exhibits widespread distribution in South China (Yuan et al., 2022). In this study, WRSG was treated to prepare RS, which is used to partially replace NS, using the grinding & dry-sieving process proposed by Wu et al. (2023) (Fig. 1). Compared with NS, RS has lower apparent density and fineness modulus, and higher crushing index and water absorption. The clay content of RS and NS is 5.5% and 0, respectively. The particle size distribution of clay particles in RS is measured. The distribution of clay particles in RS and cement particles appears to be relatively close. Fig. 3 shows the SEM micrographs of RS. The particles of RS are irregular and angular because of the weathering of granite (Liu et al., 2022), and the surface of the particles has a rough texture and a significant number of pores because of the presence of acicular microcline and lamellar kaolinite. However, the particles of NS are regular, and the surface is smooth and dense after long-term scouring by water (Singh et al., 2016).

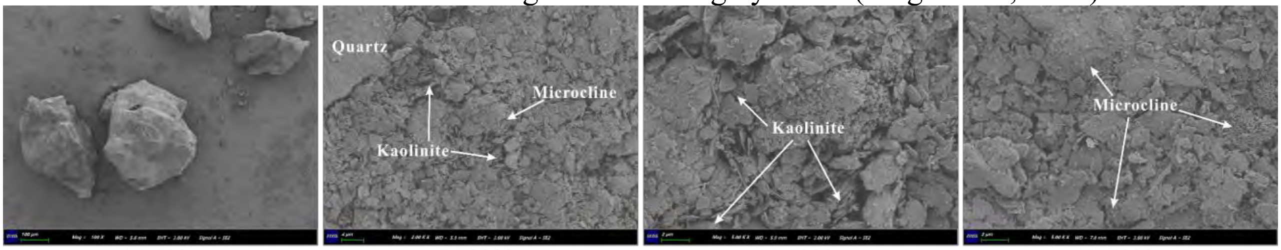

(a) 100× **(b) 2000×** **(c) 5000×** **(d) 5000×**

Fig. 3. SEM images of RS from WRSG.

The coarse aggregates used in this study were NCAs and RCAs made by crushing and sieving abandoned concrete pavements. Although RCAs and NCAs have similar particle size distributions, RCAs have a slightly lower apparent density and higher crushing index and water absorption due to the old mortar attached to the surface in comparison with NCAs. The old concrete used to produce RLs came from the abandoned support beams, and the sizes of the crushed RLs mainly ranged in 60~90 mm.

All specimens are numbered in this form W#-RS#-RCA#-RL#. In this way, W represents the effective water-cement ratio of fresh concrete, RS and RCA represent the replacement ratio of recycled sand (η_{RS}) and recycled coarse aggregates (η_{RCA}) in fresh concrete, respectively, and RL represents the replacement ratio of recycled lumps (η_{RL}).

2.2. Methods

The compressive tests were loaded by MATEST-4000kN press. During the test, displacement loading at a rate of 10×10^{-6} /s was applied.

The permeability test was conducted by HP-4.0 tester. 2.5 MPa and 1.5 MPa water pressure were used for W36 and W45 series specimens, respectively, and 0.8 MPa water pressure was used for the old concrete specimens. The specimens were split in half and water permeation was observed from the vertical split surface after 24 h.

3. RESULTS AND DISCUSSION

3.1. Compressive behavior

The variation of compressive strength and elastic modulus of RLAC at day 90 with η_{RS}, η_{RCA}, and η_{RL} are given in Fig. 4 and Fig. 5, respectively. It can be seen that: (a) The composite utilization of RCAs and RS has no statistically significant effect on the compressive strength. (b) The increase of η_{RS} led to the elastic modulus decrease, but the decrease is modest. The reason is that NS mainly consists of quartz, accounting for 93.5% of its composition, while RS is mostly composed of quartz (63.5%), microcline (30.0%), and kaolinite (4.9%). The elastic modulus of microcline and kaolinite, which are 59.9 GPa and 17.3 GPa respectively, is considerably lower than that of quartz (87.7 GPa) (Sun et al., 2021). (c) When the compressive strength (26.9 MPa) and elastic modulus (23.6 GPa) of the old concrete were significantly low, the compressive strength and elastic modulus of the RLAC decreased significantly for the utilization of RLs.

3.2. Water permeability

Fig. 6 demonstrates the variation in the permeability coefficient (Lin & Wu, 2022) of specimens with η_{RS} and η_{RL} at day 90. The data shows that: The use of RS contributes to a notable enhancement in the impermeability of concrete, with the degree of improvement growing as η_{RS} increases. In addition, when the permeability coefficient of the old concrete is relatively high (3.88×10^{-9} cm/s), the utilization of RLs leads to a substantial decrease in RLAC impermeability. However, it is vital to note that the extent of this decrease becomes progressively smaller as η_{RS} increases.

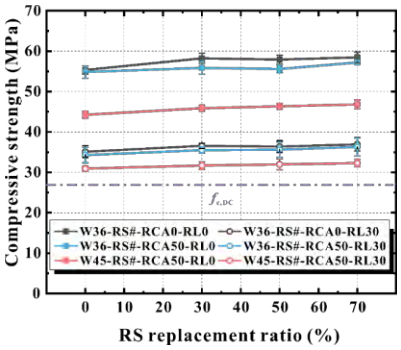

Fig. 4. Variation of compressive strength with η_{RS}, η_{RCA}, and η_{RL}.

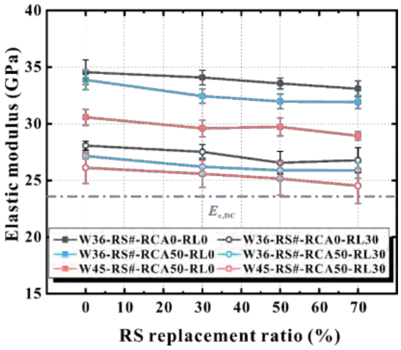

Fig. 5. Variation of elastic modulus with η_{RS}, η_{RCA}, and η_{RL}.

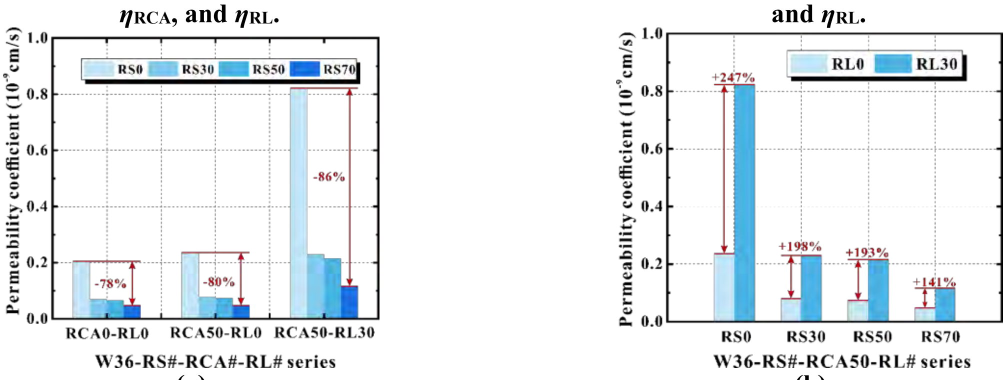

(a) **(b)**

Fig. 6. Variation of permeability coefficient with (a) η_{RS}, and (b) η_{RL}.

3.3. MIP, XRD and SEM tests

Fig. 7 shows the variation in the porosity and pore size distribution of the mortar in RLAC with η_{RS} at day 90, and the corresponding pore characteristics of the mortar are given in Table 1. According to Fig. 7 and Table 1, the total porosity, porosity of harmful pores (>100 nm), critical aperture, and the most probable pore aperture of the mortar decreased steadily as η_{RS} increased. In conclusion, the utilization of RS can improve the pore structure of the mortar.

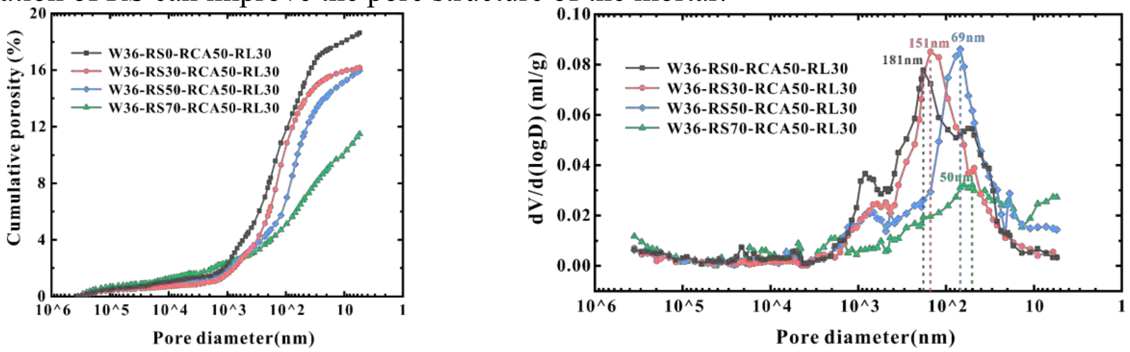

(a) Porosity **(b) Pore size distribution**

Fig. 7. Porosity and pore size distribution of the mortar in RLAC.

Table 1. Pore characteristics of the mortar in RLAC.

Specimen	Total porosity (%)	Porosity of harmful pores (%)	Critical aperture (nm)	Most probable pore aperture (nm)
W36-RCA50-RS0-RL30	18.6	10.9	1850	181
W36-RCA50-RS30-RL30	16.2	9.3	1606	151
W36-RCA50-RS50-RL30	16.0	5.7	1434	69
W36-RCA50-RS70-RL30	11.5	4.7	432	50

Fig. 8 illustrates the XRD pattern of mortar in RLAC at day 90. The test samples were mixed with α-Al_2O_3 as the internal standard at a mass ratio of 5:1 to improve the accuracy of the semi-quantitative analysis of the amorphous phase (C-S-H) and other phases. The formation of calcite can be attributed to the carbonation process of C-S-H and CH exposed to the air, soon after the grinding of mortar samples (Gervais et al., 2004). Semi-quantitative analysis was carried out using the Rietveld method for Fig. 8, and the normalized results of the hydration-related products are shown in Fig. 9. The analysis results indicate that there is a positive correlation between the content of hydration-related products and the increase in η_{RS}. RS makes the hydration of the cement more adequate, which, leads to a denser structure of the cement paste. On the one hand, the utilization of RS can significantly reduce the average value of surface spacing between neighboring aggregate grains in fresh concrete (Zhutovsky et al., 2004). Therefore, the cement paste will be more susceptible to the internal curing effect of water in aggregates pores. On the other hand, the distribution of the clay particles in RS and cement particles is closer to each other. Hence, additional nucleation sites for the precipitation of the hydration products can be provided.

Fig. 10 show the SEM micrographs of the mortar containing NS for fresh concrete and the mortar containing 70% RS for fresh concrete in RLAC at day 14. It's readily apparent from the figure that in the mortar containing NS, obvious microcracks were observed in the interfacial transition zone (ITZ) between NS and cement paste, and a number of coarse stick-like AFt could be observed in the pores of mortar, with a loose and porous microstructure. However, the microcracks in the ITZ between RS and cement paste were comparatively insignificant in the mortar containing 70% RS, and the mortar pores were filled with clay particles. The tight-knit network of C-S-H gel, and embedded CH crystals within the network, together contribute to the dense microstructure. On the one hand, RS's surface has a rough texture and a lot of pores, which can improve the cement paste's adhesion and permeability. On the other hand, RS's particle size is significantly smaller than that of NS's (RS's fineness modulus is significantly smaller than NS's), which can be better for filling. Moreover, clay particles in RS provide more nucleation sites for the precipitation of hydration products.

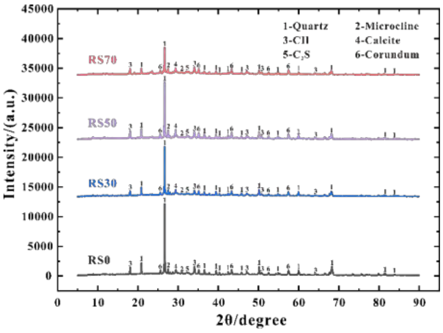

W36-RS#-RCA50-RL30 series

Fig. 8. XRD pattern of the mortar in RLAC.

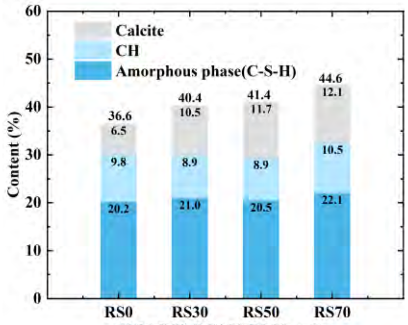

W36-RS#-RCA50-RL30 series

Fig. 9. Percentage of hydration-related products.

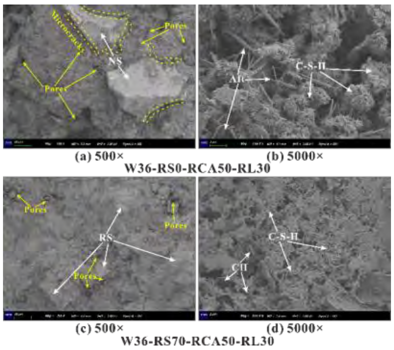

(a) 500× (b) 5000×
W36-RS0-RCA50-RL30
(c) 500× (d) 5000×
W36-RS70-RCA50-RL30

Fig. 10. SEM images of the mortar in RLAC.

4. CONCLUSION

The results showed that: (a) at the age of 90 days, RS and RCAs have no significant effect on the compressive behavior of RLAC, but RLs deteriorated the compressive strength and elastic modulus of RLAC when the source concrete of RLs showed poorer compressive behavior. (b) RLs deteriorated the impermeability of RLAC when the source concrete of RLs showed poorer impermeability, however, the adverse effect of RLs on impermeability decreased with the increase of the RS replacement rate. (c) The test results of MIP, XRD and SEM confirmed that RS can improve the pore structure and cement hydration of concrete due to the filling, nucleation, and internal curing effects of RS.

5. ACKNOWLEDGMENT

This research was financially supported by the Key-Area Research and Development Program of Guangdong Province [Project number 2019B111107003], the National Natural Science Foundation of China [Project number 52078219], and Guangdong Provincial Key Laboratory of Modern Civil Engineering Technology [Project number 2021B1212040003]. The financial supports are sincerely appreciated.

6. REFERENCES

Gervais, C., Garrabrants, A. C., Sanchez, F., Barna, R., Moszkowicz, P., & Kosson, D. S. (2004). The effects of carbonation and drying during intermittent leaching on the release of inorganic constituents from a cement-based matrix. *Cement and Concrete Research*, *34*(1), 119-131.

Lin, L., & Wu, B. (2022). Water permeability behavior of recycled lump/aggregate concrete. *Construction and Building Materials*, *323*, 126508.

Liu, X., Zhang, X., Kong, L., Wang, G., & Lu, J. (2022). Disintegration of granite residual soils with varying degrees of weathering. *Engineering Geology*, *305*, 106723.

Singh, S., Nagar, R., Agrawal, V., Rana, A., & Tiwari, A. (2016). Sustainable utilization of granite cutting waste in high strength concrete. *Journal of Cleaner Production*, *116*, 223-235.

Sun, C., Li, G., Xu, J., Rong, H., & Sun, Y. (2021). Rheological characteristics of mineral components in sandstone based on nanoindentation. *Chinese Journal of Rock Mechanics and Engineering*, *40*(1), 77-87.

Wu, B., Cao, H., & Wu, Q. (2023). Compressive and shrinkage behaviors of recycled aggregate concrete containing recycled sand from weathered residual soil of granite and MgO expansion agent. *Journal of Building Engineering*, *68*, 106154.

Yuan, B., Chen, W., Zhao, J., Li, L., Liu, F., Guo, Y., & Zhang, B. (2022). Addition of alkaline solutions and fibers for the reinforcement of kaolinite-containing granite residual soil. *Applied Clay Science*, *228*, 106644.

Zhutovsky, S., Kovler, K., & Bentur, A. (2004). Influence of cement paste matrix properties on the autogenous curing of high-performance concrete. *Cement and Concrete Composites*, *26*(5), 499-507.

Session A3

CO_2 Mineralization and Environmental Assessment

ASSESSMENT OF CARBONATED FERRONICKEL SLAG AS SUPPLEMENTARY CEMENTING MATERIALS WITH IMPROVED CARBON IMPACT AND REACTIVITY

Cyr, M[1], Laniesse, P[1,2], Dufourny, A[3], Julcour, C[3], and Bourgeois, F[3]

[1]LMDC, Université de Toulouse, UPS, INSA, Toulouse, France
[2]ECOCEM Materials Limited, Dublin, Ireland
[3]LGC, Université de Toulouse, CNRS, INPT, UPS, Toulouse, France
E-mail (corresponding author): martin.cyr@univ-tlse3.fr

Ferronickel slag is a by-product of the ferronickel production with pyrometallurgical process, either in blast furnace or in electric arc furnace. In New Caledonia, around 2 million tons of ferronickel slags are produced annually, but only 8% is re-used, mostly as sand in road applications. The chemical composition of the ferronickel slag depends on the process and temperatures, and it includes mainly SiO2, MgO, CaO, Al2O3 and Fe2O3. The mineralogical composition primarily consists of magnesium-iron silicates of the olivine group, such as ferroan forsterite ((Mg,Fe)2SiO4), and magnesium silicates of the pyroxene group, such as clinoenstatite (MgSiO3). When ferronickel slags are quenched with water, the content of amorphous phases could be higher than 50%. However, it has been shown that their use as supplementary cementing materials (SCM) in replacement of Portland cement was less attractive than ground granulated blastfurnace slags (GGBS), as the presence of magnesium silicate leads to a limited reactivity of the product.

This work assessed the feasibility of carbonating ferronickel slag to produce a more reactive material that could be used as a binder. Carbonation of such materials has indeed several advantages:

- Capture and stabilize the storage of carbon dioxide in stable minerals. Carbonation rates between 20% and 80% of the initial material was achieved by a process of attrition-carbonation in a controlled humidity/temperature carbonation device.
- Separate magnesium from silica in two distinct mineral forms: crystallized magnesite (MgCO3) and amorphous silica (SiO2). This process helped to improve the reactivity of the silica fraction with calcium hydroxide in Portland cement-based materials. A more reactive SCM was thus produced with this process.

Keywords: Mineral carbonation, ferronickel slag, carbon capture, reactivity, pozzolan

VALIDATION OF A BIM TOOL FOR THE QUANTIFICATION OF WASTE AND IMPACTS OF DEMOLITION PROJECTS

Garcia-Estevez, D.[1], Garcia-Cortes, V.[1], San-Jose, J.T.[2] and Sandonis, E.[3]

[1]TECNALIA, Basque Research and Technology Alliance (BRTA), Building 700, Astondo Bidea, 48160 Derio, Spain
[2]UPV/EHU, Department of Engineering in Mining, Metallurgy and Materials Science, Plaza Ingeniero Torres Quevedo 1, 48013 Bilbao, Spain
[3]LEZAMA DEMOLICIONES, Trapaga Elkartegia Bº Ugarte s/n- MOD 17-21, 48510 Bilbao, Spain
david.garcia@tecnalia.com

Building Information Modeling (BIM) has been widely adopted for design, construction and maintenance of buildings. This methodology and related tools can also offer numerous benefits for demolition planning and waste management, such as enhanced collaboration, accurate waste quantification, efficient planning, improved safety and reduction of landfill waste. However, there are also challenges that need to be addressed when utilizing BIM in these processes, including reality capture, complex modelling, limited adoption, data integration, time and cost.

A software named BIM4DW has been developed to avoid the dependency of complex BIM models and to reduce the time for modelling and inventory, from top pictures or drawings. BIM4DW is a web tool that runs directly on Internet browsers. Projects are stored in the cloud. BIM4DW combines a 2D/3D modelling interface, directly or using a reference layer with the available information, with parametric databases of most common building elements. Geometry, composition and densities are used to identify and quantify materials. Sequentially, the tool supports the definition of the groups, demolition techniques (including equipment and labor) and the final waste streams (using harmonized codes from the European Waste Catalogue). Additionally, BIM4DW calculates the total time, the environmental impacts and the cost of each demolition alternative, taking into account the physical demolition task, transport and waste treatment. At the end, it provides a final report (pdf) or exchangeable format file (json) to be used by other software.

This paper presents the validation of BIM4DW in three demolition projects. It provides an overview of the data entering stages and the major difficulties when using it in industrial buildings. The obtained results are compared with finally obtained waste streams. Conclusions include the accurate identification and quantification of waste, the improved control of the demolition site and the need to improve the sketching module and the environmental impacts databases.

Keywords: BIM, demolition, waste management, circular, construction

UTILIZATION OF DEMOLISHED CONCRETE WASTES FOR CO_2 CAPTURE AND MINERALIZATION IN THE CEMENT AND LIME INDUSTRY

Liang Li[1], Hai Yu[1], Song Zhou[1], Sanket Rawat[2], Vinh Dao[3], Y.X. Zhang[2]

[1]Commonwealth Scientific and Industrial Research Organisation (CSIRO), Energy Centre, NSW, 2304, Australia
[2]School of Engineering, Design & Built Environment, Urban Transformations Research Centre, Western Sydney University, NSW 2751, Australia
[3]School of Civil Engineering, The University of Queensland, Brisbane, 4072, Australia
(Corresponding author: liang.li@csiro.au)

1. INTRODUCTION

Utilization of demolished concrete wastes as host minerals for CO_2 sequestration has attracted great interest as part of the Carbon Capture, Utilization and Storage (CCUS) roadmap of the cement and lime industry (Li & Wu, 2022). A couple of large-scale demonstrations of CCUS technologies and projects have been deployed in the cement industry in the recent few years (Marmier, 2023; Srinivasan et al., 2021). In this work, the utilization of concrete wastes as CO_2 mineralization feedstock in an integrated CO_2 capture and mineralization approach is explored. The utilization route not only promotes the reuse and reprocessing of concrete wastes as valuable materials but also reduces hard-to-abate emissions in the cement and lime industry.

Before being desirable CO_2 feedstock, the collected concrete wastes are exposed to mechanical activation (by grinding). The grinding process can not only reduce the particle size of concrete wastes but also result in the production of new surfaces, defects in crystalline structures, and phase transformations, leading to an increased carbonation reactivity (Li, Yu, et al., 2023; Li & Wu, 2022). The particle size and distribution of the ground concrete wastes can significantly affect the CO_2 uptake capacity upon mineralization. However, the energy consumption associated with the mechanical activation of concrete wastes has been one of the primary barriers for the economic pre-treatment of construction wastes as CO_2 feedstock.

2. INTEGRATED CO_2 CAPTURE AND MINERALIZATION STRATEGY

After pre-treatment, the collected concrete wastes are used in an integrated CO_2 capture and mineralization process. In this study, the integrated CO_2 capture and mineralization approach developed is highly consistent with the general pathways for reaching net-zero emissions in the cement and lime sector in terms of CCUS technologies. In short, the integrated approach contains six steps, as presented in Figure 1. In the first step, direct CO_2 capture from flue gas (emitted by the cement and lime sector or other heavy industries) or ambient air is performed using alkaline chemical solutions (e.g., 2 Mol KOH (Keith et al., 2018)). During the CO_2 capture process, the pH of the chemical solution, as a monitoring indicator, reduces. Once the pH of the solution reaches around 8-9 (or even much lower), ground concrete wastes are added with a given solid-to-liquid ratio. Generally, major hydration products of cement consist of 50-70% (by mass) calcium silicate hydrate (C-S-H), 20-25% calcium hydroxide (or portlandite, CH), and some AFt and AFm phases (Li, Liu, et al., 2023). Additionally, un-hydrated cement compounds also exist, e.g. dicalcium silicate (C_2S) and tricalcium silicate (C_3S). Theoretically, all those calcium-bearing phases can react with CO_2 under suitable conditions (see Reactions 1-4), but the carbonation rate and kinetics of each calcium-bearing phase appear to be different.

With CO_2 mineralization proceeding at Step 2, the pH of the solution increases due to the consumption of carbonate ions and the formation of hydroxide ions. As the pH of the solution gets back to approximately 14, the separation of the liquid and solid of the slurry is carried out using the membrane technology (see Step 3). After separation, the obtained solid wastes can be reused as construction materials (e.g., fine aggregates and supplementary cementitious materials), while the liquid with a high pH can be recycled and reused for CO_2 capture. It should be noted that besides calcium carbonates, SiO_2 is also produced during the CO_2 mineralization process (see Reactions 1-4). Due to the high pH of the solution in Steps 2 and 3, the produced SiO_2 is usually dissolved, meaning that the recycled solution in Step 5 is silicon rich. In the following CO_2 capture process based on the silicon-rich solution, silica gel can also be obtained due to the reduced solubility as the pH of the solution declines (see Step 6).

$$Ca(OH)_2 + CO_2 \rightarrow CaCO_3 + H_2O \quad (1)$$

$$C_x\text{-}S_y\text{-}H_z + xCO_2 \rightarrow xCaCO_3 + ySiO_2 \cdot wH_2O + (z - yw)H_2O \quad (2)$$

$$2CaO{\cdot}SiO_2 + 2CO_2 + yH_2O \rightarrow SiO_2{\cdot}yH_2O + 2CaCO_3 \quad (3)$$

$$3CaO{\cdot}SiO_2 + 3CO_2 + yH_2O \rightarrow SiO_2{\cdot}yH_2O + 3CaCO_3 \quad (4)$$

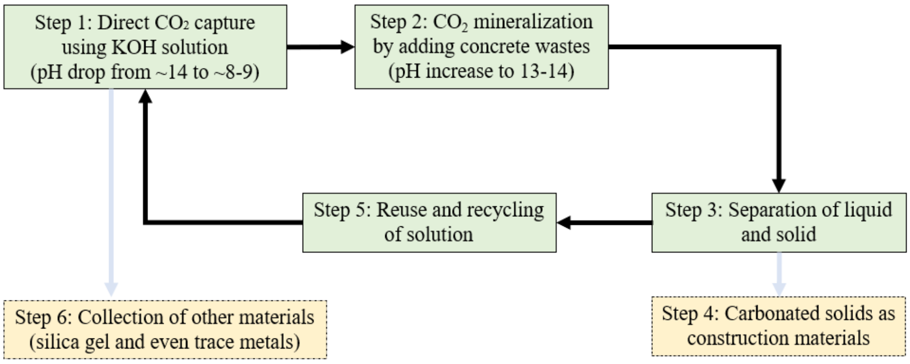

Figure 1. Integrated CO_2 capture and mineralization approach using concrete wastes

3. SUMMARY REMARKS AND PERSPECTIVE RESEARCH

In this work, the utilization of demolished concrete wastes for the decarbonization of the cement and lime industry is introduced, with a special focus on the integrated CO_2 capture and mineralization strategy using concrete wastes as CO_2 feedstock. Perspective research and key knowledge gaps in the deployment of the integrated CO_2 capture and mineralization strategy in the cement and lime sector are summarised, as follows.

- Concrete wastes with varied components tend to have considerably different carbonation kinetics and CO_2 uptake capacity, which needs further research. Besides, the life cycle assessment of concrete wastes as CO_2 feedstock in the integrated CO_2 capture and mineralization approach is also required.
- As a substitute for KOH, other chemical agents which can be used in the integrated CO_2 capture and mineralization approach should also be explored, such as amine and amino acid salts. The recovery and recycling efficiency of chemical agents used must be studied in-depth.
- Knowledge sharing and learning by doing between industry and researchers nationally and internationally can underpin the implementation of the integrated CO_2 capture and mineralization strategy. Besides desktop study, pilot plant demonstration is needed. Further research to establish CO_2 transport and storage options is also required in order to cover the whole CCUS chain in the cement and lime sector and help the sector to reach net zero emissions.

4. ACKNOWLEDGEMENT

The financial support from the CSIRO’s CarbonLock Future Science Platform is sincerely acknowledged.

5. REFERENCES

Keith, D. W., Holmes, G., St. Angelo, D., & Heidel, K. (2018). A process for capturing CO2 from the atmosphere. *Joule*, *2*(8), 1573–1594. https://doi.org/10.1016/j.joule.2018.05.006

Li, L., Liu, Q., Dao, V., & Wu, M. (2023). Dimensional change of cement paste subjected to carbonation in CO2 sequestration and utilization context: A critical review on the mechanisms. *Journal of CO2 Utilization*, *70*, 102444. https://doi.org/10.1016/j.jcou.2023.102444

Li, L., & Wu, M. (2022). An overview of utilizing CO2 for accelerated carbonation treatment in the concrete industry. *Journal of CO2 Utilization*, *60*, 102000. https://doi.org/10.1016/j.jcou.2022.102000

Li, L., Yu, H., Zhou, S., Dao, V., Chen, M., Ji, L., & Benhelal, E. (2023). Activation and utilization of tailings as CO2 mineralization feedstock and supplementary cementitious materials: A critical review. *Materials Today Sustainability*.

Marmier, A. (2023). *Decarbonisation options for the cement industry*. Publications Office. https://data.europa.eu/doi/10.2760/174037

Srinivasan, V., Temminghoff, M., Charnock, S., Moisi, A., Palfreyman, D., Patel, J., Hornung, C., & Hortle, A. (2021). *CO2 Utilisation Roadmap*. CSIRO.

CO_2 MINERALIZATION AND IN-SITU STORAGE OF INDUSTRIAL SOLID WASTE DRIVE A SUBSTANTIAL DECARBONIZATION POTENTIAL: ROLES OF UNFAVORABLE IMPURITIES

Yikai Liu[1], Qiusong Chen[2,3], Maria Chiara Dalconi[1], Luca Valentini[1], Xinyi Yuan[2],
Simone Molinari[1], Yunming Wang[2,3], Gilberto Artioli[1]

[1]Department of Geosciences and CIRCe Centre, University of Padua, Padua, Italy
[2]School of Resources and Safety Engineering, Central South University, Changsha, China
[3]Sinosteel Maanshan General Institute of Mining Research Co., Ltd., Maanshan, China
E-mail: yikai.liu@phd.unipd.it

Using metal-rich solid waste to directly capture atmospheric CO_2 is considered one of the promising technologies to utilize industrial solid waste while combating global anthropogenic CO_2 emissions. Previous estimations report that a 4.02 Gt per year mitigation potential can be facilitated through CO_2 mineralization. However, existing estimates do not take into account the impacts of impurities in solid waste, which have broad uncertainty and variability due to different industrial processes. The existence of certain impurities might influence the rate of the carbonation reaction and therefore, the amount of CO_2 captured and carbonates formed. For instance, some elements (e.g., Pb, Cd, and Mn in tailings) can enhance the CO_2 capture capacity due to the precipitation of heavy metal carbonates. While some organics (e.g., organic matter in sludge) and anions (e.g., phosphates in phosphogypsum) can influence the carbonation reactions negatively. Especially, the questionable releasing behavior of these potentially toxic elements can bring about new environmental issues when the deposited body reaches groundwater or aquifer resources. Therefore, in this work, we have attempted to clarify the roles of impurities in the mineralization process and the afterward usage period, including the accelerating or retarding effects of impurities in carbonation and the leaching behavior of potentially toxic elements. Industrial solid wastes from different sectors, such as typical mine tailings (e.g., lead-zinc mine tailings and phosphate mine tailings), industrial by-products (e.g., phosphogypsum, fly ash, red mud, and coal gasification slag), and demolition waste, are used for accelerated and atmospheric carbonation at ambient temperatures. Numerical simulations based on experimental results are further applied to estimate the amount of CO_2 storage by mineral trapping at different time scales and impurities fractions. Our study reveals that although mineralization and in-stu storage could turn industrial solid wastes into a global carbon mitigation sink, unfavorable impurities may curb abatement potential.

Keywords: CO_2 capture, CO_2 utilization, Solid waste management, Carbon mineralization, CO_2 emission reduction

PREPARATION OF HIGH-PERFORMANCE OF CO_2-CURED CONCRETE USING HYDRATED MAGNESIA CARBONATES

Shaoqin Ruan

College of Civil Engineering and Architecture, Zhejiang University, Hangzhou 310058, China

The current academic research on carbonates focuses mainly on the calcium carbonate cementitious material system, with less research on basic hydrated magnesium carbonate, especially the lack of explanation of the strength source of concrete based on this cementitious system at the micro-nano-level, making it impossible to prepare concrete products with appropriate strength grades. This study explores the effects of RMC activities, carbonate crystals structures and aggregate/paste interface properties on the strength of basic hydrated magnesium carbonate concrete by using synthetic RMC, carbonate nuclei and recycled aggregates in preparing basic hydrated magnesium carbonate concrete. Meanwhile, its strength formation mechanism is revealed through the evolution of micro nano structure and physical phase compositions.

CO_2 SEQUESTRATION AND UPCYCLING OF CARBONATED Γ-C_2S BINDERS VIA THERMAL ACTIVATION

Zhe Yu, Xiaoli Wang, Tung-Chai Ling*

College of Civil Engineering, Hunan University, Changsha 410082, Hunan, China
*Corresponding author: tcling@hnu.edu.cn

γ-C_2S demonstrated a green and potential binder for CO_2 sequestration due to its low-sintering temperature and high reactivity with CO_2. The carbonated γ-C_2S could be upcycled at the end of their service life to further benefit the concrete life cycle. This paper aims to evaluate the recyclability of carbonated γ-C_2S by direct recycling, pulverizing the γ-C_2S compact into powder, and reusing to produce construction materials (e.g. compact) through CO_2 curing. The results showed that the compressive strength of the first recycling cycle is comparable to that of the original carbonated γ-C_2S compact, demonstrating some remaining unreacted γ-C_2S can be react during second round of carbonation process. However, the further recycling of carbonated γ-C_2S (in 2nd and 3rd recycling routes), the carbonated compacts exhibited 70% and 88% strength reduction, hence direct recycling (without any pretreatment) should be prohibited when the measured carbonation degree exceeded 60%. A thermal reactivation method, via pre-sintering these carbonated γ-C_2S at elevated temperatures (800 °C-1000 °C), is then proposed to reactivate these carbonated γ-C_2S. The results show that compacts prepared by the thermal reactivated powder possessed a comparable or even higher compressive strength than those samples prepared by raw γ-C_2S. The component of thermal reactivated powder included lime, γ-C_2S, and β-C_2S. As the sintering temperature rose from 800 °C to 1000 °C, the lime content decreased from 9.3% down to 1.1%, while γ-C_2S and β-C_2S were gradually increased. This phenomenon indicated that lime was likely to react with silica gel to form γ-C_2S and β-C_2S at higher sintering temperatures. Therefore, it is recommended that 950 °C is the optimal temperature for the reactivation of carbonated γ-C_2S as the lime has adverse impacts on the mechanical properties of the carbonated compacts.

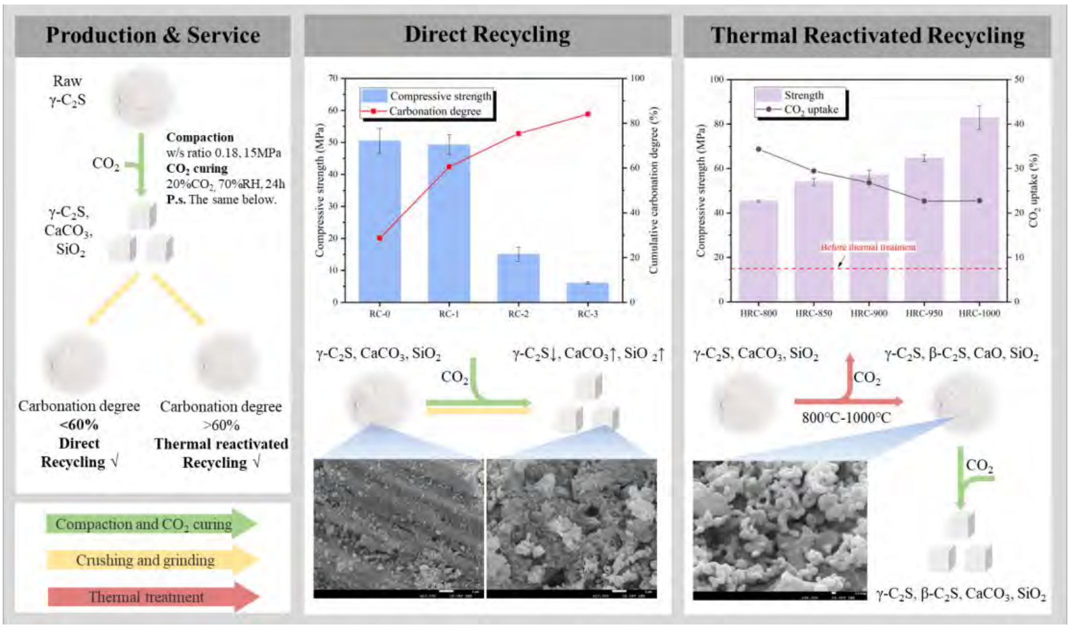

Keywords: γ-C_2S, CO_2 curing, Recycling, Thermal treatment, β-C_2S

ENHANCING THE TREATMENT EFFICIENCY OF RECYCLED CONCRETE FINES WITH AQUEOUS CARBONATION

JIANG, Y., SHEN, P., and POON, C.S.

Department of Civil and Environmental Engineering & Research Centre for Resources Engineering towards Carbon Neutrality, The Hong Kong Polytechnic University, Hong Kong, China
peiliang.shen@polyu.edu.hk (SHEN, P.), cecspoon@polyu.edu.hk (POON, C.S.)

Recycled concrete fines (RCFs, 0.3mm<<2.36mm) are the fine fractions of waste concrete generated during the recycling process. RCFs contain less natural aggregate and more residual cement paste than their coarser counterparts, thus more prone to carbonation. Although carbonation is beneficial for the microstructure and reactivity of RCFs by refining the pores and changing the phase compositions of the residual cement paste, carbonation rate is usually too slow for practical applications. In this study, two critical modifications (i.e., manipulating the initial carbonate concentrations and using elevating temperatures) were applied to aqueous carbonation of RCFs, aiming to improve the carbonation efficiency. Particularly, the rate of calcium carbonate (Cc) precipitation, the advance of Cc deposition front, the mineralogy, the development of microstructure, and the aqueous chemistry during carbonation were investigated using techniques of multiple scales. Based on the results, the rate of Cc precipitation and advancement of the Cc deposition front was significantly improved. The pore structure was drastically refined. Using elevated temperatures not only activated carbonate transport but also enhanced silicate polymerization, leading to the formation of a larger amount of silica gel as well as the increase in Q4/Q3 ratio, thus improving the reactivity of RCFs. A lab-scale production of carbonated RCFs was conducted, and the carbonation products were used for preparing cement mortars. Based on the compressive strength results, the carbonation treatment duration for RCFs could be reasonably reduced to hours and even minutes.

Keywords: Recycled concrete fines; aqueous carbonation; elevated temperature; sodium bicarbonate; efficiency

ASSESSING THE RHEOLOGY AND BUILDABILITY OF 3D PRINTED MORTAR WITH CO_2 MODIFICATION

Kaiyin Zhao, Shipeng Zhang, Chi Sun Poon

Department of Civil and Environmental Engineering, Research Centre for Resources Engineering toward Carbon Neutrality, The Hong Kong Polytechnic University, Hung Hom, Kowloon, Hong Kong
E-mail: shipeng.zhang@polyu.edu.hk

3D printing technology imposes more rigorous requirements for the rheological properties of concrete compared to traditional cast concrete. Printable concrete needs to be equipped with satisfactory pumpability and buildability. In this paper, CO_2 was selected to modify the fresh properties of mortar to enhance printability since CO_2 is both a greenhouse gas that needs to be reduced emission and a highly active additive for cement. To evaluate the effect of CO_2 on rheological properties and buildability of the mortar, different CO_2 injection parameters (flow rate and injection time) are adopted to produce modified mortar. Various 3D-printing-related rheological properties were systematically characterized, including static yield stress, thixotropy, and viscosity recovery evolutions over rest intervals (ranging from 0 to 120 minutes). In addition, the surface characterization of cement and printability of mortar after CO_2 modification are also investigated. Results show that a larger flow rate and shorter injection time of CO_2 cause higher static yield stress but lower thixotropy, which is not conducive to print. The addition of CO_2 improves the static yield stress and the structuration rate of mortar by agglomerating cement particles into large and ultra-large flocs at an early age. The flocculation mechanism results from that nanoscale products carbonation produced provide the heterogeneous nucleation sites for the sedimentation of hydration products. In addition, mortar with CO_2 modification both has a higher reversibly coagulated structure and irreversible network structure leading to an enhanced buildability.

Keywords: 3D printed mortar; CO_2 modification; Rheology; Buildability; Static yield stress

BONDING PROPERTIES BETWEEN 3D PRINTED RECYCLED COARSE AGGREGATE CONCRETE AND REBAR

Huawei Liu[1,2], Chao Liu[1], Guoliang Bai[1]

[1]Department of Civil and Environmental Engineering, The Hong Kong Polytechnic University, Hung Hom, Kowloon, Hong Kong, China
[2]Institution School of Civil Engineering, Xi'an University of Architecture and Technology, Xi'an, China
E-mail (huawei.liu@polyu.edu.hk)

With a focus on the interface bond structure between 3D printed recycled coarse aggregate concrete (3DPRAC) and ribbed rebar, the bonding properties of 3DPRAC-rebar with different rebar arrangement directions (parallel, vertical, 45°) were investigated and compared with those of 3D printed mortar (3DPM) and cast concrete. The results showed that the pore defects and recycled coarse aggregate (RCA) were found to be the main causes of the structural differences between the bonding interfaces of 3DPRAC and 3DPM with rebar. Incorporation of RCA enhanced the interface structure of 3DPRAC-rebar and introduced large volume pore defects. The partition distribution and geometric configuration of pore defects were key to decreasing the bond strength between 3DPRAC and rebar. Based on the structural composition of the 3DPRAC-rebar bond interface, a bond interface-partitioning model was proposed to elucidate the bond-slip damage mechanism. Finally, a bond-slip model of 3DPRAC-rebar was established.

Keywords: 3D printed concrete, coarse aggregate, rebar, bonding properties, bond slip

PREPARING CARBON-NEGATIVE VATERITE CEMENT FROM RECYCLED CONCRETE FINES: A PROMISING APPROACH

Jiankai Xie, Peiliang Shen*, Chi Sun Poon*

Department of Civil and Environmental Engineering, The Hong Kong Polytechnic University,
Hong Kong, China
E-mail: peiliang.shen@polyu.edu.hk (P. Shen)
cecspoon@polyu.edu.hk (C.S. Poon)

Vaterite cement is a carbon-negative cement composed entirely of reactive calcium carbonate, which is a promising approach to recover massive CO_2 emissions in cement production. In this work, vaterite collected by carbonating RCF, was utilized as the binder to prepare vaterite cement. Experiments results showed that high-purity can be collected though carbonating RCF leachate. The spontaneous crystalline transformation from vaterite to calcite provided the main source of mechanical properties in vaterite cement. The crystalline transformation was including dissolution of vaterite and recrystallisation of calcite, which was almost completed within 3d in saturated-water conditions. The final performance of vaterite cement mixtures can be enhanced by reducing water content due to less pores in mixtures. This work conducted the disposal of concrete waste and provides a promising approach towards carbon-negative concrete composite.

Keywords: Carbon-negative cement, Vaterite, Recycled concrete fines, crystalline transformation

CARBONIZED RECYCLED COARSE AND FINE AGGREGATE PREPARATION FOR CONCRETE BLOCKS TO ACHIEVE ULTRA-LOW OR NEGATIVE CARBON

Qinglong QIN, Zihan MA, Peiliang SHEN*, Chi Sun POON *

Department of Civil and Environmental Engineering, The Hong Kong Polytechnic University, Kowloon, Hong Kong

peiliang.shen@polyu.edu.hk (P.L. Shen)
cecspoon@polyu.edu.hk (C.S. Poon)

The utilization of recycled aggregates and CO_2 sequestration has been a major trend in the construction industry, however, the shortcomings of recycled aggregates themselves have seriously restricted their large-scale development and utilization. In order to promote the rapid development of recycled aggregates, recycled aggregate concrete blocks, and to achieve the purpose of carbon sequestration, this paper first carbonization of recycled coarse and fine aggregates, which not only improves the performance of recycled aggregates, but also achieves the purpose of primarily carbon sequestration. After CO_2 curing, the properties and improvement mechanisms of carbonated recycled aggregate concrete blocks are analyzed by considering the physical and mechanical properties, pore structure, microstructure and morphology of the products, and micromechanical properties of ITZ. Additionally, the CO_2 sequestration and economic value of carbonized recycled aggregate concrete is evaluated based on the life cycle assessment, which ultimately not only realizes the resourceful utilization of recycled aggregate and the industrialization of carbonized recycled aggregate concrete blocks, but also makes carbonized recycled aggregate concrete blocks ultra-low-carbon or carbon-negative. Therefore, this study demonstrates a green technology that can successfully recycle recycled aggregates.

Keywords: carbonized recycled aggregates; concrete blocks; carbonization; ultra-low or negative carbon

Session A4

High Performance Concrete Incorporating Wastes

SUSTAINABLE DREDGING AND SEDIMENT RE-USE AT THE PORT OF KOKKOLA, FINLAND

Tommi Marjamäki[1], **Michael Mengelt[1]**, and Tapio Lampinen[2]

[1]Ramboll Finland Oy
[2]Port of Kokkola
tommi.marjamaki@ramboll.fi
michael.mengelt@ramboll.fi
tapio.lampinen@portofkokkola.fi

The Kokkola Harbour fairway deepening and infrastruture improvements project is nearing completion in Finland. The project improves harbour operations to facilitate development of industry nearby. The fairway to the harbour and the harbour basin are dredged to deepen and widen them to allow access by larger vessels. The dredging masses consist primarily of highly disturbed silt units, many of which are heavily contaminated from historic harbour and vessel traffic operations. Masses of sand and gravel, and of blasted rock were also dredged. The project sustainable dredging practice and achieved 100 percent re-use of dredged material in land reclamation and harbour area construction.

The result is a modernized harbour area allowing development of the offshore wind industry and local industrial operations, achieved using a beneficial re-use policy and a low-carbon, sustainable construction product. The presentation provides overview of design and construction of the fairway and harbor, and the plans for the coming 10-year construction, expansion, and operation period.

Keywords: re-use, sustainability, stabilization, contamination, low-carbon

REUSE AND RECYCLING IN CONSTRUCTION USING CLAY AS BUILDING MATERIAL

Kalbe, U.[1], Richter, M.[1], Horn, W.[1], Schröder, S.[1], Mönig, J.[2], Klinge, A.[2,3] and Ziegert, C.[3]

[1]Federal Institute for Materials Research and Testing (BAM), Berlin, Germany
[2]NATURAL BUILDING LAB, Technical University Berlin, Germany
[3]ZRS Ingenieure GmbH, Berlin, Germany
ute.kalbe@bam.de (corresponding author)

Clay is increasingly coming back into people's consciousness with the demand for ecological, healthy and sustainable building materials.

Earthen building materials, including clay from the historical building stock, offer a high potential for their reusability and thus for saving natural resources. Unfired clay can be reused at any time and indefinitely. Dry clay only needs to be crushed and moistened with water and it can be processed again. However, there exist only a few studies on the contamination with pollutants and on the accumulation of salts in existing historic buildings regarding the evaluation of reuse potential. Within the framework of a project, preliminary tests are being carried out taking into account the previous usage of the buildings. In order to evaluate the suitability for indoor use, the potential transfer of volatile organic compounds into the air is investigated.

Fine fractions of C&D waste (particle size less than 2 mm) are currently mostly landfilled. However, such materials can be suitable for substituting primary resources of earthen building materials provided they are adequately processed. Therefore, in another research project it is investigated whether and to what extent fine and ultra-fine fractions of construction and demolition waste processed by washing can be employed for that purpose. The recycled fines are investigated considering organic and inorganic contaminants in solid matter and leaching tests are carried out to assess the potential to mobilize harmful substances. Additionally, the recycled fines are investigated in emission test chambers regarding indoor air requirements to construction products. The results will be transferred to standardization work as in Germany in standards for earthen building materials only aggregates and binders from natural sources are permitted currently.

Results of both projects will exemplary presented.

Keywords: Earthen building materials, Clay, Recycled aggregates, Resource recovery

RECOVERY OF LOCALLY DREDGED SANDS IN CONCRETE: NEW TIDAL DOCK CASE-STUDY, PORT OF ANTWERP (BELGIUM)

Hulsbosch, Niels[1], Baert, Gert[2], Bergmans, Jef[3], Dilissen, Nicole[1], Huyghe, Stijn[2], and Van den Abeele, Liesbet[3]

[1]Buildwise. Avenue P. Holoffe 21, 1342 Limelette, Belgium.
[2]Port of Antwerp-Bruges. Zaha Hadidplein 1, 2030 Antwerp, Belgium.
[3]VITO, Boeretang 200, 2400 Mol, Belgium
E-mail (corresponding author): niels.hulsbosch@buildwise.be

1. INTRODUCTION

A new tidal dock and related infrastructure are planned to be constructed in order to support container growth at the Port of Antwerp (Figure 1). To construct over 3 kilometers of quay walls, approximately 360,000 cubic meters of concrete will be required. Around 215 kilotons of natural sand, obtained from the North Sea or imported from neighboring countries, would be needed to produce this amount of concrete under the business-as-usual scenario. A considerable amount of sand can, however, potentially be resourced locally by retrieving fine construction aggregates from the excavated subsoil materials during tidal dock construction. Nonetheless, most subsoil, sandy units in the project area contain a significant fraction of glauconite (i.e. an iron potassium phyllosilicate). This presence of glauconite is commonly regarded as detrimental to the properties and application of sand within the context of construction (Westgate et al., 2023).

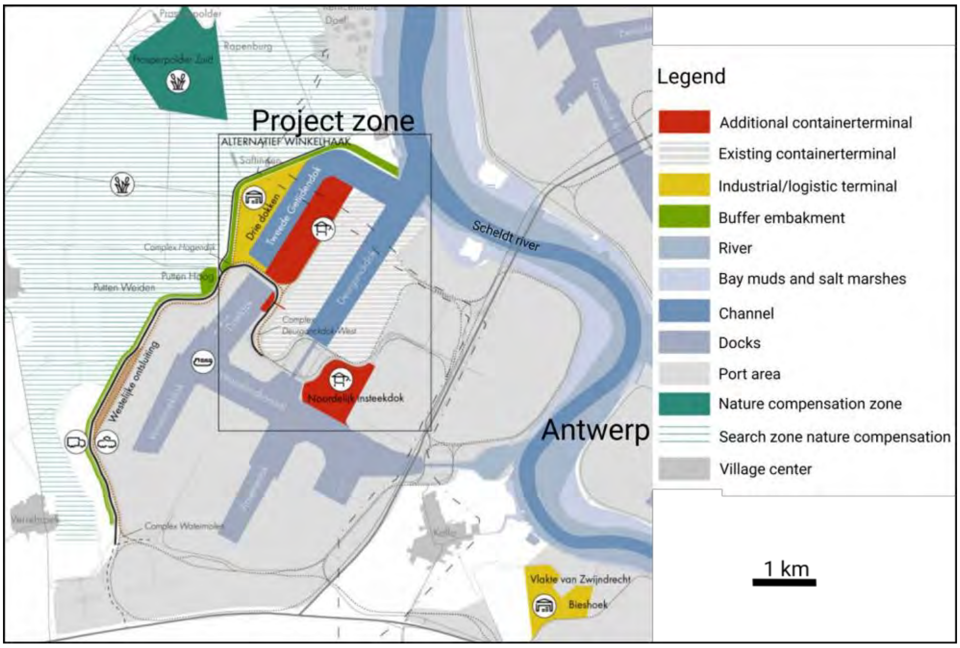

Figure 1. Map of Port area Antwerp with the location of the project zone. (Adapted from: https://www.cpeca.be/)

2. MATERIALS AND METHODS

A study in several steps has been planned to assess the feasibility of using locally dredged, glauconite-bearing sands: (1) selection of the most suitable sandy subsoil layers based on historical data, (2) sampling and characterization of these layers, (3) testing of the sands at different replacement rates in mortar and then in concrete, and (4) performing durability tests, in lab environment as well as in situ, on concrete elements to determine a service-life model. As a starting point for concrete requirements maritime infrastructure, the most demanding exposure classes (i.e. XC4, XS3, XF4 and XA1) for sea environments with tidal and splash zones are targeted conform EN 206 and its Belgian national annex B 15-001.

Existing dredged sand stocks and in-situ, geological sand units, sampled from the Port of Antwerp's docks, have been analyzed for their properties. Several 'local' subsoil layers were investigated of which four, with a high potential to be used as fine aggregates in concrete mixtures, were selected in this studied: (1) AMORAS: stock of processed, dredged material consisting of pressed filter cakes, (2) Zandstock A12: stock of excavated and dredged sand units from several docks constructed at the right bank region of the Scheldt river, (3) Lillo-Oorderen: in-situ sampled sand (12-20 m depth) in the docks near the location of the new tidal dock, and (4) Tussenzanden: in-situ sampled sand (4-7 m depth) in the docks near the location of the new tidal dock. All sand types did not contain peat but did contain glauconite. In this abstract we will report results from the sieving and fine fraction analyses (EN 933-1), density and water absorption analyses (EN 1097-6), glauconite content determination by Frantz separation (method of Adriaens and Vandenberghe (2020)) and determination of the calcareous substances' content (NBN 589-209).

Several tests were done to purify these sands and achieve a higher quality, such as dry sieving, wet sieving, hydro cyclone, and magnetic separation. The main aim was to remove shells (coarse materials), glauconite or clay fraction. With magnetic separation, the glauconite present, could be removed. Ultimately, five project sands were selected for mortar- and concrete-level testing: (Z1) AMORAS as-received, (Z2) Zandstock A12 as-received, (Z3) Tussenzanden sands as-received, (Z4) Lillo-Oorderen as-received and (Z5) Tussenzanden sands wet-sieved.

Two specific cement types were selected in order to achieve the necessary properties for concrete for medium and high strength classes and for use in massive and critical structures, such as quay walls, exposed to an aggressive seawater environment (cf. EN 206, B 15-001, EN 197-1, B 12-108, B 12-109): i.e. low hydration heat (LH), sulphate resistance (SR, HSR) and limited alkali content (LA). Specifically, (C1) CEM III/B 42.5 N-LH/SR LA and (C2) CEM V/A (S-V) 42.5 N-LH HSR LA were chosen.

A mortar test program was carried out to screen the overall impact of project sand replacement in cementitious mixtures via determination of (1) setting time (EN 480-2), (2) flexural and compressive strength at 2, 7, 28 and 91 days (EN 196-1) and (3) alkali-silica reaction (ASR) sensitivity via UAMBT (CUR Recommendation 89/Annex E). The 21 prepared mortar compositions were based on 1 kg of cement, 2.25 kg of sand and 1 kg of water. Reference mortar compositions were prepared with 100% natural sands (round siliceous sands 0/0.315 and 0/1). The test mortar compositions were prepared by replacing 50 vol% of the natural sand with the five project sands. By adding superplasticizer (SP), an attempt was made to obtain an equal, semi-plastic consistency for all mortars prepared (i.e. mini-slump 140-180 mm, NBN EN 1015-3).

A concrete test program was carried out with five different project sand replacement rates (i.e. 0%, 10%, 20%, 30% and 40% replacement of sand volume with project sand) with the determination of (1) density and water absorption of hardened concrete (EN 12390-7, 15-215), (2) compressive strength at 28 and 91 days (EN 12390-3), (3) flexural strength at 28 days (EN 12390-5), and (4) wear resistance - Böhme (EN 13892-3). Similar natural sands as in the mortar program were used, the coarse aggregates consisted entirely of natural, limestone aggregates (Dmax = 16 mm). All nine optimized concrete compositions were prepared with 375 kg/m^3 CEM III/B, a water-cement ratio of 0.45 and by adding SP and stabilizer (see discussion section). The targeted strength class is C35/45 conform EN 206.

3. RESULTS AND DISCUSSION

3.1 Characterization of sands

The analyzed soils all consist of fine sands, with a large content of material <63 µm (Figure 2).

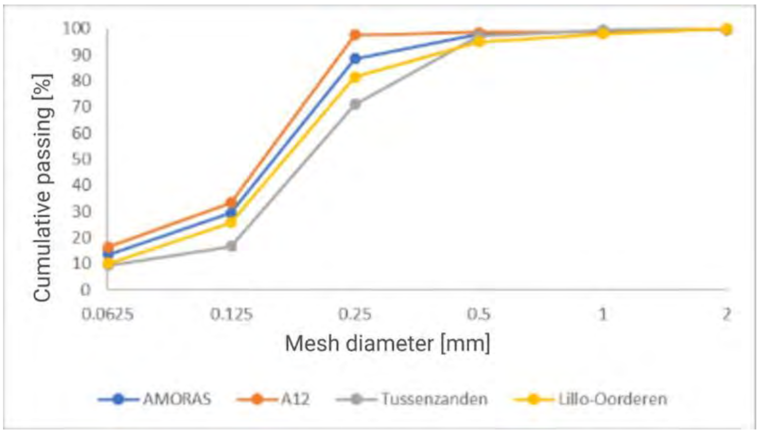

Property	AMORAS	Zandstock A12	Tussen-zanden	Lillo-Oorderen
Fraction < 63 µm [%]	14	12	20	25
Relative density [kg/dm³]	2.51	2.66	2.58	2.59
Water absorption [%]	1.1	1.4	1.2	1.6
Glauconite content [%]	10	13	5	8
Calcareous substances [%]	14	6	14	25

Figure 2. Sieving results and additional aggregate properties.

3.2 *Mortar program*

Mortars prepared with the 5 project sands showed a 14-day expansion < 0.1 % according to the UAMBT criteria, allowing the sands to be considered as non-ASR-sensitive.

Due to the very fine nature of the project sands (0/0.3-0/0.5 mm) with a large proportion of fines < 63 µm (> 10%), which, moreover, consist for a significant part of glauconite, it was difficult to obtain acceptable workability (in time) (i.e. mini-slump 140-180 mm) and this without increasing the water content and/or not exceeding the recommended dosage of the selected SP's.

In cooperation with Sika Deutschland GmbH, the effect of water absorption and polycarboxylate ether (PCE) adsorption by the project sands on workability (over time) was therefore investigated. The results showed a very high adsorption of PCE SP after 10 minutes and explained the very high dosage requirement of SP. Moreover, the further increase in PCE adsorption after 90 minutes led to a strong loss of consistency over time. By using a PCE-based stabilizer (i.e. Sika Stabilizer 920), in combination with PCE SP (i.e. Sika ViscoCrete-1550 Con30%), it was possible to: (1) obtain a blocking of the project sand grain surfaces so that PCE SP could still develop normal performance, (2) maintain the recommended dosage of PCE SP, and (3) achieve the desired processing properties.

Based on strength development profiles of the project and reference mortars, CEM III/B was selected because of obtaining higher absolute final strengths at 28 and 91 days. In terms of setting time at mortar level, there was no unambiguous influence due to the choice of cement type. Independent of the cement type used, mortars with project sands Z1 to Z4 showed equal or higher strength development compared to the reference mortars. Mortars with project sand Z5, which underwent a semi-industrial wet sieving step, showed significantly lower strength development profiles. Project sands Z1 to Z4 were then retained for testing at the concrete level.

3.3 *Concrete program*

The fresh concrete mixtures prepared with the project sands (Z1-Z4) and with CEM III/B showed stable behavior without any de-mixing. The concrete was, however, viscous but well compacted after 10 sec compaction on the vibrating table (regardless of the sand replacement rate). Retention of the targeted slump class 'S4' (EN 12350-2) was demonstrated for 60 min. A setback in consistency to slump class 'S3' (and exceptionally 'S2') was obtained for the mixtures after 90 min. The volumetric mass of the fresh concrete (2270-2305 kg/m^3) is similar to reference concrete with natural aggregates. An increased air content around 6.0% was commonly observed (regardless of sand replacement rates).

The density of the hardened concrete in oven-dry state (2170-2250 kg/m^3) was similar to normal concrete with natural aggregates (i.e. reference concrete). The water absorption by immersion of the hardened concrete (4.0-5.2 %) was equal to or lower than the reference concrete and complies with limits set in B 15-001.

The average compressive strengths on cubes (150x150x150 mm^3) of the concrete at the age of 28 days was positively correlated with the sand replacement rate. The reference concrete had a cube compressive strength of 62.0 ± 0.3 MPa. For example, for concrete with ‘Zandstock A12 asreceived', compressive strengths of 52.0 ± 1.2 MPa, 59.7 ± 2.2 MPa, 60.5 ± 1.5 MPa and 63.0 ± 1.5 MPa were obtained at 10%, 20%, 30% and 40% sand replacement, respectively. The average fourpoint flexural tensile strength at the age of 28 days amounts for the reference concrete 7.3 ± 0.4 MPa. For example, for concrete with 'Zandstock A12 as-received', flexural tensile strengths of 6.1 ± 0.2 MPa, 7.0 ± 0.3 MPa, 7.8 ± 0.2 MPa and 6.8 ± 0.2 MPa were obtained at 10%, 20%, 30% and 40% sand replacement, respectively.

The wear resistance of the concrete compositions was determined using the Böhme wear test. Both for the reference concrete and concrete with project sands, and thus independent of the sand replacement rate, wear values for unfinished, sawn surfaces were obtained that indicate an application for light loading ($12\ \text{cm}^3/50\ \text{cm}^2 < A \leq 15\ \text{cm}^3/50\ \text{cm}^2$). This is due to the high cement content (i.e. 375 kg/m3) combined with the use of limestone aggregates and the choice of a small Dmax = 16 mm. These parameters generally reduce the wear resistance of the concrete.

4. CONCLUSION

Laboratory-scale testing demonstrated that sand replacement rates up to 40 vol% are feasible while still meeting the required mechanical concrete properties. As such, excavated sand from the Antwerp subsoil can be considered as a potential target for replacing natural sand in concrete for maritime application. These excavated sands demonstrated the presence of glauconite (5-13 %), high fine fraction content <63 µm (≤20%), a significant limestone content (≤14%), and a relatively high water absorption (<1.6%).

The next phase of the study will involve in-situ monitoring of large-scale concrete elements in a representative tidal dock environment (i.e. Deurganckdok, Port of Antwerp, Belgium) as well as assessments of durability and calculation of service life predictions.

5. ACKNOWLEDGMENT

This research is part of the PIONEERS project which received funding from the European Union’s Horizon 2020 Research and Innovation Program under grant agreement 101037564 (website: https://pioneers-ports.eu/).

6. REFERENCES

Adriaens, R., & Vandenberghe, N. (2020). Quantitative clay mineralogy as a tool for lithostratigraphy of Neogene Formations in Belgium: a reconnaissance study. *Geologica Belgica*, *23*(3-4), 365-378. https://doi.org/https://doi.org/10.20341/gb.2020.018

Westgate, Z. J., DeGroot, D. J., McMullin, C., Zou, Y., Guo, D., Van Haren, S., Beemer, R. D., Zeppilli, D., Miller, K. G., & Browning, J. V. (2023). Effect of degradation on geotechnical behavior of glauconite sands from the U.S. Mid-Atlantic Coastal Plain. *Ocean Engineering*, *283*, 115081. https://doi.org/https://doi.org/10.1016/j.oceaneng.2023.115081

EVALUATION OF GRAPHENE OXIDE ON MICROSTRUCTURE AND MICROMECHANICAL PROPERTIES OF ULTRA-HIGH PERFORMANCE CONCRETE WITH RECYCLED FINE AGGREGATE

Chen, Kang[1,2], Cheng, Shukai[1,2,*], Wu, Ziyang[1,2] ,You, Xiao[1,2], Ye, Ziqian[1,2]

[1]School of Civil Engineering and Architecture, Wuhan Institute of Technology, Wuhan 430074, China
[2]Hubei Provincial Engineering Research Center for Green Civil Engineering Materials and Structures, Wuhan Institute of Technology, Wuhan 430074, China
chengsk@wit.edu.cn

1. INTRODUCTION

This study aims to explore the use of industrial-grade graphene oxide (GO) to enhance UHPC containing RFA, in order to promote the recycling of construction and demolition waste and reduce the cost of UHPC. The influence of four different contents of GO on the mechanical properties and self-shrinkage performance of UHPC is evaluated. The pore volume change and pore size distribution of the UHPC matrix under different GO contents are studied using a mercury intrusion porosimetry (MIP). In addition, the transition zone (ITZ) of UHPC is observed using scanning electron microscopy (SEM). An effective method is provided for utilizing construction and demolition waste in construction activities.

2. MATERIALS AND METHODS

2.1 Raw materials

The raw materials include cement, fly ash, silica fume, recycled sand, quartz sand, quartz powder, GO, superplasticizer (WR), steel fibers, and tap water. The industrial-grade GO used in this study is cost-effective. The steel fibers used have a diameter of 0.2mm and a length of 13mm. The superplasticizer used is a high-efficiency polycarboxylic acid with a pale yellow viscous liquid appearance.

2.2 Material design and preparation

The reference group, Q, was compared with five other groups using 100% quartz sand (QS) as fine aggregate. In the other five groups, RFA and other materials replaced 20% of QS by volume. The mass ratio of aggregate to binder was 1:1, and the water-to-binder ratio (w/b) was 0.18. Due to the water absorption of RFA during the mixing process, it needed to be saturated with tap water before mixing and then naturally dried outdoors until it reached a state of surface saturated dryness. To maintain consistent w/b ratios for each group, the total water content of the group containing RFA also needed to be reduced by the amount of water absorbed by RFA. To improve the dispersion effect of GO, a JY98-IIIN ultrasonic homogenizer with a power of 300W was used for ultrasonic treatment for 15 minutes. Then, the water reducer was quickly mixed in and added to the mixture of cementitious materials and fine aggregates by spraying. Finally, in order to reduce the agglomeration of steel fibers within the matrix, the steel fibers were added in two separate times, with 5 minutes of stirring after each addition.

2.3 Testing methods

The specimens used to measure the compressive strength of UHPC had dimensions of 100×100×100mm. According to the Chinese standard GB/T 50081–2002, the compressive strength of cubic specimens was measured at both 7 and 28 days under displacement-controlled loading. The autogenous shrinkage of UHPC was tested according to ASTM C1698. The pore structure of the mortar was measured using Mercury Intrusion Porosimetry (AutoPore IV 9500) within the pressure range of 0MPa to 420MPa. The density of the UHPC matrix, as well as the microstructure of the interfacial transition zone (ITZ) between the fine aggregate and the paste, were analyzed using scanning electron microscopy (SEM).

3. RESULTS AND DISCUSSION

3.1. Compressive strength

Figure 1 illustrates the effect of different concentrations of graphene oxide (GO) on the compressive strength of UHPC. This indicates that the addition of GO can significantly enhance the compressive strength of UHPC. The compressive strength of R decreases by 11% at 7 days compared to Q, suggesting that the early strength may decrease due to the deficiencies of RFA when partially substituting for QS. It is worth noting that at the age of 28 days, the compressive strength of R is slightly higher than that of Q. This is because RFA, as an internal curing material, releases moisture when the internal humidity decreases in later stages, promoting hydration reactions and increasing the density of the matrix, thereby improving the compressive strength.The lower purity of industrial-grade GO and other raw materials used in this study resulted in smaller strength improvement compared to the findings reported by Li et al. [1]. GO serves as a nano-filler to fill in micro-pores, and its nucleation effect enhances the extent of hydration reactions [2]. These factors contribute to the improvement of RFA deficiencies to some extent, which may be the main reason for the increased compressive strength.

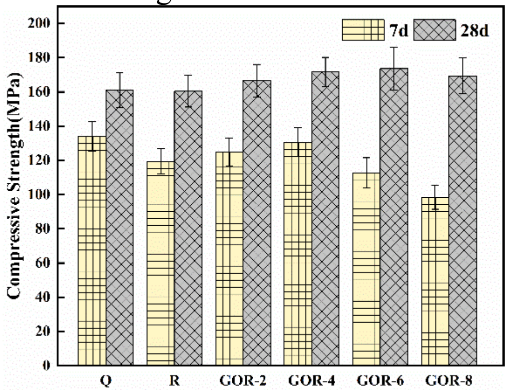

Figure. 1. Compressive strength of UHPC with different contents of GO.

3.2 Autogenous shrinkage

Figure 2 presents the trend of self-shrinkage in UHPC as the content of graphene oxide (GO) varies. Compared to Q, the self-shrinkage of R decreases by 61.07%. This indicates that the addition of RFA can significantly reduce the early self-shrinkage of UHPC. This is mainly because RFA releases internal moisture to alleviate the self-shrinkage caused by the loss of internal micropores when the internal humidity decreases.Compared to R, GOR-2 and GOR-4 exhibit increases of 5.55% and 27.68%, respectively, in self-shrinkage. This is because the addition of GO refines the pore size and increases the content of micropores, leading to increased self-shrinkage [3].

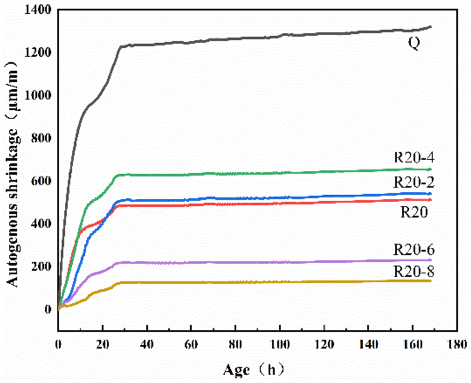

Figure. 2. Autogenous shrinkage of UHPC with different contents of GO.

3.3 Pore structure

Figure 3 illustrates the MIP (Mercury Intrusion Porosimetry) results of UHPC. As shown in Figure 3, the porosity of UHPC with R20-4 is lower than that of R, but the specific surface area is higher. This indicates the phenomenon of pore refinement. Meanwhile, the porosity of UHPC with R20-6 is higher than that of both R and R20-4, and the specific surface area is significantly increased as well. This is because the filling and nucleation effects of GO reduce the content of macropores in the matrix and increase the content of micropores. It can be seen that the volume of capillary pores with diameters ranging from 10-5000 nm increases due to the addition of graphene, mainly due to the increase in C-S-H gel and pore refinement. The pores in Region I are closely related to the compaction of the matrix, while the pores in Region II are mainly formed due to volume shrinkage and water evaporation [4]. In summary, the addition of graphene can significantly reduce the pore volume and thereby improve the mechanical strength of UHPC. This is consistent with the 28-day compressive strength results obtained in this study.

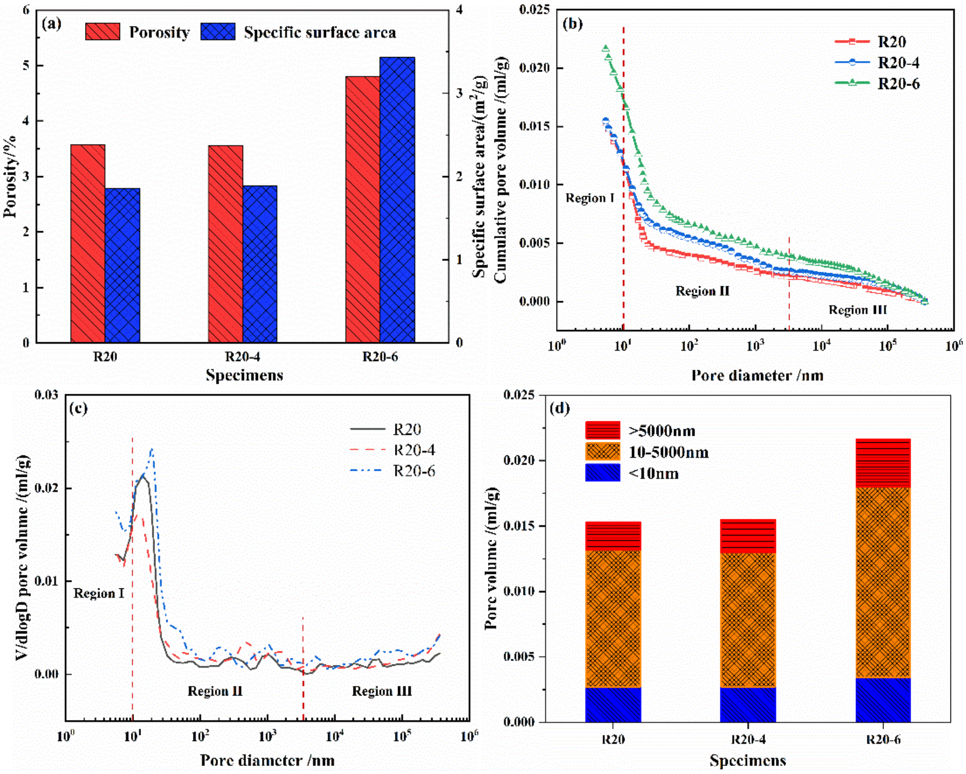

Figure. 3 Porosity and pore structure of UHPC.

3.4 Microstructure analysis

In order to investigate the influence of GO on the ITZ (Interfacial Transition Zone), we obtained SEM (Scanning Electron Microscope) images that provide more detailed microstructural information. Figure 4 shows the SEM images with different content of GO. In Figure 4, it can be observed that in the mortar without GO, there is interface non-uniformity, weak bonding, and high porosity between RFA (Recycled Fine Aggregate) and cementitious matrix. Due to the GO nanosheets providing nucleation sites for cement hydration products, GO can effectively promote the formation of hydrates around RFA. Additionally, the spray method of adding graphene oxide aids in its dispersion and promotes the formation of a denser structure.

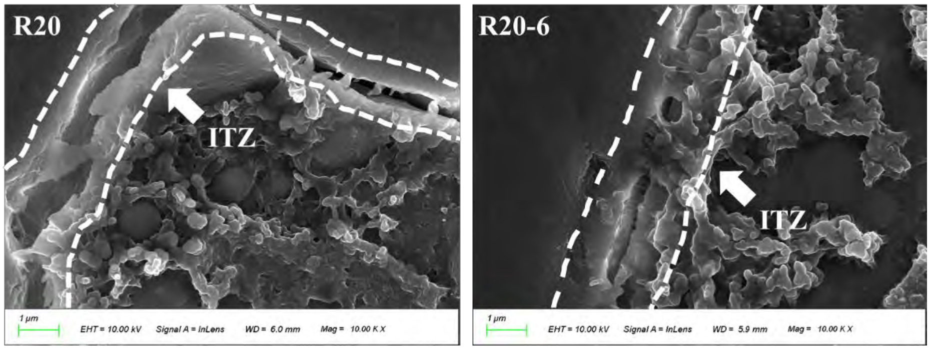

Figure. 4 SEM images of UHPC with different GO contents.

4. CONCLUSIONS

The main objective of this study is to improve the performance of UHPC (Ultra-High Performance Concrete) containing RFA by using GO and reduce production costs. GO was used to enhance the matrix of UHPC, and the effects of adding four different contents of GO in the initial mixture on the mechanical properties, volume stability, and microstructure of UHPC with RFA were evaluated. The main conclusions of the study are as follows:

1. For different contents of GO, the compressive strength of UHPC at 28 days ranged from 160.36 to 173.58 MPa, with the addition of GO resulting in the highest increase in compressive strength of 9.4% at 7 days and 4.89% at 28 days. Early strength was significantly improved.
2. For different contents of GO, the autogenous shrinkage of UHPC at 7 days ranged from 138.90 to 665.45 μm/m, with the addition of GO increasing autogenous shrinkage by 27.5% for R20-4 and reducing it by 54.7% for R20-6.
3. For different contents of GO, the porosity of UHPC ranged from 3.58% to 4.80%, and the addition of GO refined the pores in UHPC. This is why the mechanical and durability properties of UHPC produced in this study were significantly improved by adding GO.
4. According to the SEM analysis results, the interface bonding between RFA and UHPC matrix was enhanced due to the filling and nucleation effects of GO nanosheets.
5. Therefore, the use of GO effectively improved the performance of UHPC containing RFA in terms of mechanical properties, volume stability, and microstructure. This finding contributes to the development of cost-effective UHPC with enhanced properties.

5. ACKNOWLEDGMENTS

The authors gratefully acknowledge the financial supports from the National Science Foundation of China (No. 52208286), and Knowledge Innovation Program of Wuhan-Shuguang Project (No. 2022020801020362).

6. REFERENCES

[1]. W.G. Li, X.Y. Li, S.J. Chen, Y.M. Liu, W.H. Duan, S.P. Shah, Effects of graphene oxide on early-age hydration and electrical resistivity of Portland cement paste, Constr. Build. Mater. 136 (2017) 506–514.

[2]. Kong, D., Huang, S., Corr, D., Yang, Y., Shah, S.P., 2018. Whether do nano-particles act as nucleation sites for C-S-H gel growth during cement hydration? Cement Concr. Compos. 87, 98–109.

[3]. Yu, L., Wu, R., 2020. Using graphene oxide to improve the properties of ultra-high-performance concrete with fine recycled aggregate. Construct. Build. Mater. 259, 120657.

[4]. Z. Li, X.Y. Guo, Y.Y. Liu, et al. Hydration kinetics, pore structure, 3D network calcium silicate hydrate, and mechanical behavior of graphene oxide reinforced cement composites. Constr. Build. Mater. 2018, 190: 150-163.

HIGH DUCTILITY CEMENTITIOUS COMPOSITES INCORPORATING SEAWATER AND CORAL SAND (SCS-HDCC) FOR OFFSHORE ENGINEERING: MICROSTRUCTURE, MECHANICAL PERFORMANCE AND SUSTAINABILITY

Xiangpeng Fei[1], Liping Guo[1,2], and Lingyi Zhao[1]

1School of Materials Science and Engineering, Southeast University, Nanjing 211189, China
2 Jiangsu Key Laboratory of Construction Materials, Jiangsu Collaborative Innovation Center for Sustainable Civil Engineering Materials & Structures, Nanjing 211189, China
E-mail: guoliping691@163.com

1. INTRODUCTION

In order to alleviate the prominent resource conflicts, there is an urgent need to explore the development and utilization of the ocean as a potential source of raw materials, with the aim of expanding living space and improving resource efficiency (Xiao et al., 2017). The construction and development of islands and reefs have emerged as vital components of the marine economy, promoting marine resource development and protecting national maritime rights and interests. However, the transportation costs of traditional building materials are exorbitant and significantly prolonging construction time. Furthermore, ocean engineering construction, particularly on exposed islands and reefs, faces the significant challenge of extreme weather and natural disasters. Consequently, concrete must exhibit superior mechanical properties to withstand complicate mechanical loads (Huang et al., 2020). Developing a new generation of concrete materials for marine construction, that are highly performance-based, functional, environmentally friendly and cost-effective, is a critical scientific and engineering challenge.

The utilization of seawater and sea sand has proven to be a successful approach in alleviating resource scarcity, reducing engineering development costs, and saving construction time (Cheng et al., 2018). Coral aggregate has been identified as a natural ecological lightweight aggregate with unique characteristics (Cai et al., 2021). However, compared to river sand and natural gravel aggregate, the inferior strength of coral aggregate results in brittle concrete with low toughness. The concrete with coral aggregates exhibited obvious vertical and diagonal cracks and typical brittle failure characteristics under excessive loads, therefore, the application of coral aggregate in concrete is limited (Mi et al., 2016).

High Ductility Cementitious Composite (HDCC) as a special type of fiber-reinforced material exhibits strain hardening behavior and multiple cracking characteristics under uniaxial tensile load, with tensile strain capacity of 1%-8% and crack opening width less than 100μm (Li V.C, 2012). The excellent mechanical performance and strong crack control capacity make HDCC have broad application prospects in marine engineering. The application of HDCC for reinforcement or in critical components of concrete structures can effectively improve the structural bearing capacity and seismic resistance (Maalej M. et al., 2012). Therefore, the use of seawater and coral sand to prepare HDCC (SCS-HDCC) in marine environments not only meets the engineering background of using local materials and reduces costs, but the composite is also composed primarily of corrosion-resistant organic fibers, making it less susceptible to seawater (Ding et al., 2019).

To minimize the temporal and economic expenditures of transporting construction raw materials to remote islands and reefs, and to promote the sustainable development of civil engineering materials, this research investigates the feasibility of seawater and coral sand as fresh water and river sand substitutes in fabricating HDCC.

2. MATERIALS AND METHODS

The materials included Portland cement (P·I 42.5, C), Class II fly ash (FA), natural river sand

(RS) and coral sand (CS). The mixing water used in the experiments comprised of fresh water (FW) and seawater (SW). The seawater was prepared by blending chemical reagents with fresh water to conform (ASTM D1141-98, 2021). The experiment employed an additive identified as a polycarboxylic acid-based water reducing agent (WR). The fiber utilized in the study was the short cut polyvinyl alcohol (PVA) fiber with high strength and high modulus.

The compressive strength and flexural strength of HDCC were measured according to the standard (JC/T 2462-2018). The tensile strength and tensile strain capacity of HDCC were conducted by uniaxial tensile test with reference to standard (JC/T 2462-2018). The interfacial bonding performance between fibers and matrices was evaluated by single-fiber pullout experiments.White paint was applied to the surface of the test specimens with the intention of enhancing the visibility of any cracks and to facilitate the statistical determination of their number and residual widths. Subsequently, a high-definition macro digital camera was employed to capture any cracks present within the designated area of samples. The pore characteristics, including porosity and pore size distribution were analyzed by utilizing the MesoMR12-060V-I low-field nuclear magnetic resonance (LF NMR) instrument.

3. RESULTS AND DISCUSSION

From Fig.1, with the addition of seawater and coral sand, the ratio of harmful pores to less harmful pores significantly decreased , leading to a decrease in the total porosity. The increase in the proportion of harmless pores demonstrated that the combined effect of ion-induced accelerated reaction and internal curing of coral sand resulted in pore size refinement, filling of harmful pores, and reduction of porosity. However, since the strength of coral sand is relatively low, although coral sand improved the structure of the transition zone, the strength of the mortar did not increase accordingly.

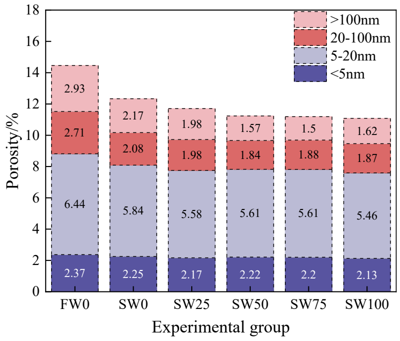

Fig. 1 Cumulative porosity of different mortars

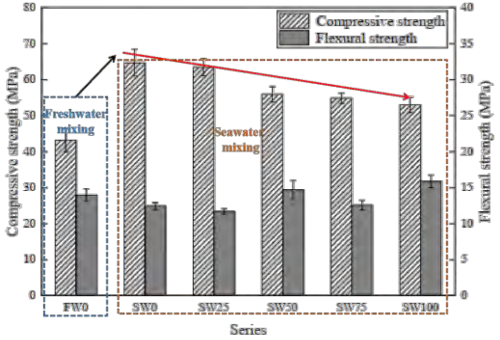

Fig. 2 Compressive and flexural strength of HDCC with different mix ratios

As Fig.2 shows, regardless of whether river sand or coral sand is used, seawater significantly enhances the compressive strength of HDCC. With the increase of coral sand substitution, the compressive strength of SCS-HDCC decreases continuously. One promising reason is that the substitution of coral sand for river sand makes the properties of the aggregate in the matrix uneven. The presence of coral sand prevents river sand from exerting its strength. However, with a significant increase in the substitution of coral sand, the properties of aggregates in the matrix tends to be consistent, the incompatibility decreases, resulting in less noticeable strength changes.

Table 1 Uniaxial tensile properties of HDCC with different mixing ratios

Mixture	First cracking tensile strength/MPa	Ultimate tensile strength/MPa	Ultimate tensile strain/%
FW0	3.54±0.59	4.92±0.32	1.47±0.32
SW0	4.85±0.07	5.47±0.10	0.39±0.06
SW25	4.12±0.21	5.44±0.28	0.97±0.25
SW50	3.53±0.45	4.91±0.31	1.04±0.14
SW75	**4.18±0.23**	**5.66±0.21**	**1.18±0.08**
SW100	4.34±0.24	6.03±0.12	0.90±0.23

Table 1 lists the uniaxial tensile properties of HDCC with varying mixing ratios. For the river sand group, compared with fresh water-mixed HDCC (FR-HDCC), seawater-mixed HDCC (SR-HDCC) significantly improved the initial crack strength and ultimate tensile strength. This improvement leads to a rapid decrease in tensile ductility and a loss of high ductility. The initial crack strength and ultimate tensile strength of SCS-HDCC are generally higher than those of FR-HDCC, but the tensile ductility is lower. It can be attributed to the fact that the abundant ions introduced from seawater and coral sand accelerate the dissolution and reaction of minerals, promoting cement hydration and pozzolanic reaction. Furthermore, the "internal curing" effect of coral sand improved the strength of the matrix. The improvement of strength was achieved at the expense of ductility, resulting in a decrease in ductility of SCS-HDCC.

The results of the uniaxial tensile tests indicate that although SCS-HDCC exhibits inferior ductility compared to FR-HDCC, experimental evidence supports the feasibility of employing seawater and coral sand to prepare SCS-HDCC.

Table 2 Cracking characteristics after uniaxial tensile testing of HDCC

Mixture	Tensile ductility/%	Number of cracks	Average cracking width/μm	Average cracking spacing/mm
FW0	1.47±0.32	24	61.32±2.56	4.17
SW25	1.04±0.14	15	69.54±4.65	6.67
SW50	0.97±0.25	14	71.06±3.08	7.32
SW75	1.18±0.08	17	71.2±6.74	6.02
SW100	0.90±0.23	13	68.70±11.56	7.69

Table 2 shows the crack distribution of HDCC with different mix ratios after uniaxial tensile testing. The results demonstrate that the average crack spacing of each HDCC group is less than 100μm, indicating excellent resistance to permeability. Although there is still a certain gap with the crack spacing of saturated multiple cracking (1-2 mm) (Yang, 2008), it confirms the feasibility of preparing HDCC with seawater and coral sand.

Table 3 Fiber/matrix interface parameter of HDCC with different mixing ratios

Series	Chemical bonding strength G_d (J/m^2)	Interface bonding strength τ_0 (MPa)	Slip-hardening coefficient β
FW0	0.43±0.14	2.58±0.65	0.21±0.04
SW0	0.30±0.11	2.71±0.62	0.24±0.06
SW25	0.78±0.46	2.25±0.64	0.24±0.06
SW50	0.65±0.48	1.86±0.39	0.25±0.07
SW75	0.68±0.33	1.61±0.65	0.26±0.05
SW100	0.43±0.23	2.04±0.66	0.26±0.05

Table 3 illustrates the fiber-matrix interface parameters of HDCC with different mixing ratios. The substitution of coral sand resulted in a random distribution of river sand and coral sand within the matrix, which led to different friction and cutting effects on the fibers during the slip process. With increasing coral sand substitution, the probability of fiber contact with coral sand increased, while low-strength coral sand weakened the friction and cutting effects on the fibers. Moreover, massive ions introduced by coral sand accelerated the hydration and pozzolanic reactions, which enhanced the friction between the matrix and fibers. Consequently, τ_0 shows a decreasing trend followed by an increasing trend as the amount of coral sand substitution increases. The slip hardening coefficient β remained almost unchanged, and all the HDCC mixtures exhibited slip-hardening behavior after fiber debonding.

For the construction of remote coral reefs, the weight of materials required per unit volume of FR-HDCC is huge, which need to be obtained from inland, generating enormous transportation costs Compared with FR-HDCC, SCS-HDCC can save energy and reduce production costs. The overall cost is 48% lower than that of the FW0 group. Therefore, this study utilizes seawater and coral sand to prepare HDCC, ensuring high ductility and demonstrating significant economic and environmental benefits, indicating the significance of further research and promotion.

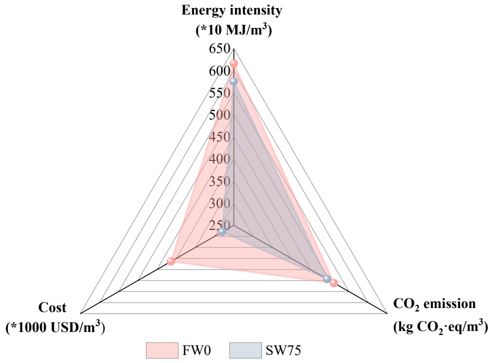

Fig.3 MSIs radar plot for HDCC with different materials

4. CONCLUSION

The action of seawater and coral sand led to a refinement of the matrix pore size. The harmful pores were reduced, and the porosity was decreased. However, the low strength of coral sand is prone to cracking perpendicular to the direction of coral growth under stress, which affects the mechanical properties.The dissolution and reaction rate of cementitious materials was enhanced by seawater, resulting in increased fracture toughness and compressive strength, as well as greatly improved initial cracking and ultimate tensile strengths of HDCC significantly. The chemical bond strength G_d between fiber and matrix dropped, the interfacial bond strength τ_0 grew, which prevented the fiber from fully transferring the energy generated by HDCC cracking. The change in the CS content had a complex and varied effect on the mechanical properties of SCS-HDCC. SCS-HDCC with satisfactory ductility was prepared, and the ductility was around 1%, with crack widths generally lower than 100μm. According to sustainability indicators, compared with FR-HDCC, SCS-HDCC prepared in this study can save energy and reduce production costs. This research provides a new approach for the construction and development of remote islands and reefs as well as promotes the sustainable development of building materials for offshore engineering.

5. ACKNOWLEDGMENT

This work was supported by a National Natural Science Foundation of P.R. China (Grant No. 52178191).

6. REFERENCES

ASTM D1141-98, 2021. Standard Practice for Preparation of Substitute Ocean Water. ASTM Committee on Standards.

Cai, X., Zhao, Q., Chen, H., 2021. Research Progress in Coral Concrete. J Chin Ceram Soc. 49(8), 1753-1764.

Cheng, S., Shui, Z., Sun, T., Yu, R., Zhang, G., 2018. Durability and microstructure of coral sand concrete incorporating supplementary cementitious materials. Constr Build Mater. 171, 44-53.

Ding, C., Guo, L., Chen, B., Deng, Z., Huang, G., Luo, D., 2019. Alkali Resistance and Surface Modification of High Strength and High Modulus PVA Fibers. J Chin Ceram Soc. 47(02), 228-235.

Huang, B., Wu, J., Yu, J., Dai, J., Christopher, K.Y.L., 2020. High-strength seawater sea-sand Engineered Cementitious Composites (SS-ECC): Mechanical performance and probabilistic modeling. Cem Concr Compos. 114, 103740.

JC/T 2462-2018. Experimental method for mechanical properties of high ductility fiber reinforced cementitious composites. Cement Products.

Li, V.C., 2012. Tailoring ECC for Special Attributes: A Review. Int. Concr. 6(3), 135-144.

Maalej, M., Quek, S.T, Ahmed, S.F.U, Zhang J, Lin V.W.J, Leong K.S., 2012. Review of Potential Structural Applications of Hybrid Fiber Engineered Cementitious Composites. Constr Build Mater. 36, 216–227.

Mi, R., Yu, H., Ma, H., Da, B., Yua, Y., Zhang, X., Zhu, H., Dou, X., 2016. Experimental research on the mechanical properties of full coral seawater concrete. Marine Eng. 34, 47-54.

Xiao, J., Qiang,C., Nanni, A., Zhang, K., 2017. Use of sea-sand and seawater in concrete construction: Current status and future opportunities. Constr. Build. Mater. 155, 1101-1111.

Yang, E., 2008. Designing Added Functions in Engineered Cementitious Composites. University of Michigan, Michigan.

APPLICABILITY OF CEMENT PASTE MIXED WITH WASTE GINGER AS PC GROUT

Maho Sato[1], Takuya Kondo[2]

[1]National Institute of Technology, Kochi College, advanced course
[2]National Institute of Technology, Kochi College E-mail (s2308@gm.kochi-ct.jp)

1. INTRODUCTION

As the performance of prestressed concrete (PC) grout should be retained, there are anticorrosion PC steel as well as integration of member and PC steel. However, the presence of poor grout filling in the sheath of a PC structure is a factor that reduces durability. Therefore, it is necessary to improve the grout performance in order to reliably perform grout during construction.

In recent years, one of the materials expected to improve the performance of grouts is cellulose. Previous studies have shown that when cellulose ether (CE) is added to grout materials, increase in viscosity with an increase in the amount of added CE leads to a decrease in fluidity while the water non-separability increases (Hisada et al. (2021)). It has also been reported from previous studies that the setting time is delayed as the amount of added CE thickener increases (Sano et al. (2000)).

In this study, discarded ginger was added to PC grout as an admixture to improve grout performance and to make effective use of waste while the fresh properties of the grout were investigated.

2. GINGER PWDER PROCESSIN

Two types of ginger were used in this study: without skin (Figure 1) and with skin (Figure 2). Ginger without skin is a piece of ginger that is removed from the skin by rubbing the ginger together which is then discharged in the process. Meanwhile, ginger with skin are those that spoil during the storage process.In this study, frozen ginger was stored for seven days in a drying furnace at 70°C to dry the ginger. Afterwards, the two kinds of ginger were separately ground for 1 minute and 30 seconds in a small powder mixer which was exclusively used for dry matter. Then, only the ginger with skin was allowed to evaporate enough water, and it was further ground for 30 seconds in a mixer. This resulting powder was used in the test.

Figure 1. Ginger without skin

Figure 2. Ginger with skin

3. STUDY SUMMARY

The test method for ginger powder is shown in Table 1. Also, the powder degree test was measured by the BET adsorption method. Test methods for ginger-added grouts are shown in Table 2. Meanwhile, the test parameters of the grout are shown in Table 3. These were tested at W/C = 45%, 40%, and 35%. Condensation tests were carried out for parameters other than water-cement ratio, flowability tests were performed using the JP funnels, and the bleeding rate was defined after 3 hours. Table 4 shows the grout mixes. The materials used were ordinary Portland cement (Specific gravity: 3.15, Specific surface area: 3380 cm 2/g), a high-performance water reducing agent for W/C = 35%, and AE water reducing agent for W/C = 40%.

Table 1. Tests on the basic properties of ginger powder

Test items	Measurement
Density test	JIS R 5201
Fineness test	JIS R 5201
Moisture content test	JIS A 1203

Table 2. Tests on the basic properties of grout

Test items	Measurement
Setting test	JIS R 5201
Fluidity test	JSCE-F 531
Bleeding rate and expansion measurement test	JSCE-F 532

Table 3. Grout type

Type	Types of Ginger	Addition amount
N	No additive	
A0.1	A：Without Skin	C×0.1%
A0.5		C×0.5%
A1.0		C×1.0%
B0.1	B：With Skin	C×0.1%
B0.5		C×0.5%
B1.0		C×1.0%

Table 4. Mix proportion of grout

W/C	Cement (g)	Water (g)	Admixture (ml)
35%	1487	520	6
40%	1384	554	4
45%	1294	583	0

4. DENSITY, FINENESS, AND MOISTURE CONTENT

Test results on the basic properties of ginger powder are shown in Table 5. There was no difference in density between A and B. Also, both showed about half the density of normal Portland cement and about 3–4 times the specific surface area of normal Portland cement. The moisture content of B was three times that of A. Although the water content of ginger cannot be uniformly compared as it depends on the drying method and storage condition, B contained more water in the ginger used for the experiment.

Table 5. Test results for ginger powder

	Density (g/cm)	Fineness (cm^2/g)	Moisture content (%)
A	1.44	12700	0.53
	1.45		
B	1.45	10700	1.60
	1.46		

5. SETTING TIME

The setting time is shown in Figure 3. A0.1 and B0.1 showed little difference from N. Meanwhile, further increase in the added amount of ginger tended to delay setting time. Comparing A and B, B showed a tendency to delay the setting time.

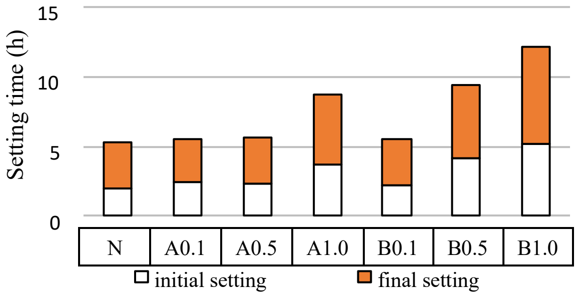

Figure 3. Setting time

6. BLEEDING RATE

The bleeding rate after 3 hours at W/C = 45% is shown in Figure 4. In both A and B, bleeding tended to decrease with an increase in the amount of ginger added. This indicates that cellulose in ginger increases viscosity, leading to a decrease in fluidity and an increase in water non-separability as described by Hisada et al. (2021). The high powder content of ginger may also be a factor in the increased viscosity.

The bleeding rate after 3 hours at W/C = 40% is shown in Figure 5. Unit water volume is reduced by decreasing the water-cement ratio. Therefore, bleeding occurred with only A0.1 and B0.1.

The bleeding rate after 3 hours at W/C = 35% is shown in Figure 6. No bleeding was observed in A. On the other hand, a small amount of bleeding was observed in B.

In all test parameters with added ginger, many bubbles were immediately observed after mixing the grout. Meanwhile, for W/C = 35%, bubbles were observed in the supernatant water of the grout even when the bleeding rate was measured after 3 hours. According to Kitabatake et al. (1987), proteins have been shown to have an excellent interfacial activity, thus aiding foam formation and suppressing bubble collapse. Therefore, the air bubbles generated during kneading may be affected by the protein contained in ginger.

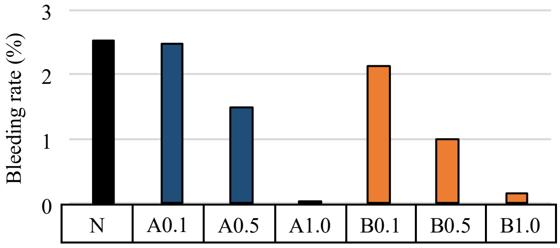

Figure 4. Bleeding rate after 3 h at W/C = 45%

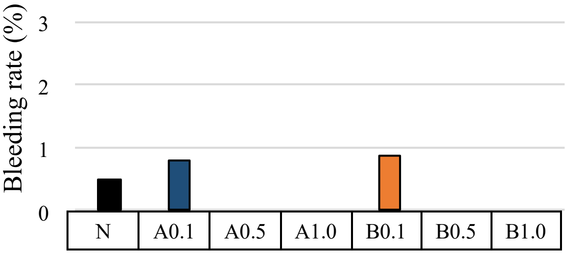

Figure 5. Bleeding rate after 3 h at W/C = 40%

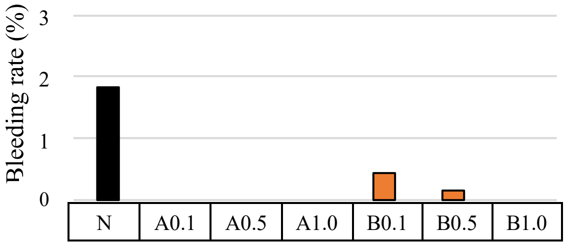

Figure 6. Bleeding rate after 3 h at W/C = 35%

7. FLUIDITY

The time course of the W/C = 45% flow down time is shown in Figure 7. B1.0 was omitted from the data because the grout was blocked in the JP funnel. When data was compared for each added amount of ginger, it could not be confirmed that A 0.1, A 0.5, and B 0.1 had a large difference in the flow time from N. Moreover, the flow time tended to be delayed with an increase in the amount of ginger added. This is thought to be due to the thickening effect of cellulose which affects the decrease in fluidity. Ginger powder has a higher specific surface area and a higher degree of powder than cement. Therefore, it is possible that the grout viscosity increased while fluidity decreased. At the same mixing level, the fluidity of B tended to be lower than that of A.

The time course of the W/C = 40% flow down time is shown in Figure 8. A1.0, B0.5, and B1.0 were excluded from the data because the grout was occluded. The flow time tended to increase with the addition of ginger. At the same mixing level, the fluidity of B tended to be lower than that of A. Compared with the case of W/C = 45%, the bleeding was suppressed while the flow time did not show a significant change for 60 minutes because the water-cement ratio was smaller and AE water reducing agent was added.

The time course of the W/C = 35% flow down time is shown in Figure 9. A1.0, B0.5, and B1.0 were excluded from the data because the grout was occluded. As with the other water-cement ratios, both A and B showed a tendency to increase the flow time with an increase in the amount of mixing. In addition, compared with the case of W/C = 40%, bleeding was further suppressed while the flow tended to be delayed against time because the water-cement ratio was smaller and a highperformance water reducing agent was added.

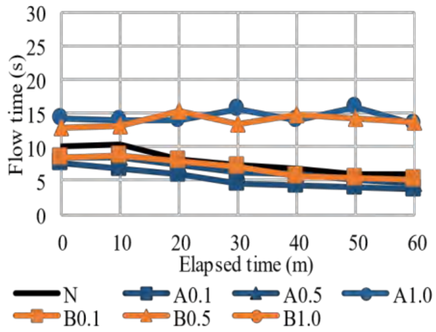

Figure 7. Flow time at W/C = 45%

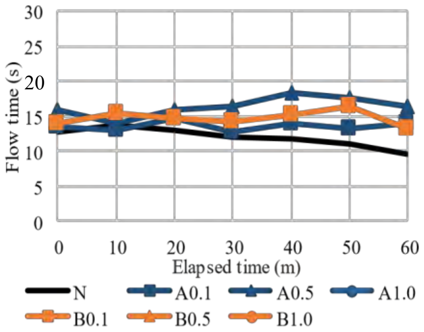

Figure 8. Flow time at W/C = 40%

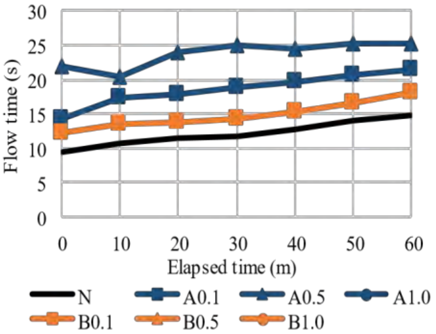

Figure 9. Flow time at W/C = 40%

8. GINGER-ADDED GROUT CHALLENGES

From test results on the fresh properties of grout using waste ginger, its applicability could be clarified. On the other hand, it is necessary to suppress air bubbles caused by an increase in the amount of ginger powder added. Therefore, in the future, tests should be conducted on strength characteristics and durability to examine the long-term applicability.

9. CONCLUSIONS

In this study, the basic physical properties of ginger powder and the fresh properties of gingeradded grout were investigated in order to improve the performance of grout material by considering the material separation resistance effect due to the thickening action of cellulose in ginger. As a result, while the amount of added ginger increased, there were trends such as delay in setting time, decrease in fluidity due to an increase in viscosity, and decrease in bleeding rate. When comparing ginger without skin and ginger with skin, the setting time of ginger with skin was more delayed and its fluidity tended to decrease. On the other hand, there was no significant difference in bleeding between the two types.

10. REFERENCES

Hisada, M., Murakami, K., Satoh, A. and Konishi, H. (2021) “Experimental Study on Various Fluidity, Underwater Separation and Compressive Strength of Grout Mixed with Cellulose Ether,” Cement Science and Concrete Technology, Vol.74: 428-434

Kitabatake, N. and Doi, E. (1987) “Properties of Foam,” Journal of food science and technology, Vol.34, No.8: 549-557

Sano, K., Matsumoto, F., Hattori, A. and Miyagawa, T. (2000) “Properties of Microstructure and Mass Transport in Self-Compacting Concrete Containing Cellulosic Viscosity Agent,” Journal of JSCE, Vol.662: 75-89

VALORIZATION AND ENHANCEMENT MECHANISM OF FERROCHROME SLAG AS AGGREGATE FOR MANUFACTURING ULTRA-HIGH PERFORMANCE CONCRETE (UHPC)

Yuanyuan Zhu[1,2], Zhidan Rong[1,2*], Maopeng Jiao[1,2], Qing Jiang[1,2], and Jiandong Wu[1,2]

[1]School of Materials Science and Engineering, Southeast University, Nanjing, 211189, China
[2]Jiangsu Key Laboratory of Construction Materials, Nanjing, 211189, China
E-mail (zdrong@seu.edu.cn)

Ferrochrome slag (FCS) is a by-product discharged in the smelting of ferrochrome alloys. This high-volume waste can be effectively valorized by utilizing it as aggregate in ultra-high performance concrete (UHPC), which is beneficial for resolving the environmental issue induced via its buildup and potential risk of chromium leaching. Additionally, it can also compensate for the shortage of natural aggregate (NA), and reduce the cost of UHPC. Its feasibility as aggregate in UHPC was explored. The enhancement mechanisms of FCS aggregate dosage, pre-wetting water, and steel fiber on the performances of UHPC were systematically investigated. The results indicated that FCS with rough texture, higher water absorption and lower strength can substitute NA in the manufacturing of UHPC. The mechanical and drying shrinkage properties of UHPC mixed with FCS were improved, which was attributed to the synergistic effects including the reduction of effective water-binder ratio and porosity, the enhanced interface structure, and the internal curing to matrix. The water film layer enriched surrounding aggregate absorbed by FCS, which reduced the enrichment and directional growth of portlandite at interface. This also inhibited the water absorption of UHPC, and may hinder the transport of harmful ions inside UHPC. With the incorporation of FCS, its autogenous shrinkage increased, this matter can be ameliorated by the pre-wetted aggregates with water not exceeding 45%-65% of the saturated water absorption rate. Furthermore, the reinforcement of steel fiber on UHPC strength gradually decreased due to the fiber dispersion was affected by the declined workability and aggregate morphology.

Keywords: Ferrochrome slag; Industrial solid waste; Porous aggregate; UHPC; Internal curing

DEVELOPMENT AND CHARACTERISTICS OF CARBONATION-ENHANCED HIGH-STRENGTH FOAM CONCRETE (HSFC): TOWARDS HIGH STRUCTURAL EFFICIENCY AND CARBON SEQUESTRATION

Dingqiang FAN, Jian-Xin LU, Chunpeng ZHANG and Chi Sun POON

Department of Civil and Environmental Engineering & Research Centre for Resources Engineering Towards Carbon Neutrality (RCRE), The Hong Kong Polytechnic University, Hong Kong, Hung Hom, Kowloon, Hong Kong, China

Excessive CO_2 emissions have caused great environmental burdens. This study innovatively developed a carbonation-enhanced high-strength foam concrete (HSFC) for maximum CO_2 sequestration and utilization. The HSFC was produced by incorporating a fine and stable foam into a dense paste matrix designed by the particle packing theory. After that, the carbonation curing regime was adopted to enhance the performance of HSFC, as well as realize CO_2 sequestration. Micro and macro tests were conducted to understand the mechanisms of carbonation curing in the HSFC system. The results revealed that the designed HSFC had a notable CO_2 uptake capacity of up to 12.6 wt% (equivalent to 90 kg CO_2 per m^3 of concrete). In the low water-to-binder (W/B) ratio system, carbonation curing can not only consume calcium hydroxide and calcium silicate hydrate (CSH) gel but also unhydrated cement (C_2S and C_3S). Hence, substantial amounts of calcium carbonates (CC) can be produced in three forms: amorphous, calcite (predominant), and aragonite (only appeared at higher levels of carbonation). Notably, the carbonation of CSH gel slightly increased the microhardness of the matrix rather than reduction, because carbonation products filled the micro pores of the matrix and reduced the porosity by 19.8%. Additionally, the generation of CC on the foam pore walls refined the pore size, further enhancing the compressive strength of HSFC (about two times higher than that of conventional foam concrete). At the same time, the carbonation curing obviously improved the durability in terms of water absorption and electrical resistance. Finally, the strategies for fabricating the HSFC with high structural efficiency, excellent performance and good environmental benefits were proposed. The outcomes of this work introduced a novel concrete system, which would contribute to the ongoing efforts towards sustainable construction practices and environmental stewardship.

Keywords: High-strength foam concrete (HSFC); Low water/binder ratio; CO_2 sequestration; Carbonation curing; Structural efficiency

GRAPHITE MODIFIED RECYCLED COARSE AGGREGATES TOWARDS A HIGHLY HEAT-CONDUCTIVE CONCRETE

Chen Chen, Pan Feng, Lijing Shao

Jiangsu Key Laboratory of Construction Materials, School of Materials Science and Engineering,
Southeast University, Nanjing 211189, China
Email: ccchen@seu.edu.cn

The problem of temperature crack caused by the poor thermal conductivity of concrete in modern concrete structure is very prominent. One of the traditional methods to improve the thermal conductivity of concrete is to add high thermal conductivity particles to the concrete. However, the problem of uneven dispersion of high thermal conductivity particles in this method makes the thermal conductivity improvement of concrete very limited. Therefore, it is necessary to improve the thermal conductivity of concrete through other more effective ways.

As we all know, the concrete is mostly made up of aggregates, and we believe that coarse aggregates may be an excellent carrier for improving the thermal conductivity of concrete. Based on this, the effects of different coating processes and different coarse aggregates on the physical properties and thermal conductivity of single coarse aggregate after coating were studied by using the surface modification technology of recycled coarse aggregates. Furthermore, the influence of heat-conductive coarse aggregates on the thermal conductivity and mechanical properties of concrete are studied, and the important role of the connectivity rate of the thermal conductivity path on the thermal conductivity of concrete is discussed in combination with experiments and simulations.

The results show that by coating graphite on the surface of the recycled coarse aggregates, the thermal conductivity of the recycled coarse aggregate is increased by 85.94%, and its physical properties are optimized. Graphite exists in the concrete in the form of a coarse aggregate coating, forming a thermal conductivity network in the concrete, and the thermal conductivity of the concrete is increased by 1.9 times. Based on low cost, simple process and green environmental protection, this study further expands the application field of recycled concrete. It provides a new idea for improving the thermal conductivity of concrete.

Keywords: concrete, thermal conductivity, recycled coarse aggregates, surface finishing, connectivity

Session B1

Waste to Geopolymer

MECHANICAL PROPERTIES AND ENVIRONMENTAL IMPACT ASSESSMENT OF GEOPOLYMER MATERIALS BASED ON MULTI-SOURCE SOLID WASTES

Xiaoshuang Shi[1,2], Yanlin Li[1]

[1]Failure Mechanics & Engineering Disaster Prevention and Mitigation, Key Laboratory of Sichuan Province, College of Architecture and Environment, Sichuan University, Chengdu 610065, China
[2]MOE Key Laboratory of Deep Earth Science and Engineering, College of Architecture and Environment, Sichuan University, Chengdu 610065, China
shixs@scu.edu.cn (corresponding author)

1. INTRODUCTION

The dual-carbon goal means implementing the development concept of green, low-carbon and recycling. As a large infrastructure country, it is of great significance for the sustainable development of China's building materials industry to give full play to the consumption capacity of the building materials industry and to utilize industrial solid waste to prepare green and low-carbon new building materials.

Cement has always been an important area of carbon emissions, and the production of ordinary Portland cement is a major contributor to carbon emissions, accounting for about 7% of global carbon emissions [1]. In addition, the production of cement is a high consumption process, with an average of 850 kcal of energy used to produce 1 kg of cement [2]. In order to reduce the amount of cement and its environmental impact, green cementing materials should be found to replace cement. Geopolymer is a cementitious material which is stimulated by industrial solid wastes such as fly ash (FA), blast furnace slag (GGBS), red mud (RM) and sewage sludge ash (SSA) in alkali activators. Geopolymer is a potential environmental protection building materials, it can not only effectively reduce the amount of waste, but also replace traditional building materials, thereby reducing the consumption of natural resources. With the continuous improvement of sustainable development awareness, the application prospects of it will be more extensive.

At present, the analysis of geopolymer is based on a single performance analysis, which cannot consider multiple target factors at the same time. In order to consider environmental benefits, mechanical properties and material costs at the same time, two quantitative evaluation indexes GS and GSC were proposed to analyze the comprehensive properties of different geopolymer, so as to guide the low-carbon application and evaluation of solid waste-based cementing materials.

2. MATERIALS AND METHODS

2.1. Materials

The main chemical composition of all materials is shown in Table 2. Fly ash (ASTM Class F) was used, but due to the timing of the tests and material batches, type I FA was used for FA-GPC and FA-GRC100, and type II FA was used for the other materials.

And, the alkali activator is prepared by sodium hydroxide (NaOH) solution and sodium silicate solution (Na_2SiO_3), and NaOH solution is prepared by dissolving deionized water and 98% pure NaOH solid. The composition of sodium silicate solution of FA-GPC and FA-GRC100 (Na_2O = 14.7%, SiO_2 = 29.4%) is different from that of other sodium silicate solutions (8.83% Na_2O, 27.64% SiO_2). The NaOH concentration of FA-GPC and FA-GRC100 is 8 mol/L, and the concentration of the others is 12 mol/L. Alkali activator is prepared 24 hours before pouring.

Table 1 Chemical components of precursor precursors used in this study.

Component	SiO_2	Al_2O_3	CaO	Fe_2O_3	MgO	K_2O	Na_2O	SO_3	TiO_2	P_2O_5	L.O.I
FA (I)	48.30	30.50	2.80	12.10	1.20	0.40	0.20	0.3	-	-	1.70
FA (II)	60.66	14.51	5.11	6.29	0.77	1.90	0.94	-	1.04	-	4.98
GGBS	28.21	13.10	35.67	0.48	7.76	0.32	0.46	-	1.69	-	12.54
RM	14.22	18.97	1.54	42.28	0.12	0.36	6.03	-	4.56	-	5.67
SSA	38.38	18.45	4.69	8.16	3.15	-	0.66	-	1.04	14.15	-

2.2. Mix design

The following ten different waste-based geopolymer materials were discussed: Ordinary Portland cement concrete (OPCC), Recycled aggregate concrete (RAC), Fly ash based geopolymer concrete (FA-GPC), Fly ash and blast furnace slag based geopolymer concrete (FA-GGBS-GPC), Fly ash based geopolymer recycled aggregate concrete (FA-GRC), Fly ash and blast furnace slag based geopolymer recycled aggregate concrete (FA-GGBS-GRC), Red mud based geopolymer pervious concrete (RM-PC), Red mud based geopolymer recycled aggregate pervious concrete (GRPC), Ordinary Portland cement pervious concrete (OPC-PC), Sewage sludge ash based geopolymer mortar (SSAB-GM). The mix ratio data for all materials are shown in Table 2.

Table 2 The mix ratio of multi-source solid geopolymer materials (kg/m^3).

	Precursor					Aggregate			Alkali activators		Added water	Curing condition
	FA	GGBS	RM	SSA	OPC	NA	RA	Sand	NaOH	Na_2SiO_3		
OPCC	-	-	-	-	364	1294	-	554	-	-	182	room temperature
RAC100	-	-	-	-	364	-	1294	554	-	-	182	room temperature
FA-GPC	368	-	-	-	-	1294	-	554	53	131	-	80°C-24h
FA-GGBS-GPC	125	375	-	-	-	1155	-	495	90	135	55	room temperature
FA-GRC100	368	-	-	-	-	-	1294	554	53	131	-	80°C-24h
FA-GGBS-GRC100	125	375	-	-	-	-	1155	495	90	135	55	room temperature
RM-PC	79	158	79	-	-	1580	-	-	21.1	105.3	31.6	room temperature
GRPC	79	158	79	-	-	-	1580	-	21.1	105.3	31.6	room temperature
OPC-PC	-	-	-	-	300	1783	-	-	-	-	99	room temperature
SSAB-GM	-	601.10	-	257.61	-	-	-	1000	43.91	294.10	203.28	room temperature

2.3. Test method

The compressive strength of the cubic specimens was tested on an electric hydraulic press according to GB/T 50081-2002[3] when they were cured at 28 days.

2.4. Environmental impact analysis

According to ISO 14040 and 14044, the LCA method is carried out in four steps [4]. The first step is to determine the objective and scope of the study, the second step is to perform a life cycle inventory (LCI) analysis, the third step is to classify the impact categories based on the inventory data and perform a life cycle impact assessment (LCIA), and the last step is to interpret the inventory and impact assessment analysis.

3. RESULTS AND DISCUSSION

3.1 Compressive strength

The 28d compressive strength (C_{28}) of all materials was measured as Table 3.

Table 3 The 28d compressive strength of multi-source solid geopolymer materials.

	OPCC	RAC100	FA-GPC	FA-GGBS-GPC	FA-GRC100	FA-GGBS-GRC100	RM-PC	GRPC	OPC-PC	SSAB-GM
C_{28}（Mpa）	49.98	44.58	85.66	66.31	54.66	43.40	27.16	10.26	22.00	41.69

3.2 LCA research

The objective of this study is to quantify the environmental impact of 1 m^3 geopolymer for the entire production process in different strength ranges from raw materials production and transportation to concrete production, so the functional unit is 1m^3 geopolymer. The system boundary is the "cradle-gate". In this study, for the reliability of LCA research, the localized data of relevant raw materials and transportation stages were queried according to the Chinese Reference Life Cycle Database (CLCD), and some missing data were obtained through enterprise real data collection, literature research, and other methods.Global Warming Potential (GWP) was chosen as an indicator for the environmental assessment, and the GWP values for all materials for each raw material and each stage are shown in Table 4.

In all geopolymer materials, GWP values meet the following laws: raw material production > concrete preparation > transportation stage. The material contribution analysis shows that the GWP value contribution of alkali activators is high. If the high temperature curing is used to ensure the compressive strength of geopolymer, the GWP environmental impact category will be further adversely affected.

Table 4 The value of GWP of multi-source solid geopolymer materials (kg CO_2 eq).

	Precursor					Alkali activators		non-cementitious materials	Transportation	Production	Sum
	FA	GGBS	RM	SSA	OPC	NaOH	Na_2SiO_3				
OPCC	-	-	-	-	266.08	-	-	4.75	21.78	1.23	293.85
RAC100	-	-	-	-	266.08	-	-	3.20	25.63	1.23	296.15
FA-GPC	8.39	-	-	-	-	20.13	163.75	4.72	24.30	204.27	425.56
FA-GGBS-GPC	2.85	16.65	-	-	-	47.11	168.75	4.22	29.40	1.23	270.21
FA-GRC100	8.39	-	-	-	-	20.13	163.75	3.17	28.15	204.27	427.87
FA-GGBS-GRC100	2.85	16.65	-	-	-	47.11	168.75	2.84	32.84	1.23	272.27
RM-PC	1.80	7.02	3.32	-	-	30.60	131.63	3.86	21.18	1.23	200.62
GRPC	1.80	7.02	3.32	-	-	30.60	131.63	1.97	30.59	1.23	208.14
OPC-PC	-	-	-	-	219.30	-	-	4.37	20.28	1.23	245.18
SSAB-GM	-	26.69	-	0.07	-	63.67	134.07	2.86	32.92	1.23	261.51

3.3 Cost research

Based on the prices of materials purchased in the laboratory, real market price surveys of companies and literature research, the prices of all raw materials were obtained to calculate the cost-effectiveness of different types of geopolymers. As shown in the Table 5.

Table 5 Price of multi-source solid geopolymer materials (Yuan/m^3).

	Precursor					Aggregate			Alkali activators		Added water	Sum
	FA	GGBS	RM	SSA	OPC	NA	RA	Sand	NaOH	Na_2SiO_3		
OPCC	-	-	-	-	138.32	131.99	-	59.83	-	-	0.69	330.83
RAC100	-	-	-	-	138.32	-	126.81	59.83	-	-	0.69	325.66
FA-GPC	66.24	-	-	-	-	131.99	-	59.83	159.00	117.90	-	534.96
FA-GGBS-GPC	22.50	97.50	-	-	-	117.81	-	53.46	270.00	121.50	0.21	682.98
FA-GRC100	66.24	-	-	-	-	-	126.81	59.83	159.00	117.90	-	529.78
FA-GGBS-GRC100	22.50	97.50	-	-	-	-	113.19	53.46	270.00	121.50	0.21	678.36
RM-PC	14.22	41.08	3.95	-	-	161.16	-	-	63.30	94.77	0.12	378.60
GRPC	14.22	41.08	3.95	-	-	-	154.84	-	63.30	94.77	0.12	372.28
OPC-PC	-	-	-	-	114.00	181.87	-	-	-	-	0.38	296.24
SSAB-GM	-	156.29	-	12.88	-	-	-	108.00	131.73	264.69	0.77	674.36

3.4 Analysis of the comprehensive performance

In order to be able to compare different materials under the same function, we considered the value of C_{28}, GWP and materials cost, and introduced the compressive strength and environment index (GS) and the comprehensive index (GSC), as shown in Eq.(1) and Eq.(2) respectively. The two evaluation index values of different types of geopolymer materials are shown in Table 6. Indicator values and ranking results are shown in Fig.1.

$$\mathrm{GS}=\frac{\mathrm{GWP}}{\mathrm{C}_{28}} \tag{1}$$

$$\mathrm{GSC}=\frac{\mathrm{GWP}}{\mathrm{C}_{28}}\times \mathrm{C} \tag{2}$$

Table 6 The two evaluation index values of multi-source solid geopolymer materials

	OPCC	RAC100	FA-GPC	FA-GGBS-GPC	FA-GRC100	FA-GGBS-GRC100	RM-PC	GRPC	OPC-PC	SSAB-GM
GS	5.88	6.64	4.97	4.07	7.83	6.27	7.39	20.29	11.14	6.27
GSC	1945.08	2163.37	2657.69	2783.11	4147.07	4255.69	2796.57	7552.28	3301.48	4230.07

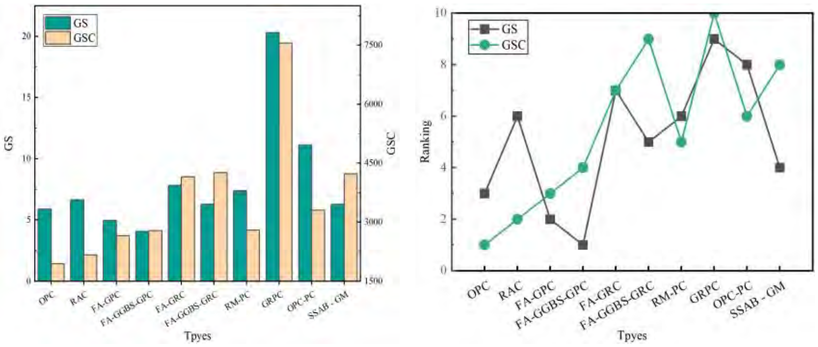

(a) (b)

Fig.1 Indicator values (a) and ranking results (b).

The larger the C_{28} of the material, the smaller the GWP, and the smaller the GS value, the better the performance. As can be seen from Fig.1 (a), the use of GGBS in geopolymer compounded with FA as precursor is better than the use of FA alone as precursor. For example, the GS of FA-GPC, FA-GGBS-GPC, FA-GRC and FA-GGBS-GRC are 4.97, 4.07, 7.83, 6.27, respectively, reduced by 18% and 20%. It was shown that incorporating a certain amount of GGBS can reduce the micro pore structure of the specimens and also ensure the mechanical properties of geopolymer concrete when cured at room temperature condition[5].

When the precursor and other raw materials and curing conditions are unchanged, all concrete using RA performs worse than concrete using NA. This is because non-cementitious materials contribute little to the GWP, but the impact of aggregate on compressive strength is significant. It can be seen from the 28d compressive strength in Table 3 that the use of RA will reduce the C_{28}.

Both geopolymer concretes have lower GS than cement-based concrete, for example, the GS of OPCC and FA-GPC are 5.88 and 4.97, respectively, and the strength of FA-GPC is increased by 71% compared with OPCC, and the GWP value is increased by 45%. The increase in compressive strength of geopolymer concrete far outweighs the increase in environmental growth, indicating that under the same strength, the performance of geopolymer materials is more low-carbon.

The overall performance of the pervious concrete was poor, which is mainly due to the fact that the aggregates have a lesser impact on the environment, but a greater impact on compressive strength, so the ratio of is significantly increased.The best performance of all types of concrete is FA-GGBS-GRC, because it did not use RA, and the precursor was compounded with FA and GGBS, where the geopolymer material ensured compressive strength while avoiding the adverse impact of high temperature curing on the environment.

As can be seen in Fig.1(b), when cost is taken into account, the rankings of all geopolymers show a decreasing trend, and the rankings of all cementitious materials increase to varying degrees, which is due to the fact that the alkali activator is higher than the level required for construction, and the price is now based on the market price instead of the production price[6], so when geopolymers are commonly applied, it may not be as costly as it should be.

4. CONCLUSION

(1)The GWP values for all materials satisfy the following laws: raw materials production> concrete preparation > raw materials transportation. Alkali activators and high temperature curing are the main contributors to GWP. (2)The comprehensive performance of GGBS and FA compound based geopolymer is better than that of FA only. (3)The effect of aggregates on GWP values is minimal, but on compressive strength is significant, which leads to the fact that the comprehensive performance of recycled aggregates concrete is worse than that of natural aggregates concrete. (4) The GS values for GPC are lower than those for OPCC, indicating that the favourable impacts of increased GPC intensity far outweigh the negative environmental impacts of increased emissions. (5)The comprehensive poor performance of pervious concrete is due to aggregates. (6)For GS, the best performer was FA-GGBS-GPC, because GGBS not only improves the pore structure but also avoids the environmental effects of high temperature curing. (7)Because of the price of Alkali activators, the advantages of geopolymers will be reduced when the cost factor is considered.

5. ACKNOWLEDGMENT

Supported by the Open Fund of Sichuan Provincial Engineering Research Center of City Solid Waste Energy and Buliding Materials Conversion and Utilization Technology (No. GF2022ZD003).

6. REFERENCES

[1] Kathirvel, P., Kaliyaperumal, S.R.M., 2016. Influence of recycled concrete aggregates on the flexural properties of reinforced alkali activated slag concrete. CONSTR BUILD MATER. 102, 51-58.10.1016/j.conbuildmat.2015.10.148.

[2] Puertas, F., García-Díaz, I., Barba, A., Gazulla, M.F., Palacios, M., Gómez, M.P., Martínez-Ramírez, S., 2008. Ceramic wastes as alternative raw materials for Portland cement clinker production. Cement and Concrete Composites. 30, 798-805.10.1016/j.cemconcomp.2008.06.003.

[3] GB/T 50081-2002. Standard for test method of mechanical properties on ordinary concrete., National Standards of the People's Republic of China.

[4] Finkbeiner, M., Inaba, A., Tan, R., Christiansen, K., Klüppel, H., 2006. The New International Standards for Life Cycle Assessment: ISO 14040 and ISO 14044. The International Journal of Life Cycle Assessment. 11, 80-85.10.1065/lca2006.02.002.

[5] Li, Z., Liu, S., 2007. Influence of Slag as Additive on Compressive Strength of Fly Ash-Based Geopolymer. J MATER CIVIL ENG. 19, 470-474.10.1061/(ASCE)0899-1561(2007)19:6(470).

[6] Abbas, R., Khereby, M.A., Ghorab, H.Y., Elkhoshkhany, N., 2020. Preparation of geopolymer concrete using Egyptian kaolin clay and the study of its environmental effects and economic cost. CLEAN TECHNOL ENVIR. 22, 669-687.10.1007/s10098-020-01811-4.

ALKALI ACTIVATION OF WASTE CONCRETE POWDER FOR THE DEVELOPMENT OF ECO-FRIENDLY CEMENTLESS BINDER

Prabhat Vashistha[1], Muse Aidarus Yonis[1], Yanchen Oinam[1], **Sukhoon Pyo**[1*]

[1]Department of Civil, Urban, Earth, and Environmental Engineering, Ulsan National Institute of Science and Technology (UNIST), 50 UNIST-gil, Ulju-gun, Ulsan 44919, Republic of Korea
* Corresponding author. E-mail (shpyo@unist.ac.kr)

1. INTRODUCTION

The construction sector is grappling with significant sustainability issues, with a primary focus on environmental conservation. One of the industry's pressing challenges is the immense production of ordinary Portland cement (OPC) worldwide, exceeding 4 billion tons, accounting for over 8% of global warming impact [1, 2]. We require the adoption of alternative cementitious binders that generate less CO_2 emissions to mitigate the human-induced impacts of global warming. On the other hand, the production of recycled aggregates from construction and demolition waste generates about 5 to 80 tons of waste concrete powder (WCP) per hour depending on plant size and type of concrete material processes. WCP is mostly composed of hydrated cement paste and can be incorporated into cementitious binders. The present research is focused on innovative investigations of the influence of high-volume WCP incorporation on the performance of cementless binder. The chemical modification treatment was utilized to modify the properties of WCP. Valorization of WCP through the development of alkali-activated cementless binders could provide a sustainable solution for binder manufacturing.

2. MATERIALS AND METHODS

The WCP was collected from the municipal Ulsan recycling plant, South Korea. The chemical composition of WCP was determined through XRF analysis, as represented in Table 1. Significant proportions of SiO_2 and CaO, which make up about 54% of the WCP were observed [3,4]. Magnesium oxide, Al_2O_3, K_2O, SO_3, and TiO_2 were other major oxides present in the WCP, with around 15% loss on ignition (LOI).

Table 1: XRF analysis WCP

	Weight (%)									
	SiO_2	Al_2O_3	Fe_2O_3	CaO	TiO_2	K_2O	MgO	SO_3	Others	LOI
WCP	25.12	5.56	13.18	29.12	1.15	2.65	1.74	1.78	2.54	15.1

The WCP based alkali activated binder was prepared by following the process as per Fig. 1. The WCP was burned to avoid organic impurities before the application of it to the alkali-activated binder. The thermal treatment of WCP was done in a Muffle furnace at a temperature of 650°C for 2 hours. After taking out the burned WCP from the furnace, it was air-cooled and used for the grinding in the ball mill. Different proportions of milled WCP (MWCP), Burnt and milled WCP (BMWCP) were prepared with the addition of metakaolinite and alkali solution. The prepared alkali activated paste was used to prepare the samples. The specimen was cured at 60 °C for 72 hours.

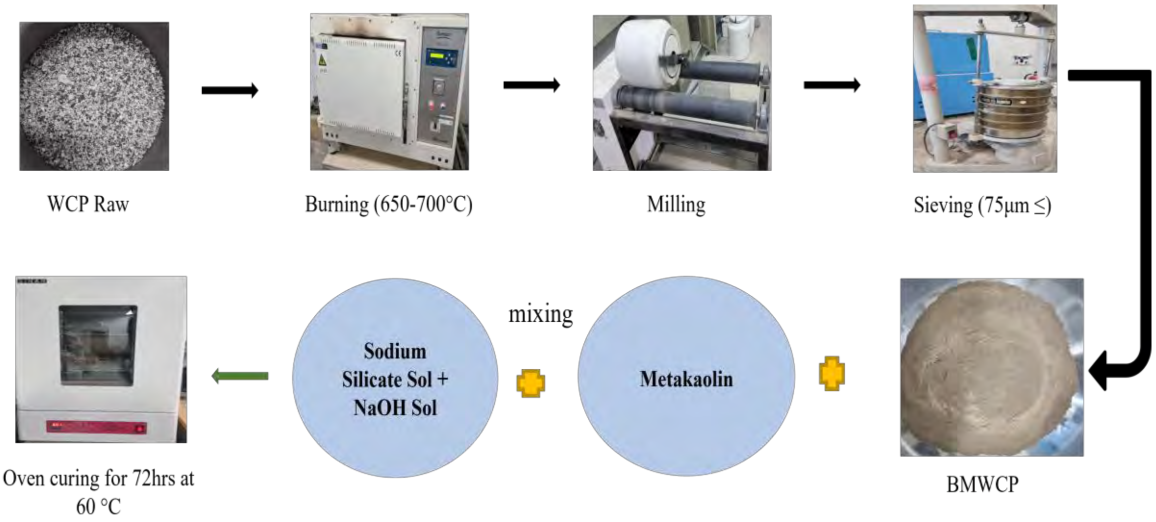

Figure 1: Method for WCP based binder preparation

The prepared samples were tested for compressive strength, mineralogical analysis, Fourier Transform Infrared Spectroscopy (FTIR) analysis**,** mercury intrusion porosimetry (MIP) analysis and Isothermal calorimeter analysis. Life cycle analysis (LCA) of the alkalai activated WCP binder was also performed to compare the environmental impacts of it with reference sample and Ordinary Portland cement (OPC).

3. RESULTS AND DISCUSSION

Figure 2 represents the compressive strength development of different blends of WCP after 72 hours of curing at 60°C. The outcome of compressive strength results indicates that BMWCP blends resulted in the development of more compressive strength than MWCP blends. The BMWCP40 blend resulted in 66% more compressive strength than the cement-based reference mix while the BMWCP50 blend developed 5% more compressive strength than the reference, which attributes to the development of more hydration products in the case of BMWCP based blends.

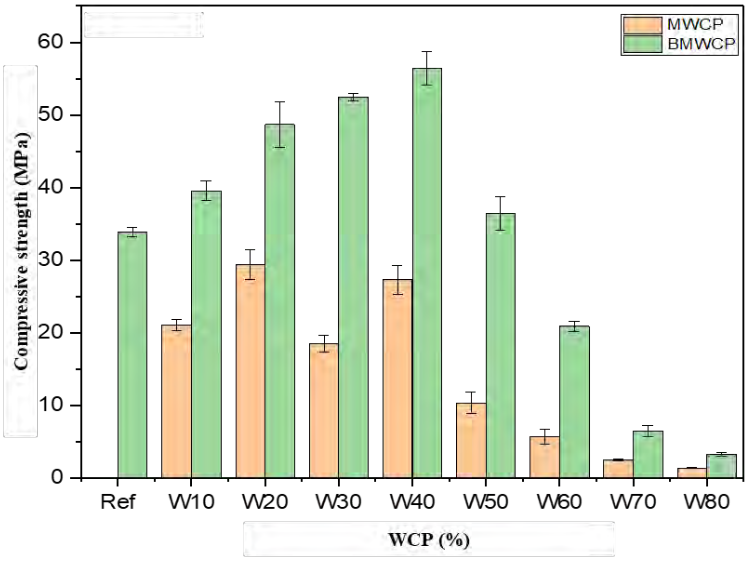

Figure 2: Impact of WCP application on compressive strength

Figure 3 represents the minerological analysis of the W40 series with reference mixture. In the case of BMWCP40, the broad hump from 2 theta 16 to 35 reflects the presence of amorphous phase, which makes BMWCP40 more reactive blend and developed more compressive strength than MWCP40 [5,6]. The intensity of calcium hydroxide (JCPDS No.: 01-84-1264) and calcite

(JCPDS:5-586) peaks also decreased in case of BMWCP 40 than MWCP40, which attributes to the development of more hydrates due to availability of reactive silica and calcium compounds in BMWCP mix [7].

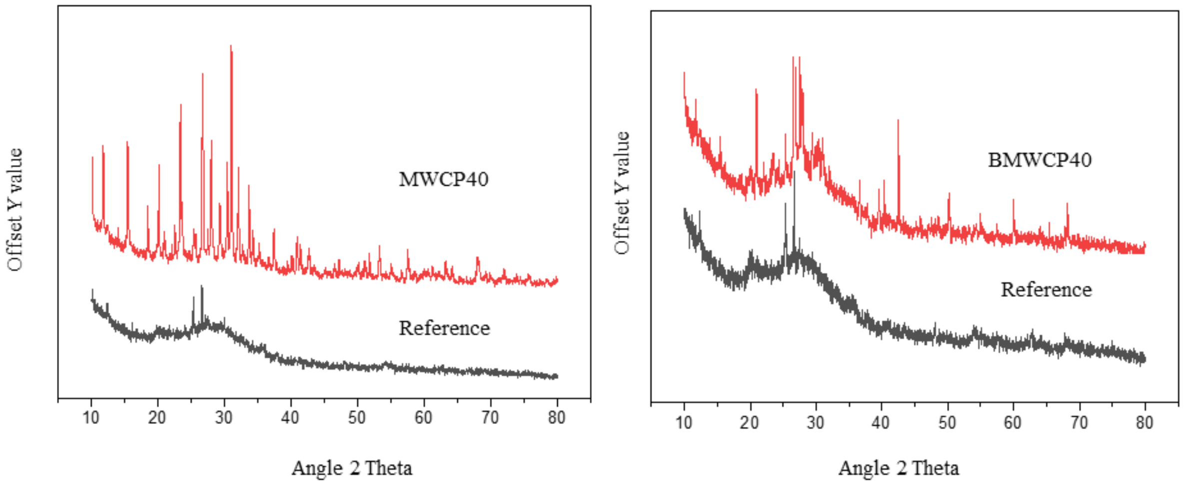

Fig. 3: XRD analysis of the hardened paste mixtures

It was found that the application of alklai activated BMWCP improved the climate change indicator the IMPACT world + Midpoint V1.01 method of the LCA analysis. The potential climate change indicator for BMWCP 40 resulted in 50% and 5% less carbon dioxide emission as compared OPC and Reference sample, respectively [8,9].

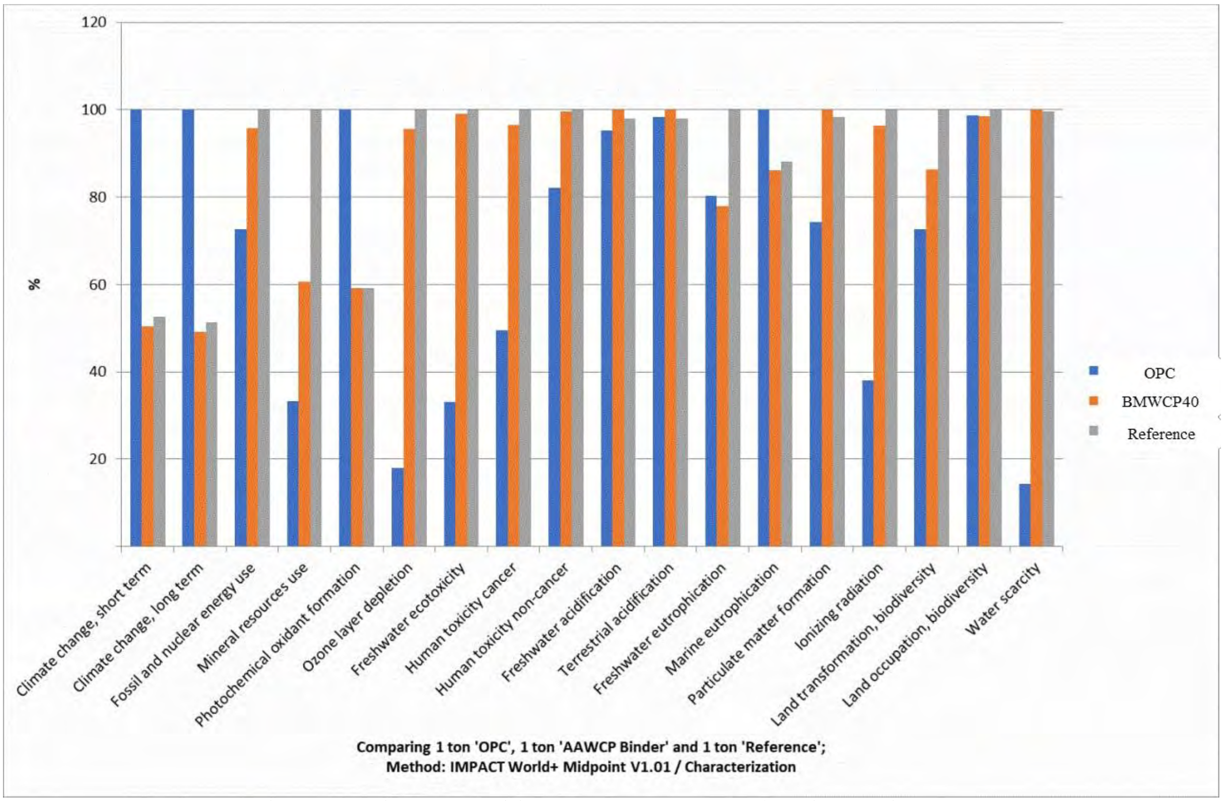

Fig. 4: Environmental impact assessment of various mixtures

4. CONCLUSION

The WCP was used as a reactive material, which contributed to the development of compressive strength through alkali activation. Up to 40% of alkali activated BMWCP can be utilized in cementless binder with improved strength properties. The performance of BMWCP based alkali activated binder was superior to that of the milled WCP in terms of utilization. The XRD results provide evidence that BMWCP resulted in a greater utilization of calcium hydroxide, leading to its transformation into calcium silicate hydrates. Likewise, the environmental analysis also referes to the emission of less carbon dioxide for alkali activated binder, however alkali activated binder consumed more energy and mineral resources than OPC production, which can be the future research recommandation on the utilization of WCP for the development of cementless binder.

5. ACKNOWLEDGMENT

This work was supported by the National Research Foundation of Korea (NRF) grant funded by the Korea government (MSIT) (No. 2021H1D3A2A02041471 and RS-2023-00212366).

6. REFERENCES

1. Hossain, M.U., et al., Techno-environmental feasibility of wood waste derived fuel for cement production. Journal of Cleaner Production, 2019. 230: p. 663-671.
2. Zhang, C.-Y., et al., Accounting process-related CO2 emissions from global cement production under Shared Socioeconomic Pathways. Journal of Cleaner Production, 2018. 184: p. 451-465.
3. Yu, K.-Q., et al., Micro-structural and mechanical properties of ultra-high performance engineered cementitious composites (UHP-ECC) incorporation of recycled fine powder (RFP). Cement and Concrete Research, 2019. **124**: p. 105813.
4. Shen, P., et al., Phase assemblance evolution during wet carbonation of recycled concrete fines. Cement and Concrete Research, 2022. 154: p. 106733.
5. Li, S., et al., Investigation of using recycled powder from the preparation of recycled aggregate as a supplementary cementitious material. Construction and Building Materials, 2021. 267: p. 120976.
6. Mehdizadeh, H., et al., Effect of particle size and CO2 treatment of waste cement powder on properties of cement paste. Canadian Journal of Civil Engineering, 2021. 48(5): p. 522-531.
7. Skibsted, J. and R. Snellings, *Reactivity of supplementary cementitious materials (SCMs) in cement blends.* Cement and Concrete Research, 2019. **124**: p. 105799.
8. Sadok, R.H., et al., *Life cycle assessment of cementitious materials based on calcined sediments from Chorfa II dam for low carbon binders as sustainable building materials.* Science of The Total Environment, 2022. **826**: p. 154077.
9. 58. Yu, J., et al., *Compressive strength and environmental impact of sustainable blended cement with high-dosage Limestone and Calcined Clay (LC2).* Journal of Cleaner Production, 2021. **278**: p. 123616.

POTENTIAL POSSIBILITY OF DREDGED SEDIMENT AS ALUMINOSILICATE PRECURSOR IN ALKALI-ACTIVATED SYSTEM

Zhenzhong Chen[1], Nanqiao You[2], Chun Chen[1], and Yamei Zhang[1]

[1]School of Materials Science and Engineering, Jiangsu Key Laboratory of Construction Materials, Southeast University, Nanjing 211189, China
[2]School of Civil Engineering, Suzhou University of Science and Technology, Suzhou 215009, China
E-mail (corresponding author): ymzhang@seu.edu.cn

Dredged sediment (DS) is a kind of solid waste containing complex mineral phases, and its activity has been neglected for a long time. In this study, a new method was proposed to evaluate the activity of DS and verify its possibility as aluminosilicate precursor in alkali-activated system. From the aspect of solid phase, the contributions of individual phases to overall dissolution characteristics of DS were compared based on TESCAN Integrated Mineral Analyzer (TIMA). With respect to the filtrate after dissolution, the variation of element concentration was dynamically monitored within 24 h. It was found that the dissolution of major phases preferred to occur at regions with high surface energy. Seven major minerals in DS were all involved in the dissolution to a different extent, and the plagioclase and zeolite phase exhibited higher activity owing to special crystal structure. Metal cations are more likely to be liberated into solution compared with skeleton atoms (Si and Al). The inconsistent relative relationships of dissolved Al and Si from solid and into solution indicates that, depolymerization and polycondensation almost occur simultaneously in solution, which consumes more Si than Al. The proposed method for evaluating activity is of wide applicability and universal significance for systems with multi-minerals. It can be applied to DS from different sources, and provides theoretical guidance for exploring DS as a potential precursor in a real sense.

Keywords: Dredged sediment; Aluminosilicate precursor; Dissolution; Activity; Alkali-activated system

SOLIDIFICATION OF HEAVY METAL ELEMENTS IN WASTE PHOSPHATE ACID ACTIVATED METAKAOLIN GEOPOLYMER

Qingxin Wei[1], Hongwei Chen[1], **Kaibao Wang**[1], and Huirong Le[1]

[1] The Future Lab, Tsinghua University, Beijing 100084, P. R. China
lehr@mail.tsinghua.edu.cn

With the rapid development of industrial modernization and economic level in China, the non-standard use and excessive use of urban construction, industrial manufacturing, mining, and living industrial wastewater have caused a large number of heavy metal wastes to be discharged into the environment. This is significantly harmful to human health and the ecological environment. As high-quality development strategic goals, such as carbon neutrality, industrial waste and heavy metal pollution treatment, and green development, have been introduced successively, how to deal with heavy metal waste more economically and effectively is an important issue to be solved. Therefore, it is crucial to develop low-carbon materials and realize efficient solidification of heavy metal ions.

By using industrial waste acid and metakaolin as raw materials to prepare geopolymers, the core issue solved in this project is the harmless treatment of industrial waste acid as well as the high cost and resource waste during the recycling of waste acid. Meanwhile, it can reduce the heavy metal pollution to the environment and carbon emissions of the construction industry. This presentation will report on our current efforts in the heavy metal solidification of waste phosphate acid-activated metakaolin geopolymer. The issues with the fabrication process are explored, including the determination of waste acid composition, curing mechanism, solidification efficiency of heavy metal ions, and mechanical properties. A few thoughts about the challenges and opportunities with this process will be given for discussion.

Keywords: Low carbon, Geopolymer, Waste phosphate acid, Heavy metal solidification, Mechanical properties

INVESTIGATION OF FUNDAMENTAL PROPERTIES OF GEOPOLYMER USING WOOD ASH

Mitsuki Hirose[1], Takuya Kondou[2]
[1]National Institute of Technology, Kochi College, Advanced Course Student
[2] National Institute of Technology, Kochi College
S2316@gm.kochi-ct.jp

1. INTRODUCTION

Recently, there has been growing interest in woody biomass power generation in Japan as an alternative energy resource to fossil fuels and as a means of more effectively utilizing forest resources to mitigate global warming as well as realize a recycling-oriented society. Woody biomass power generation uses chips and pellets made from forests, branches, and leaves as fuel material, while the combustion process generates woody biomass wood ash. However, the cost of processing wood ash, which is an industrial waste, is worsening the profitability of businesses (Maegawa et al. (2018)). It is also estimated that up to 810,000 tons of wood ash will be generated in 2023 (Ike et al. (2020)). Therefore, this study focused on construction materials to effectively utilize wood ash.

Since the components of wood ash are like those of cement, there is a possibility that it can be effectively used as a cement replacement material. In Japan, although wood ash has been used as a concrete admixture, there are few examples of its use as a cement replacement material.

Therefore, in this study, specimens of wood ash mixed with fly ash, a by-product of thermal power plants, was prepared to investigate its effective utilization and usefulness as a cement replacement material. The mixing ratio with slaked lime used as an alkali stimulant was a test factor, and the basic physical properties were examined.

Figure 1. wood ash
(Left: before drying, Right: after drying)

2. MATERIALS AND METHODS

The methodology must be clearly stated and described in sufficient detail or with sufficient references. The wood ash used in this experiment is shown in Fig.1. It was assumed to be made exclusively from unused wood, including bark and end wood, as raw material for wood chips. Wood ash is classified into three types according to its generation process: the “main ash” is residue discharged from the bottom of the combustion chamber or boiler body, the “fly ash” is the ash that is blown up by combustion in the boiler, and the “riddling ash” is the ash that falls through gaps in the furnace. From the study by Katayama and Ouchi (2015), a tendency of fly ash reacting with water and contributing to strength development was obtained. Therefore, fly ash was also used in this study. However, fly ash has a high-water absorption rate with 30% of its composition being water. If used as is, this may affect the water–binder ratio and fresh properties. For this reason, fly ash was used in this test after being oven-dried at 110°C for 24 hours. Results of the wood ash Xray fluorescence analysis are shown in Table 1, the fly ash composition table is shown in Table 2, and the density of the materials used are shown in Table 3. As shown in Table 1, the wood ash used in this study contained high amounts of calcium and potassium. However, compared to ordinary cement, the proportion of calcium and silicon attributed to strength development is low. Therefore, slaked lime (industrial grade) ($Ca(OH)_2$) was used to compensate for the lack in calcium content and as an alkaline stimulant for the wood ash. It is also known that combustion ash has a coarse particle shape which reduces fluidity immediately after mixing (Suzuki et al. (2022)). Therefore, fly ash II was employed to supplement silicon components and improve fluidity.

The parameters of this test are shown in Table 4. The water–binder ratio was 0.7, and the binders were wood ash, slaked lime, and fly ash. The water–binder ratio was determined by preliminary tests to be the minimum amount of water that provides sufficient fluidity.

Experiments were conducted without using any admixture as a basic study. Preliminary tests showed that wood ash with water did not produce sufficient strength. Therefore, slaked lime was used to gain initial strength. The same preliminary tests showed that the highest strength at 28 days was obtained at a slaked lime replacement rate of 26%. Accordingly, slaked lime replacement with a rate of 26% was used in this study.

In addition, four levels of fly ash replacement were used. Two levels of curing were used in the compressive strength test to examine the effect of moisture conditions on strength development. For kneading and mixing, the prescribed materials were placed into a 15-L industrial use bucket and mixed with a hand mixer. Thereafter, the material was cast into a cylindrical formwork of φ50 × 100 mm and de-molded after three days. Then, curing was conducted using the prescribed method. The mixing of the specimens for the flow test was conducted by JIS R 5201 Annex C.

Table 1. Results of X-ray fluorescence analysis of wood ash

Mg	0.92	Ca	33.09	Zn	0.14
Si	1.67	Ti	0.16	Br	0.02
P	0.17	Mn	0.63	Rb	0.15
Si	4.12	Fe	2.23	Sr	0.23
Cl	1.65	Cu	0.08	Ba	0.31
K	54.46	(unit: mass%)			

Table 2. Fly ash composition

Quality			Test value
SiO_2		%	63.3
Moisture content		%	0.11
Intense heat loss		%	1.9
Powder content		cm²/g	3050
Flow value ratio		%	102
Activity index	Material age 28 days	%	80
	Material age 91 days	%	93

Table 3. Density of materials

Type	Name	Mark	Density (g/cm³)
Powder	Wood ash	M	1.96
	Slacked lime	S	2.21
	Fly ash (JIS II-class)	FA	2.20

Table 4. Test parameters

Parameter	Levels
Fly-ash replacement rate(%)	10 (F10), 30 (F30) 50 (F50), 70 (F70)
Curing method	Water curing Air curing

3. FLOW TEST

The flowability evaluation of the paste is based on the slump flow test of JIS R 5201 "Physical Test Methods for Cement," along with the slump test because of the high water–binder ratio. Diameters in the orthogonal biaxial directions were measured and used as the flow value.

4. COMPRESSIVE STRENGTH TEST

After a given duration, specimens were removed and polished to a smooth surface. The ages of the specimens were 7, 14, and 28 days. Compressive strength tests were conducted on three specimens of the same mix, with the average value used as the test result.

5. RESULTS AND DISCUSSION

The maximum flow values obtained from the flow test and the orthogonal direction are shown in Table 5, while the flow after 15 strokes is shown in Figure 2.

These values tended to increase as the fly ash replacement ratio increased. This can be attributed to the high-water absorption of the wood ash. In addition, fly ash consists of smooth spherical particles which may have contributed to the improvement of workability.

Results of the compressive strength tests are shown in Figure 3. Figure 3 shows the results of inwater curing after three days, whereas Figure 4 shows the results of in-air curing after three days. Compressive strength at seven days was not performed for fly ash replacement ratios of 50% and 70% because unmolding could not be performed at three days. Meanwhile, compressive strength for the underwater curing environment was greatest at F10 wherein the amount of wood ash was the largest. However, it tended to decrease with an increasing fly ash replacement ratio. This may be due to the amount of calcium and potassium contained in the wood ash. The presence of calcium and silicon in the fly ash may have promoted the formation of C-S-H, while the presence of potassium may have accelerated the reaction. Compressive strength increased in both formulations.

Table 5. Flow value

Symbol	Flow value(mm)	
	Max	Orthogonal
F10	155	152
F30	196	194
F50	262	260
F70	300	300

Figure 2. Situation after flow test

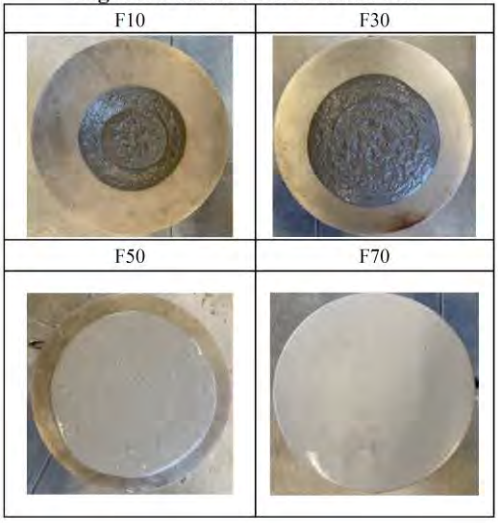

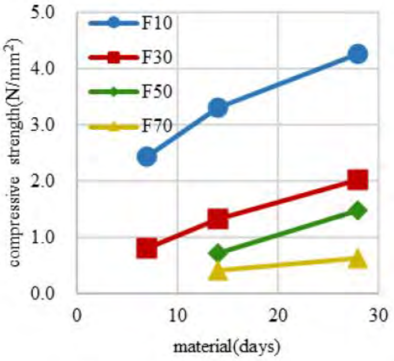

Figure 3. Water curing

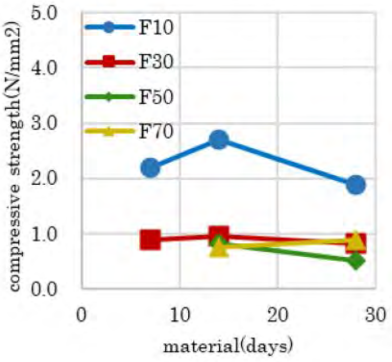

Figure 4. Air curing

Water is essential for the pozzolanic reaction, and the increase in strength over time suggests that the reaction was accelerated. Although results of this study are shown up to 28 days, the activation of the pozzolanic reaction occurs after 91 days (Hamajima and Soeda (2008)) and this trend may change in the long term. Therefore, continuous research is needed in the future.

In air curing, compressive strength tended to increase up to 14 days, although the amount was lower than that in water curing. At 28 days, the compressive strength of all specimens, except F70, showed a tendency to decrease. The strength of the specimens up to 14 days may have increased due to water remaining in the specimens after mixing along with the carbonate hardening reaction of slaked lime. However, after that time, the lack of sufficient moisture in the specimens may have prevented the pozzolanic reaction from taking place to produce strength. In addition, because of the large water–binder ratio, the drying from three days may have increased shrinkage. This may have caused cracks on the surface of the specimens which may have affected compressive strength.

6. CONCLUSION

Fly ash and slaked lime were mixed with wood ash generated at a biomass power plant. The fresh properties and compressive strength after hardening were investigated. Results showed that by mixing a large amount of wood ash, it was possible to produce a hardened compact with a compressive strength of ~4 N/mm^2 at 28 days. Since the pozzolanic reaction is the main cause of strength development, it may be possible to produce hardened compacts with even higher compressive strength by increasing the curing period.

In contrast, since the formulation required for strength development is not yet known, the optimal formulation based on various chemical analyses would be investigated in a future study. At the same time, ascertaining the physical properties for practical use, such as shrinkage properties, are of interest.

7. REFERENCES

Akihiro Maegawa, Koji Ichikawa, Shinya Matsuura, Yukitoshi Okuyama and Takahiro Sakaguchi (2018) “Fundamental study on various properties of hardened mortar mixed with woody biomass combustion ash”, Proceedings of the Annual Conference of the Japan Society of Waste Management Experts, 29:209-210

Minori Ike, Kazuyuki Oshita and Masaki Takaoka (2020) “The estimated amount of combustion ash generated at FIT-certified woody biomass power generation facilities in Japan”, Journal of the Japan Society of Material Cycles and Waste Management, 31:169-178

Akinobu Katayama and Masahiro Ouchi (2015) “Strength development of concrete with wood ash and slaked lime”, Kochi University of Technology graduation thesis:1-2

Mariko Suzuki, Yuuki Hasegawa, Kent Koide and Suto Masashi (2022) “Basic study for development of porous concrete for planting base utilizing woody biomass combustion ash”, Proceedings of the Japan Concrete Institute, 44:1138-1143

Youhei Hamajima and Masashi Soeda (2008) “Study on the Effect of Curing Conditions on Strength Development of Fly Ash Concrete”, Japan Society of Civil Engineers Western Branch research presentation:715-716

PREPARATION AND PROPERTIES OF GREEN HIGH DUCTILITY GEOPOLYMER COMPOSITES INCORPORATING RECYCLED FINE BRICK AGGREGATE

Bang-Cheng Lyu [1], Li-Ping Guo [1,2], Xiang-Peng Fei [1], Jian-Dong Wu [1], Run-Song Bian [1]

[1] School of Materials Science and Engineering, Southeast University, Nanjing 211189, P.R. China
[2] Collaborative Innovation Center for Advanced Civil Engineering Materials, Jiangsu Key Laboratory of Construction Materials, Nanjing 211189, P.R. China
guoliping691@163.com (corresponding author)

1. INTRODUCTION

Engineered cementitious composite (ECC) is a kind of composite material that realizes tensile strain hardening behavior (Li, 1998), which can also be called as High ductility cementitious composites (HDCC) (Li, 1992). However, the cement usage of HDCC is 2-3 times higher than that of ordinary concrete (Wang et al., 2007). Geopolymer with high strength, high durability, low energy consumption and low emission has attracted the attention of researchers. The high ductility geopolymer composites (HDGC) has been successfully prepared by combining fiber reinforcement with geopolymer. Studies have shown that HDGC and HDCC can also be designed using micro-mechanical models, and both have similar tensile strain behaviors to solve brittle fracture of concrete (Zhang et al., 2020. Ohno, 2018).A large amount of recycled brick aggregate is available for consumption, but fine-grained brick aggregates (BA) high ductility composites have not yet been developed. Therefore, the combination of BA and geopolymers will be beneficial for the green and sustainable development of high ductility composites and will also provide new solutions for the utilization of brick aggregates.

2. MATERIALS AND METHODS

2.1 Raw materials

Fly ash (FA) and slag (SG) were used, and alkaline solution with different silicate modulus prepared by mixing water glass, sodium hydroxide and water. Polyvinyl alcohol PVA fibers were selected as reinforcing components. River sand aggregate (RA) and brick sand aggregate (BA) were used as fine aggregates, and BA were collected from crushed and ground recycled clay brick.

2.2 Mix proportions

The maximum volume fraction of brick sand can reach 100%. Alkaline solutions with silicate modulus of 1.4, 1.6 and 1.8, and 20 wt% high-calcium slag were selected as variable components. The mix proportions of HDGC are shown in Table 1. Fly ash, slag and aggregate were mixed for 90 seconds. Then, alkaline solution was poured. Finally, the fibers were gradually added and stirred for 120 seconds. The fresh mixtures were poured into a mold and were covered with a film. After 24 hours, the test specimens were placed in a sealed bag and cured at 20 ± 2°C.

2.3 Methods

The compressive strength of HDGC specimens was tested, and the loading rate was 2400 N/s. An INSTRON 8802-10 T testing machine was used to test the three-point bending of a 40× 40×160 mm^3 rectangular notched beam specimen to determine the fracture toughness K_m. A dog-bone shaped specimen was used for the uniaxial tensile testing of HDGC. Single fiber pull-out test was used to evaluate the effect of the fiber/matrix interface properties of HDGC. The bridge residual energy J'_b was calculated according to the stress-crack opening width curve. The fractured HDGC was selected to prepare a sample with a size of about 5-6 mm. A thin film (Pt) was sputtered on the surface of the sample for SEM and EDS analysis.

Table 1 Mix proportions of HDGC

Mixture ID	FA	SG	Modulus	Activator	RA	BA	water	Fiber
1.4FARA	1.0	/	1.4	0.568	0.3	/	/	0.02
1.4FARBA	1.0	/	1.4	0.568	0.15	0.138	0.05	0.02
1.4FABA	1.0	/	1.4	0.568	/	0.276	0.1	0.02
1.4SGRA	0.8	0.2	1.4	0.568	0.3	/	/	0.02
1.4SRBA	0.8	0.2	1.4	0.568	0.15	0.138	0.05	0.02
1.4SGBA	0.8	0.2	1.4	0.568	/	0.276	0.1	0.02
1.6SGRA	0.8	0.2	1.6	0.568	0.3	/	/	0.02
1.6SGBA	0.8	0.2	1.6	0.568	/	0.276	0.1	0.02
1.8SGRA	0.8	0.2	1.8	0.568	0.3	/	/	0.02
1.8SGBA	0.8	0.2	1.8	0.568	/	0.276	0.1	0.02

3. RESULTS AND DISCUSSION

3.1 Compressive strength

Fig. 1 shows the compressive strength of HDGC. The compressive strength of HDGC decreased gradually as the fine brick aggregate increased from 0 to 100% replacement. As the slag increased and silicate modulus decreased from 1.8 to 1.4, the compressive strength of both river sand and brick sand groups showed an increasing trend.

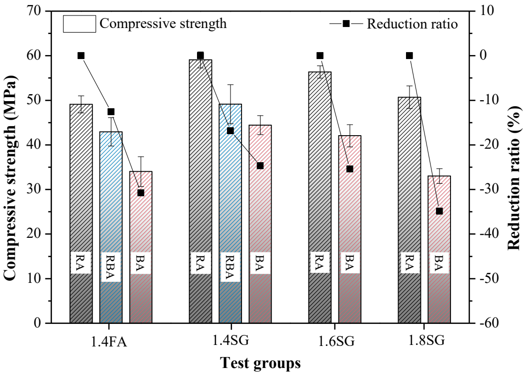

Fig. 1 Compressive strength of HDGC

3.2 Fracture properties of matrix

The fracture test results of the HDGC matrix are shown in Table 2. The E_m, K_m and J_{tip} of the matrix were reduced by the fine brick aggregate, which had a similar trend to the compressive strength. A decrease in E_m and K_m was caused by the increase of the silicate modulus, while the activity of geopolymer matrix, E_m and K_m were increased due to the slag incorporation.

Table 2 Fracture properties of HDGC matrix

Mixture ID	E_m (GPa)	K_m (MPa•m$^{1/2}$)	J_{tip} (J/m^2)
1.4FARA	4.47 ± 0.39	0.222 ± 0.02	14.95 ± 1.23
1.4FABA	3.42 ± 0.30	0.187 ± 0.03	11.86 ± 0.64
1.4SGRA	5.85 ± 0.56	0.324 ± 0.05	18.15 ± 1.48
1.4SGBA	4.14 ± 0.68	0.213 ± 0.02	11.98 ± 0.56
1.6SGRA	5.35 ± 0.46	0.297 ± 0.01	16.65 ± 2.01
1.6SGBA	3.93 ± 0.11	0.206 ± 0.06	10.66 ± 1.55
1.8SGRA	4.92 ± 0.74	0.285 ± 0.04	14.56 ± 1.23
1.8SGBA	3.47 ± 0.45	0.187 ± 0.02	9.99 ± 1.16

3.3 Tensile properties

The tensile stress-strain curves of HDGC are shown in Fig. 2. The fibers in HDGC can achieve stress transfer after the first crack occurs, and the strain increases with the increase of stress during the tensile process. When brick sand was used as aggregate, the first cracking strength of composites decreased regardless of whether the replacement rate of half or 100%. The lower the modulus and the higher the slag content, the greater the tensile strength of HDGC. The maximum tensile strength of 1.4SGBA can reach 4.41 MPa and the tensile strain was 3.77%. And meanwhile, the maximum tensile strain of 1.8SGBA was 4.27%.

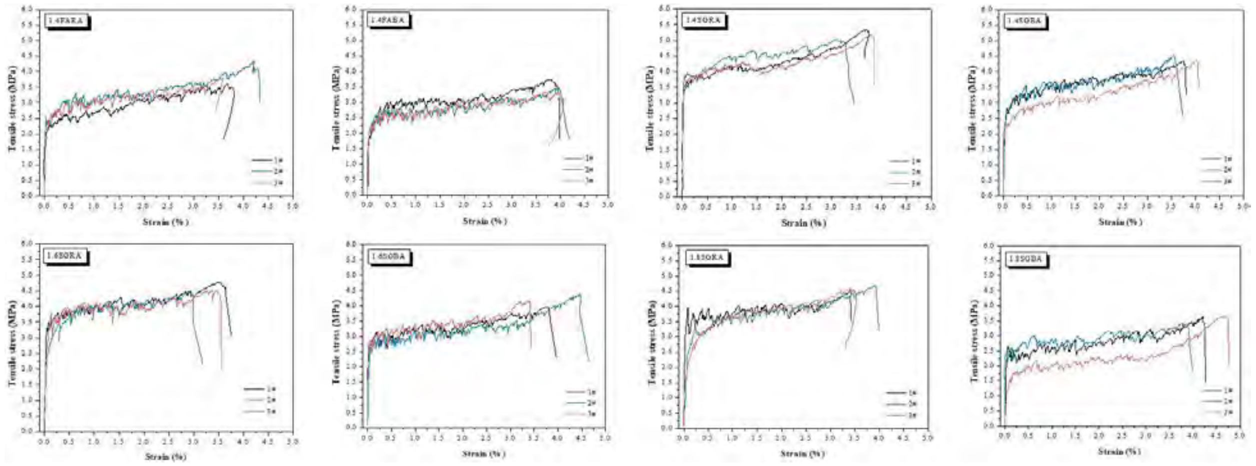

Fig. 2 Tensile stress-strain curves of HDGC

3.4 Fiber/matrix interfacial properties

Fig. 3 shows the fiber-matrix interface parameter results of the single fiber pull-out test. a low water-to-binder ratio and a high-compactness microstructure can promote stronger fiber/matrix bonding, which means higher G_d and τ_0. When brick aggregate was used, the chemical bond strength was concentrated in the range of 0.20~0.30 J/m^2. The frictional bond varied from 2.0 to 3.5MPa, basically followed the development trend of macroscopic mechanical strength and chemical bond strength. For the slip-hardening coefficients concentrated in the range of 0.20~0.27, and the value of the brick sand group is slightly higher than that of the river sand group.

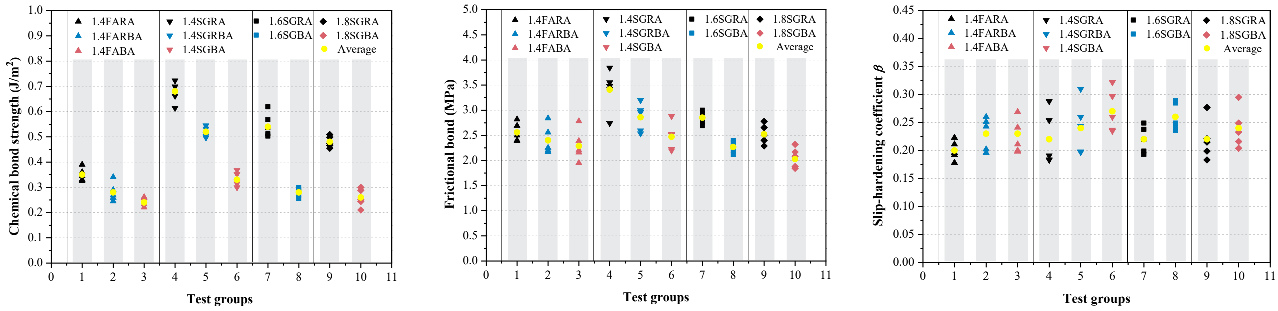

(a) Chemical bond strength (b) Frictional bond (c) Slip-hardening coefficient

Fig. 3 Fiber/matrix interfacial parameters obtained from the single fiber pull-out test

3.5 PSH criteria

Two PSH indexes, namely, the strength index $PSH_{strength}$ (σ_0 / σ_{fc}) and the energy index PSH_{energy} (J'_b / J_{tip}), are summarized in Fig. 4. The strength index results show that although the some of the $PSH_{strength}$ of all HDGC mixtures was only greater than 1.3, but most of them can exceed 1.5, which still ensured the gradual initiation and development of microcracks in HDGC. For another, PSH_{energy} was higher than the recommended threshold of 3, which indicated that microcracks can propagate stably and the bridging ability of fibers can be fully exerted during the tensile process.

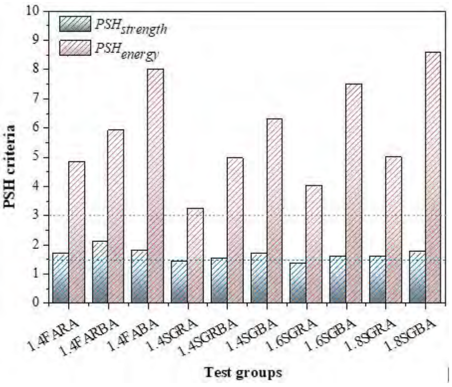

Fig. 4 PSH criteria of HDGC

3.6 Microstructure morphology

The frictional bond between the fibers and the matrix, the broken ends of the fibers were observed, as shown in Fig.5. During the fiber pull-out process, the matrix around the space occupied by the fiber was disturbed, and part of gel remained on the fiber surface. Whether river sand or brick sand was used, there were obvious scratches and filaments on the surface of the pulled fibers. The increase in the frictional bond of the fiber/matrix contributes to the improvement of the strain hardening behavior. For achieving higher J'_b, low chemical bonding and higher frictional bonding can improve the energy absorbed during fiber slippage. Therefore, HDGC incorporating fine brick aggregate still has considerable tensile stress and tensile strain in this experiment.

(a) 1.8SGRA

(a) 1.8SGBA

Fig. 5 Fiber/matrix interface

4. CONCLUSION

The main conclusions are as follows:

(1) The developed RFBA-HDGC has compressive strength of 30~50 MPa, tensile strength of 3.4~4.8 MPa and tensile strain capacity of 3.7%~4.3%. Compared to river sand aggregate HDGC, the utilization of RFBA, shows a decrease in strength, with a greater reduction in strength as the volume replacement increases.

(2) The silicate modulus and the slag content directly affect the matrix properties and tensile behavior of HDGC. Compressive strength, fracture toughness, and tensile strength decrease with increasing modulus, but tensile ductility is increased; increasing slag content leads to the opposite trend.

(3) The RFBA-HDGC prepared from recycled fine brick aggregates and low-carbon geopolymer materials has the potential for engineering applications, and can provide a new way to solve the application of waste bricks and reduce the consumption of natural resources in cement production.

5. ACKNOWLEDGMENT

This work was mainly supported by the National Natural Science Foundation of China (Grant No. 52178191).

6. REFERENCES

Li, V. C., (1998). *Engineered cementitious composites-Tailored composites through micromechanical modeling*. Canada, pp. 64-97.

Li, V. C., Leung, C. K., (1992). Steady-state and multiple cracking of short random fiber composites. *Journal of Engineering Mechanics*, 118(11), 2246-2264.

Wang, S., Li, V. C., (2007). Engineered cementitious composites with high-volume fly ash. *ACI Materials*. J. 104(3), 233-241.

Zhang, S., Li, V. C., Ye, G., (2020). Micromechanics-guided development of a slag/fly ash-based strain-hardening geopolymer composite. *Cement and Concrete Composites*, 109, 103510.

Ohno, M., Li, V. C., (2018). An integrated design method of Engineered Geopolymer Composite. *Cement and Concrete Composites*, 88, 73-85.

PERFORMANCE OF REINFORCED CONCRETE BEAM ELEMENT STRENGTHENED BY FIBER-REINFORCED GEOPOLYMER COMPOSITES

Guades, Ernesto J.[1]

[1]School of Engineering, University of Guam, Guam, USA
E-mail: guadese@triton.uog.edu

1. INTRODUCTION

Fiber-reinforced geopolymer composites (FRGC) draw interest particularly in the rehabilitation of structural concrete elements. FRGC are suitable for repairing and strengthening these elements since they are compatible with the concrete substrate (Ding et al., 2018). Currently, FRGC has been field-applied for material repair in large-diameter sewer reinforced concrete (RC) pipes, RC culverts and sewerage manholes and dam surface improvement using spray-casting technique). In the context of structural repair and strengthening of concrete elements, studies are limited, and no practical application has been documented. This issue became the motivation of conducting the present study to characterize the behavior of the strengthened beam element. In this paper, the effect of 1-side, 2-sides and 3-sides jacketing technique of the beam with different thickness layers was reported. The effect of the jacketing techniques was described in terms of the loading performance, cracking response, ductility and energy absorption capacity.

2. MATERIALS AND METHODS

The material and mixed proportions of FRGC as jacketing material adopted in this study are listed in Table 1. The fly ash used is Class F and conforms to EN 450-1 (Hasholt et al., 2019). Straight steel fiber and PVA fiber having a length of 11 mm and 18 mm, respectively with a total fiber volume content of 2% (i.e. 1% steel fiber and 1% PVA fiber) was chosen. A combination of 12 M sodium hydroxide (NaOH) solution and sodium silicate (Na_2SiO_3) was used as alkaline activator (AA) with a ratio of Na_2SiO_3/ NaOH solution of 2.5 The concrete used in casting the RC beam was made from a mixture of ordinary Portland cement, sand (0.1–2.00 mm particle size) gravel (8–16 mm particle size) and water with mixture combination displayed in Table 1. Eight RC beams (2 replicates for each jacketing configurations and 2 replicates as control specimen) were investigated in this study. All beams have length of 1,100 mm with a nominal cross section of 100 x 175, 150 x 150mm and 150 x 175, depending on the applied jacketing configurations. The thickness of the FRGC overlays for strengthened beams adopted in this study is 25 mm. Proper labels were assigned to beam specimens, where S for strengthened, 1J for FRGC overlay placed on the bottom of the beam, 2J for FRGC overlay placed on the 2 sides of the beam and 3J for FRGC overlay placed on the bottom and 2 sides of the beam. All beams were loaded in a four-point bending using a 100kN-capacity testing machine under displacement control rate of 2 mm/min.

Table 1. Mix proportion of FRGC and concrete.

Material	Unit Content (kg/cu^3)								
	Fly ash	Cement	Alkaline Activator	Sand	Gravel	Water	Superplasticizer	Steel fiber	PVA fiber
FRGC	486	–	486	1,458	–	–	–	78	13
Concrete	–	300	–	930	960	180	3	–	–

3. RESULTS AND DISCUSSION

3.1. Load-deflection relationship

The load-deflection relationship of RCB (control) and strenghtened beams are shown in Figure 1. The control specimen exhibited the expected flexural response of a ductile (tension-controlled) beam whereby the steel reinforcement yielded prior to crushing of the concrete in the compression zone. The load-deflection response of the control beam can be approximated into three stages, whereby the first stage represents the behavior during un-cracked condition. This happened at a load level of approximately 7.6 kN. The second stage describes the post-cracking condition up to yielding of steel reinforcement at 40.6 kN, which in turn represents the cracked beam that resulted in decreased moment of inertia. The last stage, representing the steel yielding up to the ultimate condition before reaching the final beam failure at 42.3 kN loading, describes the inelastic region. The load-deflection relationship of the strengthened beams (i.e., S-1J, S2J and S-3J) likewise follows a trilinear curve. S-1J exhibited slight increase in both slope and length in this region relative to RCB with crushing of concrete as the actual failure at peak loading condition. This enhancement is primarily attributed by the addition of FRGC section that consequently increased the un-cracked gross moment of inertia. At the first elastic zone (i.e., load level of 12.9 kN), S-1J remained intact and act monolithically. On the other hand, the length and slope of S-2J in the first cracking region have an intermediate values between S-1J and S-3J. S-3J exhibited the highest increase in slope and length in this zone due to the maximum equivalent addition of FRGC, hence highest relative un-cracked moment of inertia.

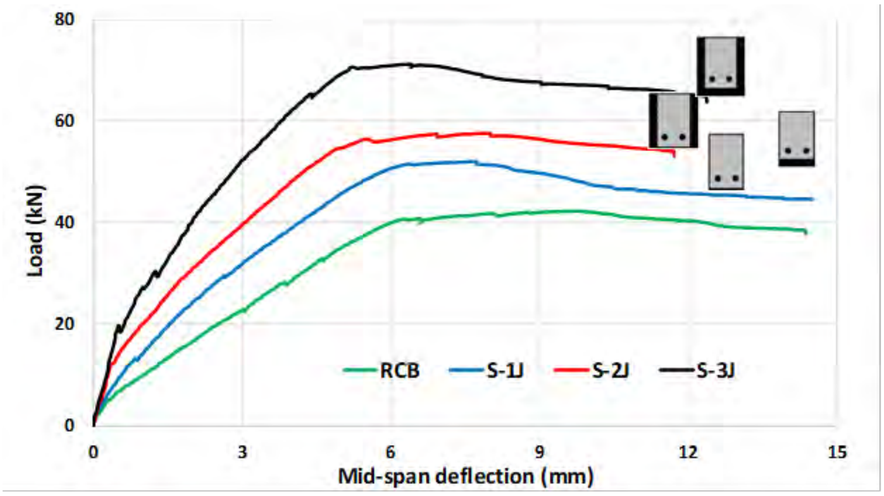

Figure 1. Load-deflection relationship of control and strengthened RC beams.

3.2. Loading capacity of tested beams at different stages

Table 2 summarizes the load values (average of 2 replicates) of beam specimens at different loading stages. In the case of jacketing at the bottom side, this technique was able to increase the load to initially crack the beam by 94% higher than the control beam, whereas jacketing at the two sides of the beam yielded 101% enhancement. Similarly, beam strengthened by 3-sides jacketing technique has improved first cracking performance showing the highest increase of 167% compared to control beam. Beams strengthened using the three jacketing techniques demonstrated yielding load ranging from 51–69 kN. Compared to the RCB, jacketing the beam only at the bottom increased the yielding load capacity by 24%. Changing the jacketing configuration from the bottom to the two sides of the specimen exhibited 36% increase of load to yield the strengthened beam. Referring from Table 2, the initial cracking load increment for S-1J and S-2J can be calculated as equal to 7% while their post-cracking-to-yielding load deviation is 12%. Meanwhile, applying a 3-side jacketing approach to strengthen the beam showed a relatively higher yielding load increase of 62% than its un-strengthened counterpart. Strengthening RC beam using bottom jacket increased the ultimate loading value by 21% while jacketing the three sides resulted to 62% load rejuvenation. The ultimate loading capacity of the beam jacketed at the two sides remained intermediate relative to beams S-1J and S-3J, obtaining 36% higher value than the control specimen.

Table 2. Load values of tested beams at different stages.

Specimen ID	First cracking Load (kN)	Yielding load (kN)	Ultimate load (kN)
RCB	6.29	41.52	42.34
S-1J	12.20	51.30	51.30
S-2J	12.62	56.34	57.59
S-3J	16.77	67.47	68.63

3.3. Ductility performance of the tested beams

In the present study, ductility was described using an index in terms of deflection and quantitatively defined as the ratio between the maximum deflection δmax and the deflection at yielding δy. Table 3 summarizes the ductility indices of the test specimens. Table 3 shows that the jacketing technique on the bottom, two and three sides of the beam provided conflicting effects on the ductility behavior of the strengthened specimens. In the case of S-1J, jacketing method provided a less favorable outcome that marginally decreased the ductility index by at least 7%. Putting equivalent thickness of 25 mm FRGC on the two sides of the beam (S-2J) increased the ductility of the RC beam by 3%. Beam S-2J exhibited higher ductility index value than S-1J since theoretically placing 25mm thick FRGC on the two sides of the beam provided smaller effect in lowering the neutral axis than putting it on bottom. As a result, S-2J required longer deflection after post-yielding of steel to reach the crushing strain of concrete in compression. Moreover, putting fiber reinforcement by virtue of FRGC on the upper part of the beam avoid a sudden and brittle concrete crushing owing to their ability of enhancing concrete toughness in compression (Meda et al., 2012), thus increased ductility

Beam S-3J demonstrated an opposing ductility performance as the index value is reduced by 11 % compared to that of RCB. While the provision of jacketing the three sides of the beam provided the highest increase of load capacity, this technique offered a ductility performance of 4 % and 16 % lower than S-1J and S-2J, respectively.

Table 3. Ductility indices of the tested beams.

Specimen ID	δ_y (mm)	δ_{max} (mm)	Ductility index, δ_{max}/δ_y
RCB	6.55	8.88	1.36
S-1J	6.23	8.88	1.26
S-2J	5.61	7.86	1.40
S-3J	5.36	6.47	1.21

3.4. Energy absorption capacity of the tested beams

Strengthened beams using FRGC jacket at the bottom, two and three sides exhibited higher absorption capacity than un-strengthened counterpart, as demonstrated in Figure 2. Jacketing at the bottom (S-1J) led to an absorption capacity value of the beam to 270 kN-mm, corresponding to 6% more energy it can absorb if the beam is not jacketed. On the other hand, S-2J and S-3J offered almost identical absorption performance exhibiting an absorbed energy of 331 kN-mm and 337 kN-mm, respectively. Although S-3J demonstrated a relatively higher ultimate load capacity than S-2J (30% in this case), its deflection to reach at the ultimate condition is shorter than the latter that resulted to a marginal difference of only 2% on their energy absorption capacity. Nevertheless, jacketing on the two and three sides of the beam can be considered effective toughening technique since they can absorb 30% and 32%, respectively, more energy than without putting jacket at all. Unlike in the case of repaired beams in which the toughness interval is solely dependent on the amount of equivalent tensile FRGC, it seems that for strengthened beams the jacketing patterns (i.e., bottom, two and three sides) also matters as evidenced by a tapered interval value of 2% between S-2J and S-3J.

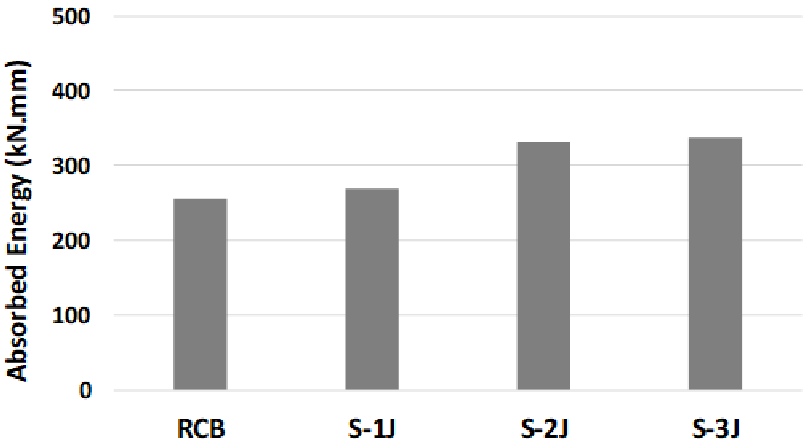

Figure 2. Comparative curve of ductility performance for strengthened beams.

4. CONCLUSION

The conclusions of this study are: Strengthening using 25 mm thick FRGC jackets on the bottom, 2 and 3 sides of the RC beam resulted to its 94–167% and 24–62% load enhancement at the first cracking and yielding conditions, respectively. On the other hand, it also increased the ultimate load value of the initial RC beam by 21–62%. RC beams strengthened along the 2 sides shown matchable ductility and 30% higher absorption capacity than the control specimen. In contrary, RC beams strengthened on the bottom and 3 sides demonstrated less ductile response, nevertheless their energy absorption value capacity is higher than their un-strengthened counterpart by 6–32%.

5. ACKNOWLEDGMENT

This project has received funding from the European Union’s Horizon 2020 Research and Innovation Programme under the Marie Sklodowska-Curie grant agreement No. 713683.

6. REFERENCES

Ding, Y and Bai, Y.L. (2018) Fracture properties and softening curves of steel fiber-reinforced slag-based geopolymer mortar and concrete, Materials, Vol. 11, 1–18.

Hasholt, M.T., Christensen, K.U. and Pade, C. (2019) Frost resistance of concrete with high contents of fly ash - A study on how hollow fly ash particles distort the air void analysis, Cement and Concrete Research, Vol. 119, 102–112.

Meda, A., Minelli, F. and Plizzari, G. A. (2012) Flexural behaviour of RC beams in fiber-reinforced concrete, Composites Part B, Vol. 43, 2930–2937.

DEVELOPMENT OF AN ECOLOGICAL AMBIENT-CURED ONE-PART GEOPOLYMER UTILIZING MUNICIPAL SOLID WASTE INCINERATION BOTTOM ASH

Syed Farasat Ali Shah[*], Shipeng Zhang, Chi Sun Poon

Department of Civil and Environmental Engineering, The Hong Kong Polytechnic University,
Hung Hom, Kowloon, Hong Kong
Email: farasat.shah@polyu.edu.hk

Incineration Bottom Ash (IBA) is the primary byproduct of municipal solid waste incineration (MSWI). Typically, the landfill disposal method is used for its disposal, which consequently results in heavy metal contamination and the squandering of huge areas. The aim of this study is to utilize incineration bottom ash (IBA) to develop an ecological ambient-cured one-part geopolymer. Alumino-silicate precursors, including ground granulated blast furnace slag (BFS) and slaked lime (CH), were used, along with anhydrous sodium silicate as an alkaline activator. Various techniques such as mechanochemical activation, calcination, and pre-foaming were employed to enhance IBA's reactivity at room temperature. Fresh properties were determined via slump flow, and setting time tests while hardened properties were measured through compressive and flexural strength tests. X-ray Diffraction analysis (XRD), Mercury Intrusion Porosimetry (MIP), and Scanning Electron Microscopy examination (SEM) investigations were performed to evaluate the chemical functional groups and microstructure of the mix. The environmental impact analysis was determined through measurement of carbon dioxide equivalent (CO_2^{-e}) of constituents. The study found that pretreatment and blast furnace slag addition improved MSWIBA's reactivity, and hardening was achieved at room temperature. The improvement in mechanical strength and hardening behavior was attributed to enhanced geopolymerization reaction and improved gel structure, as confirmed through microstructural testing.

Keywords: Municipal solid waste incineration bottom ash; One-part Geopolymer; Pretreatment; Mechanochemical activation; Rheology

THE EFFECT OF SCMS ON THE RESISTANCE OF STEAM-CURED CONCRETE TO CHLORIDE ATTACK IN THE TIDAL ZONE OF REAL MARINE ENVIRONMENT

Tengfei, Guo, Kaidong, Han, and Qianping, Ran

Jiangsu Key Laboratory of Construction Materials, School of Material Science and Engineering,
Southeast University, Nanjing 211189, Jiangsu, PR China
E-mail: qpran@cnjsjk.cn

To address the imperatives of low-carbon and environmentally sustainable practices within the construction sector, the judicious utilization of industrial byproducts is of paramount significance. Steam curing has been demonstrated as an efficacious solution to rectify the inadequate early-age performance issues associated with supplementary cementitious materials (SCMs). Of particular concern is the deleterious impact of chloride ion erosion on reinforced concrete structures. Nevertheless, the influence of SCMs on the chloride ion transport mechanisms in steam-cured concrete remains an area of limited understanding. In this study, XRD, LF-NMR, ^{29}Si-NMR, and ^{27}Al-NMR techniques are employed to investigate the microstructural evolution of steam-cured concrete amended with fly ash and slag. Subsequently, realistic marine exposure tests were conducted on steam-cured concrete incorporating SCMs to elucidate the intrinsic interplay between microstructural changes in steam-cured concrete amended with SCMs and the chloride ion erosion behavior in tidal zones. The findings reveal that the incorporation of SCMs into steam-cured concrete does not significantly alter the depth of the convection zone. However, a notable reduction in the peak concentration of chloride ions, as well as in the content of free chlorine and total chlorine, is observed. This phenomenon can be attributed to the enhancement of the Q_2/Q_1 ratio resulting from the addition of fly ash and mineral powder to steam-cured concrete. This increase leads to an elongation of the average molecular chain length and a higher degree of polymerization in the C-(A)-S-H gel. Moreover, it facilitates the conversion of silica tetrahedral dimers into polymers and refines the pores within steam-cured concrete, particularly those with dimensions exceeding 200 nm. Simultaneously, the SCMs amplifies the content of $Al(OH)_6^{3-}$ and $O_xAl(OH)_{6-x}^{3+x}$ octahedral structures. This augmentation enhances the binding affinity between steam-cured concrete and chloride ions, reducing the diffusion coefficient of chloride ions and, consequently, inhibiting the transport of free chloride ions.

Keywords: Fly ash, Slag, Steam curing, chloride ion erosion, pores

THE INTRINSIC CHANGE OF BIOCHAR IN BIOCHAR-CEMENT BASED CONSTRUCTION MATERIALS: INSIGHTS FROM STRUCTURAL, CHEMICAL AND MECHANICAL PROPERTIES

Weijian Xu[1], Xiaohong Zhu[2], and Daniel C. W. Tsang[3,*]

[1]Department of Civil and Environmental Engineering, The Hong Kong Polytechnic University, Hung Hom, Kowloon, Hong Kong, China
[2]Department of Civil and Environmental Engineering, University of California, Berkeley, CA, 94720, United States
[3]Department of Civil and Environmental Engineering, The Hong Kong University of Science and Technology, Clear Water Bay, Hong Kong, China
*Corresponding author: cedan@ust.hk

Partially replacing cement with biochar to develop biochar-cement construction materials has become a promising strategy to reduce the carbon emissions and custom-tailor the construction material. Despite the publication of a few studies evaluating the function of biochar in the performance of biochar-cement construction materials, no study on the intrinsic properties changes of biochar when exposed to cement environment has been reported. This study aims to investigate the properties change of biochar from structural, chemical, and mechanical perspectives. The results indicated that pore structure of biochar changed after degradation. The pore size of biochar was enlarged, and the biochar skeleton was observed to collapse. The decline of the aromaticity, increase of the defective and looser structure, and formation of organometallic complexes through oxygen functional groups indicated that the interaction with hydrated cement led to chemical properties changes of biochar. Furthermore, the Young's modulus of biochar decreased from 3.81 GPa to 1.55 GPa, and the hardness decreased from 0.70 GPa to 0.13 GPa after degradation due to the damage of pore structure and the occurrence of defects in the carbon matrix. Additionally, the elastic biochar exhibited elastic-plastic deformation after degradation because the de-esterification reaction damaged the carbon molecular network when exposed to alkaline environment. However, the chemical stability of biochar increased in cement due to physical isolation of the deposited salts and the decrease of reactive oxygen functional groups. Notably, although the rebound ability of biochar decreased when exposed to cement environment, the long-term rebound rate could still reach 83-95%. Moreover, due to salts crystals deposition and filling when exposed to NaCl in seawater concentration, the Young's modulus and hardness of biochar would increase 40% compared with fresh biochar and the long-term rebound rate could reach 96.6-99.2%. This provides a basis to support the feasibility of biochar applied in biochar-cement construction materials, especially those exposed to marine environment.

Keywords: Low-carbon construction; durability; biochar application; marine environment; nanoindentation.

Session B2

Blended Cements and Hydration

RESEARCH ON THE RETARDATION MECHANISM OF STEEL SLAG ON THE EARLY-AGE HYDRATION AND SETTING OF CEMENT

Qiang Wang*, Shiyu Zhuang

Department of Civil Engineering, Tsinghua University, Beijing 100084, China
E-mail (* corresponding author): w-qiang@tsinghua.edu.cn (Q. Wang)

Steel slag retards the early-age hydration and setting of cement. However, the mechanisms are still unclear. In this study, the early-age hydration kinetics and the evolution of the solid phases, aqueous species and microstructures in a cement-steel slag composite binder are investigated to explore how and why steel slag retards the early-age hydration and setting of cement. Results show that steel slag slows the depletion of gypsum, reduces the formation of ettringite, and inhibits the precipitation of CH and C-S-H. Steel slag increases the Ca concentration in the pore solution, reduces the supersaturation of the pore solution with respect to CH and inhibits the nucleation and growth of C-S-H. It was identified that $C_{12}A_7$ in steel slag plays a major role in retarding the early-age hydration of cement. The early-age hydration of C_3S is significantly retarded with the increase of $C_{12}A_7$ content. In most of cement-steel slag composite binders, the $C_{12}A_7$ content is usually at a low level, and the retarding effect of $C_{12}A_7$ on the early-age hydration of C_3S leads to prolonged setting time. When the $C_{12}A_7$ content is high enough, it leads to fast setting due to a lot of products with large specific surface areas produced by the rapid reaction of $C_{12}A_7$.

Keywords: Steel slag; Cement; Retardation; Hydration; setting

UNDERSTANDING THE IMPACT OF ALUMINUM INCORPORATION ON C-A-S-H DECALCIFICATION

Yong Tao, Yining Gao*, and Chi Sun Poon*

Department of Civil and Environmental Engineering, The Hong Kong Polytechnic University,
Hung Hom, Kowloon, Hong Kong
E-mail: cecspoon@polyu.edu.hk (C.S.Poon)

1. INTRODUCTION

Aluminum (Al), as a common foreign ion that can enter the molecular structure of Calcium Silicate Hydrate (C-S-H) gel, its impact on C-S-H structures and properties has been broadly studied. It is generally believed that Al can partly substitute silicon (Si) in C-S-H without destroying its layered structures, hence forming the so-called C-A-S-H gel. However, unlike silicon's uniformly four-coordinated structure, experimental and theoretical studies show that Al in C-A-S-H has multiple coordination numbers from 4 to 6 (Kunhi Mohamed et al., 2020). Additionally, the intrinsic electronic structure differences between Al and Si elements also result in discrepancies in the structure and properties of C-A-S-H as compared to C-S-H and have been widely investigated (Yang et al., 2018; Zhu et al., 2023). Compared to the big scale gap between the microstructure of C-A-S-H and the macro mechanical properties of hardened cement, the correlation between C-A-S-H nanostructures and the chemical properties is much more straightforward. The decalcification of C-A-S-H is the most representative research issue in this aspect. The phase evolution for decalcification of C-A-S-H has been elucidated and compared with C-S-H by experimental studies (Jin et al., 2023). However, the fundamental mechanisms of the effect of Al incorporation on C-A-S-H decalcification only remain in hypothesis. Despite previous research that explained the effect of Al on the adsorption behaviour of the C-A-S-H surface through molecular dynamics (MD) simulations (Hou et al., 2018), direct thermodynamics calculations on C-A-S-H decalcification are still lacking. Therefore, we used metadynamics-enhanced MD to calculate the free energy of non-equilibrium Ca dissolution of different C-(A)-S-H gels, which works as a bridge to link the molecular structure of C-A-S-H with macro decalcification kinetics, thereby clarifying the fundamental mechanism of the impact of Al incorporation.

2. MATERIALS AND METHODS

In this work, we used amorphous C-S-H with a typical Ca/Si ratio of 1.7 as the reference group. Al ions were introduced into C-S-H in two different forms: the first is where 20% of Si was replaced by Al with the Ca/(Al+Si) ratio remaining identical to the original C-S-H's Ca/Si ratio; the second is where an amount of Al equivalent to 20% of the Si content was additionally introduced into C-S-H with the Ca/Si ratio remaining unchanged. The former and latter models were labelled as C-A-S-H_1 and C-A-S-H_2 respectively. The crystalline 11 Å tobermorite of Hamid (Hamid, 1981) was adopted as a prototype to construct amorphous models of C-S-H. A 3×4×1 supercell was made from a rectangular unit cell of 11 Å tobermorite. The bridging [SiO_2] groups were partly randomly removed or replaced by [AlO_2] groups to achieve the target Ca/Si and Al/Si ratios of C-S-H and C-A-S-H. The [AlO_4] chains were protonated to balance the net charges engendered by the substitution of Al ions for Si ions. The developed C-S-H and C-A-S-H models were fully annealed with MD using a reactive force field (Pitman & van Duin, 2012) to release residual stress and obtain thermodynamically stable structures, which were further utilized to build the surface models for calculating the free energies of Ca ions leaching from the solid to the pore solution (**Fig. 1**). The free energy was calculated using the well-tempered metadynamics (Barducci et al., 2008) with the Plumed (Bonomi et al., 2009) package of LAMMPS (Plimpton, 1995).

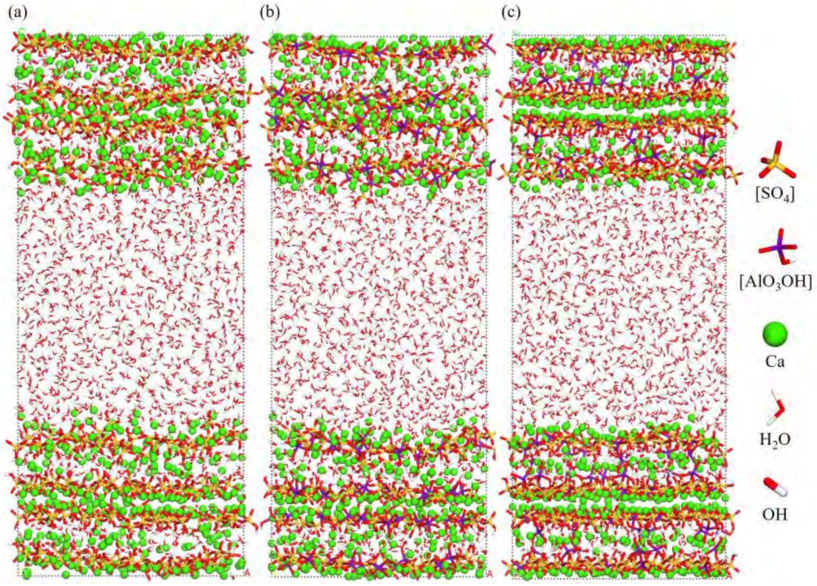

Figure 1. Molecular models of C-S-H, C-A-S-H_1, and C-A-S-H_2 for Ca dissolution simulations

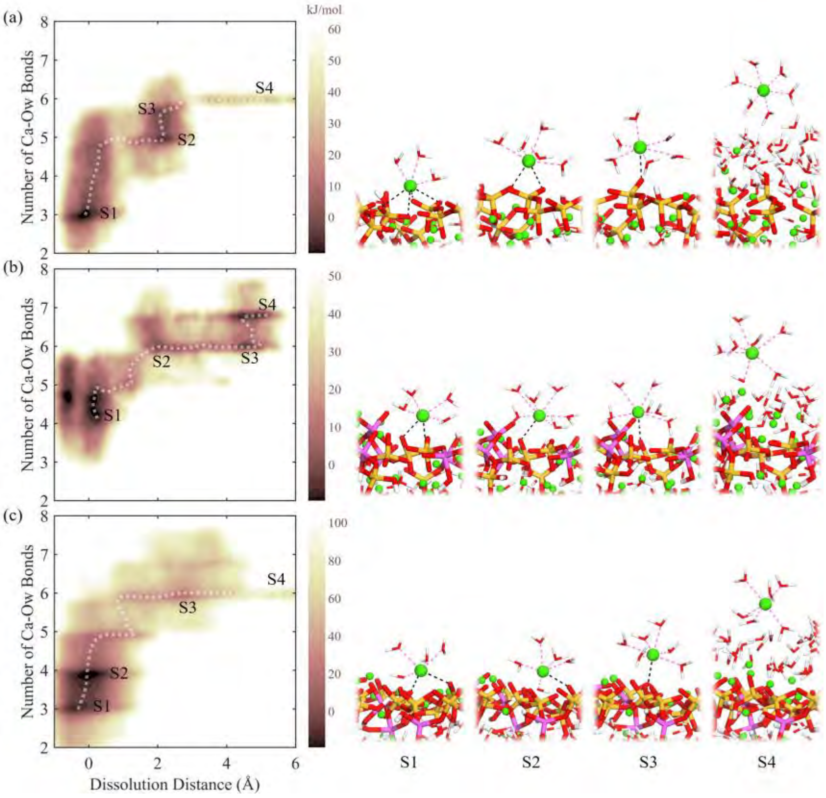

Figure 2. Two-dimensional free energy profiles as a function of dissolution distance and Ca coordination number with water for (a) C-S-H, (b) C-S-H_1, and (c) C-S-H_2 models. The minimum energy paths are plotted by the white dashed lines and the important intermediate states are illustrated by the snapshots.

3. RESULTS AND DISCUSSION

3.1 Decalcification process and energetics of C-(A)-S-H

Fig. 2 compares the dissolution process and free energy landscape of representative Ca sites on the surfaces of C-S-H, C-A-S-H_1, and C-A-S-H_2. As dissolution proceeds, the chemical bonds between Ca ions and the gel surface are gradually broken, accompanied by an increase in Ca-Ow bonds. The fully dissolved Ca ion in solution (S4) possesses a coordination number of 6-7, which is in line with previous experimental and computational results (Ohtaki & Radnai, 1993; Raiteri et al., 2015). The minimum energy paths and transition states between different states were explored using the Nudged Elastic Band method (Henkelman et al., 2000), as shown by the dashed lines in

Fig. 1. The overall Ca dissolution free energy of C-A-S-H_1 (~ 43 kJ/mol) is slightly lower than that of C-S-H (~ 47 kJ/mol), while both are far less than that of C-A-S-H_2 (~ 65 kJ/mol). Since C-A-S-H_1 and C-S-H share an equivalent Ca/(Al+Si) ratio and they are higher than that of C-A-S-H_2, the free energy results suggest that the impact of Al replacing Si on C-(A)-S-H decalcification is far less than that of a reduced equivalent Ca/(Al+Si) ratio caused by the additional inclusion of Al ions. The underlying mechanisms for this are elaborated in the following section.

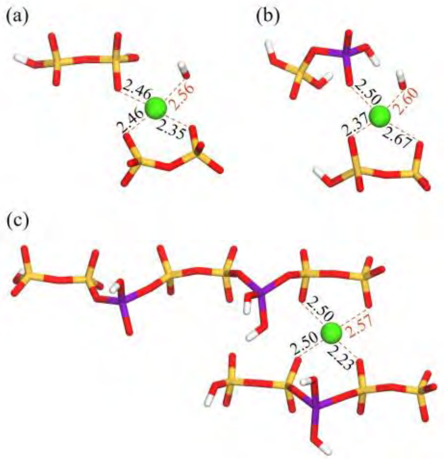

Figure 3. Typical coordination structures of surface Ca ions in the C-S-H, C-S-H_1, and C-S-H_2 models. The dashed lines show the surface constraints of the Ca ions.

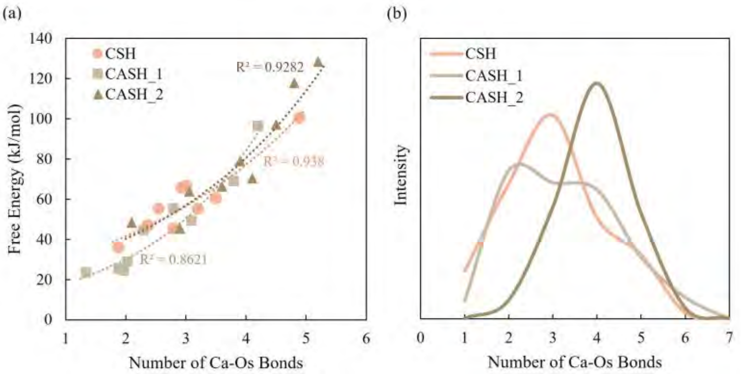

Figure 4. (a) Ca dissolution free energy as a function of the surface constraints of Ca ions and (b) the full distribution of surface constraints for all surface Ca ions in the C-S-H, C-S-H_1, and C-S-H_2 models.

3.2 Impact of Al incorporation on topological structures in C-A-S-H

When Al partly replaces Si in C-S-H (i.e., C-A-S-H_1), the number of bonds of Ca with surface O ions of the gel (known as the number of constraints) barely changes (**Fig. 3**). However, the surface constraints of Ca in C-A-S-H_2 are much different due to the elongation of aluminosilicate chains. It is noteworthy that although Oh ions on the gel surface are classified as surface O, the binding force of Ca-Oh bonds to Ca leaching is far less than other surface constraints because the OH groups can dissolve with Ca ions together as the snapshots show in **Fig. 2**. In this regard, it is understandable that C-A-S-H_2 features a higher Ca dissolution free energy since it has stronger surface constraints compared with C-S-H and C-A-S-H_1. For a statistical comparison, the number of surface constraints and corresponding dissolution free energy of multiple Ca sites from C-S-H, C-A-S-H_1, and C-A-S-H_2 are presented in **Fig. 4a**. It suggests that Ca dissolution free energy increases exponentially with the number of surface constraints, which is understandable because Ca dissolution requires overcoming surface constraints. The nine selected representative Ca sites suggest that the number of surface constraints on Ca in C-A-S-H_1 is slightly less than that in C-S-H, and both significantly less than that in C-A-S-H_2, which explains the difference in the dissolution free energy of Ca ions in the three types of C-(A)-S-H structures shown in **Fig. 2**. The full distribution of surface constraints for all surface Ca ions further confirms the differences of Ca coordination structures in the three types of C-(A)-S-H (**Fig. 4b**). Considering the Ca/(Al+Si) ratio in the three C-(A)-S-H structures, **Fig. 3** and **Fig. 4** indicate that C-(A)-S-H with a higher Ca/(Al+Si) ratio favours longer aluminosilicate chains and more constraints on the surface Ca ions, making decalcification more difficult. Indeed, previous experimental studies validated that C-S-H with a higher Ca/Si ratio exhibits faster Ca leaching (Harris et al., 2002; Trapote-Barreira et al., 2014), which is consistent with our computational results.

4. CONCLUSION

In this study, we used metadynamics-enhanced MD simulations to clarify the correlation between the Ca dissolution free energy and changes in coordination structures of C-(A)-S-H caused by Al doping. The mechanisms of Al incorporation on C-A-S-H decalcification are uncovered. The dissolution free energy of Ca indicates that the difficulty of decalcification in C-(A)-S-H is directly determined by the coordination structure of Ca ions on the gel surface, which is highly related to the cross-linking degree of C-A-S-H, the length of aluminosilicate chains, and the Ca/(Al+Si) ratio. Therefore, the effect of Al on C-A-S-H decalcification falls into two scenarios: replacing Si with Al while keeping the Ca/(Al+Si) ratio unchanged; and introducing additional Al without changing the Ca/Si ratio. The lower the Ca/(Al+Si) ratio, the longer the aluminosilicate chains, the more constraints on the surface Ca ion, and the more difficult the decalcification process. For the comparison of C-A-S-H and C-S-H with the same Ca/(Al+Si) ratio, Al replacing Si increases the disorder and cross-linking degree of C-A-S-H, leading to a slight decrease in the number of surface constraints on Ca ion, thereby promoting the decalcification process. This impact however is much less important than that from the Ca/(Al+Si) ratio variations.

5. REFERENCES

Barducci, A., Bussi, G., & Parrinello, M. (2008). *Physical Review Letters*, *100*(2), 020603.

Bonomi, M., Branduardi, D., Bussi, G., Camilloni, C., Provasi, D., Raiteri, P., Donadio, D., Marinelli, F., Pietrucci, F., Broglia, R. A., & Parrinello, M. (2009). *Computer Physics Communications*, *180*(10), 1961-1972.

Hamid, S. (1981). *Zeitschrift für Kristallographie-Crystalline Materials*, *154*(3-4), 189-198.

Harris, A. W., Manning, M. C., Tearle, W. M., & Tweed, C. J. (2002). *Cement and Concrete Research*, *32*(5), 731-746.

Henkelman, G., Uberuaga, B. P., & Jónsson, H. (2000). *The Journal of Chemical Physics*, *113*(22), 9901-9904.

Hou, D., Li, T., & Wang, P. (2018). *ACS Sustainable Chemistry & Engineering*, *6*(7), 9498-9509.

Jin, M., Ma, Y., Li, W., Huang, J., Yan, Y., Zeng, H., Lu, C., & Liu, J. (2023). *Cement and Concrete Research*, *172*, 107251.

Kunhi Mohamed, A., Moutzouri, P., Berruyer, P., Walder, B. J., Siramanont, J., Harris, M., Negroni, M., Galmarini, S. C., Parker, S. C., Scrivener, K. L., Emsley, L., & Bowen, P. (2020). *J Am Chem Soc*, *142*(25), 11060-11071.

Ohtaki, H., & Radnai, T. (1993). *Chemical reviews*, *93*(3), 1157-1204.

Pitman, M. C., & van Duin, A. C. (2012). *J Am Chem Soc*, *134*(6), 3042-3053.

Plimpton, S. (1995). *Journal of computational physics*, *117*(1), 1-19.

Raiteri, P., Demichelis, R., & Gale, J. D. (2015). *The Journal of Physical Chemistry C*, *119*(43), 24447-24458.

Trapote-Barreira, A., Cama, J., & Soler, J. M. (2014). *Physics and Chemistry of the Earth, Parts A/B/C*, *70-71*, 17-31.

Yang, J., Hou, D., & Ding, Q. (2018). *ACS Sustainable Chemistry & Engineering*, *6*(7), 9403-9417.

Zhu, X., Vandamme, M., Brochard, L., Zhang, Z., Ren, Q., Li, C., He, B., Zhang, H., Zhang, Y., Chen, Q., & Jiang, Z. (2023). *Cement and Concrete Research*, *167*, 107131.

STRUCTURAL CHARACTERIZATION OF CALCIUM ALUMINATE HYDROXIDES WITH DIFFERENT INTERCALATED ANIONS BY MULTINUCLEAR SOLID-STATE MAS NMR

Shuai Nie and Jørgen Skibsted

Aarhus University, Department of Chemistry and Interdisciplinary Nanoscience Center (*i*NANO),
Langelandsgade 140, DK-8000, Aarhus, Denmark
E-mail: shuainie@chem.au.dk, jskib@chem.au.dk

Modern cement incorporates a variety of supplementary cementitious materials, such as slag, fly ash, calcined clay, limestone, or potentially carbonated recycled concrete fines, to reduce CO_2 emissions and enhance sustainability. However, the introduction of different SCMs inevitably results in the presence of various anions, notably carbonate ions (CO_3^{2-}), within the hydrating cement system. Furthermore, when cement is employed in harsh marine environments, it encounters challenges associated with guest anions like sulfate and chloride anions. Calcium aluminate hydroxides play a crucial role in the stabilization and solidification of these anions. In this study, a variety of AFm and AFt phases have been synthesized and investigated by ^{1}H, ^{13}C, and ^{27}Al MAS NMR spectroscopy. ^{27}Al quadrupolar coupling parameters and isotropic chemical shifts (δ_{iso}) have been determined for the AFm phases. A single Al site is observed for most of the AFm phases, exhibiting similar ^{27}Al quadrupolar coupling constants around 1.2 MHz and δ_{iso} in the range of 9 – 12 ppm. Two distinct Al sites are observed for monocarbonate by ^{27}Al MAS and MQMAS NMR at very high magnetic field. Two dominant peaks are apparent in the ^{1}H MAS NMR spectra of all phases. For the AFm samples, these resonances are assigned to framework hydroxyl groups and water molecules/hydroxyls in the interlayer. For the AFt phases, the peaks are ascribed to framework hydroxyl groups in the $[Ca_6Al_2(OH)_{12}]^{6+}$ columns and water molecules associated with the Ca ions. The hydrogen connectivity network for the 22 different H atoms in monocarbonate has been further characterized using 2D ^{1}H – ^{1}H SQ-DQ experiments. The orientation of the CO_3^{2-} group in carbonate containing AFm phases has been investigated by the ^{13}C chemical shift anisotropy parameters determined from ^{13}C MAS NMR. This work significantly enhances our understanding of the local structures, dynamics, and stability of these phases in cement systems.

Keywords: Calcium aluminate hydroxides, ^{1}H and ^{27}Al MAS NMR, intercalated anions.

EFFECT OF STEAM CURING ON HYDRATION EVOLUTION OF CEMENT-BASED MATERIALS WITH RECYCLED BRICK POWDER

Xu Luo [a,b], Shujun Li [a,b], Yasong Zhao [a,b], Gaofeng Chen [a,b] ,Jianming Gao [a,b,*]

[a]School of Materials Science and Engineering, Southeast University, Nanjing, 211189, China
[b]Jiangsu Key Laboratory of Construction Materials, Nanjing, 211189, China
*Corresponding author: Jianming Gao: Prof&PhD; E-mail: jmgao@seu.edu.cn.

1. INTRODUCTION

With the increasing demand for sustainable building materials, the use of recycled brick powder (RBP) as a supplementary cementitious material (SCM) in cement-based construction materials has gained significant attention (Chang, Luo, Ailifeila, Chong, & Jiang, 2022; X. Zhang et al., 2017; Z. Zhang & Lin, 2018). Due to its lower reactivity compared to highly active materials such as blast furnace slag and fly ash, the pozzolanic activity of RBP is not readily initiated during early hydration (Berodier & Scrivener, 2014). It is widely recognized that the early hydration of cement-based materials occurs at a rapid pace. Therefore, accelerated curing methods have a significant influence on the hydration process prior to demolding (Shi et al., 2020) . Some scholars (M. Liu, Tan, & He, 2019) explored the effects of nano-SiO2 on early strength and microstructure of steam-cured high volume fly ash cement system and found that NS accelerated both the hydration of cement and pozzolanic reaction of fly ash. Liu. et al. (C. Liu & Zhang, 2021) concluded that the elevated curing temperature can accelerate the pozzolanic reaction of fly ash during the entire reaction process.And Kong et al. (Kong, Wang, & Liu, 2018) found that the hydration of Portland cement-steel slag powder forms the small size CH under steam curing when compared with that under normal curing.

Although some studies have been done on RBP as a SCM (Q. Liu, Li, Xiao, & Singh, 2020; Zhao et al., 2021), no research has been conducted on how the steam curing affects the hydration evolution of cement-based materials with RBP. In this study, the hydration properties of composite cementitious materials are investigated using methods such as calorimetry, DTG, XRD and SEM-EDS. The aim of this study is to broaden and develop the application prospects and scope of RBP as a SCM, in order to further promote energy conservation, emission reduction, and adhere to the path of sustainable development.

2. MATERIALS AND METHODS

P•I 42.5 Portland cement was utilized as the cementitious material in this research. Waste clay bricks were crushed and subsequently milled to obtain the RBP. Portland cement and RBP were mixed in accordance with the Chinese standard GB/T 1346-2011. After casting, the paste samples were cured 8 hours at steam curing condition (80°C).

The content analysis of cement pastes was conducted using an A D8-Discover X-ray diffractometer, and the Topas software was utilized to apply the Rietveld method for quantitative analysis of the phase content. The weight loss of cement pastes was determined using an STA 449F3 TGA instrument. The micro-morphology of hardened samples was analyzed using the FEI 3D field emission environmental scanning electron microscope.

3. RESULTS AND DISCUSSION

It can be observed that increasing the temperature enhances the intensity of the exothermic peak in the pastes, resulting in a notable reduction in the duration of the induction period and the emergence of a second exothermic peak. The substitution of cement with RBP decreases the available cement content for hydration. Although RBP exhibits pozzolanic activity, its reaction degree is lower compared to cement. Additionally, RBP acts as a filler and provides more nucleation sites for C-S-H gels, thereby delaying the occurrence of the peak of the second exothermic peak (Castellano, Bonavetti, Donza, & Irassar, 2016).

It is evident that neither the temperature variation nor the addition of RBP has any influence on the types of hydration products in the paste, as indicated by the similar trends observed in the DTG curves. The content of $Ca(OH)_2$ increases with the higher curing temperature in P0 and P40. In P0, the $Ca(OH)_2$ content is higher compared to P40, which can be attributed to the replacement of cement by RBP. Additionally, the pozzolanic reaction also consumes $Ca(OH)_2$. The $Ca(OH)_2$ content increases with the prolonged curing time, and the rate of increase is also influenced by the curing temperature (He et al., 2021; Shao, Gao, Zhao, & Chen, 2019).

After steam curing, it can be observed that the increase in temperature accelerates the rate of cement hydration reaction and enhances the degree of hydration. As a result, the number of unhydrated particles decreases while the amount of hydration products increases. This is reflected in the enhanced diffraction characteristic peaks of portlandite (Navrátilová & Rovnaníková, 2016).

From the SEM-EDS results, after 28 days of steam curing, it is evident that the pozzolanic reaction has taken place. The surface of the RBP shows the growth of numerous small burrs, and areas with a relative high reaction degree exhibit the presence of gel sheets.

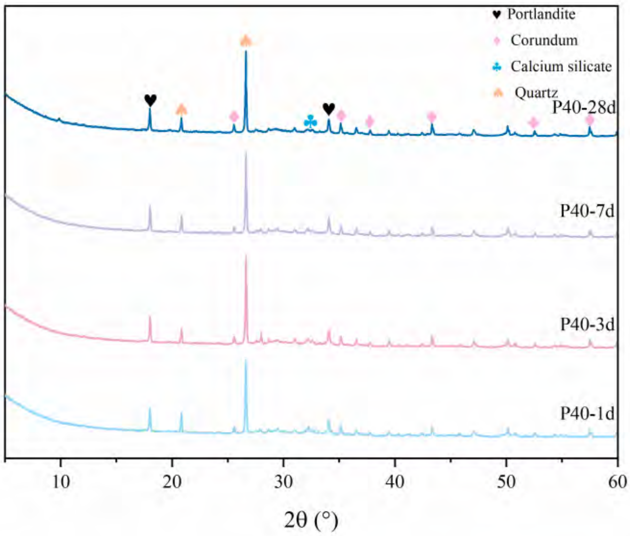

Figure 1. The XRD pattern of P40

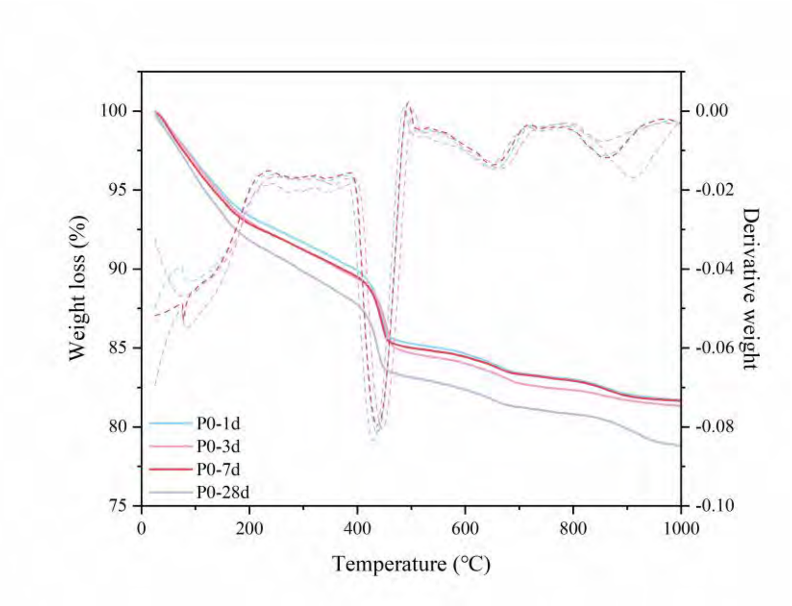

Figure 2. The weight loss of P0 at different hydration time

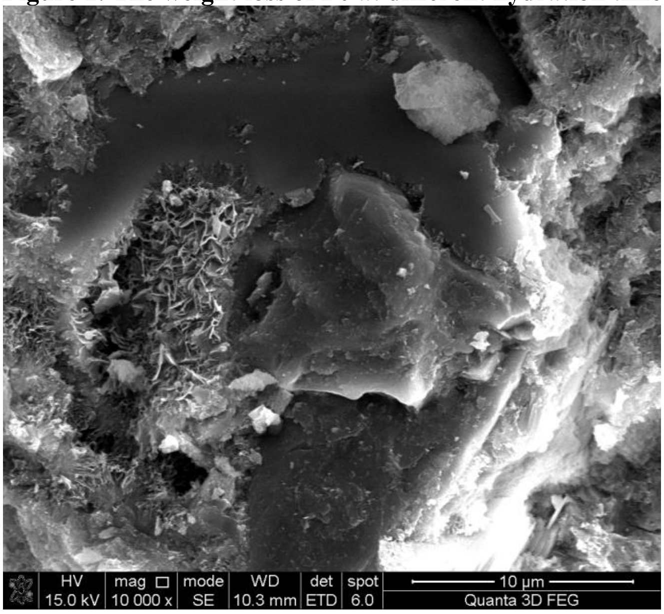

Figure 3. The SEM image of P40 at 28 days

4. CONCLUSION

In this study, the effect of steam curing on hydration evolution of cement-based materials with recycled brick powder were investigated and the following conclusions can be drawn:

1. The curing temperature is closely related to the hydration process of cement. Rising curing temperature is an effective way to promote the early hydration of cement.
2. Due to the occurrence of shrinkage and the presence of an inadequately compacted pore structure, steam-cured cement displays a phenomenon of strength retrogression during the advanced stages of hydration.
3. Steam curing conditions facilitate the pozzolanic reaction between RBP and portlandite, thereby reducing the occurrence of strength retrogression during the later stages of hydration.

5. ACKNOWLEDGMENT

The authors would like to express appreciation for the support provided by the National Natural Science Foundation of China (No. 52130210) and the Jiangsu Key Laboratory of Construction Materials.

6. REFERENCES

Berodier, E., & Scrivener, K. (2014). Understanding the Filler Effect on the Nucleation and Growth of C-S-H. *Journal of the American Ceramic Society, 97*(12), 3764-3773. doi:https://doi.org/10.1111/jace.13177

Castellano, C. C., Bonavetti, V. L., Donza, H. A., & Irassar, E. F. (2016). The effect of w/b and temperature on the hydration and strength of blastfurnace slag cements. *Construction and Building Materials, 111*, 679-688. doi:10.1016/j.conbuildmat.2015.11.001

Chang, J., Luo, S.-l., Ailifeila, A., Chong, L.-l., & Jiang, J.-q. (2022). Effects of Coarse and Fine Crushed Clay Brick Content on the Compressive Strength of Recycled Aggregate Concrete and the Microscopic Mechanism. *Geofluids*, 1-12. doi:10.1155/2022/1341185

He, Z., Shen, A., Wu, H., Wang, W., Wang, L., Yao, C., & Wu, J. (2021). Research progress on recycled clay brick waste as an alternative to cement for sustainable construction materials. *Construction and Building Materials, 274*, 122113. doi:https://doi.org/10.1016/j.conbuildmat.2020.122113

Kong, Y., Wang, P., & Liu, S. (2018). Microwave pre-curing of Portland cement-steel slag powder composite for its hydration properties. *Construction and Building Materials, 189*, 1093-1104. doi:https://doi.org/10.1016/j.conbuildmat.2018.09.088

Liu, C., & Zhang, M. (2021). Effect of curing temperature on hydration, microstructure and ionic diffusivity of fly ash blended cement paste: A modelling study. *Construction and Building Materials, 297*, 123834. doi:https://doi.org/10.1016/j.conbuildmat.2021.123834

Liu, M., Tan, H., & He, X. (2019). Effects of nano-SiO2 on early strength and microstructure of steam-cured high volume fly ash cement system. *Construction and Building Materials, 194*, 350-359. doi:https://doi.org/10.1016/j.conbuildmat.2018.10.214

Liu, Q., Li, B., Xiao, J., & Singh, A. (2020). Utilization potential of aerated concrete block powder and clay brick powder from C&D waste. *Construction and Building Materials, 238*, 117721. doi:https://doi.org/10.1016/j.conbuildmat.2019.117721

Navrátilová, E., & Rovnaníková, P. (2016). Pozzolanic properties of brick powders and their effect on the properties of modified lime mortars. *Construction and Building Materials, 120*, 530-539. doi:https://doi.org/10.1016/j.conbuildmat.2016.05.062

Shao, J., Gao, J., Zhao, Y., & Chen, X. (2019). Study on the pozzolanic reaction of clay brick powder in blended cement pastes. *Construction and Building Materials, 213*, 209-215. doi:10.1016/j.conbuildmat.2019.03.307

Shi, J., Liu, B., He, Z., Wu, X., Tan, J., Chen, J., & Jiang, J. (2020). Properties evolution of high-early-strength cement paste and interfacial transition zone during steam curing process. *Construction and Building Materials, 252*, 119095. doi:https://doi.org/10.1016/j.conbuildmat.2020.119095

Zhang, X., Shen, J., Wang, Y., Qi, Y., Liao, W., Shui, W., . . . Yu, X. (2017). An environmental sustainability assessment of China's cement industry based on emergy. *Ecological Indicators, 72*, 452-458. doi:10.1016/j.ecolind.2016.08.046

Zhang, Z., & Lin, B. (2018). Energy Conservation and Emission Reduction of Chinese Cement Industry: From a Perspective of Factor Substitutions. *Emerging Markets Finance and Trade, 55*(5), 967-979. doi:10.1080/1540496x.2018.1516638

Zhao, Y., Gao, J., Xu, Z., Li, S., Luo, X., & Chen, G. (2021). Long-term hydration and microstructure evolution of blended cement containing ground granulated blast furnace slag and waste clay brick. *Cement and Concrete Composites, 118*. doi:10.1016/j.cemconcomp.2021.103982

REACTION MECHANISM OF CLINKER-FREE BINDER WITH BIOMASS FLY ASH AND SLAG

Xuhui Liang[1], Guang Ye[1, 2]

[1]Section Materials and Environment, Faculty of Civil Engineering and Geoscience, Delft University of Technology, Delft, the Netherlands
[2]Magnel Laboratory for Concrete Research, Department of Structural Engineering, Ghent University, Ghent, Belgium
E-mail (X.Liang-1@tudelft.nl)

Biomass fly ash is one of the main by-products in bioenergy industry. Unlike conventional pozzonlanic materials such as slag and coal fly ash that are rich in aluminosilicates, the primary elements reported in biomass fly ash are calcium, alkalis, and sulfur, with a comparatively lower amount of aluminosilicates than the conventional pozzolanic materials. Consequently, the pozzolanic activity of biomass fly ash is relatively low, limiting its potential as a major component in blended cement systems. With the anticipated growth of bioenergy, a significant increase in biomass fly ash generation is expected in the coming decades, highlighting the demands for an effective recycling approach.

This study focused on the recycling of biomass fly ash as the primary constituent in the development of a clinker-free binder, in combination with slag. Mixtures with different biomass fly ash to slag ratios were systematically investigated, encompassing the analyses of reaction kinetics and microstructural evolution through multiple characterization techniques. The obtained results revealed that mixtures with larger biomass fly ash to slag ratios initially exhibited slower reactions but a more intensive reaction for the long-term hydration. The main hydration products were C-A-S-H gels, ettringite, and kuzels. Notably, the mixtures containing higher proportions of slag are more likely to generate hydrotalcite. These fundamental aspects are beneficial for effectively tailoring the properties of the binary binder, enabling further advancements in its performance.

Keywords: Biomass fly ash, clinker-free binder, waste recycling, reaction mechanism

TOWARD PERFORMANCE IMPROVEMENT OF EXCESS-SULFATE PHOSPHOGYPSUM SLAG CEMENT BY POLYALUMINUM CHLORIDE: SYNCHRONOUS REGULATION OF THE FORMATION OF ETTRINGITE AND C-(A)-S-H GELS

Xiang Liu[1], Pei Tang[2], and Wei Chen[2*]

[1] School of Materials Science and Engineering, Wuhan University of Technology, Wuhan, China
[2] State Key Laboratory of Silicate Materials for Architectures, Wuhan University of Technology, Wuhan, China
[*]E-mail: chen.wei@whut.edu.cn

1. INTRODUCTION

Phosphogypsum (PG) is the main industrial solid waste of phosphate fertilizer and phosphate chemical industry, which is generated by treating phosphate rock with sulfuric acid. With the existence of acid impurities, organic substances, heavy metal ions and radioactive substances in phosphogypsum, the outdoor stacking method would not only occupy a lot of land resources, but also cause serious environmental pollution. The application of phosphogypsum as cementitious materials can effectively solve the pollution caused by the massive storage of phosphogypsum. On the basis of supersulfated cement (SCC), Huang et al. (Huang and Lin, 2010) developed an excess-sulfate phosphogypsum slag cement with comparable engineering properties, composed of 45% PG, 10% steel slag, 35% granulated blast furnace slag and 10% limestone. However. Long setting time and low early strength limit the application of ESPSC in civil engineering, which is mainly due to the adhesion of F^- and PO_4^{3-} impurities on the surface of phosphogypsum particles and the slow hydration rate of slag. Polyaluminum chloride (PAC) is a recently developed water-soluble inorganic coagulant, which is widely used in water treatment due to its high efficiency, low cost and board applicability. The highly positively charged ionic group generated after the hydrolysis of PAC can effectively absorb the negatively charged F^- and PO_4^{3-} (Chen et al., 2022), and promote the strength development of slag cement paste (Chen et al., 2016). Therefore, PAC has the potential to solve the problems of low early strength and long setting time of ESPSC, while the underlying mechanisms have not been extensively addressed.

2. MATERIALS AND METHODS

Phosphogypsum used in this study was supplied by Hubei Changyao New Materials Co.,Ltd of China. Clinker obtained from Huaxin Cement Corp. ltd of China, which is in accordance with the Chinese standard GB/T 21372-2008. The ground granulated blast furnace slag was provided by Shaoguan, Guangdong Province. The polyaluminum chloride is a commercial production for water purification.

The preparation method of ESPSC pastes is divided into two steps. Firstly, phosphogypsum, slag, clinker and water were placed in a horizontal ball milling tank at a mass ratio of 45:1:2:28.8 and wet grinding at a speed of 500 r/min. The ground phosphogypsum slurry was sealed for one day at room temperature, and a "PG slurry" was obtained. After sealing, the ESPSC pastes was prepared by mixing PG slurry and other raw materials for 5 min according to the mix proportions given in Table 1. The fresh ESPSC pastes of all mix were cast into moulds with a size of 40 × 40 × 40mm. Then, the specimens were demoulded after sealing and maintained at room temperature for 24h, followed by 27 days of curing at 25 °C and 95% RH.

Table. 1 Mix design of ESPSC pastes

Sample	PG slurry	Slag	Clinker	PAC	Water
REF	76.8	48	4	0	11.2
1%PAC	76.8	48	4	1	11.2
2%PAC	76.8	48	4	2	11.2
3%PAC	76.8	48	4	3	11.2

The initial and final setting times of all ESPSC pastes were tested according to the Chinese standard GB/T 1346-2011. Sinc the setting time of ESPSC pastes is too long, all ESPSC pastes were placed in a constant temperature and humidity box during the test process. The compressive strength of ESPSC pastes was evaluated at 1, 3 and 7 days following the Chinese standard GB/T 17671-1999 with a loading rate of 0.6 kN/s.

The changes in the composition of the pore solution at 3 days and 7 days hydration were determined in the ESPSC pastes. The pore fluid was extracted using the Pore Fluid Expression Technique(García Calvo et al., 2010). The concentration of calcium, phosphate and aluminate in these pore solutions were tested with inductively coupled plasma optical emission spectrometry (ICP-OES).

To further explore the regulation mechanism of PAC on the early hydration of ESPSC pastes, the phase assemblage and morphology of hydration products at 1, 3, 6, 12 and 24 hours with or without PAC were characterized with XRD analysis. XRD analysis was performed with a tabletop powder X-ray diffractometer (Rigaku MiniFlex600) with CuKα incident radiation in the range of 5°-10°, a step size of 0.02° and a measuring speed of 0.1°/min. TEM analysis was conducted with JEM-1400Plus transmission electron microscope with an accelerating voltage of 100 kV.

3. RESULTS AND DISCUSSION

The initial and final setting time of all ESPSC pastes are displayed in Fig. 1 (a). The REF pastes represented a longer setting time in comparison with other ESPSC pastes. With the addition of PAC, the intial and final setting time were signifiantly shortened. The initial and final setting time of 1%PAC group ESPSC pastes are reduced by 578 min and 797 min, resprectively, referring to REF group. The addition of 1 wt% PAC presents a prominent effect on reduced setting time, which implies that the $Al(OH)_4^-$ ionic group generated by the hydrolysis of PAC can speed up the formation reaction of ettringite in ESPSC pastes(Wang et al., 2022). With the further addition of PAC, the accelerated effect was weakened. Fig. 1 (b) shows the compressive strength of ESPSC pastes. With the dosage of PAC increased from 0% to 1%, the 1 day compressive strength increased from 2.06MPa to11.88 MPa. The improvement in the early mechnical properties of ESPSC pastes was attributed to the massive formation of ettringite in the pore solution, which forms a stable structure by overlapping with each other. With the further addition of PAC, the increment tendency was gradually weakened.

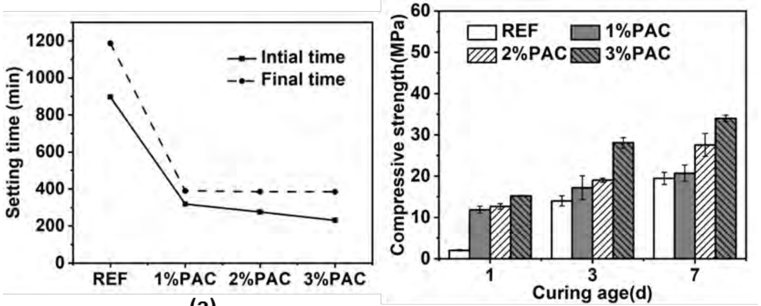

(a) (b)

Fig. 1 (a) Setting time and (b) compressive strength of ESPSC pastes.

The composition of the pore solution of ESPSC pastes after 3 days and 7 days hydration are shown in Table. 2. The content of calcium in pore solution increased with the increase of PAC content, and the content of sulfur was inversely proportional to PAC dosage. In terms of the formation reaction of hydration products, sulfur only involves the formation of ettringite, and calcium involves the formation of ettringite and C-(A)-S-H gel. The consumption rate of calcium in pore solution should be significantly higher than sulfur, but this trend is contrary to the experimental results. The main reason is that the sources of calcium are phosphogypsum, slag and clinker. The addition of polyaluminum not only promotes the dissolution of phosphogypsum, but also accelerates the dissolution of slag(Kim, 2019). Therefore, the concentration of calcium in the experimental group added with polyaluminum is higher. Sulfur is only provided by phosphogypsum. The addition of PAC accelerates the formation of ettringite, so the concentration of sulfur is reduced. In addition, the pH value of pore solution decreases with the increase of the content of PAC, which is mainly due to the consumption of hydroxide ion in the hydrolysis of PAC.

Table. 2 Composition of the pore solution of ESPSC pastes. 3 days and 7 days

Group	3d (mmol/L)				7d (mmol/L)			
	Ca	S	Al	pH value	Ca	S	Al	pH value
REF	11.62	63.97	\	12.08	13.26	118.92	0.0097	11.85
1%PAC	22.21	35.69	0.0021	11.54	25.85	134.26	0.0055	11.43
2%PAC	53.45	27.46	\	11.19	51.73	96.23	0.0072	11.06
3%PAC	54.34	31.80	\	10.87	67.86	57.83	0.0031	10.84

To further explore the regulation mechanism of PAC on the early hydration of ESPSC pastes, the XRD pattern of REF group and 3%PAC group ESPSC pastes after 1, 3, 6, 12 and 24 hours hydration are shown in Fig. 2. The hydration products of ESPSC pastes are composed of ettringite and C-(A)-S-H gels. Ettringite phase played an important role in the early setting and hardening of pastes, so this study mainly focused on the regulation of PAC on ettringite. The diffraction peak intensity of ettringite increases with the increase of hydration time. After adding PAC, the diffraction peak intensity of ettringite is significantly higher than that of REF group, and the diffraction peak intensity of ettringite in REF group after 24h hydration was the same as that of 3%PAC group after 1h hydration. This is consistent with the result of setting time and compressive strength.

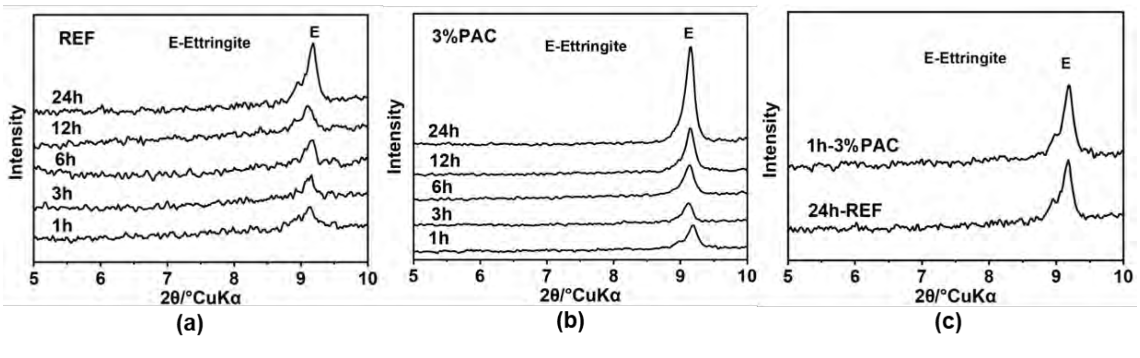

Fig. 2 XRD pattern of (a) REF group and (b) 3%PAC group ESPSC pastes after 1, 3, 6, 12 and 24 hours hydration.

XRD analysis results of early hydration products of ESPSC pastes with and without PAC cannot directly reflect the regulation of ettringite crystals size and quantity. TEM images of hydration products of REF group and 3%PAC group ESPSC pastes after 1 hour hydration are shown in Fig. 3. It can be seen that a small amount of short rodlike ettringite crystals with a length of about 130 nm appeared in the REF group pastes after 1 hour hydration. After adding PAC, a large number of needle-like ettringite crystals with length of 1-2μm are generated in the pastes. The results indicated that the incorporation of PAC greatly accelerated the nucleation and growth process of ettringite crystal, and increased the aspect ratio and quantity of ettringite crystal. The regulation of ettringite by PAC promoted the shortening of setting time and the enhancement of compressive strength of ESPSC pastes.

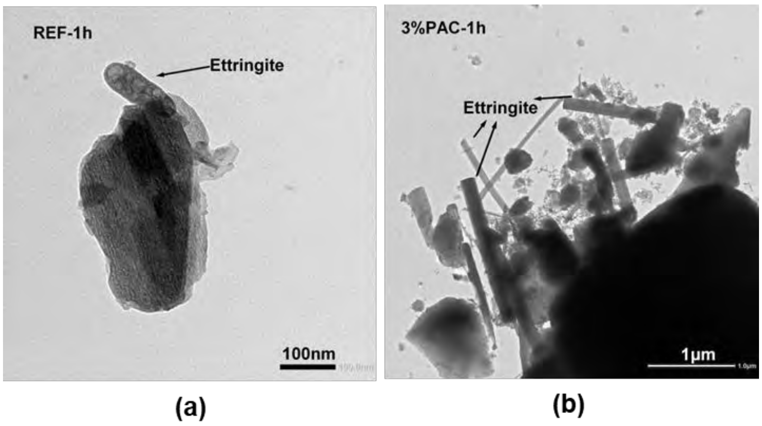

Fig. 3 TEM images of hydration products of ESPSC pastes after 1 hour hydration, (a) REF; (b) 3%PAC

4. CONCLUSION

In this study, the effect of polyaluminum chloride (PAC) on the early hydration behavior of ESPSC pastes was investigated. The regulation mechanism of PAC on the composition, structure and morphology of hydration products were characterized by various analytical techniques.

The addition of PAC accelerated the dissolution of phosphogypsum and slag in the ESPSC pastes, and calcium ions, sulfate ions and the $Al(OH)_4^-$ ionic group formed by the hydrolysis of PAC generated a large amount of ettringite in the alkaline pore solution enviornment.

The incorporation of PAC greatly accelerated the nucleation and growth process of ettringite crystal, and increased the aspect ratio and quantity of ettringite crystal, which promoted the shortening of setting time and the enhancement of compressive strength of ESPSC pastes.

5. ACKNOWLEDGMENT

This research is financially supported by the National Key Research and Development Program of China (2022YFC3902705), the National Natural Science Foundation of China (51972248, 52072279), the Key R&D Program of Hubei Three Gorges Laboratory, Hubei Three Gorges Laboratory (Grant No.SC211004), Shenzhen Science and Technology Plan Collaborative Innovation Project (CJGJZD20200617102601003).

6. REFERENCES

Chen, Q., Zhang, Q., Wang, Y., Zhang, Q. and Liu, Y. (2022) “Highly-efficient fluoride retention in on-site solidification/stabilization of phosphogypsum: Cemented paste backfill synergizes with poly-aluminum chloride activation”, *Chemosphere*, 309(Pt 2), 136652.

Chen, W., Li, B., Li, Q. and Tian, J. (2016) “Effect of polyaluminum chloride on the properties and hydration of slag-cement paste”, *Construction and Building Materials*, 124, 1019-1027.

García Calvo, J.L., Hidalgo, A., Alonso, C. and Fernández Luco, L. (2010) “Development of low-pH cementitious materials for HLRW repositories”, *Cement and Concrete Research*, 40(8), 1290-1297.

Huang, Y. and Lin, Z. (2010) “Investigation on phosphogypsum–steel slag–granulated blast-furnace slag–limestone cement”, *Construction and Building Materials*, 24(7), 1296-1301.

Kim, T. (2019) “The effects of polyaluminum chloride on the mechanical and microstructural properties of alkali-activated slag cement paste”, *Cement and Concrete Composites*, 96, 46-54.

Wang, J., Wang, Y., Yu, J., Xu, L., Li, M., Cheng, J. and Li, Z. (2022) “Effects of sodium sulfate and potassium sulfate on the properties of calcium sulfoaluminate (CSA) cement based grouting materials”, *Construction and Building Materials*, 353, 129045.

PROCESS COMPATIBLE DESULFURIZATION OF NSP CEMENT PRODUCTION: A NOVEL STRATEGY FOR EFFICIENT CAPTURE OF TRACE SO_2 AND THE INDUSTRIAL TRIAL

Tongsheng Zhang[1,2], Hui Peng[1], Chang Wu[1], Yiqun Guo[1], Jiawei Wang[3], Xinzhi Chen[4], Jiangxiong Wei[1,2], Qijun Yu[1,2,5]

[1] School of Materials Science and Engineering, South China University of Technology, 510640, Guangzhou, China
[2] Guangdong Low Carbon Technology and Engineering Center for Building Materials, 510640, Guangzhou, China
[3] Energy and Bioproducts Research Institute (EBRI), Aston University, Aston Triangle, B4 7ET Birmingham, UK
[4] Guangdong Wanyin Technology Development Co. Ltd, 510075, Guangzhou, China
[5] College of Civil Engineering, Hefei University of Technology, 230009, Hefei, China
Corresponding author. Email address: concyuq@hfut.edu.cn. (Qijun Yu)

Cement industry contributes to more and more SO_2 emission due to utilization of alternative raw materials and fuels, whereas the available calcium-based dry flue gas desulfurization (FGD) technologies present low efficiency due to slow reversible de-SO_2 reactions and short gas-solid contact time in the preheater. In the present study, the SO_2 capture potentials of $CaCO_3$, CaO, and $Ca(OH)_2$ in the preheater environment were maximized by introducing V_2O_5-based catalyst and selecting optimal reaction temperature, and the de-SO_2 mechanism was extensively discussed. The results showed that the de-SO_2 efficiency of calcium-based adsorbents increased by 10-57 times as SO_2 was effectively oxidized to SO_3 in the presence of V_2O_5-based catalyst, then maximum de-SO_2 efficiency of 75.5% was achieved using $Ca(OH)_2$ and V_2O_5-CeO_2 at 600 ºC. Furthermore, $CaCO_3$ assisted by V_2O_5-CeO_2 also had a de-SO_2 efficiency of 65.6%. Subsequently, a novel process compatible FGD technology was designed to maximize the de-SO_2 ability of raw meal in the preheater by adding V_2O_5-based catalyst and humidification, the SO_2 concentration of flue gas reduced from 1000 mg/Nm^3 to less than 100 mg/Nm^3 in the industrial-scale trial, as more sulfur was solidified into clinker in the form of alkali sulfate without reducing its properties. This novel process compatible de-SO_2 strategy is of real significance for reducing SO_2 emission of cement industry at low economic cost.

Keywords: Calcium-based adsorbents; Catalyst-assisted SO_2 capture; NSP cement production; Process compatible desulfurization; SO_2

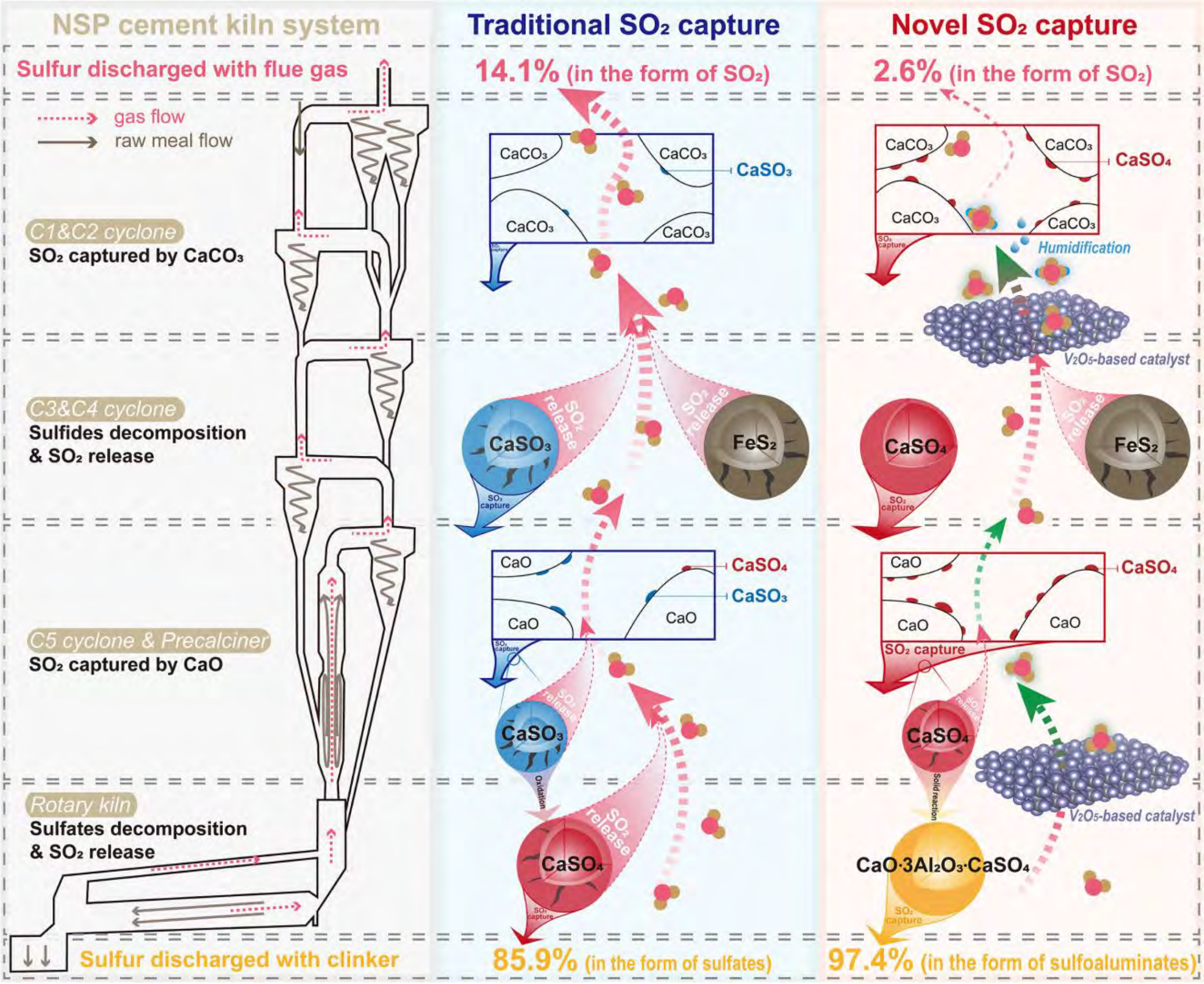

Graphic abstract: Novelty of process compatible de-SO_2 strategy.

VOLUME STABILITY OF LOW-CARBON MAGNESIUM SILICATE HYDRATE CEMENTITIOUS SYSTEM

Tingting Zhang[1], Jingbin Zhang[1], Ziyu Zhou[1], Yuan Jia[2], Chris Cheeseman[3]

[1]Faculty of Infrastructure Engineering, Dalian University of Technology, Dalian 116023, China
[2]College of Materials Science and Engineering, North China University of Science and Technology, Tangshan 063210, China
[3]Department of Civil and Environmental Engineering, Imperial College London, London SW7 2AZ, United Kingdom
E-mail: tingtingzhang@dlut.edu.cn

The cementitious system of magnesium silicate hydrate (MSH) is susceptible to significant volume deformation and cracking upon hardening. This phenomenon leads to degraded mechanical properties and durability, thereby restricting its application and development. This study aims to address this problem by conducting a more systematic investigation of the volumetric stability performance and the underlying volume change mechanism of the MSH system.

A non-contact method was used to measure the volume stability performance of the MSH system under different curing conditions. It is indicated that the MSH system exhibits expansion deformation under soaking conditions, primarily shrinkage deformation under drying and sealing conditions, and minor expansion during the later stages of drying. The volumetric stability of the MSH system was further investigated by quantitatively probing the physical phase development using a combination of XRD, DTG and NMR techniques, exploring the pore structure development through N_2 adsorption experiments, and examining the change in microscopic morphology through SEM. The results indicate that the expansion deformation of the MSH system is primarily due to solid-phase expansion resulting from the conversion of MgO to $Mg(OH)_2$. Additionally, the shrinkage deformation of the MSH system is mainly due to the collapse of micro mesopores caused by external or internal water loss. The crystal precipitation effect may be the primary reason for the paradoxical relationship between capillary stress and shrinkage rate.

Keywords: magnesium silicate hydrate; curing conditions; expansion deformation; drying shrinkage; self-shrinkage

EFFECTS OF SEAWATER ON THE HYDRATION, PROPERTIES, AND STRUCTURE OF ALUMINATE PHASES IN CEMENT

Yamei Cai, Yong Tao, Dongxing Xuan, and Chi Sun Poon*

Department of Civil and Environmental Engineering, The Hong Kong Polytechnic University, Hong Kong
E-mail: cecspoon@polyu.edu.hk

Concrete is the most widely used man-made construction material in the world. In the past few decades, along with the rapid urbanization, a great number of new infrastructural projects have been constructed. This has noticeably contributed to a growing demand for freshwater which is one of the important constituents in producing cement and concrete products. The possible use of seawater for concrete production has consequently gained increasing interest particularly in remote islands and for the construction of offshore structures.

In Portland cement, even though tricalcium aluminate (C_3A) only accounts for approximately 5-10 % by mass, C_3A, as the most reactive phase, affects the fresh properties of cementitious materials. However, research on the influence of ions in seawater on the hydration process and hydration products of C_3A system is still scarce. The purpose of this work is thus to fill in the research gap and provide new insights. The results showed that seawater can accelerate the formation of AFt, leading to a higher hydration degree of C_3A at the early age compared to the pastes mixed with deionized water (DI). After gypsum depletion to form AFt, the available Ca ions in reaction system play an important role in the later hydration degree of C_3A. The Mg ions present in seawater could enter the sites of Ca in the AFt structure, resulting in an unstable structure. The micromechanical properties of AFm phase can be strengthened by incorporation of Cl ions. Compared to the ions in seawater, the alkalinity in the reaction system seems to have a relatively significant effect on the particle size, elemental composition, and micromechanical properties of Cl-AFm phase (Friedel's salt) formed.

Keywords: Seawater, C_3A, Hydration, AFt, AFm

Session B3

Carbonatable Systems and Sustainability

IMPROVING THE HYDRATION ACTIVITY AND VOLUME STABILITY OF THE RO PHASES IN STEEL SLAG BY COMBINING ALKALI AND WET CARBONATION TREATMENTS

Wenzheng Li [a], Mingli Cao [a], Dan Wang [b], Jiuye Zhao [c,*], **Jun Chang** [a*]

[a] School of Civil Engineering, Dalian University of Technology, Dalian 116024, Liaoning, China
[b] Special Glass Key Lab of Hainan Province & State Key Laboratory of Marine Resource Utilization in South China Sea, Hainan University, Haikou 570228, China
[c] College of Transportation Engineering, Dalian Maritime University, Dalian 116026, China

Poor volume stability of steel slag (SS) is due to the existence of free-CaO, free-MgO, and RO phases. Combined treatments of alkali and wet carbonation (AWC) were conducted on the RO phases to stimulate hydration activity. The hydration degree of AWC_RO phases with MgO molar ratios of 0.84 increased from 10.6% to 57.6%. The effects of FeO-MgO-MnO proportions on the hydration activity of RO phases were investigated electronically based on the density functional theory. Results showed that Fe imparted higher inhibition effects on MgO hydration than Mn. The compressive strength of mortar with added AWC_SS was 34.4% higher than with added untreated SS at 28 days, with an expansion rate decreased from 0.0447% to 0.0298%. The main products of AWC_RO phases were $Mg(OH)_2$ and $Mg_5(CO_3)_4(OH)_2 \cdot 4H_2O$, which exhibited seed crystal effects, accelerating the early hydration of cement. This method provides guidance towards a meaningful solution to poor SS volume stability.

Keywords: Steel slag; Carbonation; RO phase; Volume stability; Density functional theory (DFT)

DEEP STABILIZATION OF SOFT CLAY SOIL WITH A LOW-CO2 BINDER GENERATED FROM WASTE STREAMS OF PULP AND PAPER MILLS

Minna Sarkkinen[1], Juha Koskinen[1], Riikka Silmu[2], Katja Viitikko[2], and Kari Saari[2]

[1]Tapojärvi Oy
[2]UPM
minna.sarkkinen@tapojarvi.com

1. INTRODUCTION

Stabilization by deep soil mixing (DSM) with hydraulic binders is a generally used technique to improve engineering properties of low bearing soils. In the method, a dry binder is mechanically mixed into the soil where it after reaction with water and soil material increases strength. Portland cement and lime have commonly been used as binders generating high amount of CO_2 emissions. To produce a low-carbon alternative cement, green liquor dregs (GLD) and biomass ashes were used as main raw materials besides minor amount of gypsum and lime kiln dust (LKD). The raw materials were mixed and calcined at temperature of 950 ºC that is lower than that of used in calcination of Portland cement (1450 ºC).

Carbon emissions were analysed by Life Cycle Analysis (LCA). According to the LCA, the new TapoEko binder had fossil emissions of 65.05 kg CO_2-eq/tonne compared to typical fossil emissions ranging from 793 to 1060 kg CO_2-eq/tonne of Portland cement (Barcelo et al., 2014) and 1,027 kg CO_2-eq/tonne (FMI, 2019) of burnt unslaked quicklime. According to the compressive strength tests, the results achieved values up to 1,550 kPa after 90 days, which is clearly higher than typical design value of 100-200 kPa (NGF, 2012). Thus, the new low-CO_2 binder indicates good suitability for use as a binder for deep stabilization of soft clayey soils including sulfidic clays common for example in Finland.

Soft clay is typically characterized by low undrained shear strength (Cu<40 kPa), high compressibility (Cc 0.19-0.44), and high moisture content (> 40 %) (BS 8004). Strength development of the produced low-CO_2 cement was tested by stabilizing three different soft clay soils with dosages from 100 kg/m^3 to 170 kg/m^3. Unconfined compressive strength (UCS) was determined after 7 days, 28 days and 90 days. In addition, leaching of hazardous substances was analysed from the stabilized crushed material by 2-phase leaching test (EN 12457-2:2002).

The results are part of a larger research work including verifying the obtained results in a plant-scale test work and piloting the end-product at test sites for external users. The research work aims at the start of industrial production and for the first time the commercial utilization of GLD.

2. MATERIALS AND METHODS

The wastes used in this study were produced by Finnish UPM-Kymmene Oyj comprising GLD from its three pulp mills, biomass fly ashes (FA) from its three plants, and LKD from its three pulp mills. In addition, phosphogypsum (PG) waste was used to replace natural gypsum. The chemical composition of the raw materials studied in X-ray fluorescence analysis is presented in Table 1.

Raw materials were mixed in the as-received condition in an electric mixer for 5 min to get a homogenous mix. The raw mix was then calcined in an electrical lab furnace in two steps: heating up to 100 ºC and then heating up to 950 ºC using dwell times of 60 min and 120 min. Quenching was executed in the air at room temperature. The calcined mix was milled by a laboratory swing mill to the fineness below 90 µm.

Table 1. Chemical composition of the dry raw materials by X-ray fluorescence analysis in mass %.

Raw material	*LOI at 950 °C*	*XRF (%)*							
	(%)	CaO	SiO_2	Al_2O_3	Fe_2O_3	SO_3	MgO	K_2O	Na_2O
GLD1	35.96	48.36	3.58	2.43	0.63	2.52	7.00	0.31	3.19
GLD2	38.75	52.22	1.84	0.48	0.19	1.06	8.01	0.21	3.09
GLD3	37.24	42.48	2.42	0.70	0.27	4.25	8.08	0.78	3.54
FA1	1.79	29.52	25.92	16.05	2,76	1.60	2.20	2.59	0.93
FA2	8.51	32.41	17.99	8.61	4.49	3.18	4.33	3.78	1.28
FA3	14.72	53.71	11.50	10.23	1.46	1.28	1.83	0.34	3.72
LKD1	38.73	56.47	0.72	0.24	0.03	0.62	0.34	0.14	3.17
LKD2	40.60	58.21	0.32	0.00	0.04	0.52	1.09	0.16	3.15
LKD3	41.26	60.13	0.39	0.13	0.04	0.57	1.26	0.15	3.12
PG	8.40	43.93	0.11	0.07	0.02	51.47	0.05	0.01	0.00

The soft clay used for the preparation of stabilized specimens was collected from 1.0 m to 2.0 m and from 5.0 to 6.0 m depths from the airfield of Malmi located in the city of Helsinki in Southern Finland. According to the x-ray powder diffraction analysis, the main mineralogical components in the first sample were Albite, Phlogopite, Clinochlore, Microcline, and Illite, and in the second sample Phlogopite, Quartz, Actinolite, Microcline, and Clinochlore. The index properties are presented in Table 2, and mineralogical compositions in Figure 1 and Figure 2.

Table 2. Index properties of soft clay.

Sampling point	*Depth (m)*	*Water content (%)*	*pH*	*Density Qm (kg/m^3)*
SP1	1.0 – 2.0	82.1	6.2	1510
SP2	5.0 – 6.0	77.3	8.9	1540

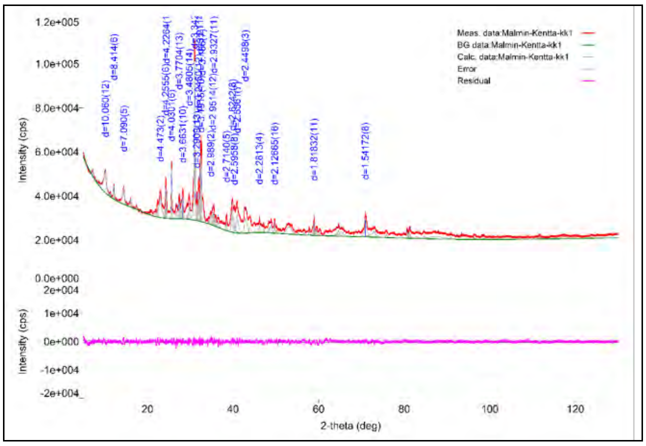

Figure 1. XRD of clay sample 1.

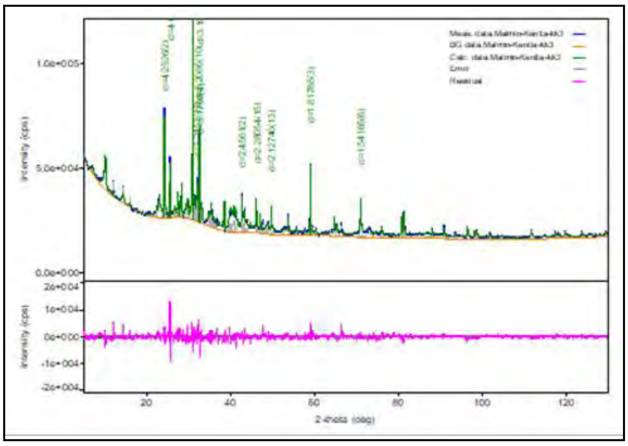

Figure 2. XRD of clay sample 2

Typically, laboratory pre-tests are needed with samples taken from different depths to optimize the binder content. The clay samples taken from the depths of 1…2 m (SP1) and 5…6 m (SP2) had slightly different water content (77.3 % and 82.1 %) and pH (6.2 and 8.9). Consequently, the calcined binder quantities from 120 kg/m^3 to 200 kg/m^3 were added into the clay samples SP1 besides 10 % or 30 % PG and binder quantities from 80 kg/m3 to 160 kg/m^3 with PG contents of 10 % and 30 % were added to the samples SP2. The mixes were blended in an electric mixer and three replicate specimens were prepared to test mechanical properties. Unconfined compressive strength and the vertical strain were measured after 28 days and 90 days curing.

Life cycle analysis (LCA) was conducted according to the standard for assessment of greenhouse gases ISO 14067, besides the standards for life cycle analysis ISO 14040 and ISO 14044. The assessed phases comprised the acquisition of raw materials (A1), their transport to the processing (A2), and the production of the final product (A3). The data was based on the information from raw material producers and the emission coefficients were from public sources. Emission from commercial gypsum was used in the LCA due to unavailable information on the emissions of the processed PG.

3. RESULTS AND DISCUSSION

Figure 3 shows average compressive strength results after 28 days and 90 days when using a binder with a PG quantity of 10 % and Figure 4 with a PG quantity of 30 %. The results indicate increased compressive strength along with higher binder quantity and higher PG quantity. All the results except SP1 120 kg/m^3 met the minimal strength requirement of 100 kPa already after 28 days. Clay samples SP2 gained higher strength (654 kPa and 1550 kPa) than clay samples SP1 (215 kPa and 764 kPa) when comparing 90 days strength results with binder quantities of 160 kg/m^3.

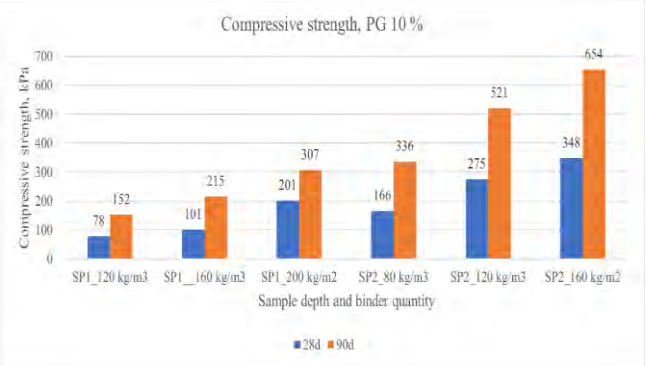

Figure 3. Strength results of the binders with PG 10 %.

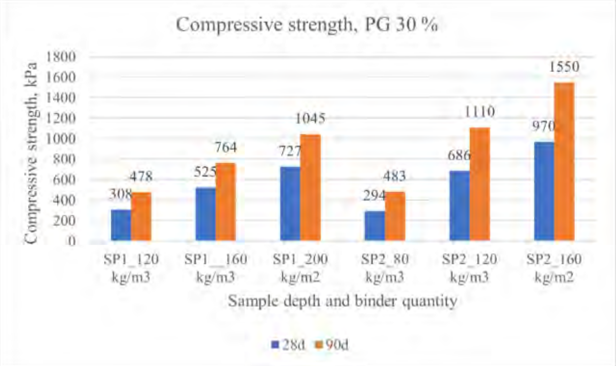

Figure 4. Strength results of the binders with PG 30 %.

Based on the compressive strength results with two PG quantities, a PG addition of 20 % was used in the LCA. Greenhouse gas emissions (GHG) from the production of one product tonne of final stabilization binder product are presented in Table 3 and Table 4.

According to the LCA, it can be stated that one tonne (1,000 kg) of TapoEko stabilization cement produces 115.5 kg CO_2-eq/tonne greenhouse gases, which of them are 65.05 kg CO_2-eq/tonne fossil and 50.45 kg CO_2-eq/tonne biogenic. Acquisition of raw materials (A1) provides only 7 %, transportation (A2) 14 % of emissions, and production 79 %. Biogenic emissions are mainly produced from the calcination process, where changes in the chemical composition of GLD release biogenic carbon dioxide.

Table 3. LCA category based GHG emissions.

Results	kgCO2e/tonne
A1 Raw materials acquisition	8.20
A2 Transport	15.90
A3 Production	91.40
Total	115.50

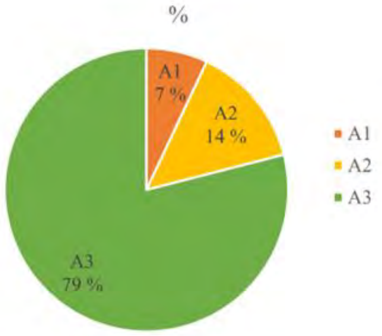

Table 4. GHG emissions from the production of one product ton of final stabilization binder product.

Life Cycle Category	kg CO_2-eq/tonne
A1 – Raw materials acquisition	8.20
A2 – Raw materials transportation	15.48
A2 – Raw materials transportation (Biogenic)	0.42
A3 – Reception and storage	0.63
A3 – Raw materials mixing	1.58
A3 – Production facilities	3.16
A3 – Transport	0.00
A3 – Calcination	35.99
A3 – Calcination (Biogenic)	50.03
A3 – Classification/milling	0.00
A3 – Pre-storage	0.00
A3 – Grinding/blending	0.00
A3 – Intermediate storage	0.00
Total	115.50

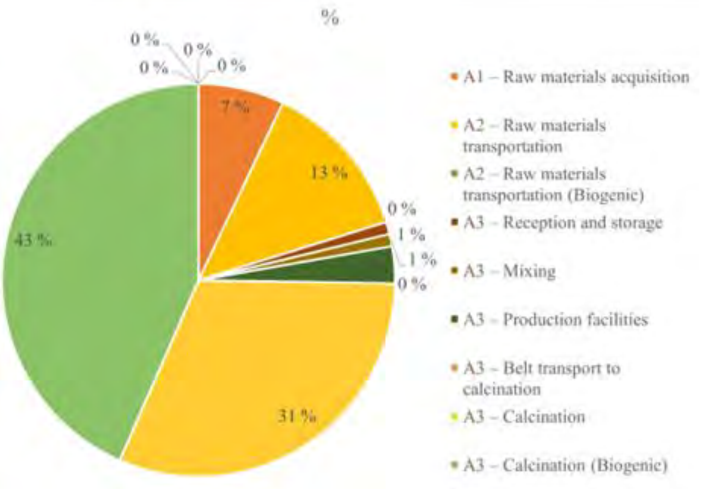

4. CONCLUSION

First, the analyses with two different soft clays and different binder quantities indicate that high (up to 1,550 kPa (90 days) compressive strength results can be gained with a moderate 160 kg/m^3 binder quantity when using a binder based on wastes generated by paper and pulp mills. In practice, a lower quantity (120 kg/m^3) with PG 10 % would be sufficient. Secondly, LCA results confirm the amount of kg CO2-eq/tonne fossil emissions providing a good potential to reduce CO_2 emissions of deep stabilization works when replacing Portland cement and quicklime. In addition, replacing natural gas with, for example, biofuel or electricity would reduce CO_2 emissions furthermore.

5. REFERENCES

Barcelo, L., Kline, J., Walenta, & G., Gartner, E. (2014). Cement and carbon emissions. *Engineering Materials and Structures,* 47, 1055-1065.

British Standard B.S:C.P. 8004, “Code of Practice for Foundations,” British Standard Institution, London, 1986.

FMI. (2019). Environmental Product Declaration burnt quicklime, Franzefoss Minerals AS.

ISO 14067:2018 Greenhouse gases — Carbon footprint of products — Requirements and guidelines for quantification

EN ISO 14040:2006+A1:2020 Environmental management. Life cycle assessment. Principles and framework

ISO 14044:2006 Environmental management — Life cycle assessment — Requirements and guidelines

NGF. (2012). Guide for deep mixing with lime-cement columns [In Norwegian]. Norwegian Geotechnical Society.

UPCYCLING WASTE POWDER INTO SUPPLEMENTARY CEMENTITIOUS MATERIALS THROUGH A TWO-STEP WET CARBONATION PROCESS

Wenwen LIAN[a], Danni QU[a], Renjie ZHOU[a], **Xiaoliang FANG**[a,*]

[a] School of Civil & Environmental Engineering and Geography Science, Ningbo University,
Ningbo, Zhejiang, China
[*]Corresponding author: fangxiaoliang@nbu.edu.cn

The powder fraction of C&D wastes lacks of reuse applications and consumes the landfill capacity of major cities. The wet carbonation approach has been proven effective for turning waste powder into potential value-added materials. This study utilized the products derived from wet carbonation methods as SCMs to benefit the cement hydration process. The chemical composition, particle size distribution, and pozzolanic activity of the Ca-rich and Si-rich products were tested and analyzed respectively. A series of comparative experiments were conducted to investigate the effects of incorporating the two products of wet carbonation into the cement hydration process. The heating rate was monitored through an Isothermal Conduction Calorimetry (ICC) device to analyze different mixtures. The chemical properties of sampled hydrated binder mixtures at the age of 3d, 7d, and 28d were determined by X-ray fluorescence, X-ray diffraction, Fourier Transform infrared spectroscopy, and Thermal gravimetric analysis. The microscopic observation was conducted through a scanning electron microscopy device. The results indicated that both the Ca-rich residue and Si-rich gel can be used as SCMs to improve cement hydration.

Keywords: recycled powder; wet carbonation; upcycling; supplementary cementitious material

METHODS FOR EVALUATING CARBONATION DEGREE OF STEEL SLAG, C_3S AND CARBIDE SLAG

Qi Zhang[1], Pan Feng[1, *], Xuyan Shen[1]

[1]Jiangsu Key Laboratory of Construction Materials, School of Materials Science and Engineering, Southeast University, Nanjing 211189, China
E-mail (corresponding author): pan.feng@seu.edu.cn

1. INTRODUCTION

Cement concrete has become an indispensable and important material for the development of the world today. However, the CO_2 emitted during the production of cement is as high as 8-9% of the total CO_2 emissions [1], and excessive carbon emissions are harmful to the ecological environment. As early as the 1970s, researchers had placed concrete under CO_2 atmosphere for curing, that is, carbonation curing [2] [3]. This allowed CO_2 to be stored in the concrete for a long time. If all cement-based materials are used for carbonation curing, a large amount of CO_2 can be absorbed and sequestered, which is of great significance for the realization of carbon neutrality in the cement concrete industry.

The carbonation degree reflects the actual amount of carbon sequestration of materials, which is an important indicator to evaluate the environmental benefits of material carbonation treatment. In practical applications, it can guide the selection of materials and the setting of carbonation environmental conditions, which is conducive to efficient and rapid fixing of CO_2, while saving costs, reducing or even avoiding secondary pollution to the environment. Therefore, it is of great significance to achieve accurate and simple measurement and calculation of carbonation degree. However, for different materials and different carbonation conditions, there is still a lack of systematic and specific research on whether the current carbonation degree calculation methods [4-6] are all applicable and can get accurate carbonation degree results.

In this paper, three evaluation methods of carbonation degree were systematically compared from the point of view of the changes of carbonation reactive phase, carbonated products and carbonation reaction process: the consumption of carbonation reactive phase, the production of $CaCO_3$ and $MgCO_3$ and the dry mass change of carbonation reaction. The carbonation degrees of steel slag, C_3S and carbide slag under w/c = 0 and w/c = 0.15 were evaluated by these three methods, the reasons for the influence of material type and water-cement ratio on the carbonation degree were explained, and the characteristics and relationships among the three methods under 6 cases were compared and analyzed. The aim is to determine one or more methods that can accurately and easily calculate the carbonation degree, so as to evaluate the actual carbon sequestration of materials and provide guidance for the improvement of carbonation process.

2. MATERIALS AND METHODS

1. Materials

Steel slag, specific surface area is 1.317 m^2/g; C_3S, specific surface area is 1.242 m^2/g; carbide slag, specific surface area is 1.413 m^2/g.

2. Carbonation condition

Respectively weigh 2 g of dry steel slag, C_3S and carbide slag, set water-cement ratio of 0 and 0.15, and put them in a PTFE box with a diameter of 4 cm and make them evenly distributed. Carbonation was carried out for 0.5 h, 2 h, 4 h, 6 h, 12 h, 1 d, 2 d, 3 d, 7 d and 14 d in a carbonation chamber with a temperature of 25 ºC, relative humidity of 60% and CO_2 concentration of 40%, respectively. The samples were dried under vacuum at 45 ºC for 3 days, and then screened with a 200-mesh screen and stored for subsequent testing.

3. Evaluation method of carbonation degree

(1) Carbonation degree based on the consumption of carbonation reactive phase

$$\alpha r_{QXRD} = \frac{\omega(initial\ carbonation\ reactive\ phase) - \omega(final\ carbonation\ reactive\ phase)}{\omega(initial\ carbonation\ reactive\ phase)} \times 100\%$$

(2) Carbonation degree based on the production of $CaCO_3$ and $MgCO_3$

$$Theoretical\ CaCO_3\ production = \frac{M(CaCO_3)}{M(CaO)} \times \omega(CaO - \frac{M(CaO)}{M(CaCO_3)} \times CaCO_3 - \frac{M(CaO)}{M(SO_3)} \times SO_3)$$

$$Theoretical\ MgCO_3\ production = \frac{M(MgCO_3)}{M(MgO)} \times \omega(MgO)$$

By QXRD:

$$\alpha g_{QXRD} = \frac{\omega(final\ CaCO_3) - \omega(initial\ CaCO_3) + \omega(final\ MgCO_3) - \omega(initial\ MgCO_3)}{Theoretical\ CaCO_3\ production + Theoretical\ MgCO_3\ production} \times 100\%$$

By TG:

$$\omega g_{CO_2-Ca} = \omega_{ML}(CaCO_3) - \omega_{rawML}(CaCO_3) \qquad \omega g_{CO_2-Mg} = \omega_{ML}(MgCO_3) - \omega_{rawML}(MgCO_3)$$

$$\omega g_{CaCO_3} = \omega g_{CO_2-Ca} \times \frac{M(CaCO_3)}{M(CO_2)} \qquad \omega g_{MgCO_3} = \omega g_{CO_2-Mg} \times \frac{M(MgCO_3)}{M(CO_2)}$$

$$\alpha g_{TG-CO_2} = \frac{\omega g_{CO_2-Ca} + \omega g_{CO_2-Mg}}{Theoretical\ CO_2\ uptake} \times 100\%$$

$$\alpha g_{TG} = \frac{\omega g_{CaCO_3} + \omega g_{MgCO_3}}{Theoretical\ CaCO_3\ production + Theoretical\ MgCO_3\ production} \times 100\%$$

(3) Carbonation degree based on dry mass change of carbonation reaction

$$\alpha m = \frac{\frac{m_d - m_0}{m_0}}{Theoretical\ CO_2\ uptake} \times 100\%$$

3. RESULTS AND DISCUSSION

Figures 1-3 shows the carbonation degree of steel slag, C_3S and carbide slag measured by several methods in section 2 when w/c = 0 and w/c = 0.15, respectively. In general, several methods of the calculated results show similar trend, and are qualitative methods to carbonation degree. Carbide slag has the highest carbonation degree, while C_3S and steel slag have a lower carbonation degree. With the increase of carbonation time, the carbonation degree increases first and then tends to be stable, and it is difficult to completely carbonate. Compared with w/c = 0, the carbonation degree of the three materials increased significantly when w/c = 0.15, indicating that liquid water promoted the carbonation reaction of the three materials, among which, compared with steel slag, liquid water had a higher promotion effect on C_3S carbonation. For C_3S, α-C_2S and β-C_2S, the carbonation process is that calcium ions are first dissolved in minerals, and then Ca^{2+} and CO_3^{2-} undergo carbonation reaction to produce $CaCO_3$ [7] [8]. C_3S has a higher dissolution rate than that of C_2S. Therefore, in the presence of liquid water, the dissolution degree of C_3S is greater than that of steel slag, which may be the reason why liquid water has a more significant promoting effect on the carbonation of C_3S.

Comparing the results of several methods, it can be seen that αr_{XRD} and αg_{XRD} are measured by quantitative XRD, ignoring the consumption or formation of amorphous phase. However, due to the small number of amorphous forms involved in the carbonation reaction, the calculated results of the two are close. αg_{XRD} and αg_{TG-Ca} are respectively measured by quantitative XRD and TG, which have the same physical meaning. Therefore, the calculated results are highly consistent, and the slight differences may be due to errors between the two testing instruments [6]. Both $\alpha g_{TG\text{-}Ca}$ and $\alpha g_{TG\text{-}CO2}$ are measured by TG. The former evaluates the degree of $CaCO_3$ and $MgCO_3$ generation, while the latter evaluates the degree of CO_2 fixation. However, due to the same calculation basis, the results show a linear relationship. $\alpha g_{TG\text{-}CO2}$ and αm are respectively measured by TG and weighing method. The former only considers the fixed CO_2 in the form of $CaCO_3$ and $MgCO_3$, while the latter assumes that all the sample quality changes before and after carbonation reaction come from the fixed CO_2. Therefore, the difference between these two methods is relatively large in general.

Through the above analysis it can be seen that there are similar results among αr_{XRD}, αg_{XRD}, $\alpha g_{TG\text{-}Ca}$ and $\alpha g_{TG\text{-}CO2}$. However, there is a large deviation between αm and the results obtained by other methods, especially when w/c=0.15. This may be due to the experimental error caused by the sample not being completely dried when αm is measured. In addition, liquid water may exist as structural water in the hydration products since the steel slag and C_3S may hydrate at w/c =0.15. Thus, the sources of increased mass in αm may include fixed CO_2 and water that is not fully dried or participating in the reaction. But the specific reasons need to be further studied.

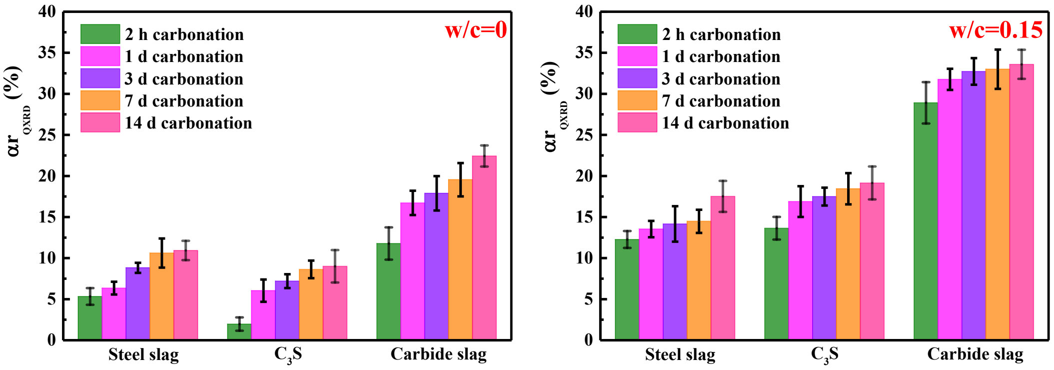

Fig.1. Carbonation degree based on consumption of carbonation reactive phase

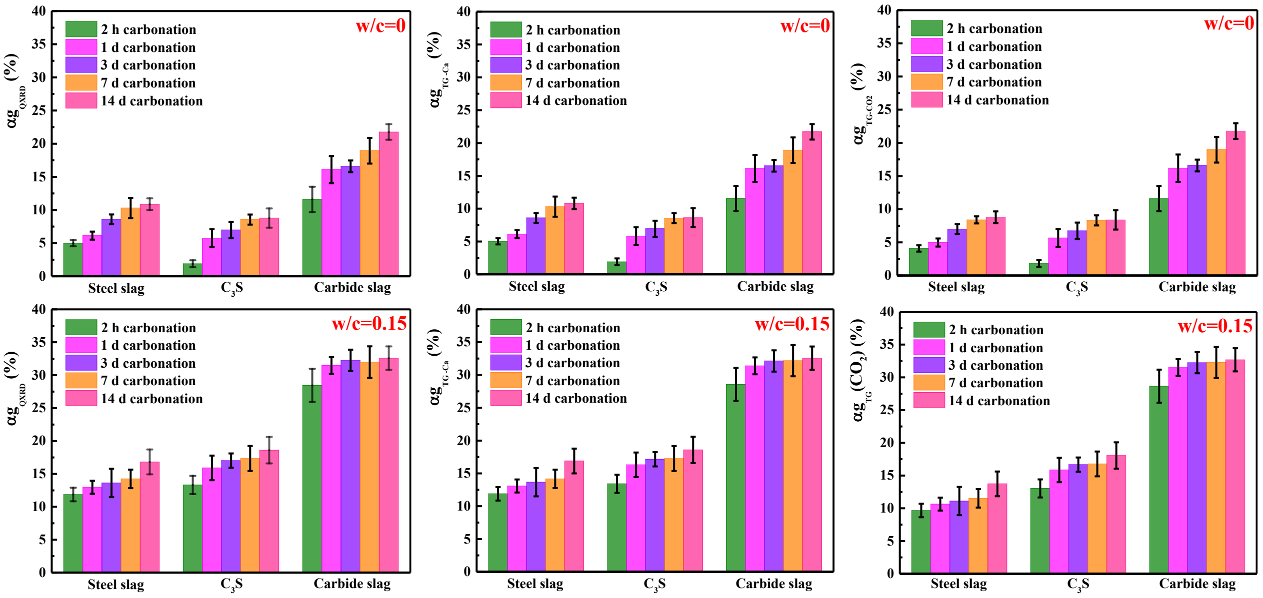

Fig.2. Carbonation degree based on the production of $CaCO_3$ and $MgCO_3$

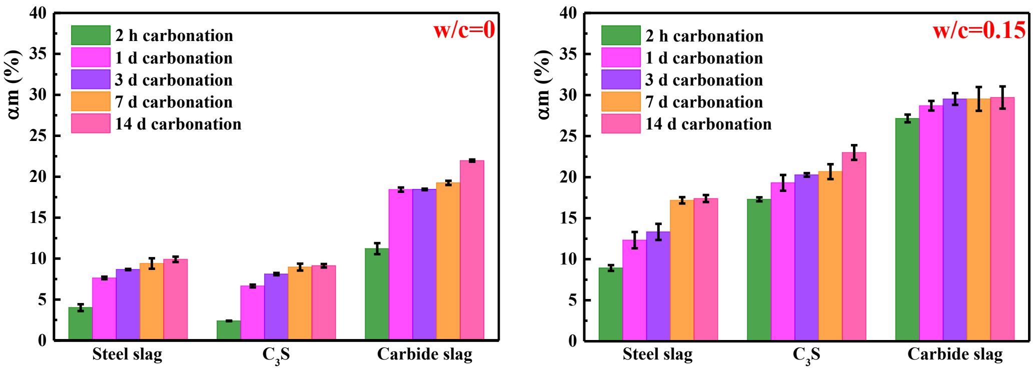

Fig.3. Carbonation degree based on dry mass change of carbonation reaction

4. CONCLUSION

1. Several methods for evaluating carbonation degree show that: compared with steel slag and C_3S, carbide slag has the highest carbonation degree because it contains the largest amount and most easily carboned phases; liquid water can significantly promote the carbonation reaction by increasing the dissolution of CO_2 and the dissolution of calcium and magnesium, and furthermore improve the efficiency of carbonation reaction.

2. The results of αr_{XRD}, αg_{XRD}, αg_{TG-Ca} and αg_{TG-CO2} are similar and there is a large deviation from αm, which is possibly related to the water that is not fully dried or participating in the reaction. αm may not be a suitable method for quantitative evaluation of carbonation degree. However, due to αm can qualitatively reflect and compare the carbonation degree of materials, and the test is relatively simple, it is also a method that cannot be ignored.

5. ACKNOWLEDGMENT

This work was financially supported by the National Natural Science Foundation of China (Nos. 51890904, 52078126, 52122802, and 51825203), Science and Technology Innovation 2025 Major Project of Ningbo (No. 2020Z040), Jiangsu Provincial Department of Science and Technology Innovation Support Program (No. BZ2022036)

6. REFERENCES

[1] T. Chen and X. Gao. (2019). Effect of Carbonation Curing Regime on Strength and Microstructure of Portland Cement Paste. Journal of CO2 Utilization, 34, 74-86.

[2] J. F. Young, R. L. Berger, and J. Brees. (1974). Accelerated Curing of Compacted Calcium Silicate Mortars on Exposure to CO_2. Journal of the American Ceramic Society, 57, 394-397.

[3] R. L. Berger, J. F. Young, and K. Leung. (1972). Acceleration of Hydration of Calcium Silicates by Carbon Dioxide Treatment. Nature Physical Science, 240, 16-18.

[4] S. Kashef-Haghighi and S. Ghoshal. (2010). CO_2 Sequestration in Concrete through Accelerated Carbonation Curing in a Flow-through Reactor. Industrial & Engineering Chemistry Research, 49, 1143-1149.

[5] D. Zhang and Y. Shao. (2016). Early age carbonation curing for precast reinforced concretes. Construction. Building. Materials, 113, 134-143.

[6] Z. Ghouleh, R. I. L. Guthrie, and Y. Shao. (2017). Production of carbonate aggregates using steel slag and carbon dioxide for carbon-negative concrete. Journal of CO2 Utilization, 18, 125-138.

[7] L. Hu et al. (2022). An insight of carbonation-hydration kinetics and microstructure characterization of cement paste under accelerated carbonation at early age. Cement and Concrete Composites, 134, 104763.

[8] I. K. Jeon, A. Qudoos, and H. G. Kim. (2021). Influence of carbonation curing on hydration and microstructure of magnesium potassium phosphate cement concrete. Journal Building Engineering, 38, 102203.

SIMULATION OF FLUE GAS FOR CURING CEMENT COMPACTS: INFLUENCE OF GAS IMPURITIES

Hao Yu[1], Tung-Chai Ling[1,*]

[1]College of Civil Engineering, Hunan University, Changsha-410082, China
*Corresponding author email: tcling@hnu.edu.cn; tcling611@yahoo.com

1. INTRODUCTION

Flue gas CO_2 curing of calcium-based construction materials has recently received great attention for its potential CO_2 sequestration ability on a large scale (He et al., 2020). Based on the literatures, flue gas with a CO_2 concentration of 10-20% (Kemache et al., 2017) can be utilized for CO_2 curing and attained considerable performance compared with reported CO_2 curing with high purity or concentration of CO_2 (> 99.9%) (Horgnies et al., 2015; Liu et al., 2010). However, industrial flue gas generally contains a small amount of typical gas impurities, including sulfur compounds (SO_2) (< 3000ppm), nitrogen oxide compounds (NO_X) (< 1000ppm), fly ash, soot (unburnt carbon) and trace elements, even after purifying process (Lin et al., 2020; Pan et al., 2017). The presence of impure components in flue gas, such as SO_2 and NO_2 may dissolve and compete with CO_2 for carbonation and hydration reactions.

Compared with CO_2 (1.7g/1kg water), SO_2 (110g/1kg water) and NO_2 have a higher solubility. Therefore, strong acid ions of SO_4^{2-} and NO_3^- would be quickly formed, leading to a significant pH reduction in the pore solution of cement paste (Li et al., 2016; Liu et al., 2010), and this will eventually alter the carbonation efficiency. The presence of SO_2 is known to interfere with CO_2 reaction, and the competing effect is highly dependent on the H_2O content for its acceleration on both carbonation and sulfation reaction of calcium oxide (Chen et al., 2021). Also, the SO_2 is expected to react with $CaCO_3$ as well as CH in a high-pressure environment, and these chemical reactions would further release water and CO_2 with precipitations of sulfate compounds, such as gypsum and ettringite. As for NO_2, it will only react with the hardened cement pastes with the presence of activated materials such as carbon powder (Horgnies et al. 2015). Since hydration and carbonation behaviors always simultaneously occur in the CO_2 curing process of cement compacts (Xian et al., 2021), gas impurities could also have a significant impact on cement hydration behavior. Therefore, it is important to understand the influence of multi-components gas impurities on CO_2 curing process.

The aim of this study is to elcidate the presence of gas impurities (SO_2 and NO_2) on CO_2 curing and hydration of cement compacts. The mechanical performance and microstructural changes of cement compacts were examined at different designed curing ages.

2. EXPERIMENTAL PROGRAM

2.1 Materials and sample preparation

Ordinary Portland cement (OPC), P.I 42.5, complying with the Chinese Standard GB8076-2008, was used for the production of dry-mix cement compact. The chemical compositions are presented in Table 1. OPC was mixed with water at a water-to-cement (w/c) ratio of 0.15, and then immediately compacted (10 Mpa) into a prismatic stainless-steel mold with a dimension of 20×20×20 mm (Li & Ling, 2020). After that, the compact samples were demolded for flue gas CO_2 curing.

Flue gas used in this study was supplied by an industrial gas manufacturer from Jining, China. To simulatethe actual flue gas emitted from incineration power plant, the flue gas was desgined with 15 vol% CO_2, 10 vol% O_2, 74.9 vol% N_2, 500 ppm SO_2, and 500 ppm NO_2. For comparision, control cement compacts was cured with 15% concentration of pure CO_2 (in which the remaining 85% was mixed with pure N_2).

Table 1 Chemical and physical properties of P.I. 42.5 Portland cement

Mineral composition of cement (% by weight)											
SiO_2	Al_2O_3	Fe_2O_3	CaO	MgO	SO_3	R_2O	f-CaO	C_3S	C_2S	C_3A	C_4AF
21.20	4.93	3.98	64.42	1.52	0.96	0.53	0.87	59.53	15.86	6.31	12.10

Physical properties						
Specific gravity (m^2/kg)	Density (g/cm^3)	Water demand for normal consistency	Setting time (min)		Compressive strength (MPa)	
			Initial setting	Final setting	3-d	28-d
357	3400	24.60%	95	156	28.0	53.5

2.2 Carbonation set-up

The obtained samples were placed into a sealed carbonation autoclave, exposed to flue gas (F) and control gas (C) CO_2 curing (20 °C, 65% RH, 0.1 MPa), respectively. All the cement compacts was cured with flue gas (F) and pure CO_2 gas (C) for 2 h at 20 °C and 65% RH, prior subsequent water curing (20 °C) until testing ages at 1, 3, 7, 14 and 28 days. The details of curing regime and notation are presented in Fig. 1. Sample notation was followed by rule of "CO_2 curing-Water curing"; for example, "F2h-W1d" represents the samples that cured with 2-h flue gas and 1-d water curing.

2.3 Testing methods

Three cement compacts were used for the determination of compressive strength. The loading rate was fixed at 0.5 N/min in accordance with Chinese Standard GB/T 17671-1999. Fractured samples obatined from most outer layer (<1mm) was used for analythical testing. Samples was immersed in isopropanol solvent for hydration stopping (Zhang & Scherer, 2011). After drying and grinding, powder samples with size below 75μm was used for Thermogravimetry Analysis (TGA) test (Rigaku TG-DTA 8121H). About 10±1 mg of the powder sample was heated from 25°C to 1000°C at a rate of 10°C/min under a 30 ml/min flow of N_2 gas. Based on TGA results, the hydration degree (HD) and carbonation degree (CD) can be calculated using Eqs. (1)-(4) (Li & Ling, 2020):

$$CO_2\ (\text{wt.\%}) = \frac{\Delta m_{500°C\text{-}950°C}}{m_{950°C}} \times 100 \tag{1}$$

$$CO_{2\text{uptake}}\ (\text{wt.\%}) = \frac{CO_{2\text{carbonated}}\ (\text{wt.\%})\text{-}CO_{2\text{initial}}\ (\text{wt.\%})}{100\text{-}CO_{2\text{carbonated}}\ (\text{wt.\%})} \times 100 \tag{2}$$

$$CD\ (\%) = \frac{CO_{2\text{uptake}}\ (\text{wt.\%})}{95\% \times TH_{CO_2}} \times 100 \tag{3}$$

$$HD\ (\%) = \frac{\Delta m_{\text{water, carbonation}}\text{-}\Delta m_{\text{water, initial}}}{M_{950°C} \times M_c \times TH_{\text{water}}} \times 100 \tag{4}$$

Where, $\Delta m_{500℃\text{-}950℃}$ is the mass loss due to the decomposition of $CaCO_3$; $m_{950°C}$ is the dry mass of sample weighed at 950°C; TH_{CO_2} is the maximum theoretical CO_2 uptake of cement (0.511) according to Xuan et al. (2018); $\Delta m_{\text{water,carbonation}}$ and $\Delta m_{\text{water,initial}}$ represent the mass loss of carbonated samples at 105-550 °C and uncarbonated samples at 105-550 °C, respectively; TH_{water} (0.24) is the theoretical required water for cement to be fully hydrated (Feng et al., 2004).

3. RESULTS AND DISCUSSION

The compressive strength of cement compacts exposed to simulated flue gas and pure CO_2 curing along with subsequent water curing is presented in Fig. 1. In general, C2h exhibited a relatively high compressive strength after 2 hours of pure CO_2 curing due to theformation of carbonation precipitates to densify the pores and enhance the mechanical rigidity of the cement paste matrix (Li & Ling, 2020). In comparison, the presence of gas impurities in flue gas CO_2 curing could lead to a

30% reduction in compressive strength due to the inhibition of CO_2 precipitation by SO_2. However, the negative impact of gas impurities became less obvious with prolonged the hydration time, particularly noticed at 1 day. The compressive strength of both compacts reached nearly 80 MPa after 28 days of subsequent water curing.

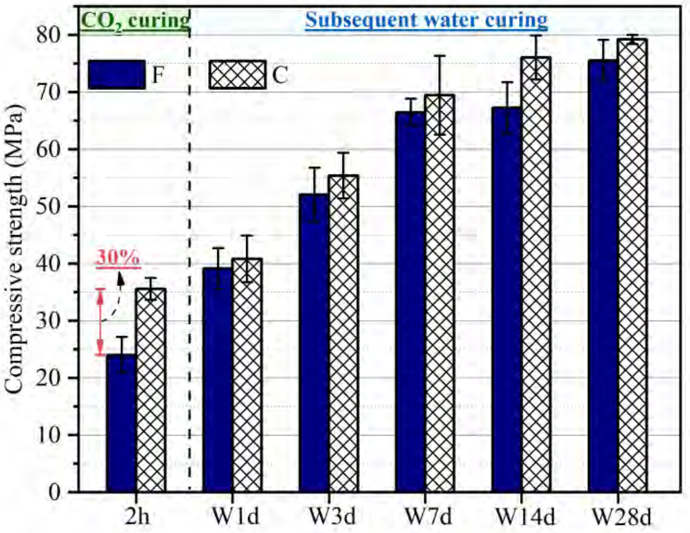

Fig. 1. Comparison of compressive strength of cement compacts exposed to flue gas and pure CO_2 curing.

The carbonation degree (CD) and hydration degree (HD) of cement compacts (F and C groups) cured at different ages are illustrated in Fig. 2. The presence of gas impuritiesreduced the carbonation efficiency due to the presence of SO_2 and NO_X. This is because these gases can compete with CO_2 and H_2O for calcium-based phases reaction (Li et al., 2016). The high solubility of such acid gases (Liu et al., 2010), endowed them with a high ability to capture calcium ions (Ca^{2+}) compared with CO_2 (Rasmussen et al., 2015). On the other hand, due to the strong oxidizing properties, SO_2 can potentially react and decompose the formed $CaCO_3$, leading to a lower carbonation efficiency in F2h sample. As water curing proceeded, CD of CO_2 curing group samples was aggressively increased until W28d. The simultaneous carbonation reaction with hydration was closely related to the continuous reaction of residual CO_2/CO_3^{2-} ions in cement pores (Li & Ling, 2020; Šavija & Luković, 2016). For flue gas cured samples, however, the carbonation degree was found to be slightly lower than that of CO_2 curing group samples despite a general increasing trend.

Similarly, an inferior hydration degree was also noticed in the F2h sample compared with corresponding C2h sample. However, this negative effect can be compensated by progressive hydration, particularly in the first 72 hours (3d). This explained the sharp increase of compressive strength observed in FC1d sample (see Fig. 1). This indicated that gas impurities, especially sulfur-kind components, can exert a positive impact on short-term hydration of the flue gas cured cement compacts. After 3-d, the increase of HD was not obvious, probably due to the simultaneous carbonation that consumed hydrates (Gunning et al., 2010).

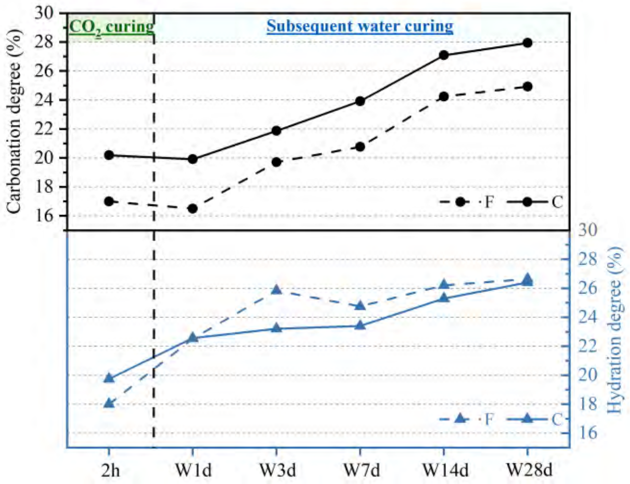

Fig. 2. Carbonation degree and hydration degree of F and C group samples at different curing ages.

4. CONCLUSION

This study examined the influence of gas impurities of flue gas CO_2 curing on the carboantion and progressive hydration of cement compacts. Experiment results showed that cement compacts subjected to 2-h of flue gas CO_2 curing attained a 33% lower compressive strength compared with that of pure CO_2, associated to the lower carbonation reactivity interferenced by the presence of acidic SO_2 and NO_X, which can compete with CO_2/CO_3^{2-} for calcium precipitation, thereby reduced the bonding efficiency of CO_3^{2-} ion. The progressive hydration alleviated this negative impact on the strength reduction, and achieved a comparable strength for both flue gas and pure CO_2 curing groups samples. Findings from this study highlight the essential consideration of gas impurities in flue gas CO_2 curing, and a need also required for exploring the durability characteristics and interactions of gas impurities at high temperature curing.

5. ACKNOWLEDGMENT

The authors would like to express appreciation for the support of National Natural Science Foundation of China (NSFC) The Research Fund for International Senior Scientists (52250710158).

6. REFERENCES

Chen, L., Dai, W., Wang, C., Wang, W., & Anthony, E. J. (2021). The combined effect of SO2 and H2O on CO2 capture performance by calcium looping. *Journal of CO2 Utilization*, *54*, 101798. https://doi.org/https://doi.org/10.1016/j.jcou.2021.101798

Feng, X., Garboczi, E. J., Bentz, D. P., Stutzman, P. E., & Mason, T. O. (2004). Estimation of the degree of hydration of blended cement pastes by a scanning electron microscope point-counting procedure. *Cement and Concrete Research*, *34*(10), 1787-1793. https://doi.org/https://doi.org/10.1016/j.cemconres.2004.01.014

Gunning, P. J., Hills, C. D., & Carey, P. J. (2010). Accelerated carbonation treatment of industrial wastes. *Waste Management*, *30*(6), 1081-1090. https://doi.org/https://doi.org/10.1016/j.wasman.2010.01.005

He, Z., Wang, S., Mahoutian, M., & Shao, Y. (2020). Flue gas carbonation of cement-based building products. *Journal of CO2 Utilization*, *37*, 309-319. https://doi.org/https://doi.org/10.1016/j.jcou.2020.01.001

Horgnies, M., Dubois-Brugger, I., Krou, N., Batonneau-Gener, I., Belin, T., & Mignard, S. (2015). Reactivity of NO2 and CO2 with hardened cement paste containing activated carbon. *The European Physical Journal Special Topics*, *224*, 1985. https://doi.org/10.1140/epjst/e2015-02515-7

Kemache, N., Pasquier, L.-C., Cecchi, E., Mouedhen, I., Blais, J.-F., & Mercier, G. (2017). Aqueous mineral carbonation for CO2 sequestration: From laboratory to pilot scale. *Fuel Processing Technology*, *166*, 209-216. https://doi.org/https://doi.org/10.1016/j.fuproc.2017.06.005

Li, X., & Ling, T.-C. (2020). Instant CO2 curing for dry-mix pressed cement pastes: Consideration of CO2 concentrations coupled with further water curing. *Journal of CO2 Utilization*, *38*, 348-354. https://doi.org/https://doi.org/10.1016/j.jcou.2020.02.012

Li, Y., Yi, H., Tang, X., Liu, X., Wang, Y., Cui, B., & Zhao, S. (2016). Study on the performance of simultaneous desulfurization and denitrification of Fe3O4-TiO2 composites. *Chemical Engineering Journal*, *304*, 89-97. https://doi.org/https://doi.org/10.1016/j.cej.2016.06.035

Lin, F., Wang, Z., Zhang, Z., He, Y., Zhu, Y., Shao, J., . . . Cen, K. (2020). Flue gas treatment with ozone oxidation: An overview on NOx, organic pollutants, and mercury. *Chemical Engineering Journal*, *382*, 123030. https://doi.org/https://doi.org/10.1016/j.cej.2019.123030

Liu, C.-F., Shih, S.-M., & Huang, T.-B. (2010). Effect of SO2 on the Reaction of Calcium Hydroxide with CO2 at Low Temperatures. *Industrial & Engineering Chemistry Research*, *49*. https://doi.org/10.1021/ie100924z

Pan, S.-Y., Wang, P., Chen, Q., Jiang, W., Chu, Y.-H., & Chiang, P.-C. (2017). Development of high-gravity technology for removing particulate and gaseous pollutant emissions: Principles and applications. *Journal of Cleaner Production*, *149*, 540-556. https://doi.org/https://doi.org/10.1016/j.jclepro.2017.02.108

Rasmussen, M. H., Wedel, S., Pedersen, K. H., Illerup, J. B., & Dam-Johansen, K. (2015). Initial reaction between CaO and SO2 under carbonating and non-carbonating conditions. *Chemical Engineering Science*, *134*, 169-177. https://doi.org/https://doi.org/10.1016/j.ces.2015.04.051

Šavija, B., & Luković, M. (2016). Carbonation of cement paste: Understanding, challenges, and opportunities. *Construction and Building Materials*, *117*, 285-301. https://doi.org/https://doi.org/10.1016/j.conbuildmat.2016.04.138

Xian, X., Zhang, D., & Shao, Y. (2021). Flue gas carbonation curing of cement paste and concrete at ambient pressure. *Journal of Cleaner Production*, *313*, 127943. https://doi.org/https://doi.org/10.1016/j.jclepro.2021.127943

Xuan, D., Zhan, B., & Poon, C. S. (2018). A maturity approach to estimate compressive strength development of CO2-cured concrete blocks. *Cement and Concrete Composites*, *85*, 153-160. https://doi.org/https://doi.org/10.1016/j.cemconcomp.2017.10.005

Zhang, D., Li, V., & Ellis, B. (2018). Optimal Pre-hydration Age for CO2 Sequestration through Portland Cement Carbonation. *ACS Sustainable Chemistry & Engineering*, *6*. https://doi.org/10.1021/acssuschemeng.8b03699

Zhang, J., & Scherer, G. W. (2011). Comparison of methods for arresting hydration of cement. *Cement and Concrete Research*, *41*(10), 1024-1036. https://doi.org/https://doi.org/10.1016/j.cemconres.2011.06.003

EFFECT OF PRESSURIZED CARBONATION DURATION ON PROPERTIES OF RECYCLED AGGREGATE CONCRETE

Long Li [a], Chi Sun Poon [bc]

[a] Department of Structural Engineering, Tongji University, Shanghai 200092, P.R. China
[b] Department of Civil and Environmental Engineering, The Hong Kong Polytechnic University, Hong Kong
[c] Research Centre for Resources Engineering towards Carbon Neutrality, The Hong Kong Polytechnic University, Hong Kong
E-mail: cecspoon@polyu.edu.hk (C.S. Poon)

The use of recycled coarse aggregate (RCA) produced from waste concrete in new concrete is an effective way to realize the recycling of construction and demolition waste. The utilization of accelerated carbonation to enhance RCA has attracted a lot attention because it can enhance performance of recycled aggregate concrete (RAC) and has potential for CO_2 sequestration. This study systematically investigated the influences of the duration of pressurized carbonation on the properties of RCA, RCA-new mortar interface, and RAC. The results showed that water absorption of carbonated RCA (CRCA) decreased with the increase of carbonation duration. But the beneficial effect of carbonation was less obvious after 1-day carbonation because most of calcium hydroxide and Ca-rich calcium silicate hydrates in RCA had reacted with CO_2 within 1 day. After using CRCA, the improvement in different performance indicators of RAC was dependent on different factors. The enhancement in compressive strength and chloride penetration resistance of RAC prepared with CRCA were dependent on the reduced porosity of CRCA. That was why they correlated with the water absorption of CRCA as carbonation duration increased. However, the decrease in initial absorption of water of RAC was mainly dependent on the denser surface layer of CRCA, rather than the reduced porosity of CRCA. This is because the denser surface layer can change water path from “penetrating through RCA” to “passing around RCA”. It is recommended to use 1-day carbonation to enhance RCA, which might have higher cost-effectiveness.

Keywords: Recycled aggregate concrete; Carbonation duration; Interface; Mechanical properties; Durabilit

CARBON(ATE) CEMENT: DREAM OR REALITY?

Min Wu

Department of Civil and Architectural Engineering, Aarhus University, Aarhus C, 8000,
E-mail: mnwu@cae.au.dk

Due to the large volume of production, the cement industry accounts for 8-10% of the global CO_2 emissions. Significant efforts have been made to reduce the carbon emissions and remarkable progresses have been achieved, such as the Limestone Calcined Clay Cement (LC3). Among the various strategies proposed, carbonate cement and concrete are an area that have attracted significant interests, since they can be directly coupled with Carbon Capture, Usage and Storage (CCUS) which is considered an essential approach to reach the demanding goal of “net-zero emissions” by 2050. Excellent work includes CO_2 curing of cement-based products, CO_2 mineralization of calcium-bearing wastes as supplementary cementitious materials, carbonated solid wastes as recycled concrete aggregates, pure calcium carbonate cement, etc.

The terminology “carbonate cement” or “carbonate binder” has been used in literature, while there is no clear definition, and the ambiguity causes confusion. This work firstly tries to provide a summary of the recent research progress on cementitious materials directly containing carbon/carbonates. Based on that, the differences among the various types of carbonate binders are discussed and the challenges are highlighted. The efforts aim to clarify potential confusions and propose clearer definitions for carbon/carbonate binders.

Keywords: Carbonate binder, CO_2 mineralization, low-carbon cement, supplementary cementitious materials, CCUS.

FROM WASTE TO VALUABLE PRODUCTS: INVESTIGATION OF CARBONATION PROCESSES WITHIN THE “BBCIRCLE” PROJECT

Masi, A.[1], Costa, G.[1]
[1]Department of Civil Engineering and Computer Science Engineering, University of Rome Tor Vergata, Rome 00133, Italy
alessandramasi96@gmail.com (corresponding author)

1. INTRODUCTION

The construction sector makes use of a very large quantity of raw materials and is characterized by a significant carbon footprint. It has been recently reported e.g. that only the materials used in the construction of buildings account for around 9% of overall energy-related CO_2 emissions (UNEP, 2022). In order to increase the sustainability of this sector, the use of alternative materials characterized by a lower associated carbon footprint, as well as suitable properties in view of the intended application, needs to be promoted. Carbonation processes can be exploited as a strategy to achieve this goal via the treatment of alkaline industrial residues.

Carbonation is the exothermic reaction between metal oxides (especially Ca and Mg-based ones) and CO_2 that leads to the formation of stable carbonate phases. This reaction occurs spontaneously in nature (silicate weathering) but it is possible to accelerate it by operating in controlled conditions. Over the years, growing interest has developed towards the use of alkaline industrial residues (rich in Ca-bearing reactive species) as feedstock for carbonation processes (Rahmanihanzaki & Hemmati, 2022), trying to valorize those waste streams that are often underutilized or disposed of in landfills (Gomes et al., 2016), as well as to store the reacted CO_2 in a permanent solid form.

Depending on the selected route (direct or indirect), different products can be obtained (Sanna et al., 2014) and many of these can also be employed in the construction sector. In this framework, carbonation can be regarded as both a strategy within the circular economy agenda and a CO_2 storage and utilization pathway. The work we present, developed in the framework of the regionally funded “BBCircle” project, was aimed at identifying and testing specific carbonation routes to treat different kinds of alkaline industrial residues generated in the Lazio region of Italy.

2. MATERIALS AND METHODS

The samples collected for this study came from different industrial sites located in the Lazio region. More in detail, we tested two types of recycled aggregates from construction and demolition waste: a fine fraction with a particle size below 4 mm (C&D_1) and a material presenting a broader size distribution with a maximum grain size of 31.5 mm (C&D_2); three residues from a biomass-fired power plant: the bottom ash (BA_b) collected from the grid, the fly ash (FA_b) collected from the boiler and the air pollution control ash (APC_b) coming from the bag filters; four residues from an RDF incineration plant: two types of bottom ash collected with wet and dry technology (BA_r1 and BA_r2), the fly ash from the electrostatic precipitator (FA_r) and another ash sample from the bag filter, which the producer named sodium residual product (PSR).

All samples were characterized from an elemental and mineralogical point of view by alkaline fusion followed by ICP-OES analysis of the obtained digestates, and XRD analysis, respectively. The environmental behavior of each material was evaluated according to the standardized EN 12457-2 leaching test, while the inorganic/organic carbon content was obtained following the UNI-EN 13137 procedure. Based on the results of the characterization phase, the residues presenting the highest content of potentially reactive Ca phases were identified and tested in preliminary carbonation tests performed under enhanced conditions (3 bar CO_2 pressure and 50°C,), pre-milling the samples to d<200 µm, if required. Two direct aqueous phase routes were tested, the thin film one, adopting a liquid to solid ratio (L/S) of 0.2 l/kg and the slurry phase one, carried out employing a L/S of 5 l/kg. On the basis of the results of these two phases, tailored direct and indirect carbonation-based treatments for producing alternative construction materials were selected and tested on specific types of residues.

In the direct route tests, carbonation was coupled with a granulation step and the effects of different combinations of the treatments were assessed in terms of product properties. Specifically, the resulting aggregates were characterized in terms of particle size distribution (ASTM D422), environmental behavior and mechanical strength (ACV test, BS 812-110:1990).

In the indirect carbonation tests aimed at producing high-purity calcium carbonate, several extracting agents were tested for enhancing the dissolution of Ca at different L/S ratios applying an extraction time of 1 h: three strong acids, two weak acids and two ammonium salts.

The influence of the molarity of the extracting agent on Ca dissolution efficiency was evaluated for nitric acid, citric acid and ammonium nitrate. Preliminary $CaCO_3$ precipitation tests were carried out bubbling CO_2 at 1 bar in the solution resulting from the extraction tests; an alkaline solution (5M NaOH) was added when necessary to buffer the pH, in order to allow the precipitation reaction to proceed.

3. RESULTS AND DISCUSSION

From the analysis of the elemental composition of the tested alkaline residues, the most abundant constituents for all of the analyzed samples resulted Al, Ca, Fe, K, Mg, Na and Si. In particular, the Ca concentration ranged from 10 to 20%wt. for the majority of the samples, with the exceptions of PSR and APC_b that presented a much lower concentration of this element and therefore a low carbonation potential. In general, it was observed that the residues collected from the waste to energy plant presented a higher concentration of constituents of potential environmental concern such as Cr, Ni, Pb, Sb, Zn and Cu. The main Ca-bearing species identified by XRD analysis were mixed Ca silicates, mainly belonging to the melilite group, which are known to be less prone to react with CO_2 (Baciocchi et al., 2010), detected in the C&D samples and in the two types of BA from the incineration plant and Ca oxides, found in samples FA_b and FA_r.

With regard to the environmental behavior, as expected, the materials that proved to be more critical were those deriving from the air pollution control treatment units of both the thermal treatment plants, especially those from the RDF incinerator, given the presence in the leachate of substances of concern such as Pb, Sb, Cl^- and SO_4^{2-} in concentrations exceeding the limits foreseen for disposal in hazardous waste landfills according to the Italian legislation.

The highest potentially reactive Ca content, associated to different mineralogical species characterized by a diverse reactivity, were obtained for FA_b, BA_r1,2 and FA_r, with values ranging from 12 to 20%wt. On these samples we decided to perform some preliminary direct carbonation tests under thin-film and slurry conditions to determine the resulting CO_2 uptake achieved (the amount of CO_2 stored measured by inorganic carbon analysis per 100 g of dry residue). The results are shown in Figure 1.

The maximum mean CO_2 uptake (12%wt.) was achieved for FA_r under slurry conditions, which seemed to be more efficient for all of the tested residues with the exception of FA_b, when considering the maximum uptake obtained.

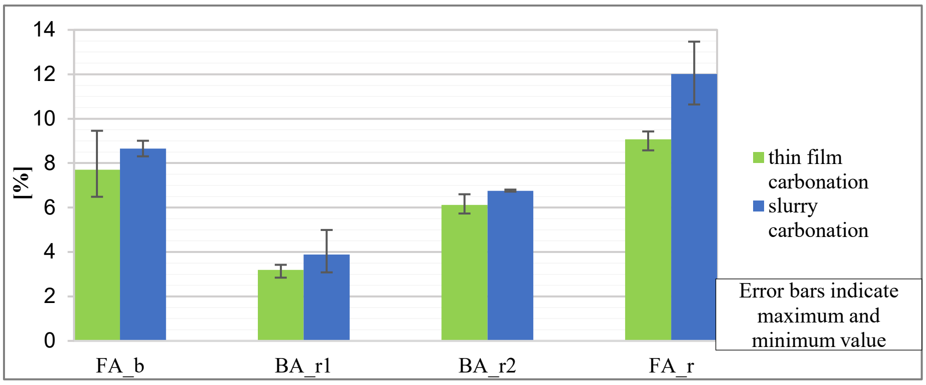

Figure 1. CO_2 uptake resulting for the thin film and slurry route tests performed on the selected residues

We then performed further leaching tests on the carbonated products to assess the effects of the tested treatments on the environmental behavior of the materials. As already observed in previous studies (e.g.: Lin et al., 2015; Baciocchi et al., 2010), carbonation proved to be effective in reducing the leachability of amphoteric constituents such as Pb and Zn, while an opposite effect was observed for oxyanionic-forming ones like Cr and Sb.

The following step allowed to identify the carbonation-based treatment routes to apply to the different materials we tested. Given their overall higher reactivity and their initial fine particle size, for FA_b and FA_r we selected a direct carbonation process coupled with a granulation phase, which might also be beneficial in improving the environmental behavior of the products, aimed at obtaining aggregates. For the BA samples, instead, we opted for an indirect treatment, which should allow to obtain a high purity $CaCO_3$ product. These routes are currently being tested.

For the direct carbonation process, we obtained aggregates from the two types of fine residues combining granulation with pre and post carbonation. The products obtained in both configurations were characterized by a much larger particle size with respect to the initial materials, exhibiting a d50 increase of roughly two orders of magnitude. The CO_2 uptake evaluated after a 28-day curing period was the highest, around 6%wt., when pre-carbonation was applied for both FA_b and FA_r. The ACV values obtained for the FA_r aggregates (FA_b aggregates could not be tested with this procedure) were never below 60%, indicating a limited strength of the product. However, the lowest values, corresponding to the highest strengths, were obtained with the post carbonation treatment. Also in this case, the implemented treatments showed to yield both positive and negative effects on the leachability of different constituents of the products, indicating that critical aspects related to the environmental behavior of these materials persist.

For the indirect route, all the tests mentioned in this work were performed on BA_r2. As shown in Figure 2, the use of different extracting agents led to different dissolution efficiencies; it is worth comparing the different behavior of hydrochloric and nitric acid, which were able to dissolve 100% of the Ca content of the residue, to that of the ammonium salts, for which the maximum amount of Ca extracted was 40%. Apart from the extraction efficiency, which is obviously of paramount importance, another key aspect is Ca affinity; in fact, the lower the affinity, the more difficult it is to obtain a pure carbonate. The results we obtained confirmed an inverse correlation of these two parameters, i.e. a higher affinity was obtained employing the ammonium salts.

Using the filtered (0.45 µm) solution obtained with 1M NH_4NO_3 at L/S=200 l/kg, preliminary carbonation tests were carried out; a high carbonation efficiency was obtained even after relatively low carbonation reaction times, reaching a maximum of 95.8% after 45 min. Other $CaCO_3$ precipitation tests are being performed employing the solutions resulting from the use of other extracting agents.

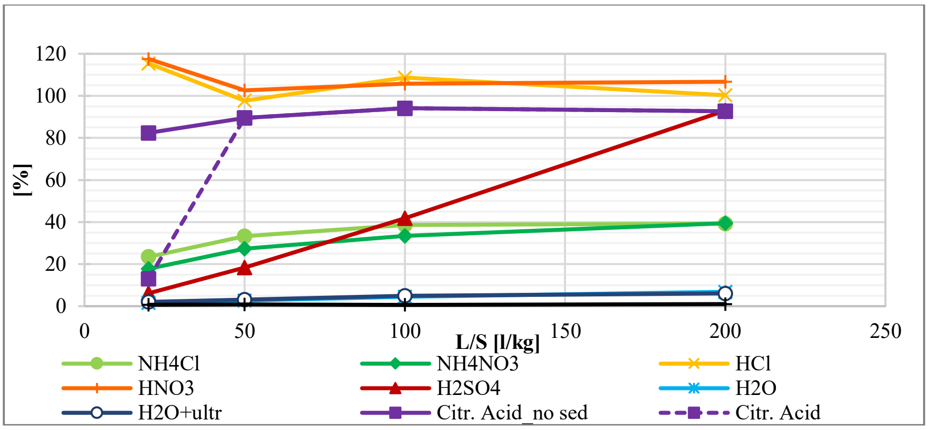

Figure 2. Ca dissolution efficiencies from BA_r2 as a function of L/S for different extracting agents

4. CONCLUSIONS

In this work, after the preliminary characterization of ten alkaline residues from different industrial facilities operating in the Lazio region, four were selected to undergo carbonation-based treatments to obtain different valuable products that could be potentially employed in the construction sector while permanently storing CO_2 in solid form. Two different routes were identified and the first tests to assess their feasibility were carried out. The products from the direct processes (aggregates) were tested according to their CO_2 uptake, environmental behavior and mechanical strength, while the analysis of the purity of the $CaCO_3$ product obtained implementing the indirect treatments will be performed in the next stages of this research. Further studies will be performed to allow to select the best operating conditions for each of the selected routes also in terms of the net carbon footprint of the construction product obtained.

5. ACKNOWLEDGMENTS

This research is part of the project “BBCircle- Biomaterials, biofuels, CO_2 storage and circularity” funded within the Public Notice "Research Groups 2020" - POR FESR Lazio 2014-2020 - Action 1.2.1 - approved with Resolution no. G08487 of 07/19/2020 - published in BURL N.93 of 07/23/2020 - amended with Resolution no. G10624 / 2020 - published in BURL n. 116 of 22/09/2020 of the LAZIO region.

6. REFERENCES

Baciocchi, R., Costa, G., Di Bartolomeo, E., Polettini, A., & Pomi, R. (2010). Carbonation of Stainless Steel Slag as a Process for CO_2 Storage and Slag Valorization. Waste and Biomass Valorization, 1(4), 467–477. https://doi.org/10.1007/s12649-010-9047-1;

Gomes, H. I., Mayes, W. M., Rogerson, M., Stewart, D. I., & Burke, I. T. (2016). Alkaline residues and the environment: A review of impacts, management practices and opportunities. Journal of Cleaner Production, 112, 3571–3582. https://doi.org/10.1016/j.jclepro.2015.09.111;

Lin, W. Y., Heng, K. S., Sun, X., & Wang, J.-Y. (2015). Accelerated carbonation of different size fractions of MSW IBA and the effect on leaching. Waste Management, 41, 75–84. https://doi.org/10.1016/j.wasman.2015.04.003;

Rahmanihanzaki, M., & Hemmati, A. (2022). A review of mineral carbonation by alkaline solidwaste. International Journal of Greenhouse Gas Control, 121, 103798. https://doi.org/10.1016/j.ijggc.2022.103798

Sanna, A., Uibu, M., Caramanna, G., Kuusik, R., & Maroto-Valer, M. M. (2014). A review of mineral carbonation technologies to sequester CO_2. Chem. Soc. Rev., 43(23), 8049–8080. https://doi.org/10.1039/C4CS00035H

UNEP, press release 9 November 2022. Available at: https://www.unep.org/news-and-stories/press-release/co2-emissions-buildings-and-construction-hit-new-high-leaving-sector

FIRST 60 MIN BEHAVIOR OF FRESH PROPERTIES AND REACTION MECHANISMS OF CEMENT PASTES INTERMIXED WITH CO_2

Shuang Luo[1], Tung-Chai Ling[1,*]

[1]College of Civil Engineering, Hunan University, Changsha 410082, China
E-mail (corresponding author): tcling@hnu.edu.cn; tcling611@yahoo.com

1. INTRODUCTION

Ready-mixed concrete (RMC) is widely used in industrial applications due to its consistent quality, time and labor savings, low material wastage, suitability for various types of project sizes, etc. (Mishra et al., 2022). However, the transportation time of RMC is essential to avoid negative effects on workability and setting time for constriction (Weiszer et al., 2020). Thus, it is usually recommended to deliver the RMC to the construction site within 60 to 90 min in order to be workable and maintain its optimal fresh properties (Lin, et al., 2010).

Notably, 70-75% of the total cement produced is used by RMC production according to the 2021 U.S. Geological Survey report. Therefore, reducing carbon emissions related to RMC production holds significant importance in addressing environmental concerns. Recently, intermixed CO_2 during the mixing process (CO_2-intermixed) of concrete has emerged as a promising approach to reducing the carbon footprint while enhancing or maintaining its mechanical properties (Monkman et al., 2017). As the intermixed CO_2 is expected to react with calcium phases in cement paste and stored as a stable $CaCO_3$ crystal, which can further refine the pore structures of the cement matrix and enhance the mechanical performance of the cement concrete (Luo et al., 2022).

It is well known that during early cement hydration, the dominant heat flow measurement arises from the reaction of C_3S and C_3A (Jansen et al., 2012). Interestingly, previous studies have shown that the intermixing of CO_2 into cement paste can significantly alter early hydration reactions. Specifically, CO_2-intermixed pure C_3S paste has been observed to exhibit lower hydration heat compared to C_3S paste without CO_2 (Monkman et al., 2020). However, in the work of Luo et al. (2022), CO_2-intermixed cement pastes attained a higher peak hydration heat than those without CO_2. Therefore, it can be inferred that minerals, especially C_3A could significantly influence the early reaction of cement paste during the fresh stage, as the C_3A can rapidly react with $CaCO_3$ to form the calcium carboaluminate in the cement paste system (Kakali et al., 2000). For this reason, this paper aims to elucidate the reaction mechanism of CO_2-intermixed cement paste within the first 60 min by injecting lower doses of CO_2 (0.033 and 0.083‰, ‰: per thousand) into the cement paste during the mixing process. The hydration heat, pH value variations, and reaction products within the initial 60 min were studied.

2. MATERIALS AND METHODS

2.1. Materials

The chemical composition of P·I 42.5 Portland cement used is detailed in Table 1. The CO_2 gas for intermixing with cement paste was industrial-grade with a purity of 99%. Pure deionized water was used throughout the entire experiment.

Table 1: Chemical compositions of P·I 42.5 Portland cement.

SiO_2	Al_2O_3	Fe_2O_3	CaO	MgO	SO_3	Na_2O	f-CaO	Cl^-	LOI
20.53	4.45	3.17	62.05	2.81	2.10	0.55	0.8	0.032	1.74

2.2. Methods

All cement pastes were prepared using an airtight mixer to avoid the injected CO_2 gas for mixing escape from the environment into the air. Initially, cement and water were mixed in that specialized mixer with a fixed water-cement ratio (W/C) of 0.4. Then, 0.033, and 0.083 ‰ (‰: per thousand) of CO_2 gas by weight of cement was injected for (named C-0.033, and C-0.083) mixing with fresh cement paste. After the completion of CO_2 mixing (specified as t = 0 min), a small portion of the cement paste was filtered for pH measurement. The freshly mixed cement paste was also soaked in isopropanol to stop hydration reactions and then dried in a vacuum chamber (20 ± 1 °C) for 7 days prior to examination of thermogravimetric analysis (TGA) and x-ray diffraction (XRD). Furthermore, to determine the initial reaction heat of CO_2-intermixed cement paste, an isothermal calorimeter measurement was performed using a closed admix ampoule equipped with a stirring motor.

3. RESULTS AND DISCUSSION

3.1. Hydration heat

Figure 1 shows the heat evolution of cement hydration. It can be seen that during the initial reaction stage, the peak heat of the C-0.033 and C-0.083 groups achieved 9.2% and 23.1% higher values than that of the C-0 group. Previous studies have indicated that the heat evolution of the cement paste during the initial reaction stage is primarily associated with the rapid dissolution of C_3S and C_3A minerals (Jansen et al., 2011). Thus, it may imply that the formation of amorphous nano-$CaCO_3$ (ACC) can promote the initial hydration reaction of C_3S and C_3A (Monkman et al., 2020). Correspondingly, after the initial reaction period, the heat release in the CO_2-intermixed group (C-0.033 and C-0.083) kept maintained a higher value up to 24 h due to the promotion of hydration reaction by the intermixed CO_2 in the cement paste.

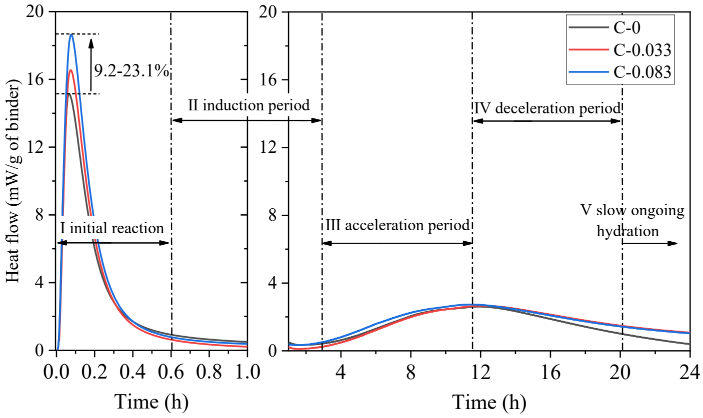

Fig. 1. Heat flow of the cement paste over the first 24h.

3.2. pH value variations in CO_2-intermixed cement pastes

The change in pH value in cement pastes within the first 60 min is depicted in Table 2. It is evident that during the reaction of 60 min, the pH value in the CO_2-intermixed cement pastes stabilizes within the range of 12.83 to 12.92, regardless of the CO_2 dose. It is well-known that a pH value ranging from 10 to 13 in cement-based materials achieves the passivation of mild steel (Payam et al., 2020). Hence, the intermixing of CO_2 at doses of 0.033-0.083 ‰ in the cement paste is unlikely to adversely affect the durability of reinforced concrete structures.

Table. 2: pH value of cement paste with in the first 60 min.

Time (min)	5	15	30	45	60
C-0	12.82	12.82	12.81	12.82	12.83
C-0.033	12.91	12.91	12.92	12.89	12.86
C-0.083	12.82	12.80	12.78	12.78	12.79

3.3. Hydration degree

Figure 2 observed that the hydration degree increases with a higher CO_2 dose, attributed to the generation of more ACC that promotes the hydration reaction. Notably, at 0 min, the hydration degree increased by 72.8% as the CO_2 dose increased to 0.083‰. However, no significant further increase in hydration degree was observed for hydration time between 5 and 60 min. This observation suggests that the enhancement of hydration primarily occurs within a few minutes after mixing CO_2 with cement paste. While the relatively stable hydration degree after 5 min may be due to the presence of ion supersaturation in the cement paste so that the hydration was gradually entering the induction period. These findings align with the hydration development presented in Section 3.1.

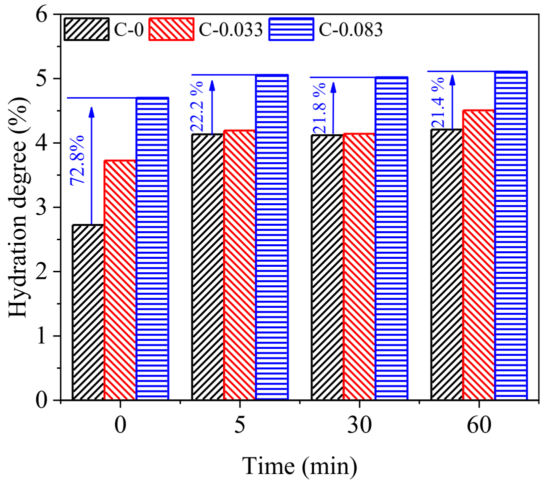

Fig.2. Hydration degree of the cement paste within the 60 min.

3.4. Phases identification

The XRD analysis of cement paste is presented in Figure 3. At 5 min, both the CO_2-intermixed group and the control group exhibited similar phase compositions. However, at 60 min, a significant consumption of gypsum was observed in the control group, leading to a prominent AFt peak due to the further reaction between C_3A and gypsum. Interestingly, the CO_2-intermixed group still contained a notable amount of gypsum, and the AFt peak was noticeably lower compared to the control group. This difference might be attributed to the preferential reaction of C_3A with ACC in the solution, resulting in the formation of calcium carboaluminate (Feng et al., 2021). It is worth noting that the XRD patterns did not exhibit obvious peaks of $CaCO_3$ and calcium carboaluminate, possibly due to their limited presence in the cement pastes within 60 min and their amorphous phase nature.

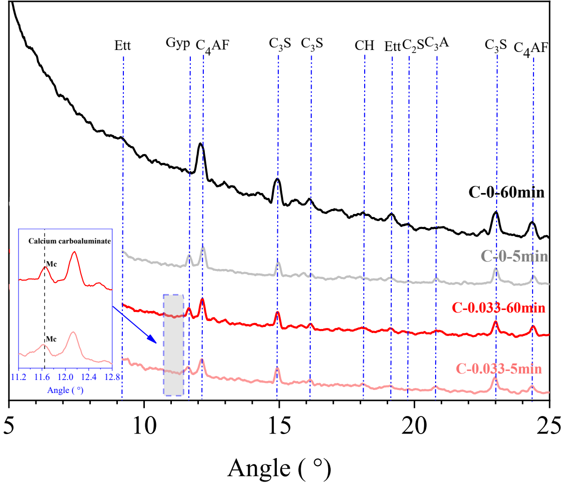

Fig. 3. XRD results of the cement paste reaction for 5 min and 60 min.

4. CONCLUSION

In this study, CO_2 intermixed with fresh cement pastes significantly influenced the cement hydration in first the 60 min. CO_2-intermixed cement pastes showed higher heat release (9.2-23.1% more at 5 min) due to the rapid reaction of C_3S and C_3A with CO_2 in the pore solution, forming ACC and calcium carboaluminate. ACC can then promote cement hydration, resulting in higher $Ca(OH)_2$ content and reasonable pH values at 60 min. The priority reaction between ACC and C_3A lowered the consumption rate of gypsum in the CO_2-intermixed cement pastes. After 60 min, XRD results revealed detectable gypsum in the CO_2-intermixed pastes, while the control paste consumed a higher amount of gypsum. Further research is required to understand the role of remaining gypsum in CO_2-intermixed pastes on cement hydration and microstructure development.

5. ACKNOWLEDGMENT

This work was supported by the Program Fund of Non-Metallic Excellence and Innovation Center for Building Materials (2023Ph.D-6).

6. REFERENCES

Busch, P., Kendall, A., Murphy, C. W., & Miller, S. A. (2022). Literature review on policies to mitigate GHG emissions for cement and concrete. *Resources, Conservation and Recycling*, *182*, 106278.

Feng, J., Yang, F., & Qian, S. (2021). Improving the bond between polypropylene fiber and cement matrix by nano calcium carbonate modification. *Construction and Building Materials*, *269*, 121249.

Jansen, D., Goetz-Neunhoeffer, F., Lothenbach, B., & Neubauer, J. (2012). The early hydration of ordinary Portland cement (OPC): An approach comparing measured heat flow with calculated heat flow from QXRD. *Cement and Concrete Research*, *42*(1), 134–138.

Jansen, Daniel, Goetz-Neunhoeffer, F., Stabler, C., & Neubauer, J. (2011). A remastered external standard method applied to the quantification of early OPC hydration. *Cement and Concrete Research*, *41*(6), 602–608.

Kakali, G., Tsivilis, S., Aggeli, E., & Bati, M. (2000). Hydration products of C_3A, C_3S and Portland cement in the presence of $CaCO_3$. *Cement and Concrete Research*, *30*(7), 1073–1077.

Lin, P.-C., Wang, J., Huang, S.-H., & Wang, Y.-T. (2010). Dispatching ready mixed concrete trucks under demand postponement and weight limit regulation. *Automation in Construction*, *19*(6), 798–807.

Luo, S., Guo, M.-Z., & Ling, T.-C. (2022). Mechanical and microstructural performances of fly ash blended cement pastes with mixing CO_2 during fresh stage. *Construction and Building Materials*, *358*, 129444.

Mishra, A. K., Sudarsan, J. S., & Nithiyanantham, S. (2022). Feasibility study on application of ready mix concrete in construction projects in Nepal.

Monkman, S., Lee, B. E. J., Grandfield, K., MacDonald, M., & Raki, L. (2020). The impacts of in-situ carbonate seeding on the early hydration of tricalcium silicate. *Cement and Concrete Research*, *136*, 106179.

Monkman, S., & MacDonald, M. (2017). On carbon dioxide utilization as a means to improve the sustainability of ready-mixed concrete. *Journal of Cleaner Production*, *167*, 365–375.

Payam, S., & Zainah, I. (2020). The pH of cement-based materials: A Review. *Journal of Wuhan University of Technology-Mater. Sci. Ed.*, *35*(5), 908–924.

Qian, X., Wang, J., Fang, Y., & Wang, L. (2018). Carbon dioxide as an admixture for better performance of OPC-based concrete. *Journal of CO_2 Utilization*, *25*, 31–38.

Weiszer, M., Fedorko, G., Molnár, V., Tučková, Z., & Poliak, M. (2020). M. Weiszer, G. Fedorko, V. Molnár, Z. Tučková, M. Poliak, Dispatching policy evaluation for transport of ready mixed concrete. Open Engineering, 10, 120-128.

GREEN RECYCLING OF CFRP COMPOSITES IN ATMOSPHERIC ENVIRONMENT

Xiangfei, Wang[1], Chun, Pei[1], Jihua, Zhu[1,*]
[1]College of Civil and Transportation Engineering, Shenzhen University, Shenzhen, Guangdong, 518061, China
E-mail: zhujh@szu.edu.cn

1. INTRODUCTION

The utilization of carbon fiber-reinforced polymer (CFRP) composites has witnessed significant growth owing to their inherent advantages such as high strength and low weight. Nevertheless, this widespread application has led to a substantial generation of waste. Projections indicate that by 2025, aircraft-related CFRP waste will reach 170,000 tons, and wind turbine blade waste will reach 225,000 tons (Wang et al., 2023; Meng et al., 2017), imposing resource wastage and environmental harm. Consequently, the quest for an efficient recycling solution for CFRP holds paramount importance as it can reduce carbon fiber costs and mitigate carbon emissions from re-production (Meng et al., 2018).Presently, mainstream recycling methods comprise mechanical recycling, thermal recycling, and chemical recycling (Karuppannan Gopalraj & Kärki, 2020). Among these, mechanical recycling involves grinding waste CFRP materials into particles of 10-50mm, followed by recycling through sieving resin-rich powder and various lengths of embedded fibers. The resultant recycled materials are primarily utilized in construction and road laying, with some serving as reinforcing materials or being re-prepared as CFRP. However, this may lead to challenges in controlling the performance of the new materials (Ogi et al., 2005; Pickering, 2006; Hirayama et al., 2017).The heat recovery method employs high temperatures in an inert gas or atmosphere with specific oxygen content to remove resin and other components, yielding internal fibers. While partially commercialized, this approach is plagued by high energy consumption, matrix resin oxidation and decomposition, and issues related to fiber size and mechanical properties (Guo et al., 2022; Meng et al., 2018; Ma et al., 2020).In contrast, the chemical recovery method dissolves the three-dimensional cross-linked resin in solution to obtain fibers. It includes supercritical/subcritical fluid recovery (high-temperature and highpressure state), electrochemical recovery, and solvent dissolution (Pei et al., 2021; Jiang et al., 2017). Compared to pyrolysis, chemical recovery is characterized by lower energy consumption and can be performed under mild conditions. Moreover, resin degradation products can be recovered in solution. The mechanical property retention rate of rCF (recycled CFRP) obtained through the chemical recovery method is higher, with minimal fiber surface oxidation, preserving the original fiber appearance to a great extent. Therefore, the development of an efficient, low pollution, and low corrosion chemical recovery system emerges as one of the effective solutions for recycling waste CFRP materials (Zhao et al., 2020). This study employs chemical methods to recycle waste CFRP materials, completing fiber recycling under mild conditions, and providing detailed characterizations. Additionally, extraction treatment on the recovered solution enables the recovery of resin degradation products, and organic solvents are tested for regeneration and utilization.

2. MATERIALS AND METHODS

2.1 Materials

The potassium hydroxide (KOH, 99.9%) used as catalyst were obtained from Shanghai Macklin Biochem Technology Co., Ltd. Dimethyl sulfoxide (DMSO, CP) as the reaction solvent was purchased from Jinan Jiangtai Chemical Company. The wasted CFRP were provided by XX company. The resin type is bisphenol A epoxy resin (DGEBA), as shown in figure 1, and information on the ratio is not disclosed.

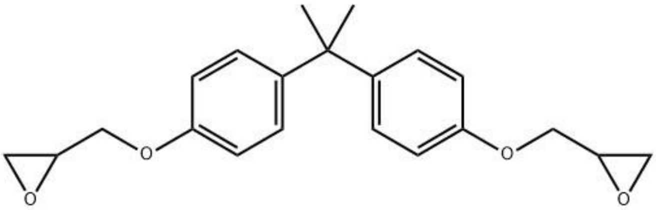

Fig. 1. Structural formula of bisphenol A epoxy resin

2.2 Methods

KOH crystals were dissolved in deionized water in a mass ratio of 1:1.1 to prepare a KOH solution. The KOH solution was mixed with an organic solution DMSO in a mass ratio of 1:10 to complete the solution preparation. The experiment was conducted using a sealed tube, heated to 180 °C in an oil bath and stirred using a magnetic stirring device, and the recycling process is shown in Figure 2. The morphology of the recovered fibers was characterized using scanning electron microscopy (SEM); As the ratio of resin and fiber content is unknown, CFRP materials were tested by Thermogravimetric analysis (TGA) to master the recovery status. The temperature is set to 25-1000 °C, the heating rate is 10 °C/min, and the atmosphere is air atmosphere; XPS was used to detect the surface element distribution and valence information of recycled fibers; Mechanical properties of recycled fibers were tested using a single fiber stretching instrument; The resin decomposition products were analyzed by FTIR.

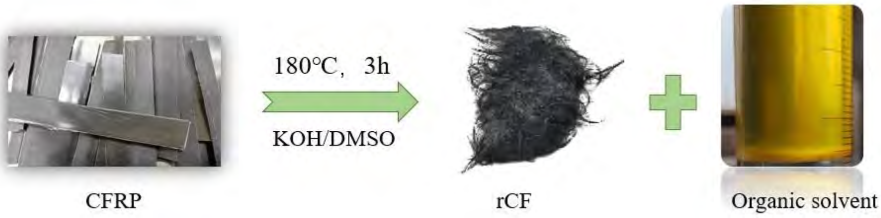

Fig. 2. Recycling process of CFRP

3. RESULTS AND DISCUSSION

The thermogravimetric curve of CFRP is shown in Figure 3, which shows that the resin material undergoes oxidation first in an air atmosphere and is divided into two main stages. Starting from 600 °C, it gradually stabilizes, followed by oxidation behavior of carbon fibers until it stabilizes at 800 °C. During this process, it can be inferred that the resin content is 35.7%.

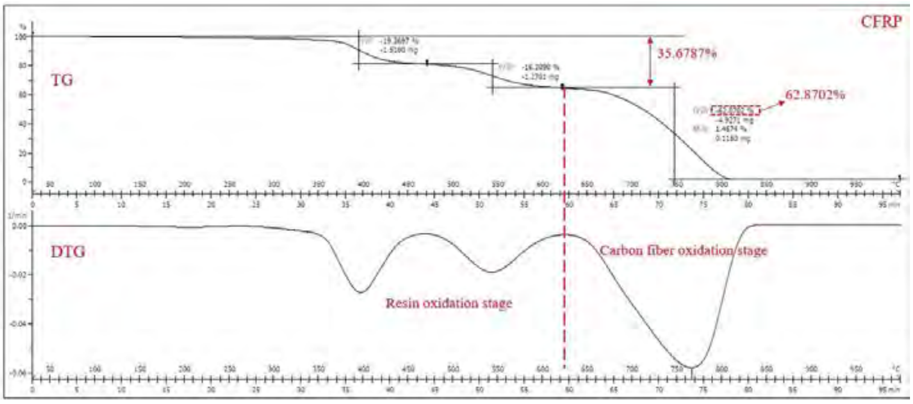

Fig. 3. Thermogravimetric curve of CFRP

Figure 4 shows the surface morphology of rCF. After recycling, the surface of the fibers is smooth and continuous, with no residual attachments or obvious signs of oxidation and corrosion, basically maintaining the original appearance of the fibers. According to statistics, the average fiber diameter is 5.3 μm.

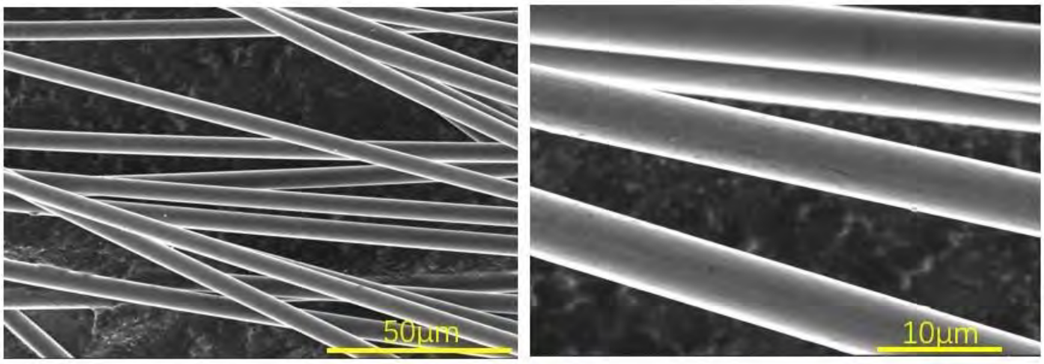

Fig. 4. SEM images of rCF

The XPS results of rCF and the single fiber tensile result are shown in Figure 5. From the broad spectrum, it can be seen that the C and O element contents of rCF are 78.36% and 2.4%, respectively. This also confirms that there is almost no oxidation behavior on the fiber surface, and mild recovery conditions are conducive to the retention of carbon fiber properties. At the same time, the peak splitting results of C 1s indicate that the C-C single bond is the main bonding bond. In addition, the surface still contains oxygen-containing functional groups such as hydroxyl and carboxyl groups, which is beneficial for enhancing the surface chemical activity of carbon fibers and improving the interfacial properties of the material. From the tensile test of a single fiber, the maximum strain reaches 0.43mm and the peak stress is 104.96N. Combining with the diameter of rCF, it can be calculated that the tensile strength of the recycled fiber reaches 4.76Gpa and the elastic modulus is 276.7Gpa.

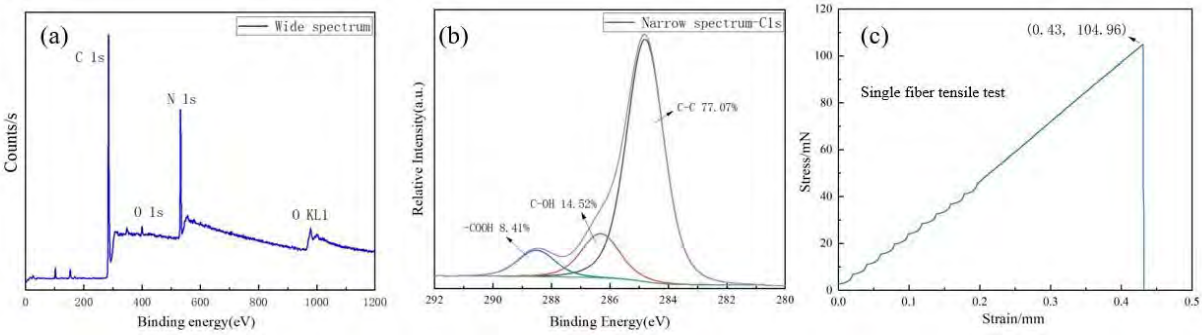

Fig. 5. a~b, XPS of rCF; c, single fiber tensile test of rCF

4. CONCLUSION

This study successfully used a KOH/DMSO mixed solution to recover waste CFRP under mild conditions, and obtained the resin content of this CFRP through TGA testing; By analyzing the surface morphology and distribution of surface functional groups of rCF, the feasibility of this recycling scheme was confirmed, and a large number of oxygen-containing functional groups were retained on the fiber surface, which is beneficial for improving the surface activity and interface performance of the fiber. In addition, the tensile test results of the fibers indicate that rCF still retains excellent mechanical properties. The degradation mechanism of resin and the analysis and recovery of degradation products are still ongoing, and this part will be supplemented in subsequent research.

5. ACKNOWLEDGMENT

The authors would like to express appreciation for the support of the Key-Area Research and Development Program of Guangdong Province [Project Number: 2019B111107002], the National Natural Science Foundation of China [Project Number: 52108231], and the Shenzhen Science and Technology Innovation Program [Project Number: 20220810140230001, 20220810160453001].

6. REFERENCES

Guo, L., Xu, L., Ren, Y., Shen, Z., Fu, R., Xiao, H., & Liu, J. (2022). Research on a two-step pyrolysis-oxidation process of carbon fiber-reinforced epoxy resin-based composites and analysis of product properties. Journal of Environmental Chemical Engineering, 10(3), 107510. https://doi.org/10.1016/j.jece.2022.107510

Hirayama, D., Saron, C., Botelho, E. C., Costa, M. L., & Ancelotti, A. C. (2017). Polypropylene Composites Manufactured from Recycled Carbon Fibers from Aeronautic Materials Waste. Materials Research, 20, 519–525. https://doi.org/10.1590/1980-5373-MR-2016-1022

Jiang, J., Deng, G., Chen, X., Gao, X., Guo, Q., Xu, C., & Zhou, L. (2017). On the successful chemical recycling of carbon fiber/epoxy resin composites under the mild condition. Composites Science and Technology, 151, 243–251. https://doi.org/10.1016/j.compscitech.2017.08.007

Karuppannan Gopalraj, S., & Kärki, T. (2020). A review on the recycling of waste carbon fibre/glass fibre-reinforced composites: Fibre recovery, properties and life-cycle analysis. SN Applied Sciences, 2(3), 433. https://doi.org/10.1007/s42452-020-2195-4

Ma, C., Sánchez-Rodríguez, D., & Kamo, T. (2020). Influence of thermal treatment on the properties of carbon fiber reinforced plastics under various conditions. Polymer Degradation and Stability, 178, 109199. https://doi.org/10.1016/j.polymdegradstab.2020.109199

Meng, F., McKechnie, J., Turner, T. A., & Pickering, S. J. (2017). Energy and environmental assessment and reuse of fluidised bed recycled carbon fibres. Composites Part A: Applied Science and Manufacturing, 100, 206–214. https://doi.org/10.1016/j.compositesa.2017.05.008

Meng, F., Olivetti, E. A., Zhao, Y., Chang, J. C., Pickering, S. J., & McKechnie, J. (2018). Comparing Life Cycle Energy and Global Warming Potential of Carbon Fiber Composite Recycling Technologies and Waste Management Options. ACS Sustainable Chemistry & Engineering, 6(8), 9854–9865. https://doi.org/10.1021/acssuschemeng.8b01026

Ogi, K., Shinoda, T., & Mizui, M. (2005). Strength in concrete reinforced with recycled CFRP pieces. Composites Part A: Applied Science and Manufacturing, 36(7), 893–902. https://doi.org/10.1016/j.compositesa.2004.12.009

Pei, C., Chen, P., Kong, S.-C., Wu, J., Zhu, J.-H., & Xing, F. (2021). Recyclable separation and recovery of carbon fibers from CFRP composites: Optimization and mechanism. Separation and Purification Technology, 278, 119591. https://doi.org/10.1016/j.seppur.2021.119591

Pickering, S. J. (2006). Recycling technologies for thermoset composite materials—Current status. Composites Part A: Applied Science and Manufacturing, 37(8), 1206–1215. https://doi.org/10.1016/j.compositesa.2005.05.030

Wang, Y., Li, A., Zhang, S., Guo, B., & Niu, D. (2023). A review on new methods of recycling waste carbon fiber and its application in construction and industry. Construction and Building Materials, 367, 130301. https://doi.org/10.1016/j.conbuildmat.2023.130301

Zhao, Q., Jiang, J., Li, C., & Li, Y. (2020). Efficient recycling of carbon fibers from aminecured CFRP composites under facile condition. Polymer Degradation and Stability, 179, 109268. https://doi.org/10.1016/j.polymdegradstab.2020.109268

ACCELERATED CARBONATION OF RECYCLED CONCRETE AGGREGATE IN SEMI-WET ENVIRONMENTS: A PROMISING TECHNIQUE FOR CO_2 UTILIZATION

Yining Gao, Yi Jiang, Yong Tao*, Peiliang Shen*, Chi Sun Poon*

Department of Civil and Environmental Engineering &
Research Centre for Resources Engineering Towards Carbon Neutrality,
The Hong Kong Polytechnic University, Hong Kong, China
*Corresponding authors: yong.tao@polyu.edu.hk (Y.Tao) peiliang.shen@polyu.edu.hk (P.L. Shen),
cecspoon@polyu.edu.hk (C.S. Poon)

The practical implementation of accelerated carbonation for recycled waste concrete is impeded by sluggish carbonation efficiency. In contrast to previous carbonation enhancement schemes using high-pressure gas and/or complex pre-/post-processing, this study introduces a novel semi-wet carbonation method that achieves high-efficiency carbonation of recycled concrete aggregates (RCA) in a practically simple way. A noteworthy carbonation degree of 10.6% was achieved within 30 minutes at room temperature and ambient pressure, which enhanced the RCA by reducing the water absorption rate and porosity by 3.6% and 20% respectively. The formed $CaCO_3$ is primarily in calcite form with poorer crystallinity and smaller grain size and the formed silica gel features a lower polymerization degree compared with those formed in wet carbonation. It is due to that the carbonation reactions for the semi-wet scenario happen at the spatially confined water film of the solid-liquid interface. Moreover, the addition of sodium bicarbonate significantly accelerated the semi-wet carbonation, which is due to the weak alkaline environment lowering the CO_2 speciation free energy as revealed by reactive molecular dynamics simulations. The proposed semi-wet carbonation method provides a promising way of pushing industrial CO_2 capture and utilization.

Session B4

Waste Treatment and Enhancement

THE UTILIZATION OF RECYCLED CONCRETE AGGREGATES FOR PAVEMENT ENGINEERING APPLICATIONS: A STATE-OF-THE-ART REVIEW

Jie Ji[1,2,*], Hao Chen[1], Zhi Suo[1,2], Wenhua Zheng[1,2], Yening Yu[1,2], Wenjuan Zhou[1,2] and Zijian Zhao[1,2]

[1] School of Civil and Transportation Engineering, Beijing University of Civil Engineering and Architecture, Beijing, 100044, China
[2] Beijing Collaborative Innovation Center for Energy Conservation & Emission Reduction and Sustainable Urban-Rural Development, Beijing, 100044, China
E-mail: jijie@bucea.edu.cn

1. INTRODUCTION

Global urbanization has spurred the need for urban renewal as a key initiative to address issues such as population growth, urban aging, and sustainable development. Organic renewal aims to optimize the functionality and efficient utilization of urban space through the reconfiguration of existing urban infrastructure and buildings, including the reuse of old buildings, the utilization of vacant land, and the enhancement of public spaces. Substantial attention has been placed on resource utilization of Construction and Demolition Waste (C&DW) (Akhtar & Sarmah, 2018). The generation of C&DW increased by a compound annual growth rate of 4.0%, rising from 2,547.9 million metric tons in 2016 to 3,094.3 million metric tons in 2021 in China. The C&DW is estimated to reach 3,618.3 million metric tons by 2026 (Zhong Shang Intelligence Network, 2022), with a projected compound annual growth rate of 3.2% between 2021 and 2026. Nowadays, recycling and reuse, landfilling, and incineration are the most commonly used methods for C&DW treatment (Ma et al, 2023). A comprehensive approach to waste management is necessary to handle C&DW, and this has been adopted by many countries around the world. These methods aim to minimize waste generation and enhance resource utilization efficiency by employing waste classification, recycling and reuse, energy recovery, and landfill control measures (Tauš et al, 2023; Shooshtarian et al, 2022; Saravanan et al, 2022). Effective management of C&DW through a series of measures, including mandatory waste classification, establishment of recycling systems, waste resource utilization, and construction of waste treatment facilities, are carried out to encourage the utilization of construction waste as a resource for energy recovery in China (Liu et al, 2022; Liu et al, 2020; Lee et al, 2020; Kurniawan et al, 2021). In addition, advanced waste treatment techniques, including construction waste crushing equipment and concrete regeneration methods are recommended to boost waste resource utilization and create an environmentally friendly livin (Lee et al, 2020). The stockpile of C&DW had exceeded 20 billion metric tons by the end of 2022 and continues to rise rapidly at a rate of 3.5 billion metric tons per year according to an incomplete statistic records. However, the overall rate of utilization has only reached about 40%, which is considerably lower than the utilization rates of 90% in European Union countries and 97% in Japan (Peng et al,2021). Therefore, it is an urgent to develop crucial technologies for resource utilization, decarbonization, scalability, and systematic application of C&DW to improve the comprehensive utilization rate.

C&DW mainly include soil, slurry, debris from construction sites, waste from demolition and renovation projects. Construction debris, demolition and renovation waste primarily consisted of inorganic non-metallic materials. These materials can be processed into recycled aggregates, recycled fines, surplus soil, etc., through crushing and classification treatments (Ministry of Transport of the People's Republic of China, 2021). Figure 1 shows that C&DW is predominantly composed of concrete, accounting for more than 70%, which can be transformed into Recycled Concrete Aggregates (RCAs). Therefore, the focus of this review is on evaluating the application of RCAs derived from demolition waste for pavement engineering.

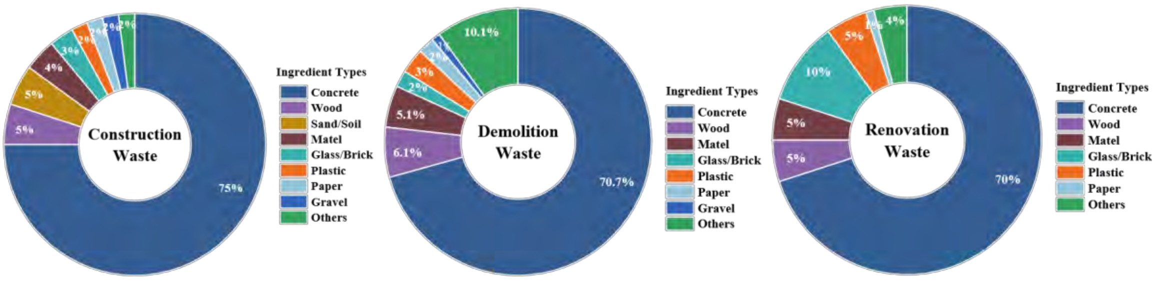

Figure 1 Typical composition of C&DW (Arabani&Azarhoosh,2012)

Around 5 billion tons of natural aggregates (NAs) are required for construction and maintenance of pavement every year in China. Certain technologies and processes can be utilized to convert C&DW into RCAs with different particle sizes to replace some of the NAs,which not only reduces engineering construction costs by allowing the utilization of various types and qualities of C&DW (Editorial Department of China Journal of Highway and Transport, 2020; Zhang & Tan, 2020), but also has a significant positive effect on the environment by minimizing the impact of NAs extraction. Given the significant construction and utilization benefits, pavement engineering will undoubtedly be one of the primary scenarios for the recycling of construction waste. RCAs present several undesired characteristics such as multiple interfaces, micro-cracks, poor particle shape and gradation, low density, high-water absorption, crushing value, and Los Angeles abrasion value. These properties are mainly caused by heterogeneity, natural degradation, processing, crushing, and surface coating of C&DW. The performance differences of RCAs with NAs pose a challenge in meeting the technical requirements for higher-grade pavements or materials in the upper layers of pavements for NAs application. At present, RCAs are primarily focused on utilizing lower-grade pavements or lower layers of pavements (such as subgrade and base layers), with limited research on upper-grade pavements and upper layers of pavements. The use of RCAs are hindered in high-grade, upper layers, and fully recycled pavements, thus limiting its value and overall utilization.

Therefore, this paper presents a comprehensively review of the processing technology, performance characterization, performance enhancement measures, and application of RCAs in pavement engineering. The aim is to evaluate the extent of differences among various influencing factors, guide the practical use of RCAs in sustainable pavement applications, and increase its overall utilization rate.

2. MATERIALS AND METHODS

In this review, Recycled Concrete Aggregates (RCAs) were selected as the research object and studied through the method of literature review. This review gives a comprehensive overview of the characteristics of RCAs and the methods used to improve their aggregate performance. Furthermore, this review examines the application of RCAs in the sub-base, cement, and asphalt surface layers of pavements.

3. RESULTS AND DISCUSSION

Multiple interfaces and microcracks, low bulk and apparent density, high water absorption, crushing value, and Los Angeles abrasion value of RCAs result in significant differences with natural aggregates. RCAs are most suitable for use in the subgrade and base layers due to their inherent characteristics. The physicochemical characteristics, heterogeneity, natural degradation, processing crushing, and, the presence of hardened cementitious paste adhering to the surface are among the factors influencing the RCA properties. Thus, the utilization of RCAs has several limitations. To improve RCAs, two techniques can be used: removing or reinforcing mortar coatings. However, single-reinforcement methods are not very effective. This suggests the use of composite reinforcement techniques instead. The crushing characteristics of RCAs should be considered during the gradation design of pavement subbases to optimize their utilization, especially when the blending proportion is low. RCAs can replace natural aggregates (NAs) completely in cement concrete pavements. Reinforcement techniques are necessary to enhance the durability of cement concrete.

RCAs can replace up to 60% of NAs in asphalt mixtures and maintain acceptable pavement performance despite exhibiting lower performance than NAs. To enhance the utilization of RCAs in pavement engineering, two or more reinforcing techniques should be utilized in the early stages of application. Optimizing the design based on existing grading and mix proportions should be performed. The purpose of this approach is to offer theoretical support for the treatment of C&DW and its utilization as recycled aggregates to enhance overall efficiency.

4. CONCLUSION

This review presents an overview of the processing of RCAs, characterization of its properties, measures to improve its performance, and applications in pavement engineering. Based on the aforementioned analysis, one can draw the following conclusions and expectations:

（1） RCAs exhibit a porous and less dense surface, lower inherent strength, and higher water absorption, resulting in inferior adhesion with asphalt. Nevertheless, most of its physical and mechanical properties comply with the requirements of standard specifications.

（2） Two categories of reinforcement methods exist for RCAs: removal of adhered mortar and strengthening of adhered mortar. The removal of adhered mortar as a reinforcement method has some drawbacks such as high energy consumption and incomplete reinforcement. Regarding the strengthening adhered mortar method, microbial mineralization has significant effect on enhancing RCAs. However, controlling the reinforcement factors is challenging. On the other hand, the performance of RCAs can be remarkably enhanced by using mineral admixtures. Nevertheless, the stability of reinforcement could be affected by engineering circumstances. Therefore, it is recommended to adopt a composite reinforcement approach by combining different methods to achieve the desired reinforcement effect.

（3） The stability of RCAs in terms of water retention characteristics, rebound modulus, and permanent deformation is affected by particle breakage under loading and temperature-humidity conditions. Understanding the impact of recycled aggregate grading, composition, and particle breakage characteristics on the above properties under various complex conditions is crucial to achieve accurate prediction and control of the service performance of recycled aggregate in pavement subgrades. However, the current research in this area is limited.

（4） RCAs can fully replace NAs in cement concrete surface layers. Certain aggregate reinforcement techniques should be applied to enhance the performance of RCAs and meet durability requirements.

（5） According to literature, RCAs have great potential for use in asphalt concrete surface layers, with reported substitution levels varying from 15% to 100%. RCAs asphalt mixes typically exhibit weaker performance compared to those with NAs aggregates, resulting in an increase in the optimal asphalt content. However, by controlling RCAs content below 60%, the performance of asphalt mixes can mostly satisfy the relevant technical specifications...

5. ACKNOWLEDGMENT

This study is sponsored by the National Key R&D Program of China (2022YFC3803403), National Natural Science Foundation of China (52078025), Beijing Natural Science Foundation and Beijing Municipal Education Commission (KZ201910016017).

6. REFERENCES

Akhtar, A., & Sarmah, A. K. (2018). Construction and demolition waste generation and properties of recycled aggregate concrete: A global perspective. *Journal of Cleaner Production*, *186*, 262–281. https://doi.org/10.1016/j.jclepro.2018.03.085

Forecast and Analysis of China’s Construction Waste Market Size and Market Driving Factors in 2022. Zhong Shang Intelligence Network. https://www.askci.com/news/chanye/20230825/093905269292754470448248.shtml

Ma, W., Hao, J. L., Zhang, C., Di Sarno, L., & Mannis, A. (2022). Evaluating carbon emissions of China's waste management strategies for building refurbishment projects: Contributing to a circular economy. Environmental Science and Pollution Research, 30(4), 8657–8671. https://doi.org/10.1007/s11356-021-18188-6

Tauš, P., Šimková, Z., Cehlár, M., Krajňáková, I., & Drozda, J. (2023). Fulfillment of EU goals in the field of waste management through energy recovery from waste. Energies, 16(4), 1913. https://doi.org/10.3390/en16041913

Shooshtarian, S., Maqsood, T., Caldera, S., & Ryley, T. (2022). Transformation towards a circular economy in the Australian construction and Demolition Waste Management System. Sustainable Production and Consumption, 30, 89–106. https://doi.org/10.1016/j.spc.2021.11.032

Saravanan, A., Kumar, P. S., Nhung, T. C., Ramesh, B., Srinivasan, S., & Rangasamy, G. (2022). A review on biological methodologies in Municipal Solid Waste Management and landfilling: Resource and Energy Recovery. Chemosphere, 309, 136630. https://doi.org/10.1016/j.chemosphere.2022.136630

Liu, J., Chen, Y., & Wang, X. (2022). Factors driving waste sorting in construction projects in China. Journal of Cleaner Production, 336, 130397. https://doi.org/10.1016/j.jclepro.2022.130397

Liu, H., Long, H., & Li, X. (2020). Identification of critical factors in construction and demolition waste recycling by the grey-DEMATEL approach: A Chinese perspective. Environmental Science and Pollution Research, 27(8), 8507–8525. https://doi.org/10.1007/s11356-01907498-5

Lee, R. P., Meyer, B., Huang, Q., & Voss, R. (2020). Sustainable Waste Management for Zero waste cities in China: Potential, challenges and opportunities. Clean Energy, 4(3), 169–201. https://doi.org/10.1093/ce/zkaa013

Kurniawan, T. A., Lo, W., Singh, D., Othman, M. H., Avtar, R., Hwang, G. H., Albadarin, A. B., Kern, A. O., & Shirazian, S. (2021). A societal transition of MSW management in Xiamen (China) toward a circular economy through integrated waste recycling and technological digitization. Environmental Pollution, 277, 116741. https://doi.org/10.1016/j.envpol.2021.116741

Peng, Z., Lu, W., & Webster, C. J. (2021). Quantifying the embodied carbon saving potential of recycling construction and demolition waste in the Greater Bay Area, China: Status quo and future scenarios. Science of The Total Environment, 792, 148427. https://doi.org/10.1016/j.scitotenv.2021.148427

Ministry of Transport of the People's Republic of China. (2021). Technical Specification for Highway Engineering Utilizing Construction Waste. China. People's Transport Press.

Arabani, M., & Azarhoosh, A. R. (2012). The effect of recycled concrete aggregate and steel slag on the dynamic properties of asphalt mixtures. Construction and Building Materials, 35, 1–7. https://doi.org/10.1016/j.conbuildmat.2012.02.036

Editorial Department of China Journal of Highway and Transport. (2020). A Comprehensive Review of Academic Research on Chinese Pavement Engineering. China Journal of Highway and Transport, 33(10): 1-66.

Zhang, Y., & Tan, W. (2020). Demolition Waste Recycling in China: New evidence from a demolition project for Highway Development. Waste Management & Research, 38(6), 696–702. https://doi.org/10.1177/0734242x20904440

MECHANICAL PROPERTIES AND MICROSCOPIC MECHANISMS OF LBM-GGBS SOLIDIFIED SALINE SOIL IN SEASONALLY FROZEN AREAS

Ming-Zhi Guo[a*], Ziqing He[a], Chenxi Dong[b], Jiang-Shan Li[b]

[a] School of Civil Engineering, Shaoxing University, Shaoxing 312000, China
[b] State Key Laboratory of Geomechanics and Geotechnical Engineering, Institute of Rock and Soil Mechanics, Chinese Academy of Sciences, Wuhan 430071, China.
[*] Corresponding author emails: guo.mz.guo@connect.polyu.hk

This study investigated the durability of saline soils solidified by Light-Burned Magnesia (LBM)-Ground Granulated Blast Furnace Slag (GGBS) under Freezing-and-Thawing (F-T) cycles in an attempt to apply the developed products in subgrade engineering in seasonally frozen regions. The effects of LBM and GGBS on the unconfined compressive strength (UCS), permeability coefficient and Cl^- leaching concentration of chloride saline soil under different freeze-thaw cycles (0, 2, 4, 6, 8, and 10) were examined. The microstructures of the LBM-GGBS modified soil were analyzed by Scanning Electron Microscope (SEM) with Energy Dispersive Spectrometer (EDS) and Mercury Intrusion Porosimetry (MIP) tests. The results showed that at a 12% total dosage of curing agent content and a GGBS to LBM ratio of 7, the residual strength of the solidified soil reached 3 MPa after 10 F-T cycles, which was the optimal mix proportion. Increasing the curing agent effectively improved the ability of the modified soil to resist F-T cycles. At a curing agent of 12%, the permeability coefficient varied within the range of an order of magnitude. The microscopic analysis revealed that LBM-GGBS reacted with Cl^- in saline soil to form a new hydration product-$3CaO\cdot Al_2O_3\cdot(0.5CaCl_2\cdot 0.5CaSO_4)\cdot 12H_2O$ (Ks). The formation of various hydration products contributed to a significant improvement in the strength and F-T resistance of the solidified soil. After undergoing F-T cycles, the total porosity of the solidified soil increased; whereas, the pores between the aggregates decreased, but the pores between the particles increased, indicating that the F-T cycle had a negligible effect on the microstructures of the solidified soil. Therefore, LBM-GGBS can be used as an excellent soil stabilizer in road filling materials in seasonally frozen areas.

Keywords: chloride saline soil; GGBS; Magnesia; freeze-thaw cycles; mechanical properties; microstructure

ENHANCED LONG-TERM VOLUME STABILITY OF CARBONATED STEEL SLAG BLOCKS WITH REDUCED IRON CONTENT: AN INVESTIGATION UNDER ACCELERATED DEGRADATION AND NATURAL ENVIRONMENT CONDITIONS

Jiaxin Deng [1,2], **Lei Gu** [1,2,*], Xiaoxiang Zhang [1,2]

[1] Changzhou Architectural Research Institute Co., Ltd., Changzhou 213015, China
[2] Jiangsu Nigao Science and Technology Co., Ltd., Changzhou 213141, China
E-mail: gulei@czjky.com

1. INTRODUCTION

Steel slag, a significant by-product of industrial steelmaking, accounts for approximately 15-20% of total crude steel production (Song et al., 2021). Despite this, less than a third of steel slag is effectively utilized in China (Bo et al., 2016). The improper disposal of steel slag not only claims large tracts of land but also degrades the soil and water quality, disrupting local vegetation growth, ecological balance, and urban air quality.

The underutilization of steel slag stems from factors such as its poor hydraulic properties, poor grindability due to high iron content (Mo, 2020) , and high free-CaO/MgO content leading to volume stability issues when employed in cement (A et al., 2018). The expansion amount are 98% and 148% when free-CaO/MgO are converted to $Ca(OH)_2$ and $Mg(OH)_2$ in the hydration process. However, it is noteworthy that the abundant free-CaO/MgO in steel slag exhibits significant reactivity during carbonation, despite its weak hydraulic characteristics.

Previous studies have extensively reported the use of CO_2 curing to prepare steel-slag blocks. Ghouleh et al. (Ghouleh et al., 2015) demonstrated that carbonation of steel slag blocks for 2 h could achieve a compressive strength of 80 MPa, under 99.5 vol% CO_2 concentration and 1.5 bar gas pressure. Moreover, Zhong et al. (Zhong et al., 2021) achieved over 50 MPa compressive strength in steel slag blocks, finding that elevated temperature and gas pressure were beneficial for strength gain, while temperatures exceeding 70 °C and pressures over 0.55 MPa had adverse effects. Similarly, Humbert et al. (Humbert et al., 2019) discovered that greater steel slag fineness, larger molding pressure (10-30 MPa), higher partial pressure of CO_2 (0.05-0.25 MPa), and longer curing time (0.5-72 hours) led to higher carbonated compressive strength steel slag products. Hou et al. (Hou et al., 2021) prepared a carbonated steel slag block under pure CO_2 for 30 min at a pressure of 0.2 MPa, no defects of the block were shown after curing in 3 MPa saturated steam for 3 h. These studies indicate that carbonation of steel slag is a viable solution for both steel slag utilization and CO_2 sequestration, particularly for industrial waste gas with low CO_2 concentration.

The carbonation process could mitigate the unsoundness of steel slag caused by high free CaO/MgO content. However, the high iron content remains in these steel slags without magnetic separation. The expansion induced by iron corrosion may also impact the long-term durability of steel slag based carbonated products, an aspect that has not been widely studied.

This research program aims to investigate the influence of residual iron content on the long-term durability of carbonated steel slag blocks under both accelerated degradation and natural environmental conditions. Measurements of compressive strength, capillary porosity, volume stability, X-ray diffraction (XRD), and scanning electron microscopy (SEM) are undertaken to unravel the deterioration properties and mechanism behind.

2. MATERIALS AND METHODS

2.1 Materials

Steel slag, provided by Zhongtian Iron and Steel Company, was utilized for this study. The steel slag with high and low iron content exhibited specific surface areas of 407 m^2/kg and 434 m^2/kg, and densities of 3.55 g/cm ^{3} and 3.49 g/cm,^{3} respectively. **Figure 1** displays the optical micromorphology of steel slag. The chemical compositions of steel slag with varying residual iron content, determined by X-ray fluorescence (XRF), are presented in **Table 1**.

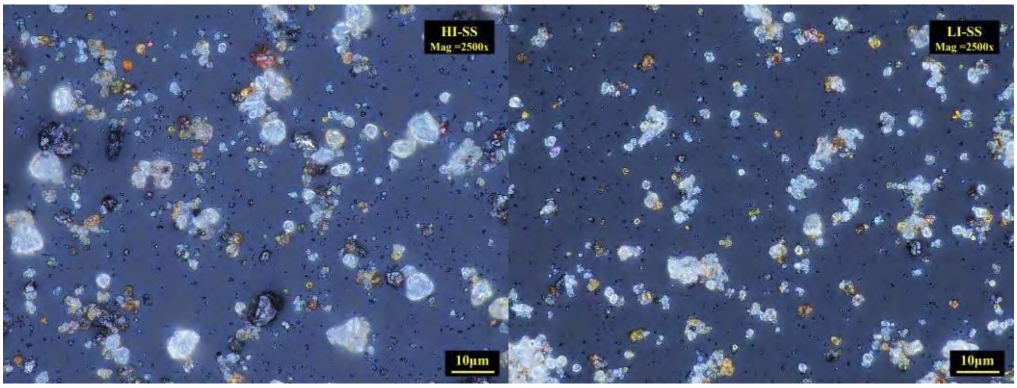

Figure 1. Optical micromorphology of steel slag

Table 1 Chemical composition of steel slag (wt.%).

Sample	CaO	SiO_2	Fe_2O_3	Al_2O_3	MgO	MnO	SO_3	TiO_2	Others
HI-SS	28.34	13.30	38.47	4.04	6.50	4.44	0.29	0.73	3.89
LI-SS	40.04	17.27	25.88	2.63	4.74	3.96	0.25	1.35	3.88

2.2 Sample Preparation

The steel slag powder, sand, and water were mechanically mixed for 5 minutes using a mortar mixer. The mortar was weighed (to keep the weight constant) and compacted into 50-mm diameter cylindrical specimens at 12 MPa. The compact specimens were demolded and placed in a carbonation chamber with a 30% CO_2 concentration at a temperature of 30°C and relative humidity of 70% at ambient pressure for 72 h. The carbonated steel slag blocks were dried at 40°C for 24 hours to control water content. Then, accelerated degradation and natural environmental conditions were set to explore the deterioration properties and mechanism of steel slag with different residual iron content. The accelerated degradation condition involved wet-dry cycles in 3.5 wt.% sodium chloride solution, with specimens immersed in the solution for 1 day and dried at 40°C for 2 days as one wet-dry cycle to accelerate corrosion (Cai et al., 2020).

2.3 Test Methods

2.3.1 CO_2 Uptake

To quantify the CO_2 uptake, the sample was dried at 105°C until reaching a constant weight, then pulverized into a fine powder. The CO_2 uptake was calculated based on the carbon content before and after carbonation, as measured by a carbon/sulfur combustion analyzer (EMIA-Pro, Horiba, Japan).

2.3.2 Compressive Strength

Carbonated steel slag blocks of dimensions φ50*50 mm were prepared for compressive strength testing. The procedure was refer to GB/T 11969-2008 “Test Methods of Autoclaved Aerated Concrete”, with a loading speed of 2 kN/s.

2.3.3 Capillary porosity

Porosity was evaluated by the weight difference between water-saturated and dried samples (Kai et al., 2016). The carbonated steel slag block was oven-dried at 40 °C until reaching a constant weight

(m_1), then immersed in water for 24 hours, and the mass of the surface-dried saturated sample was recorded as m_2. The apparent volume of the sample was measured using the drainage method.

2.3.4 Volume stability

The φ50*100 mm carbonated steel slag blocks were prepared for volume stability test refer to ASTM C157/C157M "Standard Test Method for Length Change of Hardened Hydraulic-Cement Mortar and Concrete". Initial length of samples was recorded after carbon curing and dried in 40 °C, the length and mass change were recorded under different exposure conditions.

2.3.5 X-ray diffraction (XRD)

XRD was utilized to analyze the product composition of carbonated steel slag blocks under various exposure conditions. For XRD measurements, the pure steel slag paste was oven-dried at 40°C for two days and then pulverized into powders (particle size less than 75 μm). The X-ray diffractometer with nickel-filtered Cu Kαl radiation 1.5405 Å, 40 kV voltage and 40 mA current with scanning speed of 5°/min and scanning range between 5° to 70° (2θ).

2.3.6 Scanning electron microscopy (SEM)

SEM was used to analysis the micromorphology of reaction products. The dried pure steel slag paste was cut and coated with gold to enhance the conductivity. Observations were undertaken at an accelerating voltage of 20 kV with a secondary electron (SE) detector.

3. RESULTS AND DISCUSSION

3.1 CO_2 uptake

The CO_2 uptake of steel slag increased concurrently with the duration of CO_2 curing which was shown in **Figure 2**, with the majority of absorption occurring within the first hour, accounting for nearly 70% of the total 24-hour CO_2 uptake. Steel slag with lower iron content exhibited a higher carbon sequestration efficiency, due to the persistence of more carbonation reaction minerals in LISS.

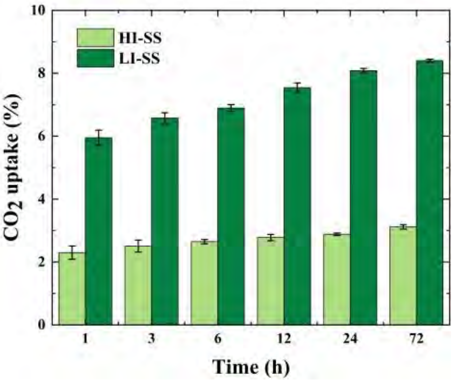

Figure 2. CO_2 uptake of steel slag with different iron content.

3.2 Compressive strength and capillary porosity

Carbonated steel slag blocks constructed with LI-SS achieved a compressive strength of 31.2 MPa, which was double the strength of blocks made from HI-SS (15.2 MPa). The more carbonated products formed in carbonated blocks with LI-SS, which is beneficial to increase the porosity of the matrix, strengthen the density of the matrix, and improve its compressive strength.

3.3 Volume stability

Preliminary results: After 3 months of accelerated deterioration experiments, slightly expansion was shown in carbonated steel slag blocks with HI-SS.

3.4 Deterioration mechanism

3.4.1 XRD

Preliminary results: After 3 months of accelerated deterioration experiments, extra hematite was observed in the HI-SS samples, indicating iron corrosion is happening.

3.4.2 SEM

Preliminary results: Porous structures were found in steel slag with high residual iron content. The EDS analysis revealed the presence of iron corrosion products on the surface of the samples with higher residual iron content (HI-SS).

4. CONCLUSION

This study investigates the impact of residual iron content on the long-term volume stability of carbonated steel slag blocks, and the following conclusions can be drawn:

(1) Carbonated steel slag blocks with lower residual iron content exhibited a compressive strength exceeding 30 MPa, with no fractures observed after autoclaving at 2 MPa for 3 hours.
(2) Higher carbon sequestration efficiency was observed in steel slag with lower iron content.
(3) After 3 months of dry and wet cycle curing, slight expansion and corrosion products were detected in HI-SS samples, while LI-SS samples remained stable. The findings suggest that magnetic separation could mitigate volume stability problems caused by residual iron.

5. REFERENCES

A, Y. J., A, T. C. L., A, C. S., & B, S. Y. P. (2018). Characteristics of steel slags and their use in cement and concrete— A review. *Resources, Conservation and Recycling*, *136*, 187-197.

Bo, Pang, Zonghui, Zhou, Pengkun, Hou, Peng, Du, Lina, & Zhang. (2016). Autogenous and engineered healing mechanisms of carbonated steel slag aggregate in concrete. *Construction & Building Materials*.

Cai, Y., Zhang, W., Yu, L., Chen, M., & Yang, K. (2020). Characteristics of the steel-concrete interface and their effect on the corrosion of steel bars in concrete. *Construction and Building Materials*, *253*, 119162.

Ghouleh, Z., Guthrie, R. I. L., & Shao, Y. (2015). High-strength KOBM steel slag binder activated by carbonation. *Construction and Building Materials*, *99*, 175-183. https://doi.org/10.1016/j.conbuildmat.2015.09.028

Hou, G., Yan, Z., Sun, J., Naguib, H. M., Lu, B., & Zhang, Z. (2021). Microstructure and mechanical properties of CO2-cured steel slag brick in pilot-scale. *Construction and Building Materials*, *271*. https://doi.org/10.1016/j.conbuildmat.2020.121581

Humbert, P. S., Castro-Gomes, J. P., & Savastano, H. (2019). Clinker-free CO2 cured steel slag based binder: Optimal conditions and potential applications. *Construction and Building Materials*, *210*, 413-421. https://doi.org/10.1016/j.conbuildmat.2019.03.169

Kai, Yang, Changhui, Yang, Bryan, Magee, Sreejith, Nanukuttan, Jianxiong, & Ye. (2016). Establishment of a preconditioning regime for air permeability and sorptivity of alkali-activated slag concrete. *Cement & concrete composites*.

Mo, L., ShuoHuang, BeiXu, LinglingFeng, ShengfaDeng, Min. (2020). Preparation, microstructure and property of carbonated artificial steel slag aggregate used in concrete. *Cement & concrete composites*, *113*(1).

Song, Q., Guo, M.-Z., Wang, L., & Ling, T.-C. (2021). Use of steel slag as sustainable construction materials: A review of accelerated carbonation treatment. *Resources, Conservation and Recycling*, *173*. https://doi.org/10.1016/j.resconrec.2021.105740

Zhong, X., Li, L., Jiang, Y., & Ling, T.-C. (2021). Elucidating the dominant and interaction effects of temperature, CO2 pressure and carbonation time in carbonating steel slag blocks. *Construction and Building Materials*, *302*. https://doi.org/10.1016/j.conbuildmat.2021.124158

PROMOTION AND TECHNICAL STUDY FOR THE WIDER USE OF GGBS CONCRETE IN THE CONSTRUCTION INDUSTRY FOR REDUCING CARBON EMISSION

Ir Jackie CK LEUNG[1], Ir Terry KF LUK[2], Ir Jack Y KWOK[3], Ir Jenny F YEUNG[4]
[1-4]Geotechnical Engineering Office (GEO),
Civil Engineering and Development Department (CEDD),
The Government of the Hong Kong Special Administrative Region

1. INTRODUCTION

According to Hong Kong's Climate Action Plan 2050, the city is targeting to achieve a carbon reduction of 50% by 2035 to pave way for carbon neutrality by 2050. The construction industry contributes to about 11% of global carbon emission, among which 8% comes from cement industry alone. The use of supplementary cementitious materials (SCM) such as Pulverised Fly Ash (PFA) and Ground Granulated Blastfurnace Slag (GGBS) in concrete production has been proven effective in reducing total carbon emission by replacing Ordinary Portland Cement (OPC). The general specifications (GS) for various works, e.g. GS for Civil Engineering Works, published by the Government have allowed the use of PFA in concrete production for public work projects in the past three decades. However, the local supply of PFA is expected to halt by 2035 when the power companies cease using coal for electricity generation. There is hence an imminent need to identify alternatives of SCM for concrete production. Despite GGBS concrete has also been allowed since 2012, its consumption was only about 1% of the total concrete consumption in 2022, contributed by the pilot use of GGBS concrete in a number of public works projects (PWP) in that year. There have generally been a few concerns over the performance of GGBS concrete, particularly on its perceived lower early strength, though recent studies may prove otherwise.

To this end, the Standing Committee on Concrete Technology (SCCT) has been tasked by the Development Bureau of the Government to promote the wider use of GGBS concrete in Hong Kong's construction industry. In order to take the lead, the SCCT has consulted the relevant stakeholders and formulated a roadmap for encouraging the use of GGBS concrete in PWP.

With a view to evaluating the performance of GGBS concrete used in the recent projects, the Public Works Central Laboratory (PWCL) of GEO, CEDD has conducted a preliminary technical study on various performance aspects, including early strength development and shrinkage properties. The PWCL is also studying the use of GGBS grout for slope upgrading works under the Landslip Prevention and Mitigation Programme (LPMitP), with emphasis on technical requirements including workability and bleeding.

This paper shares the Government's vision in promoting the wider use of GGBS concrete and presents the results of the preliminary studies.

2. TECHNICAL STUDY ON PERFORMANCE OF GGBS CONCRETE MIXES

PWCL manages a database of concrete mixes used by the PWP. In order to review the performance of the GGBS concrete used in the PWP since 2022, information of the relevant GGBS concrete mixes were retrieved from the database. The data set of GGBS concrete mixes indicates that the grade strength and GGBS replacement ratio range from Grade 25 to Grade 60 and 35% to 65% respectively. PWCL prepared concrete cubes, replicating 13 of these GGBS concrete mixes using the same cementitious content, aggregate content and water-cement (w/c) ratio in the laboratory environment for testing. The selected mixes covered various grade strengths and GGBS replacement ratios. Compressive strength tests and shrinkage tests were conducted in the laboratory conditions in accordance with CS1:2010 and BS EN 12390-16 respectively. For each of the replicated GGBS concrete mix, a control OPC mix with the same w/c ratio was also prepared for comparison purpose. A summary of the concrete mixes is shown in Table 1.

Table 1: List of GGBS concrete mixes

Mix Number	Grade	Total Cementitious Content, kg/m^3	GGBS Content %	a/c Ratio*	w/c Ratio
1	25	410	60%	4.09	0.49
2	30	406	35%	4.26	0.45
3	30	450	60%	3.61	0.46
4	40	410	50%	4.44	0.38
5	45	450	35%	3.83	0.41
6	45	480	40%	3.52	0.36
7	45	450	60%	3.8	0.42
8	45	450	65%	3.91	0.36
9	45	410	65%	4.41	0.38
10	50	450	65%	3.91	0.36
11	55	430	65%	4.2	0.35
12	55	460	65%	3.76	0.35
13	60	460	50%	3.83	0.35

* a/c ratio denotes aggregate/cement ratio

In addition to the concrete specimens prepared by PWCL, GGBS concrete and PFA concrete cubes were also obtained from the construction sites of some on-going PWP for carrying out strength tests for comparison purpose. These covered 5 GGBS concrete mixes and 2 PFA concrete mixes.

The following observations were made from the test results:

(a) The results from the compressive strength tests showed that all GGBS mixes achieved greater than 40% and 60% of the 28-day strength at 3 days and 7 days respectively, corresponding to 60% and 90% of the grade strength at 3 days and 7 days. The control OPC mixes achieved greater than 60% and 80% of the 28-day strength at 3 days and 7 days respectively, corresponding to 90% and 100% of the grade strength at 3 days and 7 days. The 7-day to 28-day strength of the GGBS mixes ranged from 0.62 to 0.76, whereas the figures of the control OPC mixes ranged from 0.81 to 0.89. Despite the early strengths at 3 days and 7 days of all GGBS mixes were consistently lower than the control OPC mixes, the actual strengths achieved by all GGBS mixes at 3 days and 7 days are considered sufficient for general civil and foundation works.

(b) The total shrinkage of the specimens was determined in accordance with BS EN 12390-16. The results from the shrinkage tests showed that 9 out 13 GGBS mixes exhibited less total shrinkage than the corresponding control mixes, while the remaining mixes exhibited the opposite behaviour. No consistent trend on the influence of GGBS on shrinkage performance could be observed in this exercise. Further study on the effect of GGBS on the autogenous shrinkage and drying shrinkage, as well as to cover longer measurement periods is recommended.

The results of this preliminary study revealed that the performance of the GGBS concrete mixes adopted in PWP were on-par with OPC concrete mixes and were suitable for general civil and foundation works. However, given that the scope of the study was relatively limited, covering only strength and total shrinkage tests, further studies on the performance of GGBS concrete, including but not limited to the durability (e.g. chloride resistance) and heat evolution, will be carried out.

3. TRIAL ON GGBS GROUT FOR SLOPE UPGRADING WORKS

Cement-based grout is widely used in slope engineering works in particular for grouting of soil nails, rock bolts and rock dowels. Traditionally, a simple and standardised cement grout mix, involving OPC and water with a w/c ratio not exceeding 0.45 has been referred to in standard specifications in the past decades. GEO has recently been exploring the potential of considerably replacing OPC by GGBS in the grout mixes for use under the LPMitP. To this end, PWCL was tasked to identify possible GGBS grout mixes that could satisfy the relevant technical requirements, such as workability and bleeding, with an optimal addition of admixtures.

With the technical support of GGBS / cement / concrete suppliers, a series of laboratory trial mixing using different grout formulas, cementitious materials and admixtures was arranged. The GGBS replacement ratio ranged from 50% to 73%. In addition, four control mixes with 50% GGBS replacement but without the use of admixtures and one control mix using pure OPC were also arranged. Compliance tests, namely flow cone tests to ASTM C939, bleed tests to ASTM C940 and compressive strength tests at various cube ages to CS1:2010 were conducted.

The following observations were made from the test results:

(a) General and workability – All GGBS grout mixes generally met the flow cone requirements for grout for geotechnical works as stipulated in the GS.

(b) Strength - The GGBS grout mixes achieved compressive strengths ranging from 46 MPa to 106 MPa at 28 days, which are beyond the requirement of 30 MPa at 28 days as stipulated in the GS.

(c) Bleeding - For all mixes, the 3-hour bleeding results were the same as the final bleeding results. Although only one series of GGBS grout mixes, having the lowest w/c ratio of 0.36, satisfied the 3-hour bleeding requirement (< 0.5%) as specified in the GS, all mixes satisfied the maximum bleeding requirement (1%). In addition, all mixes were observed to have absorbed the bled water within 24 hours.

Moreover, preliminary field trials were conducted and the initial results appeared promising. Further field trials of the preferred GGBS grout mixes will be conducted, with particular focus on resolving any field mixing operation difficulties encountered on site. Upon successful laboratory and field trials, a standard material specification will be prepared to promote the use of GGBS grout for slope engineering works.

4. ROADMAP TO PROMOTE WIDER USE OF GGBS CONCRETE

Based on the promising results of the previous and the recent technical studies on GGBS concrete, the use of GGBS concrete with a replacement ratio ranging from 35% to 75% allowed by the GS has been proven effective. With a recent review on the demand and supply of GGBS and GGBS concrete conducted through consultation with the relevant stakeholders, an ambitious target has now been set for the PWP to increase the use of GGBS concrete to 50% by volume in the financial year 2024/25. Further study on the demand and supply of GGBS concrete, and its technical requirements, with emphasis on its early strength (as early as its 1-day strength), will be conducted in parallel. With the technological advancement and the better quality of GGBS available in recent years, the feasibility of achieving higher replacement levels and higher grade strengths will also be explored. Subject to the satisfactory results of the study, the Development Bureau will consider further increase the GGBS usage to a higher percentage by 2026.

The construction industry in Hong Kong has been proud of delivering first class infrastructure projects in the world, it certainly bears the social responsibility to reduce carbon emission in the course. It is anticipated that the above initiative and studies by the Government would serve to raise the industry awareness and gear up the technical competency of industry practitioners and stakeholders to promote the wider use of GGBS concrete. It is also believed that the resulting carbon reduction will contribute to shaping Hong Kong as a more liveable city while developing into a sustainable metropolis.

5. ACKNOWLEDGEMENT

This paper is published with the permission of the Head of the Geotechnical Engineering Office and the Director of Civil Engineering and Development, the Government of the Hong Kong Special Administrative Region, China. The input and support from the various public works contracts in providing additional concrete specimens for the GGBS concrete study are gratefully acknowledged. The technical support from Excel Concrete Ltd., Greentex Construction Materials Ltd. and K. Wah Construction Materials Ltd. in the trials of GGBS grout are also gratefully acknowledged.

6. REFERENCES

Rodgers L, 2018. *Climate change: The massive CO^2 emitter you may not know about*. BBC News. <https://www.bbc.com/news/science-environment-46455844>

BSI. 2006. *Ground Granulated Blastfurnace Slag for Use in Concrete, Mortar and Grout. Definitions, Specifications and Conformity Criteria.* BS EN 15167-1: 2006. British Standards Institution, London.

BSI. 2011. *Cement – Part 1: Composition, specifications and conformity criteria for common cements*. BS EN 197-1:2011. British Standards Institution, London.

BSI. 2019. *Testing hardened concrete Part 16: Determination of the shrinkage of concrete.* BS EN 12390-16:2019. British Standards Institution, London.

HKSAR Government. 2006. *General Specification for Civil Engineering Works (2006 Edition).* The Government of the Hong Kong Special Administrative Region.

HKSAR Government. 2020. *General Specification for Civil Engineering Works (2020 Edition).* The Government of the Hong Kong Special Administrative Region.

HKSAR Government. 2010. *Construction Standard – Testing Concrete (2010 Edition)*. The Government of the Hong Kong Special Administrative Region.

Leung, W.C. Leung & Wong, H. D. 2011. *Final Report on Durability and Strength Development of Ground Granulated Blastfurnace Slag Concrete*. GEO Report No. 258. HKSAR

Wong, H.D. & Chi, R.C.Y. 2016. Use of Ground Granulated Blastfurnace Slag in Cement Grout for Geotechnical Works. GEO Technical Note No. 2/2016, 34p.

EQUIPMENT AND TREATMENT PROCESS OF DECORATION WASTE: AN INVESTIGATION OF SHANGHAI

Zhenhua Duan[1], **Minjie Hou**[1], Jianzhuang Xiao[1*]

[1]Department of Structural Engineering, Tongji University, Shanghai, 200092, China
*Corresponding author: jzx@tongji.edu.cn; Tel: 86-13621836895

Decoration waste (DW), one type of construction and demolition waste (C&DW), refers to the waste generated during the building interior decoration. The development of Chinese construction industry is making the transition from low-quality rapid development to high-quality sustainable development, which lead to the emission of C&DW will significantly reduce and the amount of DW will keep growth for a long period in the future. This study through investigating the current situation of DW treatment plants in Shanghai to fully understand the advantage and disadvantage of different processing technologies. 12 plants were statistically analyzed based on equipment, processes, funding, recycled aggregate and recycled product. The results show that DW requires additional devices for removing contaminants compared to C&DW. Main sorting equipments contain eddy current separator, magnetic separator, air separator and photoelectric sorter. The pre-removal process of fine residues can greatly improve efficiency of treatment and final aggregate quality. With the reasonable control of the whole process in recycling plant, recycled aggregates with less than 1% impurity content can be obtained through multiply crushing, sorting and screening. In addition, a disposal model for cities and towns with different development situation is proposed by the public economy and market requirement. Lastly, based on the comparison of C&DW and DW, the key difficulties and problems of DW recycling processes are identified for future strategy. The findings of this study may contribute to the technology development and recycling of DW.

Keywords: Decoration waste; recycling and utilization status; processing technology; contaminant removal; economic analysis

VALUE-ADDED RECYCLING OF WASTE POLYPROPYLENE INTO PERFORMANCE-ENHANCING BITUMEN MODIFIERS THROUGH MELTING DEGRADATION-GRAFTING REACTIONS

Tianqi Hu[1], Xiong Xu[2,*] , Yunsheng Zhu[1], Yaming Chu[2], Guoxiang Hu[2]

[1] School of Transportation and Logistics Engineering, Wuhan University of Technology, Wuhan 430063, China
[2] School of Civil Engineering and Architecture, Wuhan Institute of Technology, Wuhan, 430073, China
[*] Corresponding author. School of Civil Engineering and Architecture, Wuhan Institute of Technology, Wuhan, 430073, China.
E-mail (corresponding author): xxucea@wit.edu.cn

1. INTRODUCTION

Plastic products are widely used in our daily lives (Kulkarni, Ravekar, Rao, Waigokar, & Hingankar, 2022). Because they are not fully reused, large amounts of their waste are quickly produced and eventually become real rubbish. As most of them cannot be degraded in the natural environment for a long period like ten years. Therefore, it is of great importance and significance to seek for an effective and efficient approach to make these plastic wastes sustainable and applicable.

Plastics can be used as modifiers for asphalt to improve some technical properties, such as anti-rutting deformation and resistance to moisture damage (Modarres & Hamedi, 2014). However, in the case of polypropylene (PP), good compatibility can only be achieved if the mixing temperature of waste PP modifier and asphalt is higher than 180°C (Dalhat & Al-Adham, 2023). However, mixing temperatures above 180°C are associated with high energy consumption, serious environmental pollution and high health risks for workers (Ameri, Afshin, Shiraz, & Yazdipanah, 2020). Therefore, in the clean production of waste PP-modified asphalt binder, it is very important to solve the contradictory problems of lower modification temperature and higher performance.

This study proposes a new mechanochemical approach to prepare different modifiers by incorporating two different catalysts, N-hydroxyphthalimide (NHPI) or dibenzoyl peroxide (BPO), and degradation grafting of waste PP using phthalic anhydride (PA) as grafting monomer, for the performance improvement of asphalt binders. To better understand the physicochemical properties of the obtained modifiers and modified asphalt binders, torque rheology, thermogravimetric analysis (TG) of the waste PP-based modifiers were compared, and penetration, softening point will be performed on PP-modified asphalt binders (PPA).

2. MATERIALS AND METHODS

2.1. Raw materials

2.1.1. Waste Polypropylene (PP)

Waste PP was those sourced from disposable tableware wastes, which were mechanically crushed into the finer-sized particles for use. Through testing, its melting temperature is greater than 180°C and the density is 0.91 g/cm^3.

2.1.2. Initiator and monomer

N-hydroxyphthalimide (NHPI) and dibenzoyl peroxide (BPO) are commonly used to initiate grafting reactions in plastics and also to degrade plastics by causing β-breakage reactions in plastic polymers (Zhou et al., 2019). Phthalic anhydride (PA) improves the toughness of plastics, so an attempt was made to use PA as a grafting monomer for PP plastics. These reagents, purchased from Aladdin Reagent (Shanghai) Co., Ltd were analytically pure in grade.

2.1.3. Asphalt binder

The asphalt binder used in this study was a Pen 70 virgin bitumen supplied locally. The physical properties include softening point, penetration at 25°C, and ductility at 15°C, which were tested to 49.0°C, 63, and greater than 100cm, respectively.

2.2. Preparation of PP modifiers through thermal degradation-grafting method

30 g waste PP, 0.15 g NHPI (5‰ by weight of waste PP) and various dosages of PA (0%, 1%, 3%, and 5%, by weight of waste PP) were weighed and added to the mixing chamber of the RM-200A torque rheometer at a reaction temperature of 200 °C with a rotational speed of 60 rpm for 10 min. After thermally mixing, the reaction products were collected and then mechanically crushed and granulated into particles as asphalt modifiers. These modifiers are designated N-PP0, N-PP1, N-PP3 and N-PP5. BPO, on the other hand, needs to be reacted at a temperature of 160°C. The modifiers obtained using the BPO reaction are designated B-PP0, B-PP1, B-PP3 and B-PP5.

2.3. Thermal analysis for PP modifiers

2.3.1. TG test

TG test is commonly used to characterize the thermal properties of plastics. This study employed NETZSCH thermogravimetric analyser to investigate the thermal properties of the modifiers obtained from waste PP. The test conditions were as follows: The heating temperature range was 30-600°C, the heating rate was 10°C/min and the atmosphere was air.

2.3.2. Torque rheology

The torque rheological behaviour of the modifiers was tested using the RM-200A torque rheometer to assess the degradation state of the modifiers during the reaction. The test conditions were following the procedures shown in Section 2.2.

2.4. Preparation of modified asphalt binder

The previously prepared PP modifiers were mixed with the original asphalt binder (4% by weight of asphalt), stirred at low speed for 20 min at a temperature of 170°C, and then sheared at high speed for 30 min at 4,000 rpm. The obtained PP modified asphalt binders (PPA) (Padhan & Sreeram, 2018) were named as N-PPA0, N-PPA1, N-PPA3, N-PPA5, B-PPA0, B-PPA1, B-PPA3 and B-PPA5, respectively.

2.5. Physical properties for PPA

PPA adhesives have been tested for softening point and penetration at 25°C according to ASTM D36 and ASTM D5 to evaluate their high temperature performance and consistency.

3. RESULTS AND DISCUSSION

3.1. Thermal analysis of different PP modifiers

Fig. 1 shows the thermal stability of different PP modifiers. It is clear that the quality of the different PP modifiers gradually decreases with increasing temperature. Among the temperatures corresponding to a 2% mass loss of the modifiers, N-PP5 has the lowest temperature for a 2% mass loss, 228.7°C, and B-PP0 has the second lowest temperature for a 2% mass loss, 231.7°C. This result indicated that the best degradation among the NHPI series of modifiers is N-PP5, and the best degradation among the BPO series of modifiers is B-PP0, with N-PP5 degrading even better than B-PP0 (Xu et al., 2022). It can be explained that the addition of PA in the BPO-induced reaction hindered the degradation of PP. Fig. 2 states the rate of thermal decomposition of PP modifiers. This result is well consistent with the above-mentioned TG result.

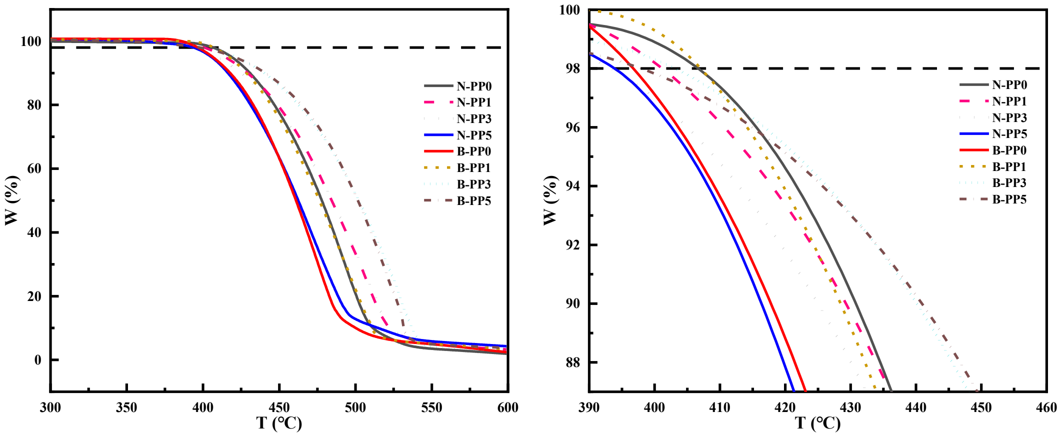

Fig. 1. Thermogravimetric (TG) analysis of the various PP modifiers

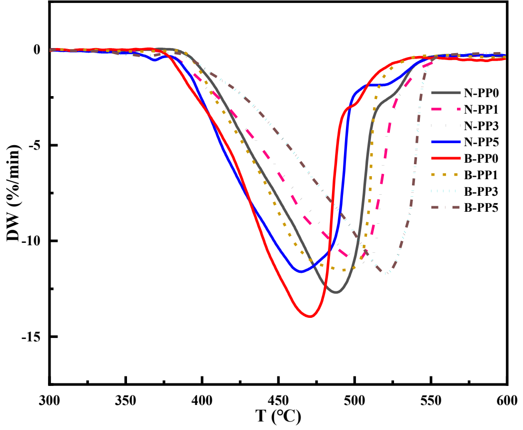

Fig. 2. DTG analysis of the various PP modifiers

3.2. Torque rheology analysis of PP modifiers

Fig. 3 shows the effect of NHPI or BPO on the torque rheological properties of PP. From the trend of the curves, the torque rheological behaviour of PP modifiers can be roughly divided into three stages: (1) solid feed stage; (2) PP modifier torque gradually increases to reach the peak stage; (3) PP modifier torque decreases from the peak to the equilibrium stage. Comparing the torque values of the PP modifiers at equilibrium, it can be seen that the torque of the NHPI series modifiers at equilibrium is not very different, and the torque of the BPO series modifiers at equilibrium is greatest for B-PP0 and least for B-PP5. The results indicated that BPO has a greater chance of cross-linking PP than NHPI, and the incorporation of PA can reduce the chance of PP cross-linking reaction.

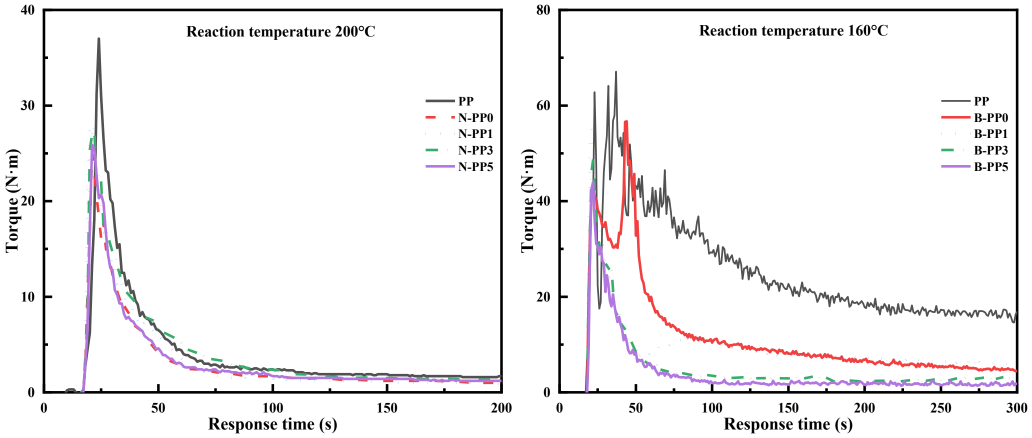

Fig. 3. Torque variation of the various PP modifiers

3.3. Effects of the modifiers on physical properties of virgin bitumen

Table 1 presents the softening point and penetration results of modified asphalt binders. It is clear that various PP modifiers increase the softening point and decrease the penetration of virgin bitumen. B-PPA0 showed the least change in softening point and N-PPA5 showed the least change in penetration compared to the virgin bitumen. This further indicates that B-PPA0 and N-PPA5 have the best degradation effect.

Table 1 Softening point and penetration at 25 °C of the asphalt binder.

Binder ID	Softening point (°C)	Penetration at 25 °C (0.1mm)
Virgin bitumen	49.0	63
N-PPA0	56.3	45
N-PPA1	55.7	47
N-PPA3	54.4	49
N-PPA5	53.9	52
B-PPA0	53.2	50
B-PPA1	57.1	43
B-PPA3	56.0	44
B-PPA5	53.3	49

4. CONCLUSIONS

In this study, NHPI and BPO were innovatively used for degradation grafting of PP, respectively, to obtain PP modifier in the case of PA as grafting monomer, and PP-modified bitumen was produced with PP modifier. The degradation efficiency of PP by NHPI and BPO was investigated by thermal analysis and torque rheology analysis of PP modifiers and the following conclusions were obtained:

(1) N-PP5 and B-PP0 had the best degradation effect, and the increasing content of PA can promote the degradation of waste PP by NHPI.

(2) The increase of PA content hinders the degradation of PP by BPO, but also reduces the chance of PP cross-linking reaction occurring.

(3) The PP modifier prepared with NHPI has a smaller chance of cross-linking reaction, and 5‰ NHPI and 5% PA are recommended for the preparation of PP modifier.

Overall, this paper provides a new way to prepare PP modifier for waste PP, but the reaction relationship between degradation and grafting of PP needs further research, in addition to the use of degradation grafted plastic modified asphalt preparation of asphalt mixes, and the road performance of the mixes, which will be explored in more depth in the subsequent research.

5. REFERENCES

Ameri, M., Afshin, A., Shiraz, M. E., & Yazdipanah, F. (2020). Effect of wax-based warm mix additives on fatigue and rutting performance of crumb rubber modified asphalt. *Construction and Building Materials, 262*, 120882.

Dalhat, M., & Al-Adham, K. (2023). Review on laboratory preparation processes of polymer modified asphalt binder. *Journal of Traffic and Transportation Engineering (English Edition).*

Kulkarni, P., Ravekar, V., Rao, P. R., Waigokar, S., & Hingankar, S. (2022). Recycling of waste HDPE and PP plastic in preparation of plastic brick and its mechanical properties. *Cleaner Materials*, 100113.

Modarres, A., & Hamedi, H. (2014). Effect of waste plastic bottles on the stiffness and fatigue properties of modified asphalt mixes. *Materials & Design, 61*, 8-15.

Padhan, R. K., & Sreeram, A. (2018). Enhancement of storage stability and rheological properties of polyethylene (PE) modified asphalt using cross linking and reactive polymer based additives. *Construction and Building Materials, 188*, 772-780.

Xu, X., Chu, Y., Chen, R., Wu, Q., Chen, X., Zou, F., & Peng, C. (2022). Thermo-mechanochemical recycling of waste polypropylene into degradation products as modifiers for cleaner production and properties enhancement of bitumen. *Journal of Cleaner Production, 379*, 134792.

Zhou, H., Plummer, C. M., Li, H., Huang, H., Ma, P., Li, L., Chen, Y. (2019). Regioselective post-functionalization of isotactic polypropylene by amination in the presence of N-hydroxyphthalimide. *Polymer Chemistry, 10*(5), 619-626.

THEORY AND APPLICATION OF CIVIL FUNCTIONAL MATERIALS PREPARED BY RED MUD WITH MULTISOURCE SOLID WASTE

Jian Zhang, Zhaofeng Li, Shucai Li

Geotechnical and Structural Engineering Research Center, Shandong University

Red mud is a major industrial waste residue from aluminum production. Based on the concept of collaborative utilization of multiple solid wastes, the reporter has developed green and high-performance red mud-based cementitious materials that can completely replace cement for different road construction projects, such as road base, subgrade, prefabricated components, and reinforcement of poor geological conditions. At present, a pilot production line with an annual output of 500,000 tons of red mud-based cementitious materials has been built, and the products have been successfully applied in the construction of Jigao Expressway, Linlin Expressway and other projects. This is the first time in China that red mud-based cementitious materials have achieved 100% substitution of cement for the construction of stable crushed stone layers on highways.

UTILIZATION OF LOW-GRADE GLASS AS A PARTIAL REPLACEMENT OF CEMENTITIOUS MATERIALS AND RIVER SAND IN ULTRA-HIGH PERFORMANCE CONCRETE: PREPARATION OF GREEN BUILDING MATERIALS FOR SUSTAINABLE USE

Xudong Zhao [a, b, c], Jian-Xin Lu [a*], C.S. Poon [a*]

[a] Department of Civil and Environmental Engineering & Research Centre for Resources Engineering Towards Carbon Neutrality, The Hong Kong Polytechnic University, Hong Kong, China
[b] State Key Laboratory of Silicate Materials for Architectures, Wuhan University of Technology, Wuhan 430070, China
[c] School of Materials Science and Engineering, Wuhan University of Technology, Wuhan 430070, China
*Corresponding author: jianxin.lu@polyu.edu.hk (J. X. Lu),
chi-sun.poon@polyu.edu.hk (C. S. Poon)

Recycling of waste glass is a serious problem in Hong Kong. Among other things, factory recycled waste glass powder contains high levels of contaminants, which may be harmful to concrete, and glass cleaning is neither economical nor sustainable. Limited studies have investigated the effect of unwashed waste glass on concrete properties, which hinders its engineering application in ultra-high performance concrete (UHPC). In this study, low-grade waste glass is combined with high value-added UHPC to explore the preparation of sustainable new high-performance building materials. Unwashed waste glass powder and sand (U-WGP and U-WGS) were used as substitutes for cement and river sand, respectively, and the results showed that the mechanical properties of UHPC were affected by using U-WGP and U-WGS. The impurities in the unwashed waste glass could act as an internal conditioner positively affecting the autogenous shrinkage and drying shrinkage of UHPC. And impurities react in alkaline environment of UHPC to produce gases that expand at the early stage, compensating for the autogenous shrinkage that occurs in the later stages of the UHPC matrix. ASR tests have shown that there was no risk of swelling when waste glass was used in UHPC, due to its low water-cement ratio and dense structure. X-ray CT and microstructural images show that swelling from impurities in the U-WGS cracks the UHPC matrix structure and degrades the ITZ between the U-WGS and the matrix. Overall, this study found that UHPC prepared with 30% U-WGP replacement cement performed better with negligible effect of contaminants in waste glass compared to 50% U-WGS replacement RS.

Keywords: UHPC; low-grade glass; shrinkage; ASR expansion; microstructure

ENCHANTMENT OF ARCHITECTURAL LUMINESCENT-GLASS MORTAR (ALM) PROPERTIES WITH WHITE-COLOR POWER ENCAPSULATION

Jinxin, Wei[1], Yujia Xiao[1], Tung-Chai Ling[1,*]

[1]College of Civil Engineering, Hunan University, Changsha 410082, Hunan, China
E-mail (corresponding author): tcling@hnu.edu.cn; tcling611@yahoo.com

1. INTRODUCTION

Luminous building materials are designed as smart and multifunctional that possesses the ability to capture solar or artificial light and emit it in the form of visible light in the dark environment. This material does not consume any electricity, which considered to be sustainable and low-carbon green material (Han et al., 2017) for the application in building decoration, roads/lanes lighting construction, as well as integrated in expressway signs/safety (Aich et al., 2013; Hai et al., 2018; Hu et al., 2017).

Architectural luminescent-glass mortar (ALM) has been developed using waste glass as aggregate and fixing luminescent powder on the glass aggregate with adhesive material (Xiao et al., 2022a). ALM exhibited good workability, mechanical properties, and proper light excitation and emission wavelength ranges. In addition, the brightness can be maintained for 8 hours in a dark environment (Xiao et al., 2022b). However, the presence of the adhesive used for encapsulating the luminescent powder on the glass surface had an adverse effect on the mechanical properties in particular the compressive strength of ALM. This was because the adhesive coating retarded the hydration of cement, resulting in weak mechanical properties and may cause some durability problems (Wang et al., 2006; Xie et al., 2020). Furthermore, the adhesive properties also resulted in the difficulty for the separation of glass aggregates prior using in the production of ALM.

This study aims to improve the performance of ALM in particular the mechanical and luminescent properties by wrapping a layer of white powder on the luminescent glass aggregate before incorporating into cement mortar. To examine the effect of white powder, six different type of powders including white cement (WC), metakaolin (MK), ground granulated blast-furnace slag (GGBS), calcium carbonate (CC), quartz (Q) and glass powder (GP) were used and studied comparatively.

2. MATERIALS AND METHODS

2.1. Materials

White cement (WC) was selected as sole binder for the production of ALM. Recycled glass (RG) was derived from discarded beverage bottles. Two sizes of glass aggregates (1~6 mm and 6~9 mm) were via crushing, cleaning and drying processes. It should be noted that only coarse glass aggregates (6~9 mm) were chosen for luminescent-glass (LG) preparation.

Luminescent powder (LP) is a yellowish-green powder with a particle size range of 10 to 100 μm, sourced from Luming Technology Group Co., Ltd. The main indexes of LP are shown in Table 2. The adhesive material (Shenzhen Poly Gold ink Technology Co., Ltd.) used was CB-Series screen printing ink, a kind of transparent synthetic resin varnish, and its chemical composition is 30~55% polyester resin, 25~55% filler (carbon black/titanium dioxide/pigment red) and 15~20% isophorone solvent. The chemical compositions and whiteness of white-color powders used are presented in Table 1.

Table 1. The chemical composition and whiteness value of white-color powders.

Powders	Chemical composition (wt%)						Whiteness
	CaO	SiO_2	Al_2O_3	MgO	SO_3	K_2O	
WC	60.14	15.35	1.69	6.86	4.42	0.56	84.9
MK	0.28	50.89	45.86	0.07	0.03	0.20	80.5
GGBS	39.76	30.16	14.53	9.21	3.43	0.35	73.4
CC	99.82	-	-	0.14	0.01	-	92.7
Q	0.04	98.59	0.96	0.03	-	0.25	82.0
GP	10.01	71.11	0.48	3.60	-	0.15	79.6

Table 2. The main indexes of luminescent powder.

	Average particle size / D_{50} (μm)	Chemical composition	Excitation Wavelength range (nm)	Emission Wavelength peak (nm)	Afterglow time (h)
LP	36.12	$SrAl_2O_4$: Eu^{2+}, Dy^{2+}	340-430	393	12

2.2. Sample preparation and curing

The LP and the transparent adhesive were first mixed at a ratio of 0.3 (LP/adhesive) to form a viscous luminescent paint. One part of coarse glass aggregate was then stirred with five parts of the prepared viscous luminescent paint. LG was prepared by covered the surface layer by white-color powder and placed for 48 h prior mixing with other ingredients for ALM production. The preparation steps involved is shown in Figure 1. After casting, all the samples were covered with plastic films in the laboratory under a temperature of 23 ± 3 °C and RH of 75% for 24 h and then demolded.

Figure 1. The flow chart of preparing LG and ALM.

2.3. Testing methods

Three 40 mm cubic samples were used for the compressive strength test in accordance with Chinese Standard GB/T 17671-2021 at 1, 7, and 28 days. Three cylindrical samples with a diameter of 40 mm were cut to expose the cross-section with LG for the examination of luminescent property of ALMs according to the Chinese standard GB/T 5838.3-2015 (Wang et al., 2021). The samples were excited by a 5.4×103 cd/m^2 light source for 30 min. The brightness was measured using the ST-86LA screen luminance meter, and the appearances of the ALMs were captured by a digital camera.

3. RESULTS AND DISCUSSION

The compressive strength of ALMs are presented in Figure 2. At 1-d, control ALM gained the lowest compressive strength, about 28.6% lower than that of white powder modified ALM. This could be mainly related to the direct contact of adhesive with surrondind cemnet paste which could delay the cement hydration at early strength. It is clear that the modified ALM with inert materials such as CC and Q showed the greater improvement in 28d-strength (acheived 65MPa), about 50% higher than the control ALM. The key reason was that the adhesive was diluted and filled with white powders, resulting in a denser luminescent layer (interfacial transition zone). The white-color powders existed in the outermost layer of the LG also created a better bond between the cement paste and LG via physical and chemical effects. In comparison, the influence of white-color powder type showed quite little effect on the strength of ALMs.

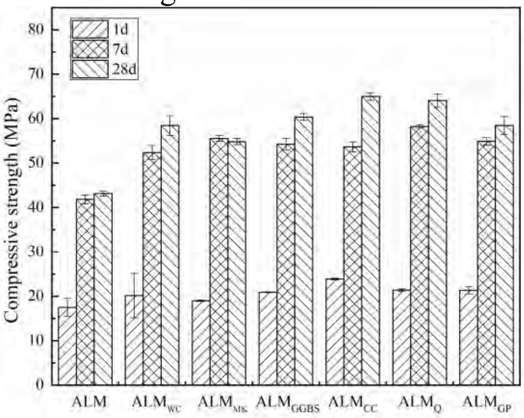

Figure 2. The compressive strength of ALMs.

Note: ALM refers to a control group without white powder.

The luminescent property of ALMs over time are shown in Figures 3 and 4. ALM$_{CC}$ exhibited the highest initial brightness and the longest afterglow time (~8h), while ALM$_{GGBS}$ had the lowest performance in luminescent property. As can be seen in Figure 4, both the initial brightness and afterglow time of ALM$_{GP}$ were the same compared to that of ALM. The ALM$_{WC}$, ALM$_{MK}$, and ALM$_{Q}$ attained the lowest in terms of afterglow time with only 4-5 h.

These results were in good agreement with the whiteness of white powders. The powder in the luminescent layer will absorb part of the light emitted by the LP, thus affecting the initial brightness and afterglow time of ALMs. Therefore, LP with high whiteness values of white powder could absorb the least light and presented better luminescent property. In addition, the addition of white powder (i.e. calcium carbonate) was beneficial to reduce the path of excited and emitting light of LP, that is, the distance from the glass aggregate, resulting in better luminescent property than ALM.

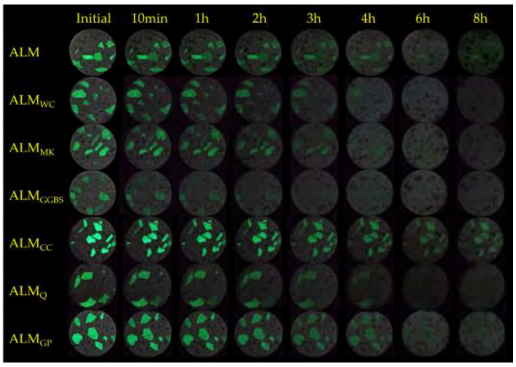

Figure 3. The luminescent property of ALMs.

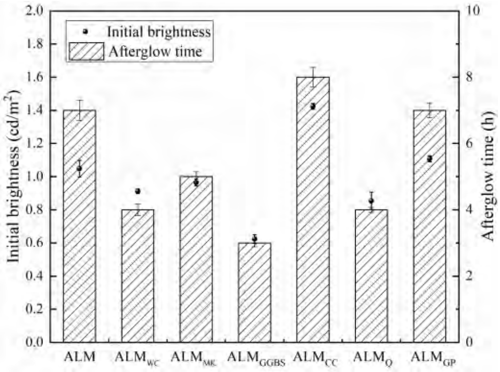

Figure 4. The initial brightness and afterglow time of ALMs.

4. CONCLUSION

The encapsulation of white powder significantly improved the mechanical properties of ALM and offset the adverse effects of the adhesive in the cement paste matrix. Due to the influence of whiteness of powder, the luminescent property of modified ALMs was slightly lower than that of ALM, except CC-modified ALM. The performance change could be attributed to the filling effect of white powder in the luminescent layer and the dilution effect on the adhesive. This paper demonstrates an enhancement approach to improve the mechanical and luminescent properties of using luminous material in glass decorative cement-based materials.

5. ACKNOWLEDGMENT

The research funding support from the Science and Technology Innovation Plan of Hunan Province (2022WZ1010).

6. REFERENCES

Aich, N., Appalla, A., Saleh, N. B., & Ziehl, P. (2013). Triboluminescence for distributed damage assessment in cement-based materials. *Http://Dx.Doi.Org/10.1177/1045389X13484100*, *24*(14), 1714–1721. https://doi.org/10.1177/1045389X13484100

Hai, O., zhang, Z., Ren, Q., Wu, X., Zhang, Q., Zeng, B., & Li, D. (2018). The preparation and fun ctional studies of the porous long afterglow luminescent materials. *Dyes and Pigments*, *156*, 16 0–166. https://doi.org/10.1016/J.DYEPIG.2018.04.007

Han, B., Zhang, L., & Ou, J. (2017). Smart and multifunctional concrete toward sustainable infrastr uctures. *Smart and Multifunctional Concrete Toward Sustainable Infrastructures*, 1–400. https:/ /doi.org/10.1007/978-981-10-4349-9/COVER

Hu, S., Lu, C., Qin, X., Zhou, G., Xu, Z., & Wang, S. (2017). Color tuning of $Lu_3Al_5O_{12}$:Dy^{3+} cera mic-based white light-emitting phosphors via Yb incorporation. *Journal of the European Cera mic Society*, *37*(1), 229–237. https://doi.org/10.1016/J.JEURCERAMSOC.2016.07.025

Wang, R., Li, X. G., & Wang, P. M. (2006). Influence of polymer on cement hydration in SBR-mo dified cement pastes. *Cement and Concrete Research*, *36*(9), 1744–1751. https://doi.org/10.101 6/J.CEMCONRES.2006.05.020

Wang, W., Sha, A., Lu, Z., Jia, M., Jiang, W., Liu, Z., & Yuan, D. (2021). Self-luminescent cement -based composite materials: properties and mechanisms. *Construction and Building Materials*, *269*, 121267. https://doi.org/10.1016/J.CONBUILDMAT.2020.121267

Xiao, Y., Pham, B. T., Guo, M. Z., & Ling, T. C. (2022a). Use of luminescent-glass aggregates for the production of decorative architectural mortar. *Journal of Building Engineering*, *50*, 104233. https://doi.org/10.1016/J.JOBE.2022.104233

Xiao, Y., Pham, B. T., Guo, M. Z., & Ling, T. C. (2022b). Influence of luminescent powder type an d characteristic on the glow light performance of architectural glass mortar. *Journal of Building Engineering*, *58*. https://doi.org/10.1016/j.jobe.2022.105021

Xie, N., Li, H., Zhang, H., Zhang, X., & Jia, M. (2020). Effects of accelerated weathering on the op tical characteristics of reflective coatings for cool pavement. *Solar Energy Materials and Solar Cells*, *215*, 110698. https://doi.org/10.1016/j.solmat.2020.110698

PRODUCTION OF LIGHTWEIGHT AGGREGATES FROM WASTE GLASS AND INCINERATED SEWAGE SLUDGE ASH

Yujie Huang, Zuwang Bian, Ziwei Chen, Weiyi Ji, Jian-Xin Lu*, Chi Sun Poon*

Department of Civil and Environmental Engineering & Research Centre for Resources Engineering towards Carbon Neutrality (RCRE),
The Hong Kong Polytechnic University, Hung Hom, Kowloon, Hong Kong
E-mail: jianxin.lu@polyu.edu.hk (J.X. Lu); cecspoon@polyu.edu.hk (C.S. Poon)

In this study, lightweight aggregates (LWAs) were prepared by waste glass (WG) and incinerated sewage sludge ash (ISSA) as materials during the process of powder sintering. The effect of ISSA content on physical properties, leaching behaviour, phase composition, pore structure of LWAs were systematically investigated. The results showed that LWAs made with WG and ISSA could be used as an environmentally safe material for civil engineering. The addition of ISSA was beneficial for the formation of various crystalline phases and the increase of viscosity of liquid phase, which enhanced the densification of LWAs and improved the pore structures. At the sintering temperature of 900 ℃, the samples prepared with 90 wt.% of WG and 10 wt.% of ISSA as raw materials, and 5 wt.% $CaCO_3$ as foaming agent possessed bulk density of 0.97 g/cm^3, bloating index of 27.7%, 24 h water absorption of 9.4%, and compressive strength of 5.7 MPa, respectively. This study realized the recycling of WG and ISSA, and provided theoretical and practical value for the preparation of LWAs.

Keywords: Waste glass; Incinerated sewage sludge ash; Lightweight aggregates; Phase composition; Pore structure

BLENDING EFFICIENCY OF RECLAIMED ASPHALT RUBBER PAVEMENT AND ITS CRACKING RESISTANCE

Danning, Li[1], Zhen, Leng[1,2]

[1]Department of Civil and Environmental Engineering, The Hong Kong Polytechnic University, Kowloon, Hong Kong
[2]Research Centre for Resources Engineering towards Carbon Neutrality, The Hong Kong Polytechnic University, Kowloon, Hong Kong
E-mail: zhen.leng@polyu.edu.hk

Despite significant number of studies on recycling of conventional reclaimed asphalt pavement (RAP) mixtures into new asphalt mixture construction, research on recycling reclaimed asphalt rubber pavement (RARP) is still quite limited. The special multiphase system of asphalt rubber (AR) binder may cause a more complicated blending condition during the recycling of RARP due to the existence of rubber particles, and the blending efficiency of RARP and virgin AR mixtures is still unclear. The main objective of this study is to investigate the mobilization tendency of aged AR binder during the recycling of RARP mixture considering both the potential mobilizations of bitumen phase and rubber particles, as well as their correlation with the cracking resistance of the RARP mixture. AR mixtures containing 40% RARP were prepared at three different mixing temperatures and one warm mix case with the inclusion of a foam-based additive. A special gradation design was used to track the mobilization of aged AR binder from RARP to virgin coarse aggregates. Mobilization indexes of bitumen and rubber were established based on Fourier transform infrared spectroscopy and thermal gravimetric analysis tests, while the cracking resistance of the RARP mixture was evaluated by the semi-circular bending test. The mobilization indexes indicated that rubber and bitumen were simultaneously mobilized, and a higher mixing temperature led to stronger mobilization tendencies. In addition, a positive correlation was found between both mobilization indexes and the cracking resistance of the RARP mixture. The foam-based WMA additive markedly improved the blending efficiency but compromised the cracking resistance of the RARP.

Keywords: Reclaimed asphalt rubber pavement, waste tire, blending efficiency, binder mobilization, chemical analysis

Session C1

Sustainable Concrete and Characterization

INSIGHT INTO THE MECHANISM UNDERLYING STEEL CORROSION RESISTANCE OF WASTE GLASS POWDER-ORDINARY PORTLAND CEMENT (WGP-OPC) BLENDS

Ligang Peng[1, 2], **Yuxi Zhao**[1], Jian-Xin Lu[2, *], and Chi-Sun Poon[2, *]

[1]Institute of Structural Engineering, Zhejiang University, Hangzhou 310058, Zhejiang, China
[2]Department of Civil and Environmental Engineering & Research Centre for Resources Engineering towards Carbon Neutrality, The Hong Kong Polytechnic University, Hong Kong 999077, China
[*]Corresponding author, jxinlu@polyu.edu.hk (J.X. Lu), cecspoon@polyu.edu.hk (C.S. Poon)

Conventional supplementary cementitious materials in partial replacement of ordinary Portland cement (OPC) might decrease the chloride threshold value due to the consumption of portlandite, posing a potential threat to the stabilization of passive film on the surface of steel bars under marine environment. Depending on the alkali-rich and pozzolanic characteristics, the waste glass powder (WGP) was utilized to enhance the steel corrosion resistance of pure OPC system in this study. The results showed that the incorporation of WGP could improve the steel corrosion resistance of WGP-OPC blends (i.e. less negative open circuit potential, higher concrete resistance, and higher polarization resistance), even better than pure OPC system. Additionally, the WGP replacement of 20% ameliorated the chloride penetration resistance at a later age without sacrificing any compressive strength. The enhanced steel corrosion resistance of WGP-OPC blends could be attributed to the refined pore structure due to the formation of secondary C-(N)-S-H gels with a lower Ca/Si ratio, and the increased alkalinity of pore solution due to the depolymerization of WGP and the released Na+ from WGP. The WGP-OPC blends exhibited lower ecological and economic costs during the life cycle of concrete structures, beneficial for the wider promotion of WGP in the construction sector.

Keywords: Waste glass powder; Steel corrosion; Chloride environment; Pore structure; Pore solution

MECHANICAL PROPERTY PREDICTION MODELS FOR RAC WITH RAS FROM DIFFERENT SOURCES

Yue Geng[1,2,3], Huan Zhang[1,2], Yu-Yin Wang[1,2]

[1]Key Lab of Structures Dynamic Behaviour and Control of the Ministry of Education, Harbin Institute of Technology, Harbin 150090, China;
[2]Key Lab of Smart Prevention and Mitigation of Civil Engineering Disasters of the Ministry of Industry and Information Technology, Harbin Institute of Technology, Harbin 150090, China;
[3]Guangdong Provincial Key Laboratory of Modern Civil Engineering Technology, Guangzhou 510641, China;
gengyue@hit.edu.cn (Yue Geng)

In order to increase the accuracy and generality of the prediction models for RAC using RAs from different sources, this study classified the mechanical properties of RAC into three types: the strength-related properties (SR), the deformation-related properties (DR), and the energy-release-related properties (ERR). The SR properties include the compressive and tensile strength; The DR properties include the short-term deformation index of elastic modulus, and long-term deformation indexes of drying and autogenous shrinkage, drying and basic creep; The ERR properties include the descending branch of stress-strain relationship and size effect. Consequently, based on systematic theoretical and experimental study, three key physical parameters were distilled to describe the influence of RA from different sources, including the residual mortar content, the source concrete water-to-cement ratio, and the additional water content. Finally, based on two-phase-composite-material theory, prediction models for DR properties were established; based on fracture-energy theory, prediction models for ERR properties were established; the SR properties were established through regression analysis.

It was found that the high absorbability of RA induced a “retarded-release effect” of the free water. This effect prolonged the rapid development process of RAC shrinkage and creep and accelerated the development of strength. Without accounting for the “retarded-release effect”, the 50-year creep deformation can be underestimated by 40%. The “compounding effect” between the influences of coarse and fine recycled aggregates was found, i.e., the influence of fine recycled aggregate (FRA) varies with the replacement ratio of coarse recycled aggregate (CRA). The theoretical models developed can well predict different mechanical properties of RAC with different RA sources, making a significant improvement in the prediction accuracy. For example, validation results using 671 sets of elastic modulus test data from 114 papers indicate that the prediction model proposed in this study has a deviation from experimental results of less than 15%, which significantly improved the previous models with a 30% deviation.

Key words: recycled aggregate; recycled aggregate concrete; model; mechanical property; aggregate source

ANTI-CORROSION BEHAVIOR OF SELF-HEALING CONCRETE WITH CENOSPHERE-BASED ARTIFICIAL AGGREGATES

Xiangyu Zhang, **Leyang Lv***, Jihua Zhu, Chun Pei, Feng Xing

College of Civil and Transportation Engineering, Shenzhen University, Shenzhen, 518060, P.R. China
E-mail: l.lv@szu.edu.cn

Self-healing concrete using encapsulated repairing agents has shown great potential in enhancing the durability of concrete. However, the capsules are generally behaved as deteriorated mechanical strength and high cost, limiting their large-scale application in practical engineering. In this study, a novel type of artificial aggregate that employs fly ash cenosphere as a carrier of repairing agent was designed and produced to improve the cost-effectiveness of the existing self-healing strategies in concrete. The feasibility of applying the prepared artificial aggregate to reduce the reinforcement corrosion was testified. To this end, reinforced concrete beams were exposed weekly to a simulated seawater solution. The electrochemical parameters were measured to determine the influence of the proposed self-healing mechanism on the corrosion process. Moreover, the weight and morphology of the rebars were examined in real-time throughout the corrosion process.

The results showed that the prepared cenosphere-based artificial aggregates (AE-CS) have good stability and compatibility with cement mortar. By replacing 5% of the fine aggregate with the AE-CS in the mortar mixture, up to 81% of the crack opening area of mortar specimens with a crack width of about 0.3 mm was autonomously healed. In addition, the self-healing behavior of the AE-CS was found significantly reduce the corrosion in the propagation stage as no visual damage to the rebars was detected on the specimens. Considering its excellent cost-effectiveness and minor side effects, the AE-CS proposed in this study can serve as an ideal self-healing artificial aggregate to enhance the durability of reinforced concrete structures in marine environments.

Keywords: Self-healing concrete; Cenospheres; artificial aggregate; Anti-corrosion

DEVELOPMENT OF MORTARS USING MAGNESIUM PHOSPHATE CEMENT FORMULATED WITH TUNDISH DESKULLING AS A MGO SOURCE

Alfocea-Roig, A.[1], Vera-Rivera, D.[1], Formosa, J.[1], Chimenos, J.M.[1], and Giro-Paloma, J.[1]

[1] Departament de Ciència de Materials i Química Física, Universitat de Barcelona
joanformosa@ub.edu (corresponding author)

The Portland cement industry (PC) is globally responsible for a quarter of CO_2 emissions and a sixth of industrial energy consumption. Specifically, 8% of global CO_2 emissions originated from the cement industry. High environmental impact is caused by a large amount of cement production, and the thermal processes used in its manufacture. Thus, it is mandatory to look for sustainable alternative cement. One of the most promising materials in this sense is magnesium phosphate cement (MPC). This study aims of promoting the circular economy and reducing the environmental impact and evaluates the possibility of revaluing a refractory waste obtained from the steelmaking industry. Tundish masses are an essential component in the process of continuous casting of steel, as it is the last container with refractory material to deliver molten metal at a controlled speed into the molds. The service life of the tundish masses depends on the service conditions and the performance of the material. But once it exceeds the lifetime, the tundish masses are replaced with new material, therefore a high amount of waste is generated and known as tundish deskulling (TUN). TUN contains impurities, and it is difficult to separate and recycle.

The present work aims to use TUN as a MgO source for developing magnesium phosphate cement (MPC). MPCs are developed by the chemical reaction between an acid and a base in water at room temperature. The most relevant MPC is obtained by means of MgO, and KH_2PO, as a base, and an acid, respectively. In this case, the final product is $KMgPO_4 \cdot 6H_2O$, K-struvite, or magnesium potassium phosphate cement (MKPC) as is reported elsewhere. The development of mortars by using TUN as a MgO source aims to demonstrate the potential of TUN waste for assessing MKPC's potential applications in the future.

Keywords: Tundish, Environmental impact, Refractory waste, Sustainable cement, Circular economy

DATA-DRIVEN DESIGN OF HEADED-STUD CONNECTIONS IN STEEL-RECYCLED AGGREGATE CONCRETE COMPOSITE FLOORS USING POLYNOMIAL CHAOS EXPANSIONS

Fu, Qiuni, and Schäfer, Markus

University of Luxembourg, Department of Engineering
E-mail (qiuni.fu@uni.lu)

1. INTRODUCTION

In the global construction industry, the consumption of aggregates for concrete is ever-increasing, accompanied by the growing outputs of construction and demolition waste (CDW) (Wang et al. 2021). Immoderate exploitation of natural resources and the disposal of CDW on land both jeopardize sustainable development. Recycling CDW into recycled aggregate is a feasible and economical way to close the loop of supply and waste chains. Due to the inferior mechanical properties and large variability of RAC, it has been mainly used in non-structural construction such as pavement. Extensive experimental investigations showed that it is feasible to use steel reinforced RAC and steel section-RAC composite members for structural applications, as summarized in review articles (Deresa et al. 2020; Li et al. 2015). However, design models for NAC (e.g., (EN 1992-1-1 2004)) may not have a satisfactory safety margin for RAC design, considering the variability of structural resistance of RAC members. This concern has not been clarified, since there were limited studies, e.g., Pacheco et al. (2020, 2021), addressing the suitability of the existing design models the RAC structures from the perspective of reliability. And the limited studies on reliability were only for reinforced concrete members, without covering steel-concrete composite members.

Steel-concrete composite slabs as a kind of secondary structural member are a good destination to promote massive applications of RAC. Shear connections between slabs and steel beams are vital to the performance of composite beams and further to the entire building. Therefore, it is crucial to quantify the uncertainty of resistance, e.g., load-bearing capacity, of commonly used headed-stud shear connections using RAC (abbr. headed-stud RAC connections), caused by high variability of RAC properties. To consider this uncertainty, the conventional way is to build a database of random resistance of headed-stud connections by analytical models or stochastic FE simulations verified by actual tests. Analytical models themselves usually have high uncertainty and stochastic simulations with accurate advanced FE models are extremely costive and time-consuming. Alternatively, polynomial chaos expansion (PCE) is widely used to quantify probabilistic uncertainty in engineering systems efficiently (Sudret 2007). In this study, PCE is used to build a mathematical surrogate model for data-driven design of headed-stud shear connections in steel-concrete composite floor systems.

2. MATERIALS AND METHODS

As shown in Eq. (1), PCE represents a random variable Y (herein is resistance) in terms of a polynomial function $\psi_{\boldsymbol{\alpha}}(\boldsymbol{X})$ of independent random variables ($\boldsymbol{X}$) multiplied with coefficients $c_{\boldsymbol{\alpha}}$.

$$Y = \sum_{\boldsymbol{\alpha} \in N^M} c_{\boldsymbol{\alpha}} \Psi_{\boldsymbol{\alpha}}(\boldsymbol{X}) \tag{1}$$

$$\Psi_{\boldsymbol{\alpha}}(\boldsymbol{X}) \overset{\text{def}}{=} \prod_{i=1}^{M} P_{\alpha_1}^{(i)}(x_i) \tag{2}$$

Herein the variables $\boldsymbol{X} = \{x_1, \ldots, x_i, \ldots, x_M\}$ indicate material properties and geometry of headed-stud connections, and M is the number of independent random variables. The array $\boldsymbol{\alpha} = \{\alpha_1, \alpha_2, \ldots, \alpha_i, \ldots, \alpha_M\}$ are multi-indices, indicating degree (α_i) of a monic polynomial $P_{\alpha i}^{(i)}$ of x_i. The polynomials $P_{\alpha i}^{(i)}$ (i=1, 2, …i, …M) are from the orthonormal family such as Hermite and Legendre. Specifically, if x_i follows a normal distribution, $P_{\alpha i}^{(i)}$ is a Hermite polynomial. If x_i follows a uniform distribution, $P_{\alpha i}^{(i)}$

is a Legendre polynomial. To obtain $P_{\alpha i}^{(i)}$, polynomial expansions need to be truncated at a certain order p. Then, the number of terms of $c_\alpha\psi_\alpha(\boldsymbol{X})$ in Eq. (1) turns to be $j = (M+p)!/M!/p!$ (Sudret 2007). Coefficients c_α need to be computed with properly designed experimental results.

For instance, based on the lead-bearing mechanisms and stud failure mode, stud diameter (d), stud height (h), stud ultimate strength (f_u) and concrete strength (f_c) are determined as the four basic variables (i.e., M=4). If a truncation order is defined as 3, $c_\alpha\psi_\alpha(\boldsymbol{X})$ has 35 terms (j=35). The four basic variables are regarded as following normal distributions according to prior knowledge. They need isoprobablistic transforms into standard normal distributions (x_1, x_2, x_3, x_4). The multivariate polynomials are arranged as follows: $\boldsymbol{\psi_\alpha}$ $(\boldsymbol{X}) = \boldsymbol{\psi}_{j=35}$ $(\boldsymbol{X}) = [1, x_1, x_2, x_3, x_4, (x_1^2\text{-}1)/2^{1/2}, (x_2^2\text{-}1)/2^{1/2}, (x_3^2\text{-}1)/2^{1/2}, (x_4^2\text{-}1)/2^{1/2}, x_1x_2, x_1x_3, x_1x_4, x_2x_4, x_2x_3, x_3x_4, (x_1^3\text{-}3x_1)/6^{1/2}, (x_2^3\text{-}3x_2)/6^{1/2}, (x_3^3\text{-}3x_3)/6^{1/2}, (x_4^3\text{-}3x_4)/6^{1/2}, x_2(x_1^2\text{-}1)/2^{1/2}, x_3(x_1^2\text{-}1)/2^{1/2}, x_4(x_1^2\text{-}1)/2^{1/2}, x_1(x_2^2\text{-}1)/2^{1/2}, x_3(x_2^2\text{-}1)/2^{1/2}, x_4(x_2^2\text{-}1)/2^{1/2}, x_1(x_3^2\text{-}1)/2^{1/2}, x_2(x_3^2\text{-}1)/2^{1/2}, x_4(x_3^2\text{-}1)/2^{1/2}, x_1x_2x_3, x_1x_2x_4, x_1x_3x_4, x_2x_3x_4]$. Based on the 192 test data points of headed-stud NAC connections controlled by stud failure , the coefficients c_α are solved out and presented in array $c_{j=35}$=[219.02, 19.74, -27.97, 34.79, 4.67, 17.10, 8.83, 1.35, 13.2, -10.82, -21.55, 25.78, -19.84, 7.08, -10.15, 0.69, -16.89, 8.04, 13.68, -13.04, 7.32, 6.30, 21.34, -50.54, 11.66, -20.03, -11.35, -23, 10.36, -16.60, 3.78, 18.10, -22.73, 20.59, 8.87]$^{\mathrm{T}}$. The surrogate model turns out to be $\boldsymbol{M}(\boldsymbol{X}) = \boldsymbol{\psi}_{j=35}$ $(\boldsymbol{X})\cdot c_{j=35}$.

In turn, the statistic of the established PCE surrogate model is evaluated with the test data using the method in EN 1990 (2002). Additionally, the PCE model was used for analyses of headed-stud RAC connections, assuming that RAC does not change the failure mode of connections. Specifically, the authors compared the the resistance distributions of headed-stud connections using different concrete, i.e., NAC, and RAC with the respective 50% and 100% replacement of coarse aggregate. The four basic variables, i.e., d, h, f_u, and f_c, are normally distributed. The stud design is the same among the three designs of headed-stud connections, as shown in Table 1. The mean values (μ) and standard deviation (σ) of d and h were derived from nominal values (i.e., d=19 mm and h=100 mm) and limit tolerance ranges suggested by (Hicks 2017). The μ of f_u was assumed to be 500 MPa. The σ of f_u is based on a coefficient of variation of 5% (Hicks 2017). Regarding the concrete, C30 (μ=38 MPa, σ=4.86 MPa) was considered for NAC, while the μ and σ of RAC were sourced from literature (Ju et al. 2019), as shown in Table 1.

Table 1. Material properties of headed-stud connections

	d (mm)	h (mm)	f_u (MPa)	f_c (MPa)		
				NAC (C30)	RAC_50%RA[a]	RAC_100%RA[b]
Mean μ	18.8	99.5	500	38	37.7	33.4
Std. σ	0.24	0.91	25	4.86	6.0	6.4

Following the distributions of the basic variables, fifty thousand ($n=5\times10^4$) samples were determined by Monte Carlo simulations (MCS). Their resistance was calculated with the PCE model and is presented in histograms in Section 3.

3. RESULTS AND DISCUSSION

Statistical evaluations of models. First, the coefficient of correlation (ρ) between the test data and PCE model predicted data was calculated to be 0.95 (Figure 1 a), indicating a sufficient correlation between them. The same evaluation procedure was performed for the calculation models in EN 1994-1-1 (2004) and Konrad (2011). Their correlations with test data (ρ=0.87 and 0.89, respectively) are not as strong as that of the PCE surrogate model (Figure 1). Furthermore, model uncertainty was evaluated by determining the statistic of bias factors (a random variable), as shown in Eq. (3).

$$\boldsymbol{\lambda} = \frac{Test\ result}{Model\ prediction} \tag{3}$$

The mean values of the bias factors (μ_λ) of PCE surrogate, EC4 and Konrad models are 0.993, 1.294, and 1.236, respectively. It means that the predictions of PCE model are closer than those of the other

---

[a] The water-to-cement ratio is in a range of 0.38 ~ 0.71 (Ju et al. 2019).

[b] The water-to-cement ratio is in a range of 0.35 ~ 0.81 (Ju et al. 2019).

two models to the actual test results. And the coefficients of variation of the bias factors (V_λ) of the respective three models are 8.9%, 12.3%, and 11.6%, showing that the PCE model has more consistent predictions or smaller uncertainty.

To ensure structural reliability for the ultimate limit state, the designed resistance (R_d) of a structural member is defined at a 0.1% fractile of the resistance distributions. In practice, engineers usually do not know the resistance distribution and they calculate characteristic resistance (R_k) deterministically with characteristic values of material properties regulated by standards. The term R_k corresponds to a failure probability of lower than 5%. Meanwhile, standards also give a partial safety factor (γ_M) to calculate R_d, i.e., $R_d = R_k / \gamma_M$.

In turn, to propose a γ_M for the PCE model, the authors calculated R_d and R_k with the probabilistic method recommended by EN 1990 (2002), as shown in Figure 1. As a result, γ_M for the PCE model (1.19) is like that for the other two models (1.21). Overall, the PCE model delivers a slightly more economical design than the others. This can be understood in a way that for a given headed-stud connection with a test result of 1, the design resistance calculated from PCE, EC4, and Konrad models are 0.685 (=1/0.993*0.68), 0.665 (=1/1.294*0.86), and 0.645 (=1/1.236*0.797), respectively. Thus, to achieve the same resistance, the design using the PCE model is more economical.

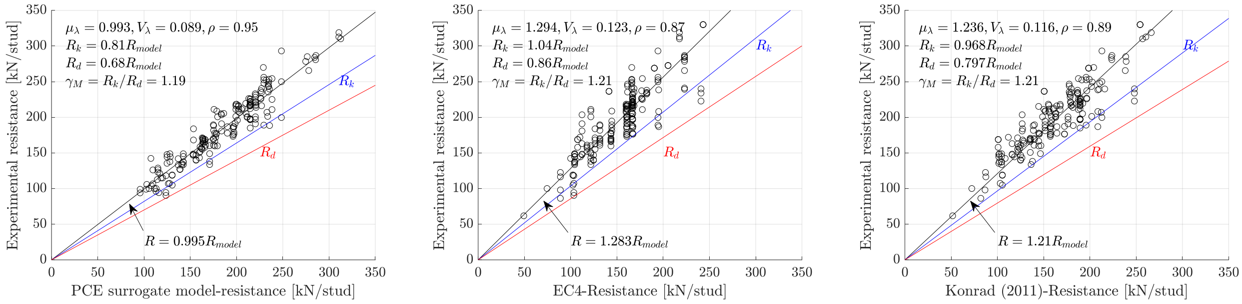

(a) PCE surrogate model (b) EN 1994-1-1 (2004) model (c) Konrad (2011) model

Figure 1. Statistical determinations of PCE surrogate model and existing mechanical models

Statistical analysis of headed-stud RAC resistance using PCE model. As the μ of RAC_50%RA is similar to μ of NAC and σ of the former is larger than the latter, the mean resistance of headed-stud connections using RAC_50%RA is not compromised (123.5 vs. 123.0 kN/stud) but the standard deviation is a bit higher compared with its counterpart (i.e., 12.23 vs. 10.30 kN/stud), as shown in Figure 2. When using RAC_100%RA instead of NAC, the mean resistance decreases slightly from 123.0 to 116.0 kN/stud and the standard deviation increases slightly from 10.30 to 11.74 kN/stud. However, the compressive strength of RAC_100%RA can be improved in many ways, e.g., by reducing water-to-cement ratio. It is promising that headed-stud connections using RAC_100%RA can achieve the same reliability as headed-stud connections with commonly-used NAC C30.

It should be noted that the above finding is drawn from the stud-failure controlled designs. Further studies are needed to address the effects of using RAC on resistance uncertainty of headed-stud connections whose ultimate failure was in concrete.

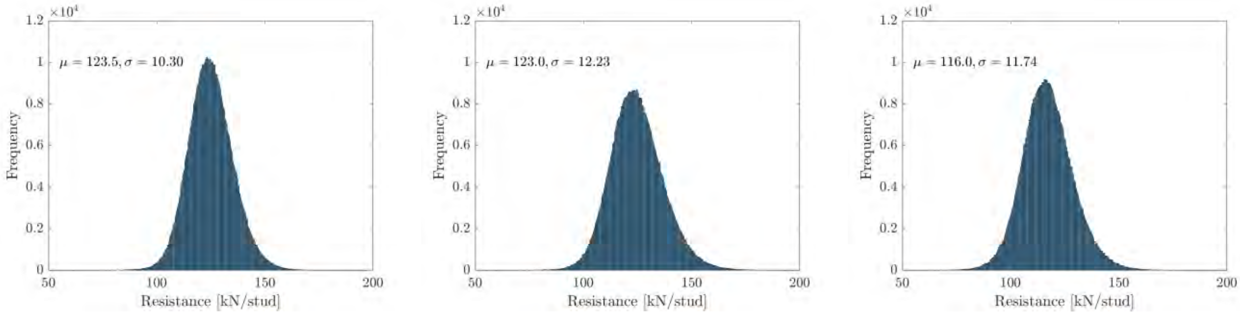

(a) NAC (b) RAC_50%RA (c) RAC_100%RA

Figure 2. Resistance distributions of NAC and RAC headed-stud connections (n=50000)

4. CONCLUSION

The study illustrated the feasibility of using PEC to predict the resistance of headed-stud connections in solid slabs with the relevant independent random variables. The PCE surrogate model has smaller uncertainty than the conventional mechanical models in EN 1994-1-1 and Konrad (2011). Besides, given a target resistance, the PCE model leads to slightly more economical design. It is expected that the uncertainty of PCE model will be further reduced, provided that the experimental design covers at best the domain of variation of the parameters. Considering these remarkable advantages, the authors propose to use data-driven PCE surrogate model for design of structural members and for quantifying the resistance reliability (uncertainty) of structural members using RAC.

5. ACKNOWLEDGMENT

The authors would like to express appreciation for the support of the European Commission Marie Skłodowska-Curie Actions Postdoctoral Fellowships [Project Number = 101103110].

6. REFERENCES

Deresa, S. T., Xu, J., Demartino, C., Heo, Y., Li, Z., and Xiao, Y. (2020). "A review of experimental results on structural performance of reinforced recycled aggregate concrete beams and columns." *Advances in Structural Engineering*, 23(15), 3351–3369.

EN 1990. (2002). "Eurocode - Basis of structural design." *CEN.*

EN 1992-1-1. (2004). "Eurocode 2: Design of concrete structures - Part 1-1: General rules and rules for buildings." *CEN.*

EN 1994-1-1. (2004). "Eurocode 4: Design of composite steel and concrete structures – Part 1-1: General rules and rules for buildings." *CEN.*

Hicks, S. J. (2017). "Design shear resistance of headed studs embedded in solid slabs and encasements." *Journal of Constructional Steel Research*, 139, 339–352.

Ju, M., Park, K., Lee, K., Ahn, K. Y., and Sim, J. (2019). "Assessment of reliability-based FRP reinforcement ratio for concrete structures with recycled coarse aggregate." *Structural Engineering and Mechanics*, 69(4), 399.

Konrad, M. (2011). *Load bearing behaviour of headed stud connectors in composite girders with transverse spanning trapezodial steel sheetings,* PhD thesis, Universität Stuttgart, in German.

Li, W., Xiao, J., Shi, C., and Poon, C. S. (2015). "Structural Behaviour of Composite Members with Recycled Aggregate Concrete — An Overview." *Advances in Structural Engineering*, 18(6), 919–938.

Pacheco, J. N., Brito, J. de, Chastre, C., and Evangelista, L. (2020). "Uncertainty of shear resistance models: Influence of recycled concrete aggregate on beams with and without shear reinforcement." *Engineering Structures*, 204, 109905.

Pacheco, J. N., Brito, J. de, Chastre, C., and Evangelista, L. (2021). "Bond of recycled coarse aggregate concrete: Model uncertainty and reliability-based calibration of design equations." *Engineering Structures*, 239, 112290.

Sudret, B. (2007). *Uncertainty propagation and sensitivity analysis in mechanical models – Contributions to structural reliability and stochastic spectral methods,* Habilitation thesis, Institut Français de Mécanique Avancée.

Wang, B., Yan, L., Fu, Q., and Kasal, B. (2021). "A Comprehensive Review on Recycled Aggregate and Recycled Aggregate Concrete." *Resources, Conservation and Recycling*, 171, 105565.

NEXT GENERATION CONCRETE MATERIALS

Mohamed Katish[1], Steve Allen[1], Adam Squares[2] & Veronica Ferrandiz-Mas[1]

[1]Department of Architecture and Civil Engineering, University of Bath
[2]Department of Chemistry, University of Bath
E-mail mak228@bath.ac.uk

1. INTRODUCTION

Industrial developments and a population boom in the last few decades have resulted in an enormous increase in energy demand. This increase in energy-demand especially that generated from fossil fuels, brought the largest environmental issue, which is climate change caused by CO_2 emission. In the built environment, space heating and cooling is the largest end use of energy with 71% of gas and electricity having been used for domestic heating in the UK [1]. A new solution using Phase Change Material (PCM) in building materials has emerged to lower energy demand for space heating and cooling. PCM is a material that stores and releases high amounts of thermal energy during phase change [2]. This thermal energy regulation can lead to energy savings and decreased CO_2e emissions, but PCM has been overlooked in the past due to incompatibility with building materials and a lack of understanding of its properties [3].

The paper proposes a cost-effective approach to generate PCM-Biochar composites that can be added to concrete to produce materials with excellent insulation and thermal storage capabilities, providing a sustainable solution to minimise waste and reducing CO_2 emissions.

2. MATERIALS AND METHODS

2.1 Materials

Biochar obtained from Soilfixer was used as an aggregate in cement-based materials due to its ability to carry PCM. The biochar bulk density was 267.7 kg/m^3 and the particle size distribution of biochar confirmed to be 0–4mm aggregates defined in BS EN 12620 [4]. Biochar sample was sieved to remove any particles smaller than 1 mm as such particles would be difficult to handle and could pass through the mesh container used during impregnation.

Octadecane, a PCM with melting point of 23 °C and latent heat energy of 227 J/g, was selected for the experiment. A technical grade (Purity of 97.9%) of this PCM was purchased from Sigma Aldrich. Portland limestone cement CEM II/A-L 32.5R purchased from Tarmac Blue Circle, UK, deionised water supplied by the University of Bath and standard silica sand purchased from Société Nouvelle Du Littoral, France.

2.2 PCM impregnation of biochar

2.2.1 Method 1: Impregnation by immersion

Biochar particles were soaked in octadecane for 60 minutes to absorb it into their pores. The container holding the molten octadecane was kept in a water bath at 50 °C and the particles were removed after 60 minutes. The PCM Percentage Absorption (PPA) was calculated from the increased mass of the biochar particles. Theoretical latent heat of octadecane-biochar particles was determined using percentage mass values.

2.2.2 Method 2: Vacuum impregnation

The process of vacuum impregnation was used to remove air from the pores of biochar using a vacuum pump. Octadecane was then forced into these pores by placing the biochar particles in a mesh basket, which was submerged in solid octadecane in a desiccator. The vacuum pressure of 1.5 bar was applied for 30 minutes, followed by increasing the temperature of PCM to 50 °C to melt octadecane. The biochar was then submerged in molten octadecane for 60 minutes, and the impregnated particles were surfaced dried after removal.

2.2.3 PCM and PCM-biochar characterisation methods

Viscosity measurement, Differential Scanning Calorimetry (DSC); and A leakage test.

2.3 Preparation of mortar samples

A series of mortar samples were produced using Ordinary Portland Cement, deionised water, standard silica sand, and octadecane-biochar particles, with the proportions specified in **Table 1**, and prepared with a water:cement mass ratio of 1:2 and cement:sand mass ratio of 1:3. The octadecane-biochar particles were added as a replacement for the sand to the total volume of mortar expressed as the apparent volume of sand (v/v%). The mortar samples were produced in accordance with BS EN 1961 [5] and were cured under controlled conditions for 1 day before being cured in water for 28 days[1].

Table 1 Mix proportions for mortar samples, percentage of sand replacement by volume

Mix	0%	10%	20%	30%	40%	50%
Sand (g)	1350	1215	1080	945	810	675
Octadecane-Biochar Particles (g)	0	45	89	134	179	223

2.4 Testing of mortar samples

The workability of fresh mortars containing octadecane-biochar particles was assessed. The compressive and flexural strengths of the mortar samples were measured after 28 days of curing using a compression machine and three-point bending test. The BS EN 1015-10 [6] method was employed to determine the dry bulk density of hardened mortars and further tests were conducted using the Hot Disk TPS 500 Thermal Analyser to determine thermal conductivity and specific heat capacity.

3. RESULTS AND DISCUSSION

3.1 Octadecane-biochar particles impregnation tests

The study found that vacuum absorption was more efficient than immersion in loading biochar with octadecane. See **Table 2**. The experiment demonstrated that biochar has a significant capacity to absorb PCM, particularly when using experimental conditions specified **above**.

3.2 Thermal Analysis of octadecane-biochar.

The thermal properties of octadecanebiochar particles were assessed using DSC to determine the enthalpy before and after phase change. The reduction in enthalpy observed in both melting and freezing processes of the octadecane-biochar loaded particles can be attributed to the biochar mass within the octadecane particles. See **Figure 1** & **Table 3**.

Table 2: Comparison between immersion and vacuum impregnation method for octadecane

Octadecane and Biochar ratio	**0.25:1**	**0.5:1**	**1:1**	**1.5.1**	**2:1**	**2.5:1**
Immersion Method (wt%)	26.34 (±0.54)	34.12 (±0.87)	42.57 (±1.20)	50.34 (±1.04)	52.41 (±0.77)	54.07 (±0.19)
Vacuum Impregnation Method (wt%)	30.23 (±0.92)	42.48 (±1.52)	53.78 (±0.99)	60.12 (±0.75)	72.18 (±0.22)	74.78 (±1.39)

---

[1] Two sets of samples were produced to also evaluate the pozzolanic activity of biochar the second set is being curing for 120 days. However, it was not included in this abstract due to time constrain.

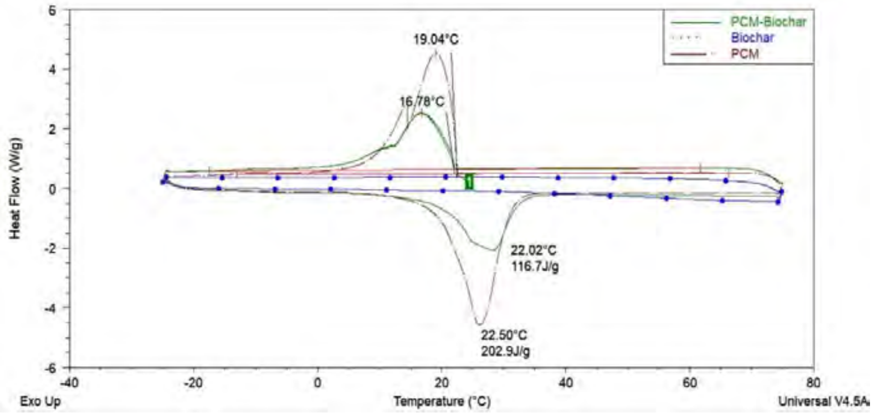

Figure 1 DSC of PCM, Biochar and PCM-Biochar

Table 3 Compressive strength, flexural strength, density, porosity, water absorption, thermal conductivity, and heat capacity of the octadecane-biochar mortars samples.[2]

Octadecane-Biochar Replacement	Compressive strength (MPa)	Flexural Strength (MPa)	Density (kg/m3)	Porosity (%)	Water Absorption (%)	Thermal conductivity (W/mK)	Heat Capacity (MJ/m3K)
0	43.35 (±1.42)	8.16 (±0.48)	2198 (±31)	17.07 (±0.10)	9.08 (±0.23)	2.81 (±0.26)	1.70 (±0.82)
10%	38.21 (±1.63)	7.08 (±0.12)	2035 (±25)	18.46 (±0.02)	12.63 (±0.12)	2.42 (±0.83)	2.00 (±0.22)
20%	35.42 (±2.19)	6.88 (±0.67)	2004 (±38)	21.17 (±0.39)	13.89 (±0.19)	2.02 (±0.39)	2.24 (±0.72)
30%	28.10 (±1.55)	6.2 (±0.33)	1968 (±26)	22.00 (±0.68)	14.67 (±0.85)	1.9 (±0.58)	2.35 (±0.39)
40%	23.63 (±1.76)	5.39 (±0.91)	1954 (±17)	23.91 (±0.08)	15.67 (±0.33)	1.6 (±0.43)	2.77 (±0.14)
50%	15.91 (±0.87)	4.40 (±0.28)	1890 (±23)	25.23 (±0.52)	17.54 (±0.76)	1.4 (±0.77)	2.80 (±0.37)

3.3 Cement mortar development test results and discussion

3.3.1 Mortar workability

Results indicate that increasing the percentage of octadecane-biochar particles led to a consistent increase in workability of the cement. This is attributed to the size and shape of the biochar particles.[3]

3.3.2 Compressive strength

The results of compressive strength testing are displayed in **Table 3**, the addition of octadecanebiochar particles to the mixture resulted in a reduction in compressive strength. The values fall below the minimum requirement for traditional concrete walls and columns as per BS EN 197-1 [7] when more than 30% sand replacement is reached. The biochar's porous nature and the increased workability of the mix caused a decrease in strength compared to sand.

Figure 2 PCM-Mortar (Lift) Mortar (Right)

3.3.3 Mortar flexural strength

The flexural strength results indicate a decrease in resistance with increased octadecane-biochar. This reduction is not significantly detrimental to the use of mortar in general construction, but there was an average decrease of 46.08% in flexural strength at a 50% octadecane-biochar loading. The standard mortar sample had an average flexural strength of 8.16 ± 0.48 MPa.

---

[2] These results plotted in origin for the sake for visual comparison are available and will be supplied in the full paper version.

[3] The water: cement ratio was kept constant to evaluate the impact of octadecane-biochar replacement to sand on cement mixtures workability.

3.3.4 Mortar porosity and water absorption

The results shown in **Table 3** indicate that the addition of octadecane-biochar particles resulted in a small increase in both porosity and water absorption, and this is due to the replacement of sand with highly porous biochar. Furthermore, this increase in porosity and water absorption was found to be positively correlated with compressive strength, which was impacted by air porosity of biochar samples and particle shape.

3.3.5 Mortar density

A slight decrease in density of mortar samples was observed when octadecane-biochar particles were added. The decrease density was correlated with both the reduction of compressive strengths and increased porosity. See density results shown in **Table 3.**

3.3.6 Mortar thermal conductivity

The thermal conductivity of construction materials can significantly affect a building's energy consumption [8]. The incorporation of octadecane-biochar into mortar mixes can lead to up to a 50.17% reduction in thermal conductivity, resulting in improved insulation properties.

3.3.7 Mortar heat capacity

The volumetric heat capacity of PCM-mortar rises with increasing octadecane-biochar particle content, as evidenced in **Table 3**. Specifically, the volumetric specific heat increased by 64.70% at the maximum 50% octadecane-biochar particle loading. However, the maximum increase in heat capacity which can be achieved without comprising mortar properties is 31.76% at octadecane-biochar particle content of 20%. These findings suggest that this material can effectively store and release large quantities of energy, making it a valuable option for thermal energy storage in building applications.

4. CONCLUSION

4.1 Octadecane-biochar impregnation

Vacuum impregnation proved to be the more effective method for impregnating biochar with octadecane due to its ability to force the octadecane into less accessible pores, as confirmed by DSC measurements. The optimal impregnation ratio was found to be 2:1 (octadecane: biochar) at a temperature of 50 ºC and pressure of 1.5 bars and CEMII being an excellent building material host for the resulting particles, but future research should consider other materials for higher thermal storage ability.

4.2 Cement mortar development

The incorporation of PCM into cement mixtures requires careful consideration due to its negative effects on strength and workability, therefore future research should focus on non-structural regions to maximise content and improve heat storage capacity, , the maximum increase in heat capacity which can be achieved without comprising mortar properties is 31.76%. The PCM-loaded particles designed in this study have the potential to reduce energy consumption in buildings by recovering excess heat, and further work is being conducted to determine which building materials are most compatible.

5. ACKNOWLEDGMENT

The authors greatly appreciate the financial support provided by Engineering and Physical Sciences Research Council (EPSRC) of UK (Grant No.: EP/T518013/1)

6. REFERENCES

[1] O. National Statistics, "UK ENERGY IN BRIEF 2021," 29 07 2021. [Online]. Available: https://assets.publishing.service.gov.uk/government/uploads/system/uploads/attachment_data/file/1032260/UK_E nergy_in_Brief_2021.pdf.

[2] Souayfane, Fardoun, and Biwole, "Phase change materials (PCM) for cooling applications in buildings: A review.," *Energy and Buildings,* vol. 129, pp. 396-431, 2016.

[3] A. S. Fleischer, Thermal Energy Storage Using Phase Change Materials: Fundamentals and Applications, Villanova, PA USA: Springer, 2015.

[4] BSI, "BS EN 12620:2013 Aggregates for concrete," BSI, London, 2013.

[5] BSI, "BS EN 196-1 Methods of testing cement. Determination of strength," BSI, London, 2016.

[6] BSI, "BS EN 1015-10:1999 Methods of test for mortar for masonry Determination of dry bulk density of hardened mortar," BSI, London, 1999.

[7] BSI, "BS EN 197-1: 2011," BSI, London, 2011.

[8] D. Kumar, M. Alam and A. J. Doshi, "Investigating the Influence of Thermal Conductivity and Thermal Storage of Lightweight Concrete Panels on the Energy and Thermal Comfort in Residential Buildings," *Buildings,* vol. 13, no. 3, p. 720, 2023.

[9] Kenisarin and M. Murat , "Thermophysical properties of some organic phase change materials for latent heat storage. A review," *Solar Energy,* vol. 107, pp. 553-575, 2014.

PERFORMANCE-ORIENTATED CONSTRUCTION MATERIAL DEIGN WITH INVERTIBLE NEURAL NETWORKS

Jie Yu[1,2], Yiwei Weng[2, *], Jiangtao, Yu[1,3,4], Jianguo Dai[2]; Kequan Yu[1, *]

[1] Department of Disaster Mitigation for Structures, College of Civil Engineering, Tongji University, Siping road 1239, Shanghai, 200092, China
[2] Department of Building and Real Estate, Faculty of Construction and Environment, The Hong Kong Polytechnic University, China
[3] School of Civil Engineering, Architecture and Environment, Hubei University of Technology, Wuhan 430000, China
[4] State Key Laboratory for Disaster Reduction in Civil Engineering, Tongji University, Shanghai 200092, China
12yukequan@tongji.edu.cn (corresponding author)
yiwei.weng@polyu.edu.hk (co-corresponding author)

1. INTRODUCTION

Strain hardening cementitious composites (SHCC) is a promising construction material due to its high tensile strain capacity and tight crack widths. It is widely known that the proportion of constituents (e.g., cement, fiber, silica fume, etc.) is the critical parameter to determine the mechanical performance of SHCC. However, traditional micromechanical-based methods (Li, 1997) fail to produce detailed ECC mixtures based on the target performance. In addition, complex tests, including single-fiber pull-out tests and fracture toughness tests, are needed to obtain the micromechanical parameters. Therefore, there is a need to develop a straightforward method that can design SHCC mixtures with desired performance.

This study presents a newly developed mixture design model for SHCC, which combines one invertible neural network (INN) (Ardizzone et al., 2019) and two artificial neural networks (ANNs) (Altayeb et al., 2021). The INN model was trained to generate new SHCC mixtures based on tensile performance, while the ANN models were used to pre-check the tensile properties of the generated SHCC mixtures without additional tests. After experimental validation, the developed model was used to produce sustainable and economical SHCC. Moreover, the model's potential to be adopted in different applications was explored by comparing the cost and carbon emissions of the generated SHCC mixtures.

2. MATERIALS AND METHODS

Framework

The framework of the SHCC mixture design model is shown in **Fig. 1**. Firstly, a dataset including 129 SHCC mixtures was built based on a review of previous literature. This dataset includes 10 mix design parameters and 2 target tensile properties of SHCC. The mix design parameters consist of: cement (C), fly ash (FA), limestone powder (LP), ground granular blast furnace slag (GGBFS), silica fume (SF), sand, water, fiber fraction, fiber diameter (F-D) and fiber length (F-L). The tensile properties are ultimate tensile strength and strain capacity, according to the JSCE standard (Japan, 2008). Subsequently, an INN model and two ANN models were developed to train with the pre-processed data. In the second step, the trained INN model was used to generate new SHCC mixtures based on the required tensile properties. Then, two ANN models were used to predict the tensile strength and strain capacity of the generated SHCC mixtures to check whether the requirements are satisfied. Finally, additional down-selection work is conducted when there are additional needs of the generated SHCC mixture. For example, mixtures with low fiber volume fraction can be produced to reduce the cost.

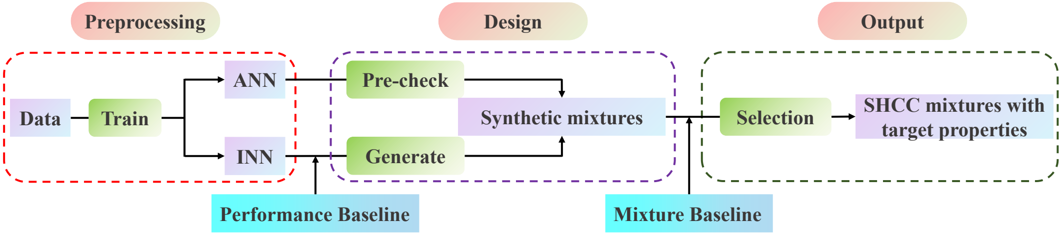

Fig. 1 The framework of the SHCC mixture design model

Materials

To verify the feasibility of the developed model for SHCC mixture design, 3 SHCC mixtures are generated and compared. As shown in **Table 1**, the economical SHCC was produced to achieve the same tensile performance with a lower fiber volume fraction. In addition, the sustainable SHCC decreases the proportions of cement and fiber volume while increasing the dosage of limestone powder to reduce the carbon emissions. Dog-bone specimens were cast, and uniaxial tensile tests were conducted according to JSCE standard (Japan, 2008).

Table 1 Generated mixtures with different targets

Mixtures	Reference	Economical	Sustainable
Expected Tensile Strength (MPa)	6	6	6
Expected Tensile Strain (%)	6	6	6
Cement (g/L)	699	826	450
Fly ash (g/L)	321	344	87
Limestone powder (g/L)	-	-	96
GGBFS (g/L)	210	145	596
Silica fume (g/L)	69	29	101
Sand (g/L)	449	434	425
Water (g/L)	364	361	349
w/b	0.28	0.27	0.26
Fiber fraction	1.9%	1.3%	1.3%
Fiber-diameter (μm)	24	24	24
Fiber-length (mm)	12	18	18
HRWR (g/L)	2	2	2
VMA (g/L)	0.5	0.5	0.5

3. RESULTS AND DISCUSSION

The comparisons between target performance and experimental results are plotted in **Fig. 2**. Based on the experimental results, the maximum difference of tensile strength was 11%, while that of tensile strain was 4%. Therefore, all the generated SHCC mixtures reached the target tensile performance. According to the embodied carbon values and material cost provided in **Table 2**, the carbon emissions and cost of each SHCC mixture were determined and compared. As shown in **Fig. 3**, the economical SHCC mixture reduced the cost by 35%, while the sustainable SHCC mixture cut the carbon emissions by 33%. Accordingly, it is evident that the developed SHCC mixture design model can generate SHCC mixtures that satisfy target requirements.

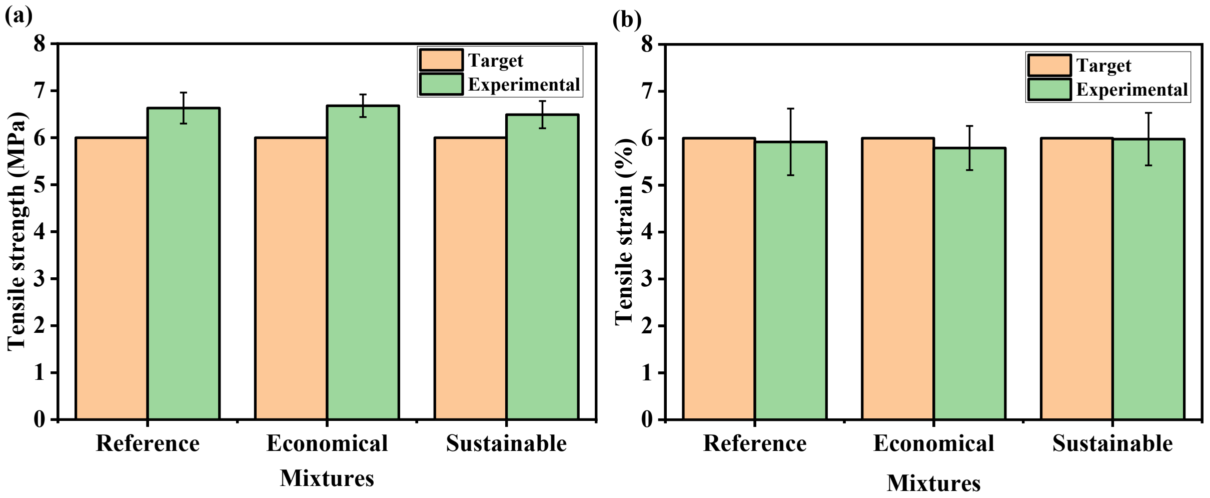

Fig. 2 Comparisons between target performance and experimental results: (a) difference of tensile strength; (b) difference of tensile strain

Table 2 Embodied carbon values and material cost of each constituent.

Constituents	Embodied carbon (kg/kg)	Cost ($/kg)
Cement	0.912	0.044
Fly ash	0.004	0.024
Limestone powder	0.016	0.13
Ground granular blast furnace slag	0.042	0.27
Silica fume	0.028	0.27
Sand	0.005	0.058
Fiber	3.3	21.49
Polycarboxylate high-range water reducer	1.88	2.98

Note: Embodied carbon values are obtained from Hammond & Jones (2019); cost values are based on the prices in Shanghai, China.

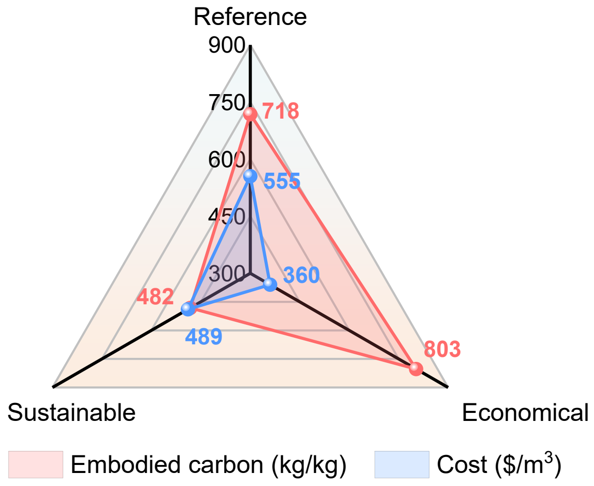

Fig. 3 Comparison of embodied carbon values and cost between different mixtures

4. CONCLUSION

An SHCC mixture design model was developed using the machine learning method in the present research. Uniaxial tensile tests were conducted to measure the tensile performance of the generated SHCC mixtures. In addition, the potential of the developed model to be used in various application scenarios has been explored. According to the experimental results and discussions, the following conclusions can be drawn:

(1) The proposed SHCC mixture design model can be used to design SHCC mixtures that satisfy the desired tensile performance.
(2) The SHCC mixture design model can generate economical materials with low cost and sustainable materials with low carbon emissions.

5. ACKNOWLEDGMENT

The authors would like to express appreciation for the support of the National Natural Science Foundation of China [51978504, 52108243]; Fundamental Research Funds for the Central Universities and Shanghai Municipal Science and Technology Commission [No. 19DZ1202500]; and The Hong Kong Polytechnic University [P0044561].

6. REFERENCES

Li, V.C. (1997). Engineered Cementitious Composites (ECC) – Tailored Composites through Micromechanical Modeling. *Canadian Society for Civil Engineering, 1–38.*

Ardizzone, L., Kruse, J., Wirkert, S., Rahner, D., Pellegrini, E. W., Klessen, R. S., Maier-Hein, L., Rother, C., & Köthe, U. (2019). Analyzing inverse problems with invertible neural networks. *7th International Conference on Learning Representations, ICLR 2019*, *August*.

Altayeb, M., Wang, X., & Musa, T. H. (2021). An ensemble method for predicting the mechanical properties of strain hardening cementitious composites. *Construction and Building Materials*, *286*, 122807. https://doi.org/10.1016/j.conbuildmat.2021.122807

Japan Society of Civil Engineers. (2008). Recommendations for Design and Construction of High Performance Fiber Reinforced Cement Composites with Multiple Fine Cracks (HPFRCC). *Concrete Engineereing Series, 82, Testing Method 6-10.* http://www.jsce.or.jp/committee/concrete/e/index.html

Hammond, G., Jones, C. (2019). Inventory of carbon & energy (ICE) version 3.0. *University of Bath*.

Session C2

Recycling of Ashes

DESIGNING LOW-CARBON CEMENTITIOUS MATERIALS FOR STABILIZATION/SOLIDIFICATION OF MSWI FLY ASH

Lei Wang

State Key Laboratory of Clean Energy Utilization, Zhejiang University, Hangzhou, 310027, China
E-mail: wanglei.leo@zju.edu.cn

Low-carbon and high-efficiency binder is desirable for safe disposal of municipal solid waste incineration fly ash (MSWI FA). In this work, CaO or MgO was used to activate ground granulated blast furnace slag (GGBS) to form calcium silicate hydrate (C-S-H) and magnesium silica hydrate (M-S-H) gel for stabilization/solidification (S/S) of hazardous MSWI FA. Experimental results showed that the potentially toxic elements (PTEs, e.g., Pb and Zn) significantly inhibited the formation of reaction products in CaO-GGBS system due to the complexation between $Ca(OH)_2$ and PTEs, whereas PTEs only had insignificant inhibition on transformation from MgO to $Mg(OH)_2$ in MgO-GGBS system, resulting in lower PTEs leachability and higher mechanical strength. Stabilization/solidification experiments demonstrated that MSWI FA (70 wt%) could be recycled by MgO-GGBS binder (30 wt%) into blocks with desirable 28-day compressive strengths (3.9 MPa) and immobilization efficiencies for PTEs (99.8% for Zn and 99.7% for Pb). This work provides mechanistic insights on the interactions between PTEs and CaO/MgO-GGBS systems and suggests a promising MgO-GGBS binder for the low-carbon treatment of MSWI FA.

Keywords: Waste incineration fly ash, Hazardous waste treatment, Low-carbon stabilization/solidification, PTEs leachability, Sustainable waste management.

THE APPLICATION OF BIO-TREATED MUNICIPAL SOLID WASTE INCINERATION FLY ASH FROM MICROBIAL ISOLATES IN MAGNESIUM PHOSPHATE CEMENT

Tangwei Mi [1,2], Birunxuan Liu [2], Jinyi Guo [2], Shuo Yan [2] and **Jun Ren** [2,*]

[1] School of Civil and Environmental Engineering, Nanyang Technological University, 50 Nanyang Avenue, 639798, Singapore
[2] Urban Construction and Digital City Teaching Experiment Center, School of Architecture and Planning, Yunnan University, Kunming 650550, P.R. China
E-mail (corresponding author: renjunking@aliyun.com)

1. INTRODUCTION

Rapid urbanization generates over 2 billion tons of municipal solid waste annually, requiring effective treatment (Zhang et al., 2021). Incineration is favored for its 90% waste reduction but leaves toxic residues like MSWI ash, which comprises 20% of waste residues and contains high levels of PCDD/Fs and heavy metals (Gutberlet, 2015). While chemical processes have successfully mitigated these toxins, they pose reagent toxicity and waste reuse issues. Recent studies have shown that microorganisms like *Bacillus megaterium* can achieve over 90% solidification efficiency, but research on bacteria derived from waste for treatment is limited.

Various methods have been explored to mitigate harmful substances in MSWIFA, including chemical processes using toxic reagents, mechanochemical methods involving grinding with additives, and microwave-assisted hydrothermal methods using chemical agents (Liu et al., 2022). While these methods have shown some efficacy in reducing PCDD/Fs and stabilizing heavy metals, they have limitations such as potential additional pollution, energy demand, and the need for chemical reagents. Despite the promising results of the microwave-assisted hydrothermal method, which achieves a PCDD/Fs removal rate of 83.7% and a heavy metal solidification rate of over 50% in a short heating time, the reusability of the resulting product is challenging (Zhang et al., 2020). Therefore, alternative environmentally friendly treatments should be considered.

The mineralization process immobilizes heavy metals in MSWIFA by incorporating them into cementitious materials, but its efficacy on PCDD/Fs removal and impact on mechanical properties of materials is unclear. This necessitates alternatives like magnesium phosphate cement (MPC), and further research on a combined treatment with MSWIFA and MPC (He et al., 2019). This study aims to develop a combined, eco-friendly treatment using *Bacillus subtilis* which was isolated from MSWIFA for biomineralization and biodegradation of dioxins and heavy metals in MSWIFA. The study will assess the performance of treated and untreated MSWIFA and MPC blended cement using various tests and analyses post 28 days of biotreatment.

2. MATERIALS AND METHODS

2.1 Materials

The RFA was collected from a Huizhou solid waste incineration plant, and after bio-treatment, detailed in section 2.3, it was labeled as BFA. MPC, with a magnesium to phosphonate ratio of 2, was sourced from Guizhou Linmei, composed mainly of MgO and $NH_4H_2PO_4$. Additionally, 98% Dibenzo[b,e][1,4]dioxine(DD) and Dibenzofuran(DF) were procured from Shanghai Macklin Biochemical Technology.

2.2 Isolation microbial and Biomineralisation/Biodegradation process for MSWIFA

To enhance biomineralization and biodegradation, alkali-resistant *Bacillus subtilis* was isolated using MS(minimal salts) culture medium with DD and DF as the only sources of carbon and energy. After identification and storage, it was used for MSWIFA biotreatment. The process involved culturing, fermenting, and centrifuging the bacteria to obtain a nutrient-rich supernatant, which was mixed with MSWIFA and a nutrient solution, oscillated, and cultured at 40 °C (Liu et al., 2023),and the preocess of isolation and biotreatment are shown in Fig. 1. After 72 hours of curing, it was used for testing and blended with MPC for pastes. Furthermore, RFA and BFA replace MPC from 20-40%, named BFAC and RFAC, respectively

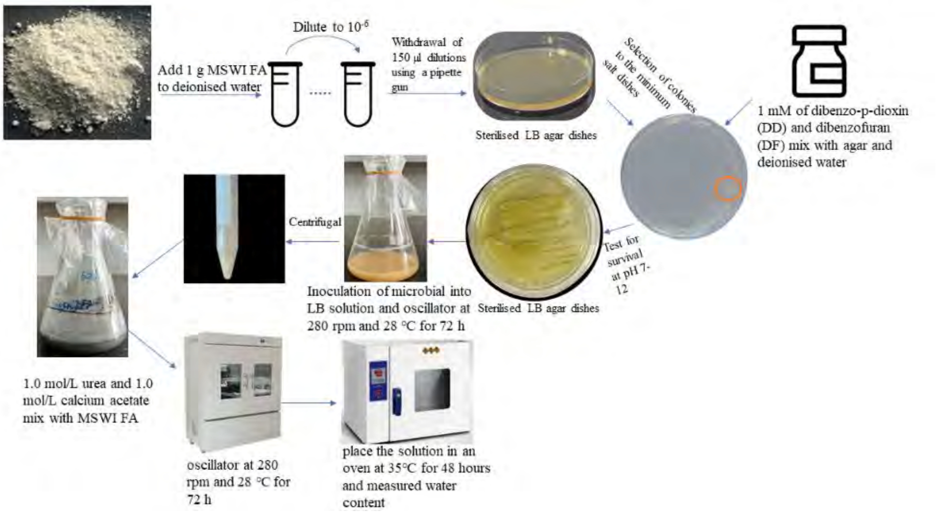

Fig. 1. Isolation and biotreatment procedure for MSWIFA.

2.3 Test methods

MPC specimens (10mm³) were compression tested after 7 and 28 days of standard curing. Three parallel specimens were tested for each mix, and the average value with a difference less than 15% was recorded. Additionally, the mineral compositions of RFA and BFA were analyzed via XRD. The XRD scan ranged from 5° to 80°, with a 0.2s scanning time per point.

3. RESULTS AND DISCUSSION

3.1 Physical properties and toxicity testing of RFA and BFA

Fig. 2(a) shows XRD patterns for untreated BFA and RFA, identifying primary components such as sylvite, halite, and quartz, among others. BFA displayed a lower peak of $CaCO_3$, a result likely attributed to the microbial treatment causing erosion of $CaCO_3$ in the RFA and subsequently leading to the formation of CaClOH. Moreover, there is more pronounced Monocarboaluminate peaks compared to RFA. Fig 2(b) shows the concentration of PCDD/Fs in BFA reduced by 99.1% compared with RFA, outperforming traditional methods in efficiency and energy consumption. Heavy metal leaching results in Fig. 2(c) and 2(d) indicate that untreated MSWIFA exceeded Chinese standards (GB18598-2019 (2020)). However, after 28-day biotreatment, BFA met Chinese standards, with heavy metal concentrations significantly lower than RFA, demonstrating the effectiveness of the biotreat process in stabilizing heavy metals.

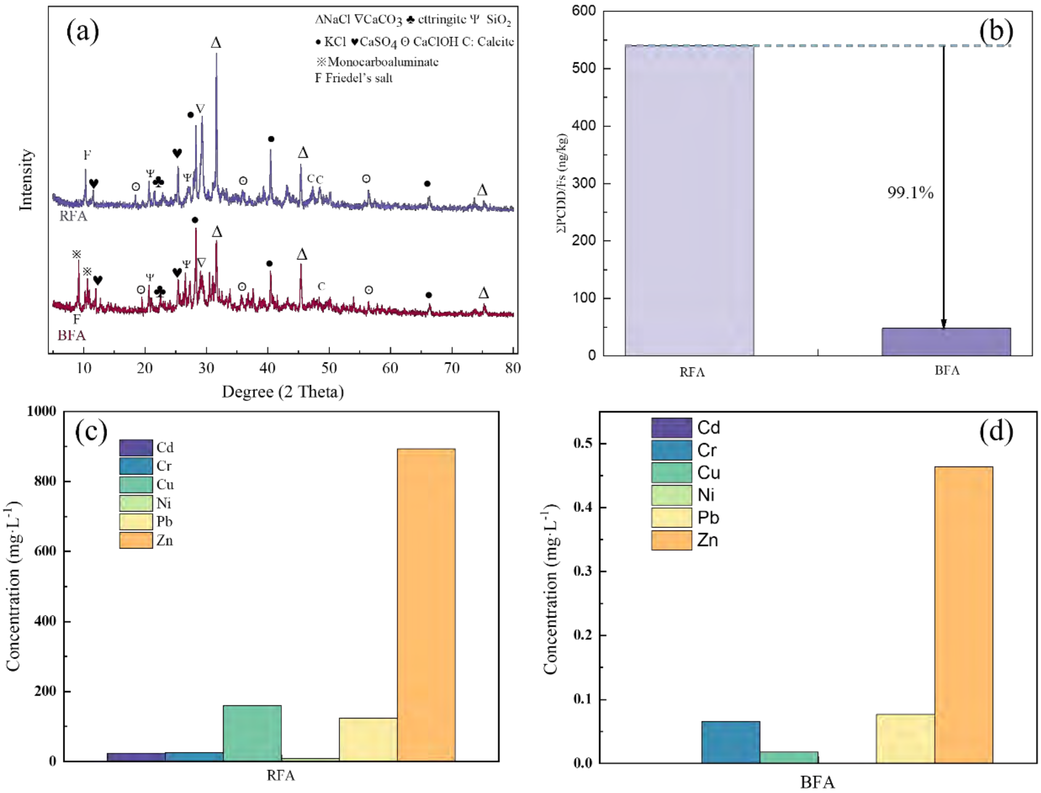

Fig. 2. XRD pattern and toxicity concentrations of BFA and RFA. (a) XRD pattern of RFA and BFA; (b) Concentration of PCDD/Fs of BFA and RFA; (c) Concentration of heavy metals in the leachate from the RFA; (d) Concentration of heavy metals in the leachate from the BFA.

3.2 Compressive strength

Fig. 3 displays the compressive strength of pastes at 7 and 28-day. MPC specimens, made with a water-cement ratio of 0.2, exhibited a compressive strength of 37.6 MPa at 7 days and 45.3 MPa at 28-day. The compressive strength of blended MSWIFA was slightly lower than pure MPC but much higher than RFA. The addition of calcium acetate increased the early compressive strength, with BFAC showing the best performance at 7-day. Moreover, the compressive strength rose with a higher MPC mix ratio. In conclusion, mixing RFA and BFA with MPC significantly strengthened the compressive strength, with the noticeable improvement in initial strength attributed to the effects of MPC and calcium acetate.

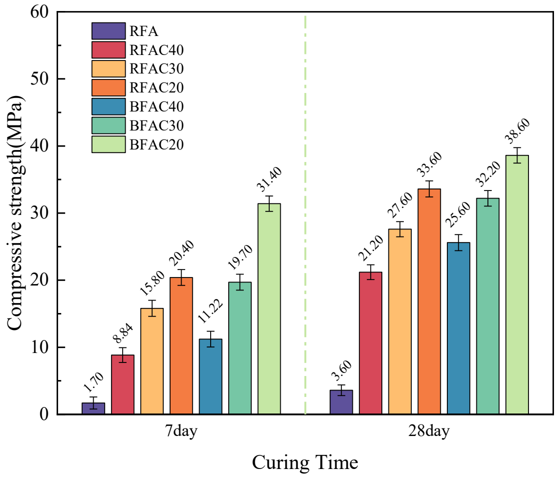

Fig. 3. The compressive strength of 7 groups at 7-day and 28-day

4. CONCLUSION

(1) Bio-treatment of MSWIFA significantly affected its physical properties, mineral composites, and environmental aspects. Notably, it enlarged the particle size, reduced chlorine content, and enabled the formation of MICP gels on the surface, indicating potential improvements in concrete strength.
(2) The bio-treatment process effectively reduced PCDD/Fs levels and stabilized heavy metals in MSWIFA, making it compliant with relevant national standards and reducing leaching concentrations.
(3) BFA blended with MPC enhanced the compressive strength of the resulting pastes, particularly in the early stages, and the addition of calcium acetate further improved early strength.
(4) The bio-treatment process significantly reduced environmental risks by lowering heavy metal concentrations in the leachate, contributing to the development of environmentally friendly MSWIFA management approaches and its beneficial reuse in construction and other applications.

5. ACKNOWLEDGMENT

The authors thank the financial supports from the National Natural Science Foundation of China (52168038, 51908526), National Natural Science Foundation of China Yunnan Province (202301AT070192), the National Key Research and Development Program of China (2022YFE0109300), Shenzhen Sustainable Development Technology Project (KCXFZ20201221173202008), the College Student Innovation and Entrepreneurship Training Project (No. 202210673087, 202210673019, S202210673064).

6. REFERENCES

Zhang, Y., Wang, L., Chen, L., Ma, B., Zhang, Y., Ni, W., & Tsang, D. C. W. (2021). Treatment of municipal solid waste incineration fly ash: State-of-the-art technologies and future perspectives. *Journal of Hazardous Materials*, *411*, 125132. https://doi.org/10.1016/j.jhazmat.2021.125132

Gutberlet, J. (2015). Cooperative urban mining in Brazil: Collective practices in selective household waste collection and recycling. *Waste Management*, *45*, 22-31.

Liu, J., Wang, Z., Xie, G., Li, Z., Fan, X., Zhang, W., Xing, F., Tang, L., & Ren, J. (2022). Resource utilization of municipal solid waste incineration fly ash - cement and alkali-activated cementitious materials: A review. *Sci Total Environ*, *852*, 158254. https://doi.org/10.1016/j.scitotenv.2022.158254

Zhang, J., Zhang, S., & Liu, B. (2020). Degradation technologies and mechanisms of dioxins in municipal solid waste incineration fly ash: A review. *Journal of Cleaner Production*, *250*, 119507. https://doi.org/10.1016/j.jclepro.2019.119507

He, Y., Lai, Z., Yan, T., He, X., Lu, Z., Lv, S., Li, F., Fan, X., & Zhang, H. (2019). Effect of Cd2+ on early hydration process of magnesium phosphate cement and its leaching toxicity properties. *Construction and Building Materials*, *209*, 32-40.

Liu, S., Cao, X., Yang, W., Liu, R., Fang, L., Ma, R., Peng, J., Zheng, S., & Ji, F. (2023). Preparation of magnesium potassium phosphate cement from municipal solid waste incineration fly ash and lead slag co-blended: Ca-induced crystal reconstruction process and Pb-Cl synergistic solidification mechanism. *Journal of Hazardous Materials*, *457*, 131690.

VALORIZATION OF FLY ASH TO PRODUCE GEOPOLYMER SPHERE AS A POTENTIAL ADSORBET IN REMOVING CADMIUM IONS FROM WASTEWATER

Tee How TAN[1], Kim Hung MO[2]

[1]Department of Construction Management, Faculty of Built Environment, Tunku Abdul Rahman University of Management and Technology, 53300 Kuala Lumpur, Malaysia
[2]Department of Civil Engineering, Faculty of Engineering, Universiti Malaya, 50603 Kuala Lumpur, Malaysia
tanth@tarc.edu.my

1. INTRODUCTION

Discharge of untreated wastewater into the water bodies is unethical and unlawful as they are generally heavily contaminated with various contaminants, including heavy metals. Cadmium is one of the heavy metals with a high toxicity level. It is primarily found in the effluent of industries like metallurgy and battery production. Exposure to cadmium, even at a low level, is extremely hazardous, which would cause lung damage, bone, and kidney toxicity (Rafati-Rahimzadeh et al., 2017). Hence, reducing the introduction of cadmium into the environment is vital. Among the various wastewater treatment approaches to remove heavy metals, adsorption has gained popularity attributed to its cost-effectiveness and protocol simplicity (Younas et al., 2021).

Recently, the potential of an geopolymer as alternative adsorbent material has been explored (Tan et al., 2020). The geopolymer adsorbent was first synthesized in the size of a powder. However, powdered geopolymer adsorbent faces limitations such as the difficulty of retrieval upon exhaustion and has led to the production of bulk-type geopolymer adsorbent. Nevertheless, the adsorption effectiveness of bulk-type geopolymer adsorbent has been found to be greatly compromised by the larger size that results in a lower surface area (Novais et al., 2016).

Spherical porous geopolymer adsorbent has been found to overcome those limitations while demonstrating a promising removal efficacy. Therefore, this work explored the potential of a porous geopolymer sphere adsorbent that was produced using direct moulding technique. This method is relatively simpler and safer while being industrially feasible. Several factors were examined to investigate Cd(II) removal effectiveness of the porous geopolymer sphere, including the pH of the Cd(II) solution, porosity, initial Cd(II) concentration, and dosage of the porous geopolymer sphere.

2. MATERIALS AND METHODS

2.1 Materials

Class F fly ash and calcined kaolin sourced from local industries were chosen as the starting aluminosilicate raw materials to produce a porous geopolymer sphere. The chemical composition of the raw materials is presented in Table 1 whereas Figure 1 demonstrates the particle size distribution of fly ash and calcined kaolin.

Table 1: Chemical composition of raw materials

Raw material	Na_2O	SiO_2	Al_2O_3	SO_3	CaO	Fe_2O_3	K_2O	MgO
Fly ash	2.02	41.13	19.77	2.23	12.13	12.91	1.28	6.27
Calcined kaolin	0.34	60.35	36.73	0.01	0.25	0.56	0.24	0.08

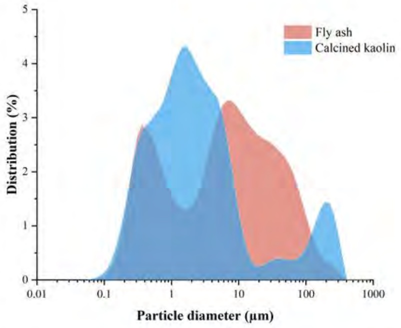

Figure 1: Particle size distribution of fly ash and calcined kaolin

Sodium silicate (Na_2SiO_3) and sodium hydroxide (NaOH) solutions were mixed at a ratio of 1:2.5 to form the alkaline activator. The silica modulus and solid content of the Na_2SiO_3 were 2.08 and 53.5%, respectively, while the molarity of the NaOH solution was 10 M. The selected foaming agent was hydrogen peroxide (H_2O_2, 30% wt./vol). Cadmium nitrate tetrahydrate ($Cd(NO_3)_2.4H_2O$) was utilized to formulate the synthetic wastewater solution containing Cd(II). All chemicals adopted were of analytical reagent grade.

2.2 Mixing process

A facile yet straightforward method, which is the direct moulding method, was adopted to produce the porous geopolymer sphere adsorbent, as illustrated in Figure 2. Firstly, fly ash and calcined kaolin were blended in a 2:1 proportion, by mass. Then, the alkaline activator and water were added and stirred for 3 min. 1.2% of H_2O_2 was then added, by mass, into the slurry for an additional 60 s to complete the mixing. Upon completion of mixing, the homogeneous slurry was immediately transferred to the spherical mould (12 mm in diameter) and subject to heat curing at 60°C for one day. The filled mould was wrapped with polyethylene film to prevent excessive moisture loss during curing.

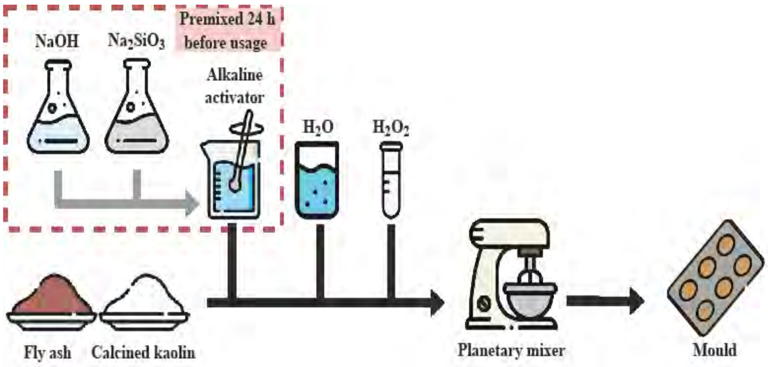

Figure 2: Schematic diagram of the mixing process

3. RESULTS AND DISCUSSION

3.1 Influence of porosity

Figure 3 shows the Cd(II) adsorption onto the porous and non-porous geopolymer sphere. The porous geopolymer sphere's Cd(II) removal capacity was 26.14 mg/g, which was approximately an 200% increment compared to that of the non-porous geopolymer sphere (8.57 mg/g). The increment is attributed to the foaming effect, which considerably increased the porosity and hence the surface area, as both spheres were made to have the same size and geometry.

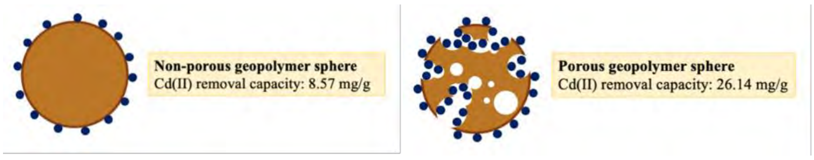

Figure 3: Adsorption of Cd(II) onto non-porous and porous geopolymer spheres

3.2 Influence of pH

Figure 4 demonstrates the influence of the pH of Cd(II) solution on the Cd(II) removal efficiency of porous geopolymer sphere. Except for pH 2, the Cd(II) removal efficiency was significantly high (100%) across the studied pH range (up to 6). At pH 2, the Cd(II) removal efficiency of the porous geopolymer sphere was only half of its peak performance (50.4%). This is due to the presence of H^+ ions that creates a vigorous competition with the Cd(II) ions for the binding sites. As a result, it can be suggested that the influence of the solution pH on the Cd(II) removal performance of porous geopolymer sphere was substantial when the solution pH was very low (pH of 2). This aligns with with the findings of Lan et al. (2019), who proposed an optimum pH of 5.

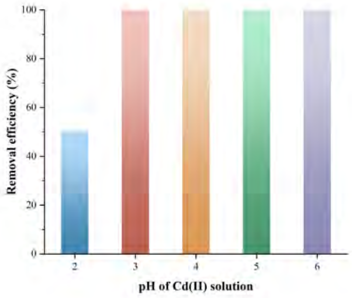

Figure 4: Influence of pH of Cd(II) solution on porous geopolymer sphere's Cd(II) removal efficiency

3.3 Influence of initial Cd(II) concentration

Figure 5 shows that as the initial Cd(II) concentration increased, the Cd(II) removal capacity increased. This implies that there were unoccupied binding sites available when the initial Cd(II) concentration was low. However, when the initial Cd(II) concentration exceeded 800 mg/L, the Cd(II) removal capacity of the porous geopolymer sphere remained constant, indicating depletion of the binding sites. On the other hand, the Cd(II) removal efficiency decreased at higher initial Cd(II) concentration, implying more unbound Cd(II) due to inadequate binding sites (Duan et al., 2016). The maximum Cd(II) removal capacity of porous geopolymer sphere was identified as 36.97 mg/g.

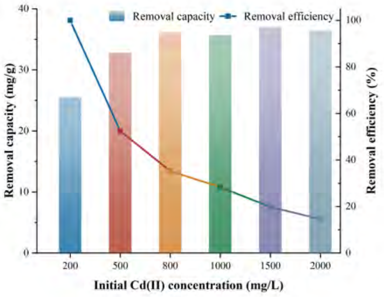

Figure 5: Influence of initial Cd(II) concentration on porous geopolymer sphere's Cd(II) removal performance

3.2 Influence of porous geopolymer sphere dosage

Figure 6 depicts the influence of porous geopolymer sphere dosage on Cd(II) removal performance. The findings showed that doubling the dosage of porous geopolymer sphere greatly improved the Cd(II) removal efficiency from 34.8% to 70.8%. However, the Cd(II) removal capacity of porous geopolymer sphere remained constant, indicating that the porous geopolymer sphere had achieved a saturated condition. Notably, the Cd(II) removal efficiency peaked at 100% when the porous geopolymer sphere dosage was tripled (3 nos.). However, the Cd(II) removal capacity was found to reduce from 36.74 mg/g (2 nos.) to 33.36 mg/g (3 nos.). The reduction of the Cd(II) removal capacity implies excessive binding sites had been offered by the porous geopolymer sphere.

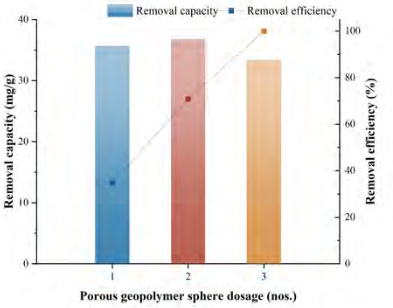

Figure 6: Influence of porous geopolymer sphere dosage on Cd(II) removal performance

4. CONCLUSION

The Cd(II) removal capacity porous geopolymer sphere is significantly improved after foaming, indicating the major drawback of bulk-type adsorbents, which tend to have a low surface area, can be offset via foaming. The porous geopolymer sphere attains a maximum Cd(II) removal capacity of 36.97 mg/g. Additionally, the optimum pH values for Cd(II) adsorption are determined to be between 3-6. When the initial Cd(II) concentration rises, the Cd(II) removal efficiency declines, which is due to the deficit of binding sites. Providing a higher dose of porous geopolymer sphere, however, can mitigate the problem. Besides the promising Cd(II) removal performance, the straightforward production method and the ability to consume industrial by-products or waste streams as the starting materials are substantial advantages, making it a sustainable adsorbent material.

5. ACKNOWLEDGMENT

The authors would like to express appreciation for the support of the sponsors [Project Number = FRGS/1/2018/TK06/UM/02/1].

6. REFERENCES

Duan, P., Yan, C., Zhou, W., & Ren, D. (2016). Development of fly ash and iron ore tailing based porous geopolymer for removal of Cu(II) from wastewater. *Ceramics International*, *42*(12), 13507-13518. https://doi.org/10.1016/j.ceramint.2016.05.143

Lan, T., Li, P., Rehman, F. U., Li, X., Yang, W., & Guo, S. (2019). Efficient adsorption of Cd(2+) from aqueous solution using metakaolin geopolymers. *Environ Sci Pollut Res Int*, *26*(32), 33555-33567. https://doi.org/10.1007/s11356-019-06362-w

Novais, R. M., Buruberri, L. H., Seabra, M. P., & Labrincha, J. A. (2016). Novel porous fly-ash containing geopolymer monoliths for lead adsorption from wastewaters. *J Hazard Mater*, *318*, 631-640. https://doi.org/10.1016/j.jhazmat.2016.07.059

Rafati-Rahimzadeh, M., Rafati-Rahimzadeh, M., Kazemi, S., & Moghadamnia, A. (2017). Cadmium toxicity and treatment: An update. *babol-caspjim*, *8*(3), 135-145. https://doi.org/10.22088/cjim.8.3.135

Tan, T. H., Mo, K. H., Ling, T.-C., & Lai, S. H. (2020). Current development of geopolymer as alternative adsorbent for heavy metal removal. *Environmental Technology & Innovation*, *18*. https://doi.org/10.1016/j.eti.2020.100684

Younas, F., Mustafa, A., Farooqi, Z. U. R., Wang, X., Younas, S., Mohy-Ud-Din, W., Ashir Hameed, M., Mohsin Abrar, M., Maitlo, A. A., Noreen, S., & Hussain, M. M. (2021). Current and Emerging Adsorbent Technologies for Wastewater Treatment: Trends, Limitations, and Environmental Implications. *Water*, *13*(2). https://doi.org/10.3390/w13020215

SAFE DISPOSAL AND RESOURCE UTILIZATION OF MUNICIPAL SOLID WASTE INCINERATION FLY ASH

Yu GAO[1], Ze LIU[1], Fuli LIU[1], Rui LIU[1], Dongmin WANG[1], Baomin WANG[2], Yan YOU[3]

[1] School of Chemical and Environmental Engineering, China University of Mining & Technology (Beijing), Beijing, 100083, China.
[2] Faculty of Infrastructure Engineering, Dalian University of Technology, Dalian 116024, China.
[3] Macau Environmental Research Institute, Macau University of Science and Technology, Macao SAR 999078, China.
lzk1227@sina.com (Ze LIU[1])

1. INTRODUCTION

In recent years, China's domestic waste incineration industry has developed rapidly, and the incineration capacity has increased year by year, exceeding 250 million tons/year. As a result, a large amount of domestic waste incineration fly ash enriched in heavy metals and dioxins pollutants has been produced.

At present, the main treatment methods of domestic and foreign domestic waste incineration fly ash are: (1) chelating agent solidification and stabilization method; (2) Plasma high temperature melting method; (3) cement kiln collaborative treatment method.

Limitations of the above methods: Chelating fly ash is the use of chelating agents to chelate heavy metal ions to fix it, chelating fly ash after the heavy metal leaching concentration reached GB/T1689-2008 into the landfill for landfill, but China's land resources are tight, according to statistics, nearly 50% of the country's cities and towns in the full load operation, and about half of the landfill in overload operation. In the Implementation Plan for strengthening the weaknesses of Urban solid waste classification and treatment Facilities, it is proposed that in principle, there will be no new primary solid waste landfills, and the operation and management level of existing landfills is low, which has the risk of secondary pollution. The plasma high-temperature melting method is to form a glass state of fly ash at a temperature above 1400℃. This technology has high energy consumption, complicated technology and high operating cost, and cannot be used on a large scale.

The main components of waste incineration fly ash are aluminosilicate minerals such as silicon dioxide, calcium carbonate and calcium sulfate, which have certain pozzolanic activity. After dechlorination and detoxification, fly ash can be used as a gelling material and realize safe resource utilization of fly ash.

The MSWI fly ash after water elution of chlorine is suitable for preparation of geopolymer due to its low soluble chlorine content. In this work, coal fly ash (CFA) and washed dechlorination MSWI fly ash (WDMFA) were taken as the raw materials, and the effects of WDMFA on the mechanical properties, microstructure, and heavy metal leaching characteristics of alkali activated CFA geopolymers were studied. It provides theoretical support for the safe utilization of fly ash from waste incineration in the field of polymers.

2. MATERIALS AND METHODS

2.1 Characterization of materials

The main ingredients were WDMFA (MSWI Power Plant in DengFeng) and CFA (Circulating fluidized bed fly ash from Shanxi Shuozhou China Coal Energy Co., LTD). The alkali-activated solution was made by mixing sodium silicate and sodium hydroxide corresponding to mix proportion in Table 2. The composition (by equivalent oxide mass) of water glass (Beijing Hongxing Soap Alkali Factory, China) was shown in Table 1. The sodium hydroxide (Shanghai Macklin Biochemical Co., Ltd, China) used were A.R. purity. Distilled water was used throughout.

2.2 Sample preparation

Geopolymer samples were prepared with the proportions as mentioned in Table1. Raw materials were mixed for 4 min (stir on low speed for 2min, stir quickly for 2min) and the homogeneous mixtures obtained were cast into the steel molds with dimensions of 30 mm × 30 mm × 30 mm, then discharged the air bubbles through compaction and vibration. Every mould was covered with plastic film to avoid moisture evaporation. These demoulded samples were packaged into a plastic bag and cured in cement maintainer with the temperature of 25 ◦C and humidity higher than 90%. Test on the samples were carried out at the time the corresponding curing age arrived.

2.3 Test method

X-ray Fluorescence (XRF-PANalytical Axios, Netherlands) and X-ray Diffraction（XRD-Rigaku Ultima IV, Japan） analyses were used to determine the chemical (Table 1) and mineral (Table 2) compositions of raw materials and specimens. A laser diffraction particle size analyser was used to measure the particle size distribution of WDMFA and CFA (Malvern Mastersizer 2000). Heavy metal contents in raw materials and specimens were measured using inductively coupled plasma optical emission spectrometry (Agilent 5110, ICP-OES) following the HJ/T299-2007 standard. SEM images were obtained from the PHENOM Pharos G1 in the vacuum environment with the thin gold-plated samples. CS200 universal servo stress testing machine was used to measure the compressive strength under 0.5 mm/min cross-head speed conditions, and the data of maximum load strength when the samples broke was recorded. For each paste, at least 3 samples were tested and the average values of these samples were usually considered as the final results

Table 1 Designed chemical compositions of WDMFA and CFA raw materials.

Compositions	WDMFA	CFA	Water glass
SiO2	18.638	46.39	32.02
Na2O	-	-	13.62
CaO	44.792	9.073	
Al2O3	6.229	30.907	
SO3	10.677	1.329	
Fe2O3	6.174	5.5	
Cl	3.493	0.101	

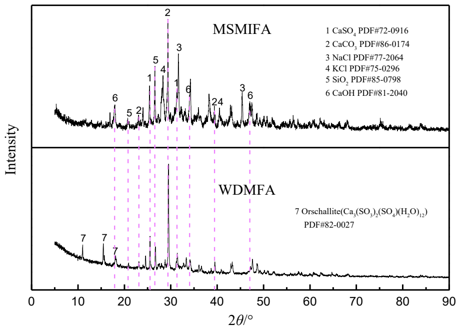

Figure 1 XRD patterns of MSWIFA and WDMFA

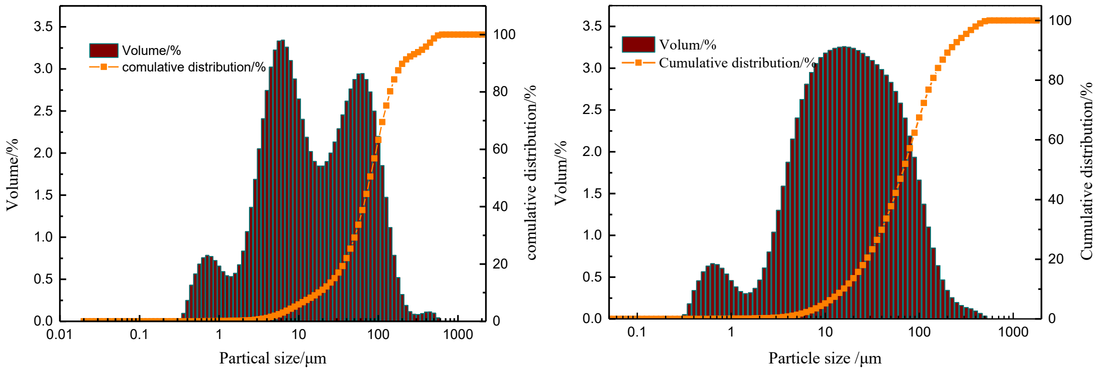

Figure 2 a Particle size of WDMFA fly ash; b Particle size of CFA.

3 RESULTS AND DISCUSSION

Configure the homogeneous slurry according to the proportion in Table 2, and after steaming for 1d, There were lots of amorphous C–S–H gels generated and dense microstructure in geopolymer , this gel contributed much to the mechanical strength of samples. The formation of gel also makes the test block become dense, and the heavy metals in the fly ash of waste incineration can be effectively solidified. However, the higher the amount of fly ash in waste incineration, the greater the expansion degree of the test block, the obvious crack of the test block and the decrease of its compressive strength directly. Compressive strength at different ages under different dosage in Figure 3.Interestingly, this phenomenon has also been mentioned in the research on cement solidified fly ash of waste incineration. This is because the fly ash of waste incineration contains some aluminum elements that cannot be completely eliminated during the process of hydration. The elemental aluminum reacts with water and sodium hydroxide in the activator to produce hydrogen, and the release of the gas causes the test block to produce bubbles, which accumulate and lead to expansion and decline in compressive strength.

Table 2 Alkali activator concentration and WDMFA dosage

	WDMFA	CFA	WG（g）	NaOH（g）	Water（g）
0	0	250	113.09	24.05	78.09
10%	25	225			
20%	50	200			

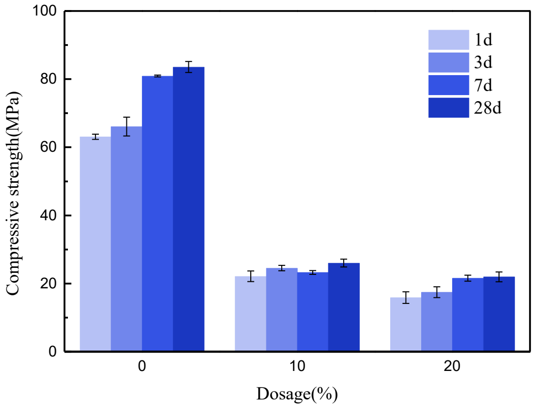

Figure 3. Compressive strength at different ages under different WDMFA content

4 CONCLUSION

In this study, we investigated the physical and chemical properties, compressive strength and heavy metal leaching characteristics of fly ash base polymer with different WDMFA content.The following conclusions can be drawn, which would facilitate the insight of the reaction mechanism of WDMFA in fly ash polymers:

(1)After washing, the soluble salt is effectively removed, and the phase of insoluble matter does not change greatly, mainly calcium carbonate, calcium sulfate and silicon dioxide

(2)After evaporation, fly ash base polymers mixed with washed fly ash all produce a large amount of C-A-S-H gel, which provides the main source of strength. However, due to the presence of aluminum in washed fly ash, and the reaction of aluminum with water in the activator and sodium hydroxide to produce hydrogen, bubbles are generated in the solidified body, and the compressive strength decreases significantly.

(3)In the fly ash base polymer mixed with washing fraction, the heavy metal ions were fixed well, and the leaching amount was in line with the HJ/T299-2007 standard.

5 ACKNOWLEDGMENT

The authors would like to express appreciation for the support of the sponsors [Joint Funds of the National Natural Science Foundation of China (U20A20324)].

6 REFERENCES

Andac, M., Glasser, F.P., 1999. Pore solution composition of calcium sulfoaluminate cement. Adv. Cem. Res. 11, 23-26.

Aubert, J.-E., Husson, B., Sarramone, N., 2006. Utilization of municipal solid waste incineration (MSWI) fly ash in blended cement: Part 1: processing and characterization of MSWI fly ash. J. Hazard Mater. 136, 624-631.

Bakharev, T., 2005. Resistance of geopolymer materials to acid attack. Cement Concr. Res. 35, 658-670.

Bakri, A.M., Kamarudin, H., Binhussain, M., Nizar, I.K., Rafiza, A.R., Zarina, Y., 2013. Comparison of geopolymer fly ash and ordinary portland cement to the strength of concrete. Adv. Sci. Lett. 19, 3592-3595.

Bolan, N., Kunhikrishnan, A., Thangarajan, R., Kumpiene, J., Park, J., Makino, T., Kirkham, M.B., Scheckel, K., 2014. Remediation of heavy metal (loid) scontaminated soilseto mobilize or to immobilize? J. Hazard Mater. 266, 141-166.

Diaz-Loya, E.I., Allouche, E.N., Eklund, S., Joshi, A.R., Kupwade-Patil, K., 2012. Toxicity mitigation and solidification of municipal solid waste incinerator fly ash using alkaline activated coal ash. Waste Manag. 32, 1521-1527.

Joseph, A.M., Van den Heede, P., Snellings, R., Van, A., 2017. Comparison of different beneficiation techniques to improve utilization potential of municipal solid waste incineration fly ash concrete. Constr. Mater. Syst. 49.

Lura, P., Jensen, O.M., 2007. Measuring techniques for autogenous strain of cement paste. Mater. Struct. 40, 431-440.

Miller, F.A., Wilkins, C.H., 1952. Infrared spectra and characteristic frequencies of inorganic ions. Anal. Chem. 24, 1253-1294.

Müller, U., Rübner, K., 2006. The microstructure of concrete made with municipal waste incinerator bottom ash as an aggregate component. Cement Concr. Res.36, 1434-1443.

Chen, T.L., Chen, Y.H., Dai, M.Y., Chiang, P.C., 2021. Stabilization-solidificationutilization of MSWI fly ash coupling CO2 mineralization using a high-gravity rotating packed bed. Waste Manag. 121, 412–421.

Chen, Z.L., Lu, S.Y., Tang, M.H., Lin, X.Q., Qiu, Q.L., He, H., Yan, J.H., 2019.Mechanochemical stabilization of heavy metals in fly ash with additives. Sci. Total Environ. 694, 133813.

Chen,Z.,Li,J.S., Zhan, B.J., Sharma, U., Poon, C.S., 2018. Compressive strength andmicrostructural properties of dry-mixed geopolymer pastes synthesized from GGBS and sewage sludge ash. Construct. Build. Mater. 182 (10), 597–607.

Chou, J.D., Wey, M.Y., Liang, H.H., Chang, S.H., 2009. Biotoxicity evaluation of fly ash
and bottom ash from different municipal solid waste incinerators. J. Hazard Mater.168 (1), 197–202.

Du, B., Li, J.T., Fang, W., Liu, Y.L., Yu, S.Y., Li, Y., Liu, J.G., 2018. Characterization of naturally aged cement-solidified MSWI fly ash. Waste Manag. 80, 101–111.

Gao, X., Yuan, B., Yu, Q.L., Brouwers, H.J.H., 2017. Characterization and application of municipal solid waste incineration (MSWI) bottom ash and waste granite powder in alkali activated slag. J. Clean. Prod. 164 (15), 410–419.

EVALUATION OF MECHANICAL AND LEACHING PROPERTIES AND CARBON FIXATION OF CARBONATED INCINERATION BOTTOM ASH

Otsuka, Y[1]., Sato. K.[1], Fujikawa, T.[1], Koga, C.[1], Tanida, K.[2], Fujita, J.[2], Hosoda, H.[2]
, and Sakanakura, H.[3]

[1] Department of Civil Engineering, Fukuoka University
[2]KOBELCO ECO-SOLUTIONS Co.,Ltd.
[3]National Institute for Environmental Studies
E-mail: td234002@fukuoka-u.ac.jp

1. INTRODUCTION

In Japan, approximately 80% of municipal solid waste (MSW) is disposed at incineration facilities, and about 3.4 million tons of incineration ash is discharged every year. Currently, the effective use of waste is being promoted in Japan, but the utilization rate of incineration ash is only 30% due to high lead concentration from the ash. On the other hand, the residual capacity of final disposal sites has been declining in recent years, and the need for effective use of incineration ash is increasing. The incineration ash is classified into incineration bottom ash (IBA) and fly ash (FA), which account for 80 % and 20 %, respectively. Since IBA has a wide grain size range and relatively low in heavy metal elution, this study focused on the effective use of IBA as base-course material. To immobilize lead in IBA, carbonation treatment of IBA with CO_2 gas was conducted in this study. In addition, modified CBR tests were performed with carbonated IBA to evaluate their applicability to base-course material. This study also focused on the carbon fixation in ash by carbonation treatment, and measured and evaluated the amount of carbon fixed by carbonation treatment.

2. MATERIALS AND METHODS

Two types of IBA discharged from a incineration facility in 2021 and 2022 were used in this study. Both IBAs of 19 mm or less in grain size were used in the study. The physical compositions of IBAs for each year is shown in Figure 1. In both years, ash and others composes the majority of the physical composition, however, focusing on glass and ceramics, there are little differences in the percentages between years of discharge.

To carbonate IBA, it was filled into two containers (640mm×440mm×320 mm). IBA was carbonated by venting CO_2 gas from the bottom of the containers under the conditions shown in Table 1. These conditions were determined based on the results of a previous study (Shigeizumi et al. 2020).

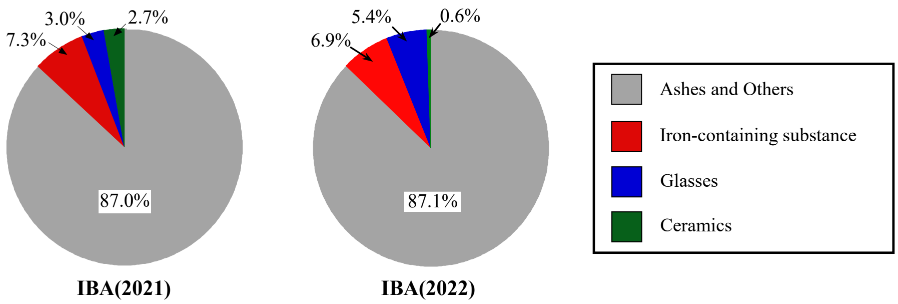

Figure 1. Physical compositons of IBA(2021) and IBA(2022)

Table 1. Experimental conditions for carbonation treatment of IBAs

Discharge year of IBA	CO_2 concentration (%)	Ventilation velocity (L/min)	Ventilation time (h)	Water content of IBA (%)	Filling density (g/cm³)	Amount of CO_2 (g/kgDW)
2021	100	30	1.5	30.6	1.00	90
2022				29.7		

To examine the effect of carbonation on lead immobilization, leaching tests were conducted on carbonated and uncarbonated IBAs in this study. The tests were performed according to the method issued by the Ministry of the Environment of Japan. IBA that passed through a 2 mm sieve were shaken for 6 hours at a liquid-solid ratio of 10, then centrifuged and filtered to make test samples which were then analyzed. In addition, compaction tests modified CBR tests were conducted on both carbonated and uncarbonated IBAs to clarify the effect of carbonation treatment on the mechanical properties of IBAs and to evaluate the applicability of them as base-course materials.

The amounts of carbon fixed in IBA through carbonation treatment were calculated using the method (Saito et al. 2022) measuring the gas pressure generated by the reaction of carbonate in ash with HCl. In this test, IBA with a dry weight of 0.5 g and 20 ml (3 mol/l) of HCl were reacted in a sealed container, and the gas pressure due to the generated CO_2 was measured. The calcium carbonate content was determined from the results, and the amount of carbon fixation was calculated using Eq. 1.

$$M_{CO_2} = m_{CaCO_3} \times \frac{MW_{CO_2}}{MW_{CaCO_3}} \times \frac{1}{m_{ash}} \qquad (1)$$

where, M_{CO_2}(kg$_{CO2}$/t DW$_{IBA}$) is the CO_2 content of IBA, m_{CaCO_3}(kg) is the $CaCO_3$ content, MW_{CO_2} is the molecular weight of CO_2, MW_{CaCO_3} is molecular weight of $CaCO_3$, m_{ash}(t) is the dry weight of IBA.

This process was performed on both carbonated and uncarbonated IBAs, and the difference in those values was estimated as the amount of carbon fixation by carbonation treatment.

3. RESULTS AND DISCUSSION

The results of leaching tests with carbonated and uncarbonated IBA are shown in Table 2. Three samples (1-3) were used for leaching tests in each condition.In both of the two years of IBA, lead leaching was not detected after carbonation treatment. It indicates the effects of carbonation treatment on the immobilization of lead in IBA. This may be due to a decrease in pH and the production of insoluble lead carbonate through carbonation. Carbonated IBAs in the tests also meet Japan's soil environmental standards in terms of lead elution concentration. These results also show that carbonation treatment of IBA can reduce the concentration of lead elution from IBA to lower than the Japan's soil environmental standard.

Table 2. The results of leaching tests between uncarbonated and carbonated IBAs

(a) Uncarbonated

Samples (IBA)	pH	Pb (mg/L)
2021 Uncarbonated 1	11.9	0.05
2021 Uncarbonated 2	11.9	0.06
2021 Uncarbonated 3	11.7	0.15
2022 Uncarbonated 1	11.7	0.05
2022 Uncarbonated 2	11.8	0.07
2022 Uncarbonated 3	11.8	0.27
Soil Enviromental Standard		0.01
Limit of Quantitation		0.01

(b) Carbonated

Samples (IBA)	pH	Pb (mg/L)
2021 Carbonated 1	10.9	N.D.
2021 Carbonated 2	10.6	N.D.
2021 Carbonated 3	10.8	N.D.
2022 Carbonated 1	10.8	N.D.
2022 Carbonated 2	10.7	N.D.
2022 Carbonated 3	10.7	N.D.
Soil Enviromental Standard		0.01
Limit of Quantitation		0.01

Compaction curves for carbonated and uncarbonated IBAs are shown in Figure 2. Although there was a slight difference in maximum dry density for the different years of IBA discharge, there was no apparent difference. The compaction curve did not change significantly after carbonation in each year's IBAs, thus it can be assumed that the impact of carbonation treatment of IBAs on compaction properties is small. On the other hand, the 95% modified CBR values for each IBA condition are shown in Figure 3. The results suggest that carbonation treatment tends to decrease the modified CBR value of IBA. This is assumed to be due to a reduction in the cohesion between ash particles as a result of carbonate formation through carbonation treatment (Fujikawa et al. 2020). In any case, the carbonated IBA also has modified CBR value above 30%, indicating that it adequately satisfied the criteria for subbase-course material.

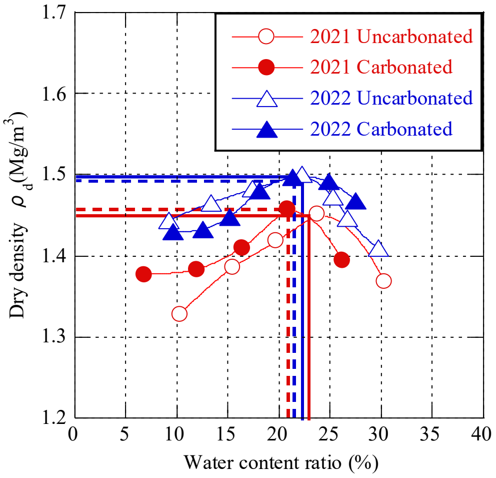

Figure 2. Compaction Curves of IBAs

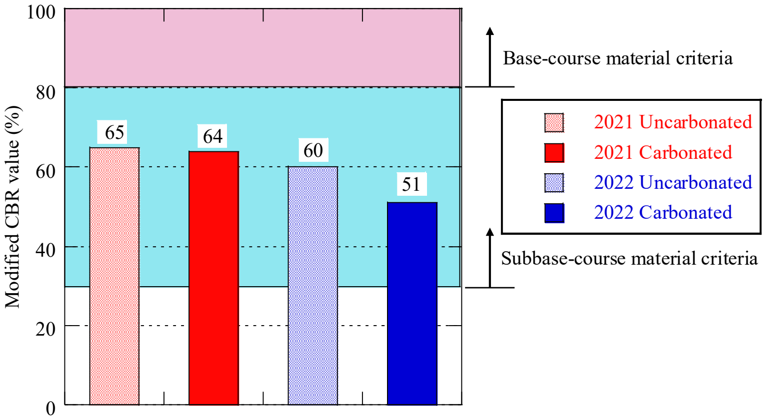

Figure 3. 95% Modified CBR Values of IBAs

The gas pressures generated by the reaction between IBA and HCl in each condition is shown in Figure 4. There were differences in the gas pressures generated in carbonated and uncarbonated IBAs, and these differences were used to determine the amount of carbonate produced by the carbonation treatments. Then, the fixation amount of CO_2 by carbonation treatment was calculated from the amount of carbonate produced and Eq. 1 to be approximately 42 kg per ton of dry weight in each year of IBA. Assuming that the percentage of IBA in the incinerated ash to be landfilled is 66% and its water content is 35%, and assuming that CO_2 is fixed in all of the IBA landfilled annually, 63,000 tons of CO_2 can be fixed in the ash in every year. The results indicate that IBA has good potential for CO_2 fixation.

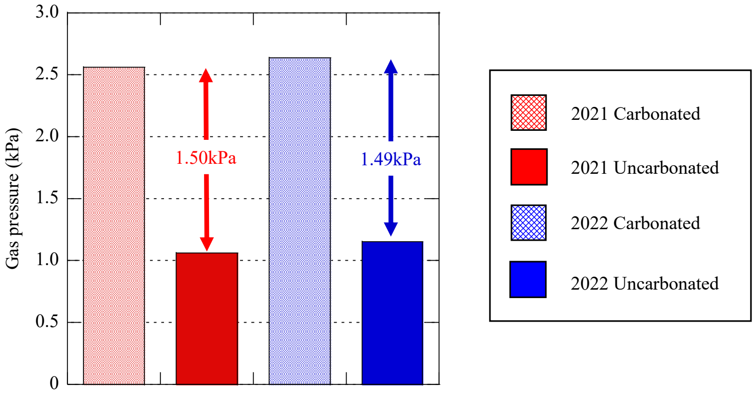

Figure 4. Differences in gas pressure generated between carbonated and uncarbonated IBAs

4. CONCLUSION

This study focused on IBA generated from MSW and evaluated the effect of carbonation treatment on lead immobilization, its applicability to base-course material, and carbon fixation by carbonation treatment, and came to the following conclusions.

1) Carbonation treatment reduces lead leaching from IBAs, and their concentrations meet soil environmental standards.in Japan.
2) The modified CBR value of IBA shows a tendency to decline with carbonation treatment, but still satisfies the material criteria for subbase-course material.
3) Approximately 42 kg of CO_2 can be fixed per ton of IBA (dry weight), which is equivalent to 63,000 tons of CO_2 fixed in the ash when converted to total IBA to be landfilled per year.

Future studies are to examine carbonation treatment using exhaust gas from incineration facilities instead of CO_2 gas, and methods to reduce lead content by efficiently sorting lead from the IBA.

5. REFERENCES

Fujikawa, T., Sato, K., Koga, C. & Sakanakura, H. (2020). Effect of Aging on Material Characteristics and Leaching Properties of Incineration Bottom Ash from Municipal Solid Waste. *Waste and Biomass Valorization*, 11, 7097-7107.

Saito, N., Yamasaki, T., Sumida, H., Nosho, K., Katsumi, T. & Takai, A. (2022). Evaluation of Carbon Fixation Method by Permeating Water Through Coal Fly Ash Waste Ground in Coastal Landfill. *Geo-Environmental Engineering 2022*, 12, 98-105.

Shigeizumi, K., Kubota, H., Kochi, H., Sato, K., Fujilkawa, T., Nagayama, Y., Sakanakura & H., Fujita, D. (2020). Elusion and Mechanical Characteristics of Municipal Solid Waste (MSW) Incineration Bottom Ash that has Undergone Accelerated Carbonation Treatment using CO_2 Recovered from Incineration Plant Exhaust. *Journal of the Japan Society of Material Cycles and Waste Management*, vol 31, 116-130.

MSWI FLY ASH CONVERSION AND PREPARATION OF CEMENTITIOUS MATERIALS: SOLIDIFICATION MECHANISM OF HEAVY METAL PB

Fuli LIU[1], Ze LIU[1], Yu GAO[1], Rui LIU[1], Dongmin WANG[1], Baomin WANG[2], Yan YOU[3]

[1] School of Chemical and Environmental Engineering, China University of Mining & Technology (Beijing), Beijing, 100083, China.
[2] Faculty of Infrastructure Engineering, Dalian University of Technology, Dalian 116024, China.
[3] Macau Environmental Research Institute, Macau University of Science and Technology, Macao SAR 999078, China.
lzk1227@sina.com (Ze LIU[1])

1. INTRODUCTION

Municipal solid waste incineration (MSWI) fly ash contains a large amount of soluble chloride salts, heavy metals, and primary carcinogen dioxins. This article proposes a safe disposal method for MSWI fly ash. After the MSWI fly ash is converted into a new solid phase mainly composed of Ettringite, the heavy metals can be effectively solidified, and the chlorine salt in the MSWI fly ash can be Recycled. The solidified body of heavy metals is effectively decomposed into dioxins after heat treatment. The final MSWI fly ash solidified body (containing dehydrated Ettringite and a small amount of anhydrous calcium sulfate) is mixed with slag to prepare gypsum slag cement. The solidified MSWI fly ash provides alkalinity and gypsum, which together stimulate the slag. With the increase of the proportion of solidified MSWI fly ash, the hydration process of slag is accelerated, and Ettringite is filled in the pores of the cementitious system to improve the overall strength.

2. MATERIALS AND METHODS

Figure 1 (a) shows the quantitative analysis of MSWI fly ash by XRD mineralogy. Its main components include Calcium hydroxide, basic calcium chloride, calcium sulfate, calcium carbonate, sodium chloride, Potassium chloride, and some amorphous components, which include carbon residue and a small amount of silicon and aluminum. The residues after MSWI fly ash conversion mainly include Ettringite and calcium sulfate dihydrate (Figure 1b). After heat treatment, the conversion residue is mainly composed of dehydrated Ettringite, anhydrous calcium sulfate, and calcium carbonate. Figure 1 (d) shows the XRD diagram of the slag used in the experiment, mainly consisting of amorphous components. The chemical composition of slag is shown in Table 1, mainly including silica, alumina, and magnesium oxide.

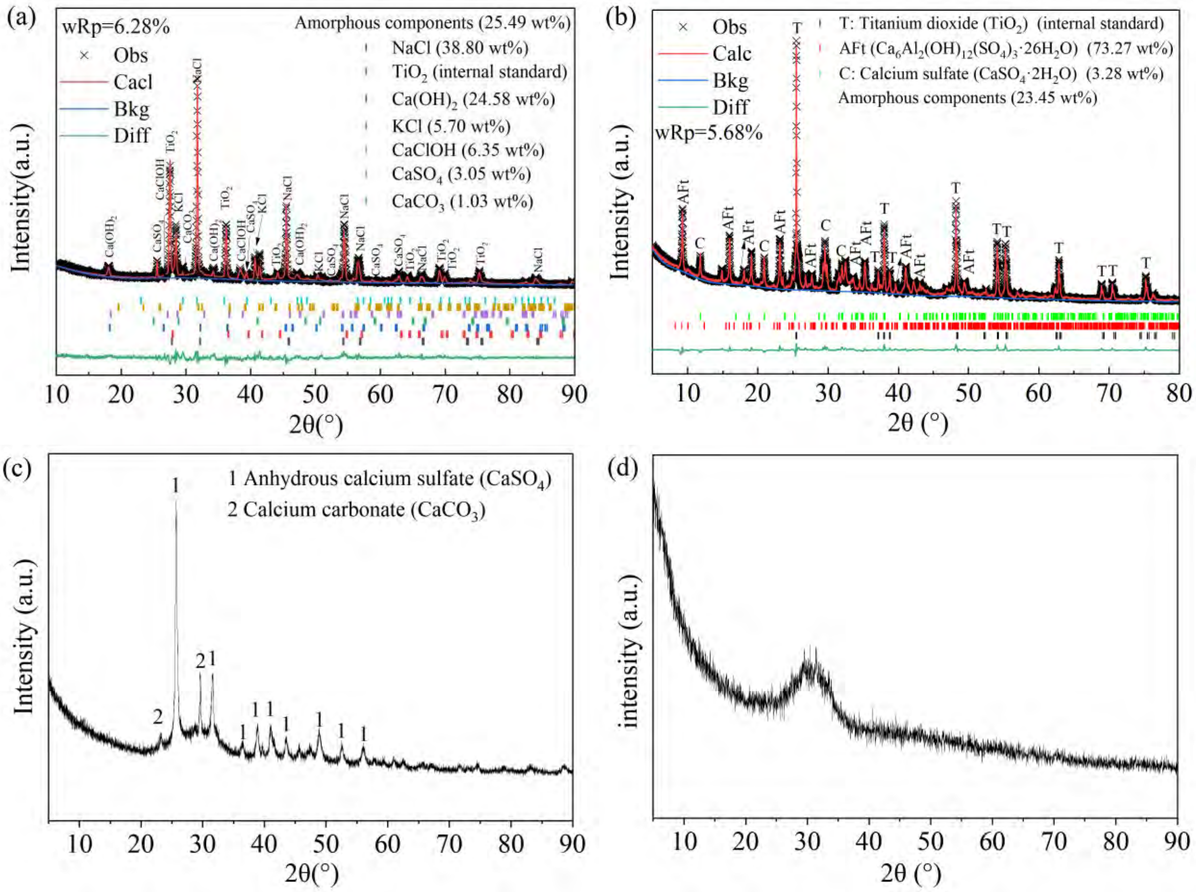

Figure 1 XRD of (1) MSWI fly ash (2) MSWI fly ash solidified body (3) Residue after roasting and separating dioxins (4) Slag

Table 1 Chemical Composition of Slag

Chemical Composition	CaO	SiO_2	Al_2O_3	MgO	SO_3	Fe_2O_3	Other
content/%	49.92	25.53	13.39	5.02	2.29	0.35	3.50

Figure 2 Conversion Path and Material Preparation Process of MSWI Fly Ash

Figure 2 shows the transformation path of MSWI fly ash, including three parts: transformation into a new solid phase dominated by Ettringite, pyrolysis of dioxin, and preparation of gypsum slag cement.

Table 2 Gypsum slag cement mix ratio

Sample name	MSWI fly ash solidified body/%	Slag/%	Water/binder ratio
DE5	5	95	0.4
DE7.5	7.5	92.5	0.4
DE10	10	90	0.4
DE12.5	12.5	87.5	0.4

Table 2 shows the mix proportion of gypsum slag cement. The MSWI fly ash solidified body can provide Ettringite, anhydrous calcium sulfate, and alkalinity, which can stimulate the slag.

3. RESULTS AND DISCUSSION

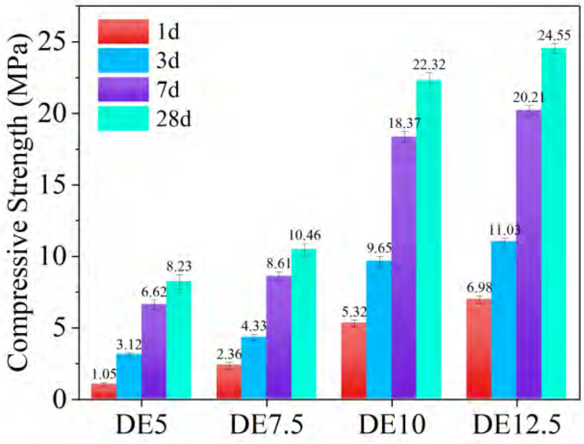

Figure 3 Compressive strength of gypsum slag cement paste

Figure 3 shows the compressive strength of the MSWI fly ash solidified body and slag cementitious system. It can be found that with the increase of the proportion of MSWI fly ash solidified body, the increase of the proportion of gypsum and alkalinity in the reaction system can promote the hydration process of slag. In addition, the increase in the proportion of Ettringite in the whole system will also lead to an increase in compressive strength. The entire hydration process has been basically completed in 7 days, and the increase in intensity at 28 days is not significant. Limited by the chloride ion content in the solidified MSWI fly ash. The maximum dosage of MSWI fly ash solidified form is about 10%.

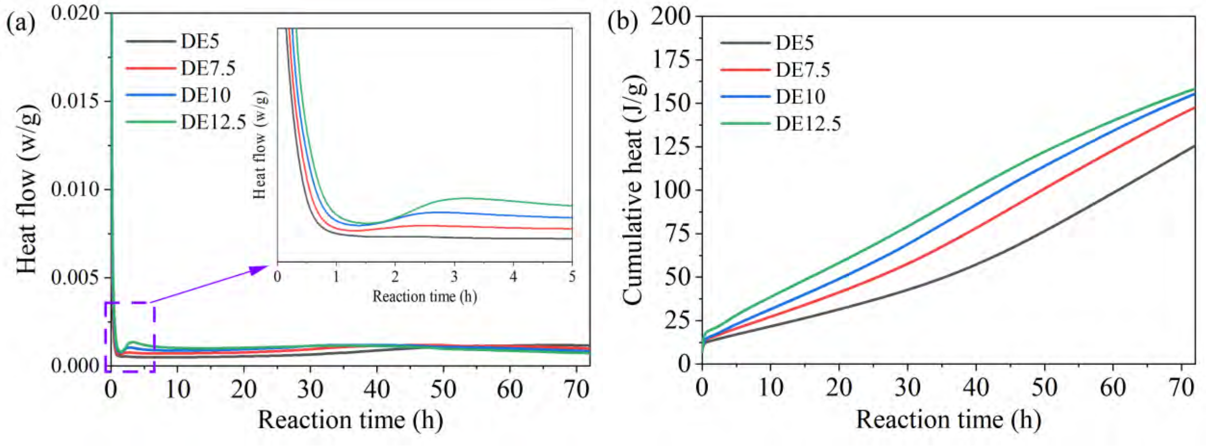

Figure 4 Heat of hydration of gypsum slag cement

Figure 4 shows the hydration heat curve of gypsum slag cement with different MSWI fly ash solidification content. From the figure, it can be observed that the increase in solidified MSWI fly ash indeed accelerates the hydration rate of slag. Accumulate more heat release.

4. CONCLUSION

The preparation of gypsum slag cement using MSWI fly ash solidified form combined with slag is a resource utilization approach for MSWI fly ash. The solidified MSWI fly ash provides alkalinity and gypsum, which together stimulate the slag. With the increase in the proportion of solidified MSWI fly ash, the hydration process of slag is accelerated. Ettringite is filled in the pores of the cementitious system to improve the overall strength.

5. ACKNOWLEDGMENT

The authors would like to express appreciation for the support of the sponsors [Joint Funds of the National Natural Science Foundation of China (U20A20324)].

6. REFERENCES

Diaz-Loya, E.I., Allouche, E.N., Eklund, S., Joshi, A.R., Kupwade-Patil, K., 2012. Toxicity mitigation and solidification of municipal solid waste incinerator fly ash using alkaline activated coal ash. Waste Manag. 32, 1521-1527.

Joseph, A.M., Van den Heede, P., Snellings, R., Van, A., 2017. Comparison of different beneficiation techniques to improve utilization potential of municipal solid waste incineration fly ash concrete. Constr. Mater. Syst. 49.

Müller, U., Rübner, K., 2006. The microstructure of concrete made with municipal waste incinerator bottom ash as an aggregate component. Cement Concr. Res.36, 1434-1443.

Chen, T.L., Chen, Y.H., Dai, M.Y., Chiang, P.C., 2021. Stabilization-solidificationutilization of MSWI fly ash coupling CO2 mineralization using a high-gravity rotating packed bed. Waste Manag. 121, 412–421.

Chen,Z.,Li,J.S., Zhan, B.J., Sharma, U., Poon, C.S., 2018. Compressive strength andmicrostructural properties of dry-mixed geopolymer pastes synthesized from GGBS and sewage sludge ash. Construct. Build. Mater. 182 (10), 597–607.

Chou, J.D., Wey, M.Y., Liang, H.H., Chang, S.H., 2009. Biotoxicity evaluation of fly ash
and bottom ash from different municipal solid waste incinerators. J. Hazard Mater.168 (1), 197–202.

Du, B., Li, J.T., Fang, W., Liu, Y.L., Yu, S.Y., Li, Y., Liu, J.G., 2018. Characterization of naturally aged cement-solidified MSWI fly ash. Waste Manag. 80, 101–111.

RECYCLING OF INCINERATED SEWAGE SLUDGE ASH AND WASTE GLASS POWDER IN CEMENTLESS BINDERS FOR SEWER REHABILITATION

Hafiz Asad Ali[1], Sun Keke[2], and Chi Sun Poon[3]

[1]Post-doctoral Fellow, Department of Civil and Environmental Engineering and Research Centre for Resources Engineering towards Carbon Neutrality, The Hong Kong Polytechnic University, Hong Kong.
[2]Post-doctoral Fellow, Department of Civil and Environmental Engineering and Research Centre for Resources Engineering towards Carbon Neutrality, The Hong Kong Polytechnic University, Hong Kong.
[3]Chair Professor, Department of Civil and Environmental Engineering and Research Centre for Resources Engineering towards Carbon Neutrality, The Hong Kong Polytechnic University, Hong Kong.
E-mail: cecspoon@polyu.edu.hk

Recent developments in alkali-activated materials (cementless binders) have been rapidly progressing. However, research on their behavior against the aggressive sewerage environment is still limited. This study investigates the performance of alkali-activated cement (AAC) mortars under an intensified artificial sewage environment. Incinerated sewage sludge ash (ISSA), a waste product generated from the incineration process of dewatered sewage sludge and containing a small amount of heavy metals, was used as a part of the precursors along with waste glass powder (GP) and ground granulated blast furnace slag (GGBS). The aim was to utilize the heavy metals in the ISSA as biocides to resist the biogenic acid attack on alkali-activated materials. The experimental results indicated the superior performance of the developed AAC mortar under the simulated biogenic acid environment. Such enhanced durability can be attributed to the presence of lower amounts of acid-soluble Ca-based reaction products in the resulting AAC gels. Furthermore, the slow release of heavy metals from the AAC gels, evidenced by leaching test results, might help inhibit microbial growth. The study results thus demonstrated that a ternary binder of ISSA, GP, and GGBS can be used to develop alkali-activated repairing mortars for sewer rehabilitation, and this provides a useful recycling route for the incinerated sewage sludge ash and waste glass.

Keywords: Alkali-activated repairing mortar; Waste glass; Incinerated sewage sludge ash; Leaching; Microbial-induced concrete corrosion

USE OF FLY ASH IN PROMOTING CARBONATION OF STEEL SLAG BLOCK

Jie Li[1], Qifeng Song[1], Tung-Chai Ling[1,]*

[1]College of Civil Engineering, Hunan University, Changsha 410082, China
E-mail (corresponding author): tcling@hnu.edu.cn; tcling611@yahoo.com

Adding fly ash to cement-based materials is found to change the pore structure, resulting in an increase in the carbonation reactivity within the cement matrix. This study aims to investigate the impact of fly ash on the carbonation reaction of steel slag compacted block and elucidate its underlying micro-mechanism. The addition of fly ash is mixed with steel slag and pressed into blocks at a water-solid ratio of 0.15 prior subjected to CO_2 curing (CO_2 concentration of 20%, pressure of 0.1 MPa) for 2 hours. As the dosage of fly ash (by weight of steel slag used) increase, the compressive strength of steel slag blocks increased and then decreased. Adding 4% fly ash attains a compressive strength of 27.8MPa, while adding 8% fly ash decrease the compressive strength to 22.1MPa. Although fly ash has a negative effect on the compressive strength of steel slag, TG results indicate that incorporating fly ash can improve the CO_2 uptake and Ca conversion of steel slag, thus compensating for the loss in overall mechanical strength of the fly ash-steel slag block. Through BSE image analysis, the addition of fly ash was found to disperse the distribution of steel slag particles in the composite structure, providing pathways for the diffusion of CO_2 during the carbonation process. Furthermore, it is observed that the Ca within steel slag particles migrate towards to the side close to the fly ash, thereby facilitates the adsorption of $CaCO_3$ by fly ash. This phenomenon inhibits the accumulation of $CaCO_3$ on the surface of steel slag particles and exposes a larger area available for carbonation.

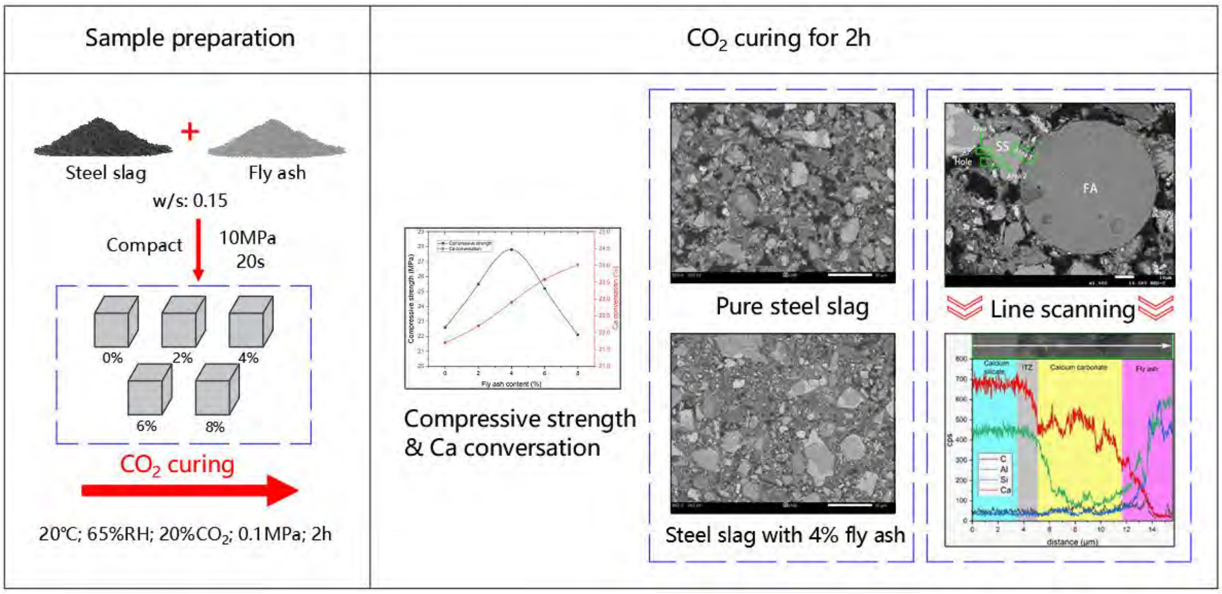

Keywords: Steel slag, Fly ash, Accelerated carbonation, Element analysis, Reaction mechanism

EMPLOYMENT OF SILICA FUME IN THE INTERFACIAL TRANSITION ZONE IN HIGH-VOLUME FLY ASH CONCRETE

Soufian EL Mghari[1], Sen Du[2]

[1]School of Civil Engineering and Mechanics, Yanshan University, Qinhuangdao 066004, China
[2]School of Civil Engineering and Mechanics, Yanshan University, Qinhuangdao 066004, China
Email: soufianmghari1998@gmaill.com,
sen.du@ysu.edu.cn

1. INTRODUCTION

As a commonly used supplementary cementitious materials (SCMs) with fine particle size and strong pozzolanic activity, silica fume (SF) can be used to strengthen the interfacial transition zone (ITZ), which is the weak region in concrete, especially in high-volume fly ash (HVFA) concrete where most of the fly ash particles remain unreacted. However, in the practice of producing HVFA concrete containing SF, SF is typically directly mixed with other ingredients, resulting in the dispersion of SF in the concrete matrix. In this case, a large amount of SF is required to improve the ITZ of concrete, which hinder its widespread use due to the high cost of SF.

The approach described in this study, which involves the preparation of SF-modified cement paste and coating the coarse aggregate with the prepared paste, allows for the construction of HVFA concrete with the improved ITZ while utilizing a tiny quantity of SF. The contributing variables and porosity of the ITZ in HVFA concrete will be modeled using the design of experiment (DoE). Furthermore, the factors analysis is carried out to find out the significant factors and the effects of these factors on the ITZ's properties.

2. MATERIALS AND METHODS

All materials used in the experiment were sourced from the local factory. Table 1 presents the chemical composition and physical properties of the cement, fly ash, and silica fume.

Table 1. Chemical composition and physical properties of cement, fly ash and silica fume

Chemical composition (wt.%)	Cement	Fly ash	Silica Fume
Al_2O_3	4.83	32.44	1.17
SiO_2	20.5	49.2	88.3
Fe_2O_3	3.24	4.76	4.76
CaO	63.2	7.47	0.48
MgO	3.22	0.81	214
Na_2O	0.15	0.51	-
K_2O	1.29	1.82	-
SO_3	2.66	0.55	1.05
			1
Physical properties			
Particle size	-	75%<40μm	0.1
Specific gravity	3.1	2.1	-
Loss on ignition(%)	0.91	2.44	2.1

In this study, the experimental design involved using Design-Expert 12 software with a central composite design (CCD) to create 26 experimental schemes. The investigation focused on five factors related to silica fume-modified cement paste: the mass ratio of water to cementitious materials (X_1: W/CM), content of slag in cementitious materials (X_2: S/CM), mass ratio of coarse aggregate to silica fume-modified cement paste (X_3: CA/CP), mixing time of silica fume-modified cement paste with coarse aggregate (X_4: T1), and drying time after coating coarse aggregate with the silica fume-modified cement paste (X_5: T2). Each factor was studied across defined ranges to understand its impact on the porosity of the ITZ: 0.3 to 0.4 for X_1, 0 to 10% for X_2, 1.5 to 4.5 for X_3, 2 to 10 minutes for X_4, and 0 to 8 hours for X_5. The specific combinations of factor settings for each experimental scheme are presented in Table 2.

Table 2. Variables and levels selected for the preparation of coated coarse aggregate

Mix	X_1, W/CM	X_2, S/CM (%)	X_3, CA/CP	X_4, T_1 (min)	X_5, T_2 (h)
1	0.38	7.8	2.2	8.2	1.8
2	0.35	5	3	10	4
3	0.35	5	3	6	4
4	0.35	5	3	6	4
5	0.35	5	4.5	6	4
6	0.35	5	3	6	4
7	0.38	7.8	2.2	3.8	6.2
8	0.35	5	3	6	8
9	0.3	5	3	6	4
10	0.38	7.8	3.8	3.8	1.8
11	0.35	5	3	6	4
12	0.32	2.2	3.8	8.2	6.2
13	0.38	2.2	3.8	3.8	6.2
14	0.32	7.8	3.8	3.8	6.2
15	0.32	7.8	3.8	8.2	1.8
16	0.35	5	3	2	4
17	0.38	2.2	2.2	8.2	6.2
18	0.35	5	3	6	0
19	0.32	2.2	2.2	3.8	1.8
20	0.35	5	3	6	4
21	0.38	2.2	3.8	8.2	1.8
22	0.35	5	1.5	6	4
23	0.35	0	3	6	4
24	0.4	5	3	6	4
25	0.32	7.8	2.2	8.2	6.2
26	0.35	10	3	6	4

In contrast to the traditional concrete production process, this experiment employs a novel approach by coating coarse aggregate with cement paste in advance. The coated aggregate was then placed in a well-ventilated and cool environment for a specified duration to allow for dryin[1]. Finally, the coated coarse aggregate was mixed with other ingredients to prepare HVFA concrete according to the mix design shown in Table 3.

Table 3. The mix proportion of HVFA concrete in this work

Cement (kg/m^3)	Fly ash (kg/m^3)	Water (kg/m^3)	Fine aggregate (kg/m^3)	Coated coarse aggregate (kg/m^3)
160	240	120	900	1000

In this experiment, scanning electron microscope (SEM) will utilize the back-scattered electron (BSE) imaging mode to capture the ITZ image of HVFA concrete. These images will be used to determine the porosity of various ITZ groups.

To process the BSE images (Figure 1), the image processing software ImageJ was employed. This software will analyze the captured images and identify the voids and cracks present in the ITZ of HVFA concrete. This identification process will be achieved by applying different gray threshold values to distinguish the pores from the matrix, as shown in Figure 2. To ensure accuracy and minimize experimental errors, a minimum of 20 BSE images from different regions will be captured for each group of HVFA concrete. These images will be used to calculate the porosity of the ITZ in a reliable and representative manner[2].

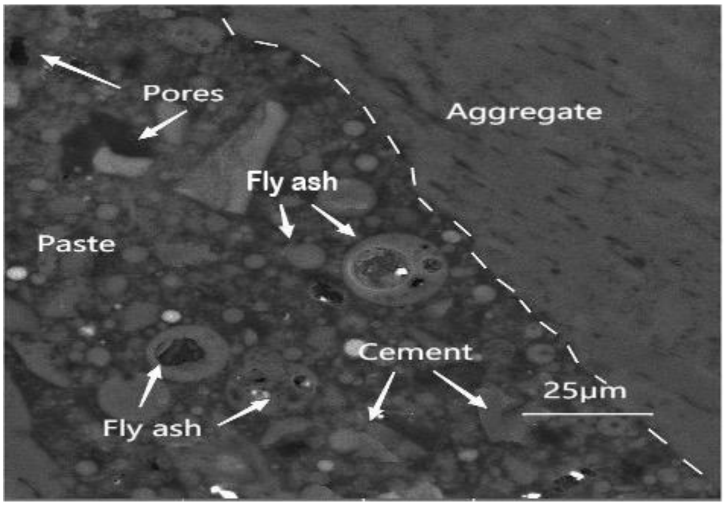

Figure 1. BSE images of the ITZ in HVFA concrete

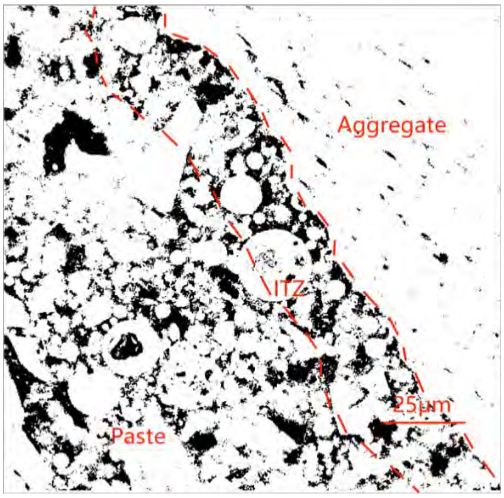

Figure 2. Pores segmented from ITZ

3. RESULTS AND DISCUSSION

The results of the porosity of the ITZ in HVFA concretes are detailed in Table 4. The numerical model analysis was conducted to reveal the relationship between the factors and the porosity of the ITZ in HVFA concrete, as shown in Equation 1. It can be seen that there existed an interaction between various factors. An increase in both silica fume content and W/CM led to an increase in the porosity of the ITZ. The porosity of the ITZ in HVFA concrete could be effectively reduced by appropriately decreasing the silica fume content and adjusting the W/CM within suitable limits.

$$Y = 401.69 - 2177.15X_1 - 6.61 + 3423.96{X_1}^2 + 0.33{X_2}^2 + 3.41{X_3}^2 \qquad (1)$$

Table 4. Porosity of the ITZ in HVFA concrete (%)

Mix	1	2	3	4	5	6	7	8	9	10
Porosity	35.6	32.4	38.3	30.9	30.5	21.7	32.9	37.0	30.9	34.6
Mix	11	12	13	14	15	16	17	18	19	20
Porosity	36.0	36.3	33.5	26.3	33.5	26.6	39.4	46.2	31.1	36.1
Mix	21	22	23	24	25	26				
Porosity	30.4	33.1	30.8	35.3	27.2	33.4				

4. CONCLUSION

In this research, a novel approach to enhance the ITZ of HVFA concrete was proposed by coating coarse aggregate with silica fume-modified cement paste. The parameters in preparing the silica fume-modified cement paste are serving as the variables, while the porosity of the ITZ in HVFA concrete served as the response. By optimizing the silica fume content and W/CM ratio of the silica fume-modified cement paste, the porosity of the ITZ in HVFA concrete can be effectively reduced.

5. ACKNOWLEDGMENT

The funding support was provided by the Natural Science Foundation of Hebei Province of China under Grant No. E2021203214.

6. REFERENCES

He Shan & Yang En Hua. (2021). Strategic strengthening of the interfacial transition zone (ITZ) between microfiber and cement paste matrix with carbon nanofibers (CNFs). *Cement and Concrete Composites*(prepublish). doi:10.1016/J.CEMCONCOMP.2021.104019.

Lin Jianjun, Chen Huisu, Zhao Qingxin & Li Mingqi. (2021). Statistical analysis of the critical percolation of ITZ around polygonal aggregates in three-phase concrete materials. *Physica A: Statistical Mechanics and its Applications*. doi:10.1016/J.PHYSA.2021.125878.

INFLUENCE OF FLY ASH ON THE EARLY-STAGE HYDRATION KINETICS OF PORTLAND CEMENT

Jiong-Huang HE[1, 2], Guang-Cheng LONG[2], Pei-Liang SHEN[1], and Chi-Sun POON[1]

[1]Department of Civil and Environmental Engineering,
The Hong Kong Polytechnic University
[2] School of Civil Engineering, Central South University
longguangcheng@csu.edu.cn

The utilization of fly ash in concrete is a crucial approach to resource conservation. To improve the efficiency, a deeper understanding of the early-stage hydration mechanism between fly ash and cement is imperative. In this study, the early hydration mechanism of fly ash was systematically investigated through the analyses of hydration exothermic behaviors, hydration kinetics model, and apparent activation energy. The results indicated that the impact of fly ash on cement hydration can be categorized into three stages: inhibition, promotion, and no significant effect. Fly ash exhibited an inhibitory effect on cement hydration within the first 10 hours, followed by a significant promotion effect between 10 and 48 hours, after which its impact gradually attenuated. The influence of fly ash unit mass with different dosages remained almost constant. Moreover, the incorporation of fly ash resulted in a significant reduction in the nucleation rate of hydration products, with a decrease of 31.37% as the fly ash content increased from 0 to 40%, which account for its inhibitory effect. Finally, the further mechanism was discussed in terms of apparent activation energy and microtopography observation. These findings provide new insights into comprehending the early hydration mechanism of fly ash-cement and the activation of fly ash.

Keywords: early-stage hydration; hydration kinetics; hydration mechanisms; apparent activation energy; fly ash

Session C3

CO_2 Sequestration and Sustainability

UTILIZATION OF RECYCLED MATERIALS IN CONCRETE TO PROMOTE SUSTAINABILITY

Xijun Shi[1]

[1]Texas State University, San Marcos, TX 78666, USA
xijun.shi@txstate.edu

Concrete is one of the most widely used construction materials. Production of portland cement, however, is carbon intensive, and the cement industry accounts for nearly 8% of global carbon dioxide (CO_2) emissions. The concrete industry also consumes significant amounts of natural aggregate. Currently, global annual production of concrete is 4.4 billion tons. Typically, 70% of concrete is aggregate, translating to 3.1 billion tons of stone and sand being harvested every year. Excessive extraction of rock and sand depletes natural resources and causes environmentally detrimental secondary effects (e.g., erosion, deforestation, and damage to river ecosystems). Steel is another important element in concrete construction. The production of steel rebar is widely considered the largest single source of greenhouse gases produced in concrete construction. For example, steel production accounts for about 51% of the total energy consumption and about 49% of the total CO_2 emission for residential buildings.

In this talk, the speaker will present three recently completed projects on using different recycled materials to replace virgin counterparts in concrete. The first study is a TxDOT research project on the use of reclaimed asphalt pavement as an aggregate replacement in concrete for pavement applications. The second study, funded by ODOT, involved a comprehensive evaluation of two existing recycled concrete aggregate based concrete pavements in Oklahoma on I-35 and I-40, highlighted by a field evaluation using a falling weight deflectometer test and distress surveys to assess pavement behavior. The third study provided a detailed experimental program on cement mortar reinforced by up to 2 vol. % recycled steel fiber from scrap tire. The team's recent effort on testing full-scale concrete pipe specimens containing the recycled steel fiber will also be presented. All three studies suggested that recycled materials are a viable option to promote sustainability and achieve cost benefits for the concrete industry.

Keywords: Concrete, sustainability, recycled aggregate, recycled steel fiber, pavement

PREPARATION OF REACTIVE CARBONATED RECYCLED CONCRETE FINE AND ITS UTILIZATION IN ORDINARY PORTLAND CEMENT

Peiliang SHEN, Ligang Peng, Yi Jiang

Department of Civil and Environmental Engineering & Research Centre for Resources Engineering towards Carbon Neutrality, The Hong Kong Polytechnic University, Hong Kong 999077, China
E-mail: peiliang.shen@polyu.edu.hk

A new wet carbonation method was developed to prepare reactive carbonated recycled concrete fine (CRCF), aiming to promote its potential applications as a low-carbon alternative to ordinary Portland cement (OPC). The phase assemblance evolution and carbonation mechanism of RCF is investigated, aiming to bring forward the basic understanding of carbonation mechanism and develop value-added products. Also, the effects of CRCF on the fresh properties, early hydration kinetics and microstructure of OPC paste. The results showed that the main carbonation products were calcite, amorphous calcium carbonate (CC), alumina-silica gel, silica gel and alumina gel. The formed CC was turned from a poorly-crystalline layer into aggregated calcite grains. In addition, CRCF not only was a highly active pozzolanic material but also an effective accelerator affecting the early hydration kinetics of OPC paste, thereby leading to an increased early compressive strength and a comparable 28-d compressive strength, even when 20% OPC was replaced by the CRCF replacement ratio. The incorporation of 20% CRCF to replace OPC could achieve a CO_2 emissions reduction of up to 25%. These indicate that the CRCF has a promising application scenario in transforming wasted concrete fines into high-value industrial products by CO_2 activation.

Keywords: Carbonation; Recycled concrete fine; Fresh properties; Hydration kinetics; Microstructure evolution

INSIGHTS ON MAGNESIUM SLAG SUPERFINE-GRINDING: THE ROLES OF MG EXPOSURE AND UNEXPECTED CARBONIZATION DURING GRINDING ON CEMENT HYDRATION

Rui Sun[1,2], and Dongmin Wang[2]*

[1] The Hong Kong Polytechnic University, Hong Kong
[2] China University of Mining and Technology-Beijing, Beijing
E-mail: wangdongmin@cumtb.edu.cn

1. INTRODUCTION

Due to its low density, excellent mechanical properties, good electrical and thermal conductivity, and machinability, magnesium alloys have gradually become important lightweight structural materials since their introduction in the field of auto parts manufacturing in the early 20th century. They have also gained favour in the aerospace industry. Magnesium alloys are widely used in various industries, including electronics, medical, and construction, earning them the title of "the green engineering metal structure material in the 21st century." Notably, China is the world's largest supplier of magnesium, with proven reserves of magnesium-containing minerals (magnesite, dolomite, etc.) reaching as high as 8.142 billion tons. In 2021, the cumulative export volume of various magnesium products reached 477,200 tons. The primary process for producing magnesium in China is the Pidgeon Process. This involves using calcined dolomite as the raw material, ferrosilicon as the reducing agent, and fluorite as the catalyst. The magnesium vapor obtained through vacuum thermal reduction is then condensed to produce metallic magnesium. However, approximately 10 tons of dolomite is consumed for every 1 ton of magnesium produced, resulting in the emission of 26-42 tons of CO_2 and 6-7 tons of Pidgeon process magnesium reduction slag (hereinafter referred to as magnesium slag). Magnesium slag is a gray-white highly alkaline slag primarily composed of dicalcium silicate (C_2S) and containing unreacted magnesium oxide (MgO), calcium oxide (CaO), and a small amount of ferrosilicon alloy from the magnesium smelting process. Unfortunately, this slag poses a serious pollution threat to soil, air, and water.

Given the large scale of the building materials industry, it has become an important channel for the consumption of industrial solid waste. As a result, the utilization of magnesium slag in the preparation of building materials has become a critical research direction. The first step in utilizing magnesium slag is the superfine-grinding treatment. However, existing research on magnesium slag grinding treatment has only focused on its effect on particle size, neglecting other physical and chemical properties. This study aimed to analyse the impact of grinding time on particle size, hydrophilicity, composition, and microstructure evolution of magnesium slag. It identified the exposure and carbonization of magnesium during the grinding process and reported on the impact of these changes on Portland cement mixed with magnesium slag. Finally, the study explained the mechanism of how the grinding treatment of magnesium slag influences the hydration process of magnesium slag-cement composite cementitious materials.

2. MATERIALS AND METHODS

2.1 Materials

The magnesium slag (MS) used in this study was initially ground into a powder with a D50 particle size of 16.55 μm by a magnesium producer in Yuling, Shaanxi province, China. A 42.5 ordinary Portland cement manufactured by China Building Materials Academy Co., Ltd. was selected to prepare the cement-magnesium slag (CMS) composite cementitious material by mixing it with MS of different particle sizes. Local tap water from Beijing was used as the mixing water, and isopropyl alcohol was used as the hydration stopping agent.

2.2 Methods

2.2.1 Grinding scheme and property measurements of MS

The grinding process was carried out using a ball mill, with grinding times set at 5 minutes, 10 minutes, 15 minutes, 20 minutes, 25 minutes, and 30 minutes, respectively. The resulting magnesium slag powder obtained from each grinding time was labelled as MSα (where α represents the specific grinding time). Various properties of MSα, including particle size distribution, hydrophilicity, chemical and mineral composition, and microstructure, were measured and analysed.

2.2.2 Mix proportion of CMS composite cementitious material

The pastes were prepared based on the mix proportions specified in Table 1, comprising two control groups (OPC and MS paste) and four CMS pastes consisting of MS with different particle sizes and OPC. The fresh pastes were poured into a steel mold to obtain equilateral cube-shaped hardened specimens with edges measuring 30 mm.

Table 1 Mix proportion of pastes

Sample ID	C	MS-16.55	MS-9.25	MS-6.68	MS-5.21	W/B
OPC	100%	0%	/	/	/	0.40
MS	/	100%	/	/	/	0.40
CMS-16.55	70%	30%	/	/	/	0.40
CMS-9.25	70%	/	30%	/	/	0.40
CMS-6.68	70%	/	/	30%	/	0.40
CMS-5.21	70%	/	/	/	30%	0.40

2.2.3 Measurements of CMS pastes

The compressive strength of CMS was tested at 3 days, 7 days, 28 days, 60 days, 90 days, and 180 days to evaluate its mechanical properties. For the analysis of the structure and composition, specimens were used at various hydration stages. The microtopography and pore structure were investigated using SEM-EDS and MIP. A detailed study on the hydrate composition of CMS was conducted using XRD, TG-DSC, FT-IR, and BSE-EDS. The hydration heat over 168 hours was measured with the ambient temperature maintained at 25 °C.

3. RESULTS AND DISCUSSION

3.1 Properties of MS after ultrafine grinding

3.1.1 Particle properties

As depicted in Fig.1, the commercially available magnesium slag powder has a median particle size of 16.55 μm. However, through the process of ultrafine grinding, the particle size of the magnesium slag powder is significantly reduced, and there is a noticeable increase in the content of particles in the 0-3 μm range. The relationship between the grinding time and the median particle size of ultrafine magnesium slag powder follows an exponential function. XRF analysis revealed that the commercially available magnesium slag powder contains only 0.81% magnesium element. However, after the grinding process, the magnesium content increases to approximately 4%. This observation leads to the speculation that grinding induces magnesium exposure within the slag particles.

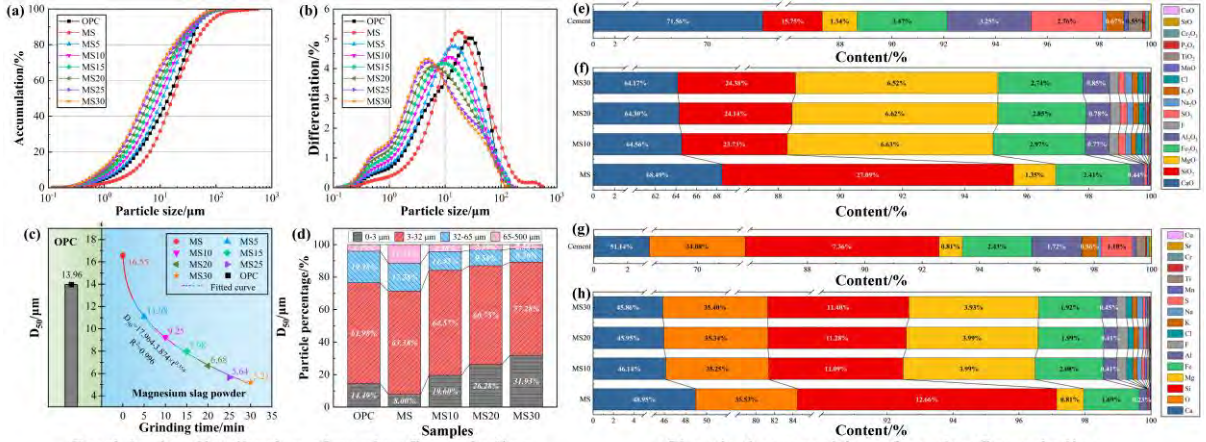

Particle size distribution after ultrafine grinding

Chemical composition after ultrafine grinding

Fig. 1 The particle size and chemical composition of ultrafine MS

3.1.2 Hydrophilicity, mineral composition, and microtopography

As illustrated in Fig. 2, the reduction in the particle size of magnesium slag contributes to improved hydrophilicity. FT-IR and TG-DTG tests clearly show the characteristic peak of carbonate, indicating that the magnesium slag has undergone a carbonization reaction after grinding, leading to the formation of magnesium carbonate. This speculation is further supported by the appearance of a magnesium carbonate diffraction peak in the XRD spectrogram. Additionally, SEM analysis reveals the presence of partial magnesium-rich particles on the surface of the magnesium slag. These particles exhibit an amorphous structure and hexagonal plates, with a particle size of less than 5 μm.

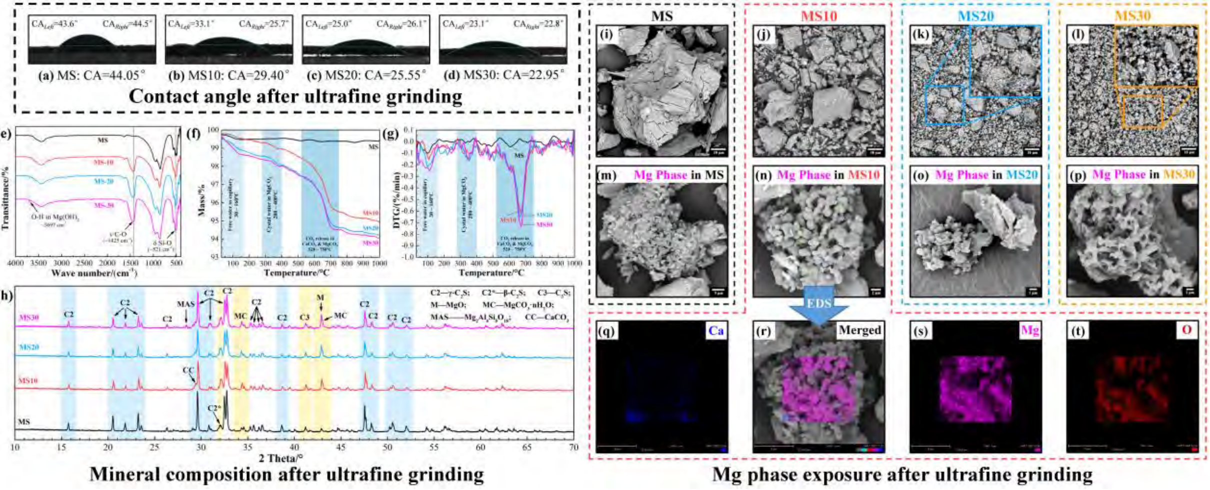

Fig. 2 The hydrophilicity, mineral composition, and microtopography of ultrafine MS

3.2 Hydration of CMS

3.2.1 Mechanical property, structure, and microtopography of CMS

As depicted in Fig. 3, the use of magnesium slag with a median particle size of 6.68 μm resulted in CMS obtaining superior mechanical properties compared to pure cement at 28 days. Notably, as the particle size of the magnesium slag decreases, the optimization of the pore structure becomes more pronounced, and there is a notable change in the Ca/Si ratio of the C-S-H gel. Furthermore, it was observed that Mg and Al tend to be enriched in the outer layer of the hydration products.

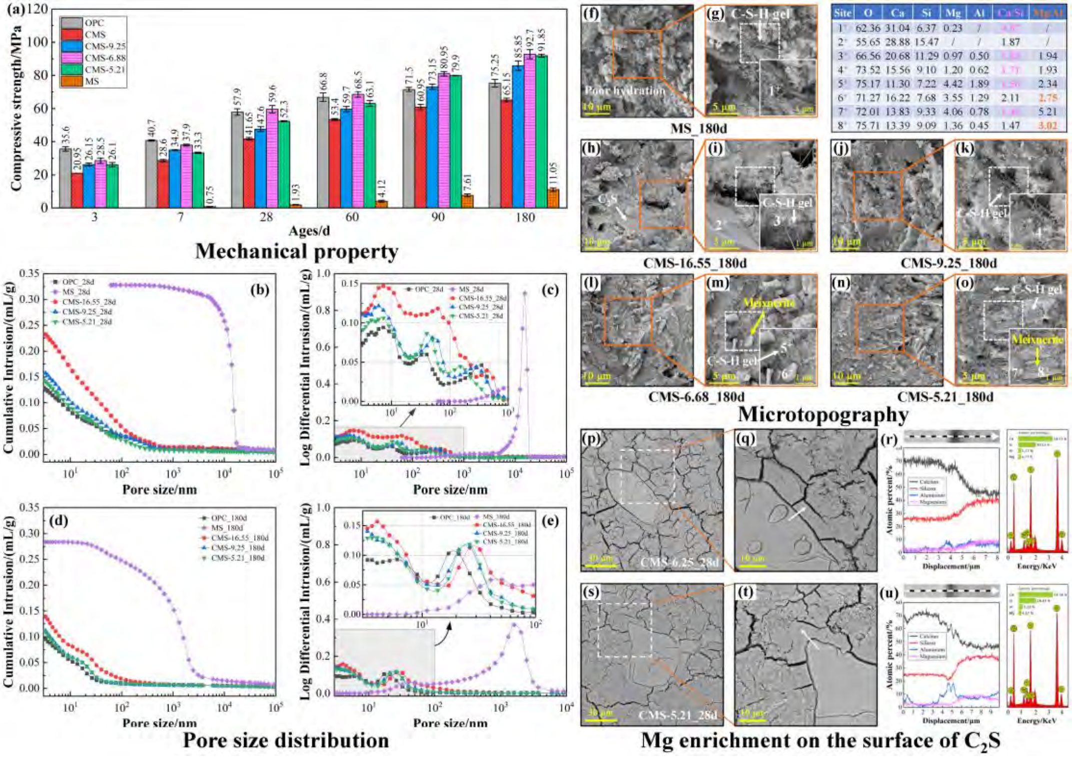

Site	O	Ca	Si	Mg	Al	Ca/Si	Mg/Al
1	62.36	31.04	6.37	0.23	/	[illegible]	/
2	55.65	28.88	15.47	/	/	1.87	/
3	66.56	20.68	11.29	0.97	0.50	[illegible]	1.94
4	73.52	15.56	9.10	1.20	0.62	[illegible]	1.93
5	75.17	11.30	7.22	4.42	1.89	[illegible]	2.34
6	71.27	16.22	7.68	3.55	1.29	2.11	2.75
7	72.01	13.83	9.33	4.06	0.78	[illegible]	5.21
8	75.71	13.39	9.09	1.36	0.45	1.47	3.02

Fig. 3 The property, pore size, microtopography and Mg enrichment of CMS pastes

3.2.2 Hydrates evaluation of CMS

The superfine magnesium slag powder enhances the hydration of C_2S and results in the formation of Meixnerite ($Mg_6Al_2(OH)_{18}\cdot 4H_2O$) in the system, which is a hexagonal sheet-like hydration product. The pozzolanic activity of ultra-fine magnesium slag powder leads to the consumption of calcium hydroxide produced during cement hydration. This, in turn, increases the content of C-S-H gel and causes the peak position of Si-O vibration bond in the infrared spectrum to shift towards higher wave numbers.

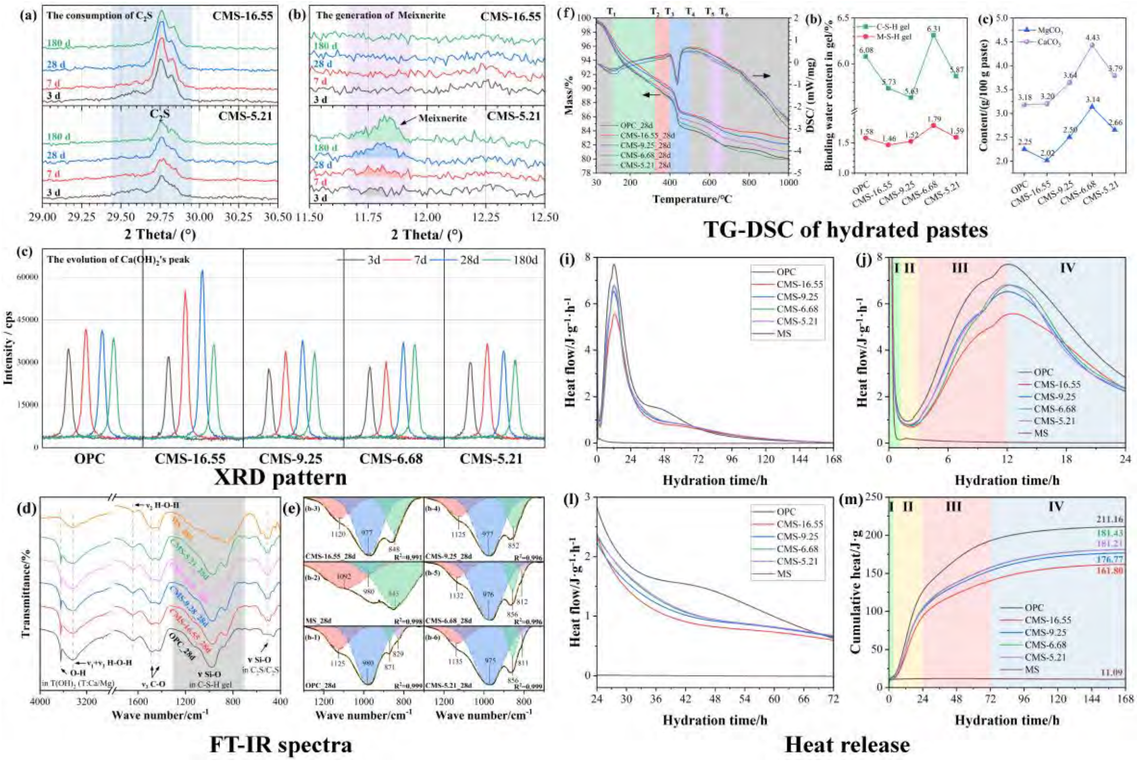

Fig. 4 The composition, chemical bonds, and heat evaluation of CMS hydration

4. CONCLUSION

(1) Ultrafine-grinding not only changes the particle size of MS but also leads to new transformations in composition distribution. Minerals containing Mg, Al, and K that were previously encapsulated in C_2S particles are exposed after ultrafine-grinding.

(2) The exposure of Mg phases during grinding presents two potential reactivities. Firstly, most of the exposed Mg is susceptible to carbonation in the air, significantly reducing the harmful effect of f-MgO in the original MS on volume stability. Secondly, the uncarbonized exposed Mg participates in the hydration of the alumina phase of OPC.

(3) The mechanical properties of CMS increase with the particle size of MS in two ways. Firstly, the pozzolanic reaction of finer MS promotes the formation of C-S-H gel and facilitates the Si in a highly polymeric state. Secondly, the filling effect of ultrafine MS contributes to a decrease in porosity.

5. ACKNOWLEDGMENT

This work was supported by the National Key Research and Development Program of China (2019YFC1907202).

6. REFERENCES

[1] Mo, L., Hao, Y., Liu, Y., Wang, F., & Deng, M. (2019). Preparation of calcium carbonate binders via CO_2 activation of magnesium slag. *Cement and Concrete Research*, *121*, 81-90.

[2] Ji, G., Peng, X., Wang, S., Hu, C., Ran, P., Sun, K., & Zeng, L. (2021). Influence of magnesium slag as a mineral admixture on the performance of concrete. *Construction and Building Materials*, *295*, 123619.

NOVEL SYNTHETIC SOL-GEL GLASSES AS SUSTAINABLE SUPPLEMENTARY CEMENTITIOUS BINDERS

Chuqing Jiang[1], D.D. Ramteke[1], Christopher Cheeseman[2], Mirja Illikainen[1] and Paivo Kinnunen[1]

[1] Fibre and Particle Engineering Research Unit, University of Oulu, P.O. Box 4300, FI-90014, Finland
[2] UKRIC Advanced Infrastructure Materials Laboratory, Imperial College London, SW7 2BU, UK
paivo.kinnunen@oulu.fi

1. INTRODUCTION

The Portland cement industry contributes to 6-8% of the annual anthropogenic CO_2 emissions (Scrivener et al., 2018). Approximately half of the CO_2 emissions stem from energy consumption and the remaining from the starting material $CaCO_3$. The investigation of supplementary cementitious materials (SCM) can offer solutions to the current CO_2 problems in the cement industry. In recent years, by-products such as fly ash, ground granulated blast furnace slag, and silica fume, have been dominantly used as SCMs (Juenger & Siddique, 2015). However, on a global scale, the quantities of these materials are declining (Serdar et al., 2019).

Novel materials with comparable cementitious properties (e.g., chemical composition, solubility/stability in water, etc.) (Fu et al., 2017) need to be explored as alternative SCMs. The possibility of synthetic glasses as an alternative cement additive is evident due to their controllable chemical and physical properties (Mascaraque et al., 2017). Chemically reactive glasses are desired products for their utilization in concrete, and the reactivity of glasses depends highly on their chemical composition. Calcium is a widely used doping element because the oxide of calcium can disturb the silicon network and depolymerize the structure, increasing the reactivity of glass (or slag). However, CaO is mainly derived from the de-carbonization reaction of $CaCO_3$. While effective, this increase in reactivity by CaO addition comes with increased raw material-related CO_2 emissions (Oey et al., 2017; Schöler et al., 2017). In our previous studies, we have proved that the addition of MgO in synthetic glasses via a sol-gel route significantly increased the reactivity of the binary MgO-SiO_2 glasses (Jiang et al., 2023). Works from (Chen et al., 2016; Sreenivasan et al., 2020) also indicate that MgO as a near-zero-carbon oxide, has great potential to improve the reactivity when added to glasses with further reduction of raw material-related CO_2 emissions.

The melt-quenching technique is widely used to synthesize glasses, which involves melting the precursors at temperatures above 1400°C and sometimes in excess of 2000°C (Fiume et al., 2020), resulting in unavoidable fuel-related CO_2 emissions. Glasses can also be prepared by the sol-gel technique, an eco-friendly route that requires much lower heat treatment temperatures at 500-800°C (Baccile et al., 2009; Dislich, 1986).

In this work, iron-bearing magnesium silicate glasses with a variable (from 0 to 55 molar ratio of Fe/(Fe+Mg)) content of iron oxide were synthesized via a modified sol-gel route, and their reactivity was evaluated by solubility experiments in water. The solubility results are used to preliminarily evaluate the practicability of the sol-gel technique for the large-scale synthesis of novel SCM associated with low CO_2 emissions in the Portland cement industry.

2. MATERIALS AND METHODS

2.1 Glass preparation

Iron-bearing magnesium silicate glasses with variable iron contents [$(Mg_{1-X}Fe_X)SiO_3$ with X_{Fe} = Fe/(Mg + Fe) from 0 to 55 mol%] and constant Mg/Si ratio [Mg/(Mg + Si) = 25 mol%] were synthesized using a modified rapid sol-gel route. Tetraethyl orthosilicate (TEOS, Fisher Scientific, 98%) was used as the alkoxy-silane monomer, and nitric acid (HNO_3, VWR J.T Baker, 65%) was used as the catalyst. Magnesium nitrate hexahydrate [$Mg(NO_3)_2{\cdot}6H_2O$, VMR BDH, 98.0-102.0%] and iron (III) nitrate nonahydrate [$Fe(NO_3)_3{\cdot}9H_2O$, VWR Alfa Aesar, ⩾98%] were used as the precursor for MgO and Fe_2O_3, respectively in the sol-gel derived glasses.

TEOS was dissolved in a solution containing deionized water and ethanol absolute (VWR BDH, ≥ 99.8%) with a molar ratio TEOS: H_2O: EtOH = 1:4:4 under continuous stirring at a temperature of ~22°C. Then HNO_3 acid was added to the mixture, and the starting pH of the solution was adjusted to 1. After one hour, $Mg(NO_3)_2{\cdot}6H_2O$ was added and the solution was stirred vigorously for an additional 1 hour. After a transparent sol was obtained, $Fe(NO_3)_3{\cdot}9H_2O$ was added to the system with continuous stirring for another 1 hour. The sol gradually turned orange to brown depending on the iron contents. Thus, the sol was maintained at room temperature for ageing until a homogeneous wet gel formed. This ageing process always took 2 to 5 days. The wet gels were dried in an oven at 60°C for 4 days and the obtained fluffy dried gels were then crushed and ground into powders. Finally, the dried gels were heat treated at 500°C for 3 hours in a high-temperature oven at a heating rate of 5°C/min.

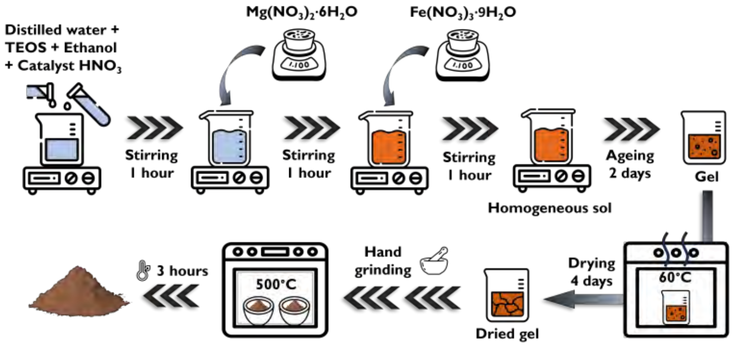

Figure 1. Procedure flow chart for the sol-gel route.

2.2 Solubility test

In this study, the reactivity of glasses was assessed by the total elemental leaching rate in water. Water dissolution experiments were performed under a fume hood where a constant level of CO_2 and water was promoted, and the room temperature was controlled at 22 ± 1°C. Milli-Q water (18 MΩcm) was bubbled with N_2 (99.997%) to ensure the absence of dissolved CO_2 before its use as the solution. The experimental setup consisted of 300 mL polypropylene vessels with 0.01 g of glass powders dissolved in 100 g of solution (L/S = 10000). Solutions were kept on a horizontal shaking table (IKA KS 260 orbital shaker) with continuous shaking at a speed of 250 rpm for 2 days. Finally, solutions were filtered through a 2 μm filter paper and acidified to pH~2 with 2% HNO_3, then stored at 4ºC. Aqueous concentrations of Fe, Mg and Si in filtered solutions were detected by inductively coupled plasma optical emission spectrometry (ICP-OES, Thermo Scientific, Model iCAP 6500 Duo).

3. RESULTS AND DISCUSSION

3.1 X-ray diffraction analysis

Powder X-ray diffraction patterns for glasses with variable iron contents are presented in Fig. 2. According to Fig. 2 (a), Glasses with X_{Fe} of 0 to 50% are confirmed to be amorphous since only a broad band between 20° and 40° (2θ) is observed. When X_{Fe} reaches 55%, some sharp peaks appear, which can be indexed to the diffraction of crystalline hematite (PDF#04-006-8177, Fe_2O_3). Based on the XRD patterns, it can be concluded that Fe-Mg-Si glasses with X_{Fe} below 50% are amorphous, while X_{Fe} reaches 55%, crystalline phases emergy within the samples.

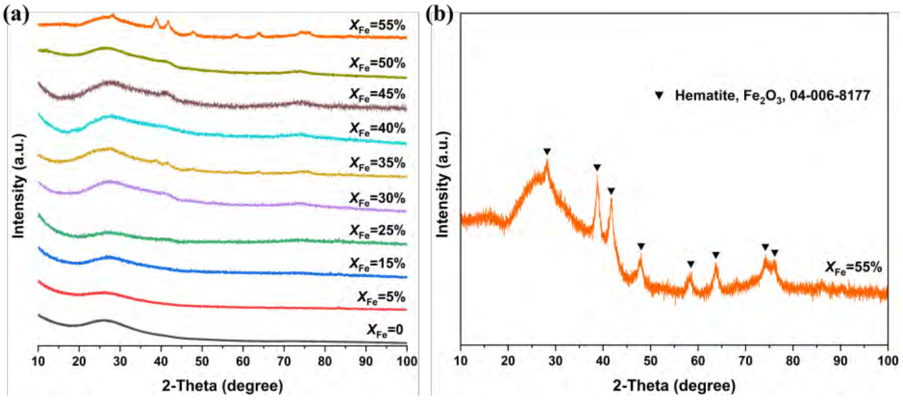

Figure 2. XRD patterns of (a) glasses with variable X_{Fe} heat-treated at 500°C for 3 hours, (b) crystalline phase identification of glasses with X_{Fe} of 55%.

3.2 Reactivity of glasses

When studying cementitious applications, the reactivity of the precursors is a major concern. In this work, the reactivity of glasses is evaluated by the leaching rate of each element (i.e., the percentage of the elements dissolved) of samples after 2 days in contact with water.

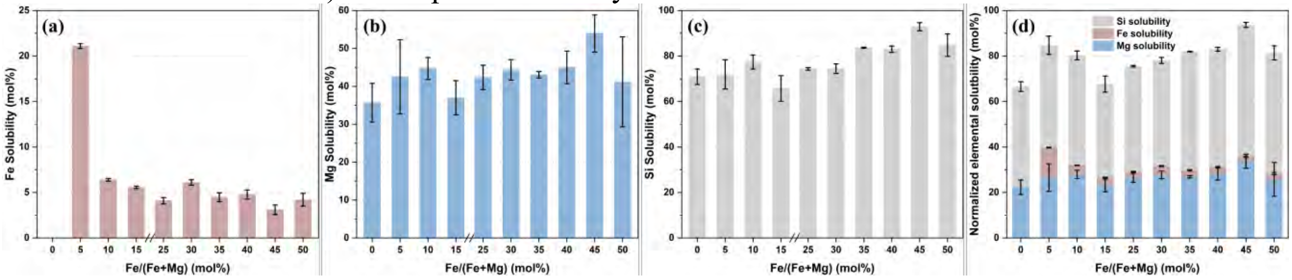

Figure 3. Leaching rate (mol%) of (a) Fe, (b) Mg, (c) Si and the sum of elemental solubility.

Based on our previous studies (Jiang et al., 2023), Mg-Si glasses with a Mg/(Mg + Si) ratio of 25 mol% showed the highest reactivity, which is taken as a reference here ($X_{Fe} = 0$). Fig. 3 indicates that all glasses doped with iron have a higher elemental leaching rate than binary Mg-Si glasses ($X_{Fe} = 0$). According to Fig .3 (d), the total leaching rate of Fe-Mg-Si glasses with X_{Fe} of 45 mol% is nearly 30% higher than that of glasses without iron. The results suggest that iron doping is beneficial to the reactivity of magnesium-based glasses. Glasses with X_{Fe} of 5% show a much higher leaching rate of iron than other samples [Fig. 3 (a)], which can be explained by the lower stability of the glass structure. The thermal stability of glasses can be demonstrated by the glass transition temperature (T_g) according to the equation $T_g = h_g/(\Sigma\Delta S_{tr,m}/N)$, where h_g is a material family constant corresponding to the activation energy for heavy atom rearrangement (Naito, 1994). A higher T_g is required for thermally stable glasses. DSC curves are present in Fig. 4. Fig. 4 (a) indicates all Fe-bearing Mg-Si glasses have lower T_g than binary Mg-Si glasses. When X_{Fe} increases from 0 to 5%, there is a significant decline in T_g, which means that glass with X_{Fe} of 5% has a much more unstable structure than glass without iron, resulting in a high leaching rate of iron.

When iron is first introduced to the glass network, part of the ions substitute Si^{4+} as the network former, while other ions occupy the voids in networks because the radius of Fe^{3+} is much lower than that of Mg^{2+} (Shannon, 1976). This causes a slight expansion of the network, and destabilizes the structure. When iron content increases, most of the voids are occupied and the networks become more compact and dense, resulting in the enhanced stability of glass structure. Thus, the reactivity of glasses slightly decreases with the increase of X_{Fe} from 5% to 25% as shown in Fig. 3.

Fe^{3+} plays a similar role to Al^{3+} in networks as an intermediate cation, meaning it can both act as a network former and modifier depending on the ion content (Kelsey et al., 2009). Because Fe^{3+}-O bonds are less stable than Si-O bonds, the amount of Fe^{3+} as the network former is limited by the Si to Fe ratio (Arslan et al., 2009). In Fe-rich glasses, network modifying Fe^{3+} is also expected. In addition, note that the substitution of Fe^{3+} for Si^{4+} produces a negative charge, which should be balanced by a cation (charge compensator). Fe^{3+} can also act as the network compensator in glasses with high iron content. When considered as the network modifier or compensator, the addition of Fe^{3+} will depolymerize networks, leading to the enhancement in reactivity. Therefore, the leaching rate increases when iron contents keep increasing until X_{Fe} reaches the maximum of 50 mol%, and the stability of glasses is also evaluated and confirmed by T_g in Fig. 4 (a).

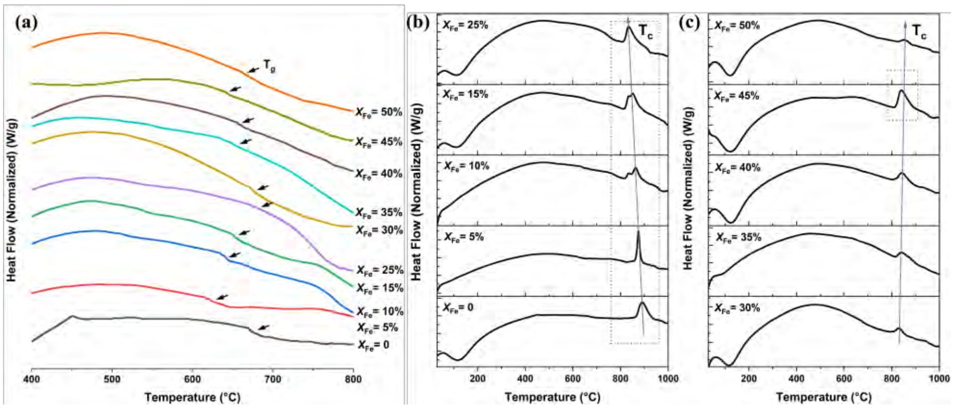

Figure 4. DSC patterns for glasses with variable iron contents including the information of (a) glass transition temperature (T_g) and (b) glass crystallization temperature (T_c).

4. CONCLUSION

Quantities of traditional SCMs such as fly ash, blast furnace slag, and silica fume are declining, which means they are insufficient to support the maximal substitution of total Portland cement consumption with SCMs in the future. In order to solve the CO_2 problem in the cement industry, novel SCMs need to be explored as alternatives. In this work, iron-bearing magnesium silicate glasses with variable iron contents were synthesized using a modified sol-gel route, with much lower raw material-related and fuel-related CO_2 emissions compared to conventional Ca-containing glasses and melt-quenching technique. Samples with X_{Fe} [Fe/(Fe + Mg)] up to 50 mol% showed an amorphous structure. The reactivity of glasses was evaluated by the elemental leaching rate via solubility tests in water. Fe-Mg-Si glasses showed an even higher reactivity compared to the highly reactive Mg-Si glasses studied in our previous work (Jiang et al., 2023) due to the complicated role of Fe^{3+} as an intermediate cation in glass networks. The high leaching rate of Si in water (nearly 90%) indicated the feasibility of the synthetic sol-gel Fe-Mg-Si glasses as a low-CO_2 sustainable concrete supplement.

5. ACKNOWLEDGMENT

The authors would like to express appreciation for the support of Academy of Finland (grant 322085) and The University of Oulu & The Academy of Finland Profi 5 (326291).

6. REFERENCES

Arslan, G., Dölekçekiç, E., & Karasu, B. (2009). Effect of transition metal oxide additions on the chemical durability of SrOMgOZrO2SiO2 glasses. European Journal of Glass Science and Technology https://www.academia.edu/32370386/Effect_of_transition_metal_oxide_additions_on_the_chemical_durability_of_SrOMgOZrO2SiO2_glasses

Baccile, N., Babonneau, F., Thomas, B., & Coradin, T. (2009). Introducing ecodesign in silica sol–gel materials. Journal of Materials Chemistry, 19(45), 8537–8559. https://doi.org/10.1039/B911123A

Chen, Y., Shui, Z., Chen, W., Li, Q., & Chen, G. (2016). Effect of MgO content of synthetic slag on the formation of Mg-Al LDHs and sulfate resistance of slag-fly ash-clinker binder. Construction and Building Materials, 125, 766–774. https://doi.org/10.1016/j.conbuildmat.2016.08.086

Dislich, H. (1986). Sol-gel: Science, processes and products. Journal of Non-Crystalline Solids, 80(1), 115–121. https://doi.org/10.1016/0022-3093(86)90384-4

Fiume, E., Migneco, C., Verne, E., & Baino, F. (2020). Comparison between Bioactive Sol-Gel and Melt-Derived Glasses/Glass-Ceramics Based on the Multicomponent SiO2-P2O5-CaO-MgO-Na2O-K2O System. Materials, 13(3), 540. https://doi.org/10.3390/ma13030540

Fu, T., Moon, R. J., Zavattieri, P., Youngblood, J., & Weiss, W. J. (2017). 20—Cellulose nanomaterials as additives for cementitious materials. In M. Jawaid, S. Boufi, & A. K. H.p.s. (Eds.), *Cellulose-Reinforced Nanofibre Composites* (pp. 455–482). Woodhead Publishing. https://doi.org/10.1016/B978-0-08-100957-4.00020-6

Jiang, C., Ramteke, D. D., Li, J., Sliz, R., Sreenivasan, H., Cheeseman, C., & Kinnunen, P. (2023). Preparation and characterization of binary Mg-silicate glasses via Sol-Gel route. Journal of Non-Crystalline Solids, 606, 122204. https://doi.org/10.1016/j.jnoncrysol.2023.122204

Juenger, M. C. G., & Siddique, R. (2015). Recent advances in understanding the role of supplementary cementitious materials in concrete. *Cement and Concrete Research*, *78*, 71–80. https://doi.org/10.1016/j.cemconres.2015.03.018

Kelsey, K. E., Stebbins, J. F., Singer, D. M., Brown, G. E., Mosenfelder, J. L., & Asimow, P. D. (2009). Cation field strength effects on high pressure aluminosilicate glass structure: Multinuclear NMR and La XAFS results. Geochimica et Cosmochimica Acta, 73(13), 3914–3933. https://doi.org/10.1016/j.gca.2009.03.040

Mascaraque, N., Bauchy, M., & Smedskjaer, M. M. (2017). Correlating the Network Topology of Oxide Glasses with their Chemical Durability. The Journal of Ph*ysical Chemistry B*, *121*(5), 1139–1147. https://doi.org/10.1021/acs.jpcb.6b11371

Naito, K. (1994). Quantitative Relations between Glass Transition Temperatures and Thermodynamic Parameters for Various Materials: Molecular Design for Nonpolymeric Organic Dye Glasses with Thermal Stability. Chemistry of Materials, 6(12), 2343–2350. https://doi.org/10.1021/cm00048a021

Oey, T., Kumar, A., Pignatelli, I., Yu, Y., Neithalath, N., Bullard, J. W., Bauchy, M., & Sant, G. (2017). Topological controls on the dissolution kinetics of glassy aluminosilicates. Journal of the American Ceramic Society, 100(12), 5521–5527. https://doi.org/10.1111/jace.15122

Schöler, A., Winnefeld, F., Haha, M. B., & Lothenbach, B. (2017). The effect of glass composition on the reactivity of synthetic glasses. Journal of the American Ceramic Society, 100(6), 2553–2567. https://doi.org/10.1111/jace.14759

Scrivener, K. L., John, V. M., & Gartner, E. M. (2018). Eco-efficient cements: Potential economically viable solutions for a low-CO2 cement-based materials industry. Cement and Concrete Research, 114, 2–26. https://doi.org/10.1016/j.cemconres.2018.03.015

Serdar, M., Bjegovic, D., Stirmer, N., & Banjad Pecur, I. (2019). Alternative binders for concrete: Opportunities and challenges. Future Trends in Civil Engineering, 199–218. https://doi.org/10.5592/CO/FTCE.2019.09

Shannon, R. D. (1976). Revised effective ionic radii and systematic studies of interatomic distances in halides and chalcogenides. *Acta Crystallographica Section A: Crystal Physics,* Diffraction, Theoretical and General Crystallography, 32(5), Article 5. https://doi.org/10.1107/S0567739476001551

Sreenivasan, H., Cao, W., Hu, Y., Xiao, Q., Shakouri, M., Huttula, M., Provis, J. L., Illikainen, M., & Kinnunen, P. (2020). Towards designing reactive glasses for alkali activation: Understanding the origins of alkaline reactivity of Na-Mg aluminosilicate glasses. PLOS ONE, 15(12), e0244621. https://doi.org/10.1371/journal.pone.0244621

LIGHTWEIGHT, PERMEABLE, AND CO_2-SEQUSTRATING CONCRETE BLOCKS ENABLED BY THE COMBINATION OF REACTIVE MAGNESIUM CEMENT AND RECYCLED BIO-MASS

Y. Tang[1], J. Qiu[1]

[1] Department of Civil and Environmental Engineering, The Hong Kong University of Science and Technology, Clear Water Bay, Hong Kong, China
E-mail: ytangck@connect.ust.hk

1. INTRODUCTION

Cement production sector accounts for 7-8% of CO_2 emission annually in the world [1]. One practical method to reduce carbon emissions in cement production stage is to replace cement partially/wholly by industrial by-products, such as coal fly ash, steel slag, silica fume etc. However, the practice of generate electricity by coal is prohibited by more and more countries, resulting the shortage of industrial by-products in the future to make greener binder. In Hong Kong, paper waste accounts for 24.5% of municipal solid waste (MSW) sent to landfills, and 2,643 tons are dumped daily with only 450 being recycled. Bio-waste represents 32.1% (3,477 tons/day) of deposited MSW and can be converted into biochar after pyrolysis, which weighs 10-20% of the original weight (348-695 tons/day) [2]. Sustainable concrete with limited carbon footprint can be made by utilizing these wastes rather than disposing of them.

Compared with Portland cement (PC), RMC has lower calcination temperature (700-900 vs. 1450°C), around 73% net CO_2 emission lower than PC during its service life [3-5]. However, the CO_2 sequestration ability is still limited due to insufficient CO_2 penetrate through dense structure. The addition of chemical admixtures [6] and porous ingredients (hollow natural fiber [7], biochar [8] etc.) can further increase their CO_2 sequestration ability and strength.

In this study, RMC concrete was developed using a high volume of biomass, including 0-24 vol.% biochar and 0-4 vol.% shredded paper pulp. The study investigates the effect of biomass dosage on mechanical properties, CO_2 permeability, and CO_2-sequestration capacity, as well as characterizing the porosity to identify microstructural changes.

2. MATERIALS AND METHODS

2.1 Raw materials, mix design, and specimen preparation

To make concrete, a mixture of RMC, silica sands (80-120 mesh), and biochar particles (less than 1mm) were used as binder, fine aggregates, and lightweight aggregates respectively. In addition, a dispersion agent, sodium hexametaphosphate ($Na(PO_3)_6$), was added. Hollow natural fibers (HNF) made from shredded paper pulp with irregular cellulose lumen structures were also incorporated.

Table 1 summarizes the mix proportions of this work. The biochar and shredded paper pulp to concrete volume ratio increases from 0 to 24 vol.% and 0 to 4 vol.% of concrete. The free water-to-cement ratio maintain 0.79.

To obtain shredded paper pulp, wastepaper was soaked in water for 24 hours then blended until a smooth pulp was formed. The lightweight composites mentioned above were mixed and cast according to Wu and Qiu [9]. The fresh mixture was cast into $40\times40\times40$ mm^3 cubes to measure dry density and compressive strength, R50×H100 mm^3 cylinders to measure carbonation degree and porosity, and $10\times45\times100$ mm^3 thin plates for CO_2 permeability testing. After curing in ambient air for 48 hours, the specimens were demolished, and the side and bottom of cylindrical specimens were sealed with paraffin. The upper face was left open to allow one-way CO_2 diffusion. All cube, cylinder, and plate specimens were then cured in an environmental chamber with a temperature of 30°C, relative humidity of 85%, and CO_2 concentration of 10 vol.% for RMC carbonation.

Table 1 Mix proportions in this work

Groups	MgO	Biochar		Silica sand	Absorbed water-biochar	Paper pulp		Absorbed water-pulp	Free Water	$Na(PO_3)_6$	Total	f_c	Dry density
	kg/m^3	Vol.%	kg/m^3	kg/m^3	kg/m^3	Vol.%	kg/m^3	kg/m^3	kg/m^3	kg/m^3	kg/m^3	MPa	kg/m^3
B0-P0	815	0	0	326	0	0	0	0	644	32	1817	55.9±2.6	1591.9±9.3
B0-P1	807	0	0	323	0	1	9	29	638	36	1841	-	-
B0-P2	799	0	0	320	0	2	18	57	631	42	1867	-	-
B0-P4	783	0	0	313	0	4	36	115	618	48	1913	-	-
B15-P0	514	15	309	216	225	0	0	0	405	20	1677	11.9±0.6	1263.5±8.1
B19-P0	412	19	412	165	301	0	0	0	325	25	1639	8.8±0.3	1140.1±6.3
B24-P0	318	24	508	127	371	0	0	0	251	45	1619	5.5±0.1	1046.6±8.4
B19-P1	408	19	408	163	298	1	9	29	322	26	1662	7.4±0.2	1075.6±9.3
B19-P2	404	19	404	161	295	2	18	57	319	31	1689	6.8±0.1	1051.4±3.7
B19-P4	395	19	395	158	289	4	36	115	312	39	1740	4.6±0.1	977.2±8.5

2.2 Test procedures

Unconfined uniaxial compressive tests were conducted to the 28-day CO_2 cured cubes with the loading rate of 0.05 mm/s; The oven-dry density was calculated by oven-dried mass of specimen divided by the sample volume obtained by water replacement method following the specification of EN 12390-7.

Mercury Intrusion Porosimetry (MIP) tests were conducted using a Micromeritics MicroActive Autopore V 9600 version 2.03. with the ability of testing pores ranging from 0.003 µm to 300 µm.

The acid digestion method was employed to measure CO_2 sequestration ability of 28-d cured samples. Slices from the same depth (0-10; 40-50 and 80-90 mm) were collected and crushed into powder respectively. A 5 vol.% sulfuric acid solution (600 ml) was prepared with excess H_2SO_4 (30 ml, 95-97%) for testing. Weight loss (ΔW) of samples and CO_2 digestion ratio (α) can be calculated by the following equations:

$$\Delta w = w_0 + w_1 - w_2 - \Delta w_c \tag{1}$$

$$\alpha = \frac{\Delta W}{W_1} \times 100\% \tag{2}$$

Here, w_0 is weight of beaker with mixture before acid digestion reaction, w_1 is sample weight, w_2 is the resulting mixture with beaker, and Δw_c is weight loss due to water evaporation.

The CO_2 sequestration ratio (β) could be approximately calculated by amount of sequestrated carbon dioxide (mol) divided by amount of magnesium (mol) in the samples. If the biochar to RMC mass ratio is x, then the derived carbonation degree can be expressed as follow:

$$\beta = \frac{\alpha \times 40 \times (1.4 + x)}{44} \tag{3}$$

The CO_2 sequestration ratio of all tested groups had subtracted the carbonates amount of pristine biochar and pulp.

Fig. 1 shows the self-designed acrylic box used for CO_2 permeability testing. The box contains a CO_2 sensor with datalogger to monitor CO_2 levels over time. The plate sample is placed on top of the box, surrounded by paraffin seal. The sealed box is then placed in an environmental chamber with 10 vol.% CO_2 level, 30°C and 85% R.H. CO_2 levels inside the box are recorded by the datalogger every two minutes till 10000 ppm.

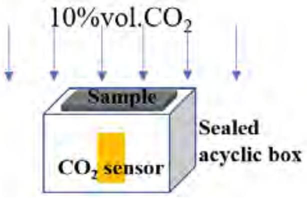

Fig.1 CO_2 permeability test schematic diagram

3. RESULTS AND DISCUSSION

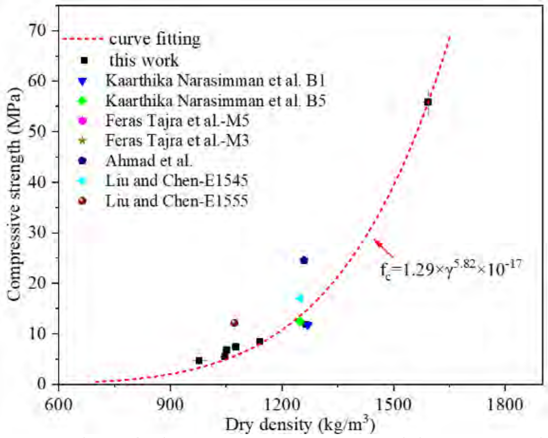

Fig.2 Comparison of f_c and dry density of biomass-based cementitious materials with other lightweight aggregate-based PC composites

28-d compressive strength is shown in the table 1. The relationship between oven-dried densities and compressive strength as well as comparison with other lightweight concretes in PC-system were also presented in Fig.2. Like other lightweight aggregate concretes in PC system [10-15], the compressive strength is depended on dry density rather than w/c ratio, the higher dry density will leads to an increased compressive strength. An empirical formula based on this work with oven-dry densities ranged from 977.2 to 1591.9 kg/m3 (for strength between 4.6 MPa to 55.6 MPa) can be given as:

$$f_c = 1.29 \times \gamma^{5.82} \times 10^{-17}$$

Herein, f_c is 28-d compressive strength (MPa), γ is 28-doven-dry density (kg/m3). And it can not only conclude the relationship between compressive strength and dry density in this work, but also well fit other researchers' work.

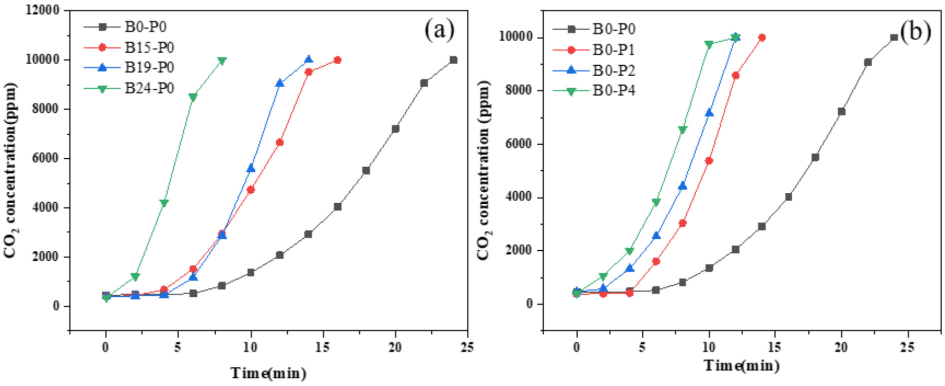

Fig.3 CO_2 permeability curves of a. biochar-RMC, b. pulp-RMC composites

Fig. 3 compares CO_2 permeability curves for biochar-RMC and pulp-RMC composites. Biochar-RMC groups' duration time decreases significantly with increasing biochar dosage, from 0 to 15 vol.% leads to a 33.3% decrease, increasing to 24 vol.% results in a 66.7% decrease. In pulp-RMC composites, increasing pulp content decreases CO_2 permeability time. CO_2 permeability time decreases from 24 minutes to 12 minutes, reflecting a significant 50% reduction with 1 vol.% pulp addition. Beyond 1 vol.%, CO_2 permeability time reduction is not significant, indicating that 1 vol.% of pulp addition is sufficient to decrease CO_2 permeability while maintaining compressive strength.

Fig.4 presents the pore size distribution curves of groups with different biochar and pulp addition. In Fig.4a, with biochar incorporated, pores size ranged from 0.003-300 μm except for 100-200 nm increased, and this trend is obvious with biochar dosage increases from 15 to 24 vol.%. In Fig.4b, the incorporation of pulp in biomass-based cementitious materials increases larger pores (1 μm to 300 nm) and smaller pores (less than 100 nm) while reducing medium size pores (0.1 μm to 1 μm) compared with groups without pulp.

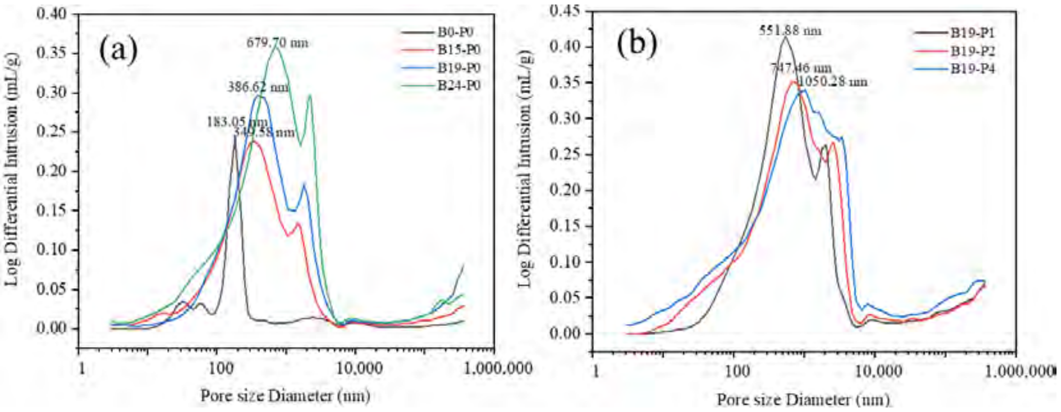

Fig.4 Pore size distribution curves of a. biochar-RMC, b. biochar-pulp-RMC composites

Fig. 5 displays the CO_2 sequestration ratio of biomass-based composites at different depths after 28-d CO_2 curing. Increasing biochar volume ratio improves the CO_2 sequestration ratio. The highest average CO_2 sequestration ratio (22.39%) is for group B24-P0, which is 2.62 times higher than group B0-P0 (8.54%). For groups with 19 vol.% biochar added, the CO_2 sequestration ratio increases then decreases with pulp volume ratio (0 to 4 vol.%). The maximum average CO_2 sequestration ratio is 35.61%, which is 1.77 times of group B19-P0 and 4.17 times of group B0-P0. The maximum CO_2 sequestration ratio always appears at the middle depth for all groups with biochar, likely due to incorporated biochar providing extra CO_2 source that alters the internal CO_2 diffusion for middle RMC carbonation.

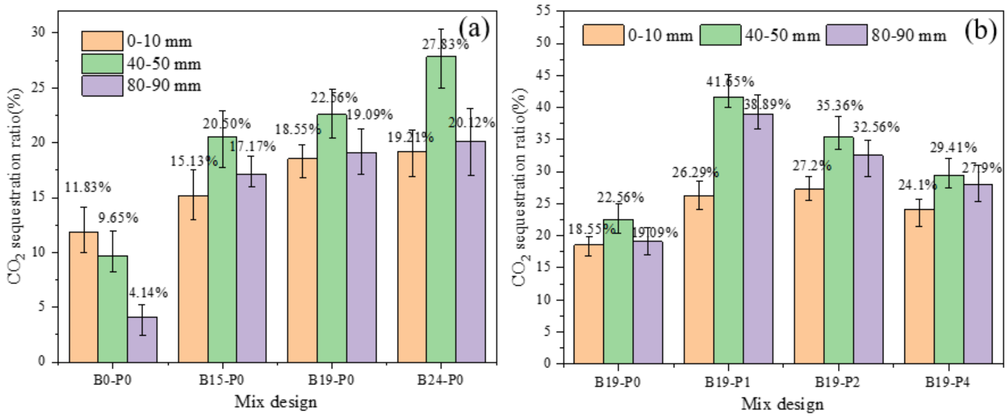

Fig.5 CO_2 sequestration ratio of a. biochar-RMC and b. biochar-pulp-RMC composites at different depth after 28-d CO_2 curing

4. CONCLUSION

This work presents the effects of high dosage of biomass on properties of RMC-based concrete, the main conclusion can be drawn as follows:

1) Lightweight-ness and 4.6-11.9 MPa 28-d CO_2 cured compressive strength can be achieved by different dosage of recycled porous biomass;
2) Compared with group without biomass, CO_2 permeability time can be significantly shortened by 50% with 1 vol.% of shredded paper pulp incorporated;
3) CO_2 sequestration ability of biomass-RMC matrix can be maximumly improved by 4.17 times compared with its counterparts without porous biomass incorporated;
4) The nano-pores (1-100 nm) and micro-pores (1 μm to 300 nm) of RMC-concrete both increased with biochar and shredded paper pulp incorporated.

5. REFERENCES

[1] Benhelal, E., Zahedi, G., Shamsaei, E., & Bahadori, A. (2013). Global strategies and potentials to curb CO2 emissions in cement industry. Journal of cleaner production, 51, 142-161.

[2] Monitoring of Solid Waste in Hong Kong Waste Statistics for 2020. 2021; Available from: https://www.wastereduction.gov.hk/sites/default/files/resources_centre/waste_statistics/msw2020_eng.pdf
[3] Unluer, C. (2018). Carbon dioxide sequestration in magnesium-based binders. In Carbon dioxide sequestration in cementitious construction materials (pp. 129-173). Woodhead Publishing.
[4] Walling, S. A., & Provis, J. L. (2016). Magnesia-based cements: a journey of 150 years, and cements for the future?. Chemical reviews, 116(7), 4170-4204.
[5] Champlin IV, J., & Heller, I. (2006). Concrete microstructure properties and materials.
[6] Dung, N. T., & Unluer, C. (2018). Improving the carbonation of reactive MgO cement concrete via the use of NaHCO 3 and NaCl. Journal of Materials in Civil Engineering, 30(12), 04018320.
[7] Wu, B., & Qiu, J. (2022). Incorporating hollow natural fiber (HNF) to enhance CO2 sequestration and mechanical properties of reactive magnesia cement (RMC)-based composites: Feasibility study. Journal of CO2 Utilization, 57, 101874.
[8] Wang, L., Chen, L., Poon, C. S., Wang, C. H., Ok, Y. S., Mechtcherine, V., & Tsang, D. C. (2021). Roles of biochar and CO2 curing in sustainable magnesia cement-based composites. ACS Sustainable Chemistry & Engineering, 9(25), 8603-8610.
[9] Wu, B., & Qiu, J. (2022). High-performance Reactive Magnesium Cement Incorporating Hollow Natural Fiber and Silica Sand. In MATEC Web of Conferences (Vol. 364). EDP Sciences.
[10] Shannag, M. J. (2011). Characteristics of lightweight concrete containing mineral admixtures. Construction and Building Materials, 25(2), 658-662.
[11] Narasimman, K., Jassam, T. M., Velayutham, T. S., Yaseer, M. M. M., & Ruzaimah, R. (2020). The synergic influence of carbon nanotube and nanosilica on the compressive strength of lightweight concrete. Journal of Building Engineering, 32, 101719.
[12] Nahhab, A. H., & Ketab, A. K. (2020). Influence of content and maximum size of light expanded clay aggregate on the fresh, strength, and durability properties of self-compacting lightweight concrete reinforced with micro steel fibers. Construction and Building Materials, 233, 117922.
[13] Islam, M. M. U., Li, J., Wu, Y. F., Roychand, R., & Saberian, M. (2022). Design and strength optimization method for the production of structural lightweight concrete: An experimental investigation for the complete replacement of conventional coarse aggregates by waste rubber particles. Resources, Conservation and Recycling, 184, 106390.
[14] Ahmad, M. R., & Chen, B. (2019). Experimental research on the performance of lightweight concrete containing foam and expanded clay aggregate. Composites Part B: Engineering, 171, 46-60.
[15] Liu, N., & Chen, B. (2014). Experimental study of the influence of EPS particle size on the mechanical properties of EPS lightweight concrete. Construction and Building Materials, 68, 227-232.

TURNING STEEL SLAG INTO A VALUE-ADDED CEMENT MATERIAL VIA EARLY-AGE AMBIENT PRESSURE CARBONATION CURING

Xiangping Xian[*]

Assistant Professor, Department of Architecture and Civil Engineering,
City University of Hong Kong (*Corresponding author)
Email: xiangping.xian@cityu.edu.hk

Steel slag (SS), an industrial waste by-product from the steel-making process. This study proves that early-age ambient-pressure (AP) carbonation can convert steel slag into a cement material with reduced energy consumption as compared to high pressure (HP), which allows production to be feasible on an industrial scale. AP carbonation-activated SS compacts have comparable CO_2 uptake and compressive strength as those subjected to HP carbonation. Through multiple microstructural characterization techniques including X-ray diffractometer (XRD), thermogravimetric analysis (TGA), Fourier transform infrared spectroscopy (FTIR), and scanning electron microscopy (SEM), AP carbonation generates significant calcium carbonates which densify SS compacts contributing to the improved performance. Additionally, the life cycle assessment (LCA) demonstrates that AP presents a smaller global warming potential (GWP) value than HP. The application of AP carbonation for concrete production exclusively using steel slag reduces carbon emissions, energy usage, and natural resource consumption.

PRODUCTION OF PURE VATERITE VIA LEACHING-CARBONATION OF BOFS

Qifeng Song[1], Tung-Chai Ling[1,*]

[1]College of Civil Engineering, Hunan University, Changsha 410082, China
*Corresponding author email: tcling@hnu.edu.cn; tcling611@yahoo.com

Carbonation of basic oxygen furnace slag (BOFS) is considered one of the most attractive options for CO_2 sequestration. Leaching of Ca^{2+} ions into the leachate followed by indirect wet carbonation, offers a promising approach to produce high-purity precipitated calcium carbonate (PCC) for various industrial applications. However, the synthesis of PCC predominantly favors the formation of the more thermodynamically stable calcite phase, posing challenges in obtaining pure metastable crystal structures. This research proposes to produce high-purity vaterite through the extraction of Ca^{2+} from BOFS using NH_4Cl and followed by aqueous carbonation. The effect of different experimental parameters on the leaching and carbonation in maximizing Ca^{2+} and CO_2 sequestration is investigated. Under the optimized condition, a Ca^{2+} leaching rate of 60.3% can be attained within 10 minutes. Aqua-ammonia addition achieved a 99.5% carbonation ratio, producing vaterite with purity over 98%. High ammonia concentration and alkaline pH conditions induce CO_3^{2-} aggregation, resulting in supersaturation and a higher CO_3^{2-}/Ca^{2+} ratio, which promotes vaterite formation. Then, adsorption of NH_4^+ and metal cations on vaterite's surface reduces its surface free energy, inhibiting its transformation to calcite. Thus, the prepared vaterite structure remains stable under various carbonation conditions and post-treatment methods. Furthermore, from an environmental perspective, the carbonation filtrate can be recycled for at least five cycles with a sustained extraction-carbonation efficiency of over 60%. The solid residue forms an amorphous gel, which may exhibit pozzolanic activity. Further research is needed to explore its potential reuse in the construction materials field.

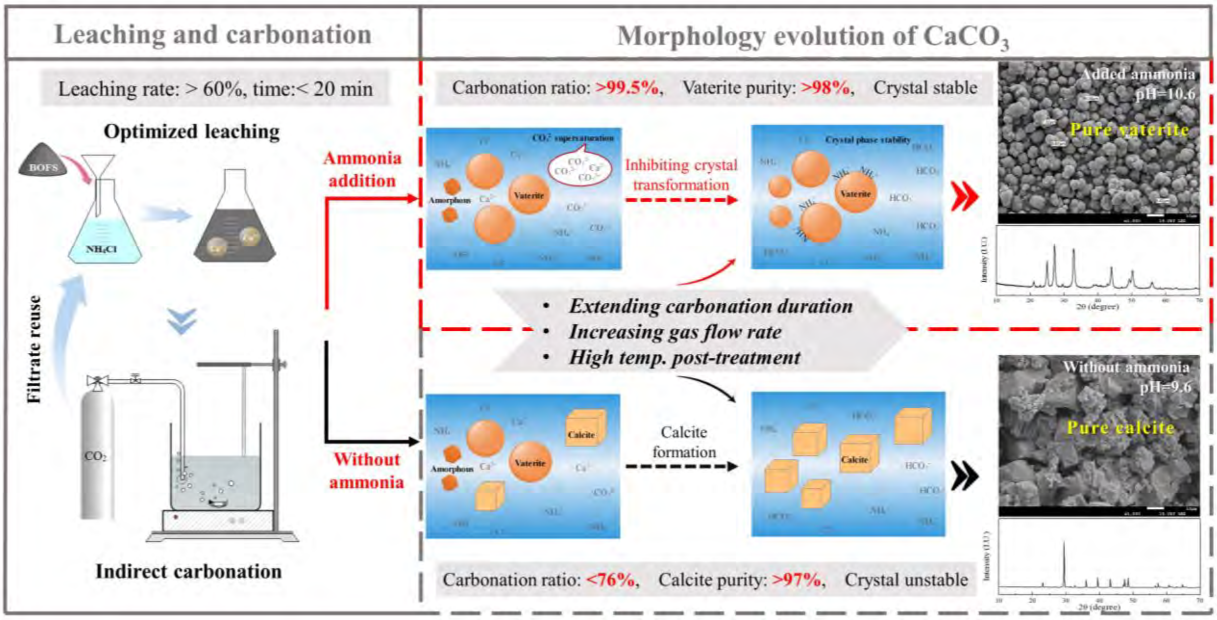

Keywords: Indirect carbonation, basic oxygen furnace slag, vaterite, aqua-ammonia

MECHANOCHEMICAL CARBONATION OF RECYCLED CONCRETE FINES: TOWARDS A HIGH-EFFICIENCY RECYCLING AND CO_2 SEQUESTRATION

Yingliang ZHAO [1], Yong ZHENG [1, 2], Zihan MA [1], Peiliang SHEN [1 *], Chi Sun POON [1 *],
Guangmin PENG [3], Ruilai GUO [3], Daohui XIA [3]

[1] Department of Civil and Environmental Engineering, The Hong Kong Polytechnic University,
Kowloon, Hong Kong
[2] Research Center of Space Structures, Guizhou University, Guiyang, China
[3] China Resources Power Holdings (Hezhou) Co., Ltd., Guangxi, China

Email: peiliang.shen@polyu.edu.hk (P.L. Shen)
Email: cecspoon@polyu.edu.hk (C.S. Poon)

The relative slow carbonation efficiency for conventional wet and dry carbonation of recycled concrete fines (RCF) limits its resource industrial utilization. In this study, an innovative mechanochemical carbonation (MC) method was developed. The carbonation kinetics, phase assemblage and microstructure evolution of RCF during the MC process were extensively examined. The results exhibited a substantial enhancement in the carbonation efficiency and CO_2 utilization rate, as evidenced by the achievement of a notable carbonation degree within 10 min. This accomplishment surpassed what could be achieved even after a prolonged 2 h period of wet carbonation, and the CO_2 uptake capacity and utilization rate achieved via MC reached more than 0.3 g-CO_2/g-RCF and 80%, respectively. The superior performance of MC were ascribed to the influence of mechanochemical effects. These effects contributed to refinement in geometrical characteristics of RCF, exfoliation of passivating layers and facilitating CO_2 dissolution, which favored the structure disintegration of RCF and carbonation progress. Another distinctive aspect of MC treatment was the production of a greater proportion of metastable CC characterized by reduced crystalline size, which was attributed to modifications on the carbonation environment and the structural alterations induced by mechanochemical effects. Moreover, the precipitation of silica gels commenced at approximately 4 min in the MC process, a notably earlier onset when compared with wet carbonation; additionally, a greater abundance of silica gels was observed in the current MC procedure, resulting from the higher carbonation degree caused by mechanochemical effects. The encouraging conclusions in the present work validated the feasibility of producing carbonated RCF more efficiently and paved the way for future industrial practice.

Keywords: Recycled concrete fines; mechanochemical; carbonation; passivation layer; crystalline structure

UTILIZING WASTE CEMENT FOR CARBON DIOXIDE SEQUESTRATION AND CAPTURE: THE ROLE OF WATER CONTENT ON THE GROWTH OF CALCIUM CARBONATE DURING THE CARBONATION PROCESS OF HYDRATED CEMENT

Zihan Ma[1], Long Jiang[1], Yi Jiang[1], Peiliang Shen[1, *] Yong Tao[1],
Jiangshan Li[2, 3], Chi-sun Poon[1, *]

[1] Department of Civil and Environmental Engineering & Research Centre for Resources Engineering towards Carbon Neutrality, The Hong Kong Polytechnic University, Hong Kong 999077, China

[2] State Key Laboratory of Geomechanics and Geotechnical Engineering, Institute of Rock and Soil Mechanics, Chinese Academy of Sciences, Wuhan 430071, China

[3] IRSM-CAS/HK PolyU Joint Laboratory on Solid Waste Science, Wuhan 430071, China

High-alkaline waste cement possesses significant potential for effectively capturing and sequestering carbon dioxide, transforming it into calcium-rich, highly reactive supplementary cementitious materials. Water plays a pivotal role in facilitating this reaction, yet there is a conspicuous absence of extensive research in this domain. This study elucidates the mechanisms by which water affects the growth behavior (precipitation and crystallization) of calcium carbonate (Cc) in hydrated cement paste during carbonation. The findings indicated that the presence of water dramatically affected Cc's polymorphs, morphology, and crystal properties. With an increase in water content from RH=55% to a liquid-solid ratio of 40, the calcite grain size underwent significant enlargement from less than 200nm to over 400nm. Moreover, as the water content increased, the different Cc polymorphs evolved into mainly calcite, and the polycrystalline Cc was transformed into monocrystalline calcite. Insufficient water elevated the local pH and ion concentration, resulting in prolonged supersaturation duration. Meanwhile, nano-sized water film restricted the Cc growth and hindered Ostwald ripening, leading to the preservation of amorphous calcium carbonate (ACC) and poor crystallization of Cc.

Keywords: Recycled cement powder; Carbonation; polymorphs; Calcium carbonate; Crystallization

Session C4

Waste Utilizing in Concrete

EVALUATION OF DURABILITY AND ENVIRONMENTAL SAFETY OF COAL ASH-STEELMAKING SLAG MIXED MATERIAL APPLIED TO BASE COURESE MATERIAL

Fujikawa, T[1], Sato, K[1], Koga, C[1], Yuma, Otsuka[1], and Yanagi, M[2]

[1]Fukuoka University
[2]NIPPON STEEL SLAG PRODUCTS CO. LTD.
E-mail takuro-f@fukuoka-u.ac.jp

1. INTRODUCTION

By-products such as coal ash discharged from thermal power plants and steelmaking slag generated in the steelmaking process need to be effectively utilized due to the large amount generated. Among these by-products, coal ash (CA) has been used as coal ash mixed material (mixed by coal ash, water, and cement) (Jcoal, 2015), mainly as a subbase-course material. However, further study is required to expand its use to base-course materials or geotechnical materials in the future. On the other hands, steelmaking slag (SS) has already been used as a base-course material because of its hydraulic property and expected improvement in bearing capacity. It also has a high abrasion resistance, a large friction angle, and high particle density and unit volume weight, making it effectively used in various applications such as construction materials and ground improvement materials.

Therefore, this study aims to expand the use of coal ash mixed material by developing CA and SS mixed material (CA-SSM), focusing on the strengthening of the slag skeletal structure and its ability to immobilize the elution of heavy metals and metalloids. Furthermore, two types of mixing methods, pre-mix and post-mix, are investigated based on the difference in timing of mixing SS with CA as shown in Figure 1. This manuscript describes the applicability of the materials prepared by pre-mix methods as base-course materials, also evaluation of durability using wetting and drying tests, and long-term safety to the surrounding environment using the outdoor exposure tests.

2. MATERIALS AND METHODS

CA generated from thermal power plants and SS from steel mills were used in this study. The SS was steam-aged in consideration of material expansibility. Blast furnace slag cement B (BB) and hydrated lime were used as solidifiers to produce the CA-SSM. Table 1 shows the testing conditions for the effects of different mixing ratios of SS. Considering that SS was used as part of the CA, SS with a grain size of 4.75 mm or less is mixed at an internal ratio of 0, 10, 30 % to the mass of CA. Each sample was mixed using a hobart mixer according to the test conditions. After mixing, the specimens were prepared by 3 layers of 12 blows at 1 E_c (550 kJ/m^3) of compaction energy using 1.5 kg rammer in a PVC mold of diameter D=5 cm and height H=10 cm. After demolding, the specimens were heat-humidified and cured at 50°C and 90% humidity for 2 days. The specimens were then cured in a constant-temperature room at 20°C for 7 and 28 days, and then performed to unconfined compression test (JIS A 1211).

Figure 1. Two types of mixing methods

Table 1. Testing condition of CA-SSM

CA : SS	CA (%)	SS (%)	Cement (%)	Water (%)	Hydrated lime (%)
10 : 0	100	0	25	24.2	3
9 : 1	90	10			
7 : 3	70	30			

*Cement and Hydrated lime are mass ratios to CA and SS

*Water is mass ratio to CA, SS and cement

After 28 days curing, CA-SSM was crushed to less than 40 mm, and CBR tests (JIS A 1211) were conducted to evaluate its performance as base-course material. The CBR index provides a measurement of the impact resistance of compacted crushed CA-SSM through the E-b method (using a 4.5 kg rammer and drying method with a non-repeating sample). The water content of the crushed CA-SSM was adjusted to the optimum water content based on the compaction test results.

To evaluate the long-term durability of CA-SSM, wetting and drying tests were conducted according to ASTM D-4843. Samples were prepared using crushed CA-SSM less than 40 mm and compacted into molds 100 mm in diameter and 127.5 mm high. Then, samples were oven-dried at 60 ± 3 °C for 24 h and then air-cooled at 20 ± 3 °C prior to wetting. Subsequently, the samples were completely immersed and soaked for 23 hours in water. 15 wetting and drying cycles were applied. At the end of each cycle, the height, diameter, and mass of each sample were measured. After 5, 10, and 15 cycle, Cone index test (JIS A 1228) was conducted to measure penetration resistance.

It is important to understand the leaching properties of heavy metals and metalloids in CA-SSM. Japanese Leaching Test No. 46 (Notifications No. 46 by the Ministry of Environment, Japan, JLT 46) was used to measure the concentrations of heavy metals and metalloids in the CA-SSM. The samples were crushed and sieved to less than 2 mm, and a solvent was added so that the liquid-solid ratio (L/S) was 10.

Considering the use of CA-SSM as a civil engineering material, it is necessary to understand the long-term elution characteristics of heavy metals and metalloids. Therefore, an outdoor exposure test was conducted. Each CA-SSM of less than 40 mm was filled in a Wagner pot with a diameter of 250 mm to a depth of 200 mm and a density of 1.0 Mg/m^3, and installed outdoors. Leachate generated through rainwater was sampled every 3000 mL and filtered through a 0.45 μm membrane filter to measure the heavy metals and metalloids. The test period was 1 year and 8 months, from November 2021 to July 2023. This study focused on boron (B), and fluorine (F) and hexavalent chromium (Cr (VI)) as they are included in the Japanese environmental standard values for soils and are present in the CA.

3. RESULTS AND DISCUSSION

Figure 2 shows the unconfined compression test results. It can be seen that unconfined compression strength (UCS) increases with the increase in the number of curing days for each condition. Furthermore, the UCS tends to increase as the slag mixing ratio increases. This is thought to be due to the solidification effect of the hydraulicity of the steel slag, as well as the effect of improving the grain size of the mixed material by mixing SS with larger grain size.

Figure 3 shows the CBR test results. Similar to the unconfined compression test results, the CBR values increased with increasing SS mixing rate. It is also clear that the 7:3 condition satisfies the criteria (CBR=80% or more) for the base-course material. Thus, it can be seen that mixing SS is an effective way to increase the effective use of coal ash mixed materials.

Figure 4 shows the wetting and drying test results. Regardless of the slag content, no significant increase or decrease in strength with increasing number of cycles is observed, and the cone index is stable, indicating that CA-SSM is a durable material. Figure 5 also shows the relationship between the number of cycles and mass change of CA-SSM. Although leakage of fine grains was observed from the specimen, there was no significant mass change regardless of the mixing method, indicating that the mass change remained constant.

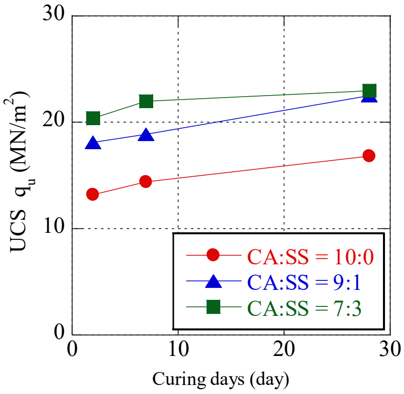

Figure 2. Relationship between number of cycles and UCS

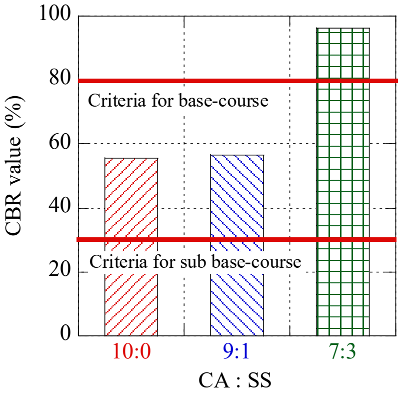

Figure 3. CBR test results

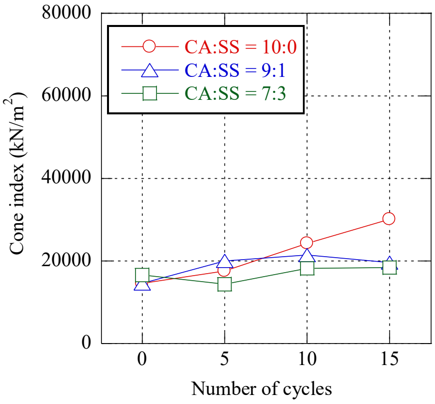

Figure 4. Wetting and drying test results (Relationship between number of cycles and cone index)

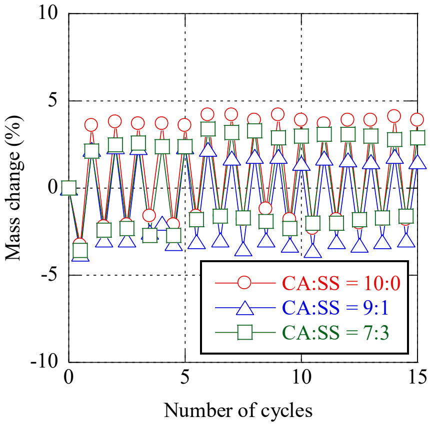

Figure 5. Wetting and drying test results (Relationship between number of cycles and mass change)

Table 2 shows the batch leaching test results of CA-SSM. It can be seen that the crushed material developed in this study satisfies the soil environmental standard in Japan. For long-term environmental safety evaluation, Figure 6 shows the results of outdoor exposure tests. pH shows alkalinity and remains at a constant value in Figure 6 (a). No elution of cadmium (Cd) and lead (Pb) was observed under all conditions. Figure 6 (b) and (c) show the relationship between the concentrations of fluorine (F) and hexavalent chromium (Cr (VI)) and the cumulative liquid-solid ratio, respectively. Both of them showed a gradual decreasing trend, indicating that they are unlikely to show high values over a long period of time and are sufficiently stable.

Table 2. Batch leaching test results

Sample	pH	Consentration [mg/L]				
		Cd	Pb	Cr(VI)	F	B
SS	12.9	N.D.	N.D.	N.D.	N.D.	0.10
CA-SSM (CA:SS = 10:0)	11.6	N.D.	N.D.	0.02	0.31	0.48
CA-SSM (CA:SS = 9:1)	11.5	N.D.	N.D.	0.03	0.28	0.30
CA-SSM (CA:SS = 7:3)	11.8	N.D.	N.D.	0.02	0.21	0.22
Environmental Standard		0.003	0.01	0.05	0.8	1

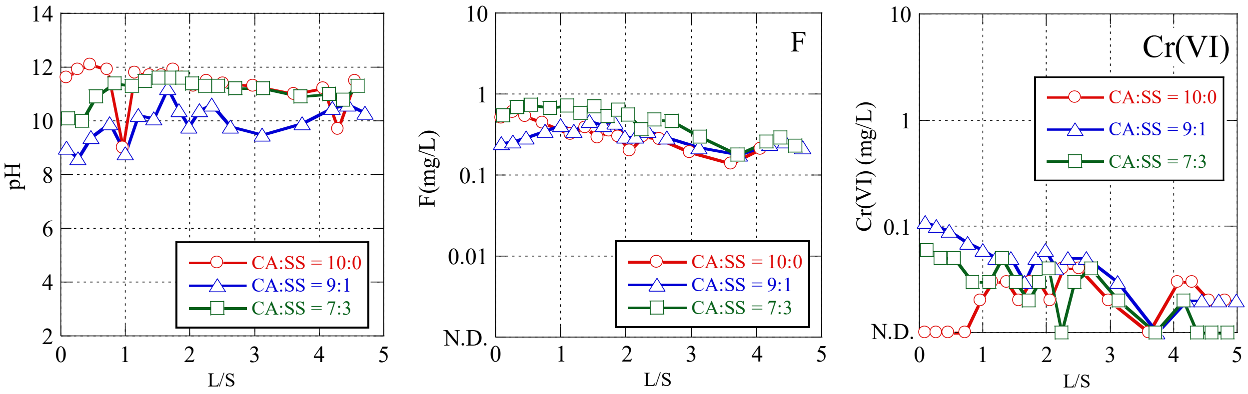

(a) pH **(b) F** **(c) Cr(VI)**

Figure 6. Outdoor exposure test results

4. CONCLUSION

1) Mechanical properties of CA-SSM can be improved with increasing slag addition rate.
2) CA-SSM can be effectively used as a base-course material.
3) CA-SSM was found to be a geomaterial with durability and long-term safety for the surrounding environment.

5. REFERENCES

ASTM (2009) D 4843-88(2009): Standard test method for wetting and drying tests of solid wastes. ASTM International, West Conshohocken, PA, USA.

Jcoal (2015) Guidelines for Effective Use of Coal Ash Mixed Material (High Standard Road Embroidery). Jcoal, Tokyo, Japan (in Japanese).

https://www.jcoal.or.jp/ashdb/ashguideline/ (accessed 17/07/2023).

JIS, 2020A. A 1211: The Method for the California Bearing Ratio (CBR) of soils in laboratory. Japan Industrial Standard, Japanese Industrial Standards Committee, Tokyo, Japan.

JIS, 2020B. A 1228: The Method for Cone Index of Compacted Soils. Japan Industrial Standard, Japanese Industrial Standards Committee, Tokyo, Japan.

Ministry of the Environment of Japan. Notifications No.46 by the Ministry of Environment, Environmental Quality Standards for Soil Pollution (accessed 18/07/2023). https://www.env.go.jp/en/water/soil/sp.html

ASSESSMENT OF CHLORIDE TRANSPORT IN METAKAOLIN-FLY ASH-LIMESTONE BLENDED CEMENTITIOUS MATERIALS

Shiyu Sui[1,2,3*], Yalong Shan[1], Gongrui He[1], Shaochun Li[1], Fengjuan Wang[2,3], Jinyang Jiang[2,3]

[1] School of Civil Engineering, Qingdao University of Technology, Qingdao, China
[2] School of Materials Science and Engineering, Southeast University, Nanjing, China
[3] Jiangsu Key Laboratory of Construction Materials, Nanjing, 211189, China
suishiyu0913@hotmail.com (Shiyu Sui)

1. INTRODUCTION

Ordinary Portland cement serves as a fundamental building material for concrete and stands as one of the most extensively utilized construction materials across the globe. Nonetheless, the excessive production of cement carries significant environmental repercussions. Moreover, the robustness and longevity of such materials are crucial factors influencing their practicality. Concrete frequently faces exposure to aggressive infiltrating agents like chloride salt, particularly in coastal settings (Shi et al., 2012). When the concentration of chloride ions around steel reinforcement surpasses a certain critical level, the protective layer of the steel becomes compromised. This breach in the protective layer paves the way for the onset of steel corrosion. Numerous researchers have dedicated efforts to studying the mechanism of chloride diffusion in cementitious materials. In order to slow down the migration of chloride ions towards the vicinity of steel reinforcement, the incorporation of novel supplementary cementitious materials (SCMs) has emerged as a strategy to improve the durability of cement-based materials. This proactive approach aims to mitigate the potential detrimental effects of chloride intrusion and increase the overall lifespan of these materials.

The combination of calcined clay and limestone (LS) composite exhibits the potential to enhance both the pore structure and the resulting hydration products within cementitious materials. This characteristic renders it a viable candidate for substituting cement clinker without compromising the materials' resistance to chloride penetration. Beyond the conventional filler effect and dilution influence, limestone has demonstrated reactivity with the aluminum (Al) phase present in clinker or SCMs. A fraction of limestone engages in hydration reactions in the presence of aluminates, leading to the formation of calcium carboaluminate hydrates. As early as 1965, the reaction between pure tricalcium aluminate (C_3A) and calcium carbonate ($CaCO_3$) to create carboaluminate compounds was documented by Feldman et al. (Feldman et al., 1965). These carboaluminate phases include monocarboaluminate (Mc) and hemicarboaluminate (Hc). When chloride ions migrate within cementitious materials, they engage in chemical interactions with C_3A or its associated hydrates (AFm), giving rise to the creation of compounds such as Friedel's salt ($C_3A.CaCl_2.10H_2O$), or they physically adhere to calcium-silicate-hydrate (C-S-H) phases. These phenomena are often referred to as "bound chloride." A material's capacity to bind a larger quantity of chloride correlates with a diminished chloride transport towards areas containing steel reinforcement. This outcome contributes positively to the structural integrity.

In this study, metakaolin (MK) and fly ash (FA) were employed to replicate diverse grades of calcined clay, thereby eliminating the impact of clay impurities. Subsequently, the study delves into the investigation of OPC-MK-FA-LS mortar specimens concerning chloride exposure, as assessed via Rapid Chloride Migration tests (RCM). As a secondary focus, the research explores the impact of limestone and metakaolin on the electrochemical parameters. This exploration aims to elucidate the underlying mechanisms governing the effects of limestone and metakaolin on the transport of chloride ions within cementitious materials.

2. MATERIALS AND METHODS

2.1 Experimental materials

In this study, a commercial Portland cement (P·I 42.5), high purity MK, LS and fly ash were applied for the specimen. Deionized water was used for the paste samples while tap water was used for the mortar preparation.

2.2 Test procedure

Five mixtures were prepared. Among them four mixtures were with MK, LS or FA inside, with MK+FA content kept as 30% (MK/(MK+FA) changing from 100%, 60%, 40% and 20%) and LS content as 15%. The other one OPC was used as the reference. In addition, 2% gypsum was added to the systems with MK to avoid the flash setting. The water to binder ratio was 0.5 and the sand to binder ratio was kept as 3. For Electrochemical Impedance Spectroscopy (EIS) test, mortars were cast in moulds with the dimensions of 40 mm ×40 mm ×160 mm for one day, and then stored in a standard curing room (95 ± 5% RH, 20 ± 2 °C) for 28 days after demolding. For X-ray Diffraction (XRD) test and porosity test, paste was prepared, which was cured in 50ml plastic bottle for 28 days until the test.

3. RESULTS AND DISCUSSION

3.1 Influence of MK content on the chloride transport

The resistance of the systems against the ingress of chloride was evaluated through the employment of the RCM test. Figure 1 illustrates the chloride diffusion coefficients across five distinct mixes. Notably, the OPC sample exhibits the highest coefficient, suggesting that the inclusion of MK contributes positively to chloride resistance. Furthermore, there is a significant reduction in the chloride diffusion coefficient with an increase in MK content. For the 100MK system, the coefficient diminishes by an impressive 98%. Even in the case of the 20MK system, containing just 20% metakaolin within the MK+FA blend, the chloride diffusion coefficient outperforms the reference mixture. This underscores MK's potential as a viable material for environments demanding heightened durability. Chloride ingress is influenced by two key factors: a physical effect related to pore structure and a chemical effect associated with chloride binding. As per prior research by Zunino & Scrivener (2021), it has been established that limestone, metakaolin, and fly ash collectively contribute to denser structural formations and the creation of Mc and Hc phases, which have the capacity to bind chloride ions. To delve further into the intricate mechanisms underlying the effects of LS, MK, and fly ash, an in-depth microstructure analysis was conducted.

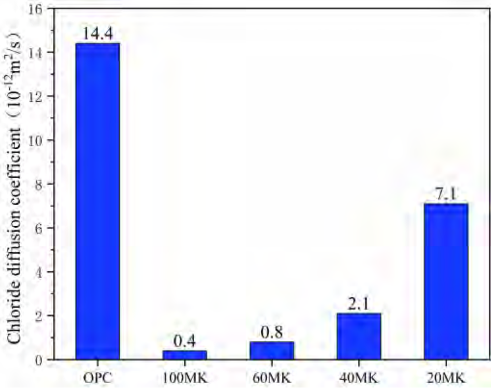

Figure 1 Chloride diffusion coefficient comparison for the investigated systems

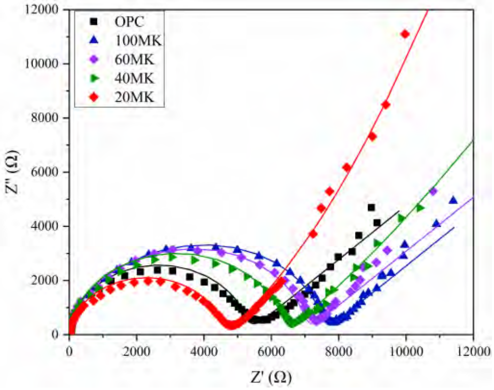

Figure 2 Nyquist curve of the investigated cement mortars

3.2 Influence of MK content on the EIS test

Electrochemical Impedance Spectroscopy (EIS) is harnessed to delve into the microstructure intricacies of blended cementitious materials. For EIS analysis, an enhanced equivalent circuit model - $R_s(Q_1(R_{ct1}W_1))(Q_2(R_{ct2}W_2))$ - is adopted, as proposed by Dong et al. (2017). Within this model, R_{ct1} symbolizes the electrical resistance tied to ion transfer processes intrinsic to cement-based materials. The Nyquist plot depicting the examined cement mortars is depicted in Figure 2, and the parameter outcomes of fitting the model to MK blended cement at 28 days are itemized in

Table 1. The discernment of the influence of MK content on the coefficient values of R_{ct1} unveils its prominence as a pivotal gauge for chloride-related behavior.

Table 1 R_{ct1} values of the blended cement mortar with different MK/FA ratios

$R_s(Q_1(R_{ct1}W_1))(Q_2(R_{ct2}W_2))$	
Sample	R_{ct1}
OPC	5177
100MK	7340
60MK	6938
40MK	5941
20MK	4552

3.3 Influence of MK content on the phase assemblage of the various systems

Upon integration of SCMs into cementitious systems, they can react with the hydration byproducts, thereby inducing alterations in the phase assemblage. Such modifications inherently exert an influence on the transport of chloride ions. As shown in Figure 3, the introduction of MK yields the production of Hc and Mc phases. In contrast, the OPC system primarily exhibits minimal presence of AFt and virtually little AFm. The emergence of AFm phases is constructive, contributing to the refinement of pore structure and the capacity to bind chloride ions. These effects collectively result in a deceleration of chloride migration.

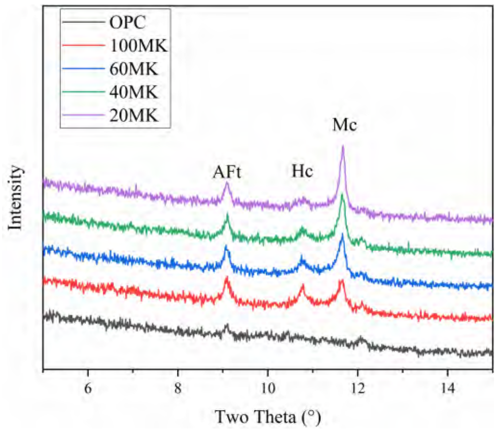

Figure 3 AFm phases change for the systems

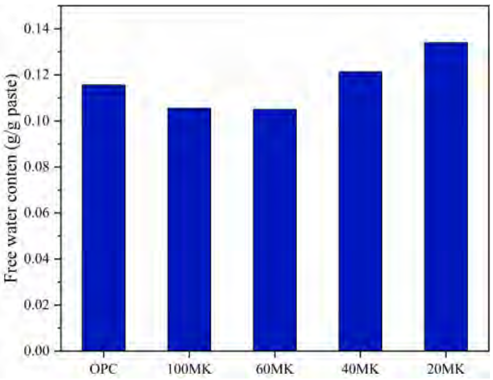

Figure 4 Free water content for the systems

3.4 Influence of MK content on the free water content

Given that chloride ions travel through water-filled pores, the presence of free water becomes a pivotal determinant of chloride resistance. The alteration in free water content corresponding to varying levels of MK within the system is illustrated in Figure 4. Notably, systems characterized by higher MK content exhibit diminished quantities of free water compared to the OPC. Furthermore, as the MK content progresses from 20MK to 100MK, a notable decline in free water content is observed. This result suggests the efficacy of introducing MK and FA in contrast to OPC, as it fosters the generation of enhanced hydration products, thereby resulting in a reduced porosity within the composite cementitious material. Consequently, this contributes to the optimization of pore structure.

3.5 Relationship between the chloride diffusion coefficient and the EIS parameters

The relationship between chloride transport and the parameter derived from the EIS examination is depicted in Figure 5. The correlation coefficient, denoted as R^2 and measuring 0.85, signifies a substantial linkage between the chloride diffusion coefficient and R_{ct1}. This result substantiates the viability of prognosticating the chloride resistance of OPC-MK-FA-LS blended materials by utilizing the electrical resistance (R_{ct1}) obtained from electrochemical impedance spectroscopy, grounded in the established EC model.

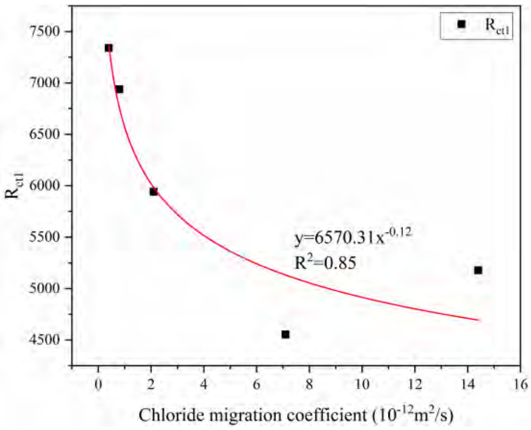

Figure 5 Relationship between the chloride diffusion coefficient and the parameters from EIS tests

4. CONCLUSION

This paper delved into the assessment of how the inclusion of MK, FA, and LS influences the chloride diffusion characteristics within cementitious materials, employing the EC model of EIS. The key conclusions drawn from this study encompass the following:

1) Because the high reactive materials content increased as the MK content increased, the number of hydrates was also improved. In addition, the reaction of the MK with hydration products and LS would refine the pore structure and phase assemblage.

2) The relationship between chloride diffusion coefficient and R_{ct1} is highly correlated. Thus, the parameter R_{ct1} from EIS can be used to predict the chloride resistance of the MK blended cement materials.

5. ACKNOWLEDGMENT

The study was funded by the National Natural Science Foundation of China (52108225), and the open research fund of Jiangsu Key Laboratory of Construction Materials, Southeast University (No. 202202).

6. REFERENCES

Dong, B. , Li, G. , Zhang, J. , Liu, Y. , Xing, F. , & Hong, S. . (2017). Non-destructive tracing on hydration feature of slag blended cement with electrochemical method. Construction and Building Materials, 149, 467-473.

Ramachandran, V. S. , Sereda, P. J. , & Feldman, R. F. . (1965). Influence of caco3 on the hydration of 3cao·al2o3. Journal of the American Ceramic Society, 48(1), 25-30.

Shi, X. , Xie, N. , Fortune, K. , & Gong, J. . (2012). Durability of steel reinforced concrete in chloride environments: an overview. Construction & Building Materials, 30, 125-138. https://doi.org/10.1016/j.conbuildmat.2011.12.038

Zunino, F. , & Scrivener, K. . The reaction between metakaolin and limestone and its effect in porosity refinement and mechanical properties. Cement and Concrete Research, 140.

DEVELOPMENT OF LOW-CARBON HIGH-PERFORMANCE LIGHTWEIGHT CONCRETE WITH WASTE MATERIALS

Jian-Xin Lu and Chi Sun Poon

Department of Civil and Environmental Engineering & Research Centre for Resources Engineering Towards Carbon Neutrality (RCRE), The Hong Kong Polytechnic University, Hung Hom, Hong Kong, China
E-mail: jianxin.lu@polyu.edu.hk

Lightweight concrete is usually limited to non-loadbearing blocks, developing high performance lightweight concrete (HPLC) capable of loading bearing purposes is essential to meet the demanding requirements of modern construction. The adoptions of special supplementary cementitious materials and high-strength eco-friendly lightweight aggregates contribute to developing low-carbon HPLC. Incorporating lightweight materials into sustainable ultra high-performance concrete (UHPC) can successfully produce the HPLC, characterized by low density, ultra high strength and superior durability. The utilization of waste glass in forms of powder and cullet is able to make a desirable UHPC binder for HPLC. Moreover, combining the waste glass powder with other solid waste, such as incinerated sewage sludge and bottom ashes, can produce high-strength lightweight aggregates for the HPLC production. Apart from solid wastes, waste flue gas (CO_2) is also introduced into UHPC paste for preparing a durable high-strength HPLC. In addition, a superhydrophobic structure is designed to further improve the durability of foamed HPLC. This study provides substantial solutions for enhancing the performance of lightweight concrete, which would be promising for the practical applications in floating structures and modular integrated constructions.

Keywords: High-performance lightweight concrete; Ultra high strength; Lightweight aggregates; Foam concrete; Durability

METHODOLOGY TO EVALUATE THE SUITABILITY OF SECONDARY SAND AGGREGATES FOR THE USE IN CONCRETE: VALORISATION OF A NORMATIVE STUDY IN BELGIUM

Dilissen, Nicole[1], Hulsbosch, Niels[1], Dooms, Bram[1], Mosselmans, Gunther[2], Pierre, Christian[2]

[1]Buildwise. Avenue P. Holoffe 21, 1342 Limelette, Belgium.
[2]CRIC-OCCN. Avenue Buyl 87, 1050 Brussels, Belgium
E-mail (corresponding author): nicole.dilissen@buildwise.be

1. INTRODUCTION

Belgian concrete production amounted to 23 Mm^3 in 2021[1], for which ~16 Mm^3 of aggregates were required, mainly from primary resources. Europe and Belgium pursue societal transitions towards green and circular economies (Green Deal, Circular Action Plan). The standards NBN EN 206 and NBN B 15-001 permit the use of coarse air-cooled blast furnace slag and recycled aggregates from construction and demolition waste (d > 4mm), yet no framework exists for finer aggregates of secondary origin (D ≤ 4 mm). The GRANISEC project, a Belgian federal pre-standardization study, scientifically supported the development of the recently published national standard NBN B 15-105:2022, in which an evaluation methodology is presented for the suitability of secondary inert aggregates in concrete. The suitability of fine secondary aggregates in concrete was specifically considered. Existing test methods were evaluated, adapted and optimized where needed for this particular scope.

2. MATERIALS AND METHODS

Based on Belgian waste-streams, eleven secondary sands and one filler (Figure 1) were evaluated through thirty-two production lots. Thirty-seven aggregate characterization methods (i.e. mineralogical, geometrical, physical and chemical) were evaluated, among which testing on soluble chlorides (NBN EN 1744-1 §7), potential alkali-silica reactivity (ASR) (ASTM C1260: Oberholster test), acid and water-soluble sulfates (NBN 1744-1 §12 and §10) and free lime content (NBN EN 1744-1 § 18.2 and 18.5). The sands were classified based on their properties by means of hierarchical cluster analyses (HCA) and principal component analyses (PCA) with Origin Pro 2020b into six groups of secondary sand types (Figure 2): i) residues of stainless steel (SS) slag, ii) physico-chemically treated (PCT) sands, iii) copper (Cu) slag, iv) bottom ash (BA), v) concrete and mixed (c&m) sands and vi) lead (Pb) slag (*cf.* Figure 1).

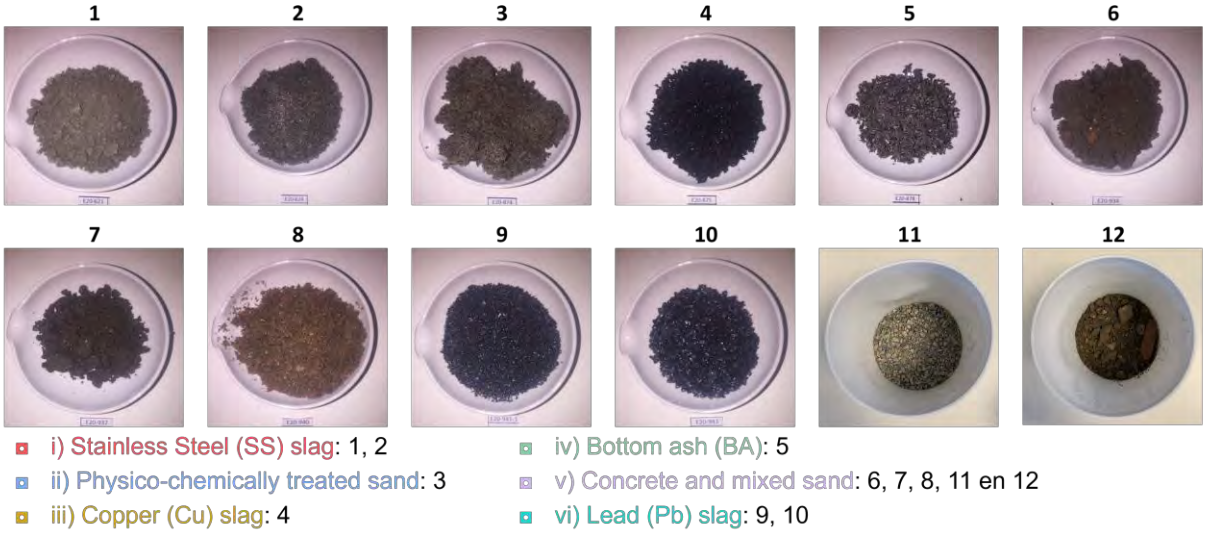

Figure 1: Sands used in the GRANISEC project, categorized in 6 groups.

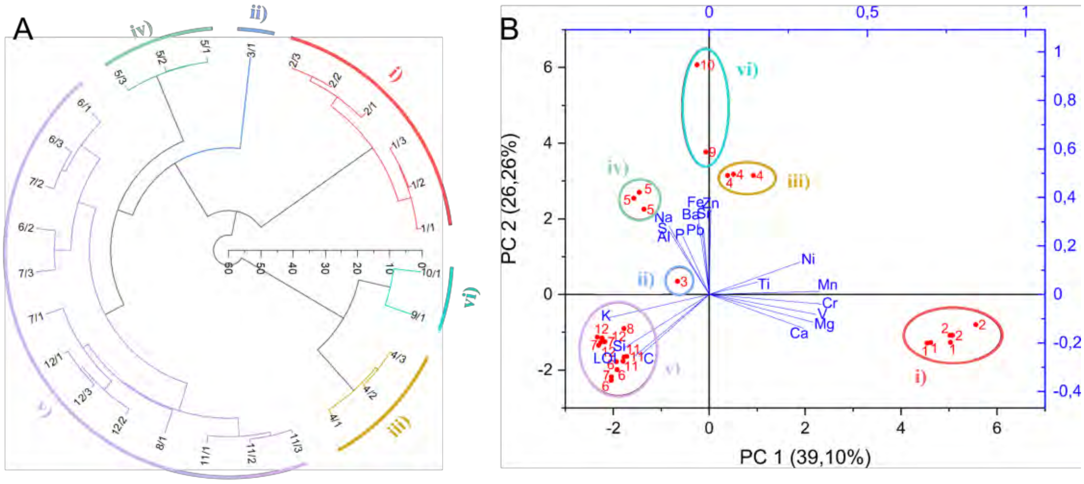

Figure 2: A) HCA dendogram with hierarchical relationships in between clusters and B) PCA multivariate statistical technique identify 6 groups based on chemical composition. Groups i) to vi) are named in Figure 1.

A set of suitable testing methods on mortar and concrete-level was evaluated. This included, among others, (1) verification of certain physico-mechanical concrete properties and relationships in correspondence with NBN EN 1992-1-1, (2) determination of durability behavior in function of exposure classes and (3) development of a testing method for acid resistance of concrete.

Mortars were prepared according to NBN EN 196-1 with w/c 0.5 and reference mortars consisting of 1350 g standardized CEN-sand, 450 g CEM I 52.5 N-SR0, 225 g effective water (13.5 g absorption water after 15 minutes pre-saturating the sand). Mortars with the secondary sands consisted of a 100 vol% replacement of the 1350 g CEN-sand, the amount in weight was calculated via the real density ρ_{rd}. Water absorption WA_{24} was calculated according to NBN EN 1097-6. The six types of secondary aggregates have a large variety in ρ_{rd} and WA_{24}, which has an influence on the workability of fresh mortar. In order to reach comparable consistency, adapted stabilizers and superplasticizers are recommended. The mortar test program screened the influence of replacement sands through the impact on initial setting time (NBN EN 480-2), expansion in sulfate solution (CUR-48) expansion in water (adjusted CUR-89 UAMBT: without NaOH, PSD adjusted to sand).

Concrete was mixed (procedure: NBN EN 480-1) with w/c 0.5 and 320 kg/m^3 CEM I 52.5 N-SR0 according to NBN B 15-001 with S4 consistency and corresponding to exposure classes XF3 and XC4. 20 vol% replacement of natural sand by secondary sand was used (Table 1).

Table 1: Raw materials used in concrete mixes

Raw material [kg/m^3]	Ref.	#2	#3	#4	#5	#6	#7	#8	#9	#10	#11	#12
CEM I 52,5 N	320	320	320	320	320	320	320	320	320	320	320	320
Effective water	160	160	160	160	160	160	160	160	160	160	160	160
Absorption water	7	19	9	9	33	31	37	25	5	8	27	36
River sand 0/1	263	119	93	394	189	182	115	134	397	395	305	182
River sand 0/4	493	243	290	40	192	262	314	260	0	24	126	243
Secondary sand	0	414	423	516	253	303	278	321	493	515	312	294
Limestone 6/14	570	594	563	508	568	485	499	548	561	528	507	512
Limestone 14/20	592	585	593	608	591	610	605	595	594	602	609	605
Superplasticizer	0,64	0,64	0,64	0,64	1,92	1,52	3,20	2,56	0,64	0,96	0,64	0,64
Total	**2405**	**2454**	**2451**	**2556**	**2309**	**2354**	**2331**	**2365**	**2531**	**2553**	**2365**	**2351**

The concrete test program included (1) testing on fresh concrete, such as consistency (NBN EN 12350-2), air content (NBN EN 12350-7), density (NBN EN 12350-6) and bleeding (NBN B 15-226), (2) mechanical properties testing on hardened concrete, such as density and water absorption (NBN EN 12390-7 and NBN B 15-215), compressive strength (NBN EN 12390-3), tensile strength (NBN EN 12390-6), E-modulus (NBN EN 12390-13), shrinkage (NBN EN 12390-16) and physico-mechanical performance (NBN B 15-105 and NBN EN 1992-1-1 ANB) and (3) durability properties testing on hardened concrete, such as resistance to carbonation (NBN B 15-105 and NBN EN 13295), chloride intrusion (NBN B 15-105 and NT Build 492), acid and sulfate attack (NBN B 15-105 and ASTM C267-1) and alkali-silica reaction (NBN B 15-105 and 15-001).

There is no standardized testing method for resistance to acid attack following NBN B 15-105, but the standard states (1) evaluation of mass loss after a series of degradation cycles and (2) reference concrete with mass loss > 5 wt%. The GRANISEC project proposed a testing method with mass loss over 6 degradation cycles of 7 days and 3 samples per concrete composition with 3 acid types: acetic (*cf.* glues, plastics), lactic (*cf.* silage feed) and sulfuric acid (*cf.* car batteries, sewers). Acid concentrations were 30 g/L. Mechanical brushing was applied to collect the mass loss. No renewal of acids after each cycle was applied, in order to assess the neutralizing effects of the concrete.

3. RESULTS AND DISCUSSION

3.1. *Characterization and properties of secondary sands*

Geometrical and physical characterization techniques of aggregates showed Cu and Pb slags and c&m sands with the most coarse calibers and with the highest variability in particle size distribution (PSD). Higher amount of fines (< 63 μm) corresponds mostly to aggregates of BA and c&m sands (e.g. ≥ 10 %), although some of these latter sands have low amounts of fines. High amounts of fines have an important impact on the water demand of mortars and concrete containing such sands. Mainly this is due to the fraction pulverized cement stone. The higher amount of water demand causes complex water management that leads to the reduction of strength, durability and increased shrinkage[2]. Therefore, the NBN B 15-001 (for coarse recycled aggregates) holds the limits of 10 % (± 2 % of the declared value) and 15 % (± 2 %) for concrete aggregate type A+ and mixed aggregate type B+, respectively. High amounts of soluble chloride (> 0.10 %) are found for BA, which may cause accelerated initial setting (here, not the case) and may exceed the maximum levels of chlorides allowed in concrete (*cf.* NBN EN 206 for chloride initiated corrosion), whereas all other sand types have < 0.06 %. Higher amounts of acid soluble sulfates (> 0.8 %) are found in Cu slag, BA and c&m sands. Higher amounts of in water soluble sulfates (> 0.2 %) are found in c&m sands. Higher amounts of free lime (> 1 %) are found in SS slags and BA. Soluble sulfates, as well as free lime may cause swelling in concrete. Sand types that show potential ASR (> 0.1 %) are BA and c&m sands. Based on these test results, testing methods for aggregates in NBN B 15-105 can be extended: per sand type a minimal range of tests shall be performed in function of their properties.

3.2. *Mortars*

The initial setting time (NBN EN 480-2) shows that mortars with BA and recycled sand (i.e. with higher soluble chloride content) have accelerated setting. Expansion in sulfate solution (CUR-48) of mortars shows a relationship with aggregate properties on free lime, sulfate and gypsum. Expansion in water (adjusted CUR-89 UAMBT,) examines the influence of free lime, sulfate and periclase. Only aggregate nr. 2 (SS slags; Figure 1) shows expansion due to the free lime content.

3.3. *Concrete*

For fresh concrete, all specimens reached S3-S4 consistency with the addition of superplasticizer. The air content ranged 1.3-2.9 % with the specimens containing BA as outlier (11.5 %), while traditional concrete has 1.5-2.0 %. The high air content in the BA specimens is due to the reactivity with water of the sand aggregate: the specimens contain metallic Al, which can form hydrogen gas through hydrolysis in water: $2Al + 6H_2O \rightarrow 2Al(OH)_3 + 3H_2$ [3]. Moreover, the BA-specimens show crack formation during curing. The density of fresh concrete ranges 2320-2550 kg/m^3, for which the differences are mainly due to the density of the secondary aggregates, except the BA-specimens 2110 kg/m^3, which is due to the high air content. Bleeding ranges 0.4-3.3 wt% water, with outliers 5.6 wt% for Cu slag specimens and 0.0 wt% for BA specimens. Notably, there is a negative correlation between the bleeding and the WA_{24} of the secondary sands: likely high WA_{24} sands still absorb water after mixing. This is thus mainly the case for BA and c&m sands.

Mechanical characterization on hardened concrete shows negative correlation between density and water absorption of hardened concrete, that slag specimens are in the same range as the reference concrete (high density, ≤ 5.0 % WAI) and that they comply with criteria from NBN 15-001 (≤ 6.0 % WAI). Not all c&m sands specimens comply (> 6.0 % WAI), but are all ≤ 6.5 % WAI. The BA specimens reach almost 7.5 % WAI. The compressive and tensile strength, as well as E-modulus is mainly higher for slag specimens (> 50 MPa; > 3.5 MPa; > 40 GPa), followed by c&m sand and PCT sand specimens (> 40 MPa; > 2.5 MPa; > 30 GPa), while BA specimens are < 20 MPa, > 2.0 MPa and < 20 GPa, respectively. The least shrinkage after 91 days (< 430 µm/m) is seen for slag specimen concrete, followed by specimens with PCT sands and c&m sands (< 500 µm/m), while BA-specimens has shrinkage > 680 µm/m. It is evident that metallic Al in BA causes quality degradation in concrete and BA should hence be treated to avoid it.

Physico-mechanical performance of concrete can be evaluated. For all concrete specimens, except BA specimens, compressive strength is related to tensile strength in accordance with NBN B 15-105. For BA specimens, the compressive strength is too low, due to the hydrolysis with metallic Al. The relationship between compressive strength and E-modulus shows that slag specimens have E-modulus higher than the limits posed by NBN B 15-105. Notably, this is also for the reference concrete, and several specimens with c&m sands. The formula for calculating the limits conform NBN B 15-105 likely should be reconsidered, especially for specimens containing higher density aggregates. The relationship between strength evolution and shrinkage is conform NBN B 15-105 for all specimens, even for BA specimens, considering that limits are very broad (306 – 894 µm/m).

Durability of hardened concrete. The carbonation depth at 56 days, as well as the chloride diffusion coefficient is lowest for slag specimens (3 – 6 mm; 18 – 24 x 10^{-12} m^2/s), followed by PCT and c&m sand specimens (6-8.5 mm; 22 – 32 x 10^{-12} m^2/s). BA specimens show 15 mm and 66 x 10^{-12} m^2/s, respectively, due to the high air content giving high porosity and permeability for CO_2 and chloride to penetrate. For the sulfuric acid attack, secondary sands showed more resistance with 5.5 – 11 wt% mass loss after 6 cycles compared to the reference (13 wt%). Mass loss of secondary sand specimens was similar as the reference under acetic (1.1-1.7 wt%) and lactic acid (1.8-2.6 wt%). The resistance to swelling under influence of sulfates is according to NBN B 15-105 below limits (< 1.2 ‰) for all concrete specimens. The resistance to ASR after 20 days on the other hand is lowest for the reference sample (0.018 %), nevertheless all specimens are below the swelling limit of 0.1 % and therefore seen as non-reactive. The BA specimens, however, reach 0.097 %.

4. CONCLUSIONS

Test methods for aggregates (physico-chemical, mechanical and environmental health) were identified, (partially) adapted and more developed, based on 6 sand types as classified in the GRANISEC project. A mechanical and durability testing program on mortar and concrete level with secondary sands was established. For some properties new testing methods had to be developed such as resistance to acid attack. Translation into the standard NBN B 15-105 was successful and can be transferred to developments at mechanical and durability level in European standards.

5. ACKNOWLEDGMENT

This research is part of the GRANISEC project (program 192040) which received funding from the FOD economie of Belgium under grant agreement 19B06.

6. REFERENCES

[1]*FedBeton – The Belgian Federation of Ready-Mixed Concrete - represents the companies of the concrete production, transport and pumping industry in Belgium (www.fedbeton.be).*

[2] Théréné, F., Keita, E., Naël-Redolfi, J., Boustingorry, P., Bonafous, L., & Roussel, N. (2020). Water absorption of recycled aggregates: Measurements, influence of temperature and practical consequences. Cement and Concrete Research, 137, 106196. https://doi.org/https://doi.org/10.1016/j.cemconres.2020.106196

[3] Wang, H., Lu, J., Dong, S. J., Chang, Y., Fu, Y. G., & Luo, P. (2014). Preparation and Hydrolysis of Aluminum Based Composites for Hydrogen Production in Pure Water. MATERIALS TRANSACTIONS, 55(6), 892-898. https://doi.org/10.2320/matertrans.M2013425

IMPROVING THE INTERFACIAL TRANSITION ZONE OF HIGH-VOLUME FLY ASH CONCRETE USING RESPONSE SURFACE METHODOLOGY

Tianyu Xiao[1], Sen Du[2]

[1]School of Civil Engineering and Mechanics, Yanshan University, Qinhuangdao 066004, China
[2]School of Civil Engineering and Mechanics, Yanshan University, Qinhuangdao 066004, China
Email: sen.du@ysu.edu.cn (Sen Du)

1. INTRODUCTION

High-volume fly ash (HVFA) concrete, an environmentally friendly concrete that contains more fly ash than cement in the binder, has received the attention of many scholars in recent years due to its superior durability performances, such as lower water absorption and improved resistance to chloride ion penetration[1]. However, the weak frost resistance is the main hurdle that limits its wide application in the cold climates if no appropriates measures are taken[2]. As the weakest area of concrete, the interface transition zone (ITZ) loses its integrity firstly during the freezing-thawing damage. On the other hand, the improvement of the ITZ can effectively enhance the freezing-thawing resistance of concrete, especially for HVFA concrete where most of the fly ash particles remain unreacted and thus the ITZ is even a weaker area than the normal concrete[3]. In general, supplementary cementitious materials (SCMs) such as slag can be incorporated into concrete to improve the ITZ through filling and pozzolanic effects. However, slag is usually directly incorporated into concrete and eventually enters the concrete matrix, which weakens the improvement effect on the ITZ[4].

This study proposed a method to improve the ITZ in HVFA concrete through coating the coarse aggregate with slag-modified cement paste. Cement paste containing slag covered on the surface of the coarse aggregate would form the new ITZ after the hardening of HVFA concrete, aiming at improving this area more directly. By changing the variables in the process of preparing coated coarse aggregate, the porosity of the ITZ in HVFA concrete was measured as a response[5]. The effect of variables on the porosity of the ITZ was investigated using response surface method.

2. MATERIALS AND METHODS

All the materials used in the experiment are from a local market. Table 1 lists the chemical composition and physical properties of cement, fly ash and slag.

Table 1. Chemical composition and physical properties of cement, fly ash and slag

Chemical composition (wt.%)	Cement	Fly ash	Slag
Al_2O_3	4.83	32.44	12.1
SiO_2	20.5	49.2	37.65
Fe_2O_3	3.24	4.76	3.23
CaO	63.2	7.47	33.3
MgO	3.22	0.81	10.9
Na_2O	0.15	0.51	-
K_2O	1.29	1.82	-
SO_3	2.66	0.55	-
MnO	-	-	1.3
Physical properties			
Particle size	-	75%<40μm	10μm
Specific gravity	3.1	2.1	2.9
Loss on ignition(%)	0.91	2.44	1.52

Central composite design (CCD) was used to design 50 experimental schemes. There were five factors used in the study, namely mass ratio of water to cementitious materials in the slag-modified cement paste (X_1: W/CM), content of slag in cementitious materials (X_2: S/CM), mass ratio of coarse aggregate to slag-modified cement paste (X_3: CA/CP), the mixing time of slag-modified cement paste with coarse aggregate (X_4: T_1), and drying time after coating coarse aggregate by the slag-modified cement paste (X_5: T_2). The following ranges were set for the factors: 0.3 to 0.4 for X_1, 0 to 10% for X_2, 1.5 to 4.5 for X_3, 2 to 10 min for X_4, and 0 to 8 h for X_5. The specific experimental design is shown in Table 2.

Table 2. Variables and levels selected for the preparation of coated coarse aggregate

Mix	X_1, W/CM	X_2, S/CM (%)	X_3, CA/CP	X_4, T_1 (min)	X_5, T_2 (h)	Mix	X_1, W/CM	X_2, S/CM (%)	X_3, CA/CP	X_4, T_1 (min)	X_5, T_2 (h)
1	0.3	2.9	3.63	7.7	2.3	26	0.37	7.1	3.63	4.3	5.7
2	0.37	2.9	2.37	7.7	5.7	27	0.33	7.1	2.37	4.3	2.3
3	0.37	7.1	2.37	4.3	5.7	28	0.37	7.1	3.63	7.7	2.3
4	0.37	2.9	2.37	4.3	5.7	29	0.37	7.1	2.37	7.7	5.7
5	0.35	5	3	6	4	30	0.4	5	3	6	4
6	0.35	5	3	10	4	31	0.33	2.9	3.63	4.3	2.3
7	0.33	2.9	2.37	7.7	2.3	32	0.33	7.1	2.37	7.7	2.3
8	0.33	7.1	2.37	7.7	5.7	33	0.35	5	1.5	6	4
9	0.33	7.1	3.63	4.3	5.7	34	0.33	2.9	2.37	7.7	5.7
10	0.33	2.9	3.63	4.3	5.7	35	0.35	5	3	6	4
11	0.33	7.1	2.37	4.3	5.7	36	0.35	5	3	6	4
12	0.37	7.1	3.63	7.7	5.7	37	0.35	5	3	6	4
13	0.37	2.9	3.63	4.3	2.3	38	0.35	5	3	6	0
14	0.35	5	3	6	8	39	0.33	2.9	2.37	4.3	2.3
15	0.37	2.9	2.37	7.7	2.3	40	0.37	2.9	3.63	7.7	5.7
16	0.35	5	3	6	4	41	0.33	2.9	3.63	7.7	5.7
17	0.37	7.1	2.37	7.7	2.3	42	0.35	5	3	6	4
18	0.37	7.1	3.63	4.3	2.3	43	0.37	7.1	2.37	4.3	2.3
19	0.37	2.9	2.37	4.3	2.3	44	0.35	5	3	6	4
20	0.33	7.1	3.63	7.7	5.7	45	0.35	5	3	6	4
21	0.35	5	4.5	6	4	46	0.35	10	3	6	4
22	0.37	2.9	3.63	4.3	5.7	47	0.37	2.9	3.63	7.7	2.3
23	0.35	0	3	6	4	48	0.33	7.1	3.63	7.7	2.3
24	0.33	7.1	3.63	4.3	2.3	49	0.3	5	3	6	4
25	0.35	5	3	2	4	50	0.33	2.9	2.37	4.3	5.7

Different from the traditional concrete mixing process, this study coated coarse aggregate using cement paste in advance. Then the coated coarse aggregate was placed in the ambient temperature to dry for a specified time. After drying, the coated coarse aggregae was mixed with sand, cement, fly ash and water to prepare HVFA concrete[6]. The fresh HVFA concrete was cast into the mold with the size of 100 × 100 × 100 mm and covered with a plastic membrane. After 1 day, HVFA concrete was demolded and cured in the curing room for another 89 days. The amount of each material used to prepare HVFA concrete is shown in Table 3.

Table 3. The mix proportion of HVFA concrete in this work

Cement (kg/m^3)	FA (kg/m^3)	Water (kg/m^3)	Fine aggregate (kg/m^3)	Coated coarse aggregate (kg/m^3)
160	240	120	900	1000

The back-scattered electron (BSE) imaging was used to capture the image of the ITZ in HVFA concrete (Figure 1), which was further used to calculate the porosity of the ITZ. Software ImageJ was used to segment the pores from the BSE images with the help of the grey-level threshold segmentation method, resulting in the pores showing as black pixel in the binary image, as shown in Figure 2. In order to improve the stastistical reliability, at least 20 BSE images of different regions were required for calculating the porosity of the ITZ in HVFA concrete[7].

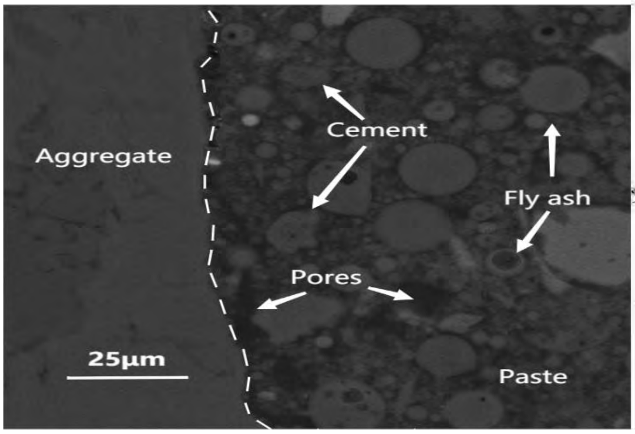

Figure 1. SEM-BSE images of ITZ

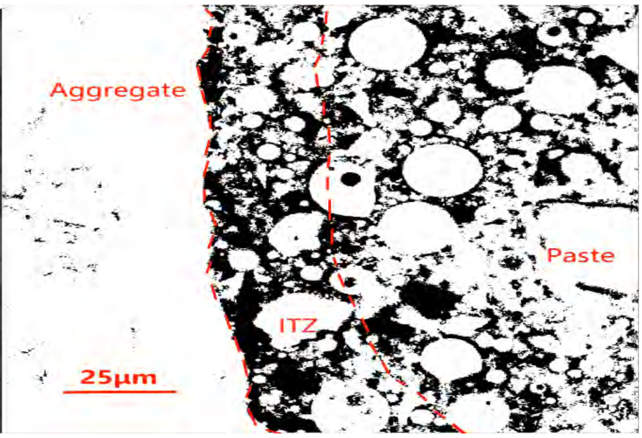

Figure 2. Pores segmented from ITZ

3. RESULTS AND DISCUSSION

The results of the porosity of the ITZ in 50 groups HVFA concrete were listed in Table 4. With the help of software Design-Expert 12, the relationship between the influential factors and porosity of the ITZ can be establised, as expressed in Equation (1). The equation in terms of significant factors can be used to make predictions about the response for given levels of each factor. Figure 3 shows the 3D surface diagram of the effects of W/CM and slag content on the porosity of ITZ. It can be seen from Figure 3 that there existed the combination of the optimal W/CM and slag content, at which the ITZ in HVFA concrete featured the lowest porostity.

$$Y^{1.09} = 38.41 + 5.43X_1 + 6.40X_2 + 12.84{X_1}^2 + 12.43{X_2}^2 + 11.39{X_3}^2 \tag{1}$$

Table 4. Porosity of the ITZ in HVFA concrete (%)

Mix	1	2	3	4	5	6	7	8	9	10
Porosity	34.6	31.4	37.3	29.9	29.5	20.7	31.9	36.0	29.9	33.6
Mix	11	12	13	14	15	16	17	18	19	20
Porosity	35.0	35.3	32.5	25.3	32.5	25.6	38.4	45.2	30.1	35.1
Mix	21	22	23	24	25	26	27	28	29	30
Porosity	29.4	32.1	29.8	34.3	26.2	32.4	33.3	28.3	35.8	43.4
Mix	31	32	33	34	35	36	37	38	39	40
Porosity	31.4	34.7	35.8	33.6	28.7	28.8	27.4	27.6	34.2	30.4
Mix	41	42	43	44	45	46	47	48	49	50
Porosity	34.0	27.8	44.6	27.2	26.9	36.8	34.5	37.3	24.6	31.6

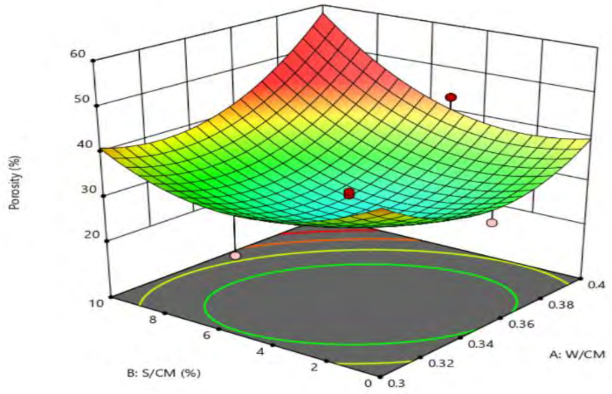

Figure 3. 3D surface diagram of the porosity of the ITZ

4. CONCLUSION

In this study, a method for improving the ITZ of HVFA concrete by coating the coarse aggregate with slag-modified cement paste was proposed. The porosity of ITZ was used as the response to reflect the effect of variables on the improvement of ITZ in HVFA concrete. For the porosity of ITZ in HVFA concrete, two significant factors were W/CM and slag content in the slag-modified cement paste. The ITZ in HVFA concrete can achieve the lowest porosity at the combination of optimal W/CM and slag content.

5. ACKNOWLEDGMENT

The funding support was provided by the Natural Science Foundation of Hebei Province of China under Grant No. E2021203214.

6. REFERENCES

Gao Yuan,Jing Hongwen,Yu Zixuan,Li Luan,Wu Jiangyu & Chen Weiqiang.(2022).Particle size distribution of aggregate effects on the reinforcing roles of carbon nanotubes in enhancing concrete ITZ. *Construction and Building Materials*. doi:10.1016/J.CONBUILDMAT.2022.126964.

Chang Xiangxiang,Liu Songhui,Zhang Cheng,Shen Peiliang,Xuan Dongxing,Guan Xuemao & Shi Caijun.(2022).Carbonation-hardening properties and ITZ microstructure of low-calcium CO2 sequestration binder mortar. *Construction and Building Materials*. doi:10.1016/J.CONBUILDMAT.2022.127589.

Tu Yan,Yu Hongfa,Ma Haiyan,Han Wenliang & Diao Yitong.(2022).Experimental study of the relationship between bond strength of aggerates interface and microhardness of ITZ in concrete. *Construction and Building Materials*. doi:10.1016/J.CONBUILDMAT.2022.128990.

Mazzucco G.,Salomoni V.A. & Majorana C..(2021).A cohesive contact algorithm to evaluate the mechanical behaviour of concrete ITZ at different roughness conditions. *Construction and Building Materials*. doi:10.1016/J.CONBUILDMAT.2021.123479.

Lyu Kai,Sun Baoyin,Liu Xiaoyan,Xie Xian & Liu Ruidan.(2022).Evaluation of the ITZ modification efficiency via aggregate surface coating with nano SiO2 (NS) and its influence on properties. *Case Studies in Construction Materials*. doi:10.1016/J.CSCM.2022.E01488.

Lin Jianjun,Chen Huisu,Zhao Qingxin & Li Mingqi.(2021).Statistical analysis of the critical percolation of ITZ around polygonal aggregates in three-phase concrete materials. *Physica A: Statistical Mechanics and its Applications*. doi:10.1016/J.PHYSA.2021.125878.

Shi Mengxiao,Wang Qiang & Zhou Zhikai.(2015).Comparison of the properties between high-volume fly ash concrete and high-volume steel slag concrete under temperature matching curing condition. *Construction and Building Materials*. doi:10.1016/j.conbuildmat.2015.08.134.

VALORISATION OF GLASS AND ALUMINIUM RECYCLING WASTES AS ALKALI-ACTIVATED BINDER PRECURSORS

Mañosa, J.[1], Maldonado-Alameda, A.[1,2], Formosa, J.[1], Chimenos, J.M.[1]

[1] Departament de Ciència de Materials i Química Física, Universitat de Barcelona, C/Martí i Franquès, 1-11, 08028, Barcelona, Spain.
[2] Fundación Centro Tecnológico de Investigación Multisectorial (CETIM); Parque empresarial de Alvedro, Rúa H, 20, 15180 Culleredo, A Coruña, Spain.
chimenos@ub.edu

Ceramic-stone-porcelain (CSP) is generated in the soda-lime glass waste recycling process. Through the optical classification of glass, the opaque fragments are separated from the transparent ones. CSP contains mainly thick glass or glass with labels, with a composition of around 84% of glass, 4% of ceramic and 4% of porcelain. PAVAL is an Al-rich waste generated during the recycling process of salt aluminium slag. A silica-rich waste (CSP) and an alumina-rich waste (PAVAL) could be valorised by mixing them to produce alkali-activated binders (AABs), increasing the sustainability of the material and contributing to the circular economy.

The main goal of this work was to produce AABs using CSP and PAVAL as precursors and NaOH solution as the alkaline activator. The effect of the Na_2O/Al_2O_3 ratio was evaluated by varying the NaOH concentration (4 and 6 M) and the L/S ratio. A complete physicochemical characterisation of the binders was performed through FT-IR, XRD and SEM, while the mechanical, physical and environmental properties were assessed by measuring the compressive strength, porosity, apparent density, water resistance and leaching potential.

The formation of C-A-S-H, N-A-S-H, and (C,N)-A-S-H gels in the cement was monitored through XRD, FT-IR and SEM-EDS. The binders presented a very high porosity due to the reaction of NaOH and the aluminium nitride form PAVAL, limiting the mechanical properties in the most porous formulations. The highest compressive strength was obtained in the formulation with NaOH 6M and a Na_2O/Al_2O_3 ratio of 1.2. The environmental characterisation demonstrated the severe activation of some heavy metal(loid)s such as As, Sb, and Se with the high pH. However, the encapsulation efficiency of these heavy metal(loid)s improves over time. The properties of the binders suggest their feasible application for non-structural purposes or thermal and acoustic insulation.

Keywords: Alkali activation; waste glass; aluminium salt slag; waste valorisation; sustainable binders

INFLUENCE OF TREATMENT METHODS AND GRADATION OF RECYCLED AGGREGATE FROM CONSTRUCTION DEMOLITION WASTE (CDW) FOR A GREENER CONCRETE

Madhavi Latha Kasulanati, Rathish Kumar Pancharathi
National Institute of Technology, Warangal
madhavi@student.nitw.ac.in (corresponding author)

1. INTRODUCTION

The constructional activities utilize about 32% of world's resources, of which more than 75% is being discarded, according to the report by Green Building Council, Australia in 2009 (1). The Construction and Demolition waste (C & D Waste) account for about 50% of total municipal solid waste (2). The utilization of recycled materials from C & D Waste for a finite number of times of recycling of concrete is a novel approach for the effective recycling of waste, even after the end of life span of recycled concrete (3). The problem of disposal of demolished material or the discarded material not meeting the quality standards during the manufacture of high strength concrete or pre-cast concrete works requiring huge dumping yards can be overcome. The usage of conventional aggregate can be economized, thereby the non-renewable energy resources are conserved, improving the sustainability in the construction sector (4).

Aggregates occupying about 60-70 % of volume of concrete, form the skeleton and contribute to the strength and stability of concrete structure. The voids present in concrete should be minimised by improving the gradation of aggregate, to surpass the deterioration in the concrete quality due to the utilisation of recycled aggregate (5). The optimum gradation of aggregate can be achieved by using particle packing methods, where the proportion of each sized aggregate is designed to attain maximum packing density and minimum void ratio. The quantity of cement required to fill the voids in concrete is also reduced due to increase in the packing density. The Particle packing methods therefore improve the concrete skeletal structure, also accounting for the sustainability of concrete at the same time (6).

The present study utilizes Compressible Packing Model (CPM) (7) for gradation of multi-recycled aggregate, and the aggregate proportions corresponding to the maximum packing density are considered in the mix design of multi-recycled concrete (8). The quality constraint of recycled aggregate due to the presence of adhered mortar content and quality of parent concrete limits the utilization of the same for different applications. Recycled aggregate is found to have lower quality, compared to conventional aggregate, and the quality further decreases with the increase in the generation of recycling (9). The quality of recycled concrete can be improved using various methods such as surface coating of the aggregate using mineral admixtures prior to usage (10), using the aggregate in saturated surface dry condition to account for excess water absorption (11), treatment of inferior aggregate using carbon dioxide (12), removal of adhered mortar content from the aggregate surface. The present study investigates the removal of adhered mortar content from multi recycled aggregate surface using various methods viz., water soaking, mechanical treatment method (abrasion), thermo-mechanical treatment and chemical treatment.

2. MATERIALS AND METHODS

A laboratory investigation of aggregates of three generations of recycling obtained using Jaw crusher is part of the study. The physical properties viz., bulk density and specific gravity of natural and multi-recycled aggregate are determined and the gradation of aggregate is determined using Compressible Packing Model (CPM) of particle packing methods (13). The corresponding packing density, void ratio and the cement content to fill the voids are determined. The first, second and third generation recycled aggregate are subjected to surface treatment methods, to determine the optimum method of removal of adhered mortar content from the surface of aggregate.

In the first method of aggregate treatment, the multi-recycled aggregate, each of 250g is soaked in water for a period of 2 hours, air dried, subjected to abrasion and the weight is determined. In the second method, a set of samples of multi-recycled aggregate are subjected to a temperature of 300^0C for a period of 2 hours and then subjected to abrasion before determining the final weight of aggregate. In the third method, the recycled aggregates are subjected to heat treatment alone at a temperature of 500^0C for about 5 hours and the final weight of aggregate is determined. In the fourth method, the aggregates are initially soaked in Hydrochloric acid of 35% purity and sulphuric acid of 98% purity, 2M each. Trials are conducted by considering two volumetric ratios (V_{acid}/V_{agg}) of 2.5 and 5 for both the acids, considering 1kg of each sample. After soaking for a period of 24 hours, the aggregate samples are washed to remove the remains of acid particles, oven dried for a period of 1 hour and then subjected to abrasion.

3. RESULTS AND DISCUSSION

The variation of physical properties viz., bulk density and specific gravity of recycled aggregate of different generations compared to natural aggregate as per the sizes according to ASTM C33/C33 M-18 are shown in Table 1.

Table 1: Properties of Multi Recycled Aggregate

Sieve size (mm)	γ_b (NA)	γ_b (R1)	γ_b (R2)	γ_b (R3)	G (NA)	G (R1)	G (R2)	G (R3)
37.5-25	1430.00	1217.00	1090.00	1042.00	2.65	2.54	2.53	2.46
25-19	1414.00	1195.00	1085.00	1030.00	2.64	2.52	2.50	2.42
19-12.5	1376.00	1184.00	1060.00	1014.00	2.62	2.48	2.42	2.40
12.5-9.5	1392.00	1198.00	1073.00	1025.00	2.64	2.54	2.52	2.46
9.5-4.75	1360.00	1170.00	1048.00	1002.00	2.60	2.46	2.40	2.32
4.75-2.36	1490.00	1282.00	1148.00	1098.00	2.45	2.34	2.30	2.26
2.36-1.18	1516.00	1305.00	1168.00	1117.00	2.46	2.36	2.33	2.28
1.18-0.60	1492.00	1284.00	1150.00	1099.00	2.44	2.32	2.24	2.18
0.60-0.30	1450.00	1251.00	1121.00	1071.00	2.45	2.34	2.28	2.20
0.30-0.15	1420.00	1242.00	1150.00	1056.00	2.44	2.31	2.22	2.14

γ_b - Bulk Density; G – Specific gravity

It can be inferred from Table 1 that the properties of recycled aggregate are inferior than natural aggregate and the quality decreases with increase in the generation of recycling of concrete, due to the presence of adhered mortar content on the surface. The surface of aggregate smeared with adhered mortar for different generations of recycling are shown in Figure 1.

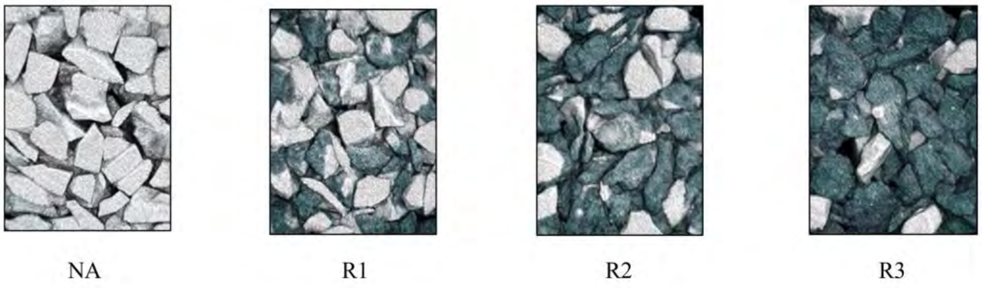

Fig.1: Multi-recycled aggregate (Thomas et al. 2018)

The aggregate percentage is shown in white colour while the adhered mortar is represented in grey colour to show the percentage increase in adhered mortar. The gradation of coarse aggregate as per the empirical relations of compressible Packing Model (14) to stabilize the aggregate skeleton and reduce the cement paste thickness required in the volume of concrete is represented in the form of a ternary diagram shown in Figure 2.

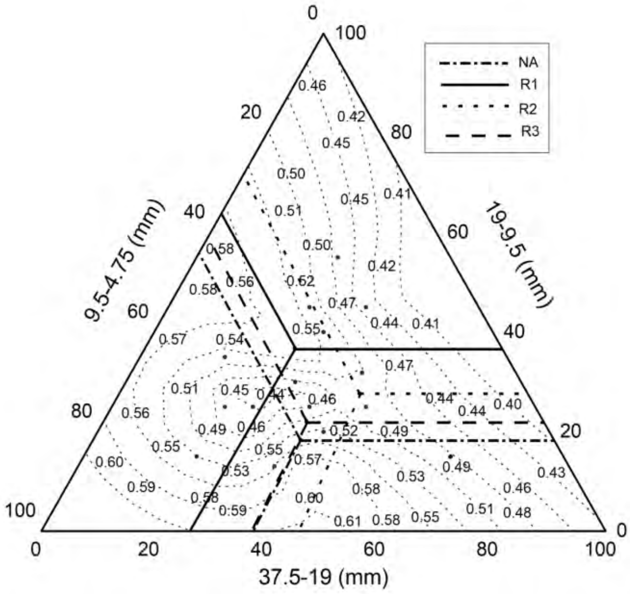

Fig.2: Ternary diagram of multi-recycled aggregate

Figure 2 shows the optimum percentage of different size fractions of coarse aggregate required for maximum packing density of aggregate in concrete volume. The fineness modulus of multi-recycled aggregate for fine aggregate (NFA, RF1, RF2 and RF3) is determined and is shown in Figure 3.

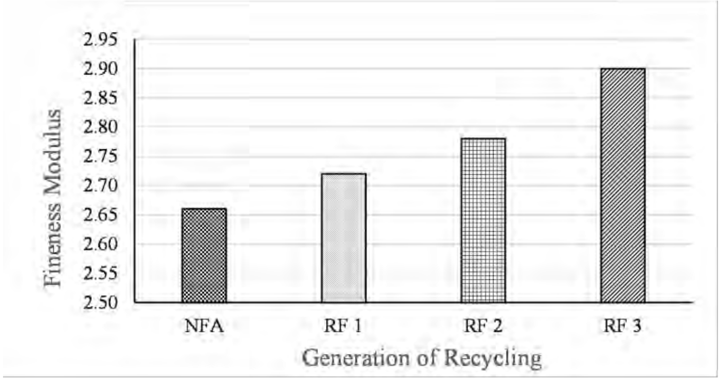

Fig.3: Fineness Modulus of Fine Multi-recycled Aggregate

The Fineness modulus is maximum for third-generation recycled aggregate, indicating increased coarseness of aggregate with increase in the generation of recycling attributed to the process of recycling.

To improve the properties of multi-recycled aggregate and for the aggregate to have properties as that of natural aggregate, the removal methods of adhered mortar are utilized. The methods of adhered mortar and the percentages removed by using the four methods considered in the present study are shown in Table 2.

Table 2: Percentage of Adhered mortar separated

Treatment method	**Percentage of adhered mortar separated**			
Generation of Recycling	**Water soaking**	**Thermal treatment**	**Thermo-Mechanical Treatment**	**Acid Treatment ($2M$-H_2SO_4)**
R1	8.40	10.00	56.60	61.00
R2	10.00	13.00	59.00	66.60
R3	12.80	14.60	61.50	71.80

The maximum percentage of adhered mortar content is removed using Acid Treatment method, as can be observed in Table 2. The Percentage removal increased with an increase in the generation of recycling indicating the weaker interfacial transition zone of third-generation recycled aggregate.

The properties of multi-recycled coarse aggregate after the removal of adhered mortar using acid soaking are shown in Table 3.

Table 3: Physical properties of Multi-Recycled Aggregate after treatment

Sieve size (mm)	γ_b (R1)	γ_b (R2)	γ_b (R3)	G (R1)	G (R2)	G (R3)
37.5-25	1340.00	1280.00	1265.00	2.60	2.57	2.50
25-19	1285.00	1278.00	1250.00	2.58	2.54	2.48
19-12.5	1270.00	1265.00	1242.00	2.54	2.50	2.48
12.5-9.5	1290.00	1270.00	1248.00	2.60	2.56	2.50
9.5-4.75	1210.00	1250.00	1230.00	2.52	2.48	2.40

From Table 3, it can be observed that the bulk density and specific gravity are increased after the treatment, due to the removal of adhered mortar. The aggregate properties are found to be similar to the natural aggregate (NA) for first-generation recycled aggregate (R1).
The gradation of coarse recycled aggregate of first, second and third generation before and after removal of adhered mortar are shown in Figure 4 (a), (b) and (c) respectively.

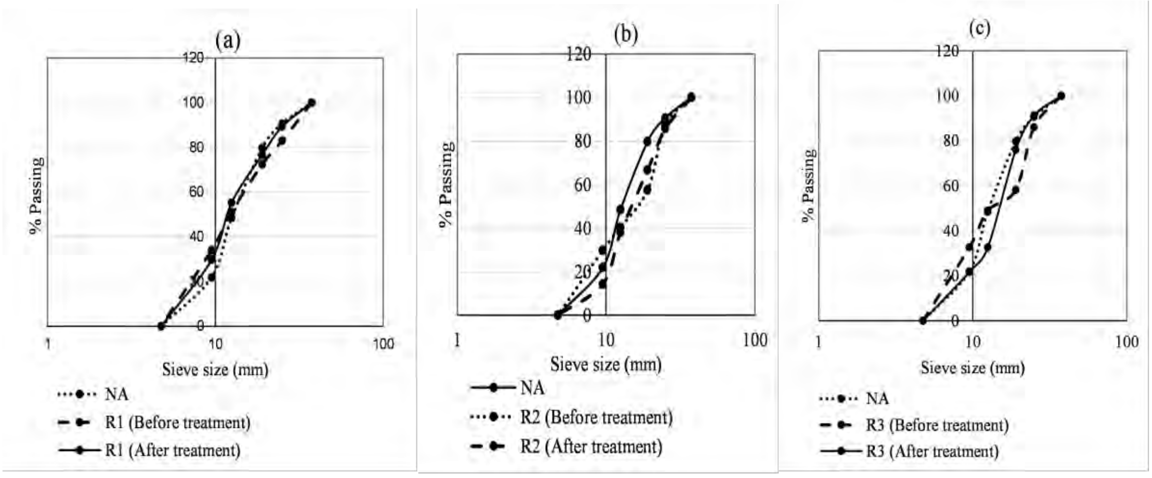

Figure 4: Gradation of Multi-Recycled Coarse Aggregate

From the above Figures, it can be observed that the gradation curves are aligned similarly to that of natural aggregate after treatment (acid soaking), compared to the gap-graded curves of multi-recycled coarse aggregate before treatment. Acid treatment method can be approved as the appropriate method for removal of adhered mortar, however, the concentration and the type of acid have to be chosen according to the type of aggregate, to avoid chemical reactions. Also, the aggregate has to be cleaned thoroughly, air dried prior to usage, as the acid particles may remain on the aggregate surface interfering with the aggregate quality.

4. CONCLUSIONS

1) The properties of aggregate deteriorate with an increase in the generation of recycling due to the presence of adhered mortar on the aggregate surface and the recycling process.
2) The roughness of aggregate increases with generation of recycling, as the fineness modulus of R3 is about 8.30%, 6.21% and 4.13% higher than NA, R1 and R2 respectively.
3) The average percentage of removal of adhered mortar content is about 10.40% using water soaking method, 12.53% using Thermal treatment, 59% using Thermo-mechanical treatment and 66.47% using acid soaking method making the acid soaking the appropriate procedure.

4) The properties of multi-recycled aggregate can be improved by optimum gradation of aggregate and by using appropriate treatment methods of adhered mortar removal, for the utilisation of aggregate in constructional activities.

5. REFERENCES

1) GBCA (2009) http://www.gbca.org.au/green-star/green-star-overview/. Retrieved 15 Oct 2009.
2) USEPA (U.S. Environmental Protection Agency) (1995) Construction and demolition waste landfills. Prepared by ECF Incorporated, Contract No. 68-W3-0008, February. http://www.epa.gov/epaoswer/hazwaste/sqg/const/cdrpt.pdf. Accessed 24 Nov 2011
3) Abreu, V., Evangelista, L., & De Brito, J. (2018). The effect of multi-recycling on the mechanical performance of coarse recycled aggregates concrete. *Construction and Building Materials*, *188*, 480-489.
4) McGinnis, M. J., Davis, M., de la Rosa, A., Weldon, B. D., & Kurama, Y. C. (2017). Quantified sustainability of recycled concrete aggregates. *Magazine of Concrete Research*, *69*(23), 1203-1211.
5) Pradhan, S., Kumar, S., & Barai, S. V. (2017). Recycled aggregate concrete: Particle Packing Method (PPM) of mix design approach. *Construction and Building Materials*, *152*, 269-284.
6) Fennis, S. A. A. M., & Walraven, J. C. (2012). Using particle packing technology for sustainable concrete mixture design. *Heron*, *57*(2), 73-101.
7) Karadumpa, C. S., & Pancharathi, R. K. (2021). Influence of particle packing theories on strength and microstructure properties of composite cement–based mortars. Journal of Materials in Civil Engineering, 33(10), 04021267.
8) Roquier, G. (2017). The 4-parameter Compressible Packing Model (CPM) for crushed aggregate particles. *Powder technology*, *320*, 133-142.
9) Zhu, P., Hao, Y., Liu, H., Wei, D., Liu, S., & Gu, L. (2019). Durability evaluation of three generations of 100% repeatedly recycled coarse aggregate concrete. *Construction and building materials*, *210*, 442-450.
10) Li, J., Xiao, H., & Zhou, Y. (2009). Influence of coating recycled aggregate surface with pozzolanic powder on properties of recycled aggregate concrete. *Construction and Building Materials*, *23*(3), 1287-1291.
11) Tam, V. W., Tam, C. M., & Le, K. N. (2007). Removal of cement mortar remains from recycled aggregate using pre-soaking approaches. *Resources, Conservation and Recycling*, *50*(1), 82-101.
12) Xuan, D., Zhan, B., & Poon, C. S. (2016). Assessment of mechanical properties of concrete incorporating carbonated recycled concrete aggregates. *Cement and Concrete Composites*, *65*, 67-74.
13) Karadumpa, C. S., & Pancharathi, R. K. (2021). Developing a novel mix design methodology for slow hardening composite cement concretes through packing density approach. Construction and Building Materials, 303, 124391.
14) Kasulanati, M. L., & Pancharathi, R. K. (2023). Particle Packing Approach for Proportioning Recycled Aggregate from Building Demolition Waste (BDW)—A Sustainable Solution. *Journal of The Institution of Engineers (India): Series A*, *104*(1), 207-222.

Session D1

Fibre Reinforced Materials

UTILISATION OF ELECTROLYTIC MANGANESE RESIDUE AS A SULPHATE ACTIVATOR IN PRODUCING CONCRETE BLOCKS WITH HIGH-VOLUME FLY ASH

Wenjie Luo[1,2], **Bo Li**[1,3,4], Gang Yang[2,4], Mengxia Xu[2,3,4], Chengheng Pang[2,3,4], Kien-Woh Kow[2,3], Two Wu[2,3,4]

[1]Department of Civil Engineering, University of Nottingham Ningbo China, 199 Taikang Road, Ningbo 315100, China
[2]Department of Chemical and Environmental Engineering, University of Nottingham Ningbo China, 199 Taikang Road, Ningbo 315100, China
[3]Key Laboratory for Carbonaceous Wastes Processing and Process Intensification Research of Zhejiang Province, University of Nottingham Ningbo China, Ningbo 315100, China
[4]New Materials Institute, University of Nottingham Ningbo China, Ningbo 315100, China
E-mail (corresponding author): bo.li@nottingham.edu.cn

ABSTRACT

Electrolytic manganese residue (EMR) is a by-product of the electrolytic manganese metal industry, and its generation and accumulation have raised concerns about sustainability. This paper investigates the feasibility of using pre-treated EMR and fly ash (FA) in the production of concrete blocks. Pre-treated EMR serves as an activator to interact with Al_2O_3 and $Ca(OH)_2$ in the mix. Engineering properties and durability of the blocks with pre-treated EMR are evaluated, including permeable porosity, compressive strength, and drying-wetting performance. Their microstructures and the leaching behaviour of hazardous elements are also studied. The results indicate that replacing sand with 0-30 wt% pre-treated EMR can improve the blocks' compressive strength while decreasing the permeable porosity. Nonetheless, increasing the pre-treated EMR content degrades the blocks' resistance to water as a result of the presence of dihydrate gypsum. Replacing 0-30 wt% of ordinary Portland cement (OPC) with FA supplies reactive SiO_2 and Al_2O_3 to the system with pre-treated EMR as a sulphate activator. This leads to the formation of ettringite, which interconnects micro particles and fills pores. The resulting concrete blocks with OPC and FA have comparable properties to those with OPC only. Leaching tests demonstrate that the hazardous elements in EMR can be effectively solidified in the concrete blocks. Incorporating 0-30 wt% FA further strengthens the solidification of Mn in the blocks due to the more intense ion substitution and physical encapsulation that stem from the enhanced formation of ettringite. Overall, this study proposes a sustainable technical solution for the utilization of EMR in concrete blocks with high-volume FA.

Keywords: electrolytic manganese residue; fly ash; sulphate activation; concrete block; mechanical properties.

1. INTRODUCTION

Electrolytic manganese residue (EMR) has been widley used as raw materials in cement production [1,2], supplementary cementitious materials (SCMs) [3-5], concrete fillers [6,7], road base materials [8,9], and aggregates in concrete blocks [10-13]. Among them, utilising EMR in concrete block fabrication has attracted significant attention, as it has potential to consume a considerable quantity of EMR. The content of EMR in concrete blocks can reach 15–90 wt% of solid raw materials. Additionally, national policies strongly encourage the use of industrial solid waste into non-sintered concrete blocks. Zhou *et al.* [10], Du *et al.* [11], Li *et al.* [12], and Wang *et al.* [13] have reported the concrete blocks containing EMR can achieve a compressive strength ranging from 20 MPa to 23.5 MPa and a permeability coefficient of 2.3×10^{-2}–4.1×10^{-2} cm/s. However, the role of EMR in the concrete blocks has been not clearly revealed yet, which necessitates a further investigation.

On the other hand, the use of high-volume fly ash binder (*e.g.*, ≥30 wt% coal fly ash of cement [14]) has many economic and environmental benefits [15-17]. However, the blocks containing high-volume FA binder but without additives show a low mechanical strength, which can be significantly improved by the addition of gypsum [18-20]. This is mainly induced by the densified microstructure achieved by the pore filling behaviour of ettringite (AFt). The AFt is formed by gypsum interacting with FA-dissolved reactive alumina and portlandite via the "sulphate activation" [9]. Since EMR contains a high content of gypsum, it could potentially serve as not only a substitute for aggregates in concrete blocks but also an efficient sulphate activator for high-volume FA cement. Nonetheless, there are limited studies focusing on utilising EMR and high-volume FA in the production of concrete blocks.

Therefore, this paper aims to systematically investigate the role of EMR in concrete blocks and explore the feasibility of using EMR as a sulphate activator in the blocks with high-volume FA. The engineering properties of the concrete blocks are evaluated, including the volume of permeable voids, compressive strength, and wetting-drying performance, while their microstructure is analysed in terms of reaction heat release, phase change, micromorphology, and elemental composition. In addition, the leaching behaviour of the concrete blocks is also studied to validate the stabilization of hazard elements. This study can guide the mix design and production of concrete blocks with EMR and high-volume FA.

2. MATERIALS AND METHODS

Pretreated EMR, low-calcium fly ash (FA), $42.5^{\#}$ ordinary Portland cement (OPC), river sand, and tap water were used to prepare the concrete block samples. The river sand (fully oven-dried at 105 °C) was first replaced by PEMR (fully oven-dried at 60 °C) at a level of 0–60 wt%. The FA was then added to further replace OPC at a level of 0–60 wt% when the PEMR content kept constant at 30 wt%. The mixtures incorporated with FA but without PEMR were designed as control groups, whereby the influence of sulphate activation achieved by PEMR can be examined. It should be noted that the effective water-to-binder ratio (i.e., w/b ratio) and the aggregate-to-binder ratio remained constant at 0.25 and 6, respectively.

The volume of permeable voids, compressive strength, drying-wetting of the concrete blocks were measured according to various standards. The samples used for the micro-analyses were collected from the mid-section of the concrete blocks. The reaction of the sample was terminated by immersing in isopropanol for 24 hours, followed by vacuum desiccation at 40 °C for 24 h. Heat release of reaction was monitored by isothermal calorimeter at a constant temperature of 20 °C for 14 d. The crystalline compositions of the concrete blocks were examined by X-ray diffraction (XRD), which was conducted on powdered samples at a scan rate of 0.02 °/step and 5 °/min via Cu-Kα radiation (λ = 1.54 Å) over an angular range of 5–20°. Attenuated total reflectance Fourier transform infrared spectroscopy (ATR-FTIR) was performed on powdered samples at a wavenumber interval of 2 cm^{-1} over a wavenumber range of 400–4000 cm^{-1}. The thermogravimetric analysis (TGA) was conducted through heating up 40 mg of powdered sample in a nitrogen atmosphere from 30 to 500 °C at a heating rate of 10 °C/min. The flow rate of nitrogen adopted was fixed at 50 ml/min. Back-scatter electron imaging coupled with energy dispersive spectroscopy (BSE-EDS) was performed on the polished samples at an acceleration voltage of 20 kV, whilst secondary electron imaging coupled with energy dispersive spectroscopy (SE-EDS) was performed on crushed samples at an acceleration voltage of 5–10 kV depending on different samples. The leaching test was carried out for EMR, PEMR, and concrete blocks with PEMR.

3. RESULTS AND DISCUSSION

The volume of permeable voids, compressive strength, drying-wetting performance of the concrete blocks containing different amounts of PEMR and FA will be presented and analysed. The reaction products in the blocks will be characterized by XRD, TG, ATR-FRIT, SEM-EDX to reveal the role of EMR in cement hydration. Moreover, the leaching behaviour of hazardous elements (e.g., Mn, Co, Ni, and Zn) from the EMR, PEMR, and concrete blocks was examined according to toxicity characteristic leaching procedure (TCLP).

4. CONCLUSION

This paper investigated the feasibility of combinedly utilising EMR and fly ash in the manufacture of concrete blocks. The volume of permeable voids, compressive strength, drying-wetting performance, microstructure, and leaching behaviour of the concrete blocks with different contents of PEMR and FA were characterised. Based on the results and discussion, conclusions can be drawn as follows. For the concrete blocks with 30 wt% PEMR, substituting 0–30 wt% of OPC by FA can maintain the permeable porosity and the 56-day compressive strength of the blocks. The FA with reactive Al_2O_3 and SiO_2 can be activated by the PEMR through sulphate activation, promoting the formation of AFt that can better fill up pores and bridge micro-particles to densify the microstructure. However, a substitution ratio above 30 wt% triggers a remarkable rise in the porosity and compromises the compressive strength due to the reduced formation of C-(A)-S-H and AFt.

5. ACKNOWLEDGMENT

The authors wish to acknowledge the financial support from Zhejiang Provincial Department of Science and Technology under Zhejiang Provincial Key R&D Programme (No.: 2023C03146) and Zhejiang Commonweal Programme (No.: LGF22B060009), Ningbo Municipal Bureau of Science and Technology under Commonweal Programme (No.: 2022S177 and 2021S097), and Zhejiang Provincial Key Laboratory for Carbonaceous Wastes Processing and Process Intensification Research funded by the Zhejiang Provincial Department of Science and Technology (2020E10018).

6. REFERENCES

[1] F. Wang, G. Long, M. Bai, J. Wang, Y. Shi, X. Zhou, J.L. Zhou, A new perspective on Belite-ye'elimite-ferrite cement manufactured from electrolytic manganese residue: Production, properties, and environmental analysis, Cement and Concrete Research. 163 (2023) 107019. https://doi.org/10.1016/j.cemconres.2022.107019.

[2] P. Hou, J. Qian, Z. Wang, C. Deng, Production of quasi-sulfoaluminate cementitious materials with electrolytic manganese residue, Cement and Concrete Composites. 34 (2012) 248–254. https://doi.org/10.1016/j.cemconcomp.2011.10.003.

[3] F. Wang, G. Long, M. Bai, J. Wang, J.L. Zhou, X. Zhou, Application of electrolytic manganese residues in cement products through pozzolanic activity motivation and calcination, Journal of Cleaner Production. 338 (2022) 130629. https://doi.org/10.1016/j.jclepro.2022.130629.

[4] X. Liu, Y. Li, L. Zhang, D. Cang, S. Zhou, Phase transitions relating to the pozzolanic activity of electrolytic manganese residue during calcination, J. Shanghai Jiaotong Univ. (Sci.). 18 (2013) 105–110. https://doi.org/10.1007/s12204-013-1372-7.

[5] D. Wang, J. Fang, Q. Wang, Y. Liu, Utilizing desulphurized electrolytic-manganese residue as a mineral admixture: A feasibility study, Cement and Concrete Composites. 134 (2022) 104822. https://doi.org/10.1016/j.cemconcomp.2022.104822.

[6] N. Chousidis, I. Ioannou, G. Batis, Utilization of Electrolytic Manganese Dioxide (E.M.D.) waste in concrete exposed to salt crystallization, Construction and Building Materials. 158 (2018) 708–718. https://doi.org/10.1016/j.conbuildmat.2017.10.036.

[7] C. Yang, X. Lv, X. Tian, Y. Wang, S. Komarneni, An investigation on the use of electrolytic manganese residue as filler in sulfur concrete, Construction and Building Materials. 73 (2014) 305–310. https://doi.org/10.1016/j.conbuildmat.2014.09.046.

[8] Y. Zhang, X. Liu, Y. Xu, B. Tang, Y. Wang, E. Mukiza, Synergic effects of electrolytic manganese residue-red mud-carbide slag on the road base strength and durability properties, Construction and Building Materials. 220 (2019) 364–374. https://doi.org/10.1016/j.conbuildmat.2019.06.009.

[9] Y. Zhang, X. Liu, Y. Xu, B. Tang, Y. Wang, E. Mukiza, Preparation and characterization of cement treated road base material utilizing electrolytic manganese residue, Journal of Cleaner Production. 232 (2019) 980–992. https://doi.org/10.1016/j.jclepro.2019.05.352.

[10] C. Zhou, B. Du, N. Wang, Z. Chen, Preparation and strength property of autoclaved bricks from electrolytic manganese residue, Journal of Cleaner Production. 84 (2014) 707–714. https://doi.org/10.1016/j.jclepro.2014.01.052.

[11] B. Du, C. Zhou, Z. Dan, Z. Luan, N. Duan, Preparation and characteristics of steam-autoclaved bricks produced from electrolytic manganese solid waste, Construction and Building Materials. 50 (2014) 291–299. https://doi.org/10.1016/j.conbuildmat.2013.09.055.

[12] J. Li, Y. Lv, X. Jiao, P. Sun, J. Li, L. Wuri, T.C. Zhang, Electrolytic manganese residue based autoclaved bricks with Ca(OH)2 and thermal-mechanical activated K-feldspar additions, Construction and Building Materials. 230 (2020) 116848. https://doi.org/10.1016/j.conbuildmat.2019.116848.

[13] Y. Wang, S. Gao, X. Liu, B. Tang, E. Mukiza, N. Zhang, Preparation of non-sintered permeable bricks using electrolytic manganese residue: Environmental and NH3-N recovery benefits, Journal of Hazardous Materials. 378 (2019) 120768. https://doi.org/10.1016/j.jhazmat.2019.120768.

[14] M. Mccarthy, R. Dhir, Development of high volume fly ash cements for use in concrete construction, Fuel. 84 (2005) 1423–1432. https://doi.org/10.1016/j.fuel.2004.08.029.

[15] P.R. de Matos, M. Foiato, L.R. Prudêncio, Ecological, fresh state and long-term mechanical properties of high-volume fly ash high-performance self-compacting concrete, Construction and Building Materials. 203 (2019) 282–293. https://doi.org/10.1016/j.conbuildmat.2019.01.074.

[16] I.R. Mocharla, R. Selvam, V. Govindaraj, M. Muthu, Performance and life-cycle assessment of high-volume fly ash concrete mixes containing steel slag sand, Construction and Building Materials. 341 (2022) 127814. https://doi.org/10.1016/j.conbuildmat.2022.127814.

[17] D.K. Panesar, D. Kanraj, Y. Abualrous, Effect of transportation of fly ash: Life cycle assessment and life cycle cost analysis of concrete, Cement and Concrete Composites. 99 (2019) 214–224. https://doi.org/10.1016/j.cemconcomp.2019.03.019.

[18] X. Aimin, S.L. Sarkar, Microstructural study of gypsum activated fly ash hydration in cement paste, Cement and Concrete Research. 21 (1991) 1137–1147. https://doi.org/10.1016/0008-8846(91)90074-R.

[19] C.S. Poon, S.C. Kou, L. Lam, Z.S. Lin, Activation of fly ash/cement systems using calcium sulfate anhydrite (CaSO4), Cement and Concrete Research. 31 (2001) 873–881. https://doi.org/10.1016/S0008-8846(01)00478-1.

[20] A. Thymotie, T.-P. Chang, H.-A. Nguyen, Improving properties of high-volume fly ash cement paste blended with β-hemihydrate from flue gas desulfurization gypsum, Construction and Building Materials. 261 (2020) 120494. https://doi.org/10.1016/j.conbuildmat.2020.120494.

ADVANCING CEMENTITIOUS COMPOSITES: UNLEASHING THE POTENTIAL OF RECYCLED CARBON FIBERS FOR ENHANCED MECHANICAL AND FUNCTIONAL PERFORMANCE

Chun PEI[1], Zhenxuan LIANG[1], and Ji-Hua ZHU[1*]

[1]Guangdong Province Key Laboratory of Durability for Marine Civil Engineering, College of Civil and Transportation Engineering, Shenzhen University, Shenzhen, Guangdong, People's Republic of China
E-mail: zhujh@szu.edu.cn

1. INTRODUCTION

Cementitious materials, due to their relative affordability, ease of sourcing, and high compressive strength, have been widely adopted in the civil engineering industry[1,2]. Nevertheless, conventional cementitious materials suffer from issues such as low tensile strength, poor toughness, and significant self-weight, leading to a propensity for brittle failure and an inability to meet durability requirements. The incorporation of fibers into cementitious materials has proven effective in addressing these challenges. Among them, carbon fibers have garnered significant attention owing to their high specific strength, stiffness, lightweight, and corrosion resistance, which can enhance the structural and durability properties of cementitious materials[3,4]. However, the practical application of virgin carbon fibers (vCFs) in cementitious materials is limited due to their poor dispersion, weak interfacial bonding performance, and, especially, high cost.

The utilization of recycled carbon fibers (rCFs) derived from carbon fiber reinforced polymers (CFRP) waste can provide a dual benefit in terms of resource conservation and environmental impact. This paper presents a comprehensive study on the influence and mechanism analysis of rCFs, obtained through our previously developed non-destructive CFRP recycling technique[5–8], on the mechanical and functional properties of cement mortar. It is demonstrated that the performance of cementitious composite materials reinforced with rCFs is comparable to that of the vCFs-reinforced cementitious composites, highlighting the significant potential of rCFs for practical application for enhancing cementitious composites.

2. MATERIALS AND METHODS

2.1 Materials

The cementitious material was composed of cement, fly ash, and silica fume. The cement (P.O.42.5) used in this study sourced from Longshan Cement Co., Ltd. The fly ash (Class II) was obtained from Zhong Yong Tong Industrial Development Co., Ltd. The high-purity silica fume was provided by Henan Borun Casting Materials Co., Ltd. The aggregate fine sand (particle size: 250μm, maximum particle size ≤800μm, specific gravity: 2.55) was procured from Fujian Weineng Building Materials Co., Ltd. High-performance polycarboxylate-based water-reducing agent (solid content: 25%, water-reducing rate ≥40%) was produced by Guangdong Foshan Futian New Materials Co., Ltd.

The vCFs (GQ-3522, average diameter: 7μm) were manufactured by Weihai Guangwei Composite Materials Co., Ltd. The rCFs were obtained through recycling carbon fiber composite waste, and further details regarding the specific process and parameters can be found in the reference provided[5–8].

2.2 Methods

The matrix mix proportions of carbon fiber-reinforced cementitious composites are presented in Table 1.

Table 1Proportions of constituents in the matrix

Matrix Type	Cement	Fly Ash	Silica Fume	Sand	Water	Superplasticizer
Cement Mortar	1	0.3	0.1	1	0.38	0.009
Cement Paste	1	-	-	-	0.38	0.009

Carbon fiber-reinforced cement pastes and mortar with vCFs and rCFs were prepared accordingly. The flexural strength, compressive strength, electrical conductivity, and thermal conductivity tests were conducted on prismatic specimens measuring 160mm×40mm×40mm according to GB-T17671-1999, ASTM G57-2006(2012), and GB/T 10297-2015, respectively. Tensile splitting tests and dispersion tests were performed on cubic specimens with a side length of 40mm according to GB/T 50081-2019. For porosity tests, cubic specimens with a side length of 10mm were utilized. After molding, the specimens were demolded and kept under normal temperature and pressure conditions for one day, then transferred to standard curing conditions (T = 20±2°C, humidity⩾ 95%) until reaching the designated testing age.

3. RESULTS AND DISCUSSION

The specimens of 40mm×40mm×40mm were prepared and cut into 4 pieces along the lateral direction at equal intervals, forming three cross-sectional surfaces. Each surface was divided into 25 small observation areas. The maximum interclass variance method[9] was employed to convert the original images into binary images. The slice dispersion coefficient was calculated respetively.

The dispersion characteristics and dispersion coefficients of carbon fiber in the composite materials are shown in Figure 1. It can be observed that both vCFRM and rCFRM dispersion coefficients exhibit an increasing trend with the rise in the carbon fiber content, indicating that a higher content leads to a decrease in the dispersion of carbon fiber in the cementitious matrix. Furthermore, rCFs have a higher carbon-oxygen functional group content than vCFs, which improves their hydrophilicity and enhances their interfacial adhesion with the cementitious matrix. Consequently, the aggregation of rCFs during the mixing process is reduced. As a result, at various carbon fiber contents, the dispersion coefficients of rCFs are lower than those of vCFs, implying that rCFs are more likely to achieve uniform dispersion in the cementitious matrix compared to vCFs. Longer carbon fibers are more prone to entanglement, leading to aggregation and reduced dispersion within the cementitious matrix as their length increases. However, under the same conditions, optimized rCFs are less likely to become entangled, and thus, their dispersion is superior to that of vCFs.

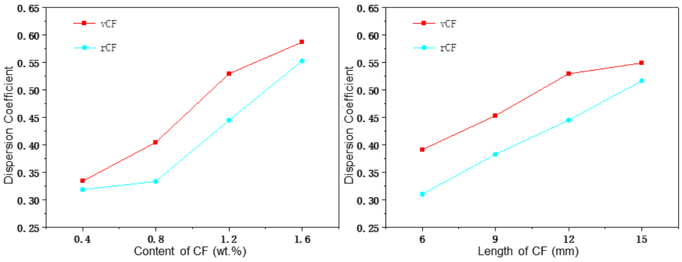

Figure 1 Dispersion coefficient of CFRM with different carbon fiber content and length

The dispersion of carbon fibers in cement mortar was observed using the SEM cross-sectional observation method, as shown in Figures 2. The distribution of rCFs (reinforcing carbon fibers) and vCFs (vapor-grown carbon fibers) in SEM images[10] was found to be similar to that obtained from digital image quantification analysis. This indicates that the distribution pattern of rCFs in cement mortar is consistent with that in the cementitious matrix and is superior to the distribution of vCFs. The experimental results of mercury intrusion porosimetry (MIP) (Figure 3) revealed that the porosity of rCFRM (carbon fiber-reinforced mortar) was lower than that of vCFRM. However, rCFRM had a smaller proportion of harmful and detrimental pores, indicating a more favorable microstructure[11,12].

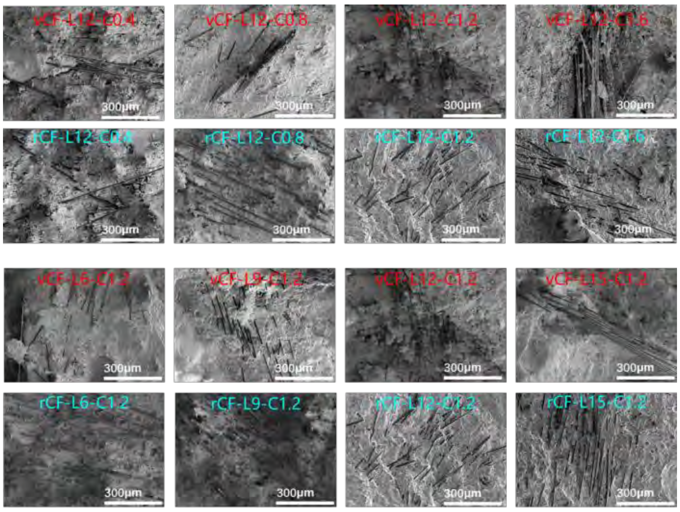

Figure 2 SEM profile of vCFRM and rCFRM with the change of carbon fiber content

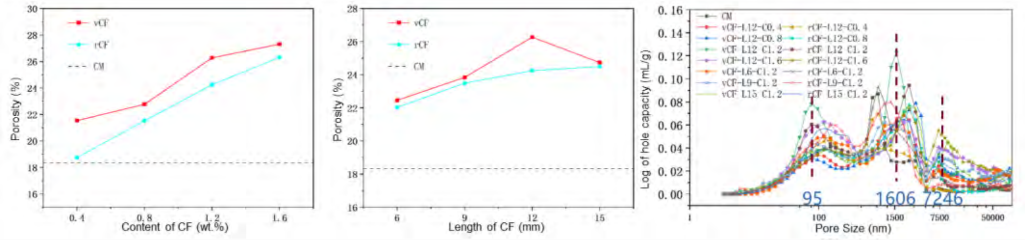

Figure 3 Porosity analysis of vCFRM and rCFRM

The flexural strength (Figure 4) of rCFRM and vCFRM was generally comparable, with a difference of within ±5%. The flexural strength of rCFRM exhibited a trend of initially increasing and then decreasing with an optimal rCFs content of 1.2 wt%. On the other hand, the flexural strength of rCFRM displayed a trend of first slowly decreasing, then sharply increasing, and finally declining with an optimal rCFs length of 12mm. At a content of 1.2wt% and length of 12mm, the flexural strength reached 11.5 MPa, representing a 19.1% improvement over the traditional CM material. rCFRM demonstrated a slight advantage in compressive strength compared to vCFRM (Figure 4). The compressive strength of rCFRM varied with the content and length of rCFs in a manner similar to the flexural strength variation. The optimal content of rCFs was 1.2wt%, and the best length was 6mm, resulting in a compressive strength of 78.1 MPa, a 12.8% increase compared to CM. In comparison to vCFRM, the fracture behavior of rCFRM remained unchanged, while the ultimate load capacity for fracture increased (Figure 4). At a content of 1.2wt% and length of 12mm, the fracture strength was 9.06 MPa, representing a significant 51.0% improvement over CM.

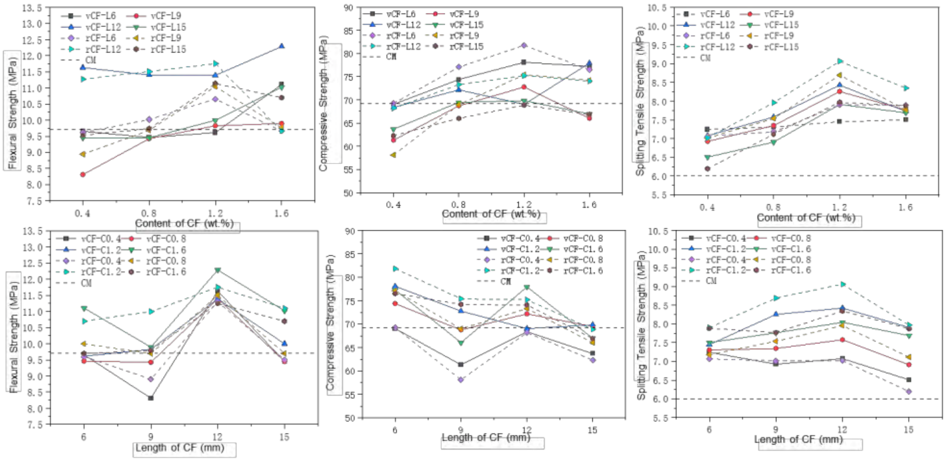

Figure 4 Mechanical properties of CFRM with different carbon fiber content and length

Both vCFs and rCFs effectively reduced the electrical resistivity of cement mortar (Figure 5). The optimal electrical resistivity for vCFRM was 153.4 Ω.cm, a 99.6% reduction compared to CM, while for rCFRM, the optimal resistivity was 215 Ω.cm, a 99.4% decrease compared to CM. Furthermore, rCFRM exhibited a maximum thermal conductivity value of 1.79 W/(m.K), representing a 16.5% enhancement compared to CM (Figure 5)..

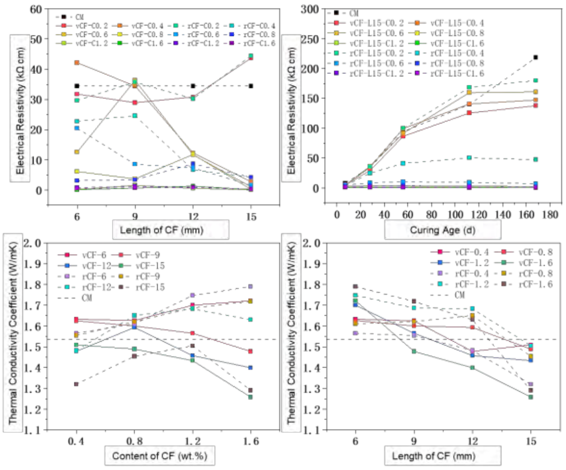

Figure 5 Functional properties of CFRM with different carbon fiber content and length

4. CONCLUSION

Based on the previous research achievements of our research group concerning the favorable interfacial properties of rCFs with cementitious materials, this study aims to explore the incorporation of rCFs to enhance cement mortar and compare it with vCFRM. The results of this investigation demonstrate that rCFs exhibit superior dispersion and lower porosity compared to vCFs, thereby indicating that the macroscopic performance of rCFRM is comparable to or slightly better than vCFRM. This study not only addresses the environmental pollution caused by waste CFRP but also overcomes the cost bottleneck associated with large-scale application of carbon fiber-reinforced concrete, thus providing a practical and feasible approach for the circular utilization of carbon fiber materials in civil engineering applications.

5. ACKNOWLEDGMENT

The authors would like to express appreciation for the support of the National Natural Science Foundation of China [Project Number: 52108231], the Key-Area Research and Development Program of Guangdong Province [Project Number: 2019B111107002], and the Shenzhen Science and Technology Innovation Program [Project Number: 20220810140230001, 20220810160453001].

6. REFERENCES

(1) Khan, M. I.; Abbas, Y. M.; Fares, G. Review of High and Ultrahigh Performance Cementitious Composites Incorporating Various Combinations of Fibers and Ultrafines. *Journal of King Saud University - Engineering Sciences* **2017**, *29* (4), 339–347. https://doi.org/10.1016/j.jksues.2017.03.006.

(2) Wang, C.; Yang, C.; Liu, F.; Wan, C.; Pu, X. Preparation of Ultra-High Performance Concrete with Common Technology and Materials. *Cement and Concrete Composites* **2012**, *34* (4), 538–544. https://doi.org/10.1016/j.cemconcomp.2011.11.005.

(3) Pei, C.; Wei, L.; Qin, Z.; Yu, H.; Zhu, J.-H.; Xing, F. Behavior and Design of Nano/Micro-Scale Carbon Modified Multifunctional Cementitious Composites. *Construction and Building Materials* **2022**, *314*, 125506. https://doi.org/10.1016/j.conbuildmat.2021.125506.

(4) Yu, H.; Lei, Y.; Pei, C.; Wei, L.; Zhu, J.-H.; Xing, F. Enhancing the Mechanical and Functional Performance of Carbon Fiber Reinforced Cement Mortar by the Inclusion of a Cost-

Effective Graphene Nanofluid Additive. *Cement and Concrete Composites* **2022**, *134*, 104777. https://doi.org/10.1016/j.cemconcomp.2022.104777.

(5) Chen, P.; Pei, C.; Zhu, J.-H.; Su, M.; Xing, F. Sustainable Recycling of Intact Carbon Fibres from End-of-Service-Life Composites. *Green Chemistry* **2019**, *21* (17), 4757–4768. https://doi.org/10.1039/C9GC01847F.

(6) Pei, C.; Chen, P.; Kong, S.-C.; Wu, J.; Zhu, J.-H.; Xing, F. Recyclable Separation and Recovery of Carbon Fibers from CFRP Composites: Optimization and Mechanism. *Separation and Purification Technology* **2022**, *278*, 119591. https://doi.org/10.1016/j.seppur.2021.119591.

(7) Pei, C.; Guo, P.; Zhu, J.-H. Orthogonal Experimental Analysis and Mechanism Study on Electrochemical Catalytic Treatment of Carbon Fiber-Reinforced Plastics Assisted by Phosphotungstic Acid. *Polymers* **2020**, *12* (9), 1866. https://doi.org/10.3390/polym12091866.

(8) Zhu, J.-H.; Chen, P.; Su, M.; Pei, C.; Xing, F. Recycling of Carbon Fibre Reinforced Plastics by Electrically Driven Heterogeneous Catalytic Degradation of Epoxy Resin. *Green Chemistry* **2019**, *21* (21), 1635–1647. https://doi.org/10.1039/C8GC03672A.

(9) Otsu, N. A Threshold Selection Method from Gray-Level Histograms. *IEEE Transactions on Systems, Man, and Cybernetics* **1979**, *9* (1), 62–66. https://doi.org/10.1109/TSMC.1979.4310076.

(10) Khushnood, R. A.; Muhammad, S.; Ahmad, S.; Tulliani, J. M.; Qamar, M. U.; Ullah, Q.; Khan, S. A.; Maqsom, A. Theoretical and Experimental Analysis of Multifunctional High Performance Cement Mortar Matrices Reinforced with Varying Lengths of Carbon Fibers. *Materiales de Construcción* **2018**, *68* (332), e172. https://doi.org/10.3989/mc.2018.09617.

(11) Baeza, F. J.; Galao, O.; Zornoza, E.; Garcés, P. Effect of Aspect Ratio on Strain Sensing Capacity of Carbon Fiber Reinforced Cement Composites. *Materials & Design* **2013**, *51*, 1085–1094. https://doi.org/10.1016/j.matdes.2013.05.010.

(12) Díaz, B.; Guitián, B.; Nóvoa, X. R.; Pérez, C. Analysis of the Microstructure of Carbon Fibre Reinforced Cement Pastes by Impedance Spectroscopy. *Construction and Building Materials* **2020**, *243*, 118207. https://doi.org/10.1016/j.conbuildmat.2020.118207.

INCORPORATION OF CALCINED BAUXITE AGGREGATE AND MICRO FIBRILLATED CELLULOSE FOR IMPROVED PROJECTILE IMPACT RESISTANCE OF CEMENTITIOUS COMPOSITES

Zhong, R., **Ai, Xianbing**, and Wang, J.

Engineering Research Center of Safety and Protection of Explosion & Impact of Ministry of
Education, School of Civil Engineering, Southeast University, Nanjing 211189, China
E-mail: cerzhong@seu.edu.cn

This experimental study evaluated the effectiveness of passive and active strategies in improving the projectile impact resistance of cementitious matrices. The principle of the passive approach is to reinforce the matrix by substituting weak Van de Waal’s forces between hydration products with covalent bonds which possesses orders of magnitude higher dissociation energy. A silane coupling agent (SCA) and micro fibrillated cellulose (MFC) were selected as the vehicles to engineering the bond scheme at the molecular scale by forming a covalently linked organic-inorganic hybrid. The mechanism of the active strategy is to aggravate damage to the projectile and thus leave less energy available for the penetration process. This is achieved by incorporating exceptionally hard calcined bauxite aggregates (CBA). Impact tests were conducted utilizing 8-mm-diameter conical-nosed steel projectiles at a designed velocity of 650 m/s. Damage was quantified by the depth of penetration (DOP) and equivalent crater diameter (ECD). Results indicated that the SCA and MFC modified matrices resulted in a 30% and 20% reduction in DOP, respectively. The crack intensity was decreased tremendously or even absent for the SCA and MFC modified matrices compared with the prominent cracks of the control radiated from the cratering region. Matrices incorporating fine CBA or siliceous aggregates led to a 55% and 38% smaller DOP, respectively. Crushing of aggregates and appreciable deformation, severe scratches, and significant mass loss of retrieved projectiles were observed. Matrices including fine CBA or siliceous aggregate maintained excellent integrity and drastically less severe cracking on the impact surface as well as the interior region compared with the control.

Keywords: Calcined bauxite aggregate; micro fibrillated cellulose; silane coupling agent; projectile impact; penetration depth

A TARGETED APPROACH OF USING GRAPHENE OXIDE TO ENHANCE THE INTERFACIAL TRANSITION ZONE IN RECYCLED AGGREGATE CONCRETE

Dong Lu[1], Zhen Leng[1,2,*], and Jing Zhong[3,*]

[1]Department of Civil and Environmental Engineering, The Hong Kong Polytechnic University, Kowloon, 999077 Hong Kong, PR China
[2]Research Centre for Resources Engineering towards Carbon Neutrality, The Hong Kong Polytechnic University, Kowloon, 999077 Hong Kong, PR China
[3]School of Civil Engineering, Harbin Institute of Technology, Harbin 150090, PR China
E-mail: zhen.leng@polyu.edu.hk (Z. Leng), zhongjing@hit.edu.cn (J. Zhong).

Recycled concrete aggregate (RCA) is composed of virgin aggregate and adhered mortar, and the latter has been demonstrated to cause several drawbacks of RCA, such as high porosity, water absorption, and crushing value. This is primarily due to the formation of weak interface transition zones (ITZs) when the RCA is admixed, significantly impairing its mechanical and durability properties. To address this issue, this study proposes a targeted approach to enhance the ITZ property of RCA by utilizing graphene oxide (GO) pre-wet RCA (referred to as GO@RCA) instead of adding GO into the cement matrix. Experimental results exhibit remarkable enhancements in the 28-day compressive and splitting tensile strength of RAC by approximately 30% and 40% respectively, when employing GO@RCA to replace RCA. Further, the GO coating significantly reduces the water absorption coefficient and the total charge passed of the concrete by around 15% and 60% respectively, ensuring its long-term durability. These improvements in the mechanical and durability properties of RCA is mainly attributed to the sub-nanometer thickness of GO coated on the surface of RCA and its hydrophilic functional groups, which locally promote cement hydration at the ITZ.

Keywords: Recycled aggregate concrete; Nano-engineering; Graphene oxide; Interface transition zone; Renewable resource

FRESH AND HARDENED PROPERTIES OF RECYCLED STEEL FIBER REINFORCED SUSTAINABLE SELF-COMPACTING CONCRETE WITH RECYCLED CONCRETE AGGREGATES

Yi liu[1], Shanli Lin[1], Qingyang Zhang[1], **Zhanggen Guo**[1,*], Ben Cai[1], Weidong Lin[1]

* Corresponding author at: School of Civil Engineering, Nanjing Tech University, 30 Puzhu Road(S), Nanjing, 211800, China. E-mail: zhgguo@njtech.edu.cn

1. INTRODUCTION

The rapid development of the construction industry has generated large amounts of construction and demolition waste. To solve these challenges, researchers have been focusing on the recycling of waste concrete. Nevertheless, extensive investigations have demonstrated that the incorporation of recycled coarse aggregates (RCAs) commonly has a negative influence on the mechanical properties. In recent years, several investigations found that the incorporation of pozzolanic materials, such as metakaolin, Fly ash (FA), ground granulated blast furnace slag (GGBFS), and silica fume (SF) improved the workability and durability properties of RAC (Guo et al., 2020; Kapoor et al., 2016). Moreover, several studies have shown that the incorporation of steel fibers significantly enhanced the mechanical properties of RAC (Ramesh et al., 2019). Nevertheless, the production of virgin fibers led to significantly environmental pollution. On the other hand, the rapid expansion of the automotive industry has led to a significant increase in the scrap tires all over the world. Several recent research has demonstrated that recycled steel fibers (RSFs) derived from scrap tires exhibited similar performance compared to virgin steel fibers. Several studies have explored the feasibility of using RSFs as alternative for conventional industrial steel fibers as the reinforcement for concrete production (Caggiano et al., 2017; Simalti and Singh, 2021).

Based on the above research, a more sustainable, low-carbon and cost-effective RSCC was proposed by combined addition of RSFs and industrial waste, with the objective of addressing multiple waste recycling problems (waste concrete, scrap tires, and industrial by-products).

2. MATERIALS AND METHODS

NCAs, RCAs, river sand, RSFs, cement, mineral admixtures, superplasticizer were used. Crushed natural limestone was used as NCAs and the physical properties were determined according to the Chinese code (JGJ 52-2006) (SAC, 2006). RCAs were prepared using waste concrete. The physical properties of NCAs and RCAs were evaluated following the Chinese code GB50119-2013 (SAC, 2013) and GB/T25177-2010 (SAC, 2010). RSFs obtained from discarded tires were utilized in this study. The mix proportion of RSF-RSCC is implemented according to EFNARC (EFNARC, 2005), Chinese standards JGJ/T 283-2012 (SAC, 2012).

Table 1. Mixture proportions (kg/m^3).

Mix code	Binder				water	NCA	RCA	Sand	RSF	Addtional Water	SP
	OPC	FA	GGBFS	SF							
0-0-0	498	0	0	0	184	818	0	808	0	0	4.98
75-0-0	498	0	0	0	184	205	574	808	0	21	4.98
A-75-50-2	249	124.5	124.5	0	184	205	574	808	0	21	4.98
A-75-50-3	249	99.6	99.6	49.8	184	205	574	808	0	21	4.98
A-75-75-3	124.5	161.85	161.85	49.8	184	205	574	808	0	21	4.98
B-75-50-2	249	124.5	124.5	0	184	205	574	808	28.5	21	4.98
B-75-50-3	249	99.6	99.6	49.8	184	205	574	808	28.5	21	4.98
B-75-75-3	124.5	161.85	161.85	49.8	184	205	574	808	28.5	21	4.98
C-75-50-2	249	124.5	124.5	0	184	205	574	808	57	21	4.98
C-75-50-3	249	99.6	99.6	49.8	184	205	574	808	57	21	4.98
C-75-75-3	124.5	161.85	161.85	49.8	184	205	574	808	57	21	4.98
D-75-50-2	249	124.5	124.5	0	184	205	574	808	85.5	21	4.98
D-75-50-3	249	99.6	99.6	49.8	184	205	574	808	85.5	21	4.98
D-75-75-3	124.5	161.85	161.85	49.8	184	205	574	808	85.5	21	4.98

In this study, all fresh mixtures were subjected to slump flow, J-ring, and segregation resistance tests as per EFNARC (EFNARC, 2005) and Chinese standard CECS 13-2009 (SAC, 2009). Compressive strength and static modulus of elasticity were evaluated as per the Chinese Standard

GB/T50081-2002 (SAC, 2002). Four-point bending tests were conducted in accordance with ASTM C1018 (ASTM C1018; 1997) and CECS13-2009 (SAC, 2009).

3. RESULTS AND DISCUSSION

The fresh test results of all RSCC mixtures are shown in Table 2. The incorporation of RSFs impaired the workability of RSCC mixtures. The flow diameter value reduced and the T_{500} flow time increased as well as the SF-JF increased with the addition of various RSFs. However, the incorporation of various SCM combinations significantly enhanced the fresh properties of RSF-RSCC mixes and most of RSF-RSCC mixtures exhibited satisfactory workability.

Table 2. Fresh properties of RSF-RSCC mixtures.

mix code	Slump flow Value-SF (mm)	T_{500} Slump Flow time (sec)	J-Ring flow-JF (mm)	SF-JF (mm)	Segregation rate (SR)
0-0	631	4.9	607	24	11
75-0	693	4.1	668	25	9
A-75-50-2	772	2.1	758	14	22
A-75-50-3	729	3.5	706	23	17
A-75-75-3	680	4.2	650	30	18
B-75-50-2	735	2.7	710	25	20
B-75-50-3	702	3.7	668	34	14
B-75-75-3	608	5.4	572	36	16
C-75-50-2	705	3.8	668	37	17
C-75-50-3	647	4.5	605	42	7
C-75-75-3	561	7.4	512	49	11
D-75-50-2	643	4.7	586	57	9
D-75-50-3	576	6.8	514	62	5
D-75-75-3	500	7.8	422	78	7
Limitation	550-850	3-7	-	0-50	≤20

[b]Note: The limitations were determined according to ENFARC-2005, JGJ/T 283-2012.

The mechanical properties of all RSF-RSCC are displayed in Table 3. It is evident from Table 3 that the compressive strength of RSCC was influenced by the various SCM combinations. The compressive strength of A-75-50-3 (20% FA, 20% GGBFS, 10% SF, and 0.0% RSFs) was equivalent to that of control mix 75-0-0. Moreover, the addition of RSFs led to a significant enhancement in the compressive strength. The maximum enhancement (5.29% to 38.32%) in compressive strength was obtained by the incorporation of 1.0% RSFs.

Table 3. Mechanical properties of RSF-RSCC.

Mix No.	Compressive strength (MPa)			Flexural strength (MPa)	Elastic modulus (GPa)
	7d	28d	120d		
0-0-0	32.78	44.78	47.21	2.81	36.18
75-0-0	29.79	39.67	44.14	2.60	31.75
A-75-50-2		37.28			
A-75-50-3		40.40			
A-75-75-3	21.22	33.32	38.94	2.28	30.48
B-75-50-2		43.12			
B-75-50-3		41.38			
B-75-75-3	26.20	38.76	43.91	3.47	32.96
C-75-50-2	35.86	51.56	62.01		
C-75-50-3		42.53			
C-75-75-3	28.55	40.39	48.36	3.65	33.75
D-75-50-2		40.05			
D-75-50-3		47.93			
D-75-75-3	25.31	38.93	45.82	4.06	32.70

The relationship between compressive strength of RSF-RSCC and curing age is depicted in Fig. 1. It is observed from Fig. 1 that the compressive strength continuously improved as curing age increased. The 120-day compressive strength of quaternary mix C-75-50-2 with 1.0% RSFs and 50% SCMs is about 62.01 MPa, which is much higher than that of normal SCC (47.21 MPa). Fig. 2 demonstrates the enhancement of 7-day, 28-day, and 120-day compressive strength in RSF-RSCC resulted from the synergistic effect of RSFs and various SCM combinations. A remarkable increase (29.98%) in compressive strength was achieved with the combined in-corporation of 1.0% RSFs, 25% FA, and 25% GGBFS compared to mix 75-0-0. Furthermore, the 120-day compressive strength of RSF-RSCC containing 50% SCMs and 1.0% RSFs increased by 40.49%, indicating a significant enhancement in the compressive strength at a later stage. It can be observed from Table 3 that the incorporation of RSFs led to a decline in the elastic modulus, which might be due to the rubber particles adhered to RSFs and the extra voids created by the rubber particles. As shown in

Fig.3, with the increase of RSF content, the flexural strength of RSF-RSCC consistently increased. For instance, compared to mix A-75-75-3, the inclusion of 0.5%, 1.0%, 1.5% RSFs increased the flexural strength by 52.19%, 60.09%, and 78.07%, respectively. Fig. 4 shows the flexural load–displacement curves of RSF-RSCC. As depicted in Fig. 4, the inclusion of various RSFs had almost no influence on the pre-peak stiffness, whereas improved the post-peak mechanical behavior of RSF-RSCC mixtures.

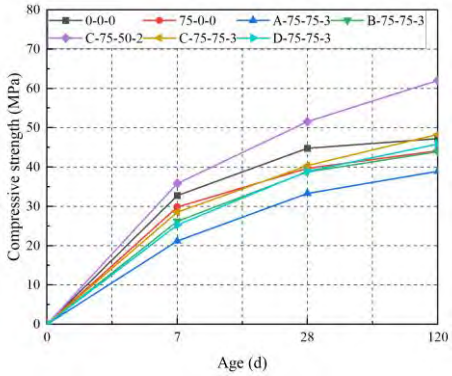

Fig. 1. Compressive strength versus curing time.

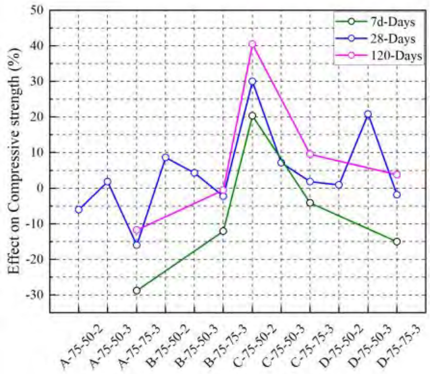

Fig. 2. Synergistic effect of RSFs and SCMs on the compressive strength of RSCC w.r.t mix 75-0-0.

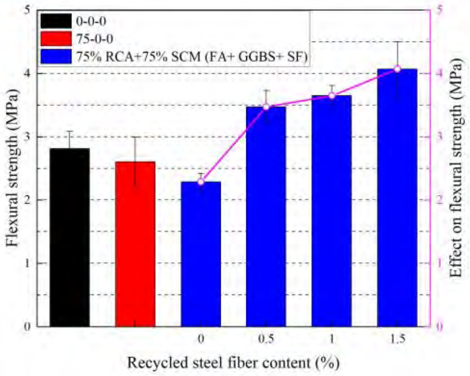

Fig. 3. Effect of RSF content on the flexural strength of RSF-RSCC.

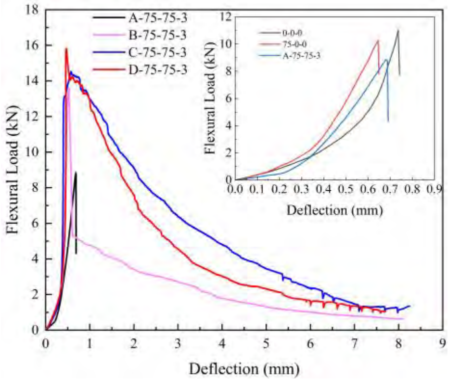

Fig. 4. Flexural load–displacement curves of RSF-RSCC mixes.

The test results demonstrates that the incorporation of RSF enhanced the mechanical properties of RSF-RSCC mixtures. This is due to the bridging action of the RSFs within the concrete matrix, which effectively restrained the propagation of cracks and improved the overall structural integrity. Moreover, the combined incorporation of RSFs and SCMs led to a remarkable improvement in mechanical properties. The improvement resulted from the combined incorporation of RSFs and various SCM combinations is higher than enhancement obtained by the individual incorporation of RSFs and SCMs. This is primarily for several reasons. First, the addition of different combinations of SCMs led to an improvement in the workability of RSCC and the even dispersion of RSFs. In addition, addition of different combinations of SCMs enhanced the packing density and reduced the porosity of the cement matrix. Secondly, the bridging effect of RSFs sustained the internal stresses and avoided the stress concentration and local fractures. Finally, the incorporation of SCMs with different combinations enhanced the ITZ between RSFs and the cement matrix. The SCM particles effectively filled the micro pores and enhanced the bond between RSFs and the cement matrix. As a result, the concurrent effect produced by the combined incorporation of RSFs and SCMs led to a net gain in mechanical properties (including compressive strength and flexural strength) as well as the ability for post-crack energy absorption.

4. CONCLUSION

The recycling of waste concrete, mineral admixtures and RSFs offers a promising solution for optimizing the fresh and hardened properties of RSCC, effectively addressing the potential challenges in workability associated with the addition of RSFs. The conclusions achieved from the current study may have limitations on the size distribution of RSFs and the combination of SCMs employed in this research. The fresh and mechanical properties of RSF-RSCC mixes are adversely influenced by the presence of rubber particles attached to the fibers. Therefore, it is necessary to maintain a low content of rubber particles before the practical engineering application.

5. ACKNOWLEDGMENT

This work was supported by National Natural Science Foundation of China (Grant No. 52178144). The authors wish to gratefully acknowledge the support for this study.

6. REFERENCES

ASTM C1018, 1997. Standard Test Method for Flexural Toughness and First-CrackStrength of Fiber-Reinforced Concrete (Using Beam with Third-Point Loading).ASTM International, West Conshohocken, PA, United States.

Caggiano, A., Folino, P., Lima, C., Martinelli, E., & Pepe, M. (2017). On the mechanical response of Hybrid Fiber Reinforced Concrete with Recycled and Industrial Steel Fibers. Construction and Building Materials, 147, 286-295. doi:https://doi.org/10.1016/j.conbuildmat.2017.04.160

EFNARC, 2005. Specification and Guidelines for Self-compacting Concrete. European Association for Producers and Applicators of Specialist Building Products.EFNARC Association House, Farnham ,UK.

Guo, Z., Jiang, T., Zhang, J., Kong, X., Chen, C., & Lehman, D. E. (2020). Mechanical and durability properties of sustainable self-compacting concrete with recycled concrete aggregate and fly ash, slag and silica fume. Construction and Building Materials, 231. doi:10.1016/j.conbuildmat.2019.117115

Kapoor, K., Singh, S. P., & Singh, B. (2016). Durability of self-compacting concrete made with Recycled Concrete Aggregates and mineral admixtures. Construction and Building Materials, 128, 67-76. doi:https://doi.org/10.1016/j.conbuildmat.2016.10.026

Ramesh, R. B., Mirza, O., & Kang, W.-H. (2019). Mechanical properties of steel fiber reinforced recycled aggregate concrete. Structural Concrete, 20(2), 745-755. doi:https://doi.org/10.1002/suco.201800156

SAC, 2002. GB/T 50081-2002: Standard for Test Method of Mechanical Properties on Ordinary Concrete. China.

SAC, 2006. JGJ 52-2006: Standard for Technical Requirements and Test Method of Sand and Crushed Stone (Or Gravel) for Ordinary Concrete. China.

SAC, 2009. CECS 13-2009: Standards test method for fiber reinforced concrete, China Planning Press. Beijing, China.

SAC, 2010. GB/T25177-2010: Recycled Coarse Aggregate for Concrete. China.

SAC, 2012. JGJ/T283-2012: Technical specification for application of self-compacting concrete. China.

SAC, 2013. GB 50119-2013: Technical specification for application of concrete admixture. China.

Simalti, A., & Singh, A. P. (2021). Comparative study on performance of manufactured steel fiber and shredded tire recycled steel fiber reinforced self-consolidating concrete. Construction and Building Materials, 266. doi:10.1016/j.conbuildmat.2020.121102

PHYSICOCHEMICAL RECYCLING OF WASTE GLASS FIBER-REINFORCED POLYMER INTO MODIFIER FOR ITS APPLICATION IN ASPHALT PAVEMENT: PREPARATION AND PERFORMANCE EVALUATION

Yi Luo[1,2], Nannan Yang[1,2], Shanshan Li[1,2], Xiang Zhang[1,2], Xiong Xu[1,2*]

[1]School of Civil Engineering and Architecture, Wuhan Institute of Technology, Wuhan 430073, China
[2]Hubei Provincial Engineering Research Center for Green Civil Engineering Materials and Structures, Wuhan Institute of Technology, Wuhan 430073, China
E-mail (corresponding author): xxucea@wit.edu.cn

1. INTRODUCTION

Due to the high strength and light weight, easy molding, flexible design, good corrosion resistance, good thermal performance and other superior performance, glass fiber-reinforced polymer (GFRP) composite materials are widely used in construction, chemical industry, automobile and railway transportation, electrical industry, communication engineering and other industries. It has become an irreplaceable functional material for different uses. However, it is because of their high performances that these discarded GFRP composites are not that easy to be treated and commonly disposed at stockpiles, resulting in some serious environmental issues, such as global warming, atmospheric pollution, soil pollution, and so on. Although many studies have reported some technical approaches to recycle and reuse them for further use [1-3], the aspects on the consumption and high-quality use are proved in fact not ideal. It is necessary to consider how to well solve the worrying points for realizing the upgrade of these recycled GFRP to some new applications. Therefore, this study attempted to prepare the finer glass fiber-reinforced polymer (GFRP) modifier through the combined treatments from silane coupling agents γ-aminopropyl triethoxy silane (KH550) and styrene-butadiene rubber (SBR) in mechanical and physicochemical approaches for its application in asphalt pavement, and then comparatively investigated the differences in mixture properties by contrast to SBS modified asphalt mixture.

2. MATERIALS AND METHODS

The used asphalt modifiers were obtained by using different surface modification processes for recycled waste powdered GFRP. The specific preparation process is shown in Figure 1. Firstly, the recycled GFRP were placed in the crusher for crushing treatment, and then passed through a 60 mesh sieve to obtain the powdered GFRP modifier. Secondly, prepare a hydrolysis solvent of deionized water and absolute alcohol (mass ratio 0.9:1), and let it stand at room temperature for 10~20 minutes to fully alcoholize. Then, KH550 at 1.4%, by weight of GFRP modifier, was dissolved in a hydrolysis solvent prepared in the previous step to obtain the KH550 hydrolysis solution, heated in a water bath at 80 ℃ for 20 minutes and stirred evenly. After the KH550 solution was left at room temperature for 1 hour, GFRP modifier was slowly added to the solution and soaked for 30 minutes to fully react. After then, the treated GFRP modifier, which was filtered and repeatedly rinsed to remove residual KH550 solution, was placed in a 160 ℃ air drying oven for 2 hours to obtain the Si-GFRP modifier. Finally, Si-GFRP and SBR were mixed in a 1:0.4 ratio in a torque rheometer, Finally, Si-GFRP modifier and SBR were mixed in a torque rheometer at a ratio of 1:0.4, with mixing conditions of 130 ℃, 50 rpm, and 5 minutes. The Developed-GFRP modifier was prepared by crushing and sieving the mixture obtained from the internal mixing into 60 mesh powders.

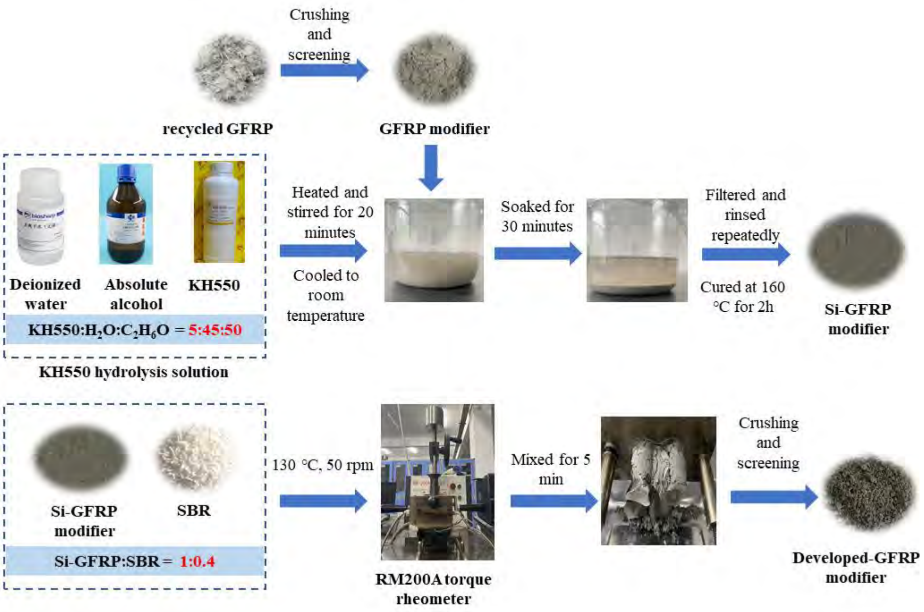

Figure 1. Schematic flow chart for the preparation of GFRP modifiers

The study used 5% GFRP modified asphalt binder to prepare AC-20 asphalt mixture, and determined the optimal asphalt content (OAC) of the mixture to be 4.3% to ensure volume parameters and Marshall loads. Modified asphalt mixture was prepared by replacing SBS with Developed-GFRP modifier in different proportions, with replacement rates of 0, 30%, 70%, and 100% by weight of SBS. Then comparatively investigated the differences in mixture properties by contrast to modified asphalt mixture with different substitution rates of Developed-GFRP modifiers, such as rutting resistance, low-temperature crack resistance, and moisture-induced damage resistance, for better understanding the performances of GFRP modifier. In addition, through aging tests, further research was conducted on the impact of different substitution rates of Developed GFRP modifiers on the durability of asphalt pavement. The research flowchart of this study is displayed in Figure 2.

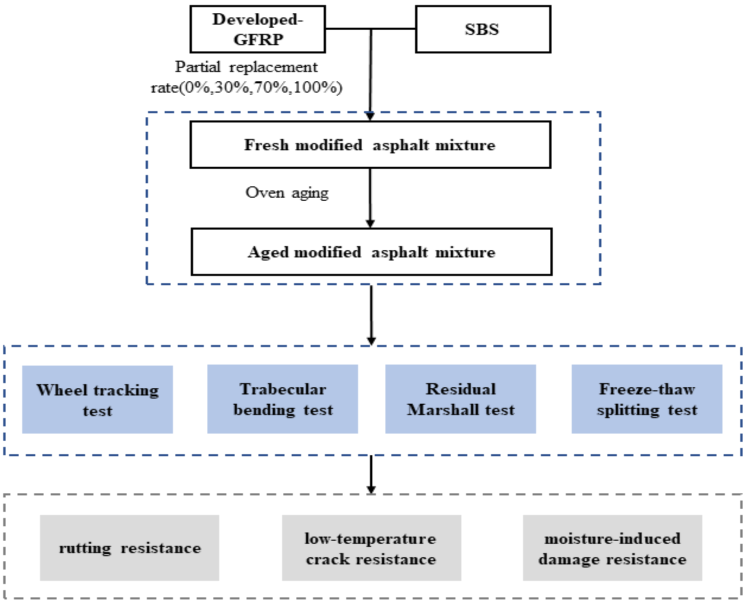

Figure 2. Research flowchart of this study

3. RESULTS AND DISCUSSION

3.1 Residual Marshall tests

With respect to the changes of target mixtures before and after aging in the MS_0 value, the results are calculated and presented in Figure 2. It was clear that the fresh SBS modified asphalt mixture decreased dramatically from 89.42% to 75.04% after aging. It can be seen that after thermal oxygen aging, the moisture-induced damage resistance of SBS modified asphalt mixture will decrease sharply. When the substitution rate was 0, the MS_0 value of the aged Developed-GFRP modified asphalt mixture increases from 90.14% to 97.87%, which was higher than that of SBS modified asphalt mixture. This shows that compared with SBS, Developed-GFRP modifiers have stronger resistance to moisture-induced damage in asphalt pavement. When the Developed-GFRP replacement rate is 30%, the MS_0 value of modified asphalt mixture before and after aging is greater than that of the modified asphalt mixture with the replacement rate of 70%, indicating that the replacement rate of Developed-GFRP should not be too large, and the asphalt mixture with small content replacing SBS has better resistance to moisture-induced damage. Thus, 30% GFRP replacement rate is the optimal proportion of the modifier.

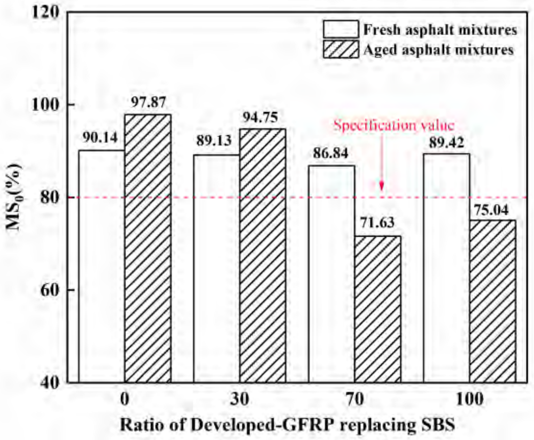

Figure 3. Effects on different replacement rates of Developed-GFRP on the residual Marshall load ratio of asphalt mixtures before and after aging

3.2 Freeze-thaw splitting tests

Figure 3 shows the effects of different replacement rates on TSR of target mixtures before and after aging after one freeze-thaw cycle. From the results, the TSR value of fresh mixtures decreases from 95.41% to 89.50%, indicating that aging will reduce its resistance to freeze-thaw damage. The TSR values of the fresh asphalt mixtures added with Developed-GFRP after a freeze-thaw cycle are relatively close. In addition, the TSR value of the asphalt mixtures with a replacement rate of 30% is 96.53%, which is higher than that of the fresh SBS modified asphalt mixture. This indicates that the incorporation of Developed-GFRP increases the adhesion between asphalt and aggregate, reduces the damage effect, and thus improves the resistance to moisture-induced damage of the SBS modified asphalt mixture. Besides, the TSR values of aged asphalt mixtures added with Developed-GFRP are relatively close, and all of them are higher than those before aging. The TSR value of asphalt mixture with a replacement rate of 30% is relatively stable before and after aging.

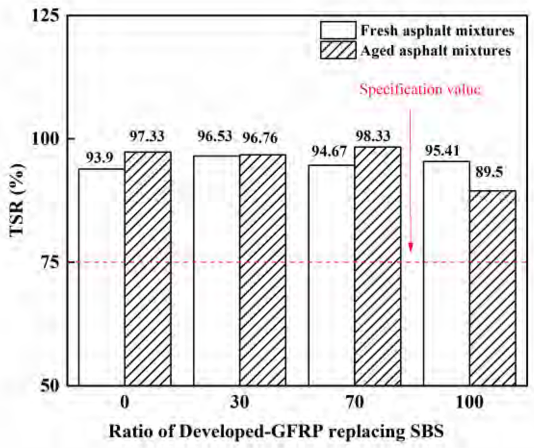

Figure 4. Effects on different replacement rates of Developed-GFRP on the frozen-thaw and split residual strength ratio of asphalt mixtures before and after aging

4. CONCLUSION

This study adopted the prepared GFRP modifiers to replace SBS modifier for mainly investigating the performance properties, especially moisture damage resistance. Through properties test, some valuable conclusions can be drawn:

(1) The prepared GFRP modifier can improve the adhesion of asphalt binder to the aggregates, thereby significantly improving the resistance of asphalt mixtures to moisture damage.

(2) No more than 30% replacement of SBS will almost not negatively influence the residual Marshall stability but improve a little bit, and the corresponding GFRP/SBS composite modified asphalt mixture has a MS_0 value of 89.13% and 94.75% before and after aging.

(3) By contrast to SBS modified asphalt mixture, GFRP/SBS composite modified asphalt mixtures have comparable resistances to the freeze-thaw damage, reaching a TSR value of more than 95%, even after aging.

5. ACKNOWLEDGMENT

The authors would like to express appreciation for the support of the Open Fund of Key Laboratory of Road Structure and Material of Ministry of Transport (Changsha University of Science & Technology) [kfj220304]

6. REFERENCES

Chukov Dilyus,Torokhov Valerii,Sherif Galal & Tcherdyntsev Victor.(2020).Thermal treatment as an effective method of carbon/glass fibers surface modification for high-performance thermoplastic polymer matrix composites. *Materials Today: Proceedings*(P4).

Mengfan Jing,Junjin Che,Shuman Xu.(2018).The effect of surface modification of glass fiber on the performance of poly(lactic acid) composites: Graphene oxide vs. silane coupling agents. *Applied Surface Science.*

Pouya Rajaee,Faramarz Ashenai Ghasemi,Mohammad Fasihi & Mohammadhossein Saberian.(2019).Effect of styrene-butadiene rubber and fumed silica nano-filler on the microstructure and mechanical properties of glass fiber reinforced unsaturated polyester resin. *Composites Part B.*

INVESTIGATION OF RECYCLED CARBON FIBER FELT AS A PROMISING MATERIAL FOR CAPACITIVE DEIONIZATION (CDI) ELECTRODES IN INDUSTRIAL APPLICATIONS

JiuYi Liu[1], Chun Pei[1], Jihua Zhu[1, *]
[1]College of Civil and Transportation Engineering, Shenzhen University, Shenzhen, Guangdong, 518061, China
E-mail: zhujh@szu.edu.cn

1. INTRODUCTION

Capacitive deionization (CDI) is a promising method for desalination of drinking water, involving the adsorption of dissolved salts onto electrode surfaces to form electric double-layers (Huang et al., 2017). The concept of capacitive deionization (CDI) was first introduced in the 1960s at the University of Oklahoma by G.W. Murphy and D.D. Caudle (Jia & Zhang, 2016).CDI technology, recognized for its pollution-free, environmentally friendly, and energy-efficient characteristics, demonstrates significant potential in various industrial applications, surpassing conventional desalination methods such as thermal distillation, reverse osmosis, and electrodialysis. The performance of CDI electrode materials is influenced by diverse factors, including material properties such as surface area, pore size, and distribution, external potential, solution conditions, and ion concentration(Suss et al., 2012). Among the materials considered for CDI electrodes, carbon fiber stands out due to its notable high specific surface area and uniform pore distribution (Jia & Zhang, 2016).Previous studies have explored the suitability of various materials, such as activated carbon (Chen et al., 2018), carbon felt (Ayranci & Conway, 2001), carbon nanotubes (Li et al., 2008), and carbon aerogels (Jung et al., 2007), for CDI electrode fabrication. However, the potential of utilizing recycled carbon fiber felt (rCFRP) for CDI electrodes remains relatively underexplored, despite its favorable attributes, including high specific surface area, uniform pore distribution, cost-effectiveness, and reduced carbon emissions compared to other materials.This study aims to comprehensively examine the viability of rCFRP as a suitable material for CDI electrode fabrication. Through the construction of CDI cells using rCFRP, a thorough investigation of their physical properties, adsorption performance, and surface morphology before and after adsorption is conducted. The research findings shed light on the applicability of rCFRP as a promising material for CDI electrodes and offer valuable insights for further advancement in this field.ls.

2. MATERIALS AND METHODS

The wasted carbon fiber-reinforced polymer (CFRP) samples were generously provided by XX company. The resin type used in the CFRP was bisphenol A epoxy resin (DGEBA).

To obtain the recycled carbon fibers, the CFRP samples were subjected to ambient-temperature soaking. Mechanical properties and characterizations of the recycled carbon fibers were measured. Subsequently, the recycled carbon fibers were utilized to fabricate carbon fiber felt using a wet-lay process.

The carbon fiber felt was then cut into dimensions of 25 cm × 25 cm and used along with acrylic plates, silicone gaskets, nylon cloth, and current collectors to construct the capacitive deionization (CDI) electrodes, as shown in figure 1. The acrylic plates served as the support, while graphite sheets were utilized as the current collectors, placed on the backside of the electrodes. The assembly was sealed with 1.5 mm-thick silicone gaskets, and two permeable nylon cloths (with a mesh size of 300) were placed between the anode and cathode for electrical isolation. Two holes (1 cm in diameter) were drilled on the acrylic plates to serve as the water outlet and inlet, as shown in figure 2.

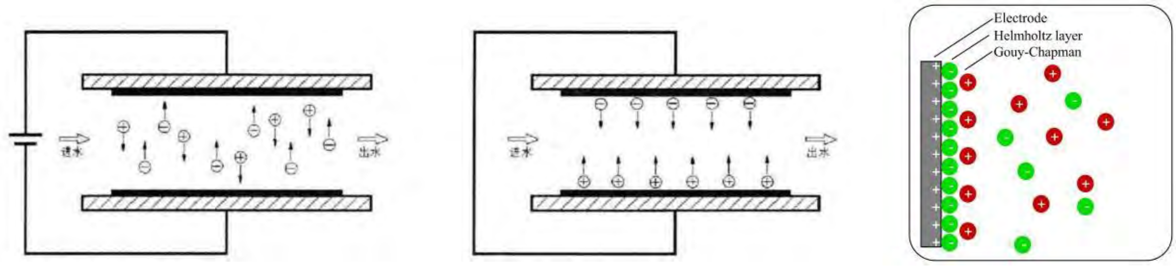

Figure 1. schematic diagram of CDI reactor

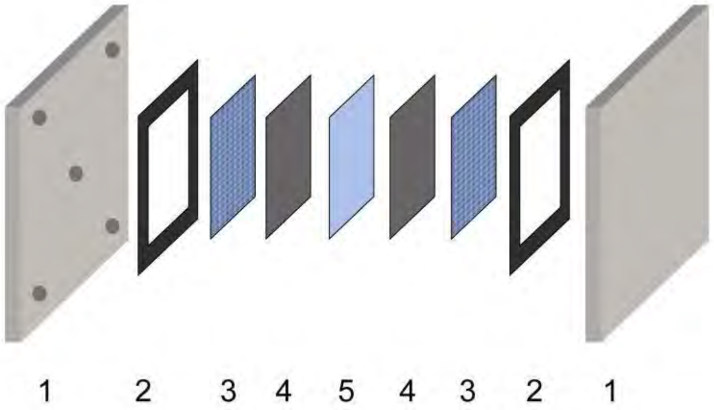

1. Acrylplatte 2. Silikon-Dichtung 3.Current controller 4.recycled carbon felt

Figure 2. Schematic diagram of CDI reactor

The experimental setup consisted of a direct current power supply, CDI electrodes, a peristaltic pump, a conductivity meter, a pH meter, a water reservoir, and a magnetic stirrer. The experiment was conducted in a batch mode, where the salt solution was pumped from the water reservoir to the CDI device and then returned to the water reservoir. The CDI electrode adsorption performance was evaluated based on the pH concentration in the water reservoir during the cycling operation, as shown in figure 3.

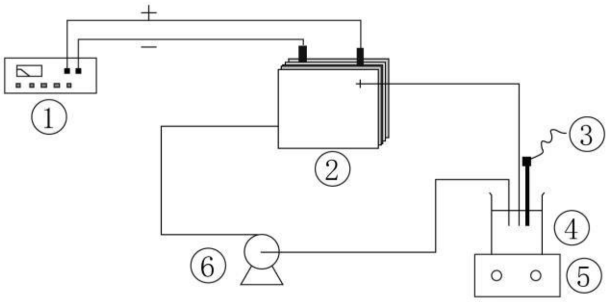

1. DC power supply 2. CDI system 3. conductivity meter 4. Beaker 5. magnetic mixer 6. peristaltic pump

Figure 3. Module of the CDI reactor

3. RESULTS AND DISCUSSION

This research explores the synthesis of CDI electrodes using recycled carbon fiber felt as shown in figure 4. in combination with suitable adsorbents or functional materials, aiming to enhance the electroadsorption desalination capacity of the composite material while optimizing its adsorption efficiency and regeneration performance in figure 5. Comparative characterization of the surface morphology and adsorption performance between CDI and recycled CDI (rCDI) systems was carried out using electron microscopy. The results indicate that the utilization of recycled carbon fiber felt for CDI electrodes does not significantly alter their surface morphology, and the adsorption capacity of the rCDI system closely matches that of the conventional CDI system. Enhanced adsorption performance further contributes to improved cathodic protection and structural reinforcement capabilities within the ICCP-SS system, concurrently reducing costs and mitigating carbon dioxide emissions.

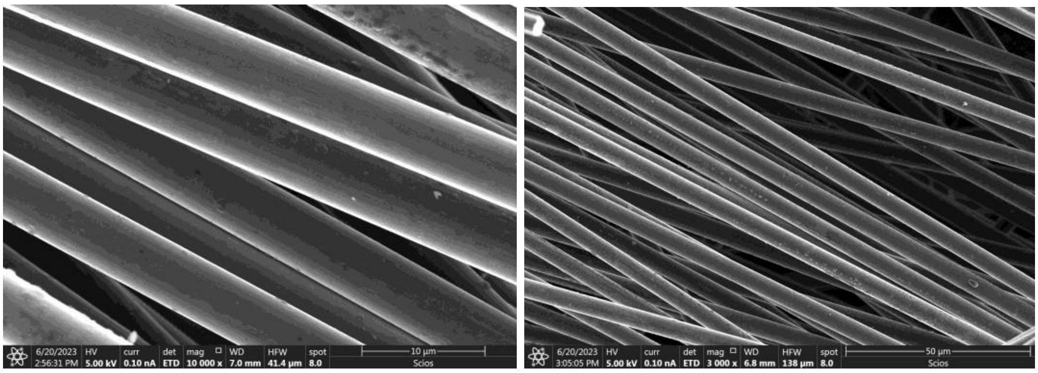

Figure 4. SEM images of rCF

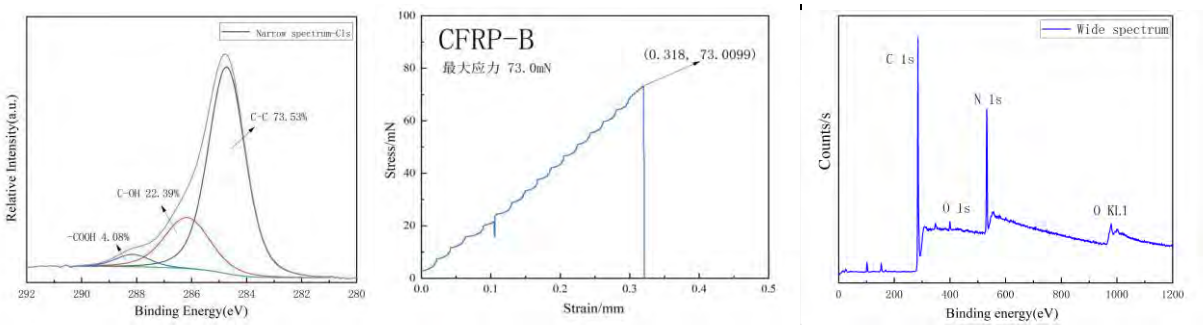

(a) (b) (c)

Figure 5. a\c XPS of rCF; b Single Fiber Tensile Test of rCF

4. CONCLUSION

In this study, we successfully utilized recycled carbon fiber-reinforced polymer (rCFRP) to fabricate carbon fiber felt. A comprehensive series of tests were conducted to assess its suitability as a material for capacitive deionization (CDI) electrodes. The rCFRP exhibited favorable characteristics, including high specific surface area, conductivity, and uniform pore distribution, qualifying it as a promising raw material for CDI electrodes. This research proposes a more environmentally friendly and cost-effective method for CDI electrode fabrication, harnessing the potential of recycled carbon fiber to reduce carbon emissions and production expenses. These findings hold paramount significance in fostering sustainable development within high-demand industries.

5. ACKNOWLEDGMENT

The authors would like to express appreciation for the support of the Key-Area Research and Development Program of Guangdong Province [Project Number: 2019B111107002], the National Natural Science Foundation of China [Project Number: 52108231], and the Shenzhen Science and Technology Innovation Program [Project Number: 20220810140230001,20220810160453001].

6. REFERENCES

Huang, Z.-H., Yang, Z., Kang, F., & Inagaki, M. (2017). Carbon electrodes for capacitive deionization.Journal of Materials Chemistry A, 5(2), 470–496. https://doi.org/10.1039/C6TA06733F

Chen, Z., Zhang, H., Wu, C., Luo, L., Wang, C., Huang, S., & Xu, H. (2018). A study of the effect of carbon characteristics on capacitive deionization (CDI) performance. Desalination, 433, 68–74. https://doi.org/10.1016/j.desal.2017.11.036

Jia, B., & Zhang, W. (2016). Preparation and Application of Electrodes in Capacitive Deionization (CDI): A State-of-Art Review. Nanoscale Research Letters, 11(1), 64. https://doi.org/10.1186/s11671-016-1284-1

Suss, M. E., Baumann, T. F., Bourcier, W. L., Spadaccini, C. M., Rose, K. A., Santiago, J. G., & Stadermann, M. (2012). Capacitive desalination with flow-through electrodes. Energy & Environmental Science, 5(11), 9511–9519. https://doi.org/10.1039/C2EE21498A0

Ayranci, E., & Conway, B. E. (2001). Removal of phenol, phenoxide and chlorophenols from waste-waters by adsorption and electrosorption at high-area carbon felt electrodes. Journal of Electroanalytical Chemistry, 513(2), 100–110. https://doi.org/10.1016/S0022-0728(01)00529-0

Li, H., Gao, Y., Pan, L., Zhang, Y., Chen, Y., & Sun, Z. (2008). Electrosorptive desalination by carbon nanotubes and nanofibres electrodes and ion-exchange membranes. Water Research, 42(20), 4923–4928. https://doi.org/10.1016/j.watres.2008.09.026

Jung, H.-H., Hwang, S.-W., Hyun, S.-H., Lee, K.-H., & Kim, G.-T. (2007). Capacitive deionization characteristics of nanostructured carbon aerogel electrodes synthesized via ambient drying. Desalination, 216(1), 377–385. https://doi.org/10.1016/j.desal.2006.11.023

GEOTECHNICAL APPLICABILITY OF CEMENT-STABILIZED FIBER-REINFORCED INCINERATOR BOTTOM ASH COMPOSITES

Kumar, Sanjeev[1], and Singh, Davinder[1]

[1]Dr BR Ambedkar National Institute of Technology Jalandhar, Punjab (India) -144011
Sanjeevk.ce.19@nitj.ac.in

1. INTRODUCTION

In the wake of extensive industrialization and inevitable population growth, the effective management of municipal solid waste (MSW) has evolved into a global challenge, necessitating innovative approaches for waste disposal and resource utilization (Bansal et al., 2023; Kumar & Singh, 2023b). This challenge extends beyond underdeveloped nations, with developed countries seeking sustainable solutions to combat this pressing issue. Poorly managed and improperly disposed MSW triggers socio-environmental problems and substantially hinders a country's economic growth. The challenges associated with MSW disposal demand urgent attention, particularly in developing nations, from soil and water contamination to various ecological impacts.

In this complex landscape, municipal solid waste incinerator ash (MSWIA), a byproduct of waste-to-energy processes, emerges as a significant factor. Contemporary waste management practices often contribute to the accumulation of MSWIA in landfills, urging a reevaluation of its potential as an eco-friendly alternative with diverse applications. Despite ending directly in the landfill, the MSW incinerator bottom ash (MSW-IBA) has been utilized in brick manufacturing, concrete, and asphalt mix preparations, and as filler material in embankments. This leads to limited usage due to its physiochemical properties, which must be advanced for long-term and eco-friendly usage. Waste-to-energy (WtE) conversion technologies refer to any waste treatment process that generates energy in the form of fuel or electricity. This approach is beneficial since it helps to minimize the volume of waste that would have otherwise been sent to landfills while at the same time generating energy (Astrup et al., 2016; Blasenbauer et al., 2020). The importance of incinerator bottom ash (MSW-IBA) and its constituents makes treating MSW-IBA an essential step before it can be used for a specific application. MSW-IBA treatment can be initiated chemically, mechanically, and through thermal treatment options.

Incineration techniques in India have been undergoing upgrades to recover most of the high metal content found in the ash. This metal recovery process can potentially lead to environmental issues or result in ash unsuitable for reuse (Sormunen et al., 2018; Sormunen & Kolisoja, 2017). Two approaches are commonly employed to address this: removing hazardous compounds or stabilizing them using various methods. While ash washing has been a conventional treatment technique, stabilizing MSW-IBA is now becoming a prominent trend in waste treatment (Alam et al., 2022, 2023).

Cement-based materials are added in a defined ratio to stabilize MSW-IBA, effectively immobilizing heavy metals within the cement matrices using binding materials. However, MSW-IBA stabilization outcomes depend on environmental factors such as pH, temperature, and humidity, which can lead to varying results (Pastapure et al., 2022, 2023). Enhancing the stabilization process, powdered fish bones and specific chemical stabilizers have yielded better results (Kumar & Singh, 2023a; Singh & Kumar, 2019). Furthermore, thermal and hydrothermal treatments of incineration ash are being considered for metal removal. Recent studies have shown that effective microwave heating combined with hydrothermal treatment offers the best results for removing polychlorinated dibenzo-p-dioxins (PCDD) (Qiu, Chen, et al., 2019; Qiu, Jiang, et al., 2019).

Since the work targets stabilization of MSW-IBA using cement addition, the other treatment methods of bottom ash are not in the scope of the study. The chemical stabilization of MSW-IBA using cementitious materials has proven effective in advancing the physiochemical characteristics, leading to improved strength properties. The addition of Fibers has been a great area of interest for researchers working in this field for wider geotechnical and geoenvironmental applications. As suggested by the previous studies related to fiber-reinforced cement stabilized composites experienced in the field of improvement of soil structure and strength behaviour, the present study focuses applicability of these residues in a stabilized form for various civil engineering applications.

2. MATERIALS AND METHODS

In this study, MSW-IBA was collected from centralized incineration facilities in Delhi, the capital of India. Ordinary Portland Cement (OPC-43), conforming to IS 8112 specifications, was commonly available as the binding material to investigate the stabilized composites. For the reinforcement of cement-stabilized composites, polypropylene fibers are used. The geotechnical properties of the MSW-IBA and cement composites, Unconfined Compression Strength (UCS), Splitting tensile strength test (STS), and California Bearing Ratio (CBR) tests were cast at their respective moisture content and dry density levels. Standard procedures, ASTM D2166-98 (1998), ASTM C496-11 (2005), and ASTM D1883-05, were followed for UCS, STS and CBR tests.

3. RESULTS AND DISCUSSION (headlines: Bold, 12pt)

Results of Unconfined Compressive Strength Behaviour

A remarkable improvement in UCS values was noticed from the experimental program performed on MSW-IBA specimens, on standard curing durations for fiber content ranging from 0.5 to 1% for cement-stabilized fiber reinforced MSW-IBA samples. As shown in Fig. 1(a), the highest amount of UCS strength was observed for 3 percent fiber content and 1% 19 mm fiber. When these values are checked at different curing durations, as shown in Fig. 1 (b), the UCS values for the 90-day curing period were remarkably higher for the same cement and fiber concentrations when compared with unreinforced cement-stabilized MSW specimens.

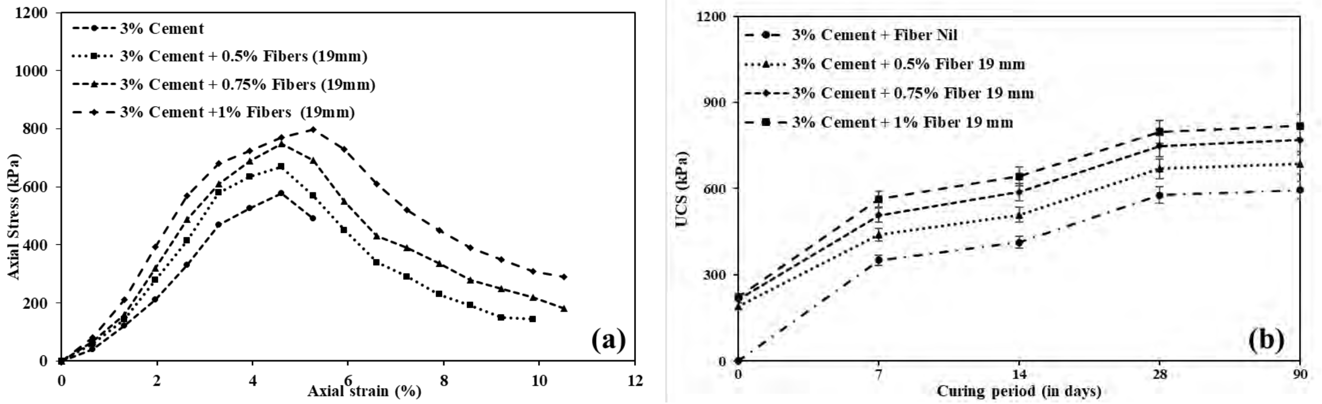

Figure 1. (a) Observed stress-strain behaviour for UCS test (b) UCS values for different percentages of fiber

Results of Splitting Tensile Strength Behaviour

The pozzolanic nature of MSW-IBA and its stabilization with cement leads to enhanced Splitting Tensile Strength values when tested under standard lab conditions. As shown in Fig.2, the improved behaviour of STS values for higher cement content can be noticed for a higher curing duration. The STS values of 100, 120, and 153 kPa are attained at 28 days of curing for specimens with 0.5, 0.75, and 1% fiber content. This shows that reinforced MSW-IBA composites successfully attain better STS values when compared to unreinforced specimens.

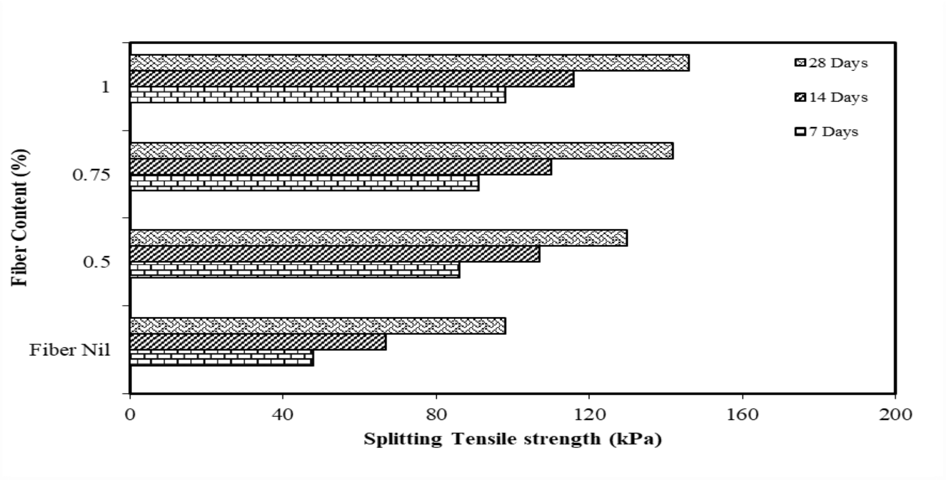

Figure 2. Splitting Tensile Strength values observed for different curing periods at different fiber percentage

Results of California Bearing Ratio Tests

Results obtained from the CBR test are used to design the flexible pavement and depths of its various layers. Fig. 3 (a) and (b) show the experimental results on fiber-reinforced MSW-IBA specimens. From the load penetration curves, it can be commented that for higher fiber content and keeping the cement percentage constant, the reinforced MSW-IBA specimens performs better for higher load. A higher value of CBR signifies a better material for flexible pavement design. Therefore, from Fig. 3(b), a higher percentage of cement content and high fiber concentration leads to better CBR results.

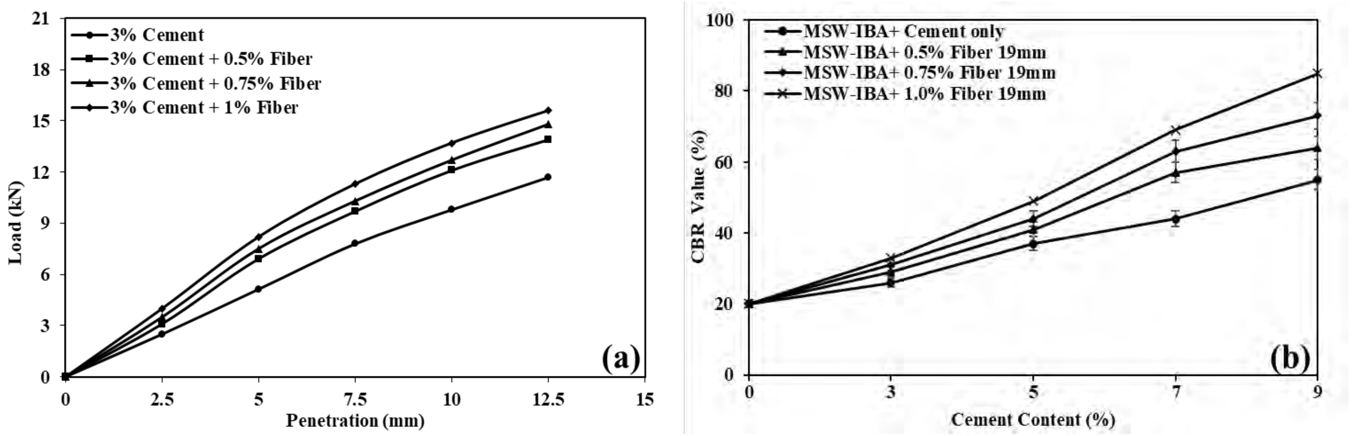

Figure 3. (a) Load Penetration curve for CBR test (b) CBR values for different percentages of fiber for 28 days curing

4. CONCLUSION

The comprehensive investigation into the mechanical properties of stabilized fiber-reinforced ash specimens has shed light on the significant influence of curing duration on their performance. The study revealed a consistent and noteworthy trend: the UCS, STS, and CBR values steadily increased as the curing duration extended. This strengthening effect was particularly pronounced within the 28-day curing period, demonstrating the expeditious enhancement in the specimens' durability due to the bottom ash's pozzolanic nature. Remarkably, the inclusion of 3% cement and 1% fiber (19mm) over 7, 14, and 28 days exhibited incremental UCS improvements of 112.74%, 134.89%, and 178.83%, respectively. These findings underscore the efficacy of incorporating both cement and fiber in enhancing the mechanical integrity of bottom ash specimens over time.The substantial improvement in CBR and STS values in the case of MSW bottom ash stabilization highlights the potential for this approach to be utilized in practical engineering applications. As future work, further investigations could explore the underlying mechanisms responsible for these enhancements and delve into optimizing the proportions of cement and fiber for even more efficient stabilization outcomes.

5. ACKNOWLEDGMENT

The authors would like to express appreciation for the support of the Department of Civil Engineering, Dr. B.R Ambedkar, National Institute of Technology Jalandhar.

6. REFERENCES

Alam, P., Kumar, S., Singh, D., & Kumar, T. (2023). Recovery Techniques and LCA Involved with Municipal Solid Waste Bottom Ash Treatment: A Review. Lecture Notes in Civil Engineering, 281, 83–93. https://doi.org/10.1007/978-981-19-4731-5_8

Alam, P., Singh, D., & Kumar, S. (2022). Incinerated municipal solid waste bottom ash bricks: A sustainable and cost-efficient building material. Materials Today: Proceedings, 49, 1566–1572. https://doi.org/10.1016/J.MATPR.2021.07.346

Astrup, T., Muntoni, A., Polettini, A., Pomi, R., Van Gerven, T., & Van Zomeren, A. (2016). Treatment and Reuse of Incineration Bottom Ash. Environmental Materials and Waste: Resource Recovery and Pollution Prevention, 607–645.

Bansal, D., Gupta, G., Ramana, G. V., & Datta, M. (2023). Environmentally responsible disposal and reuse of MSW incineration bottom ash: assessment from two Indian plants. Clean Technologies and Environmental Policy 2023, 1–16.

Blasenbauer, D., Huber, F., Lederer, J., Quina, M. J., K., Pająk, T., … Fellner, J. (2020). Legal situation and current practice of waste incineration bottom ash utilisation in Europe. Waste Management, 102, 868–883.

Kumar, S., & Singh, D. (2023a). Prediction of UCS and CBR behavior of fiber-reinforced municipal solid waste incinerator bottom ash composites using experimental and machine learning methods. Construction and Building Materials, 367, 130230.

Kumar, S., & Singh, D. (2023b). Transforming waste into Sustainable solution: Physicochemical and Geotechnical Evaluation of Cement Stabilized Municipal Solid Waste Incinerator Bottom Ash for Geoenvironmental Applications. Process Safety and Environmental Protection.

Pastapure, V., Singh, D., & Kumar, S. (2022). Engineering behavior of municipal solid waste incinerated bottom ash with the addition of lime. Materials Today: Proceedings.

Pastapure, V., Singh, D., & Kumar, S. (2023). Effects of Open Dumping of Municipal Solid Waste on Surrounding Soil Characteristics: A Review. 47–54.

Qiu, Q., Chen, Q., Jiang, X., Lv, G., Chen, Z., Lu, S., Ni, M., Yan, J., Lin, X., Song, H., & Cao, J. (2019). Improving microwave-assisted hydrothermal degradation of PCDD/Fs in fly ash with added Na2HPO4 and water-washing pretreatment. Chemosphere, 220, 1118–1125. https://doi.org/10.1016/j.chemosphere.2018.12.166

Qiu, Q., Jiang, X., Lü, G., Chen, Z., Lu, S., Ni, M., Yan, J., & Deng, X. (2019). Degradation of PCDD/Fs in MSWI fly ash using a microwave-assisted hydrothermal process. Chinese Journal of Chemical Engineering, 27(7), 1708–1715.

Singh, D., & Kumar, A. (2019). Mechanical characteristics of municipal solid waste incineration bottom ash treated with cement and fiber. Innovative Infrastructure Solutions 2019 4:1, 4(1), 1–7. https://doi.org/10.1007/S41062-019-0247-7

Sormunen, L. A., Kaartinen, T., & Rantsi, R. (2018). MSWI BA treated with Advanced Dry Recovery: a field scale study on materials' leaching properties. Int. J. Sustain. Eng., 11(4), 261–271. https://doi.org/10.1080/19397038.2018.1444679

Sormunen, L. A., & Kolisoja, P. (2017). Construction of an interim storage field using recovered municipal solid waste incineration bottom ash: Field performance study. Waste Management, 64, 107–116. https://doi.org/10.1016/j.wasman.2017.03.014

DESIGNING MAGNESIUM PHOSPHATE CEMENT FOR STABILIZATION/SOLIDIFICATION OF ZN-RICH ELECTROPLATING SLUDGE

Yuying Zhang[1], Daniel C.W. Tsang[2*]

[1] Department of Civil and Environmental Engineering, The Hong Kong Polytechnic University, Hung Hom, Kowloon, Hong Kong, China.
[2] Department of Civil and Environmental Engineering, The Hong Kong University of Science and Technology, Clear Water Bay, Hong Kong, China
*Corresponding author: cedan@ust.hk

Electroplating sludge is a hazardous waste due to its high potential to leach toxic elements into the natural environment. To alleviate this issue, we tailored magnesium phosphate cement (MPC) as a low-carbon material for stabilization/solidification (S/S) of Zn-rich electroplating sludge. The interaction between MPC and ZnO was investigated to clarify the precipitate chemistry, microstructure transition, and chemical environment of Zn species in the MPC-treated Zn sludge system. Comprehensive characterization (*i.e.*, X-ray diffraction (XRD), ^{31}P nuclear magnetic resonance (NMR), and extended X-ray absorption fine structure spectra (EXAFS)) and thermodynamic modeling results revealed that the incorporated ZnO preferentially reacted with phosphate to form $Zn_3(PO_4)_2 \cdot 2H_2O/Zn_3(PO_4)_2 \cdot 4H_2O$, changing the orthophosphate environments in the MPC system. A stronger chemical bonding between Zn and phosphate in comparison to the bonding between Mg and phosphate also resulted in the formation of amorphous $Zn_3(PO_4)_2 \cdot 2H_2O/Zn_3(PO_4)_2 \cdot 4H_2O$. $Zn_3(PO_4)_2 \cdot 4H_2O$ precipitate appears to predominate at high $\{K^+\}\{H^+\}\{HPO_4^{2-}\}$ values, and the formation of $Zn_3(PO_4)_2 \cdot 2H_2O/Zn_3(PO_4)_2 \cdot 4H_2O$ competed for the Mg sites in MPC system, leading to the inhibition of forming Mg-phosphate precipitates. Overall, this work uncovers the precipitate chemistry and microstructure transition of Zn species in the MPC system, providing new insights into the sustainable S/S of Zn-contaminated wastes by adopting MPC.

Keywords: Industrial sludge treatment; Metal leaching; Stabilization/Solidification; Sustainable waste management.

A ZERO-WASTE STRATEGY TO TRANSFORM BAYER RED MUD INTO CLEAN GLASS FIBER AND CAST IRON

Ziwei Chen[1], Lili Liu[2], and Chi Sun Poon[1,*]

[1] Department of Civil and Environmental Engineering, The Hong Kong Polytechnic University,
Hung Hom, Kowloon, Hong Kong 999077, PR China
[2] School of Materials Science and Engineering, Peking University, Beijing 100871, PR China
E-mail ([*]corresponding author): chi-sun.poon@polyu.edu.hk

Bayer red mud (BRM) is a hazardous alkaline residue resulting from the Bayer process of extracting alumina from bauxite ores. The existing approaches of recycling BRM usually produce secondary residue and require complex routes and high cost, which hinders the large-scale utilization of BRM. Hence, we reported a scalable strategy to totally transform BRM into clean glass fiber and cast iron via a short high-temperature process, while hazardous substances were immobilized in vitreous fibers. Here limestone tailings and quartz tailings were used as alkaline and acidic component modifiers, respectively. Thermodynamic calculations and molecular dynamics simulations were adopted to design the smelting-reduction and melt fiberization processes. The laboratory-scale production of glass fiber and cast iron was conducted by the smelting-reduction and fiber-blowing integrated technology. The structure, performance and environmental impact of products was further analyzed. The results showed the recovery rate of Fe was at a high level, ranging from 95.10% to 99.34%. The content of main impurity of concern (sulfur) in cast iron was less than 0.07 wt.%, which reached the recommended standard of China's ferrous metallurgy industry. The produced glass fiber showed excellent properties, such as a fibrosis rate above 83 %, a mean fiber diameter of 0.97 to 4.12 μm, and a mean fiber tensile strength varying from 1450 to 7110 MPa. The highest Na^+ leaching concentration did not exceed 1.26 mg/L and the Na^+ solidification rate was over 99.9%, showing a satisfactory environmental benefit. The mechanistic study and successful production provide new insights into the high value-added utilization of BRM.

Keywords: Total utilization; Atomic structure; smelting reduction; process design; Glass solidification

EFFECT OF WASTE GLASS POWDER ON IMPROVING THE RESISTANCE ABILITY OF ELEVATED TEMPERATURE FOR ULTRA-HIGH PERFORMANCE CONCRETE

Weichen Tian, Jian-Xin Lu, and Chi Sun Poon

Department of Civil and Environmental Engineering, The Hong Kong Polytechnic University,
Hung Hom, Kowloon, Hong Kong
jianxin.lu@polyu.edu.hk (J.-X. Lu) and cecspoon@polyu.edu.hk (C.S. Poon)

The large amount of waste glass generation is causing a serious concern in Hong Kong due to the gradually running out of landfill sites in Hong Kong. The high-value added use of waste glass in concrete construction is beneficial for reducing the carbon emission and relieving the burden of the disposal problem for waste glass in Hong Kong.

In this work, waste glass powder (WGP) was used to replace cement to prepare ultra-high performance concrete (WGP-UHPC), aiming to improve the high-temperature resistance of the specimen. Results showed the introduction of WGP would not affect the compressive strengths of WGP-UHPC even at a high replacement ratio of 40 wt%, for the specimens with 0~40 wt% WGP replacement, the compressive strengths were all around 140 MPa, while the high-temperature resulted in the strength degradation of the specimens, and the use of WGP could effectively refine this strength degradation phenomenon. Moreover, the specimens exhibited an obvious further strength reduction phenomenon after exposure to elevated temperatures with a further air curing condition, and this was induced by the microstructure degradation of the specimen. WGP could also relieve this strength reduction. Microstructural characterizations including XRD、TG、MIP、Micro-CT and SEM-BSE analyses were conducted to better understand the beneficial effect of WGP on UHPC exposed to elevated temperatures.

Keywords: Waste glass powder, Ultra-high performance concrete; Elevated temperature, Performance degradation, Microstructure analysis

PREPARATION AND CHARACTERIZATION OF POROUS GLASS LIGHTWEIGHT AGGREGATE

Weiyi Ji, Jian-Xin Lu*, Chi-Sun Poon*

Department of Civil and Environmental Engineering, The Hong Kong Polytechnic University,
Hung Hom, Kowloon, Hong Kong
*Corresponding authors: **jianxin.lu@polyu.edu.hk**; **chi-sun.poon@polyu.edu.hk**

Waste glass presents a pressing environmental concern in Hong Kong, and the reclamation of waste glass to prepare artificial lightweight aggregate help save landfill space and natural resources. In this paper, local waste glass and calcium carbonate were used to produce foamed glass by high-temperature sintering. The influence of varying sintering temperatures and the concentration of the foaming agent on the resultant density and microstructural attributes of the foamed glass were investigated. It was found that the increase of sintering temperature and foaming agent content significantly affected the sample properties, which showed that the volume of open pores increased, and the mechanical properties decreased. The effects of different parameters on pore number, size and volume distribution were further determined by SEM and X-ray CT. The theoretical effect of high temperature decomposition products of foaming agent on glass matrix was studied by thermodynamic calculation software, and the calculated results were verified by XRD.

Keywords: Incinerated sewage sludge; Lightweight aggregate; Self-foaming; Microstructure; Sintering;

Session D2

Alkali Activation and Artificial Aggregates

ARTIFICIAL AGGREGATES DERIVED FROM SOLID WASTES

Tang, P.[1], Li, Y.X.[2], Guo, S.F.[2], and Chen, W.[1]

[1]State Key Laboratory of Silicate Materials for Architectures, Wuhan University of Technology, Wuhan 430070, China
[2]School of Materials Science and Engineering, Wuhan University of Technology, Wuhan 430070, China
E-mail: (Tang, P.) pei-tang@whut.edu.cn

The recycling of various solid wastes into artificial aggregates is a beneficial way to reduce environmental risk and save natural resources. The types and properties of solid wastes, mixture proportions, manufacturing and curing of artificial aggregates have significant influence on the properties of artificial aggregates. The physical, chemical and mechanical properties of the artificial aggregates have great impact on its application sufficiency. The relationships between solid waste properties, production procedure, etc. of artificial aggregates should be well established.

Keywords: integral recycling, high volume, aggregate replacement

SUSTAINABLE ALTERNATIVE AGGREGATE FROM MSWI BOTTOM ASH THROUGH GRANULATION AND ALKALI ACTIVATION

Priyadharshini Perumal, and Mirja Illikainen

Fibre and Particle Engineering Research Unit, University of Oulu, Finland.
Priyadharshini.perumal@oulu.fi

Municipal solid waste is piling up due to lifestyle changes and urbanization in recent days. Waste to Energy plants is designed to utilize such wastes as source for fuel and helps in reducing the volume of these wastes. However, in this process, secondary residues such as fly ash, bottom ash, air pollution control residue and boiler slag are formed. Without addressing these residues and formulating a potential application, this process does not reach the circularity or sustainability. There are several research works in the related field to utilize incinerated residues as construction materials, especially as cement supplements, sand replacement in non-structural elements or in geotechnical applications as backfills, subbase layer and embankments.

In this study, locally sourced municipal solid waste incinerated bottom ash is attempted to be used as a raw material in manufacturing granulated artificial aggregate. Granulated aggregates are relatively well studied materials and commercialized with clay for the use as lightweight aggregate and in fertilizer industries. These materials are mainly produced by sintering the clay granules at high temperature around 700 – 1200 °C, making this process highly energy intensive. Alkali activation came as alternative to avoid high temperature sintering, where alkali solutions are used during granulation and curing happens at lower temperature of 60 – 100 °C or even at room temperature. However, considering the overall carbon footprint, addition of alkali creates an impact almost similar to that of sintering at high temperatures. In the present study, an attempt is made to use bottom ash and alternative alkali sources from different industrial side streams to understand the feasibility of making alkali activated granules for aggregate application. The outcomes are encouraging, and a carbon footprint calculation gives a positive note on the process parameters.

Keywords: Granulation, MSWI bottom ash, lightweight aggregate, alkali activation, carbon footprint

PREPARATION OF GLASS-CERAMIC-BASED ARTIFICIAL AGGREGATES USING MULTIPLE SOLID WASTES

Yunpeng Liu*, Xianzheng Dong, and Wenhao Wan

State Key Laboratory of Silicate Materials for Architectures, Wuhan University of Technology,
Wuhan, 430070, China
E-mail: liuyunpeng@whut.edu.cn

1. INTRODUCTION

Lightweight aggregate concrete (LWAC) has attracted wide attention due to its lightweight, improved durability, thermal insulation, and other multi-functions. Lightweight aggregates (LWAs) mainly include sintered aggregates and cold-bonding aggregates. Of which, sintered LWAs are calcined in a rotary kiln at a high temperature (1 000 – 1 300 °C) with natural clay and shale as the primary raw materials. Harmful solid waste could be disposed of during the high-temperature sintering and rapid cooling process. In China, the primary raw materials for LWAs are gradually transformed into sludge, muck, and other industrial solid wastes. However, the chemical compositions of industrial wastes are complex, which poses new challenges to the calcination process and the phase and microstructure design of LWAs(Ren, Ling, & Mo, 2021).

Although the raw material of LWAs has undergone significant changes, the sintered LWAs still have the drawbacks of low strength and high water absorption rate, which restricts the performance of LWAC. In addition, LWAs have a high water absorption rate and often need pre-saturated, which increases the difficulty of pumping construction and the risk of freeze-thaw damage. Therefore, using multi-industrial solid waste to prepare high-performance LWAs with high strength and low water absorption rates is essential.

The mineral phase composition of LWAs has an essential effect on their strength. The main phase composition of current LWAs is mainly quartz (SiO_2), mullite (SiO_2-Al_2O_3), etc. This is because the LWAs are usually designed according to the Riley scheme (SiO_2–Al_2O_3–flux), which includes SiO_2, Al_2O_3 and flux ($CaO+MgO+Na_2O+K_2O+Fe_2O_3$). A few new mineral phases could be formed by increasing the flux contents. However, the improvement in aggregate strength is not obvious. Motivated by introducing a high-strength phase in LWAs, diopside-based LWAs have been prepared according to the main chemical compositions of diopside rather than the Riley scheme(Liu et al., 2022). This extended abstract mainly introduces some new discussions on the challenges of the practical use of these novel LWAs.

2. MATERIALS AND METHODS

The materials and test methods are in References (Liu et al., 2022).

3. RESULTS AND DISCUSSION

The diopside-based aggregates were prepared using engineering residue and waste glass as the primary raw materials, which had a bulk density grade of 700, a single particle strength of approximately 20.0MPa, and a water absorption rate of only 0.9%. Compared with the mineral composition of ordinary LWAs, diopside was precipitated from the prepared aggregate, contributing to a significant strength increase. Moreover, a dense glassy layer was formed outside the aggregates, significantly reducing the aggregate's water absorption rate. The detailed crystallization mechanism has been investigated by (Liu et al., 2023).

The first challenge for industrial use is the calcination regime. The aggregates mentioned above are prepared according to the calcination regime glass-ceramic. It is pre-firing at 800 °C for 60 minutes at a slow increase rate of 5 °C/min and calcined at 1 120 – 1 200 °C for 60 min to ensure the of the analytical crystals. However, LWAs are manufactured by rapid heating (above 10 °C/min) and rapid calcination (calcination time 10 - 20min) in the rotary kiln. So, a modified calcination regime was adopted, which was increased to 600 ° C at 10 ° C/min and maintained for 10 minutes. Then, the temperature was increased to 1000 - 1200℃ at 10 ° C/min and maintained for 30 min.

Figure1 shows the microstructure of the obtained aggregates. The modified regime showed a marginal effect on the crystal phase composition and microscopic morphology, and the crystallites can be grown in a short calcination time. By using the modified regime, three glass-ceramic-based artificial aggregates, including diopside, anorthite, and wollastonite aggregates, have been prepared (Liu et al., 2023).

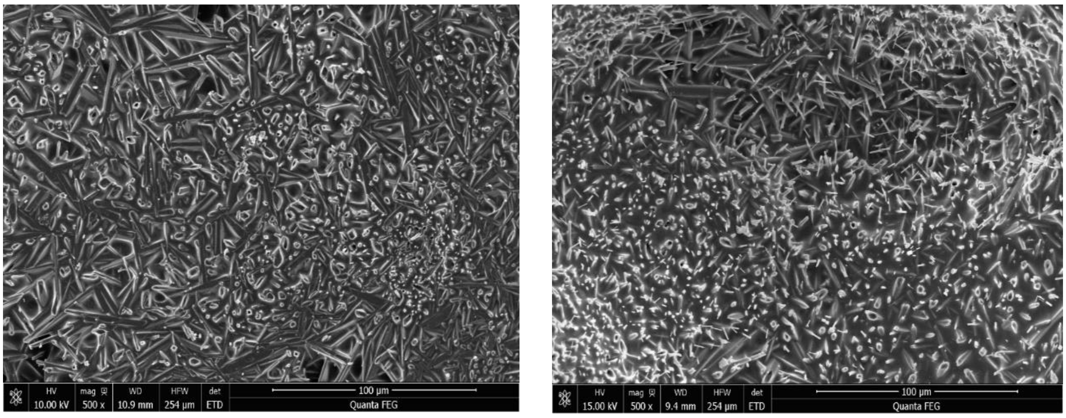

a.Orignal calcination regime b. Modified calcination regime

Figure 1. Microstructure of two aggregates prepared with different regimes

The second challenge is the different viscosity of the aggregates compared to ordinary LWAs. To facilitate the crystallization of diopside, increased CaO and MgO contents were introduced in the raw materials of LWAs, which theoretically decreased the viscosity of the liquid phase because CaO and MgO are usually recognized as the flux contents. The decreased viscosity may make keeping the aggregate's spherical shape in the rotary kiln challenging. Moreover, the gas is easier to escape during bloating, making it difficult to control the density.

At last, the improvement in the prepared concrete strength needs to be investigated. The formation of the dense glassy surface contributed to the decrease in the water absorption rate and the improvement in the strength of the aggregate. On the other hand, it should be noted that the glassy surface may reduce the interface bonding between the aggregates and cement paste. Moreover, whether the glassy surface of obtained aggregates has pozzolanic reactivity needs to be verified and investigated.

4. CONCLUSION

a. Introducing diopside in the LWAs has contributed to the increase in the aggregate's strength. However, several studies need to be further investigated.

b. The most crucial part is whether a novel design methodology could be established to balance between crystallization process and viscosity control.

c. The improvement of the concrete performances by incorporating these novel aggregates needs to be investigated.

5. ACKNOWLEDGMENT

The authors would like to express appreciation for the support of the State Key Laboratory of Solid Waste Reuse for Building Materials Open Funding. [Project Number = 20191h0592].

6. REFERENCES

Liu, Y., Wan, W., Lu, J.-X., Poon, C. S., Hu, S., & Wang, F. (2023). Preparation of glass-ceramic-based artificial aggregates using multiple solid wastes: Crystallization mechanism. *Journal of Cleaner Production, 421*, 138298. doi:https://doi.org/10.1016/j.jclepro.2023.138298

Liu, Y., Wan, W., Yang, F., Hu, C., Liu, Z., & Wang, F. (2022). Performance of glass-ceramic-based lightweight aggregates manufactured from waste glass and muck. *Ceramics International, 48*(16), 23468-23480. doi:https://doi.org/10.1016/j.ceramint.2022.04.342

Ren, P., Ling, T.-C., & Mo, K. H. (2021). Recent advances in artificial aggregate production. *Journal of Cleaner Production, 291*, 125215. doi:https://doi.org/10.1016/j.jclepro.2020.125215

DEVELOPMENT OF ALKALI-ACTIVATED CONCRETE USING MSWI BOTTOM ASH AS COARSE AGGREGATES FOR SUSTAINABLE ROAD CONSTRUCTION

Boyu Chen[1], Ivana Mariam Paul[1], Luiz Miranda de Lima Junior[1], Patrick Holthuizen[1], Shan He[1], and Guang Ye[1,2]

[1]Department of Materials and Environment (Microlab), Faculty of Civil Engineering and Geoscience, Delft University of Technology, Delft, the Netherlands
[2]Magnel-Vandepitte Laboratory, Department of Structural Engineering and Building Materials, Ghent University, 9052 Ghent, Belgium
E-mail: B.Chen-4@tudelft.nl

In recent years, municipal solid waste incineration (MSWI) has gained increasing attention due to its potential to recover energy. MSWI bottom ash is the primary residue that needs to be disposed of after waste incineration. In this work, a new type of alkali-activated concrete (AAC) was developed for road construction by using MSWI bottom ash as coarse aggregate. Before being used to prepare AAC, MSWI bottom ash was treated with NaOH solution to eliminate the adverse effect of metallic aluminum (Al) on strength development. NaOH solution-treated MSWI bottom ash aggregates were used to partially replace natural aggregates (NA) in blast furnace slag-based AAC. The mechanical properties (including compressive strength, split tensile strength, and flexural strength), freeze-thaw resistance, and leaching potential of developed AAC were tested. The microstructure of developed AAC was analyzed with scanning electron microscopy (SEM) and X-ray computed tomography (CT) scan. The test results showed that the highest achievable replacement level of NaOH-solution treated MSWI bottom ash was 30 % in AAC. Although the compressive strength of AAC prepared with 30% NaOH solution-treated MSWI bottom ash aggregates and 70 % natural aggregates (30BA-70NA AAC) was lower than that of the AAC prepared with 100 % natural aggregates, the strength level of 30BA-70NA AAC still met the requirement for road pavements exposed to de-icing salt in the Netherlands. The lower compressive strength of 30BA-70NA AAC can be attributed to the fact that replacing NA with MSWI bottom aggregates increased the porosity of AAC. The bonding between MSWI bottom ash aggregates and the alkali-activated slag pastes in AAC is weaker than that between NA and the binder. The leaching of heavy metals from 30BA-70NA AAC is below the upper limit for granular materials specified in the Dutch regulations, indicating that it is safe to use developed AAC for road application.

Keywords: MSWI bottom ash aggregates, alkali-activated concrete, NaOH solution treatment, road construction, life cycle assessment

POTENTIAL OF PALM OIL FUEL ASH IN THE PRODUCTION OF COLD-BONDED LIGHTWEIGHT AGGREGATES BY ONE-PART ALKALI-ACTIVATED METHOD

Jiayi Lin[1], Yingxin Goh[2], **Kim Hung Mo**[1,*]

[1] Department of Civil Engineering, Faculty of Engineering, Universiti Malaya, 50603 Kuala Lumpur, Malaysia
[2] Department of Mechanical Engineering, Faculty of Engineering, Universiti Malaya, 50603 Kuala Lumpur, Malaysia
[*]Corresponding author: khmo@um.edu.my

In this study, artificial lightweight aggregate was developed from palm oil fuel ash (POFA) using cold-bonded one-part alkali-activation method. Firstly, the influence of granulation parameters (the ratio of precursor (POFA) and additive (GGBS), activator content ($Na_2SiO_3.5H_2O$), water content, rotation angle, and rotation speed) on granulation efficiency and granulation duration were evaluated. Specifically, the rotation angle and rotation speed were optimized by response surface methodology (RSM) modeling. Results showed that the water demand for the POFA-based alkali-activated aggregates (PFAAs) with different combination ranged from 0.3–0.46. Increasing the GGBS and $Na_2SiO_3.5H_2O$ content improved the granulation efficiency up to 87.4% and shortened the granulation duration to 7 min. RSM modeling revealed that the optimum rotation angle and rotation speed were 55° and 50 rpm, respectively, resulting in a maximum granulation efficiency of 88.2%.

Secondly, the physical properties including loose bulk density, water absorption and crushing strength of PFAAs were further investigated. The result showed the produced PFAAs with a loose bulk density, water absorption and crushing strength from 718.3 kg/m^3 to 742.3 kg/m^3, 14.8% to 18.2% and 2.1 MPa to 2.7 MPa, respectively, which met the requirement of lightweight aggregate in EN13055.

Furthermore, the phase analysis of the PFAAs was examined to ascertain the mechanism of alkali-activation and strength development of the aggregates. The phase analysis result showed that C-S-H was identified after alkali-activation and the GGBS enhances the effect of alkali-activation. Overall, this study demonstrated the feasibility of using palm oil fuel ash to produce artificial lightweight aggregates through cold-bonded one-part alkali activation method, which can be effectively utilized in concrete production.

Keywords: Palm oil fuel ash; Granulation parameters; Artificial lightweight aggregate; Cold-bonded aggregate; One-part alkali-activation

MODIFICATION OF RECYCLED COARSE AGGREGATE USING ENZYME-INDUCED CARBONATE PRECIPITATION (EICP) TECHNOLOGY

Bingcheng Chen, Ligang Peng, Keqiong Yu, Yuxi Zhao*

Institute of Structural Engineering, Zhejiang University, Hangzhou 310058, Zhejiang, PR China
*Corresponding author, yxzhao@zju.edu.cn (Y.X. Zhao)

1. INTRODUCTION

The relentless progress of the economy and urbanization necessitates a substantial quantity of concrete, especially in China, India, and densely populated developing nations. Conversely, the extensive waste generated from construction and demolition activities [1], has led to catastrophic waste management crises. Consequently, recycled coarse aggregate (RCA) has garnered worldwide recognition as an eco-friendly alternative to natural coarse aggregate (NCA). Nonetheless, during the crushing process, cracks may occur in RCA, and the old mortar adheres to the surface of the original aggregate [2], resulting in inferior physical and mechanical properties of RCA, such as water absorption, crushing index, and apparent density [3]. The subpar performance of RCA significantly hampers the construction, mechanical properties, and durability of concrete derived from recycled materials, thereby imposing severe restrictions on the widespread utilization of recycled aggregate concrete (RAC) in the construction sector. Consequently, addressing the defects of RCA to enhance its quality assumes paramount importance in bolstering its utilization.

In recent years, bio-deposition treatment has emerged as a promising approach for addressing defects in RCA. Microbial-induced carbonate precipitation (MICP) [4] has received considerable attention among the various investigated technologies for improving the quality of RCA. Specifically, the decomposition of urea by ureolytic bacteria results in the production of CO_3^{2-}. Additionally, the incorporation of Ca^{2+} from external calcium sources promotes the formation of $CaCO_3$ precipitation [5].

In the realm of RCA biomineralization, Wang et al. [6] employed bacteria with urease-producing capability to conduct biomineralization treatment on recycled aggregates. Their findings showed a significant 19% reduction in the water absorption of RCA after MICP treatment. Similarly, Zeng et al. [7] observed an improvement in the compressive strength of concrete using modified RCA and attributed this enhancement to the increased microhardness of the ITZ after MICP treatment. Furthermore, Zhao et al. [8] reported different levels of improvement in the flexural strength and resistance to carbonation of recycled concrete mortar following MICP modification. However, Wang et al. also [6] investigated the pore size distribution of RCA before and after MICP treatment. The research findings showed a significant decrease in macro-pores (1-10 μm) in RCA, while a considerable number of micro-pores smaller than 1 μm remained. The limited size of bacteria (1-3 μm) hindered their ability to penetrate micro-pores smaller than 1 μm, thereby limiting the formation of $CaCO_3$ at deeper levels [9]. Additionally, bacteria tended to block the pores [10], resulting in $CaCO_3$ formation mainly on the aggregate surface. Despite the surface enhancement effects, the internal micro-pores were not sufficiently repaired, negatively impacting the durability of RCA. Hence, further investigation is required to develop techniques capable of effectively repairing defects at deeper levels.

Enzyme-induced carbonate precipitation (EICP) technology [11], another significant biomineralization approach, utilizes free urease instead of bacteria for urea hydrolysis. Zulfikar et al. [12] employed EICP technology to repair concrete cracks and observed a 95% reduction in the permeability of the cracked concrete after four treatment cycles. Likewise, Dakhane et al. [11]

discovered that mortar treated with an EICP solution exhibited an approximate 30% increase in flexural strength and a doubling of fracture toughness. These studies established the feasibility of EICP technology for concrete applications. Furthermore, the short lifespan of urease activity enables rapid carbonate production, while enzymatic degradation mitigates long-term effects on concrete. Nanoscale urease (~10 nm) [13] can infiltrate micro-pores and micro-damage, facilitating $CaCO_3$ precipitation in confined spaces. In contrast to bacteria, EICP technology can bypass unknown and uncertain factors associated with bacteria, such as oxygen availability and complex soil hydraulic dynamics. However, limited reports are currently available on the application of EICP technology on RCA.

In this study, three different types of RCA (i.e., recycled mortar aggregate (RMA), recycled brick aggregate (RBA) and recycled granite aggregate (RGA)) were modified using EICP technology. The effects of calcium acetate concentration on the changes in weight and water absorption of recycled aggregates were investigated to obtain the optimal EICP treatment process. Scanning electron microscopy (SEM) and Energy-dispersive spectroscopy (EDS) were used to reveal the microstructure of the bio-deposits. Mercury intrusion porosimetry (MIP) tests were conducted to analyze the pore structure of the modified recycled aggregates after the optimal process. Finally, compressive strength tests and nanoindentation experiments were performed on the modified recycled aggregate concrete to reveal the modification mechanism.

2. MATERIALS AND METHODS

C&D wastes are a complex mixture consisting primarily of materials such as concrete, red bricks, ceramic tiles, and mortar. Different types of aggregates exhibit varying effects when subjected to specific modification processes. Therefore, this study focuses on investigating the potential of mortar and red bricks found in C&D wastes. In particular, aggregates derived from crushed concrete may have different levels of old mortar adhering to their surfaces, which can influence the EICP process. To minimize interference caused by material instability, the study used laboratory-prepared mortar specimens that were cured for 28 days. These specimens were crushed using a jaw crusher to obtain RMA. Additionally, industrial red bricks was used as raw materials and crushed to produce RBA, respectively.

3. RESULTS AND DISCUSSION

Several important findings were observed when the optimal EICP treatment process was established in present work. Firstly, the concentration of calcium acetate had a significant impact on the weight increase and water absorption reduction of three types of recycled aggregates. After EICP modification, the aggregates exhibited varying degrees of weight improvement, with RMA showing the highest weight increase rate due to the presence of calcium hydroxide. At a calcium acetate concentration of 0.5 mol/L, the modified aggregates reached their maximum weight increase rates. Beyond this concentration, the weight increase rates of RMA and RBA diminished, due to the inhibitory effect of higher calcium ion concentrations on urease activity.

Furthermore, different modification methods and the number of modification cycles on the weight increase and water absorption reduction of RMA were evaluated. Different modification methods yielded varying improvements in aggregate weight and significant reductions in water absorption. M-S method demonstrated superior effectiveness compared to M-I and I-S methods. Immersing RMA directly in the mixed medium solution (M-I method) resulted in uneven $CaCO_3$ distribution (which is easily accumulated on the upper surface of the aggregate by gravity), allowing water to enter from other surfaces. However, uniform spraying of the solution (M-S method) achieved a more uniform $CaCO_3$ deposition, sealing pores and cracks and enhancing performance. The rate of weight increase and water absorption reduction reached a stable level after multiple modification cycles. Three modification cycles using different methods showed substantial improvements compared to a single cycle. Considering economic factors, the optimal EICP treatment involves 0.5 mol/L of calcium acetate, modification method 4, and two modification cycles.

The SEM observations revealed that EICP modification led to the formation of dense $CaCO_3$ precipitates on the surface of the aggregates, effectively filling the pores and cracks and reducing water absorption. These precipitates exhibited strong bonding to the substrate, contributing to improved aggregate quality. Pore size distribution analysis indicated a decrease in pore volume and an improvement in pore size distribution after EICP modification, suggesting a reduction in porosity. This finding is crucial as lower porosity can enhance the durability and performance of concrete. Moreover, the compressive strength of concrete using EICP-modified recycled aggregates was significantly improved compared to unmodified aggregates. The EICP modification repaired surface defects, reduced water absorption, and enhanced the performance of ITZ, resulting in enhanced concrete strength.

Overall, these findings demonstrate the effectiveness of the EICP modification in enhancing the properties of recycled aggregates and improving the performance of concrete. The study provides valuable insights into the optimization of EICP treatment processes and offers potential applications in sustainable construction practices. Further research could focus on exploring the long-term durability and mechanical properties of concrete incorporating EICP-modified recycled aggregates.

4. CONCLUSION

The focus of this study is to optimize the EICP treatment process for enhancing the properties of RCA. Multiple evaluation criteria were employed to assess the impact of modifications on both RCA and concrete specimens. The following conclusions were drawn:

(1) The concentration of calcium acetate exhibited influence over the weight increase and reduction in water absorption of RAs. Optimum results were achieved with a concentration of 0.5 mol/L, resulting in maximum weight increase and water absorption reduction.

(2) The optimal EICP treatment process involves adding 0.5 mol/L of calcium acetate, implementing M-S method (uniform spraying of the mixed medium solution), and repeating the modification cycle twice.

(3) SEM observations and XRD analyses demonstrated that the EICP modification led to the formation of a compact layer of CaCO3 precipitates on the aggregate surface, effectively filling pores and cracks and reducing water absorption. The precipitates exhibited cohesive interconnection and strong adhesion to the substrate. Furthermore, the MIP test revealed a reduction in pore volume within specific ranges following the EICP modification, signifying a decrease in porosity and an enhancement in pore size distribution.

(4) Concrete incorporating EICP-modified RAs exhibited enhanced compressive strength compared to unmodified RAs. The EICP modification effectively addressed surface defects, minimized water absorption, and improved the performance of the ITZ, thereby contributing to the observed strength improvement.

5. ACKNOWLEDGMENT

Financial support from the special support plan for high-level talents in Zhejiang Province (2021R52035) is gratefully acknowledged. Bo Zhang would like to express gratitude for the financial support received from two R&D programs: “Leading Goose” R&D Program of Zhejiang (2023C01154) and "Unveiling the List" program of Dinghai, Zhoushan (2022C1113).

6. REFERENCES

[1] Ibrahim, M., Alimi, W., Assaggaf, R., Salami, B. A., & Oladapo, E. A. (2023). An overview of factors influencing the properties of concrete incorporating construction and demolition wastes. Construction and Building Materials, 367, 130307.

[2] Yang, X., Liu, Y., Liang, J., Meng, Y., Rong, H., Li, D. & Liu, Y. (2023). Straightening methods for RCA and RAC—a review. Cement and Concrete Composites, 105145.

[3] McNeil, K., & Kang, T. H. K. (2013). Recycled concrete aggregates: A review. International journal of concrete structures and materials, 7, 61-69.

[4] Liu, M., Xia, J., Chin, C. S., & Liu, Z. (2020). Improving the properties of recycled aggregate pervious pavement blocks through bio-mineralization. Construction and Building Materials, 262, 120065.

[5] Qian Chunxiang, Ruixing, W. , & Liang], C. . (2009). Corrosion protection of cement-based building materials by surface deposition of caco3 by bacillus pasteurii. Materials Science and Engineering: C.

[6] Wang, J., Vandevyvere, B., Vanhessche, S., Schoon, J., Boon, N., & De Belie, N. (2017). Microbial carbonate precipitation for the improvement of quality of recycled aggregates. Journal of Cleaner Production, 156, 355-366.

[7] Zeng, W., Zhao, Y., Poon, C. S., Feng, Z., Lu, Z., & Shah, S. P. (2019). Using microbial carbonate precipitation to improve the properties of recycled aggregate. Construction and Building Materials, 228, 116743.

[8] Zhao, Y., Peng, L., Zeng, W., sun Poon, C., & Lu, Z. (2021). Improvement in properties of concrete with modified RCA by microbial induced carbonate precipitation. Cement and Concrete Composites, 124, 104251.

[9] De Muynck, W., Leuridan, S., Van Loo, D., Verbeken, K., Cnudde, V., De Belie, N., & Verstraete, W. (2011). Influence of pore structure on the effectiveness of a biogenic carbonate surface treatment for limestone conservation. Applied and Environmental Microbiology, 77(19), 6808-6820.

[10] Cui, M. J., Lai, H. J., Hoang, T., & Chu, J. (2021). One-phase-low-pH enzyme induced carbonate precipitation (EICP) method for soil improvement. Acta Geotechnica, 16, 481-489.

[11] Dakhane, A., Das, S., Hansen, H., O'Donnell, S., Hanoon, F., Rushton, A., ... & Neithalath, N. (2018). Crack healing in cementitious mortars using enzyme-induced carbonate precipitation: Quantification based on fracture response. Journal of Materials in Civil Engineering, 30(4), 04018035.

[12] Zulfikar, R. A. , Putra, H. , & Yasuhara, H. . (2021). The utilization of soybean as a catalyst material in enzyme-mediated calcite precipitation (emcp) for crack healing concrete. Journal of the Civil Engineering Forum, 7(1), 59-70.

[13] Blakeley, R. L., & Zerner, B. (1984). Jack bean urease: the first nickel enzyme. Journal of molecular catalysis, 23(2-3), 263-292.

LOW-CARBON ALKALI-ACTIVATED SLAG FOR ULTRA-DURABLE CONCRETE INFRASTRUCTURE

Hailong YE
Department of Civil Engineering, The University of Hong Kong, Pokfulam, Hong Kong, China
* Corresponding author (Email: hlye@hku.hk)

Concerns about the CO_2 emission related to ordinary portland cement manufacturing have driven the innovation and development of low-carbon construction materials. Cement-free alkali-activated material - sometimes called geopolymer cement - has been a promising option, as it could offer up to 90% reduction in CO_2 emission and its production is primarily based on the use of industrial byproduct, including granulated ground blast-furnace slag (GGBS). Nevertheless, the broad application of cement-free GGBS-based binders and concrete in the industry has been hindered partially due to the unclear durability performance. In this work, the durability performance of GGBS-based materials in extreme service conditions is discussed, particularly in the marine and sewer environments. In addition, this work introduces several innovative GGBS-based materials for both general and special applications, including marine binders, antimicrobial coatings, fire-resistant high-strength green concrete, "just add water" cement-free binders with comparable performance as conventional cement, and soil stabilizing agents.

ULTRA-STABILIZED FOAM IMPROVED BY AMPHIPHILIC NANO SILICA FOR FOAM CONCRETE

Chunpeng Zhang, Dingqiang Fan, Jian-Xin Lu *, Chi Sun Poon *

Department of Civil and Environmental Engineering & Research Centre for Resources Engineering
Towards Carbon Neutrality (RCRE), The Hong Kong Polytechnic University, Hung Hom,
Kowloon, Hong Kong, China
* Corresponding Emails: jxinlu@polyu.edu.hk; chi-sun.poon@polyu.edu.hk

Foam concrete is increasingly used in construction due to its light weight, good thermal insulation and fire resistance, and environmental sustainability, but its low strength limits its further popularization and application. To enhance the stability and performance of foam concrete, amphiphilic nano silica (ANS) was firstly used to modify the sodium dodecyl sulphate (SDS) based foaming agent. Then, the designed foam was utilized to fabricate foam concrete, of which micro/macro performance was analyzed in detail. The results showed that ANS-modified foam exhibited superior stability and thicker foam wall thickness, contributing to enhanced foam stability during mixing and in the cement matrix. The foam concrete with ANS had higher strength compared to the control groups at different density levels. The analysis of pore structures revealed that ANS modification resulted in a more rounded and uniform pore shape, with a higher percentage of small pores and a smaller average pore size. Chemical composition analysis indicated that the use of ANS did not significantly alter the cement hydration process, but it improved the overall compactness of the foam concrete. These findings demonstrate the potential of ANS as an effective foam stabilizer for foam concrete production, leading to improved mechanical properties and enhanced foam stability. Overall, the use of ANS offers promising prospects for enhancing foam concrete performance and applications in construction industry.

Keywords: Foam concrete; Amphiphilic nano silica; Foaming agent; Experimental study; Pore structure

UTILIZATION OF CONTAMINATED AIR POLLUTION CONTROL RESIDUES FOR THE PREPARATION OF ALKALI/SULFATE-ACTIVATED SLAG/GLASS POWDER

Keke Sun, Chi Sun Poon*

Department of Civil and Environmental Engineering and Research Centre for Resources Engineering towards Carbon Neutrality, The Hong Kong Polytechnic University, Hung Hom, Kowloon, Hong Kong, China

The conventional alkali-activated materials (AAMs) are usually formed by reactions between aluminosilicate precursors and a concentrated corrosive aqueous solution of alkali metal silicates or hydroxides or their combinations, such as sodium silicate, sodium hydroxide, potassium silicate, potassium hydroxide. However, the use of these high pH activating solutions usually results in an undesirable rapid setting, large shrinking cracks, and subsequent deterioration of strength. To achieve adequate strengths with controlled setting and shrinkage, the high pH alkali silicates or hydroxides can be partially replaced with near-neutral salts.

Air pollution control (APC) residues are waste materials generated during the sewage sludge incineration process, and the high content of heavy metals and sulfate salts makes it challenging to utilize them effectively. In this study, an exciting recycling route of the APC residue was identified by using it as a source of sulfate salts and aluminosilicate for the formulation of alkali/sulfate-activated slag/glass powders (ASAMs). In the ASAMs, the high pH alkali silicates or hydroxides can be partially replaced with the Na_2SO_4 from the APC residues as hybrid activators, thereby reducing the energy-intensive manufacturing processes of the activator. The ASAMs demonstrate adequate strength with controlled setting and shrinkage, and the leaching of heavy metals from the APC residues could be controlled by the solidification and stabilization mechanism of the binder. Furthermore, the ASAMs possess certain acid buffers and acid-neutralizing capacities to retard the dealumination process of the gels phase upon acid attack. This excellent acid resistance of the ASAMs was closely related to the structural characteristics and content of the gels. Overall, the ASAMs can be considered more environmentally friendly compared to the conventional AAMs due to their ability to effectively reuse industrial by-products as aluminosilicate precursors and their potential to reduce CO_2 emissions through proper design and implementation.

Keywords: Alkali/sulfate-activated materials; Air pollution control residues; Physical property; Acid-resistance; Solidification/stabilization.

THE POTENTIAL USE OF CARBONATED RECYCLED CONCRETE FINES WITH SODIUM META-ALUMINATE FOR SYNTHESIZING ALKALI-ACTIVATED MATERIALS

Weiwei Chen, Peiliang Shen, Chi Sun Poon

Department of Civil and Environmental Engineering, Research Centre for Resources Engineering
toward Carbon Neutrality, The Hong Kong Polytechnic University,
Hung Hom, Kowloon, Hong Kong

The utilization of carbonated recycled concrete fines (CRCF) as construction materials has attracted significant attention in recent years. This study aimed to employ sodium meta-aluminate (SMA) solutions with varying contents as an alkaline activator for the preparation of alkali-activated carbonated recycled concrete fines (AACRCF) materials. The results reveal that AACRCF hydration primarily involves carbonate-aluminate reactions and alkaline reactions on both the calcium carbonate and silica-alumina gel phases of CRCF grains. An increase in SMA content initially enhances the hydration degree of AACRCF, resulting in higher pirssonite and Mc content. However, excessive SMA content triggers early katoite formation, delaying the formation of these phases. The influence of SMA content on the compressive strength of AACRCF paste exhibits a strong positive correlation with the amount of pirssonite and Mc. Furthermore, the reduced compressive strength of AACRCF pastes activated with SMA content less than 40 wt.% can be attributed to the decomposition of thermonatrite and pirssonite, as well as the declining polymerization of C-N-A-S-H gels over time.

Keywords: Construction materials, Alkali-activated CRCF, Hydration mechanism, Carbonate-aluminate reaction, Alkaline reaction

Session D3

Contaminant Leaching and Environmental Impact

EVALUATION OF THE UTILISATION POTENTIAL OF PRODUCTS FROM BOTTOM ASH TREATMENT VIA A RISK-BASED METHODOLOGY BASED ON THE RESULTS OF LEACHING AND ECOTOXICOLOGICAL TESTS

Acampora, L[1], **Costa, G.**[1], Lombardi, F.[1], Maggi, L.[2], Mensi, C.[3], Messinetti, S.[3], Tediosi, E.[3], Verginelli, I.[1]

[1]Department of Civil Engineering and Computer Science Engineering, University of Rome Tor Vergata, Rome 00133, Italy
[2]Chemservice S.r.l. - Lab Analysis Group, Via F.lli Beltrami 15, 20026 Novate Milanese, Milan, Italy
[3] A2A Ambiente S.p.A., Cascina Maggiore, 27010 Giussago (PV), Italy
costa@ing.uniroma2.it (corresponding author)

1. INTRODUCTION

Waste-to-Energy is an established technology for residual waste management in Europe, which allows to recover not only energy but also valuable materials from the treatment of its most abundant solid residue: bottom ash (BA). Technologies for ferrous and non ferrous metals recovery from BA are being increasingly implemented all over Europe (Šyc et al., 2020). The mineral fraction (over 75% by weight) of BA is currently employed in construction applications in several Countries, but neither harmonized procedures, nor End of Waste criteria have been issued at a European level for establishing the environmental requirements for its utilization (Saveyn et al., 2014). Each Country has developed its own rules that make use of different methodologies, mainly based on several types of leaching test methods. In Italy, which presents one of the highest utilisation rates (85%) (Blasenbauer et al., 2020), BA is typically sent to large-scale treatment plants that besides ferrous and non ferrous metals recovery separate mineral fractions that are generally employed as aggregates or sand substitutes in concrete or asphalt mixtures, or in cement or ceramics manufacturing. End of waste criteria have not been issued for the mineral fraction products and utilisation is decided by local authorities case by case, leading to uncertainties for BA producers, treatment plants and final users of the products. The main potential risk posed to the environment and human health by these materials is the release of metals, metalloids and salts (mainly chlorides and sulphates) into percolating rainwater that may subsequently migrate to contaminate soil, groundwater and surface water, therefore potentially impacting terrestrial and aquatic ecosystems, as well as drinking water quality.

In this work, we present a methodology that was applied to assess if the use as unbound fillers or aggregates of mineral fractions from BA treatment may pose potential risks to the environment and human health. This approach employs of the results of both leaching and ecotoxicological tests carried out on products collected from full-scale industrial plants and evaluates them through a risk assessment procedure, assuming worst reasonable scenarios.

2. MATERIALS AND METHODS

Specifically, ten different products collected from four Italian BA treatment plants, termed in this paper 1, 2, 3 and 4, were analysed. Table 1 reports the acronyms of the analysed samples, their particle size and their utilisation modes.

Table 1. Ten samples analysed in this work.

Plant	Sample	Size [mm]	Utilisation
Plant 1	**1A**	0<d<25	cement/ceramics production
	1B	0<d<25 (d<10 81%)	aggregates cement/ceramics production
	1C	0<d<25 (d<10 82%)	aggregates cement/ceramics production
Plant 2	**2D**	0<d<16	cement/ceramics production
	2E	0<d<6	aggregates cement/ceramics production
	2F	0<d<8	aggregates cement/ceramics production
Plant 3	**3G**	0<d<8	aggregates
	3H	0<d<11.6	aggregates
Plant 4	**4I**	0<d<6.3	aggregates
	4L	0<d<12.5	aggregates

As for the analysis of the leaching behaviour of the products, three types of standardized tests (i.e. column percolation test - EN 14405, batch compliance test - EN 12457-2 and pH dependence test - CEN/TS 14429) were carried out. The samples collected were analysed for the major and trace constituents, including anions such as chlorides and sulfates and Dissolved Organic Carbon (DOC).

Composite samples of the eluates of the column percolation tests were also employed to carry out acute and chronic ecotoxicological tests on aquatic organisms, that are typically employed for waste classification according to the EU's CLP regulation, i.e. the OECD 201 Freshwater Alga and Cyanobacteria Growth Inhibition test, the OECD 202 Daphnia sp. Acute Immobilisation test, the OECD 203 Fish Acute Toxicity test and the OECD 211 Daphnia magna Reproduction test. For the mineral fractions that are typically utilised as aggregates or fillers, terrestrial ecotoxicological tests were also carried out employing organisms of different groups (plants, soil organisms and microorganisms).

As for the evaluation of risk-based guideline values to which compare the obtained leaching test concentrations, following a conservative approach, it was considered that the products would be employed as unbound fillers or aggregates in large parking lots or road sub-base layers. As shown in Figure 1, the results of the different types of characterization leaching tests applied, which allow also to assess the release mechanism (e.g. solubility or washout), were used as input data, and depending on the scenario considered, different dilution factors were calculated according to fate and transport models reported in the ASTM (2000) guidelines to estimate the concentrations resulting in the groundwater (point of compliance).

To evaluate the risks for the groundwater resource, two different approaches were adopted. The first consists in comparing the concentrations expected at the point of compliance with drinking water quality criteria set by specific legislation. In the second approach the risks were instead calculated for the water ingestion pathway using the equations proposed by ASTM (2000).

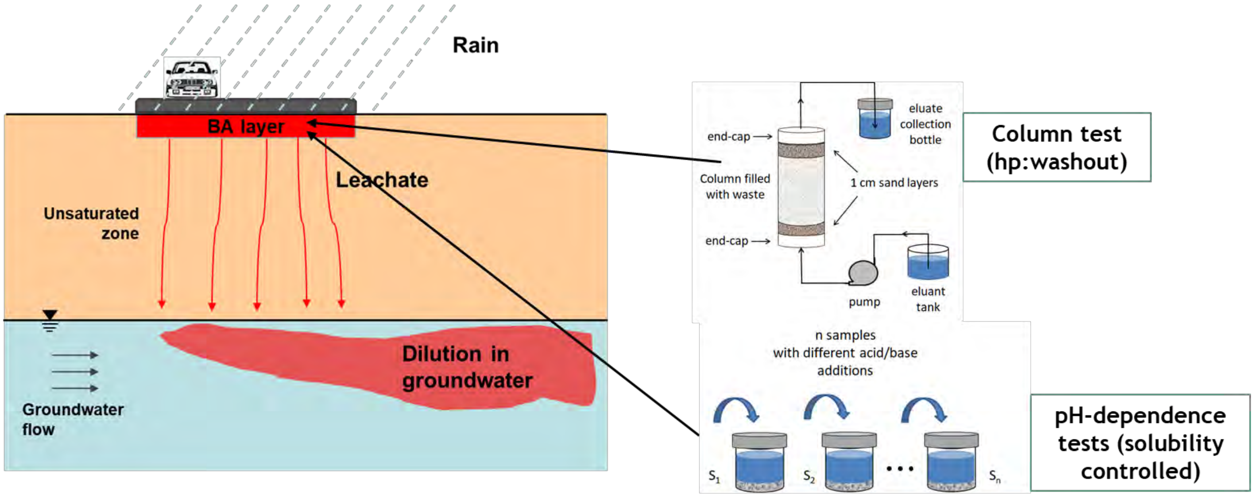

Figure 2. Scheme of the risk assessment procedure adopted.

To evaluate the risks for aquatic organisms, the results of the ecotoxicological tests were expressed as dilution factors and compared to the ones calculated for the assumed utilisation scenarios. Finally, also the results of the terrestrial ecotoxicity tests were statistically analysed to derive EC50 and EC10 to evaluate the risk for different scenarios.

3. RESULTS AND DISCUSSION

Figure 2 shows an example of the results obtained applying the two types of characterization leaching tests employed in this work, plotted as a function of the applied liquid to solid ration (L/S) for the percolation tests and pH, in the case of the pH-dependence test.

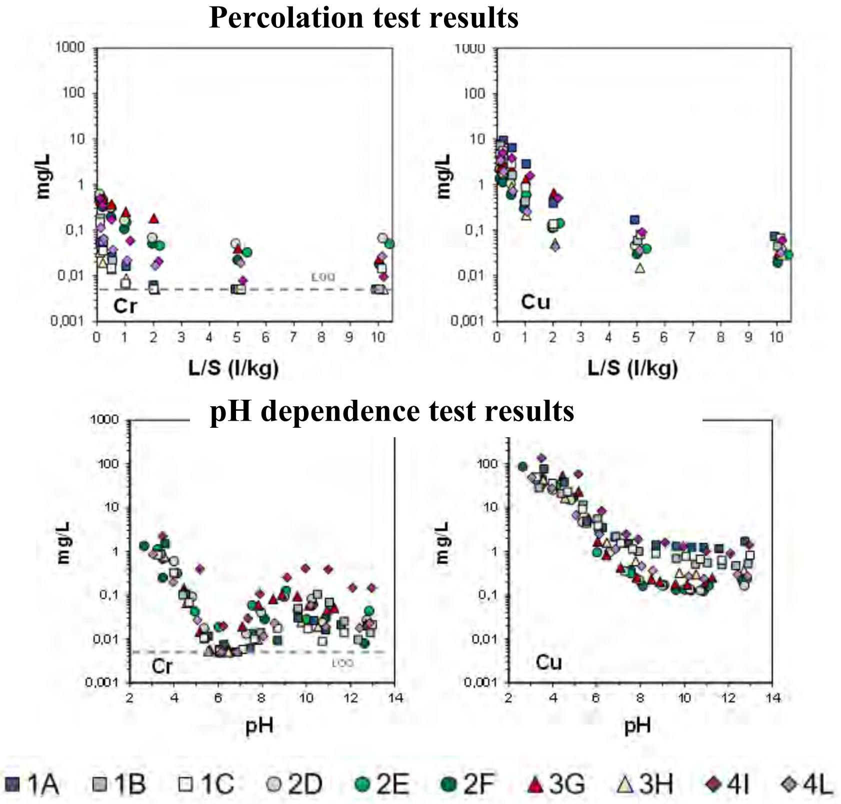
Percolation test results

pH dependence test results

Figure 2. Examples of the average results of the leaching test performed for each type of sample.

For most of the analysed constituents, the trends of the release curves obtained applying either type of test were quite consistent for the ten different samples analysed, although concentrations values showed to vary (e.g. of 1 order of magnitude in the case of Cu) depending on the type of sample. Based on the results of the leaching tests, the concentrations of the target contaminants to be used for the risk assessment were identified. For the pH-dependence leaching test, the maximum concentration obtained for pH values higher than 7 was selected, whereas for the percolation test, the maximum concentration values obtained for all of the tested L/S ratios were considered. The maximum concentrations detected from the different types of leaching tests were compared with the limit values calculated considering three utilisation scenarios and the associated Leaching Factors. For the use of the product without restrictions ("no restrictions"), the maximum concentrations in the eluate obtained from the pH dependence leaching tests and the column percolation tests for most of the target contaminants showed to be incompatible with utilisation. In particular, the most critical constituents in terms of exceedance of the risk-based limits set for the no restrictions scenario were Al, Cr, Cu, Mo, Pb, Sb, chlorides and fluorides. For the use of the products as aggregates in unbound form for large-scale applications, excluding some specific isolated cases, the maximum concentrations detected for the different indicator contaminants in the different leaching tests were lower than the calculated limit values. For the use of the products in unbound form as road sub-base materials ("worst reasonable case") no exceedance of the limit concentrations was detected for any of the indicator contaminants.

Interestingly, the results of the ecotoxicological tests provided the same type of response, indicating that the risk for aquatic organisms related to use with no restrictions would not be acceptable, while that for large-scale applications safe in most cases, and that for worst-reasonable cases always acceptable.

4. CONCLUSIONS

In this study a combined methodology to assess the environmental compatibility of the utilisation of mineral fractions obtained by BA treatment was proposed and tested for 10 samples produced by industrial plants. The procedure can be used to identify utilisation scenarios that may lead to acceptable risks to human health and aquatic and/or soil ecosystems, but also to identify the critical contaminants to be treated or managed before utilisation of the product, in order to achieve acceptable risk-based levels.

5. REFERENCES

ASTM, 2000. Standard Guide for Risk-Based Corrective Action. American Society for Testing and Materials. Standard E2081-00. West Conshohocken, PA.

Blasenbauer D., Huber F., Lederer J., Quina M.J., B. Biscarat D., Bogush A., Elza Bontempi E., Blondeau J., Chimenos J.M., Dahlbo H., Fagerqvist J., Giro-Paloma J., Hjelmar O., Hyks J., Keaney J., Lupsea-Toader M., O'Caollai C.J., Orupõld K., Pajak T., Simon F.G., Svecova L., Šyc M., Ulvang R., Vaajasaari K., Van Caneghem J., van Zomeren A., Vasarevičius S., Wégner K. & Fellner J., 2020. Legal situation and current practice of waste incineration bottom ash utilisation in Europe. Waste Manage. 102, 868-883.

Saveyn H., Eder P., Garbarino E., Muchova L., Hjelmar O., van der Sloot H., Comans R., van Zomeren A., Hyks J. & Oberender A., 2014. Study on methodological aspects regarding limit values for pollutants in aggregates in the context of the possible development of end-of waste criteria under the EU Waste Framework Directive. Institute for Prospective Technological Studies: Seville, Spain.

Šyc, M., Simon, F.G., Hyks, J., Braga, R., Biganzoli, L., Costa, G., Funari, V. & Grosso, M., 2020. Metal recovery from incineration bottom ash: State-of-the-art and recent developments. J. Hazard. Mater. 393, 122433.

LEACHING BEHAVIOR OF POLYCHLORINATED NAPHTHALENES FROM INCINERATION FLY ASH: EVALUATION BASED ON PERCOLATION TEST USING HUMIC ACID AS A LEACHANT

Mizutani, S.[1], Ito, K.[2], Kawahara, Y.[1] and Yabuki, Y.[2]

[1]Osaka Metropolitan University, Japan
[2]Research Institute of Environment, Agriculture and Fisheries Osaka Prefecture, Japan
E-mail miz@omu.ac.jp

Polychlorinated naphthalenes (PCNs) are one of the chemicals regulated by Stockholm Convention on Persistent Organic Pollutants. PCNs are generated in thermal process unintentionally and are found in solid waste incineration ash. In this study, the leaching behavior of PCNs from incineration fly ash were evaluated using up-flow percolation test, of which distilled water or humic acid are used as leachant.

An image of the percolation test is shown in Fig. 1. The 40 fractions of the leachate, approximately 1000 mL (each L/S=10 and total L/S=400) for each column were sampled followed by measurements of PCNs, TOC, pH and turbidity.

Total PCNs (i.e. total from monochloride to octachloride naphthalenes) concentration in each leachate fraction was 14 - 420 pg/L (for distilled water test) and 14 - 4300 pg/L (for humic acid test). Final leached ratios of total PCNs were 0.0086% and 0.098% respectively. The leached quantity of PCNs (especially highly chlorinated congeners) increased with increasing humic acid concentration in leachate. These results suggest that humic acid promotes the leaching of PCNs.

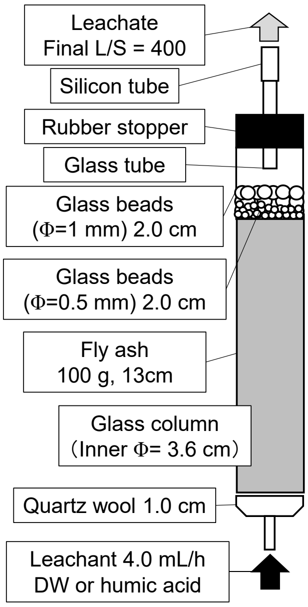

Fig.1 An image of the percolation test

Keywords: PCNs, Percolation test, Humic acid, TOC, incineration fly ash

ENVIRONMENTAL IMPACT OF MONOLITHIC PORTLAND CEMENT VERSUS HYBRID CEMENT USING DYNAMIC SURFACE LEACHING TEST

Salas, I[1], Cifrián, E[1], Fernandez-Jimenez, A[2], Maltseva, O[2], Palomo, A[2], Andrés, A[*1]

[1]Department of Chemistry and Process & Resources Engineering – ETSIIT, University of Cantabria, Santander, Spain
[2]Materials Department. Eduardo Torroja Institute (CSIC). Madrid, Spain
*andresa@unican.es (corresponding author)

The environmental assessment criteria for construction products are proposed by the European regulation framework for the protection of the environment and human health and dealing with their entire life cycle. Therefore, the prediction of the long-term release of dangerous substances is important with respect to the evaluation of release behavior of a construction product during its service life in their intended use. To this purpose, it is necessary to identify the main release mechanisms, in order to predict the long-term behavior by extrapolation of experimental data. In this article, a comparative study of the evaluation of the release of trace elements of a commercial Portland cement (CEM-I) and a hybrid cement (CEM-H) (clinker + fly ash + 5% activator) has been carried out. It has been applied the following leaching standards: Compliance leaching test (EN 12457-4) for determining the maximum concentration of pollutants from granular samples and dynamic surface leaching test (DSLT, CEN/TS 16637-2) for determining the release per unit of surface area as a function of time of potentially dangerous substances from monolithic samples. The results obtained allow to determine the leaching potential of contaminants through different stages of the life cycle: as a granular and as a monolithic material. The comparison of the long-term mobility of As, Cr, Mo, Sb, Se and V of both cements as a function of time (64 days) and the release mechanisms for monolithic materials was determined. Diffusion controlled leaching of trace elements is predominant in both type of cements. The mobility of trace elements is slightly higher in CEM-H than in CEM-I. However, both cements are considered suitable for construction application according to SQD leaching limits proposed by the Dutch Building Materials Decree.

Keywords: Portland cement, hybrid cement, leaching behavior, DSLT, long-term assessment

PRODUCING CLINKER FROM METALLURGICAL WASTE: THE CONTAMINATION PROBLEM

Pesce, C, Baral, A, Shenbagam, V K, and **Hanein, T**

Department of Materials Science and Engineering, The University of Sheffield, UK
t.hanein@sheffield.ac.uk

1. INTRODUCTION: PRESENCE OF CONTAMINANTS IN UPCYCLED WASTES

The production of Portland cement (PC) clinker is responsible for 8% of global anthropogenic CO_2 emissions and cement demand is only expected to grow in the next decades, leading to a substantial effort by the cement industry to reduce its carbon footprint. Integrating a circular economy (CE) approach to make the cement industry more sustainable is essential to ensure that environmental benefits are accompanied by business benefits. Applying a CE approach to clinker production entails finding novel solutions that increase efficiency and introduce recycling loops i.e., by using other industries' end-of-life wastes as resources. Industrial by-products and wastes can be used as alternative raw materials (ARM) to produce clinker if they contain the necessary elements for clinkering reactions to occur, are largely available, and their composition and availability are fairly stable in the long term. Also, solid waste upcycling reduces landfilling with large amounts of industrial waste being incorporated into building materials. However, one of the main barriers encountered when applying CE recycling loops to cement manufacturing is the occurrence of fluctuations in waste composition and volume, which negatively influence cement quality control and cost (Ada et al., 2023). Therefore the cement community must understand the effects of the chemistry of the solid waste used as ARM in clinker production on the cement/concrete properties.

Wastes used as ARM during clinker production are often categorised based on the main element they supplement (usually Ca, Si, Al, or Fe). Whilst clinkers produced using Ca- and Si-rich industrial wastes have been extensively studied, the properties of clinkers produced with Al- and Fe-rich wastes are still not well known, despite the suitability and large availability of these types of waste.

Two Al- and Fe-rich ARMs have been selected as the focus of this study: steel slags and aluminium dross. Steel slags have the largest global production volume (est. 280 Mt per year) among Fe-rich wastes suitable for clinker production (Peys et al., 2022). Aluminium dross is a by-product of the aluminium production process and one of the most abundant hazardous wastes (est. between 8.4 and 11.2 Mt globally per year) (Mahinroosta & Allahverdi, 2018).

A variety of minor elements in variable amounts are present in steel slags and aluminium dross as contaminants (**Table 1**). It is known that some of these elements even in small dosages can greatly affect the properties and performance of cement. In this work, we aim to review the effects of contaminants on clinker properties, reactivity, and leaching performance. In this extended abstract, we have focussed on two contaminants of particular interest because of their pervasiveness in industrial wastes and related effects and hazards: magnesium (Mg) and chromium (Cr).

Table 1. Composition of steel slag and aluminium dross.

	SiO_2	Al_2O_3	Fe_2O_3	CaO	**MgO**	SO_3	Na_2O	**Cr_2O_3**	MnO	P_2O_5	Others
Steel slag [Chenhai 2023]	16.1	6.5	20.4	40.0	**7.49**	0.9	-	**0.14**	1.45	1.28	-
Al dross [Shen 2022]	4.6	79.3	3.9	1.5	**5.7**		0.9	**0.2**			3.9

2. EFFECTS OF CONTAMINANTS DURING CLINKERING PROCESS

Minor elements, including Mg and Cr, affect clinker phase assemblage and substitute different atoms during the clinkering process. The presence of MgO affects melt formation, essential for belite conversion into alite, by reducing the temperature at which the liquid phases start to form and the viscosity of the melt phase, both of which affect the crystallization leading to the formation of smaller alite particles. The proportion of the C_3S phase also increases in the presence of MgO, stabilising the

M_3 polymorph of C_3S. For example, C_3S formation is generally hindered by SO_3, yet the addition of MgO promotes the formation of C_3S in alite-ye'elimite (Calcium sulfoaluminate-based cement) clinkers (Li et al., 2014; Liu et al., 2002). Similarly, the amount of ferrite (C_4AF) formed is increased at the expense of the aluminate (C_3A). In the alite-ye'elimite system, the presence of MgO also reduces the free lime content, an indicator of the burnability of the clinker (Liu et al., 2002).

On the other hand, the presence of Cr is generally reported to increase the amount of free lime; however, at high dosages (>10%) the amount of free lime is reduced as other Cr-containing phases start to form consuming the excess Ca (Suthatip Sinyoung et al., 2011). The presence of Cr also reduces the formation of alite, promoting belite formation and stabilizing the β-C_2S phase (Stephan et al., 1999).

The changes induced by the presence of minor elements can be attributed to the partial substitution of their ions in the main clinker phases. The presence of Mg in PC clinker is distributed in all phases, with Mg replacing Ca ions in C_3S, C_2S and C_3A and partially replacing Ca and Fe ions in C_4AF (Zhao, Zhang, Fan, et al., 2021). Similarly, Cr ions replace S and Fe ions in the ye'elimite and ferrite phases respectively (Zhao, Zhang, Guo, et al., 2021). Based on the crystal structure lattice, the amount of ion replacement is limited, and beyond the solubility limit the elements form periclase or other chromium-based phases – spinel can also form. There is no consensus on the solubility limit value in the literature, with different authors reporting the formation of periclase at different dosages of MgO.

3. EFFECTS OF CONTAMINANTS ON CLINKER HYDRATION

Clinker hydration is generally retarded by Cr. Wang et al. (2023) added Cr^{VI} in the form of sodium chromate tetrahydrate to a mixture of ultra-high performance concrete (UHPC), and ^1H-NMR relaxometry showed that the presence of Cr inhibits water consumption starting from 9.5 hours after mixing, attributed to the slow precipitation during early hydration of $CaCrO_4$, which covers cement particles and delays the hydration process. In terms of mechanical properties, the presence of Cr in PC systems improves compressive strength after 28-90 days of curing because of the precipitation of Cr-containing phases such as $CaCrO_4 \cdot 2H_2O$ which reduces the porosity forming a denser microstructure. However, in UHPC such an effect is less notable and a decrease in strength is observed instead due to Cr-containing phases covering cement particles and inhibiting the hydration process. Similarly, Zhang et al. (2023) show that cement prepared with Cr^{III}-containing glass admixture exhibits lower mechanical properties with increasing Cr_2O_3 content because of inhibition effects. Further insights are provided by Lu et al. (2017) who studied the reactivity of pure C_3S in the presence of Cr^{III} at concentrations ranging from 0.5 to 3.0 wt.%. Calorimetry results show that Cr^{III} accelerates the hydration process at dosages up to 1.0%, whilst at 1.5% the induction period is prolonged, but the hydration rate is higher during the acceleration period, and at 3.0% the induction period is further prolonged and both acceleration and deceleration period rates are lower, thus indicating that Cr^{III} exhibits a retardation effect, and that hydration is greatly hindered (**Figure 1a**).

A comprehensive review of the effects of MgO on clinker properties has been recently published by Song et al. (2021). The effects of MgO on C_3S hydration depend on the dosage, with low peaks at 0.8 and 1.7% and a central high peak at ~1.35% which corresponds to the T→M C_3S transition. MgO also affects the second exothermic peak of C_3S hydration, which is reported to appear higher and wider (**Figure 1b**), likely due to Mg^{2+} ions substituting the C_3S lattice. Effects of MgO on C_3A are complex: hydration is generally delayed in the presence of Mg however, in the presence of gypsum it is accelerated at dosages >1.5%, while at lower dosages it is delayed due to the formation of periclase and mayenite ($C_{12}A_7$).

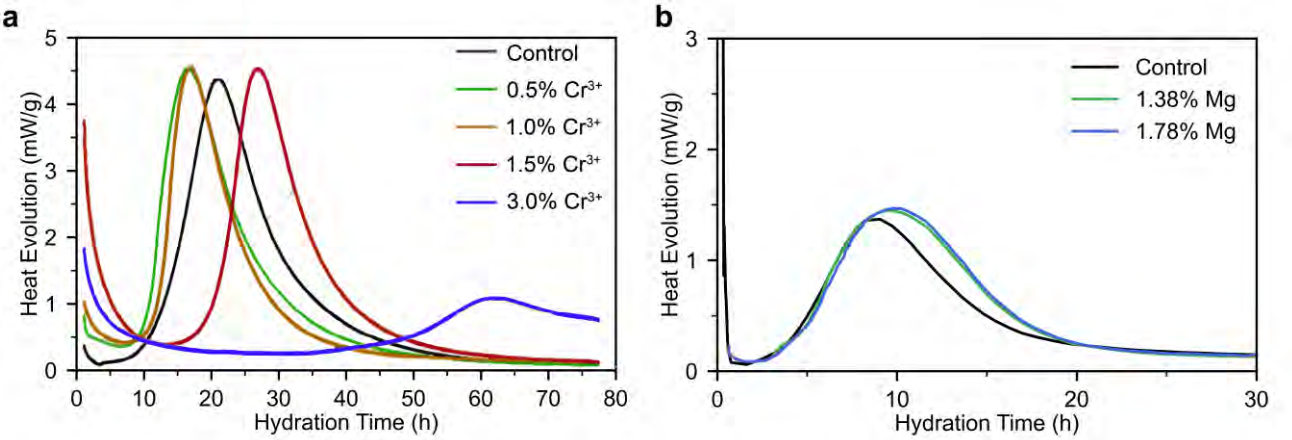

Figure 1. Effect of Cr (a) and Mg (b) on C_3S hydration. Graphs replotted from Lu et al. (2017) (a) and Bazzoni et al. (2014) (b).

4. EFFECTS OF CONTAMINANTS ON LEACHING PERFORMANCE

The leaching performance of clinker containing minor elements mainly depends on the hydration products formed, as well as the leaching test procedure utilised. While Mg leaching is not considered toxic, Cr leaching can be of significant concern depending on its oxidation state. Cr^{III} is considered essential for human health, while Cr^{VI} is carcinogenic, hemotoxic, and genotoxic, and WHO recommends a maximum of 0.05 ppm Cr^{VI} in drinking water. However, most leaching tests only recommend a total Cr concentration limit without differentiating between Cr^{III} and Cr^{VI}, such as the UK waste acceptance criteria and the US EPA Toxic Characteristic Leaching Procedure (TCLP). Conversely, Chinese standards GB 16889-2008 specify both total Cr content and Cr^{VI} content for disposal in non-hazardous landfills.

Cr is an anion-type heavy metal forming CrO_4^{2-} species in cement pore solution and does neither precipitate nor is strongly adsorbed into hydration products other than AFm phases (Wang & Wang, 2022). It has been argued that AFt and C-S-H play a role in fixing and adsorbing Cr ions, however, the leaching of Cr^{VI} was higher than other heavy metals (Halim et al., 2004). Hydrated PC mortars with PC containing as little as 0.1 wt.% Cr_2O_3 is classified as hazardous in the TCLP test (S. Sinyoung et al., 2011). Cr leaching performance of hydrated cement can be reduced by using additives such as NaCl to promote ettringite formation (Pang et al., 2022). Carbonation of concrete increases Cr leaching as the hydrated products (AFm, AFt, and C-S-H) that bind Cr decompose with the carbonation reaction (Yu et al., 2005). Researchers are equivocal on the effect of water-to-binder ratio (Bakhshi et al., 2019) or of the use of ground granulated blast furnace slag as clinker raw material on Cr leaching (Król, 2020; Yu et al., 2005).

5. CONCLUSIONS

In order to cut the high CO_2 emissions of clinker production, it is paramount to introduce CE approaches. Utilising ARMs for clinker production is a promising pathway; however, one of the main barriers is their variability or inconsistency in composition. The presence of minor elements in Al- and Fe-rich wastes induces effects on clinker structure and properties that reflect on the final concrete and that are yet to be well understood. This work aims at setting the agenda for laying a knowledge foundation, gathering the available data on the effects of contaminants. The presence of Mg promotes the formation of smaller C_3S particles and more ferrite at the expense of C_3A and ions are homogeneously distributed across phases. Cr promotes and stabilises β-C_2S and affects free lime content depending on dosage; Cr ions replace Fe in the ferrite phase. During hydration, Cr acts as a retardant. Notably, there is no consensus on solubility limits of Mg or Cr in clinker phases. Cr is not generally well immobilised in cementitious materials, with significant concerns regarding Cr^{VI} leaching. There is ambiguity on which hydrated phases best fix Cr^{VI} and on the effects of additives and mix design parameters on Cr^{VI} leaching.

6. ACKNOWLEDGEMENTS

C.P., A.B., and T.H. are funded by the UKRI EPSRC project EP/W018810/1; V.K.S. and T.H. are funded by the UKRI FLF project MR/V023829/1.

7. REFERENCES

Ada, E., Kazancoglu, Y., Mangla, S. K., & Aydin, U. (2023). Barriers to Cement Industry Towards Circular Economy. *International Journal of Mathematical, Engineering and Management Sciences*, *8*(4), 612-631.

Bakhshi, N., Sarrafi, A., & Ramezanianpour, A. A. (2019). Immobilization of hexavalent chromium in cement mortar: leaching properties and microstructures. *Environmental Science and Pollution Research*, *26*(20), 20829-20838.

Bazzoni, A., Ma, S., Wang, Q., Shen, X., Cantoni, M., & Scrivener, K. L. (2014). The Effect of Magnesium and Zinc Ions on the Hydration Kinetics of C3S. *Journal of the American Ceramic Society*, *97*(11), 3684-3693.

Halim, C. E., Amal, R., Beydoun, D., Scott, J. A., & Low, G. (2004). Implications of the structure of cementitious wastes containing Pb(II), Cd(II), As(V), and Cr(VI) on the leaching of metals. *Cement and Concrete Research*, *34*(7), 1093-1102.

Król, A. (2020). Mechanisms Accompanying Chromium Release from Concrete. *Materials*, *13*(8).

Li, X., Xu, W., Wang, S., Tang, M., & Shen, X. (2014). Effect of SO3 and MgO on Portland cement clinker: Formation of clinker phases and alite polymorphism. *Construction and Building Materials*, *58*, 182-192.

Liu, X., Li, Y., & Zhang, N. (2002). Influence of MgO on the formation of Ca3SiO5 and 3CaO·3Al2O3·CaSO4 minerals in alite–sulphoaluminate cement. *Cement and Concrete Research*, *32*(7), 1125-1129.

Lu, L., Xiang, C., He, Y., Wang, F., & Hu, S. (2017). Early hydration of C3S in the presence of Cd2+, Pb2+ and Cr3+ and the immobilization of heavy metals in pastes. *Construction and Building Materials*, *152*, 923-932.

Mahinroosta, M., & Allahverdi, A. (2018). Hazardous aluminum dross characterization and recycling strategies: A critical review. *J Environ Manage*, *223*, 452-468.

Pang, F., Wei, C., Zhang, Z., Wang, W., & Wang, Z. (2022). The migration and immobilization for heavy metal chromium ions in the hydration products of calcium sulfoaluminate cement and their leaching behavior. *Journal of Cleaner Production*, *365*, 132778.

Peys, A., Isteri, V., Yliniemi, J., Yorkshire, A. S., Lemougna, P. N., Utton, C., Provis, J. L., Snellings, R., & Hanein, T. (2022). Sustainable iron-rich cements: Raw material sources and binder types. *Cement and Concrete Research*, *157*, 106834.

Sinyoung, S., Asavapisit, S., Kajitvichyanukul, P., & Songsiririthigul, P. (2011). Speciation of Cr in cement clinkers obtained from co-burning with Cr2O3. *Nuclear Instruments and Methods in Physics Research Section A: Accelerators, Spectrometers, Detectors and Associated Equipment*, *649*(1), 210-212.

Sinyoung, S., Songsiririthigul, P., Asavapisit, S., & Kajitvichyanukul, P. (2011). Chromium behavior during cement-production processes: a clinkerization, hydration, and leaching study. *J Hazard Mater*, *191*(1-3), 296-305.

Song, Q., Su, J., Nie, J., Li, H., Hu, Y., Chen, Y., Li, R., & Deng, Y. (2021). The occurrence of MgO and its influence on properties of clinker and cement: A review. *Construction and Building Materials*, *293*, 123494.

Stephan, D., Maleki, H., Knöfel, D., Eber, B., & Härdtl, R. (1999). Influence of Cr, Ni, and Zn on the properties of pure clinker phases Part I. C 3 S. In (Vol. 29, pp. 545-552).

Wang, D., & Wang, Q. (2022). Clarifying and quantifying the immobilization capacity of cement pastes on heavy metals. *Cement and Concrete Research*, *161*.

Wang, J. N., Chen, F. X., Yu, R., Fan, D. Q., & Zhang, T. S. (2023). Effect of heavy metal (Mn, Pb and Cr) on the properties and hydration in low water/binder cement-based composites (LW/B-CC). *Construction and Building Materials*, *386*, 131567.

Yu, Q., Nagataki, S., Lin, J., Saeki, T., & Hisada, M. (2005). The leachability of heavy metals in hardened fly ash cement and cement-solidified fly ash. *Cement and Concrete Research*, *35*(6), 1056-1063.

Zhang, S., Zhang, Y., Wu, S., Yu, K., Gao, M., Zhao, Z., Wu, Y., Zhang, Y., & Zhang, Z. (2023). Feasibility of using Cr-containing vitrification product as cement admixture: Structural evolution and chromium immobilization. *Journal of Cleaner Production*, *417*, 138055.

Zhao, R., Zhang, L., Fan, G., Chen, Y., Huang, G., Zhang, H., Zhu, J., & Guan, X. (2021). Probing the exact form and doping preference of magnesium in ordinary Portland cement clinker phases: A study from experiments and DFT simulations. *Cement and Concrete Research*, *144*, 106420.

Zhao, R., Zhang, L., Guo, B., Chen, Y., Fan, G., Jin, Z., Guan, X., & Zhu, J. (2021). Unveiling substitution preference of chromium ions in sulphoaluminate cement clinker phases. *Composites Part B: Engineering*, *222*, 109092.

BINARY HETEROJUNCTIONS OF MG/AL-LDH AND CARBON-BASED MATRIXES DERIVED FROM SELF-ASSEMBLY SYNTHESIS FOR INHIBITION OF PYRENE PHOTOPOLYMERIZING: ELUCIDATION OF LDHS PROTECTING BITUMEN AGAINST UV AGING

Xinyu Cong[1], Shuang Lu[2], Yiqiu Tan[3]

[1] School of Transportation Science and Engineering, Harbin Institute of Technology, Harbin, China
[2] School of Civil Engineering, Harbin Institute of Technology, Harbin, China
[3] School of Transportation Science and Engineering, Harbin Institute of Technology, Harbin, China
E-mail (lus@hit.edu.cn; tanyiqiu@hit.edu.cn)

Layered double hydroxides (LDHs) have been found to protect bitumen against UV aging that was a culprit to shorten service life of new paved roads and burden environment with toxic volatiles in case of repaving roads time and again. Utilizing LDHs to improve the UV resistance to bitumen is desirable but the corresponding mechanism is still not be clarified. In this work, a simple self-assembly strategy is used to synthesize binary-heterojunction catalysts consisting of Mg/Al-LDH and carbon-based matrixes, aiming at obtaining copious mesopores and tailoring photocatalytic routes. By virtue of the self-assembly synthesis, the specific surface areas of the binary-heterojunction catalysts reached 193.94 and 156.31 m^2/g for Mg/Al-LDH@biocarbon and Mg/Al-LDH@g-C_3N_4, respectively.

It was found that the as-synthesized catalyst of Mg/Al-LDH@g-C_3N_4 was an outstanding inhibitor in photopolymerizing polycyclic aromatics, which was verified by photochemical experiments using pyrene (PY) as a target. The Mg/Al-LDH@g-C_3N_4 enabled to decrease the proportion of exciplex of PY to 8.63% upon UV irradiation, while the proportion was as high as 39.81% in the absence of Mg/Al-LDH@g-C_3N_4. The present study expounded the mechanisms of monophyletic Mg/Al-LDH and binary-heterojunction Mg/Al-LDH@g-C_3N_4 changing the photochemical reactions of PY upon UV irradiation. The test results revealed that photogenerated holes and photogenerated electrons were responsible for accelerating the photodegradation process of PY and suppressing the photopolymerization of PY molecules, respectively. The binary-heterojunction Mg/Al-LDH@g-C_3N_4 showed its outstanding photocatalytic activities under UV irradiation, including avoiding PY molecules from degradation and macromolecular polymerization, which was attributed to the new channel for electron-hole recombination and built-up photocatalytic routes between Mg/Al-LDH and g-C_3N_4. This work provided a perspective for tailoring promising protective agents for bitumen anti-UV aging through building reasonable photocatalytic routes for heterogeneous structures.

Keywords: Mg/Al-LDH, carbon-based matrix, photocatalyst, photodegradation, photopolymerization

ENVIRONMENTAL ASSESSMENT OF ALKALI-ACTIVATED MATERIALS BASED ON BIOWASTE ASHES AS SILICA SOURCE USING HORIZONTAL LEACHING TESTS

Salas, I[1], Cifrián, E[1], Soriano, L[2], Monzó, J[2] and Andrés, A[1]

[1]GER – Green Engineering and Resources Research Group, Department of Chemistry and Process & Resources Engineering – ETSIIT, University of Cantabria, Santander, Spain
[2]GIQUIMA – Grupo de Investigación en Química de los Materiales de Construcción – Instituto de Ciencia y Tecnología del Hormigón – Polytechnic University of Valencia, Valencia, Spain
andresa@unican.es (corresponding author)

1. INTRODUCTION

Recent advances in the development of sustainable alkali-activated materials (AAMs) formulations are focusing on substituting the conventional alkali and silica activators for industrial by-products/waste (Soriano et al., 2021). Understanding the leaching behaviour of these new materials is essential to determine the potential adverse effects of the interactions with the environment during the life cycle of the material, as a result of the release of hazardous substances. In this study, the leaching behaviour of three Blast Furnace Slag-based AAMs activated with almond biomass ash (ABA) as a source of potassium and three solid silica sources from the agricultural industry was studied. The three silica sources used were rice husk ash (RHA), diatomaceous earth from wine filtration (DEW) and bamboo leaf ash (BLA). European Construction Products Regulation proposes Horizontal Leaching tests for the environmental assessment of monolithic and granular materials. These tests were used in this work to determine the release of substances as a function of time in the monolithic Dynamic Surface Leaching Test (CEN/TS 16637-2) and as a function of the liquid-to-solid ratio in the granular Up-flow Percolation test (CEN/TS 16637-3), to evaluate the behaviour in the service and end-of-life scenarios, respectively. The obtained results allow to determine the leaching mechanisms that can be used to estimate the long-term release of hazardous substances from the materials.

2. MATERIALS AND METHODS

Three AAM mixtures were prepared with Blast Furnace Slag (BFS) as the main aluminosilicate precursor, Almond Biomass Ash (ABA) as the main alkali source, rich in potassium oxides, and three agro-industrial by-products that are rich in silica oxides: rice husk ash (RHA), diatomaceous earth from wine filtration ash (DEW) and bamboo leaf ash (BLA), and the following samples were obtained, AAM-RHA, AAM-DEW and AAM-BLA (Table 1). The novelty of this AAM system is that the alkaline solution normally used in the AAM mixtures (potassium/sodium hydroxide and potassium/sodium silicate) was substituted by the addition of silica and potassium as solid component with the precursor, obtaining the denominated one-part solid.

Samples were mixed as one-part AAMs as if they were cements used in the mortar mixtures described in the standard UNE-EN 196-1. The water/binder and sand/binder ratios were 0.45 and 3, respectively. The mixtures were casted in cubic moulds of 4 cm^3 and cured during 28 days in a chamber at 25 ºC and 90 % of relative humidity.

Table 1. Mixture design of AAMs

	Materials (kg/m^3)						
Sample	BFS	ABA	RHA	DEW	BLA	Sand	Water
AAM-RHA	337.5	56.25	56.25	-	-	1350	202.5
AAM-DEW	337.5	56.25	-	56.25	-	1350	202.5
AAM-BLA	337.5	56.25	-	-	56.25	1350	202.5

First, the Compliance leaching test (EN 12457-4) was performed to study the leaching behaviour of the raw materials and the AAMs in chemical equilibrium conditions as a granular material (< 10 mm). Second, the Dynamic Surface Leaching Test (DSLT) (CEN/TS 16637-2) was applied to the monolithic specimens, and the Up-flow Percolation Leaching test (CEN/TS 16637-3) was carried out to granular shape AAMs (< 22.4 mm). Both were used to determine the release mechanisms with time and at different L/S ratios, respectively. Analytical determination of the eluates was performed via ICP-MS in an Agilent 7900x and ionic chromatography (IC) with a Metrohm 930 Compact IC Flex. All the leaching tests were performed in duplicate.

3. RESULTS AND DISCUSSION

Mobility of elements in equilibrium conditions from compliance leaching test (EN 12457-4) is presented in Figure 1. Values obtained are normalized with the limits adopted from the Waste Acceptance Criteria (WAC) in inert waste landfills (Council Decision 2003/33/CE).

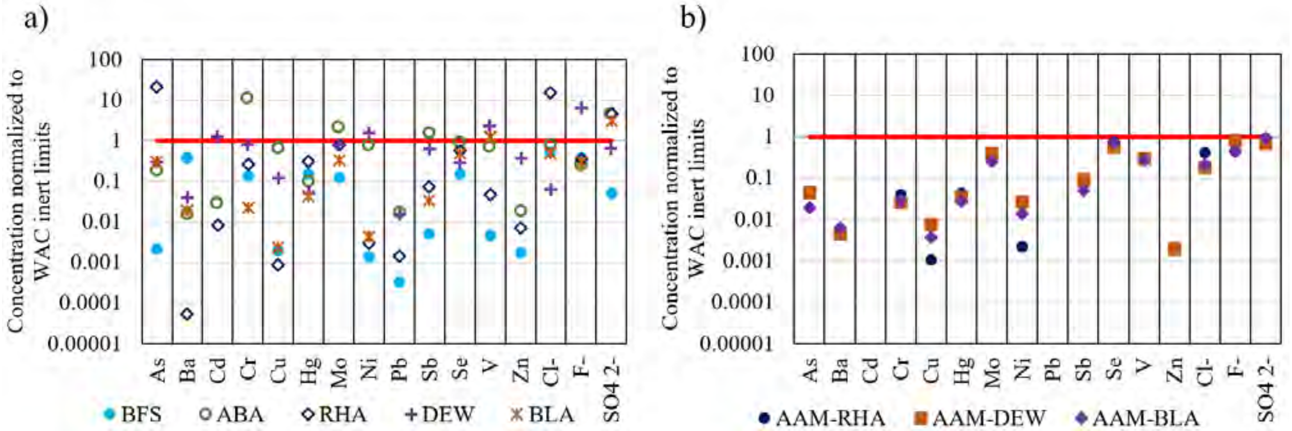

Figure 1. Concentration of elements in eluates normalized to WAC inert limits for a) raw materials and b) AAM, from the Compliance leaching test EN 12457-4

All the raw materials studied, except for BFS, surpass some limits considered for inert materials (Figure 1a), while the three AAMs are below the regulatory limits, which indicate the effectivity of the inertization by waste-based alkali activation process (Figure 1b). However, Mo, Sb, Se and V mobility are close to the inert waste limit. In the literature, it has been shown that the retention of oxyanionic elements in AAM is limited (Lancellotti et al., 2015). For this reason, the release of As, Cr, Mo, Sb, Se and V is considered in the following horizontal leaching tests.

- The concentration of elements As, Cr, Mo, Sb, Se and V in the DSLT (Dynamic Surface Leaching Test) leachates is depicted in Figure 2. pH and conductivity values are similar between the three samples ranging in all stages between 9.5-11 and 200-500 µS/cm, respectively. In all cases, a slight increase release over time is observed and similar behaviour in the three samples, except for the As release in the AAM-RHA sample due to its high content in RHA silica source (Figure 1a). However, all cumulative release values (mg·m^{-2}) at 64 days of the three AAMs (Table 3) comply with the Soil Quality Decree (2007) regulatory limits from the Netherlands for monolithic building materials.

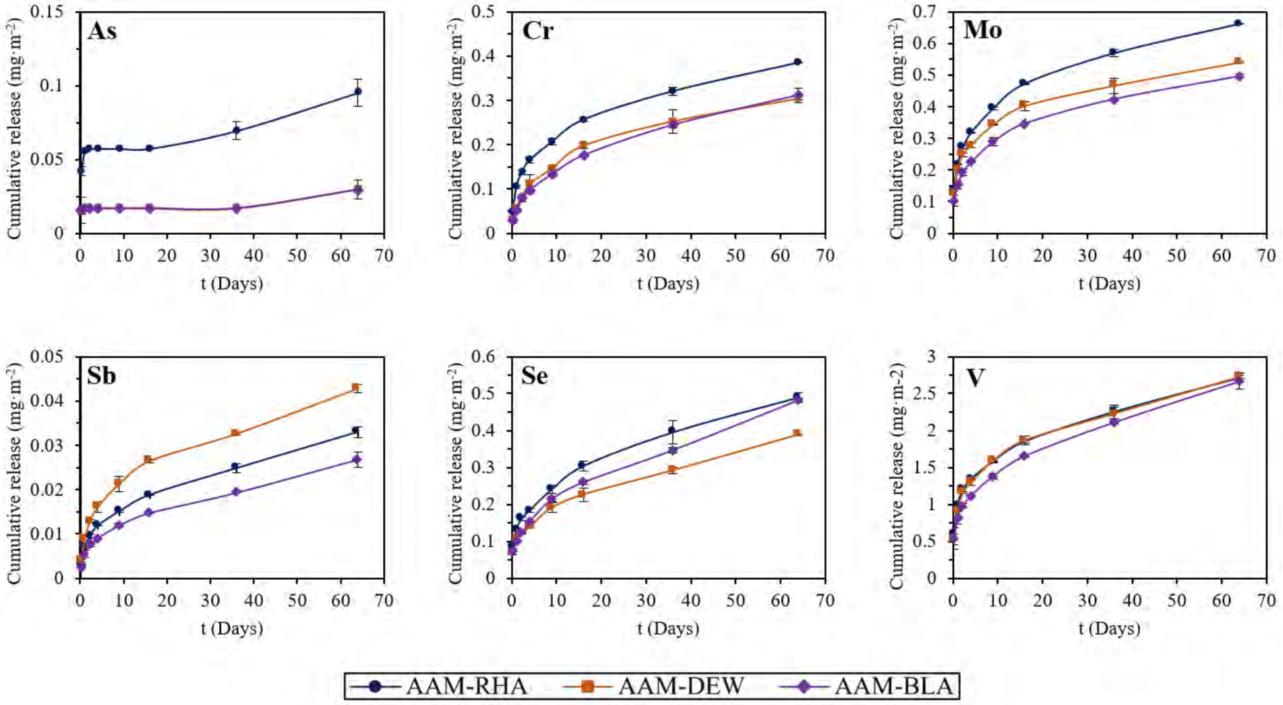

Figure 2. Cumulative release (mg·m^{-2}) of monolithic AAM mixtures in DSLT (CEN/TS 16637-2)

Table 2. Cumulative release values of AAMs at 64 days and SQD limit values for monolithic building materials

	Cumulative release per exposed area (mg·m^{-2}) as per DSLT					
Sample	As	Cr	Mo	Sb	Se	V
AAM-RHA	0.095	0.38	0.66	0.033	0.49	2.72
AAM-DEW	0.029	0.30	0.54	0.042	0.39	2.72
AAM-BLA	0.029	0.31	0.50	0.027	0.48	2.67
SQD limits (mg·m^{-2})	260	120	144	8.7	4.8	320

Release mechanisms of chemical elements considered of three monolithic AAMs samples (Table 3), from the experimental data, are found to be the same, except in Mo. Surface wash-off (SWO), diffusion and a combination of both mechanisms (SWO preceding diffusion) are the prevalent. This will allow to estimate the long-term release of potentially hazardous substances from AAMs.

Table 3. Release mechanisms of trace elements for monolithic AAM mixtures

Sample	As	Cr	Mo	Sb	Se	V
AAM-RHA	Surface wash-off	Diffusion	Surface wash-off	Diffusion	Diffusion with SWO	Diffusion with SWO
AAM-DEW	Surface wash-off	Diffusion	Surface wash-off	Diffusion	Diffusion with SWO	Diffusion with SWO
AAM-BLA	Surface wash-off	Diffusion	Diffusion	Diffusion	Diffusion with SWO	Diffusion with SWO

In relation to the Up-flow Percolation test (CEN/TS 16637-3), the cumulative release (mg·kg^{-1}) results versus at cumulative L/S ratio (Figure 3) show a depletion of all the trace elements. pH values decreased from 12.5 to 11.5, and conductivity values severely decreased from 15000 to 2500 µS/cm in the three samples in average. The release of Mo, Sb and V from AAM-DEW sample is slightly higher than the other samples. However, cumulative release at the highest L/S tested, 10 L/kg, are below the compliance leaching values in all elements, consequently below the inert materials limits. Thus, the released levels of chemical elements in the Up-flow Percolation test for granular samples are considered not harmful.

The release mechanism determined according with mathematical conditions included in the technical specification CEN/TS 16637-3 is apparent depletion for all the trace elements in the three studied samples, which is in line with the experimental tendency described as a function of the L/S ratio in Figure 3.

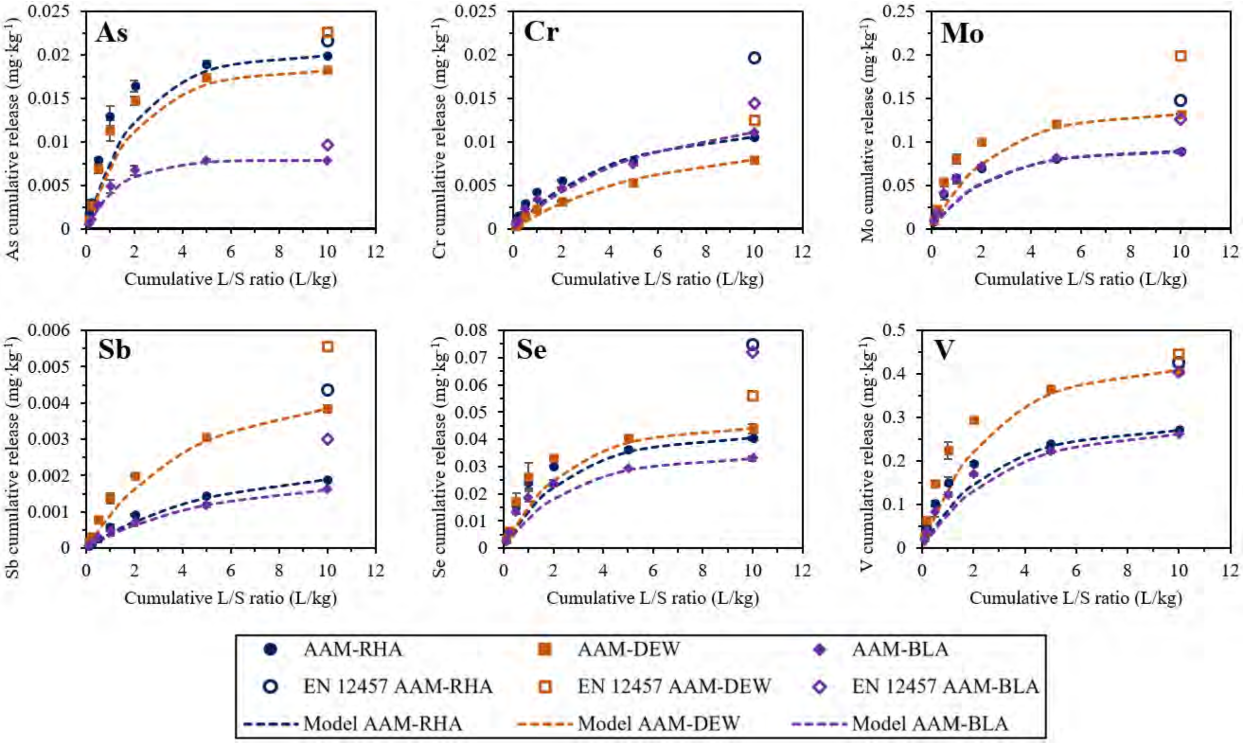

Figure 3. Cumulative release (mg·kg^{-1}) of granular AAM samples in Up-flow Percolation test (CEN/TS 16637-3), Compliance leaching test values at L/S = 10 L/kg and mathematical model derived from experimental data

4. CONCLUSION

The release mechanisms of As, Cr, Mo, Sb, Se and V have been derived from the Dynamic Surface Leaching Test (monolithic) and Up-flow Percolation Leaching test (granular) results in order to predict the long-term behaviour. From it can be concluded that the incorporation of agro-industrial by-products, like biowaste ashes, as a silica source in waste/BFS-based AAM does not suppose an environmental risk throughout the life cycle of the material under the actual applicable leaching standards in European construction products regulations.

5. ACKNOWLEDGMENT

The authors would like to thank the Spanish Ministry of Science and Innovation for the financial support of this work via ECOSOST RTI-2018-097612-B-C21 and ECOSOST RTI2018-097612-B-C22 grants.

6. REFERENCES

Lancellotti, I., Barbieri, L., & Leonelli, C. (2015). Use of alkali-activated concrete binders for toxic waste immobilization. *Handbook of Alkali-Activated Cements, Mortars and Concretes* (pp. 539–554). Woodhead Publishing Limited.

Soriano, L., Font, A., Tashima, M. M., Monzó, J., Borrachero, M. V., Bonifácio, T., & Payá, J. (2021). Almond-shell biomass ash (ABA): A greener alternative to the use of commercial alkaline reagents in alkali-activated cement. *Construction and Building Materials*, *290*, 123251.

SOLIDIFICATION/STABILIZATION AND IMMOBILIZATION MECHANISM OF PB(II) AND ZN(II) IN ETTRINGITE

Chengcheng Fan*, Baomin Wang
Faculty of Infrastructure Engineering, Dalian University of Technology, Dalian 116024, China
*Corresponding author: E-mail: fancc995@126.com

Ettringite, as the dominant hydration product in cement materials, plays a significant role in the solidification/stabilization of heavy metals. However, the combination and immobilization mechanism of heavy metal ions in ettringite crystals have yet to be fully understood. In this study, ettringite crystals were synthesized using the solution reaction method to investigate the adsorption and chemical encapsulation reactions of Pb^{2+} and Zn^{2+}. In addition, the microstructures of the ettringite crystals doped with heavy metals were characterized by XRD, FTIR and SEM/EDS to elucidate the immobilization mechanism of Pb^{2+} and Zn^{2+} on ettringite crystals. The results indicated that ettringite has a high specific surface area of 64.456 m^2 /g and considerable mesopore and macropore volumes. The optimal adsorption efficiency of Pb^{2+} and Zn^{2+} in ettringite, accounting for 98.7 % and 99.9 %, respectively, was realized in an initial liquid with a pH of 10. The adsorption kinetics results showed that the equilibrium adsorption capacities of Pb^{2+} and Zn^{2+} were 196.04 and 185.57 mg/g, respectively. In addition, the adsorption reaction of Pb^{2+} in ettringite was predominantly characterized by a chemisorption process; whereas the adsorption reaction of Zn^{2+} in ettringite was characterized by the simultaneous action of physisorption and chemisorption. The multi-peaks Gaussian fitting curves of the FTIR patterns indicated that Pb^{2+} and Zn^{2+} promoted the formation of ettringite and induced more H-O-H groups. Moreover, this study proposed and confirmed that significant differences exist between the immobilization mechanisms of Pb^{2+} and Zn^{2+} in ettringite. The lattice constant and coordination chemistry analysis revealed that Pb^{2+} mainly substituted Ca^{2+} and Al^{3+} in ettringite via lattice substitution. In contrast, Zn^{2+} predominantly induced some lattice distortion in the ettringite crystal structure and formed a solid solution via interstitial doping. Furthermore, the micro channel architecture and hydrogen bond network significantly contributed to the adsorption and solidification of heavy metals. Overall, the chemical bonding mechanism was more prominent for the solidification of Pb^{2+} than that of Zn^{2+} in ettringite, and ettringite exhibited a superior adsorption capacity and stronger binding affinity for Pb^{2+}.

SUSTAINABLE REUSE OF MODIFIED INCINERATION SEWAGE SLUDGE ASH (M-ISSA) FOR STABILIZATION OF HIGHLY AS-CONTAMINATED SOIL

Shengya Gao[a,b], Qiming Wang[a,d], Hui Yin[b], Zihan Ma[c], Jiang-shan Li[c,d#], Chi Sun Poon[a,d#]

[a] Department of Civil and Environmental Engineering, The Hong Kong Polytechnic University
[b] Key Laboratory of Arable Land Conservation (Middle and Lower Reaches of Yangtse River), Ministry of Agriculture, College of Resources and Environment, Huazhong Agricultural University, Wuhan 430070, China
[c] State Key Laboratory of Geomechanics and Geotechnical Engineering, Institute of Rock and Soil Mechanics, Chinese Academy of Sciences, Wuhan, 430071, China
[d] IRSM-CAS/HK PolyU Joint Laboratory on Solid Waste Science, Hung Hom, Kowloon, Hong Kong
[#]E-mail: jsli@whrsm.ac.cn; cecspoon@polyu.edu.hk

1. INTRODUCTION

Arsenic (As) is a teratogenic and carcinogenic metalloid element with potential threats to human beings (Ko et al. 2015). It is often found in contaminated soil caused by natural or human activities, such as volcanic activity, agriculture and so on. In soils, As concentration ranges from 0.2 to 40 mg/kg due to natural weathering of As-bearing minerals (Koo et al. 2012). Due to a large number of accidental exposures to As at work, may lead to acute arsenic poisoning, mainly damage to the intestinal system, respiratory system, etc. Therefore, various technologies for the remediation of As-contaminated soil have been developed, including chemical stabilization, Phyto stabilization and so on (Tiberg et al. 2016).

In the past few decades, in situ immobilization method based on chemical stabilization has received extensive attention (Cutler et al. 2014, Doherty et al. 2017). The immobilizing of As contaminated soil by metal (especially Fe) oxides including goethite, ferrihydrite, hematite and lepidocrocite is widely investigated. Yan et al. (Yan et al. 2020) synthesized an amorphous colloidal material by mixing starch with $FeSO_4$ and $KMnO_4$ as a remedial reagent that transformed As in soil to the more stable forms. Zialame et al. (Zialame et al. 2021) utilized reagents, including MnCl2•6H2O, $FeCl_3$•$6H_2O$, NaOH, and carboxymethyl cellulose (CMC), and produced manganese ferrite that enhanced the As immobilization. Their projects, either directly or indirectly through applying their precursors (iron grit or Fe(III) solutions), aim to lower the bioavailability and mobility of As, and minimize the possible risk of environmental contamination, leaching and uptake by humans. In addition, compared with goethite and iron grit, the adsorption efficiency of As by ferric sulfate is higher (Hartley et al. 2004). Whereas, the addition of ferric sulphates gives rise to soil acidification, thus requiring alkaline input to neutralize soil, which in turn could mobilize As (Manzano et al. 2014, Fresno et al. 2016). In addition, soil remediation techniques should strive to reduce the dosage of amendments. It is necessary to develop long-term, cost-effective, and environmentally friendly materials to tackle this problem.

In Hong Kong, in order to properly manage the growing production amount of incinerated sewage sludge ash (ISSA) (around 150 tons per day) (Zhou et al. 2020), disposal in landfills is necessary due to the lack of effective recycling technologies. The TCLP results in the previous literature showed that the leaching concentration of heavy metals in the ISSA was lower the limit value of hazardous waste (GB5085.3–2007), and thus the health and environmental risks associated with ISSA were potentially very low (Nie et al. 2021). It is therefore possible to develop options for recovery and recovery of beneficial resources from ISSA. These options include using ISSA as an additive to

Portland cement (Chiou et al. 2006), as a cementitious material (Wang et al. 2012) and as a raw material for the fabricating of bricks (Chen and Lin 2009). Due to the moderate pozzolanic reactivity of ISSA (Yusuf et al. 2012, Zhou et al. 2020), ISSA has the potential to be used in the stabilization of contaminated soils and in the improvement soil hardness together with ordinary Portland cement (OPC) as a kind of supplementary cementitious material (Li and Poon 2017). ISSA was also applied to replace the OPC and quick lime as lime-ISSA binder for marine sediments solidification/stabilization that contributed to the formation of hydrated cementitious compounds among the sediments, ISSA, and lime (Wang et al. 2018, Li et al. 2019). Most studies mainly focus on using ISSA as an auxiliary material for stabilizers rather than directly putting it to contaminated soils, and thus, the application of ISSA stability in soil should be further studied.

ISSA contains high concentrations of various metals, including silicon (Si), aluminum (Al), iron (Fe) and phosphorus (P) and is often considered as a waste material (Wang et al. 2019). The ISSA resourced from Hong Kong found iron levels to be very high and was used to treat wastewater based on the $FeCl_3$ chemical precipitation process (Pan and Tseng 2001), making ISSA potentially adsorb heavy metals. Our previous study indicated that the ISSA was modified by a combination of acid leaching and alkali precipitation and its removal capacity of As(V) in wastewater was greatly improved (Gao et al. 2021). Furthermore, considering that the As in wastewater may also spill into the soil, it would be of great significant interest to evaluate the stabilizing effect on As-containing soil using modified ISSA.

The main aims of this study were: (1) synthesize and characterize the novel modified ISSA; (2) evaluate the leaching characteristics of the stabilization of As-contaminated soil; (3) investigate the efficiency and mechanisms of stabilization in As-containing soils; (4) explore the interactions between modified ISSA and As.

2. MATERIALS AND METHODS

2.1 Preparation of As-bearing soil

In this study, the uncontaminated soil employed in this study was silt sourced from Hong Kong. The soil was air dried, pulverized and sieved to remove stones, some gelatinous material and large particles. According to dry mass (as measured by wet sieving and hydrometer tests), the soils consisted of 1.31% clay, 44.99% sand and 53.70% silt size fraction. The concentration of major elements was analyzed after $HNO_3/HClO_4$ digestion. The pH of soil was equalized in 1:1 soil: DI water for 2 h and measured by pH meter that was calibrated in advance by standard buffers of 7.00 and 4.01. It should be noted that the as-received soil had a low As concentration not exceeding the legal limit set by Urban/Rural Residential Soil Risk-based Remediation Goals (RBRGs), based on the Guidance Manual for Use of RBRGs for Contaminated Land Management (HK 2007).

First, soils with As concentrations of 100, 500, 1000 mg/kg, respectively were prepared by adding $Na_2HAsO_4.7H_2O$ solutions. These concentrations were significantly greater than the environmental quality standard for agricultural soil (GB 15618-2018) set by the Ministry of Ecology and Environment of China. Then, in order to achieve a moisture content of 20% in the As-contaminated soil, it was by adding DI water to it. The As-containing soil was stirred thoroughly, cured for 28d under ambient temperature, allowing adequate reactions of As and soil. The resulting samples were then used to characterize for their properties and subsequent stabilization experiments. Information related to soil characteristics and metal contents is given in Table 1.

Table 1 Properties of the As-containing soils

Compositions	100mg/kg soil	500mg/kg soil	1000mg/kg soil
pH	7.64±0.01	8.13±0.03	8.30±0.02
Al (%)		0.60±0.01	
Mg (%)		0.04±0.00	
Fe (%)		0.88±0.02	
As (%)	0.01±0.00	0.05±0.00	0.85±0.00
Sand (%)		44.99±0.01	
Silt (%)		53.70±0.01	
Clay (%)		1.31±0.00	

2.2 Preparation of modified ISSA

Two amendments, modified ISSA and ISSA, were used in this study. The modified ISSA was prepared by a combined acid leaching and preparation process. The detailed preparation steps were given in our previous study (Gao et al. 2021). In simple terms, the impurities are removed by adding 0.5 M HCl to ISSA. In the next step, ISSA was soaked in 6 M HCl with a solid-to-liquid of 1:10 and heated up to 60 ºC and constantly shaken for 2 h. Afterward, the sample was removed and cooled to room temperature. Then, the solution with the pH of 6.0-7.0 was prepared by the addition of 1 M NaOH solution. The suspension was stirred for 2 hours, centrifuged with a speed of 4000 rpm. The resulting modified ISSA washed several times using deionized (DI) water. Lastly, the product went through a series of operations such as freeze-drying, grinding, sieving, etc., and was placed in a desiccator for immobilization experiments. The properties of ISSA and M-ISSA are given in Table 2.

Table 2 Physicochemical properties of M-ISSA and ISSA

Items		ISSA	M-ISSA
Physical properties	BJH desorption average pore diameter (nm)	28.02	5.11
	BET surface area (m^2/g)	1.36	131.35
	pH_{pzc}	8.00	3.5
Chemical composition (%)	Na_2O	4.68	2.7
	MnO	0.10	0.11
	ZnO	0.32	0.57
	SiO_2	31.30	41.20
	P_2O_5	10.70	2.10
	K_2O	2.01	1.16
	SO_3	1.85	0.10
	Fe_2O_3	17.90	32.70
	CuO	0.11	0.13
	Al_2O_3	17.60	14.80
	TiO_2	0.71	1.07
	MgO	2.88	1.22
	CaO	9.37	0.53
	Cl	0.07	1.17

2.3 Stabilization experiments

To investigate the effectiveness of M-ISSA for stabilizing As in soils, 20 g of the As-bearing soil was weighed and mixed with different amounts of ISSA/M-ISSA thoroughly at weight ratio of 1%, 2% and 5%, respectively. For all the As-contaminated soil, the moisture content of each mixture was kept at 25% by adding water. Control experiments (CK) were conducted with deionized (DI) water. Samples of the mixture of soil and solution were cured under room temperature for 0, 7, 28 days mixing thoroughly every day and samples were collected. Three parallel trials were conducted for all experiments and average values with standard errors were reported.

2.4 Test methods

2.4.1 Leaching tests

The TCLP method (TCLP; U.S. EPA Method 1311) is applied to determine whether a waste should be categorized as hazardous. The soil samples were collected after curing for 7/28 days. Then the soil samples were leached and rotated in a glacial acetic acid solution with a pH of 4.93±0.05 (liquid-to-solid of 20 mL/g, frequency of 30 rpm) for 18 h at room temperature. After leaching, the samples were centrifuged, filtered by 0.45 um membrane filter before analysis.

According to U.S. EPA Method 1312, the synthetic precipitation leaching procedure (SPLP) was adopted for simulating acid rain, i.e., a solution with a pH of 4.20±0.05 was prepared as the leachant by the addition of DI water and sulfuric acid/nitric acid solution with a mass ratio of 6:4. and the other test conditions were the same as those of TCLP.

The speciation of As was characterized by the sequential extraction method(Wenzel et al. 2001), analyzing the possible risks of As. In Wenzel's method, metals are partitioned into the following five operationally defined fractions. After each step of extraction, the tube was immediately centrifuged at 4000 rpm and the supernatant solution was collected by filtration for subsequent analysis, while the solid residue was further extracted in next steps as shown in Table 3.

Table 3 Five procedures of sequential extraction of As in soil

Stage	Soil Speciation	Procedure	SSR
S1	Non-specifically adsorbed	0.05 M $(NH_4)_2SO_4$ for 4 hours at 20 ℃	1:25
S2	Specifically-bound	0.05 M $NH_4H_2PO_4$ for 16 hours at 20 ℃	1:25
S3	Amorphous hydrous oxide-bound	0.2 M $(NH_4)_2C_2O_4$ (pH of 3.25) for 4 hours at 20 ℃ in the dark	1:25
S4	Crystalline hydrous oxide bound	0.1 M ascorbic acid and 0.2 M $(NH_4)_2C_2O_4$ (pH of 3.25) for 0.5 hours at 96 ℃	1:25
S5	Residual phases	3 mL $HClO_4$, 5 mL HNO_3 and 5 mL HF at 123 ℃	1:50

The extraction of amorphous iron oxides from soils were conducted with 0.2 M acid ammonium oxalate (Li et al. 2015). Briefly, 50 mL 0.2 M acid ammonium oxalate was added into 1.0 g soil sample and wrapped by tin foil to maintain the samples in the dark. Then the samples were putted in 25 ºC DI water and vibrated for 2 h.

Considering the important role of amorphous Fe in the remediation of As(V) in soil, the contents of amorphous iron and total iron in the samples were tested. The dithionite citrate bicarbonate method was carried out to extract the total Fe oxides (Mehra & Jackson, 2013). Briefly, 40 mL 0.3 M $Na_3C_6H_5O_7\cdot 2H_2O$ and 5.0 mL 1 M $NaHCO_3$ were added into 1.0 g soil and heated to 80 ºC in a water bath. Then 1.0 g $NaHCO_3$ was added and continued to react for 30 mins. After reaction, the suspensions were centrifuged and analyzed the total Fe content after filtering with a 0.45 μm-mesh mixed cellulose ester (MCE).

2.4.2 Characterization

The mineral phases in solid samples were recorded on a Rigaku Smart Lab X-ray diffraction (XRD, CuKα radiation (λ= 0.154 nm)) with the operation condition of 40 kV and 40 mA. Scans were obtained in the angular range 5-70 2θ range at 0.01° step size. The SEM images were captured by using a Tescan VEGA3 operating at 20 kV with energy dispersive X-ray energy spectrometer (SEM-EDX), identifying morphology changes and analyzing the elemental compositions on typical samples before and after stabilization. The interaction between As and the M-ISSA in the soil samples were characterized by Thermo Scientific Nexsa X-ray photoelectron spectrometer (XPS) and the spectra was analyzed by XPSPEAK 4.1 software. The specific surface area of each material was obtained by a Micromeritics ASAP 2020 plus analyser (N_2-BET) and Porosimetry System. The main compositions of ISSA and M-ISSA could be analyzed by Rigaku Supermin200 X-ray fluorescence spectrometry (XRF).

3. RESULTS AND DISCUSSION

3.1 Properties of soils and amendments

The physicochemical properties of soil sourced from Hong Kong (Table. 1) indicate that the soil pH is 7.64, corresponding to a slightly alkaline environment. And the As content in the soil is also consistent with the added As solution. The ICP data show these metal elements in soils are Al (0.6%), Fe (0.88%), and Mg (0.04%).

It is known that physicochemical properties of amendment are crucial for the immobilization of contaminants in soils. ISSA and M-ISSA were characterized by SEM-EDX to check the morphology and surface elemental compositions. As shown in Fig. 1, the surface of ISSA was porous and loose, which was similar to previous reports (Fig. 1 (a)) (Fang et al. 2018). Compared with ISSA, the surface of the M-ISSA became more flatter and smoother and even some flocculating substances appeared on its surface (Fig. 1 (b)). Besides, the elemental analysis of EDX manifested that the content of iron was low in ISSA. But the weight percentage of Fe in M-ISSA was notably higher than that in the raw ISSA, which was consistent with the XRF result. This result revealed that considering the high utilization rate of waste, M-ISSA was designed as an environmentally friendly material, which could have a high As immobilization efficiency possibly due to its higher Fe amount.

Besides iron content, the iron mineral phases are also crucial to stabilize As in soils (Wang et al. 2018, Ouyang et al. 2020). The information about mineral phases in solid samples can be found in the XRD analysis before and after ISSA modification (Fig. 2. (a)). By comparison with standard PDF cards, it can be concluded that hematite (Fe_2O_3), quartz (SiO_2), and whitlockite ($Ca_3(PO_4)_2$) had obvious characteristics in ISSA as consistent with the literature reports (Donatello and Cheeseman 2013, Wang et al. 2021). After modification, the hematite peaks disappeared due to the transformation to $KFeO_2$ (PDF 39-0892), which has good removal capacity for pollutions, especially As (Asere et al. 2019). The N_2 adsorption/desorption isotherms (Fig. 2 (b)) indicated the BET surface area of M-ISSA was 131.35 m^2/g and the average pore diameter was 5.11 nm. The shape of the BET curve indicated that there are very few pores in M-ISSA. The desorption isotherm curve is a typical V-type isotherm curve consisted with the International Union of Pure and Applied Chemistry (IUPAC), showing pores were mainly mesoporous (Fig. 2 (c)). The modification greatly improved the pore volume and specific surface area of M-ISSA, consequently providing more active sites for the retention of As when applied as an amendment in soil (Su et al. 2020).

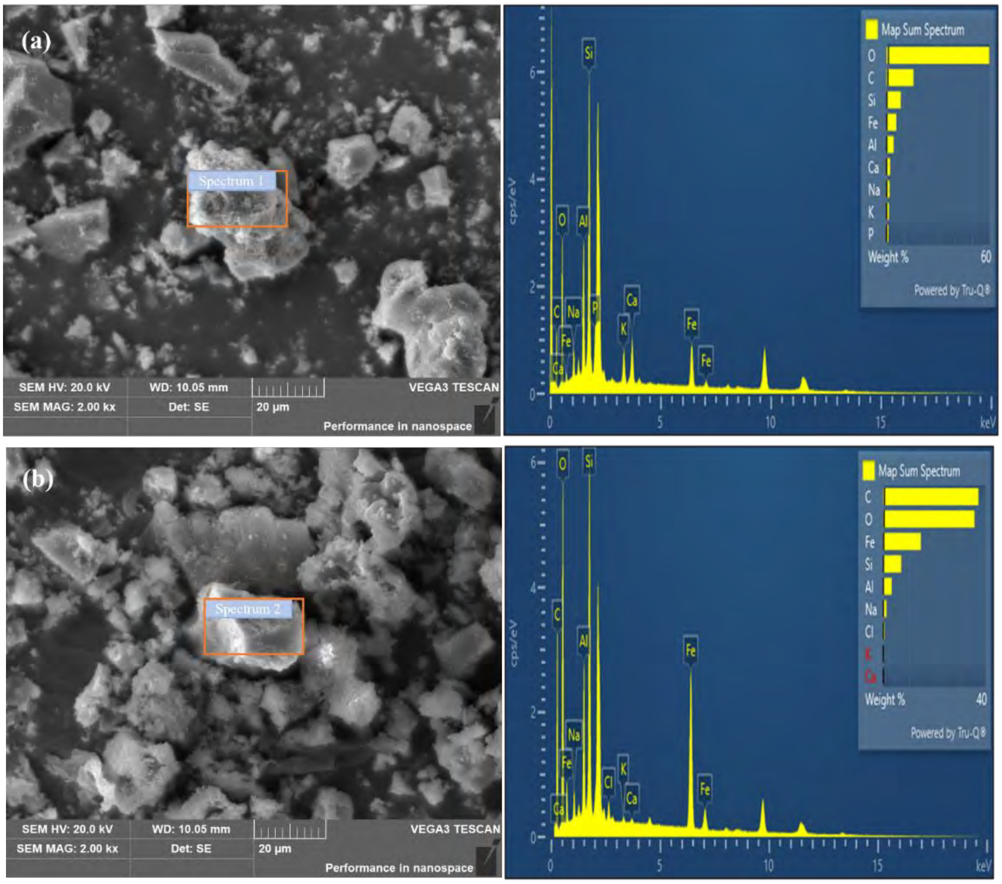

Fig. 1 SEM-EDX images of raw ISSA (a) and M-ISSA (b). The EDS spectra show analysis from the area within the square.

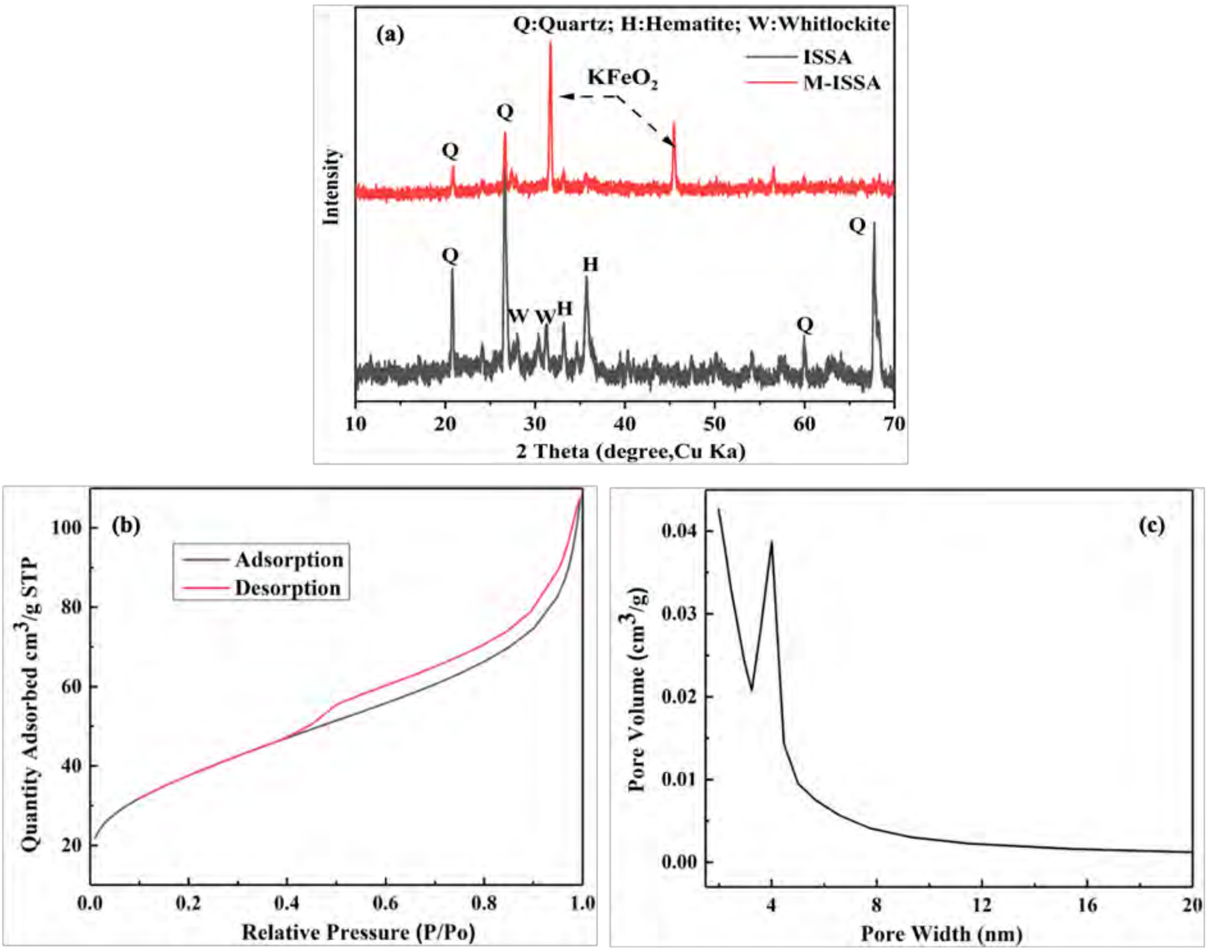

Fig. 2 The XRD pattern of raw ISSA and modified ISSA (a), N_2 adsorption and desorption isotherms and (b) pore size distribution of modified ISSA

3.2 Leaching test results

3.2.1 TCLP test

The leachate concentration of As and final pH of the TCLP test for soil containing 1000mg/kg As are listed in Fig. 3(a) and (c), respectively. ISSA showed limited As immobilization efficacy, and a 5% ratio addition of ISSA slightly reduced the leaching concentration of As from 20 mg/L to 15 mg/L after 28 d curing. On the other hand, M-ISSA significantly reduced As leaching concentration and enhanced As immobilization with increasing M-ISSA dosage and curing time. The leached As concentration was significantly decreased from 21.45 to 0.725 mg/L when 5% M-ISSA was incorporated, which was related to the increased specific surface area and enhanced retention of As by active sites on surfaces of M-ISSA compared with ISSA(Luo et al. 2020). After modification, M-ISSA contained more iron oxides ($KFeO_2$), which reacted with H_2O and formed amorphous iron during the stabilization process. So it has a better adsorption capability than ISSA (Gao et al. 2021). The final pH values of the leachates were similar around 4.5 for all the samples, which did not change with the extension of curing time and amendments incorporation ratio. According to the theory and experiment reported, high sorption and efficiency of As by melanterite and hematite in an acidic environment (pH 1.5-4.0) were best. That is because this low pH provided H^+ promoting the formation of a strong coating on As-rich minerals that could suppress both minerals oxidation and As release(Tabelin et al. 2020). Fig. 4 exhibited the As concentration and pH of leachates from soil containing 100mg/kg and 500mg/kg As. In general, the effectiveness of stabilization was primarily related to M-ISSA addition amount and, to a lesser extent, the curing time. Overall, TCLP-leachable As was considerably reduced with incubation time and the addition of M-ISSA, indicating that the environmental risk of the soil after stabilization declined significantly.

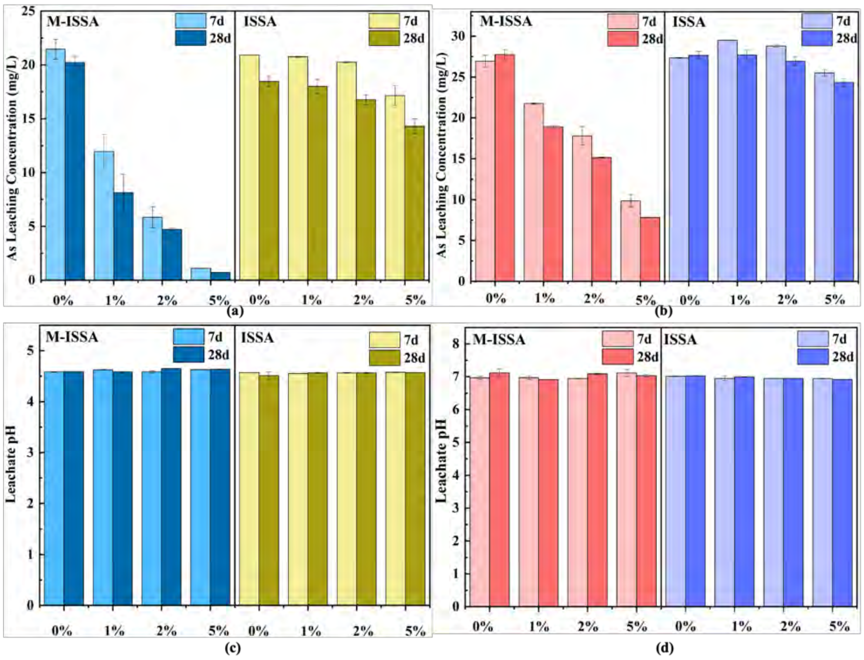

Fig. 3 Leachate As concentration (a), (b) and final pH (c), (d) from stabilization samples based on TCLP and SPLP leaching tests, respectively.

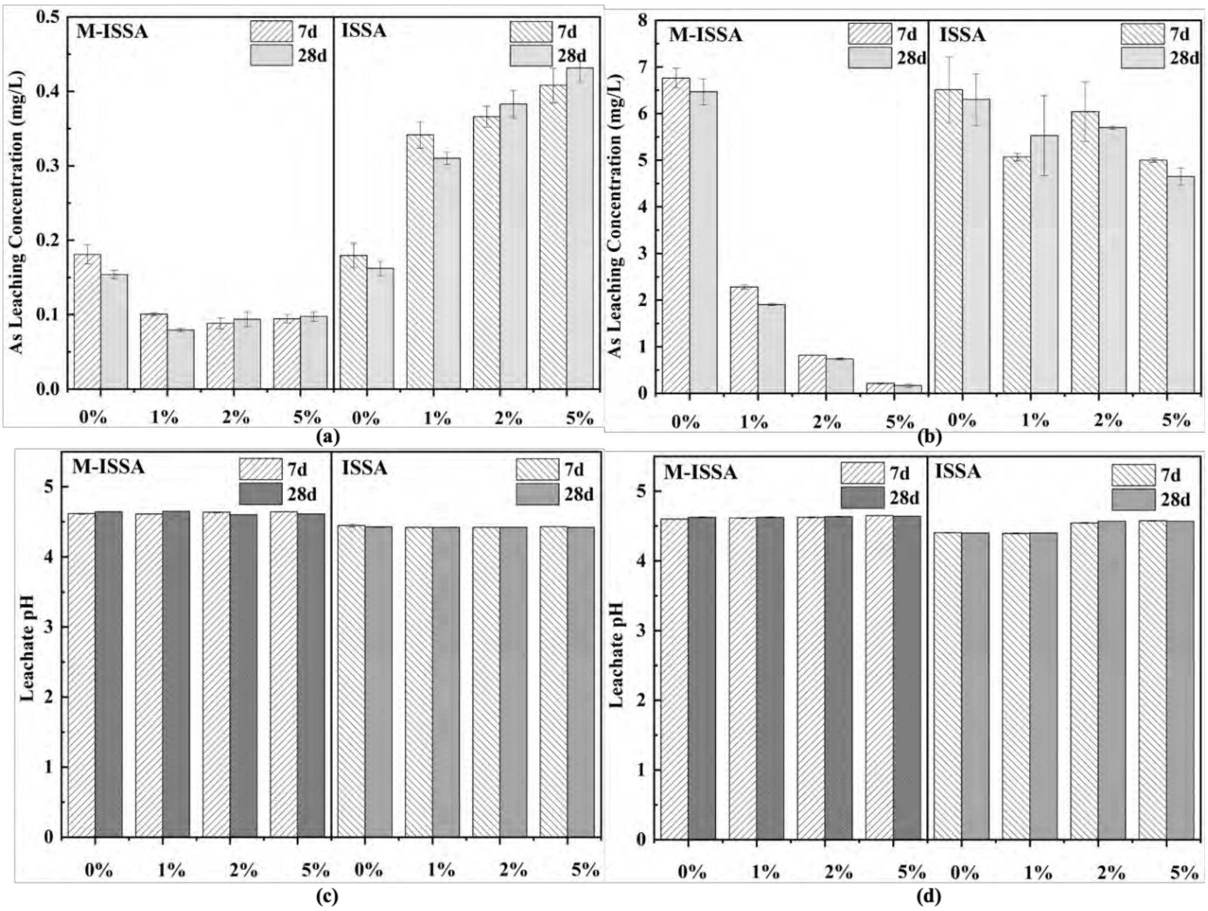

Fig. 4 As concentration and Leachate pH from stabilization samples based on TCLP test

3.2.2 SPLP test

Fig. 3 (b) and (d) display the leached As concentration and final pH from SPLP tests of the 1000mg/kg soils. It should be noted that As concentrations leached in SPLP tests were significantly higher than in TCLP tests. This was because the pH-dependent characteristics of As leaded to an increase in its mobility. The final pH of the leachates from SPLP test was around 7, which enhanced desorption of As from M-ISSA (Lee et al. 2009). It may be due to the release of rich alkaline salts like calcium (Ca) and potassium (K) into the soils resulting in this neutral pH (Madejón and Lepp 2007, Hartley et al. 2009). The final pH of TCLP tests (around 4.5) were lower than that of SPLP tests. SPLP extracted a larger proportion of As than TCLP solutions, since As was an oxyanion, it was more easily desorbed from the oxide surface under alkaline conditions (Moon et al. 2015). As leaching concentration obviously dropped with the rise of incorporation ratio and aging time of M-ISSA, compared with ISSA. For soils containing 1000 mg/kg As after 28 d of aging, the concentration of leached As significantly dropped from 27.75mg/L to 7.83mg/L, when the addition ratio of M-ISSA was 5%. The addition of ISSA however slightly reduced the leaching concentration of As irrespective of the curing time and the addition ratio, suggesting the ineffectiveness of stabilization of As by ISSA. Fig. 5 demonstrates the As concentration and pH of leachates from soil containing 100mg/kg and 500mg/kg As. In general, a higher addition ratio of M-ISSA and a longer stabilization time resulted in less SPLP leachable As from soils.

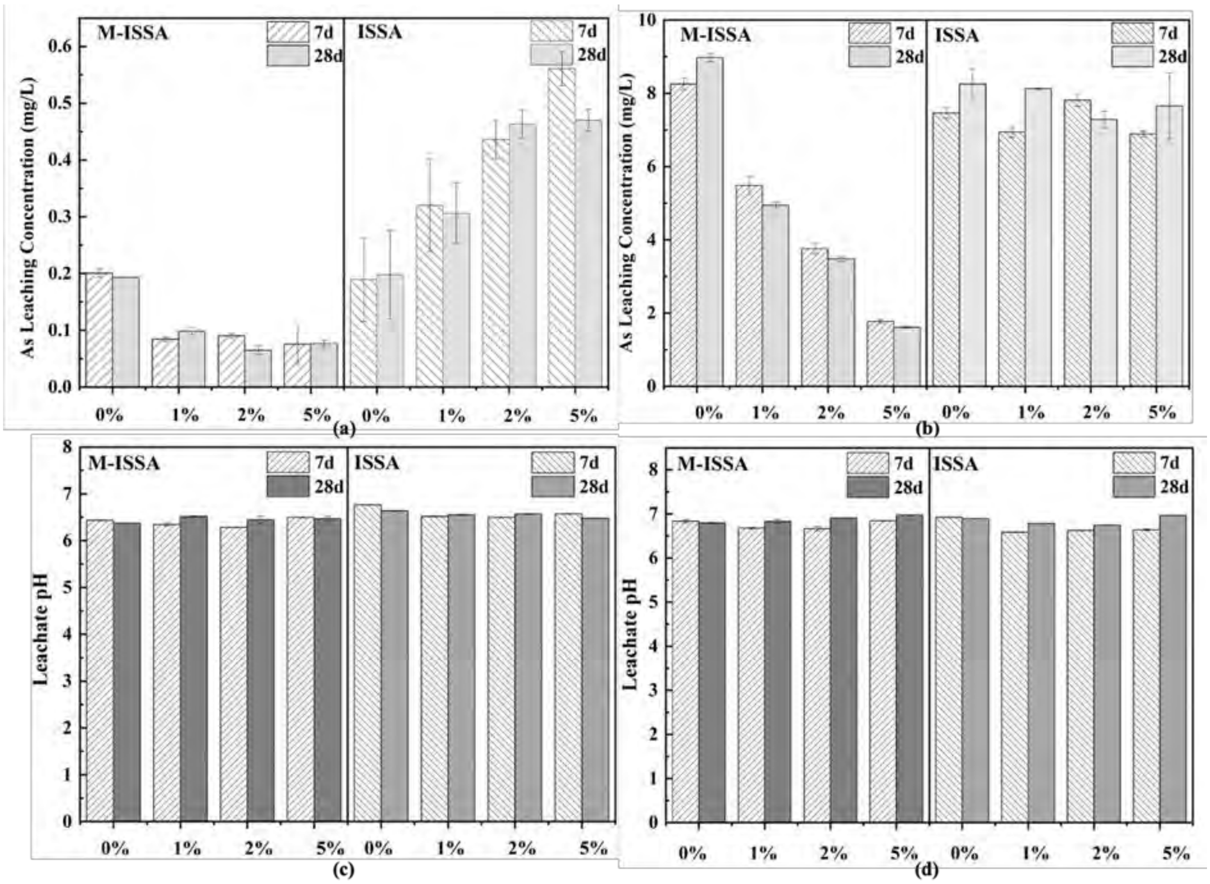

Fig. 5 As concentration and Leachate pH from stabilization samples based on SPLP test

3.3 Fractionation of As in stabilization soils

The fractions of As in 1000 mg/kg soil after 28d incubation were estimated by sequential extraction procedure (SEP) and the results are given in Fig. 6. The predominant species of As in raw soil were F1 and F2 which accounted for 69% of the total As, which would pose a high environmental risk (Karak et al. 2011). It is obvious that proportions of F1 and F2 fractions were fell while F3, F4 and F5 fractions rose with the addition of M-ISSA indicating M-ISSA had effective stabilization effects on soil As by transforming mobile As to stable forms (Yan et al. 2020). When it comes to ISSA, there was no significant difference in As fractions irrespective of ISSA addition amount. Overall, application of M-ISSA successfully transformed the labile As (F1+ F2) to more steady fractions (F3+F4+F5). Moreover, the dramatic growth was found in stable fractions, from 31% to 60%. M-

ISSA could react rapidly with H_2O to form highly reactive FeOOH, while providing the accessible active sorption sites for As(Frick et al. 2019) According to previous results, As(V) was the predominantly form present of geogenic As in the soils, and Fe(III) oxides were the coordination environment(Cui et al. 2018, Li et al. 2018). As a result, the interaction between the freshly formed amorphous iron oxides and As promoted the immobilization of As in soils (Liang et al. 2017).

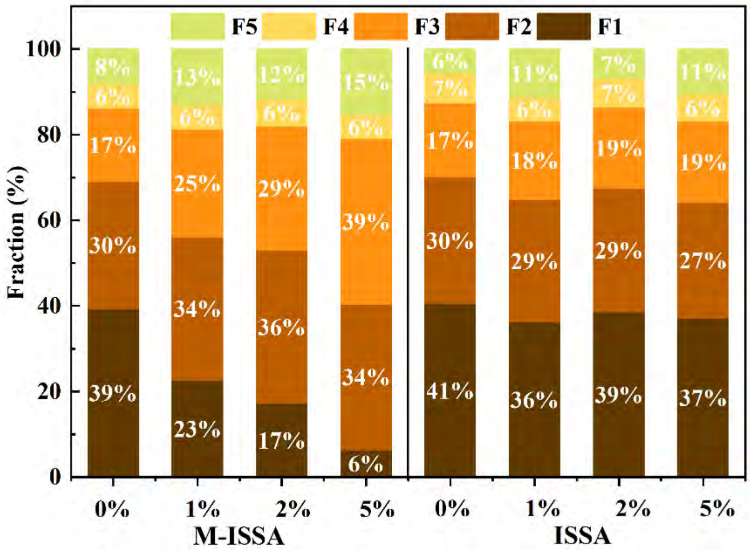

Fig. 6 As fraction in soil before and after stabilization treatment

3.4 As stabilization and iron transformation

According to the above results, M-ISSA was more effective in stabilizing As in soils compared with ISSA. It is worth mentioning that amorphous iron plays an importation role for the retention of As(V) in soil(Kim et al. 2012). Fig. 7 shows contents of amorphous and crystalline Fe in soil (1000 mg/kg) samples immobilized by M-ISSA/ISSA after 28d curing. Our results illustrated after the addition of ISSA, the contents of crystalline iron and amorphous iron in the soil remained unchanged, which was consistent with the original soil content, so the stabilization effect was not good. Crystalline Fe decreased in the soil with the treatments of M-ISSA while the amorphous Fe increased substantially. The addition of M-ISSA significantly increased the amount of amorphous Fe in soil, and it was reported that amorphous Fe played an essential role in the stabilization of As in soil. Amorphous iron had been reported to be responsible for As immobilization by coprecipitation or sorption (Fan et al. 2020). Amorphous Fe has amphoteric properties and is an effective anionic and cationic adsorbent. Its surface can be positively or negatively charged depending on the pH value of the soil (Kumpiene et al. 2008). Thus, the addition of M-ISSA obviously improved the curing effect of As (Hou et al. 2020). Regard to the soil treatment by ISSA, the concentration of these two fractions remained unchanged. These results indicated that the amorphous iron has a high ability for sequestering As in soil by forming that remain relatively stable.

The XPS full spectra of the 1000mg/kg soil samples of pre-stabilization and post-stabilization of 28 d by 5% M-ISSA treatment are shown in Fig. 8. The As XPS spectra of the soil before and after stabilization showed that the valence state of As(V) was kept unchanged, indicating that no redox reaction occurred during the stabilization process. Previous studies found that Fe(III) oxide surface had a high affinity for As(V), capable of forming inner-spere bidentate, binuclear As(V)-Fe(III) complexes(La Force et al. 2000, Zhu et al. 2019). Kim(Kim et al. 2003) reported that strong reaction of As is more likely to be due to the formation of binuclear complexes with iron oxides on the basis of the results of sequential extraction and FTIR analysis. The primary mechanism of As stabilization may be precipitation and/or physicochemical adsorption of specific As compounds. However, when it comes to specific reactions, they were usually difficult to distinguish and quantify. The possible reactions of M-ISSA and As in soil could be illustrated by the following equations:

$$F_eOOH + 3H_2A_sO_4^- + 3H^+ \rightarrow Fe(H_2A_sO_4)_3 + 2H_20$$

$$A_sO_4^{3-} + F_e^{3+} + Ca^{2+} + S_iO_3^{2-} \rightarrow (F_e, C_a)A_so_4 \cdot S_iO_3\ (s)$$

$$A_sO_4^{3-} + F_e^{3+} + Al^{3+} + SiO_3^{2-} \rightarrow (F_e, Al)A_sO_4 \cdot SiO_3\ (s)$$

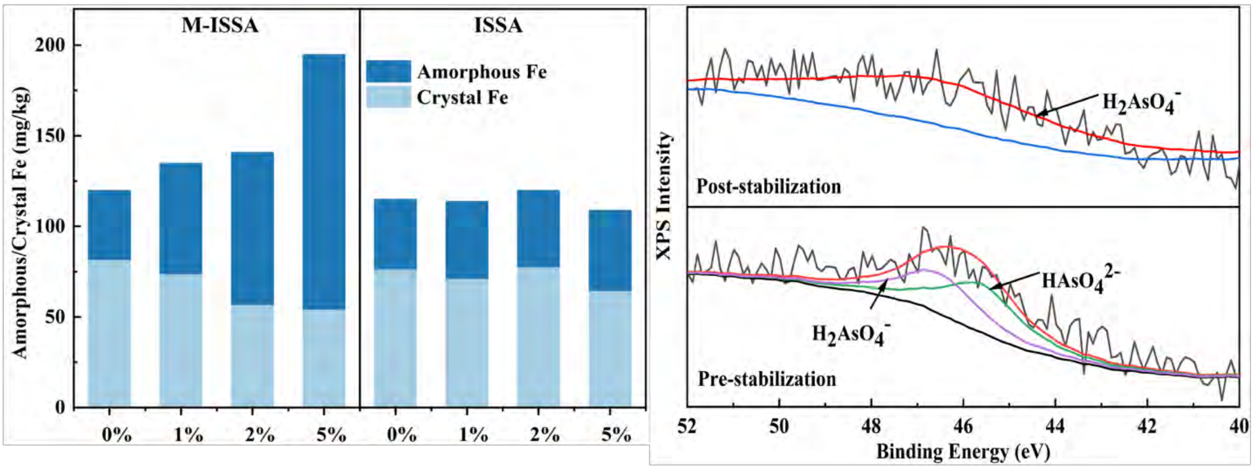

(a) (b)

Fig. 7 Amorphous and crystal Fe from two soils (1000mg/kg) with M-ISSA/ISSA treatment after 28d curing (a) and XPS of As(V) in soil before and after stabilization (b)

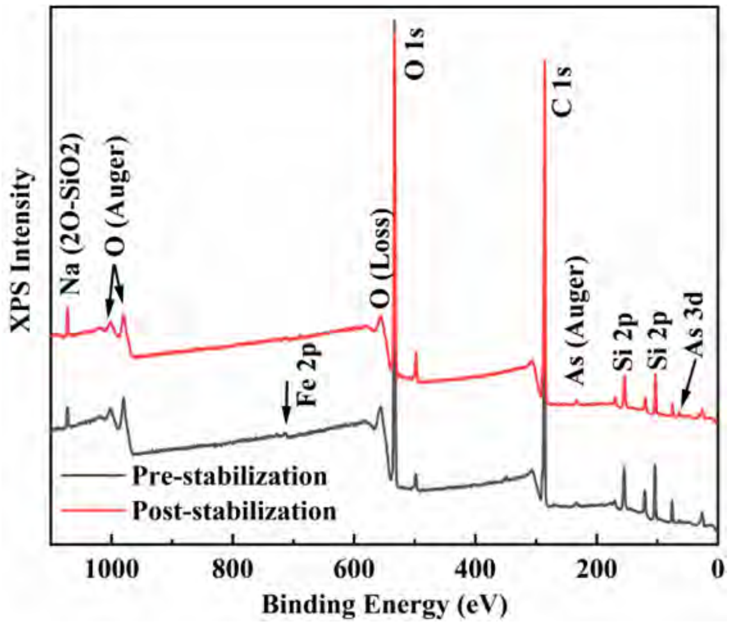

Fig. 8 XPS wide scan of soil of before and after stabilization

Overall, the main mechanism of immobilization of As(V) by M-ISSA in soils were: firstly, the addition of M-ISSA resulted in an decrease in soil pH, which subsequently caused a weakened competition of anionic (e.g. OH^-), making it easier for As(V) and metal ions to be combined into a relatively more stable form. As(V) is sensitive to pH and immobilized better at low pH. Meanwhile, the large specific surface area and porous structure of M-ISSA could promote As(V) removal. In addition, the iron in M-ISSA could adsorb and coprecipitate with As(V) and Ca or Al in soil(Suda and Makino 2016). When M-ISSA is mixed with soil, it can be sprayed onto the ground or go deep underground for restoration, expanding the range of restoration. Therefore, in this study, the recovery of ISSA into stabilizers is a very sustainable and environmentally friendly program, while the site selection and economic issues in field work should be further assessed in the future.

4. CONCLUSION

This work investigated the effects of M-ISSA on the stabilization of As-contaminated soil though a series of leaching experiments including TCLP and SPLP. The characterization results of M-ISSA using XRD, XRF, SEM-EDS, and BET were studied. Furthermore, the As immobilization mechanism was determined based on the results of amorphous and crystal Fe and XPS tests. According to this study, the following conclusions can be summarized:

1. Compared with other incinerated sewage sludge treatment methods like landfills and raw materials, the iron in ISSA was rearranged after modification and formed $KFeO_2$, which had been recently reported as a better adsorbent for As(V) removal in wastewater.
2. The characterization results of M-ISSA showed that the synthesized material had a better pore structure with a mean pore diameter of 5.11 nm and a larger specific surface area of 131.35 m^2/g compared with raw ISSA.
3. Leaching results from TCLP and SPLP illustrated that the M-ISSA could effectively stabilize As contaminated soils, while ISSA had negligible effect for As immobilization. This is because M-ISSA successfully transformed mobile As(V) fractions in soils to more stable fractions as assessed by SEP. The number of stable fractions saw a sharp rise from 31% to 60% when the M-ISSA addition was 5%. These results suggested that M-ISSA can be used as an additive for the stabilization of As(V) in soil.
4. The stabilization mechanism was predominantly associated with adsorption and coprecipitation between As(V) and iron oxides which was formed after modification in M-ISSA. In summary, the results obtained from our present study indicated that the M-ISSA could be an efficient and environmentally friendly immobilizer to remediate As contaminated soil, which provides a cleaner production strategy for the treatment of soil contaminated by heavy metals.

In the previous paper, the results suggested the feasibility of M-ISSA on As removal in waste water. In this study, M-ISSA is successfully recycled to convert wastes into useful products by saving energy, resources, and costs, which is reflected in the stabilization of arsenic-bearing soil. In addition, the comprehensive utilization of M-ISSA for remediation of As-rich soil should be tested under field conditions and the co-stabilization effect of M-ISSA on multi-metals contaminated soil should be demonstrated in the further research.

5. ACKNOWLEDGMENT

The authors wish to sincerely thank the National Natural Science Foundation of China (project no. 51861165104), and Hong Kong Research Grants Council Joint Research Scheme (N_PolyU511/18) as well as the Environment and Conservation Fund of the Hong Kong SAR government (No. P0014071) for the support of this study.

6. REFERENCES

Asere, T. G., et al. (2019). "Use of (modified) natural adsorbents for arsenic remediation: A review." Science of The Total Environment 676: 706-720doi.org/https://doi.org/10.1016/j.scitotenv.2019.04.237.

Chen, L., et al. (2009). "Applications of sewage sludge ash and nano-SiO2 to manufacture tile as construction material." Construction and Building Materials 23(11): 3312-3320doi.org/https://doi.org/10.1016/j.conbuildmat.2009.06.049.

Chiou, I.-J., et al. (2006). "Lightweight aggregate made from sewage sludge and incinerated ash." Waste Management 26(12): 1453-1461doi.org/https://doi.org/10.1016/j.wasman.2005.11.024.

Cui, J.-l., et al. (2018). "Speciation, mobilization, and bioaccessibility of arsenic in geogenic soil profile from Hong Kong." Environmental Pollution 232: 375-384doi.org/https://doi.org/10.1016/j.envpol.2017.09.040.

Cutler, W. G., et al. (2014). "Iron amendments to reduce bioaccessible arsenic." Journal of Hazardous Materials 279: 554-561doi.org/https://doi.org/10.1016/j.jhazmat.2014.07.043.

Doherty, S. J., et al. (2017). "Evaluation of amendments to reduce arsenic and antimony leaching from co-contaminated soils." Chemosphere 174: 208-217doi.org/https://doi.org/10.1016/j.chemosphere.2017.01.100.

Donatello, S., et al. (2013). "Recycling and recovery routes for incinerated sewage sludge ash (ISSA): A review." Waste Management 33(11): 2328-2340doi.org/https://doi.org/10.1016/j.wasman.2013.05.024.

Fan, J., et al. (2020). "One-pot synthesis of nZVI-embedded biochar for remediation of two mining arsenic-contaminated soils: Arsenic immobilization associated with iron transformation." Journal of Hazardous Materials 398: 122901doi.org/https://doi.org/10.1016/j.jhazmat.2020.122901.

Fang, L., et al. (2018). "Phosphorus recovery and leaching of trace elements from incinerated sewage sludge ash (ISSA)." Chemosphere 193: 278-287doi.org/https://doi.org/10.1016/j.chemosphere.2017.11.023.

Fresno, T., et al. (2016). "Assessing the combination of iron sulfate and organic materials as amendment for an arsenic and copper contaminated soil. A chemical and ecotoxicological approach." Chemosphere 165: 539-546doi.org/https://doi.org/10.1016/j.chemosphere.2016.09.039.

Frick, H., et al. (2019). "Assessment of biochar and zero-valent iron for in-situ remediation of chromated copper arsenate contaminated soil." Science of The Total Environment 655: 414-422doi.org/https://doi.org/10.1016/j.scitotenv.2018.11.193.

Gao, S., et al. (2021). "Arsenate(V) removal from aqueous system by using modified incinerated sewage sludge ash (ISSA) as a novel adsorbent." Chemosphere 270: 129423doi.org/https://doi.org/10.1016/j.chemosphere.2020.129423.

Hartley, W., et al. (2009). "Arsenic mobility in brownfield soils amended with green waste compost or biochar and planted with Miscanthus." Environmental Pollution 157(10): 2654-2662doi.org/https://doi.org/10.1016/j.envpol.2009.05.011.

Hartley, W., et al. (2004). "Arsenic and heavy metal mobility in iron oxide-amended contaminated soils as evaluated by short- and long-term leaching tests." Environmental Pollution 131(3): 495-504doi.org/https://doi.org/10.1016/j.envpol.2004.02.017.

HK, E. (2007). Guidance manual for use of risk-based remediation goals for contaminated land management.

Hou, Q., et al. (2020). "The bioaccessibility and fractionation of arsenic in anoxic soils as a function of stabilization using low-cost Fe/Al-based materials: A long-term experiment." Ecotoxicology and Environmental Safety 191: 110210doi.org/https://doi.org/10.1016/j.ecoenv.2020.110210.

Karak, T., et al. (2011). "Fractionation and speciation of arsenic in three tea gardens soil profiles and distribution of As in different parts of tea plant (Camellia sinensis L.)." Chemosphere 85(6): 948-960doi.org/https://doi.org/10.1016/j.chemosphere.2011.06.061.

Kim, J.-Y., et al. (2003). "Stabilization of Available Arsenic in Highly Contaminated Mine Tailings Using Iron." Environmental Science & Technology 37(1): 189-195doi.org/10.1021/es020799+.

Kim, K.-R., et al. (2012). "Arsenic stabilization in mine tailings using nano-sized magnetite and zero valent iron with the enhancement of mobility by surface coating." Journal of Geochemical Exploration 113: 124-129doi.org/https://doi.org/10.1016/j.gexplo.2011.07.002.

Ko, M.-S., et al. (2015). "Field assessment of arsenic immobilization in soil amended with iron rich acid mine drainage sludge." Journal of Cleaner Production 108: 1073-1080doi.org/https://doi.org/10.1016/j.jclepro.2015.06.076.

Koo, N., et al. (2012). "Increased As load to the Uchen stream due to mine drainage and soils in the abandoned Kangwon mining district of Korea." Environmental Earth Sciences 65(3): 689-697doi.org/10.1007/s12665-011-1116-7.

Kumpiene, J., et al. (2008). "Stabilization of As, Cr, Cu, Pb and Zn in soil using amendments – A review." Waste Management 28(1): 215-225doi.org/https://doi.org/10.1016/j.wasman.2006.12.012.

La Force, M. J., et al. (2000). "Arsenic Speciation, Seasonal Transformations, and Co-distribution with Iron in a Mine Waste-Influenced Palustrine Emergent Wetland." Environmental Science & Technology 34(18): 3937-3943doi.org/10.1021/es0010150.

Lee, K.-Y., et al. (2009). "A Novel Combination of Anaerobic Bioleaching and Electrokinetics for Arsenic Removal from Mine Tailing Soil." Environmental Science & Technology 43(24): 9354-9360doi.org/10.1021/es901544x.

Li, J.-S., et al. (2018). "Effects of low-alkalinity binders on stabilization/solidification of geogenic As-containing soils: Spectroscopic investigation and leaching tests." Science of The Total Environment 631-632: 1486-1494doi.org/https://doi.org/10.1016/j.scitotenv.2018.02.247.

Li, J.-s., et al. (2019). "Development of a Novel Binder Using Lime and Incinerated Sewage Sludge Ash to Stabilize and Solidify Contaminated Marine Sediments with High Water Content as a Fill Material." Journal of Materials in Civil Engineering 31(10)doi.org/10.1061/(asce)mt.1943-5533.0002913.

Li, J., et al. (2017). "Innovative solidification/stabilization of lead contaminated soil using incineration sewage sludge ash." Chemosphere 173: 143-152doi.org/https://doi.org/10.1016/j.chemosphere.2017.01.065.

Li, S.-W., et al. (2015). "Arsenic bioaccessibility in contaminated soils: Coupling in vitro assays with sequential and HNO3 extraction." Journal of Hazardous Materials 295: 145-152doi.org/https://doi.org/10.1016/j.jhazmat.2015.04.011.

Liang, Y., et al. (2017). "Stabilization of arsenic sludge with mechanochemically modified zero valent iron." Chemosphere 168: 1142-1151doi.org/https://doi.org/10.1016/j.chemosphere.2016.10.087.

Luo, M., et al. (2020). "The influence of corncob-based biochar on remediation of arsenic and cadmium in yellow soil and cinnamon soil." Science of The Total Environment 717: 137014doi.org/https://doi.org/10.1016/j.scitotenv.2020.137014.

Madejón, P., et al. (2007). "Arsenic in soils and plants of woodland regenerated on an arsenic-contaminated substrate: A sustainable natural remediation?" Science of The Total Environment 379(2): 256-262doi.org/https://doi.org/10.1016/j.scitotenv.2006.08.051.

Manzano, R., et al. (2014). "Amendment Application in a Multicontaminated Mine Soil: Effects on Trace Element Mobility." Water, Air, & Soil Pollution 225(2): 1874doi.org/10.1007/s11270-014-1874-4.

Moon, D. H., et al. (2015). "Stabilization of As-, Pb-, and Cu-contaminated soil using calcined oyster shells and steel slag." Environ Sci Pollut Res Int 22(14): 11162-11169doi.org/10.1007/s11356-015-4612-6.

Nie, J., et al. (2021). "Novel recycling of incinerated sewage sludge ash (ISSA) and waste bentonite as ceramsite for Pb-containing wastewater treatment: Performance and mechanism." Journal of Environmental Management 288: 112382doi.org/https://doi.org/10.1016/j.jenvman.2021.112382.

Ouyang, X., et al. (2020). "Immobilization and release risk of arsenic associated with partitioning and reactivity of iron oxide minerals in paddy soils." Environ Sci Pollut Res Int 27(29): 36377-36390doi.org/10.1007/s11356-020-09480-y.

Pan, S. C., et al. (2001). "Sewage sludge ash characteristics and its potential applications." Water Science and Technology 44(10): 261-267doi.org/10.2166/wst.2001.0636.

Su, B., et al. (2020). "Impact of green synthesized iron oxide nanoparticles on the distribution and transformation of As species in contaminated soil." Environmental Pollution 258: 113668doi.org/https://doi.org/10.1016/j.envpol.2019.113668.

Suda, A., et al. (2016). "Functional effects of manganese and iron oxides on the dynamics of trace elements in soils with a special focus on arsenic and cadmium: A review." Geoderma 270: 68-75doi.org/https://doi.org/10.1016/j.geoderma.2015.12.017.

Tabelin, C. B., et al. (2020). "Acid mine drainage formation and arsenic mobility under strongly acidic conditions: Importance of soluble phases, iron oxyhydroxides/oxides and nature of oxidation layer on pyrite." Journal of Hazardous Materials 399: 122844doi.org/https://doi.org/10.1016/j.jhazmat.2020.122844.

Tiberg, C., et al. (2016). "Immobilization of Cu and As in two contaminated soils with zero-valent iron – Long-term performance and mechanisms." Applied Geochemistry 67: 144-152doi.org/https://doi.org/10.1016/j.apgeochem.2016.02.009.

Wang, L., et al. (2018). "Recycling dredged sediment into fill materials, partition blocks, and paving blocks: Technical and economic assessment." Journal of Cleaner Production 199: 69-76doi.org/https://doi.org/10.1016/j.jclepro.2018.07.165.

Wang, L., et al. (2012). "Sintering characteristics of sewage sludge ashes at elevated temperatures." Fuel Processing Technology 96: 88-97doi.org/https://doi.org/10.1016/j.fuproc.2011.12.022.

Wang, Q., et al. (2019). "Recycling of incinerated sewage sludge ash as an adsorbent for heavy metals removal from aqueous solutions." Journal of Environmental Management 247: 509-517doi.org/https://doi.org/10.1016/j.jenvman.2019.06.115.

Wang, Q., et al. (2021). "Novel recycling of phosphorus-recovered incinerated sewage sludge ash residues by co-pyrolysis with lignin for reductive/sorptive removal of hexavalent chromium from aqueous solutions." Chemosphere 285: 131434doi.org/10.1016/j.chemosphere.2021.131434.

Wenzel, W. W., et al. (2001). "Arsenic fractionation in soils using an improved sequential extraction procedure." Analytica Chimica Acta 436(2): 309-323doi.org/https://doi.org/10.1016/S0003-2670(01)00924-2.

Yan, X., et al. (2020). "Arsenic stabilization performance of a novel starch-modified Fe-Mn binary oxide colloid." Science of The Total Environment 707: 136064doi.org/https://doi.org/10.1016/j.scitotenv.2019.136064.

Yan, X., et al. (2020). "Stabilization of soil arsenic by natural limonite after mechanical activation and the associated mechanisms." Science of The Total Environment 708: 135118doi.org/https://doi.org/10.1016/j.scitotenv.2019.135118.

Yusuf, R. O., et al. (2012). "Use of sewage sludge ash (SSA) in the production of cement and concrete–a review." 12(2-4): 214-228

Zhou, Y.-f., et al. (2020). "Recycling incinerated sewage sludge ash (ISSA) as a cementitious binder by lime activation." Journal of Cleaner Production 244: 118856doi.org/https://doi.org/10.1016/j.jclepro.2019.118856.

Zhou, Y.-f., et al. (2020). "Sewage sludge ash: A comparative evaluation with fly ash for potential use as lime-pozzolan binders." Construction and Building Materials 242: 118160doi.org/https://doi.org/10.1016/j.conbuildmat.2020.118160.

Zhu, N., et al. (2019). "Arsenic immobilization through regulated ferrolysis in paddy field amendment with bismuth impregnated biochar." Science of The Total Environment 648: 993-1001doi.org/https://doi.org/10.1016/j.scitotenv.2018.08.200.

Zialame, A., et al. (2021). "Stabilized magnetite nanoparticles for the remediation of arsenic contaminated soil." Journal of Environmental Chemical Engineering 9(2): 104821doi.org/https://doi.org/10.1016/j.jece.2020.104821.

BUILDING A SUSTAINABLE FUTURE: EVALUATING ENVIRONMENTAL IMPACT AND ECO-EFFICIENCY OF PREFABRICATED VS. CAST-IN-SITU CONSTRUCTION IN RAPIDLY URBANIZING INDIA

Harshal Tikam[1], and Abhiram Shukla[1]

[1]PhD Student, Indian Institute of Technology Kanpur, Kanpur, India
E-mail (harshall@iitk.ac.in)

1. INTRODUCTION

The construction sector serves as a crucial driver of social and economic development; however, its adverse environmental impact, characterized by substantial greenhouse gas emissions (GHGs) that contribute to global warming, presents significant challenges. It is the largest global consumer of resources and least sustainable sector of the economy. Rapid urbanization in India further exacerbates resource depletion and environmental pressures. In response, active promotion of the adoption of building prefabrication, a construction method reliant on in-plant manufacturing and on-site assembly of building components, offers advantages such as expedited construction, cost savings, and design flexibility. Notably, in developing countries, the preference for prefabrication is growing due to its potential to address the environmental challenges posed by rapid urbanization when compared to conventional cast-in-situ methods. Acknowledging the environmental performance of construction methodologies might exhibit discrepancies in diverse geographic areas, it becomes essential to conduct site-specific environmental evaluations of these approaches. Limited research exists regarding mitigation of greenhouse gas emissions through alternative construction methodologies, such as off-site prefabrication compared to conventional methods. This study, therefore, conducts a comparative Life Cycle Assessment (LCA) to evaluate the environmental impact of prefabricated and conventional methods of construction, utilizing case study of residential hostel buildings with similar characteristics.

2. MATERIALS AND METHODS

Goal and scope definition: The study compares the GHG emissions of prefabricated and conventional construction method based on case study of a residential hostel building in India using Life cycle assessment (LCA) model considering system processes from cradle to grave. Study presents assessment of GHG emissions of prefabricated and standard construction practices in India. Different phases of building considered are production of materials, transportation, construction, and demolition except operating phase. To analyze differences of systems and relative scenarios, a comparative LCA examining two complete life cycles of building is developed. The comparison is conducted based on emission per floor area. Finally, emission reduction recommendations are drawn for reduction in GHG emission for building sector through application of prefabrication technique.

Selection of quantitative method: To assess the environmental effects of a building, two primary methodologies are employed, process-based approach and the input-output method [1]. Limited database of GHG emission database of construction materials and economic input–output data, from all potential transactions upstream in the supply chain in India, constrains the application of software-oriented life cycle assessment methodologies. Hence, a process-based micro-bottom-up approach is embraced. This model can be employed to delineate and confine the origins and extent of greenhouse gas emissions for the purpose of computation [1,2]. Therefore, the only possible approach for assessment of GHG emissions is the process-based micro bottom-up method which is adopted in this study [1,2,3].

Building LCA for GHG emissions can be divided into embodied and operational carbon emissions. As a result, we confine the calculation elements to (1) embodied GHG emissions of materials (E1), (2) GHG emissions associated with transportation of material and waste (E2, E3) (3) GHG emissions from material and fuel consumption by equipment in construction stage(E4). (4) GHG emissions from demolition stage (E5). (5) GHG emissions reduction from material recycling (E6).

Quantitative model of GHG emissions: GHG emissions from buildings primarily consist of CO2, CH4, and N2O, with other gases being rarely emitted in this context. The Global Warming Potential (GWP) value is a standard metric utilized to quantify the climate impact of various gases. The cumulative GHG emissions for a specific stage were determined by summing emissions from all individual processes within that stage. For each process or material, GHG emissions were calculated in CO2-equivalent by multiplying the quantity of material or energy consumption with corresponding GHG emissions factor, sourced from relevant databases specific to India [4,5].

Case study: The developed LCA allows to assess environmental benefits resulting from prefabricated structure in contrast to the traditional one intended for eventual demolition and recycling. Considering an entire multi-story building constructed as a functional entity, this paper employed process-based quantitative model for detailed GHG emissions calculation and comparative study. Project A is built using prefabrication and conventional in-situ construction method was adopted for project B. Project A is an extension of project B exemplifying a significant representation of the extent to which prefabrication is employed in India. Both projects share analogous pivotal structural characteristics and profiles that influence factors such as project quality, performance, and material consumption (such as floor plan, room aspect ratio, foundation, basement, and floor-to-floor height), thus rendering them comparable. To ensure a uniform calculation basis for comparing these two projects, GHG emission per unit floor area is used to represent a unit of order for comparison [2]. The combination of site-specific data and existing emission factor databases was adopted for LCA study. Site-specific documents like Bill of quantity, tender reports, building plans and semi-structured interview was conducted to obtain all required data like structural system, flooring area, room dimension, floor elevation and other significant data for the buildings [1].

Assumption- All the building material and machinery used for both cases are sourced from the same dealer and location. Operation and maintenance of building are similar therefore it cancels out in comparative study. Both structures are demolished at the end of design life. Demolition closely mirrors the present approaches to demolition and waste management of steel, concrete and other materials adapted in India. The 50/50 allocation method was used for calculation of GHG emission reduction due to open loop recycling of steel material for the process based LCA study [6]. Calculation for resource, machinery and energy consumption for demolition stage were based on the inventory provided by Brambilla et al. (2019) for demolition of prefabricated buildings [7].

3. RESULTS AND DISCUSSION

Elaborated GHG emssions from different stages for prefabrication and conventional method are presented in Table 1. Cumulative GHG emissions till construction phase for conventional and prefabrication method are 1026 and 678 kg CO2eq/m2, respectively. Reduction of 348 kg CO2eq/m2 was observed for prefabrication, 33.9% lesser than emissions from conventional construction. This reduction is significant and aligns with prior similar studies.

For conventional construction, 90.8% of total GHG emissions upto construction stage results from embodied emissions of construction materials; 8.2% from conveyance of materials, waste, and soil; and only 0.9% from fuel combustion by machinery on site. For prefabricated construction, 86.9% of GHG emissions upto construction stage come from embodied emissions of construction materials; 11.7% from transportation; and 1.4% from fuel combustion by machinery on site.

Table 1. Total GHG emissions in conventional and prefabricated construction (unit: kgCO2-eq/m2)

Source of GHG emissions	GHG emission in CO2eq/m2				Reduction %
	Conventional Building		Prefabricated building		
E1	932.35	92.14%	589.18	98%	36.8
E2	83.84	8.29%	79.1	13%	5.6
E3	0.79	0.01%	0.52	0.1%	34.8
E4	9.17	0.1%	9.35	1.56%	-2
E5	19.85	2%	11.76	2%	40.8
E6	-34.5	-3.41%	-90.88	-15.4%	163.3
Total	**1011.5**	**100%**	**599.1**	**100%**	**40.8**

Embodied emissions of materials emerge as primary major contributor to GHG emissions in both prefabrication and traditional construction approaches, constituting 90.8% and 86.9% of total emissions, respectively. Notably, steel, concrete, and bricks emerge as major contributors. Specifically, for conventional construction, concrete, brick, plaster, and steel accounts for 17.9%, 64%, 5.5%, and 12.5% of emissions, respectively. For prefabrication approach, the distribution shifts to 23.7% for concrete, 12.5% for AAC blocks, 11% for plaster, and 51.5% for steel.

Total GHG emissions linked to transportation activities are 84.6 kg CO2eq/m2 and 79.6 kg CO2eq/m2 for conventional and prefabrication methods, respectively. The relatively lower GHG emissions in the prefabrication method, even with the extra transportation involved in handling prefabricated steel sections, can be attributed to two key factors. Firstly, the prefabrication process exhibits a reduced consumption of building materials compared to the conventional method. Secondly, the shorter distance from distribution center of steel sections to construction site contributes to this reduction, as compared to the logistics of transporting steel reinforcement suppliers. The shift to prefabrication leads to a net increase in overall GHG emissions resulting from fuel consumption in machinery operations. While diesel usage decreases for concrete delivery pumps due to reduced concrete requirements in prefabrication compared to the conventional method, there is an additional diesel consumption by forklifts and cranes involved in unloading, preparation, placement, and connection of steel sections for prefabrication method. In contrast, the adoption of prefabrication results in reduction of GHG emissions during the demolition stage, with a significant decrease of 40.1% compared to emissions from conventional construction. This reduction can be attributed to lower diesel consumption by hydraulic excavators, crawler loaders, and trucks. Additionally, the ease of demolishing prefabricated steel structures using hydraulic shears compared to demolishing larger quantities of concrete and brick structures typically found in conventional construction.

The comprehensive assessment of net GHG emissions across all stages of the building lifecycle, excluding the operational phase, highlights a significant reduction with the prefabrication approach in comparison to the conventional construction method. More specifically, emissions decreased notably from 1011.5 CO2/m2 to 599 kg CO2/m2 for prefabricated buildings. This substantial reduction of 40.75% can be attributed to a range of factors, including diminished emissions during various stages such as material production, reduced transportation-related emissions, decreased emissions from demolition activities, and an enhanced recycling capacity in the prefabrication method compared to the conventional approach. The case study results indicate that adopting prefabrication can lead to significant carbon reduction compared in construction sector compared to conventional method. The correlation between prefabrication adoption and carbon reduction suggests that need for increased utilization of prefabrication methods in residential building projects. The case study highlights that while prefabricated buildings exhibit lower carbon emissions, they also consume more fossil fuels and steel. To promote prefabrication technique effectively, development and utilization of cleaner energy sources are essential to alleviate the environmental consequences from steel and fossil fuel consumption [8]. Incorporating green electricity and replacement of diesel with biodiesel and natural gas can enhance the environmental friendliness of buildings. Additionally, actively advocating for autoclaved aerated concrete blocks can enhance economic and social benefits compared to traditional clay brick usage. The study collectively emphasize that GHG emssions associated with buildings can be reduced by altering construction techniques, utilizing alternative building materials, and adopting cleaner energy sources. Given the projected popularity of prefabricated buildings in the future, enhancing relevant measures within prefabricated construction is essential.

4. CONCLUSION

Prefabrication stands as an alternative construction approach to the conventional cast-in-situ method, encompassing distinct construction technologies and processes. The present study investigated an analytical framework for quantifying the disparities in GHG emissions between prefabrication and the traditional cast-in-situ approach. This study identified emissions at each stage, including production of materials, transportation, construction, and demolition phases, utilizing a quantitative process-based model. The GWP impact results of comparative study of conventional and prefabrication method observed emissions reduction from 1011.5 CO2/m2 to 599 kg CO2/m2 for prefabricated building. This substantial reduction of 40.75% is attributed to a range of factors, including diminished emissions during various stages such as material production, reduced transportation-related emissions, decreased emissions from demolition activities, and an enhanced recycling capacity in the prefabrication method compared to the conventional approach. The most significant factor contributing to the reduction of GHG emissions are embodied emissions associated with construction materials and the demolition phase, accounting for reduction of 36.8%, 40.8% respectively and can substantially decrease the global warming potential impact. However, emission from machinery usage for field installation produced higher GHG emissions compared to conventional method. In comparison to conventional cast-in-situ structures, prefabricated buildings exhibit higher consumption of steel bars and diesel. Future studies can also focus on a comparative analysis of construction methodologies, encompassing economic and social dimensions, including the operational phase of the building.

5. ACKNOWLEDGMENT

The authors would like to express appreciation for the financial support by Indian Institute of Technology Kanpur, Kanpur through research fellowship and travel grant.

6. REFERENCES

1. Pervez, H., Ali, Y., & Petrillo, A. (2021). A quantitative assessment of greenhouse gas emissions from conventional and modular construction: A case of developing country. *Journal of Cleaner Production*,*294* 26210.
2. Mao, C., Shen, Q., Shen, L., & Tang, L. (2013). Comparative study of greenhouse gas emissions between off-site prefabrication and conventional construction methods: Two case studies of residential projects. *Energy and Buildings*, *66*, 165-176.
3. Yan, H., Shen, Q., Fan, L. C., Wang, Y., & Zhang, L. (2010). Greenhouse gas emissions in building construction: A case study of One Peking in Hong Kong. *Building and Environment*, *45*(4), 949-955.
4. India Construction Materials Database of Embodied Energy and Global Warming Potential METHODOLOGY REPORT. (2017). International Finance Corporation, World Bank Group.
5. Mir, K. A., & Ijaz, M. (2016). Greenhouse gas emission inventory of Pakistan for the year 2011–2012. *Minist Clim Chang*, 1-136.
6. Lee, K. M., & Inaba, A. (2004). *Life cycle assessment: best practices of ISO 14040 series*. Center for Ecodesign and LCA (CEL), Ajou University.
7. Brambilla, G., Lavagna, M., Vasdravellis, G., & Castiglioni, C. A. (2019). Environmental benefits arising from demountable steel-concrete composite floor systems in buildings. *Resources, Conservation and Recycling*, *141*, 133-142.

8. Zhou, F., Ning, Y., Guo, X., & Guo, S. (2023). Analyze Differences in Carbon Emissions from Traditional and Prefabricated Buildings Combining the Life Cycle. *Buildings*, *13*(4), 874.

ECO-CEMENT SYNTHESIZED FROM MUNICIPAL SOLID WASTE INCINERATION BOTTOM ASH AND RECYCLED CONCRETE FINE

Hanxiong Lyu[1], Shipeng Zhang[1,2,*], Chi-sun Poon[1,2]

[1]Department of Civil and Environmental Engineering, The Hong Kong Polytechnic University, Hong Kong
[2]Research Centre for Resources Engineering towards Carbon Neutrality, The Hong Kong Polytechnic University, Hong Kong
*E-mail: shipeng.zhang@polyu.edu.hk

There are two major solid waste streams in modern society: municipal solid waste incineration bottom ash (IBA) and recycled concrete fine (RCF). Thus, the recycling and reusing of IBA and RCF are of great significance. An eco-cement was developed by this study exclusively from IBA and RCF through clinker raw feed design, clinkering process optimization, and performance validation. The key mineral phase in this innovative eco-cement system, sintered at 1100 °C, is β-C_2S, which exhibits remarkable reactivity when exposed to the greenhouse gas CO2. this eco-cement achieved an impressive CO_2 uptake of 12.5%, resulting in an exceptional compressive strength of 113.7 MPa after just one day of carbonation curing, significantly outperforming the reference Ordinary Portland Cement (OPC) at 48.8 MPa. The carbonization process yielded two principal products, calcium carbonate, and low Ca/Si C-S-H, which played a crucial role in enhancing the microstructure of cement pastes, ultimately leading to high strength. The heavy metals leaching test proves that this eco-cement satisfies the US EPA standard without detrimental environmental impact.

Five keywords: Incineration bottom ash, Recycled concrete fine, Sustainable cement, Carbonation curing, Waste management

Session D4

Life Cycle Assessment and Others

INTEGRATION OF UNCERTAINTY AND VARIABILITY ANALYSIS IN LIFE CYCLE ASSESSMENT OF COAL GANGUE COMPOSITE CEMENT

Lufan LI[1], Xin SHAO[2], and Tung-Chai LING[2]

[1] Department of Civil Engineering, Hangzhou City University, 310015, Hangzhou, China.
[2] College of Civil Engineering, Hunan University, 410082 Changsha, China.
E-mail tcling611@yahoo.com; tcling@hnu.edu.cn

Cement production is accounted for vast majority of CO_2 emissions, and various solid wastes have been recycled as cement replacement to produce composite. Recent Life Cycle Assessment (LCA) studies of composite cement involving solid wastes always claimed to be more environmentally friendly but the environmental burden from upstream material and property degradation are neglected, which may cause significant inequities between LCA models. This paper aims to present a systematic LCA of composite cements, which incorporates coal gangue, limestone, and ground granulated blast furnace slag as cement replacements. The uncertainty caused by the variation of calcination temperature and kaolinite content of coal gangue were assessed by Monte-Carlo analysis. Results show that ternary composite cement is more recommended in comparison to binary composite cement, considering little emissions from limestone production. Calcination temperature of 600°C is the most recommended owing to the wider selection kaolinite content range of coal cangue. The quaternary composite cement was determined to achieve the most satisfying performance from both mechanical and global warming potential perspectives, but taking the allocation method into consideration, additional attention should be paid to the deterioration of other environmental impacts, such as freshwater quality and human carcinogenic toxicity.

Keywords: Investigation, Methodology, Visualization, Formal analysis, Writing

ECO-TOXICITY ASSESSMENT OF SUSTAINABLE MAGNESIUM PHOSPHATE CEMENTS (Sust-MPCs) USING LUMINESCENT BACTERIA AND SEA URCHIN EMBRYOGENESIS BIOASSAYS

V. Muñoz-Ruiz[1], A. Alfocea-Roig[2], J. Santos[1], **E. Cifrian**[1], J. Formosa[2], J.M. Chimenos[2] and A.Andres[1]

[1] GER – Green Engineering and Resources Research Group, Department of Chemistry and Process & Resources Engineering –University of Cantabria, 39005, Santander, Spain.
[2] DIOPMA Design and Optimization of Processes and Materials Research Group, Departmen de Ciència de Materials i Química Física, Universitat de Barcelona, 08028 Barcelona, Spain
andresa@unican.es (corresponding author)

1. INTRODUCTION

Chemically bonded phosphate cements (CBPCs) are a more sustainable alternative to conventional cements due to their lower environmental impact and the promotion of the Circular Economy by incorporating industrial waste. An example of the CBPCs is magnesium phosphate cement (MPC), which is usually produced by an acid-base ($MgO-KH_2PO_4$) reaction at room temperature in water. The use of two secondary materials, Low Grade-MgO by-product (Lg-MgO) collected as a cyclone dust material from the air pollution control system during calcination of natural magnesite and Tundish deskulling waste (TUN) obtained from the steelmaking industry, as a source of MgO in the formulation of new Sustainable MPCs (Sust-MPCs), MPC-Lg-MgO and MPC-TUN was technologically verified. The aim of this work was to determine the environmental impact assessment of the new cements over marine biological life. For this purpose, using the eco-toxicity criteria proposed by the European Construction Products Regulation (Gartiser et al., 2017), the Compliance leaching test UNE-EN 12457-4, as well as two different toxicity bioassays (luminescence reduction of the marine bacteria *Vibrio fischeri* UNE-EN 11348-3 and the success of embryo-larval development of sea urchin *Paracentrotus lividus*) were conducted.

2. MATERIALS AND METHODS

2.1. Materials

The materials evaluated in this work have been, on the one hand, the secondary raw materials Low Grade-MgO by-product (Lg-MgO) and Tundish deskulling waste (TUN) used as a source of MgO, and the new Sustainable MPCs developed from them, MPC-Lg-MgO and MPC-TUN, respectively.

2.2. Leaching test

The compliance leaching test EN 12457-4:2003 was used to determine the release of trace elements from the cement mortars in equilibrium conditions. The test was conducted at a liquid/solid ratio (L/S) of $10 L\cdot kg^{-1}$ of dry matter (< 10 mm) into a rotating equipment (10 rpm) for 24 h at room temperature using as leaching agent, deionized water or seawater, depending on subsequent bioassay. The obtained leachates were filtered (0.45µm) and analysed using Inductive Coupled Plasma Atomic Emission Spectrometry (ICP-AES) (Agilent, 7700) according to ISO quality control standards. The results were obtained in triplicate and the mean values are shown.

2.3. Bioluminescence test

The bioluminescence test has been carried out according to the international standard ISO 11348-3:2007 using MICROTOX LX model bioluminescence toxicity analyser. Nine sample dilutions of each deionized water leachate and a blank were used: 0, 0.32, 0.64, 1.28, 2.56, 5.12, 10.24, 20.48, 40.95, and 81.9%. The pH values were adjusted (6.5–7.5) by adding different aliquots of NaOH or HCl (0.1 N) and the osmotic adjustment (20 g/L of NaCl). The luminescence emitted by the bacteria was measured before and 30 min after the bacteria have been come into contact with the leachate dilutions (in triplicate). The ecotoxicity is measured through the reduction in luminosity between both measurements for each dilution. Modelling these results two parameter were obtained, the EC_{20} value, that corresponds to the concentration of leachate that produced a luminescence inhibition of 20%, and the lowest ineffective dilution factor (LID), that correspond to the dilution factor that produced the EC_{20}.

2.4. Sea Urchin Embryogenesis bioassay

The embryogenesis assay was performed using the procedure described in Fig. 1.

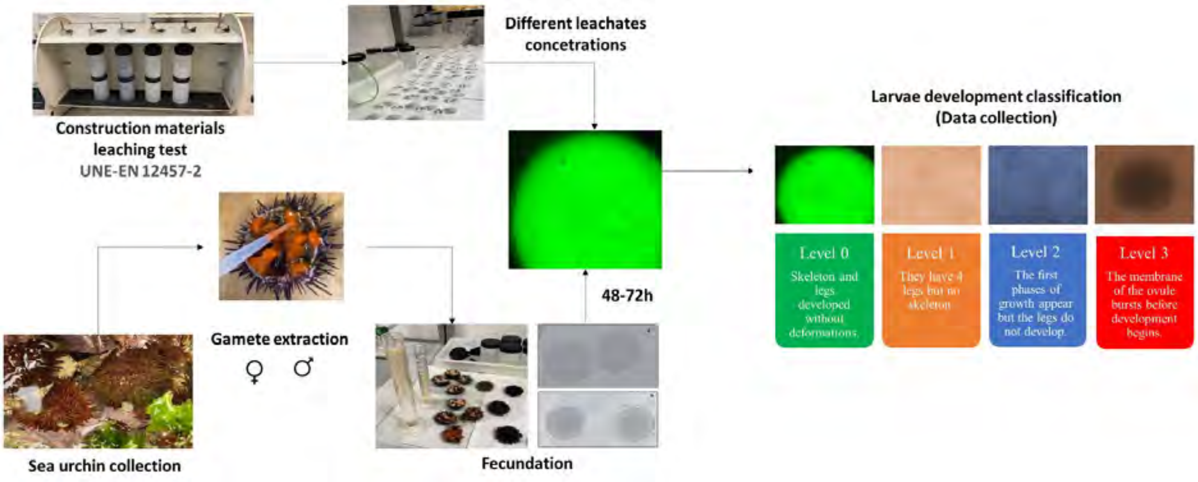

Figure 1. Embryogenesis assay adapting the procedure described by Garmendia et al., (2009)

Briefly, vials (20 mL) were filled with the different selected dilutions (5 replicates per dilution: 10, 25, 50, 75 and 100%) of each leachate and approximately 500 fertilized eggs were placed in each vial. The fertilized eggs were incubated for 48 hours at 20 °C under dark conditions. After the incubation period, the larvae were observed under inverted microscope and the percentage of the larvae developed according to the different levels of development, per 100 organisms were recorded in each replicate (Khosrovyan et al., 2013). The control treatment was used to ensure the acceptability of the tests (> 90% normal larval development).

3. RESULTS AND DISCUSSION

3.1. Leaching Behaviour

The concentration of contaminants in the leachates is shown in Table 1, using as leaching agent deionized water (DW) and seawater (SW). The conductivity and pH values are also displayed. The values obtained for each of the elements in DW are very low, all of them below the values taken as reference for non-hazardous waste. Comparing the raw materials with its corresponding product, it can be seen that some elements become inert in the MPC, such as Ba, Cr, Hg, Pb or Zn, while for other elements the mobilization increases when producing the MPC, such as, As, Mo, Se or V.

Table 1. Leaching concentration values (mg/kg) according to Compliance leaching test EN 12457-2 using as leaching agent, deionized water (DW) and seawater (SW).

Elements (mg/kg)	*DW Lg-MgO*	*DW MPC-Lg-MgO*	*DW TUN*	*DW MPC-TUN*	*NH Limits **	*SW MPC-Lg-MgO*	*SW MPC-TUN*	*SW***
As	0.0004	0.1053	0.001	0.4202	2	0.0627	0.0659	0.0299
Ba	2.375	<0.001	2.608	<0.001	100	0.0074	0.0077	0.0354
Cd	<0.0001	<0.0001	<0.0001	0.0002	1	0.0001	0.0002	0.0005
Cr	0.0611	0.0128	0.0571	0.0269	10	0.023	0.0165	0.0130
Cu	<0.0003	<0.0003	0.0009	0.0085	50	0.0145	0.0120	0.0089
Hg	0.00015	<0.00004	0.0006	0.00070	0.2	<0.00004	0.00056	<0.00004
Mo	0.0168	0.1791	0.2194	1.0836	10	0.4357	1.1154	0.1047
Ni	0.0008	0.0020	0.0093	0.0086	10	0.0166	0.0625	0.0037
Pb	0.00035	<0.00003	0.3055	0.00095	10	0.00025	0.00051	0.00056
Sb	0.0204	0.0337	0.0048	0.0396	0.7	0.0444	0.0098	0.0023
Se	0.0274	0.1434	0.4217	0.5838	0.5	0.4106	0.5885	0.0756
V	0.1414	7.1835	0.0240	4.2928	-	11.3198	1.2016	0.0350
Zn	0.0079	<0.0004	0.0858	0.04244	50	0.0252	0.0028	0.0272
pH	10.72	11.31	12.52	11.03				
Cond. (mS/cm)	5.63	5.93	2.31	2.72				

* Limit values for Non Hazardous waste according to EU Landfill Waste Acceptance Criteria 2003/33/EC; ** SW: Control; clean seawater used as reference leachate.

3.2 Bioluminescence test

The bioluminescence reduction test has been applied to two replicates of the leachates of the two secondary raw materials and MPCs (Figure 2).

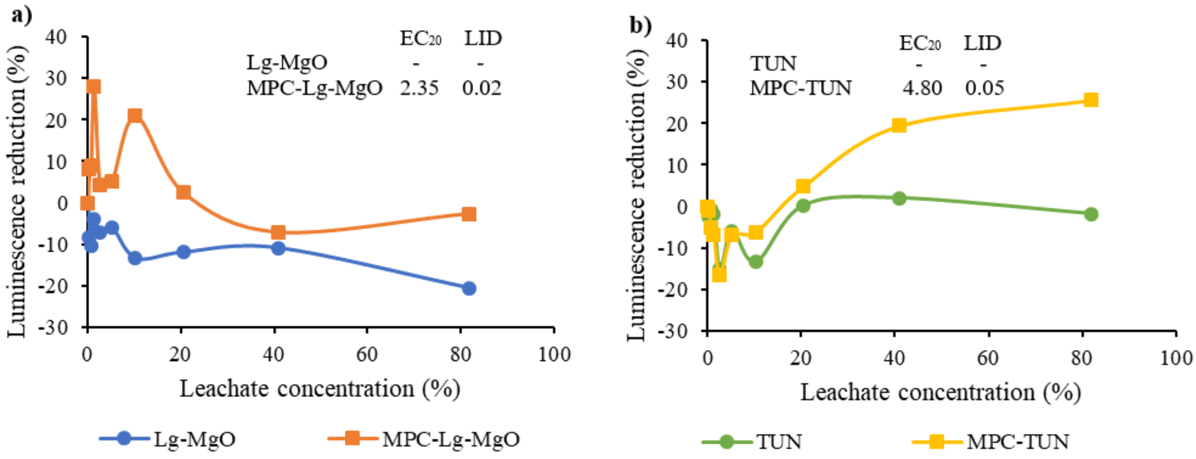

Figure 2. Bioluminescence test results expressed as percentage of light emission reduction of Vibrio fischeri after 30 min exposure as a function of leachate concentration from: a) Lg-MgO and MPC-Lg-MgO and b) TUN and MPC-TUN.

The samples do not present toxicity, obtaining results of LID much lower than 8, threshold dilution value proposed in the framework of construction products as toxicity pass criteria (CEN/TR 17105:2017). The bioassay at higher leachate concentrations performed, never exceeding a 30% reduction in luminescence.

3.3 Sea Urchin embryogenesis bioassay

Due to the fact that the raw materials did not show toxicity in the bioluminescence test, the sea urchin embryogenesis bioassay has been applied only to the MPCs (Figure 3). The results show that the four legs larvae development (level 0 and level 1) is presented until a 25% of leachates concentration in contact with the embryos, being MPC-TUN the one with the highest percentage of these embryos developed. Respect to the level 3, the results show significant effects from 50% and 75% of concentration of MPC-Lg-MgO and MPC-TUN leachates, respectively. This worse behaviour of MPC-Lg-MgO may be associated with higher level of vanadium (Santos et al., 2023).

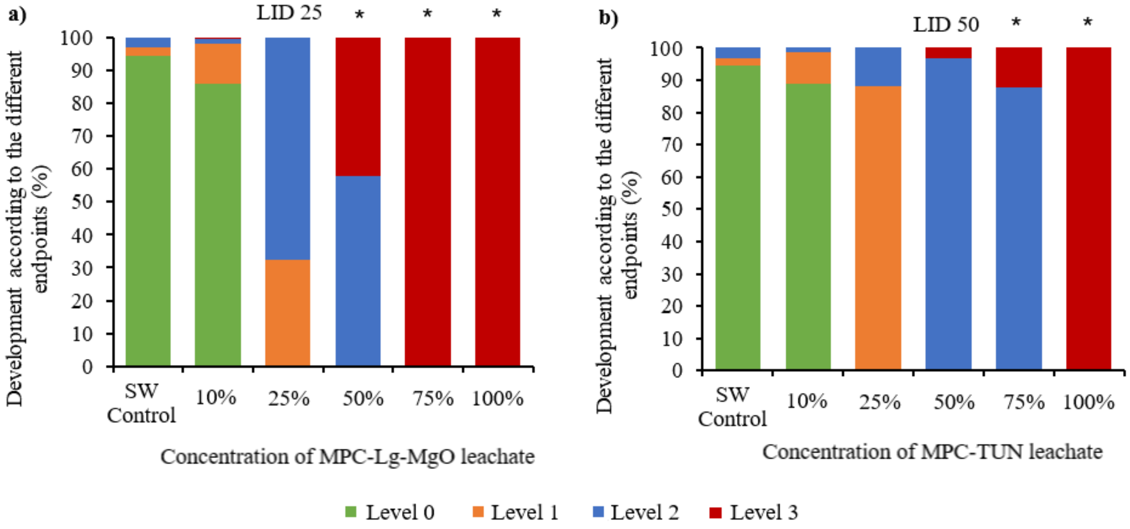

Figure 3. Sea urchin embryogenesis test results: Percentages of Paracentrotus lividus embryos incubated according to the endpoints classification for the different leachate concentrations: (a) MPC-Lg-MgO and (b) MPC-TUN. Asterisks refer to significant differences in toxicity level 3 to the control ($p<0.05$*). LID values expressed as the highest leachate concentration that no produces significant difference with the control.

4. CONCLUSION

From the leaching perspective, it should be noted that the mobility of all trace elements was considered to meet the non-hazardous landfill limits, with exception of Se mobility, in the MPC-TUN sample. No significant effects were observed on the bioluminescent bacteria within the leachate concentration range (until 80%). In the sea urchin embryogenesis bioassay it was observed that the MPC-TUN sample showed lower toxicity than the MPC-Lg-MgO sample, for toxicity level 3. The development of sea urchin embryogenesis with respect to bacteria bioassay has allowed the eco-toxicity assessment of Sust-MPCs in marine ecosystem by incorporating a bigger number of toxicity levels. In summary, the results obtained from both bioassays show consistency with the leaching behaviour of Sust-MPCs.

5. REFERENCES

Garmendia, J.M. Menchaca, I. Belzunce, M.J. Revilla, M. (2009) "Induction to Maturation of the Sea Urchin Paracentrotus lividus (Lamarck, 1816) under Laboratory Conditions" *Environ Technol*, 30(13):1441-6

Gartiser, S. Heisterkamp, I. Schoknecht, U. Bandow, N. Burkhardt, N.M. Ratte, M. Ilvonen, O. (2017). "Recommendation for a test battery for the ecotoxicological evaluation of the environmental safety of construction products". *Chemosphere* 171: 580–587.

Khosrovyan, A. Rodríguez-romero, A. Salamanca, M.J. Valls, T.A. Riba, I. Serrano, F. (2013). "Comparative performances of eggs and embryos of sea urchin (Paracentrotus lividus) in toxicity bioassays used for assessment of marine sediment quality". *Mar. Pollut. Bull.* 70: 204–209.

Santos, J., Rodriguez-Romero, A., Cifrian, E., Maldonado-Alamenda, A., Chimenos, J.M., Andres, A. (2023) "Eco-toxicity assessment of industrial by-product-based alkali-activated binders using the sea urchin embryogenesis bioassay". *J Env. Manag.* 341, 118100.

TECHNICAL FEASIBILITY AND LIFE CYCLE ASSESSMENT FOR TURNING CORN STRAW WASTES INTO SUPPLEMENTARY CEMENTING MATERIALS OF CEMENT MORTARS

Xiaoyu Shang[1*], Bin Gong[1], Jianin Chang[1], Yuqi Chen[1], Jingwei Yang[2], Guangfeng Ou[3]

[1]School of Civil Engineering and Architecture, Northeast Electric Power University, Jilin 132012, PR China
[2]Department of Civil and Environmental Engineering, Seoul National University, Seoul 08826, Korea
[3]Department of Civil Engineering, University of Tokyo, Tokyo 113-8654, Japan
E-mail shangxiaoyu@neepu.edu.cn

1. INTRODUCTION

As a kind of bulk agricultural waste, corn stalk has always been a disturbing issue in developing countries, and its unreasonable disposal brought a serious burden to the environment (Memon & Khan, 2018). The purpose of this study was to investigate the feasibility of turning corn straw waste (CSW) into supplementary cementing material (SCM) for cement mortars. Therefore, a three-step process was proposed to treat CSW into corn straw ash (CSA), including washing pretreatment, pyrolysis, and milling. The study focused on the effects of washing pretreatment (unwashed, distilled water washing, hydrochloric acid washing), pyrolysis temperatures (500 °C, 600 °C, 700 °C), and pyrolysis durations (1 h, 2 h, 3 h) on CSA activity. Also, the performance of prepared CSA-containing mortar was investigated by introducing the different types of CSA and blending amounts of CSA (3 wt.%, 5 wt.%, and 10 wt.%). Finally, LCA methods are used to assess the environmental impact of CSA-containing mortars.

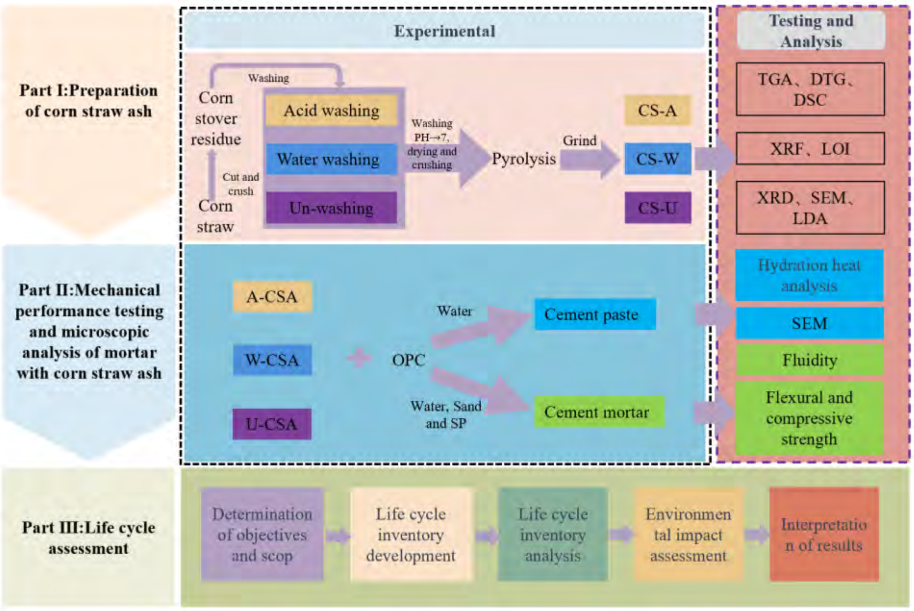

Fig. 1. Technical framework for the review.

2. MATERIALS AND METHODS

2.1 Corn straw ash

Corn straw was initially cut into small pieces (1-2mm) and then further crushed into fine particles (100-150μm) using a grinder. The crushed straw was immersed in a solution (70°C distilled water and 0.5 mol/L hydrochloric acid) and stirred for 4 hours before filtering. After washing, the straw residue was washed with distilled water, dried, and labelled as unwashed (-U), water-washed (-W), and acid-washed (-A) straw, respectively. The straw ash was then refined at different maximum pyrolysis temperatures and durations, as detailed in Table 1 (Rithuparna et al., 2021). Finally, the obtained ash was ground for 30 minutes using a ball mill (100 r/min, ball ratio of 21). Thermogravimetric analysis (TGA, DTG, DSC), chemical composition analysis (XRF), phase composition analysis (XRD) and particle size distribution analysis (LDA) of CSA with different treatment processes were carried out.

Table 1 The preparation conditions of CSA samples.

Sample code	Washing method	Pyrolysis temperature	Heating rate	Pyrolysis duration	Grinding time
A52	-U, -W, -A	500℃	10℃/min	2 h	30 min
A53		500℃		3 h	
A61		600℃		1 h	
A62		600℃		2 h	
A63		600℃		3 h	
A71		700℃		1 h	
A72		700℃		2 h	

*Washing methods: -U means unwashed. -W means pure water washed. -A means acid-washed

2.2 Mortar Mix Design

The mixture proportion of the prepared mortar samples is shown in Table 2. The mortars with a water/binder ratio of 0.5 and sand/binder ratio of 3:1 were mixed by a mortar blender for 3 mins, cast into 40 mm x 40 mm x 160 mm molds, vibrated for 2 mins, and then cured in humid air at 20°C±2 °C for 1 day. After demolding, the mortars were cured in water at 20 °C±2 °C until the scheduled age. The fluidity of mortar was tested according to GB 2419-2005. Prepared 7-day with a water-to-binder ratio (w/b) of 0.5, soaked them in anhydrous ethanol, and then vacuum dried and ground for SEM testing. Hydration heat was measured using CALMETRIX I-CAL 8000 HPC at 25°C.

Table 2 Mix-proportion details of mortar sample.

Series	Cementitious materials (wt. %)		water/binder ratio	SP(wt. %)	sand/binder ratio
	cement	CSA			
OPM	100	-	-	-	3
A-CSA3	97	3	0.5	0.15	3
A-CSA5	95	5	0.5	0.15	3
A-CSA10	90	10	0.5	0.15	3
U-CSA5	95	5	0.5	0.15	3
W-CSA5	95	5	0.5	0.15	3

2.3 LCA method

The LCA method was used to assess the environmental impact of using CSA in terms of carbon dioxide emissions and energy consumption. The functional unit selected for calculations and comparability of results is 1 m^3 of mortar (Schaubroeck, 2022). The evaluation considers the system boundary 'from cradle to gate'. Most of the inventory data is sourced from the database, with some supplemented from existing research and actual conditions.

3. RESULTS AND DISCUSSION

3.1 Characteristics of CSA

The test results showed that the amorphous silica content of CSA treated with water and acid was higher than that of untreated corn straw, which was close to 80 %. The removal rate of alkali metals and chloride ions can reach 95 %. After water and acid treatment, the average particle size decreased from 23.762 μm to 14.711 μm and 11.829 μm, respectively. With the increase of pyrolysis temperature and time, the silica content of CSA increases gradually.

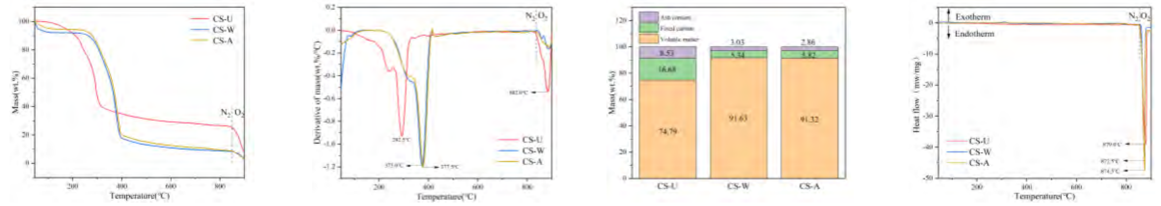

(1) TGA **(2) DTG** **(3) Composition ratio** **(4) DSC**

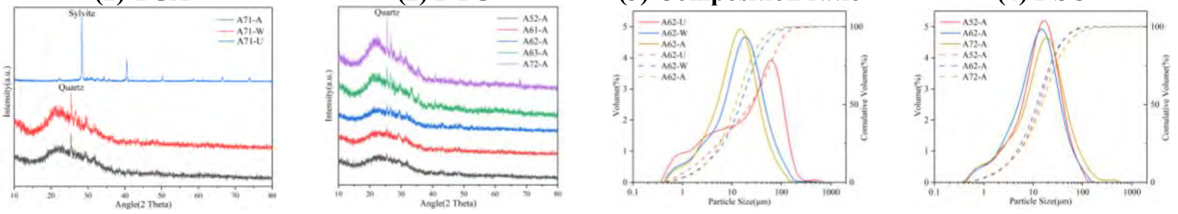

(5) XRD-1 **(6) XRD-2** **(7) PSD-1** **(8) PSD-2**

Fig.2. Test results of corn straw ash.

3.2 Properties of CSA-containing mortar

The hydration heat experiment showed all CSA after treatment possess higher activity than the control group. The more the content of CSA was introduced, the earlier the peak of hydration heat appears. The effect of water and acid washing treatment on accelerating the heat flow peak is higher than that of untreated CSA (Shakouri et al., 2020). The fluidity experiment showed that the pretreatment methods would lead to an increase in water absorption of CSA with the fluidity U-CSA5 > W-CSA5 > A-CSA5. The compressive and flexural strength experiments show that water and acid washing treatment have a significant improvement on the strength of mortars. The compressive strength of pickling and washing at 5 % dosage is 13.6 % and 4.9 % higher than that of the control group mortar, respectively. SEM images show that many C-S-H hydration products are generated in the mortars mixed with CSA. C-S-H gel hydration products grow increase with CSA contents increasing. C-S-H morphology in the sample by acid washing treatment is obviously better than that of water washing and untreated.

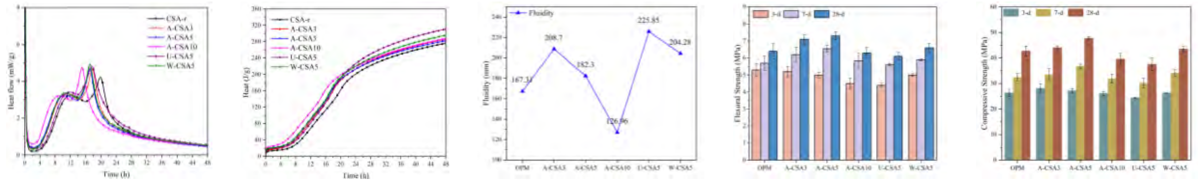

(1) Heat flow **(2) Heat** **(3) Fluidity** **(4) Flexural strength** **(5) Compressive strength**

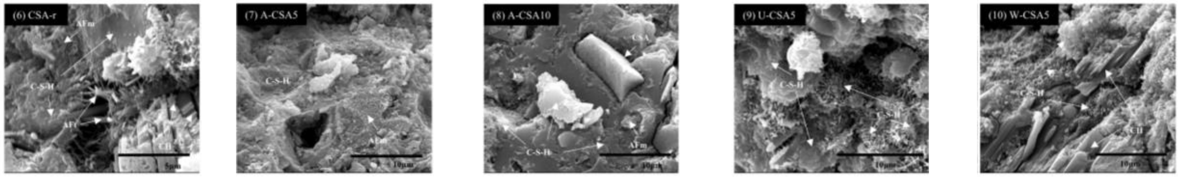

(6) CSA-r **(7) A-CSA5** **(8) A-CSA10** **(9) U-CSA5** **(10) W-CSA5**

Fig.3. Test results of mortar.

3.3 LCA

LCA shows that different CSA contents and washing treatment methods have an impact on the energy consumption and carbon emissions of mortar. The results show that with the increase of CSA contents, energy consumption increases and carbon emissions decrease. In the CSA-containing mortar produced by different washing methods, the energy consumption of unwashed is the lowest, followed by water washing, and the energy consumption of pickling is the highest. However, the washing method has little effect on CO_2 emissions. The contribution of each material and stage to energy consumption and carbon emissions shows that cement contributes the most, followed by CSA, and other materials contribute less.

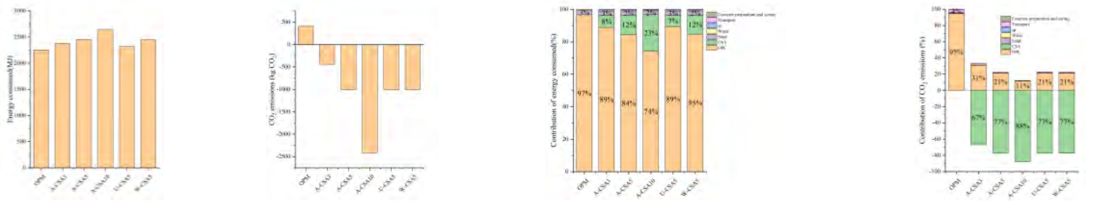

(1) Energy consumption results (2) Carbon emissions results (3) Contribution of energy consumption (4) Contribution of carbon emissions.

Fig.4. Results of LCA

Table 3 The ratio of energy consumption and carbon emissions to strength of concrete.

Number	Strength(MPa)	Energy consumed/Strength	CO_2 emissions/Strength
OPM	42.7	52.74	9.47
A-CSA3	44	54.02	-10.05
A-CSA5	47.7	51.43	-21.11
A-CSA10	28.6	66.75	-61.09
U-CSA5	37.5	61.79	-26.96
W-CSA5	43.5	56.22	-23.16

4. CONCLUSION

(1) The water and acid washing treatment can reduce the content of Cl and K_2O, LOI, and median particle size and increase the content of active SiO_2 in CSA. The effect of pyrolysis temperature on the crystallization of SiO_2 is much greater than that of pyrolysis duration. CSA showed good pozzolanic activity at 600 °C for 2h.

(2) CSA with high activity after water and acid washing can accelerate the hydration of C_3S, promote the formation of hydration products and improve the early strength of prepared mortars. However, the pretreated CSA will lead to a decrease in the fluidity of the mortars due to the high water absorption.

(3) The addition of CSA can improve the microstructure of C-S-H of the cement matrix. SEM results of CSA with untreated, water and acid washing methods show that the morphology of C-S-H changes from the honeycomb, fibrous to dense gel. The high the CSA straw ash generates the clear the dense gel-like C-S-H product.

(4) The results of LCA show that introducing CSA to cement mortar can greatly reduce carbon emissions. The compressive strength of prepared mortars can reach 40 MPa, and A-CSA5 has the lowest energy consumption and carbon emission ratio simultaneously.

5. ACKNOWLEDGMENT

We would like to acknowledge the financial support from the Natural Science Foundation of Jilin province, China (20210402076 GH).

6. REFERENCES

Memon, S. A., & Khan, M. K. (2018). Ash blended cement composites: Eco-friendly and sustainable option for utilization of corncob ash. J. Clean. Prod. 175, 442–455.

Rithuparna, R., Jittin, V., & Bahurudeen, A. (2021). Influence of different processing methods on the recycling potential of agro-waste ashes for sustainable cement production: A review. J. Clean. Prod. 316, 128242.

Schaubroeck, T. (2022). Sustainability assessment of product systems in dire straits due to ISO 14040–14044 standards: Five key issues and solutions. J. Ind. Ecol. 26, 1600–1604.

Shakouri, M., Exstrom, C. L., Ramanathan, S., Suraneni, P., & Vaux, J. S. (2020). Pretreatment of corn stover ash to improve its effectiveness as a supplementary cementitious material in concrete. Cem. Concr. Compos.112, 103658.

MODIFICATION OF RECYCLED AGGREGATES BY BIO-DEPOSITION TREATMENT FROM THE INTERIOR TO THE SURFACE

Rui Zhang, Dezhi Xie, and Jianyun Wang*

Department of Civil Engineering, Xi'an Jiaotong University, Xi'an, 710049, China
E-mail: jianyun.wang@xjtu.edu.cn

Abstract: The recycled aggregates with many interior and surface defects (pores and micro-cracks) is critically limited their application in recycled concrete. In order to improve the utilization efficiency of recycled aggregates in concrete, it is important to repair the pores and micro-cracks of the recycled aggregates. Biogenic $CaCO_3$ from microbially and enzyme-induced carbonate precipitation (MICP and EICP) has been proved to be a promising strengthening material due to its environmental friendliness and super compatibility with cementitious matrix. In this study, EICP treatment and sodium alginate (SA) aided MICP treatment were applied to modify the aggregates. The influence of single treatment and combined treatment on the modification efficiency of aggregates were investigated. Results shown that due to the small size of the urease molecule, single EICP treatment mainly repaired the internal defects of the aggregate and less surface repair, and the final water absorption was decreased by 20.97%. The surface defects on the aggregates were repaired by single SA-aided MICP treatment because of the effect of Ca-algiante fixing bacteria, and the water absorption was decreased by 35.75%. Interestingly, the combined treatment can accumulate the effect of both, so that the decrease rate of water absorption reached the highest 39.79%. It can be concluded that the interior and surface defects of recycled aggregates can be comprehensively modified by the combined EICP and SA-aided MICP treatment.

Keywords: Recycled aggregates, MICP, EICP, Sodium alginate, Water absorption.

1. INTRODUCTION

The utilization of recycled aggregates in concrete production is a popular approach on the recycling of construction waste. However, the old mortar on the aggregates surface contains of many defects, such as harmful pores and micro-cracks, leading to the highwater absorption and crushing value, which significantly decreases the mechanical property and durability of recycled aggregate concrete (Katz, 2003). Therefore, it is important to improve the properties of the recycled aggregates. Currently, the modification methods include mechanical grinding, microwave heating, thermal grinding, acid leaching (Zhang, Xie, Wu, & Wang, 2023). However, these methods have limitations, such as secondary damage to aggregates, high consumption of energy, and introduction of corrosive ions. And hence, the environmentally friendly and efficient methods, the MICP and EICP technologies were widely applied in the current research.

The modified principle of recycled aggregates based on MICP and EICP is that the generated biogenic precipitates repair the pores and micro-cracks. The difference between them is that EICP directly uses urease for the deposition reaction, while MICP uses bacteria, where the bacterial urease performs the deposition reaction by inducing urea decomposition (Xie, Zhang, & Wang, 2023). Single EICP or MICP treatment was applied for the modification of aggregates in many published researches, and also resulting in some improvement of the performance of aggregates (Wang et al., 2017). The SA-aided MICP treatment was considered as the optimal method for improving the distribution uniformity of biogenic calcium carbonate. Yet, the single treatment still have many limitations, such as the uneven distribution of precipitates of single EICP treatment, and the less repair of inner pores of aggregates as for the single SA-aided MICP treatment.

Therefore, in this study, EICP treatment and SA-aided MICP treatment were applied to modify the aggregates. The influence of single treatment and combined treatment on the modification efficiency of aggregates were investigated and evaluated by the appearance of treated aggregates, decrease rate of water absorption, and porosity of aggregates. The purpose is to achieve the comprehensive modification of recycled aggregate from the interior to the surface.

2. MATERIALS AND METHODS

2.1. Bacterial cultivation

Bacillus sphaericus LMG 22257 (Belgian Coordinated Collection of Microorganisms, Ghent) was used in this study. It is a urease producing strain, which catalyses urea decomposition about 10^{14} times faster than that of the un-catalyzed reaction. The growth medium was composed of 20 g/L yeast extract and 20 g/L urea. The bacteria were grown aseptically under batch cultivation conditions. Cultures were obtained after subsequent culturing (two times and 2% inoculum) from a -80 °C stock culture. The cultivation was in a shaker (28 °C, 150 rpm) for 24 h. Then the bacterial pellets were obtained by centrifuging at 7000 rpm for 10 min (Eppendorf 5430) and the harvested bactria were resuspended in 8.5 g/L saline solution. The obtained bacterial pellets solution (approximately 10^7 cells/mL) were fresh made and stored in 4 °C fridge for the following use.

2.2. Urease extraction

Bacterial urease was extracted through a series of ultrasonic cell disruption steps. Before the ultrasonic disruption, the above bacterial pellets were resuspended in deionized water to avoid introducing Cl^- to the system. The obtained bacterial suspension (200 mL) was placed in ice water and it was lysed at 90% of the maximum power of the ultrasonic homogenizer (SCIENTZ, JY92-Ⅱ N). The frequency was kept at 25 kHz. The ultrasonic process lasted for 30 min and was carried out by 5 s outburst and 5 s pause to allow the bacterial suspension to cool down. After ultrasonic disruption, the lysed bacterial suspension was subjected to centrifugation at 7000 rpm and 4 °C for 10 min, and the supernatant was the fresh urease solution. The obtained urease solution (around 9.86 U/mL) were stored in 4 °C fridge for the following use.

2.3. Bio-deposition treaments

The recycled aggregates were came from a local factory in Xi'an, Shaanxi Province. The particle size (10-20 mm) of aggregates were sieved and used in this research. Four treatments were designed in this study. Treatment 1, the control group, the dried recycled aggregates (100±1 g) were immersed in deionized water (100 mL) for 3 days. Treatment 2, the single EICP group, the dried recycled aggregates (100±1 g) were firstly immersed in urease solution for 12 hours, and then transferred into deposition solution consisting of equimolar $CO(NH_2)_2$–$Ca(NO_3)_2$ (0.5 M, 100mL) for 3 days. Treatment 3, the single SA-aided MICP group, the dried recycled aggregates (100±1 g) were firstly immersed in the mixture solution, consisting of bacterial pellets (10^7 cells/mL) and sodium alginate (SA, 0.5 wt%), for 12 hours, and then transferred into deposition solution (0.5 M, 100 mL) for 3 days. Treatment 4, the combined EICP and SA-aided MICP group, the dried recycled aggregates (100±1 g) were bio-treated by successively Treatment 2 and Treatment 3. Three replicates were conducted for each group.

3. RESULTS AND DISCUSSION

3.1. Visualization of treated aggregates

The appearance of treated aggregates was photographed by a stereo microscope (Leica LED3000RL) at 100x magnification, as shown in Figure 1. It was found in Figure 1(a) and (b) that the distribution of precipitates formed by single EICP treatment was extremely uneven, with only on the top surface, merely not on the bottom surface. While in Figure 1(c) and (d), it can be observed that the uniformity distribution of precipitates generated by single SA-aided MICP treatment on the top and bottom surface of aggregates, which was consistent with previous research (Zhang et al., 2023). And also, uniformly distribution of precipitates produced by combined EICP and SA-aided MICP treatment was found in Figure 1(e) and (f), which indicated that the structure of Ca-alginate could "fix" bacteria on the aggregates, leading to the in situ precipitation on the aggregates and improving the uniformly distribution of precipitates (Zhang et al., 2023). Additionally, the precipitates of Figure 1(a) were looser than those in Figure 1 (c) and (e), which is caused by the rapid precipitation rate, indicating that urease molecules without the protection of cell wall decompose urea at a faster rate than bacteria. This proves that SA-aided MICP is an essential treatment for modified aggregate surface.

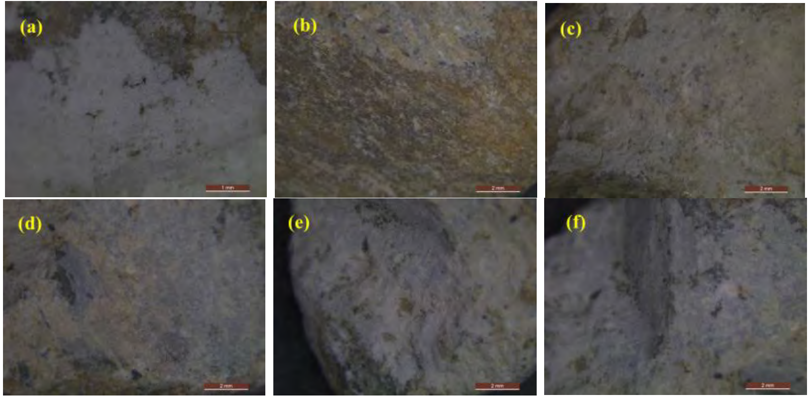

Figure 1. The appearance of (a) top and (b) bottom surface of single EICP group, (c) top and (d) bottom surface of single MICP group, and (e) top and (f) bottom surface of combined EICP and MICP group

3.2. Decrease rate of water absorption

The decrease rate of water absorption (w%) of aggregates could evaluate the efficiency of bio-deposition treatment, which was measured according to BS EN 2002 (Standard, 2002). As shown in Figure 2, though the precipitates on the aggregates surface were relatively less, the decrease rate of w% of aggregates treated by a single EICP was considerable, 20.97% on average. This indicates the interior pores of aggregates might be plugged. Due to the larger pores and micro-cracks on the aggregates surface, the surface repair under SA-aided MICP treatment resulted in a 35.75% decrease in water absorption. The decrease rate of w% under this combined treatment reached the highest average of 39.79%. Therefore, the combined EICP and SA-aided MICP treatment can repair both the internal pores and the surface pores and micro-cracks, realizing the comprehensive repair of aggregates from the interior to the surface.

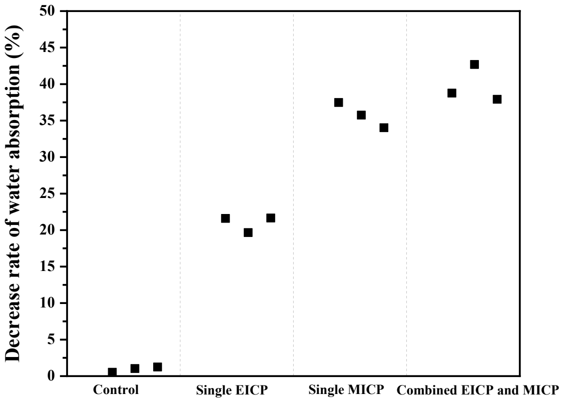

Figure 2. The decrease rate of water absorption of aggregates after various treatments

3.3. Porosity of recycled aggregates

The porosity of aggregates was measured by mercury intrusion porosimetry (MIP, Autopore IV 9500). In Figure 3, the porosities of untreated aggregates, treated by single EICP, single SA-aided MICP, and combined EICP and SA-aided MICP were 27.9%, 23.08%, 18.55%, and 14.56%, respectively. The difference between untreated group and single EICP group was approximately 4 precents, and interestingly, the difference between single MICP group and combined EICP and MICP group was also around 4 percents. This indicates that EICP can repair the internal pores and MICP can repair the surface pores and micro-cracks, and the combined treatment can superimpose the effect of both, thus the aggregates can be entirely modified from the interior to the surface.

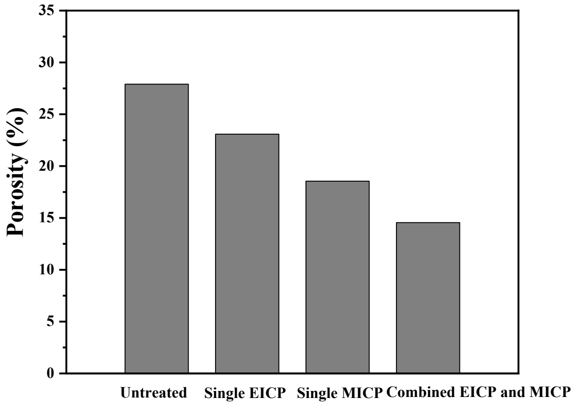

Figure 3. The porosity of recycled aggregates after various treatments

4. CONCLUSION

In this study, it was found that a single EICP treatment is hardly effective in repairing surface defects due to uneven distribution of precipitates and rapid enzymatic reactions (without the protection of cell wall) resulting in loose precipitate particles. A single SA-aided MICP treatment mainly repairs the surface defects of the aggregate, while it is difficult for bacteria to enter the internal pores, resulting in many internal pores of the aggregates still unable to be repaired. While, due to the small size of the urease molecules, it is easy to enter the internal pores, and the network structure of Ca-alginate can effectively fix bacteria on the surface of the aggregates, resulting in the in-situ precipitation, which demonstrated that EICP and SA-aided MICP treatment are focus on the repair of the internal defects and surface defects, respectively. And thus, the combined EICP and SA-aided MICP treatment could efficiently modify the aggregates from the interior to the surface. The future development needs to optimize the technological process and concentration of this combined treatment to make it suitable for large-scale application.

5. ACKNOWLEDGMENT

The authors would like to express appreciation for the support of the National Natural Science Foundation of China (No.51908459), Natural Science Foundation of Shaanxi Province (No.2020JM-040), and ‘Young Talent Support Plan’ of Xi’an Jiaotong University.

6. REFERENCES

Katz, A. (2003). Properties of concrete made with recycled aggregate from partially hydrated old concrete. *Cement and Concrete Research, 33*(5), 703-711. doi:10.1016/S0008-8846(02)01033-5.

Standard, B. (2002). Aggregates for concrete. *BS EN, 12620*.

Wang, J., Vandevyvere, B., Vanhessche, S., Schoon, J., Boon, N., & De Belie, N. (2017). Microbial carbonate precipitation for the improvement of quality of recycled aggregates. *Journal of Cleaner Production, 156*, 355-366. doi:10.1016/j.jclepro.2017.04.051

Xie, D. Z., Zhang, R., & Wang, J. Y. (2023). The influence of environmental factors and precipitation precursors on enzyme-induced carbonate precipitation (EICP) process and its application on modification of recycled concrete aggregates. *Journal of Cleaner Production, 395*. doi:ARTN 13644410.1016/j.jclepro.2023.136444

Zhang, R., Xie, D., Wu, K., & Wang, J. (2023). Optimization of sodium alginate aided bio-deposition treatment of recycled aggregates and its application in concrete. *Cement and Concrete Composites, 139*, 105031. doi:10.1016/j.cemconcomp.2023.105031

INTEGRATED DEEP LEARNING AND LIFE-CYCLE COST ANALYSIS MODEL TO ESTIMATE THE SUSTAINABILITY OF TALL BUILDINGS IN HONG KONG WITH THE CLIMATE CHANGE IMPACTS

Siqi Cao[1], Jiayao Wang[1]*, K.T. Tse[1], and Sunwei Li[2]

[1] Department of Civil and Environmental Engineering, The Hong Kong University of Science and Technology, Clear Water Bay, Kowloon, Hong Kong
[2]Shenzhen International Graduate School, Tsinghua University, Shenzhen, China
E-mail: jiayao.wang@connect.ust.hk

1. INTRODUCTION

Threats from typhoons have caused considerable damage to tall buildings in Hong Kong throughout their lifetimes. Meanwhile, typhoons simulated by physical models indicate that their phenomenon may be severely affected by climate change. The traditional typhoon intensity prediction can be roughly divided into three categories: numerical models based on partial differential equations of meteorological motion; predictions established by satellite images; and statistical regression models (Xu et al., 2022). The first two methods are relatively time-consuming and high computation power. With the development of deep learning algorithms, we can easily use deep neural networks to quickly evaluate the impact of climate change on typhoon intensity and accurately predict future wind speeds.

Moreover, as a result of climate change, typhoon intensity and frequency may fluctuate, which may also have an effect on wind-induced damage and, consequently, life-cycle costs. Therefore, an integrated deep learning and life-cycle cost analysis model to evaluate and quantify the financial losses caused by wind hazards on tall buildings is essential for designers to conduct performance-based design. In this study, the integrated life-cycle cost contains the economic cost, the social cost and the environmental cost. The economic cost can be calculated using the uncertainty of structural damping and the fragility of the building; the social cost is examined from the downtime loss caused by the acceleration that exceeds the root-mean-square acceleration threshold at the top floor; and the environmental cost can be obtained by quantifying the carbon emissions of the structure.

2. MATERIALS AND METHODS

A deep neural network is applied to predict typhoon wind speeds based on historical data as shown in Figure 1. This neural network includes seven input parameters: translation speed, central pressure deficit, approaching angle, distance of approach, radius of maximum wind (RMW), occurrence rate, and sea surface temperature. Here, the occurrence rate within 30 years is assumed to be constant. Therefore, six parameters are used to train this deep neural network model. The choice of six parameters is based on the numerical model proposed by (Huang & Xu, 2012). Additionally, two hidden layers are built and each of them contains ten nodes. The final output layer contains one parameter, which is typhoon wind speed at 90 meters height.

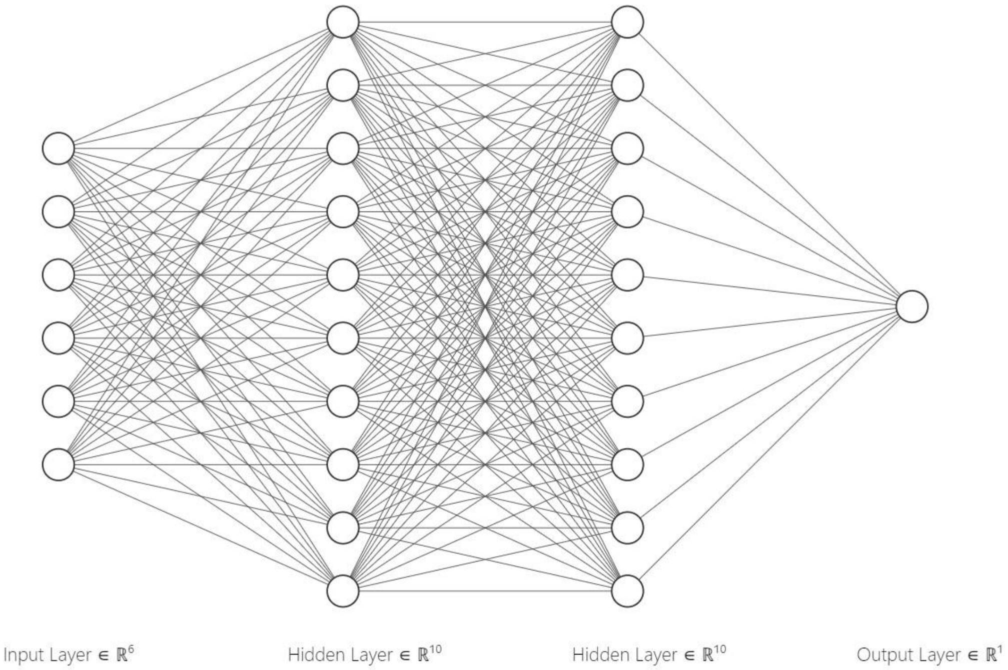

Figure 1. Deep neural network utilized to predict typhoon wind speeds in Hong Kong.

The fragility curve is used to evaluate wind-induced damage losses over the life cycle of buildings. In the life-cycle analysis (LCA) framework, the total cost is obtained by using Eq. (1), where $E[\cdot]$ is the expected total cost at the time t; C_0 is the initial cost of the building under investigation calculated by Eq. (2); C_f is the serviceability failure cost, which includes the damage cost and the out-of-service cost (in Eq. (3)); C_m is the maintenance cost covering the expanses of the maintenance activities and the financial evaluation of the environmental impacts (in Eq. (5)). The initial construction cost consists of the building material, the transportation fee, the labor cost, the equipment cost, and other on-site expenses. i is the specific type of concrete; j is a specific type of rebar or steel; α_i and α_j are the waste ratios during construction processes for concrete i and rebar/steel j, respectively; V_i and V_j are quantity of concrete i, and of rebar/steel j in m^3, respectively; CC_i and CC_j are the construction cost of concrete and rebar/steel per unit volume; ρ_j is the density of rebar/steel in the unit of kg/m^3; $e^{-\lambda t}$ is the discount factor at the time t; and λ is the constant discount rate.

$$\boldsymbol{E[C(t)] = C_0 + C_f + C_m} \tag{1}$$

$$\boldsymbol{C_0 = \left[\sum_{i=1}^{I}(1+\alpha_i)V_i CC_i + \sum_{j=1}^{J}(1+\alpha_j)\,\rho_j V_j CC_j\right]\cdot e^{-\lambda t}} \tag{2}$$

$$\boldsymbol{C_f = E\left[\sum_{l=1}^{L}\sum_{k=1}^{K} C_k P_k e^{-\lambda t_l}\right]} \tag{3}$$

$$\boldsymbol{P_k = \int\int F_k(V) f(V,t)\,dV dt} \tag{4}$$

$$\boldsymbol{C_m = \int_0^t c_m e^{-\lambda t}} \tag{5}$$

3. RESULTS AND DISCUSSION

The 5000 sets of historical data of six parameters were divided into a training set and a test set that includes 25 percent of total data. Figure 2 shows the loss function with respect to the training times, which indicates the accuracy of our deep neural network model. The total process ran around 116 seconds, which is much faster than the physical models using Monte Carlo simulation.

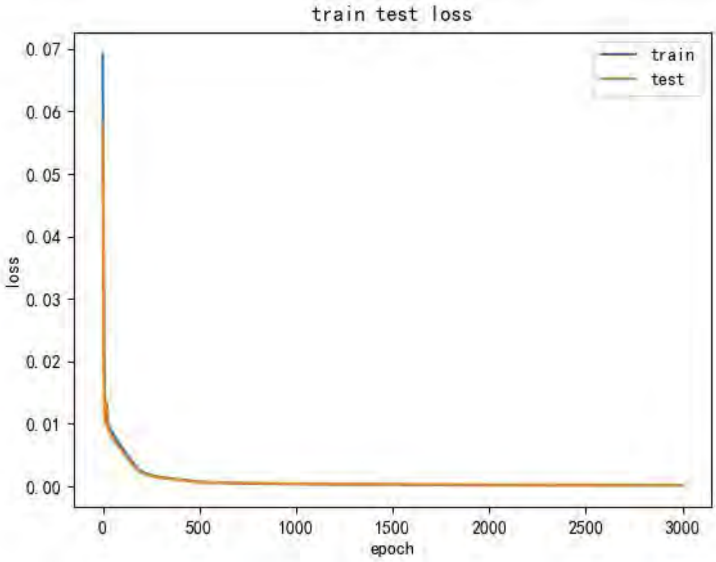

Figure 2. Loss function.

The state-of-art climate change scenario, i.e., the Shared Socioeconomic Pathways (SSPs) is considered in this paper. SSP climate change scenarios will change the distribution of the first five input parameters in the deep neural network, while will definitely increase future sea surface temperature. After simulating the climate change effects on these six parameters, future typhoon wind speeds may be predicted by using the built deep neural network. Figure 3 shows the comparison between typhoon wind speeds subject to normal climate and SSP5-85 conditions, which indicates that climate change effects will make typhoon wind speeds more intense. Eventually, the values of parameters in the LCA framework are adopted from (Cao et al., 2023). Monte Carlo simulations were conducted to derive the estimated life-cycle cost subject to typhoon wind speeds considering three different climate change scenarios. Figure 4 demonstrates that with the intensification of climate change, the difference in life-cycle wind-induced costs within 60 years can be as high as 10%.

4. CONCLUSION

To examine the life-cycle cost caused by typhoon hazards, a deep neural network is employed to predict future typhoon wind speeds fast and accurately. A 240 m height second-generation benchmark building is adopted to estimate the integrated life-cycle cost as the case study, proving that the climate change may eventually affect the life-cycle wind-induced damage of buildings. It should be claimed that the integrated analysis process is only applicable to typhoon research in Hong Kong.

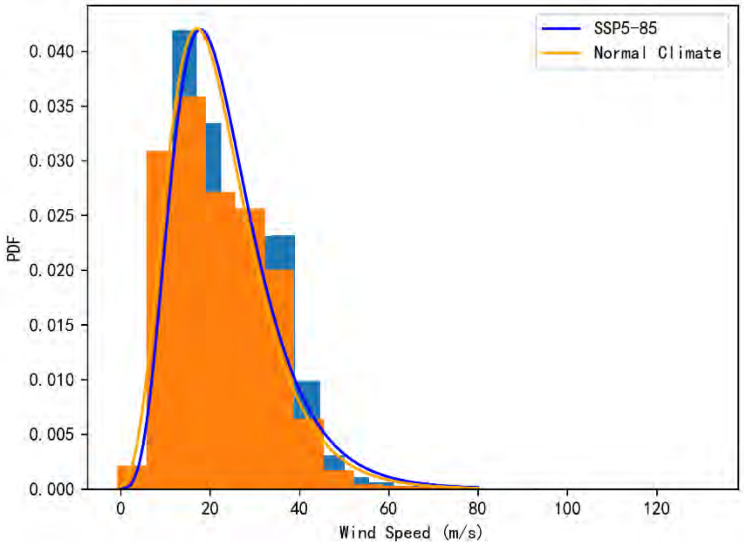

Figure 3. Normal climate wind speeds vs SSP5-85 wind speed.

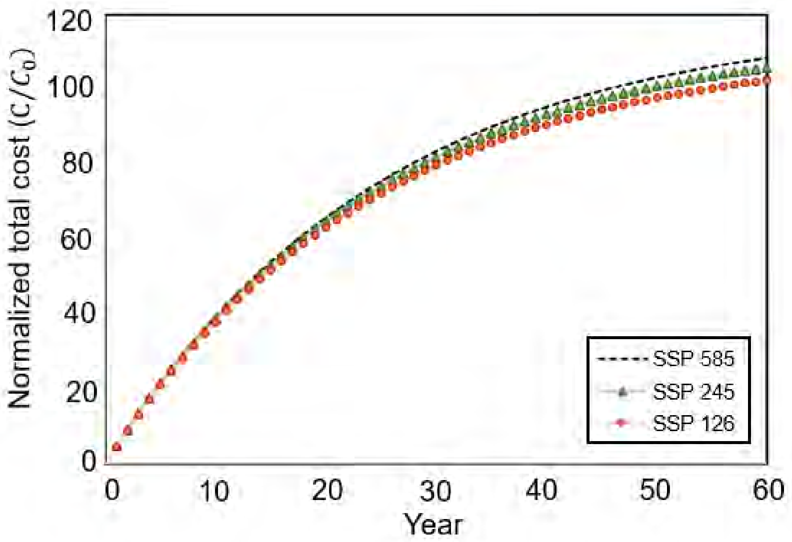

Figure 4 The normalized total life-cycle cost of the second-generation benchmark building in Hong Kong.

5. ACKNOWLEDGMENT

The work described in this article was supported by the grants from the Research Grants Council (RGC) of the Hong Kong Special Administrative Region (HKSAR), China with GRF No. 16207118.

6. REFERENCES

Cao, S., Wang, J., & Tse, T. K. (2023). Life - cycle cost analysis and life - cycle assessment of the second - generation benchmark building subject to typhoon wind loads in Hong Kong. The Structural Design of Tall and Special Buildings, e2014.

Huang, W. F., & Xu, Y. L. (2012). A refined model for typhoon wind field simulation in boundary layer. Advances in Structural Engineering, 15(1), 77-89.

Xu, G., Lin, K., Li, X., & Ye, Y. (2022). SAF-Net: A spatio-temporal deep learning method for typhoon intensity prediction. Pattern Recognition Letters, 155, 121-127.

A ROADMAP FOR ENVIRONMENTAL ASSESSMENT IN BUILDING CONSTRUCTION: INTEGRATING LCA WITH INDIA-SPECIFIC FOOTPRINT

Abhiram Shukla[1], and Harshal Tikam[1]

[1]PhD Student, Indian Institute of Technology Kanpur, Kanpur, India
E-mail: abhirams@iitk.ac.in

1. INTRODUCTION

The construction sector influences approximately one-third of global sustainable development goals, making its role crucial in achieving India's national SDGs by 2030 [1]. Construction contributes heavily to energy consumption, carbon emissions, resource use, and waste generation. India is projected to witness a significant rise in building construction and infrastructure development in the foreseeable future. However, the environmental repercussions could be significant if unsustainable, conventional approaches are employed. Despite significant schemes like the Smart Cities Mission, neglecting sustainability principles in construction could harm the environment, undermining progress in climate action, public health, and ecosystems [2]. Lifecycle assessment (LCA) tools help quantify these impacts and inform eco-friendly decisions [3]. However, research gaps exist, particularly in India, due to limited site-specific data and localized factors. To bridge these gaps, this study showcases a comprehensive life cycle assessment for Indian building projects. It compiles detailed inventory data, transforms it into a bill of materials, and integrates India-specific environmental factors, shedding light on the project's overall environmental footprint.

2. MATERIALS AND METHODS

2.1 Case study & collection of data

The quantity survey document or bill of quantity (BOQ) was obtained to build an academic block at the National Institute of Electronics & Information Technology (NIELIT) in Agartala, located in Tripura, India. The BOQ, sourced from the institute's website, provides a detailed breakdown of individual construction tasks, contractual terms, and cost estimates [4]. It encompasses 12 main categories of work, such as earthwork, concrete, steel, and more, along with 145 sub-items.

2.2 Converting the BOQ to bill of materials (BOM)

The transformation of the building’s quantity survey data or bill of quantities (BOQ) data into material inventory data or bill of materials (BOM) was executed through reference to the analysis of rates (AOR) for Delhi document, as furnished by the central public works department (CPWD) [5]. Moreover, the quantum of diesel consumption by on-site construction machinery, crucial for the execution of varied itemized tasks, was sourced from the overseeing construction agency. The rendered bill of materials assumes the nomenclature of "materials inventory data" within the realm of life cycle assessment literature. The BOM, explicated in Supplementary Table S2, encapsulates the enumeration of 161 distinct materials that found deployment in the course of the project's realization. In addition to assessing the environmental impacts of building materials, we also quantified the effects of diesel consumption. This included evaluating the environmental consequences of transporting materials from factories to the construction site and operating machinery like hydraulic excavators and concrete mixers. Total diesel use was computed considering factors like truck capacity, distance of travel, consumption of fuel, and fuel, referring past Indian literature [6].

2.3 Environment and energy characterization factors

Primarily, we utilized the Indian construction materials database (ICMD), established by the International Finance Corporation [7]. This databse provides impacts per kg of construction material across six environmental domains. Alternate sources were consulted for materials without ICMD data (Supplementary Table S3).

2.4 Environmental life cycle assessment of academic building

The life cycle assessment (LCA) comprises four stages: Goal and Scope Definition, Life Cycle Inventory Analysis, Life Cycle Impact Assessment, and Results Interpretation [8]. Our study's goal was to calculate environmental impact from constructing the academic building, utilizing material inventory data and Indian material enviornmnetal impact coefficinet. Our LCA's scope covered raw material extraction, processing, material transportation, and on-site construction, excluding other phases due to data limitations. For impact assessment, we multiplied material quantities with corresponding characterization factors for each environmental domain, summing across materials. Normalization factors were employed to facilitate inter-domain comparisons. Results interpretation identifies major contributors to environmental impact, considering materials, processes, and life cycle stages.

3. RESULTS AND DISCUSSION

3.1 Overall environmental impact of building (Cradle to site)

The construction of the academic building resulted in notable environmental impacts: 27 million MJ energy consumption, 2327 tons CO_2eq. emissions, 0.035 kg CFC-11 eq. ozone depletion, 10.82 tons SO_2eq. acidification, 0.86 tons PO_4eq. eutrophication, and 0.74 tons C_2H_4 eq. photochemical ozone creation (See Table 1). Energy, global warming, and acidification impacts are approximately 100 times greater than photochemical oxidant and eutrophication, and nearly 1000 times greater than ozone depletion.

Table 1. Environmental impacts of the building for all three life cycle stages

Stage	**Embodied energy (Million MJ)**	**Global warming potential (Tons CO_2 eq.)**	**Ozone creation potential (g CFC-11 eq.)**	**Acidification potential (Tons SO_2 eq.)**	**Eutrophication potential (Tons PO_4 eq.)**	**Photochemical ozone creation potential (Tons C_2H_4)**
Material production stage	26.07 (96.6%)	2258 (97%)	0.007 (21%)	10.58 (97.8%)	0.82 (95.7%)	0.50 (68%)
Transportation stage impacts	2.51 (21%)	189.24 (27%)	77 (63%)	0.23 (2.1%)	0.036 (4.2%)	0.23 (31%)
Construction stage impacts	0.04 (0.2%)	2.53 (0.1%)	0.0007 (2%)	0.39 (0.1%)	0.001 (0.1%)	0.006 (0.1%)
Total impacts	27	2327	0.035	10.82	0.86	0.74
Normalized impacts	6.0E-08	5.6E-08	3.9E-11	3.2E-08	6.5E-09	7.7E-09

3.2 Environmental consequences at each stage of the lifecycle

The allocation of impact among the three life cycle phases concerning the building's environmental impact across all six categories is illustrated in Figure 1. Material production dominates the overall impact for energy use (97%), GHG emissions (97%), acidification potential (98%), eutrophication potential (96%), and POCP (68%). Transportation notably influences ozone depletion potential (77%) due to significant diesel use and its characterization factor (Supplementary table S5). On-site construction contributes 15-35% of the total impact, driven by diesel, petrol, and electricity use in various operations (Supplementary table S6).

3.3 Material wise environmental impact

In Figure 2, significant materials driving the academic building's environmental impact are showcased. Depending on the environmental category, key contributors include bricks (20-40%), aluminum sections (8-17%), steel bars (10-17%), cement (10-18%), and aggregates (2-5%)—except for ozone depletion. Significantly, the major contributors to ozone depletion potential are granite stone, cast iron pipe, and the utilization of diesel. Diesel's significant contribution is evident in both transportation and the operation of machinery during construction operation.

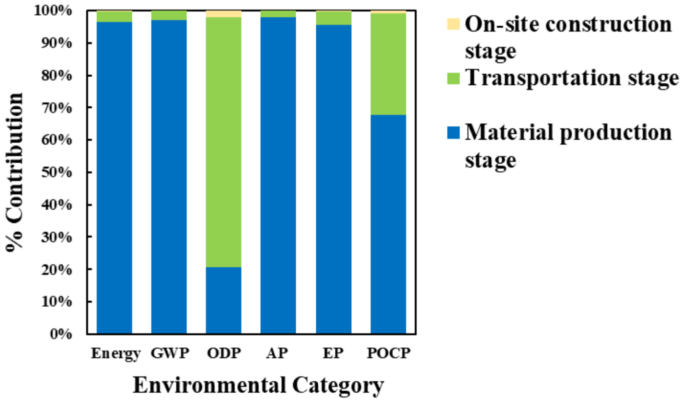

Figure 1. Percentage distribution of various stages in the building's life cycle contributing to its overall environmental impact

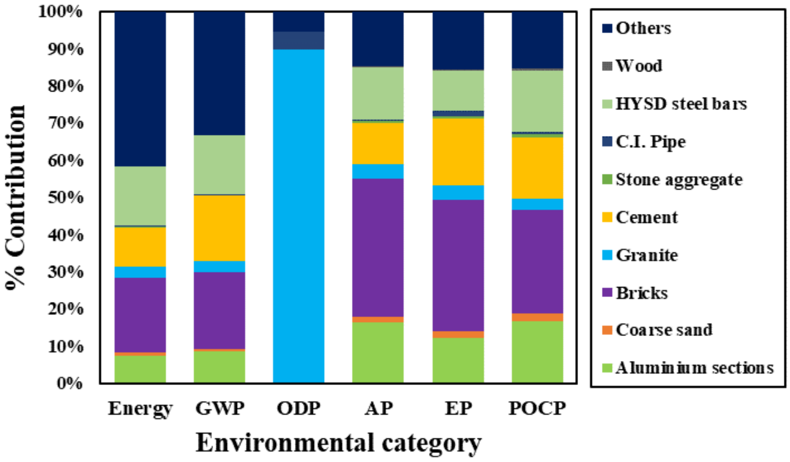

Figure 2. The distribution of the total environmental impact across different building materials is depicted as percentages. Refer to Supplementary Table S4 for detailed impacts of all 161 materials.

3.4 Item-wise environmental impact

Figure 3 displays that among 14 work items, 'brick item work (No.4)' (20-40%), 'reinforced cement concrete item work (No.3)' (20-25%), and 'aluminum item work (No.11)' (12-20%) dominate the building's environmental footprint across most categories, except ODP, energy use, and GWP. ODP is primarily influenced by marble work (88%), while 'earth work' drives energy use and GWP (30% and 25% respectively). Flooring, waterproofing, finishing, and concrete work contribute 2-5% to most categories, while wood, roofing, drainage, and water supply have <2% impact. See Supplementary Table S7 for details.

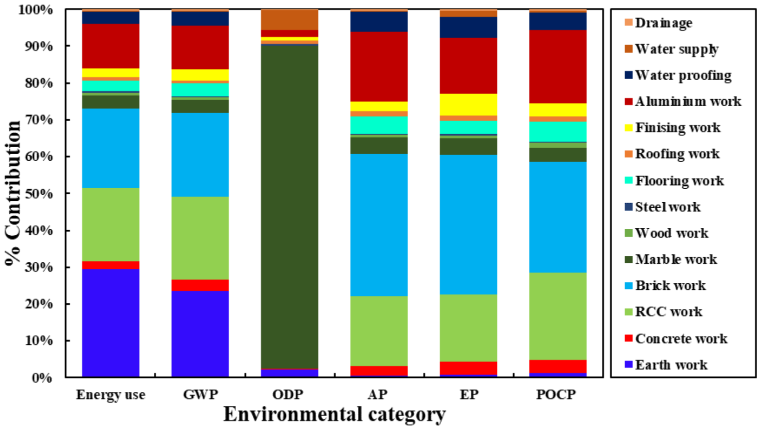

Figure 3. The distribution of environmental impact across different building item works is presented as percentages. Refer to Supplementary Table S7 for detailed impacts.

4. CONCLUSION

Our investigation demonstrates that the production phase of building materials holds the most substantial sway over a building's overall environmental footprint. Following closely is the transportation of these materials to construction sites. Particularly noteworthy are the significant contributions of materials such as bricks, aluminium sections, steel bars, and cement to these impacts. Our novel approach, which leverages publicly accessible data encompassing quantity survey document, analysis of rate for Delhi (DAR), and environmental impact coefficient from India, presents an accessible avenue to appraise the comprehensive environmental repercussions of construction projects, from inception to the construction site. We recommend heightened endeavors in data collection and platforms to facilitate all-encompassing from raw material extraction (cradle) to end of life (gravel) life cycle assessments for residential and commercial buildings, incorporating impacts during usage and the final demolition phase.

5. ACKNOWLEDGMENT

The first author would like to acknowledge the IIT Kanpur for providing institute assistantship.

6. REFERENCES

1. Wen, B., Musa, S. N., Onn, C. C., Ramesh, S., Liang, L., Wang, W., & Ma, K. (2020). The role and contribution of green buildings on sustainable development goals. *Building and Environment*, *185*, 107091.
2. Randhawa, A., & Kumar, A. (2017). Exploring sustainability of smart development initiatives in India. *International Journal of Sustainable Built Environment*, *6*(2), 701-710.
3. Nwodo, M. N., & Anumba, C. J. (2019). A review of life cycle assessment of buildings using a systematic approach. *Building and Environment*, *162*, 106290.
4. NBCCL (2012). *Construction of Permanent Campus for NIELIT at Bodhjung Nagar, Agartala, Tripura State*. National Building Construction Corporation Limited. Available at: https://www.nielit.gov.in/sites/default/files/agartal_volI3.pdf (Accessed on: Jun 30, 2023).
5. CPWD (2019). *Analysis of Rates for Delhi, Part-1*, Central Public Works Department, New Delhi, India.
   Available at: https://cpwd.gov.in/Publication/CivilDAR_2019_Vol_1.pdf (Accessed on: Jun 30, 2023).
6. Pinky Devi, L., & Palaniappan, S. (2019). Life cycle energy analysis of a low-cost house in India. *International Journal of construction education and research*, *15*(4), 256-275.
7. ICD (2017). India Construction Materials Database of Embodied Energy and Global Warming Potential Methodology Report. European Union, International Finance Corporation, (2017). Available at: https://www.edgebuildings.com/wp-content/uploads/2017/12/IFC-India-Construction-Materials-Database-Methodology-Report.pdf (Accessed on: Jun 30, 2023).
8. ISO, I. (2006). 14040. Environmental management—life cycle assessment—principles and framework, 235-248.

LIFE-CYCLE ASSESSMENT OF LOW AND HIGH WATER MIXED CEMENT PASTES: COMPARATIVE STUDY OF FAST-CURING METHODS

Xin Shao[1], Lufan Li[1], and Tung-Chai Ling[1]

[1] College of Civil Engineering, Hunan University, 410082 Changsha, China
E-mail: tcling@hnu.edu.cn

In the precast concrete industry, steam curing is commonly used to accelerate early (first few hours) strength development of concrete. Recently, CO_2 curing has emerged as an alternative method, claiming several advantages such as lower carbon footprint and anticipating fast curing for cementitious materials. However, the environmental impacts of these fast-curing methods compared to conventional standard curing (rely mainly on hydration), have not been thoroughly justified. To address this knowledge gap, this study conducted a comparative life-cycle assessment (LCA) to evaluate both low and high water mixed (water-to-cement ratio of 0.15 and 0.35) cement pastes that adopted with different curing methods. The environmental impacts of each group, including global warming potential (GWP), ecosystem quality potential (EQP), and human health potential (HHP), were quantified. The results of the evaluation revealed that both CO_2 and steam curing could reduce greenhouse gas (GHG) emissions by 20%–50% compared to standard curing for both low and high water mixed cement pastes. Additionally, using flue gas instead of purified CO_2 gas for CO_2 curing could further reduce GHG emissions by up to 80%. Examining the GWP/strength ratio over the investigated times, the CO_2 curing method exhibited the highest environmental benefits during the initial 3 days of curing. It is important to highlight that by incorporating renewable energy sources, the environmental impact of CO_2 and other GHG can be further reduced at a significant level, fostering the carbon neutrality target in construction field.

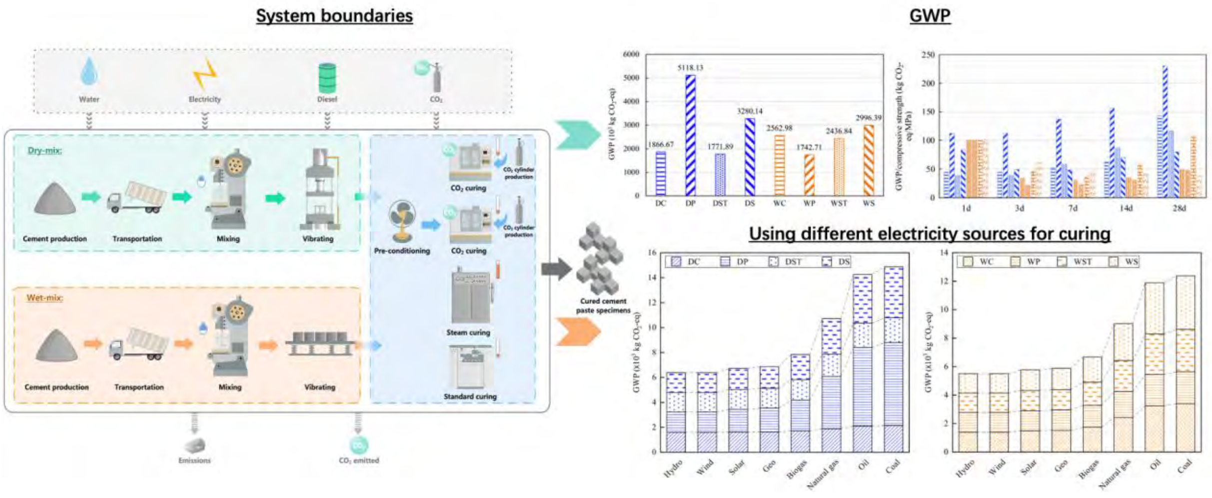

Keywords: Dry-mix; Wet-mix; Cement paste; Fast-curing method; Life-cycle assessment (LCA)

A NOVEL FOAMING-SINTERING TECHNIQUE FOR DEVELOPING ECO-FRIENDLY LIGHTWEIGHT AGGREGATES FOR HIGH PERFORMANCE CONCRETE

Zuwang Bian[1], Yujie Huang[1], Yunpeng Liu[2], Jian-Xin Lu[1], Dingqiang Fan[1], Fazhou Wang[2], Chi Sun Poon[1]

[1]Department of Civil and Environmental Engineering &
Research Centre for Resources Engineering towards Carbon Neutrality (RCRE),
The Hong Kong Polytechnic University, Hung Hom, Kowloon, Hong Kong
[2]State Key Laboratory of Silicate Materials for Architectures, Wuhan University of Technology, Wuhan, China
E-mail: jianxin.lu@polyu.edu.hk (J.X. Lu), cecspoon@polyu.edu.hk (C.S. Poon)

To tackle the scarcity of natural aggregates and reduce energy consumption of the concrete industry, a sustainable lightweight aggregate (LWA) was developed using a self-foaming and sintering technique, employing waste glass powder as the primary precursor and incineration bottom ash as a foaming agent. The influence of NaOH content (0 M, 2 M, and 8 M) on the physical properties of LWA was investigated. Manufactured sand was replaced with sintered LWA (0 M-LWA and 2 M-LWA) by 50 vol% and 100 vol% to investigate their effect on the physical properties, mechanical properties, shrinkage, and alkali-silica reaction of high performance concrete (HPC). The HPC prepared with 0 M-LWA exhibited a density of 2127 kg/m^3 and compressive strength of 108.7 MPa, which were slightly lower than that with manufactured sand. The porous and lightweight nature of 2 M-LWA resulted in a significant reduction in the density and compressive strength of HPC as the volume of 2 M-LWA increased. Nevertheless, HPC with 100 vol% 2 M-LWA showed satisfying density of 1835 kg/m^3 and compressive strength of 50 MPa. The use of 2 M-LWA effectively mitigated autogenous shrinkage in HPC due to the internal curing effect. The alkali-silica reaction expansion of all LWA was innocuous.

Keywords: Waste glass powder; Incineration bottom ash; Lightweight aggregate; High performance concrete; Internal curing

A NEW SUPERHYDROPHOBIC INTERFACE CONSTRUCTION TECHNOLOGY FOR LOW CARBON CONCRETE: IN-SITU SELF-GENERATION OF MICRO-/NANO-STRUCTURES

Long Jiang, Peiliang Shen*, Chi Sun Poon*

Department of Civil and Environmental Engineering, The Hong Kong Polytechnic University,
Hong Kong, China
E-mail: peiliang.shen@polyu.edu.hk (P. Shen)
cecspoon@polyu.edu.hk (C.S. Poon)

Superhydrophobic interface has excellent water resistance because of its special micro-nano structure, which can reduce the penetration of external water and greatly improve the durability of concrete buildings. In this work, a new in-situ self-generation micro-/nano-structure method for constructing superhydrophobic interface on concrete was proposed by impregnate carbonation. Experiments results showed that the concrete surface presented high superhydrophobicity by 2 hours of carbonation (CA=170.5 ± 0.8°, SA=1.9 ± 0.5°). With the proceeding of carbonation, the early-phase of carbonation is mainly the nucleation and growth of $CaCO_3$ on concrete surface, forming micro-sized structures. However, the late-phase of carbonation is the new nucleation and growth of $CaCO_3$ manipulated by Mg^{2+} on the micro-sized $CaCO_3$ particles, forming micro-/nano-structures. In the mixed system, all newly generated $CaCO_3$ particles were modified by silane, lowering the surface energy of concrete. The low surface energy and micro-/and nano-structure constructed the superhydrophobic concrete interface.

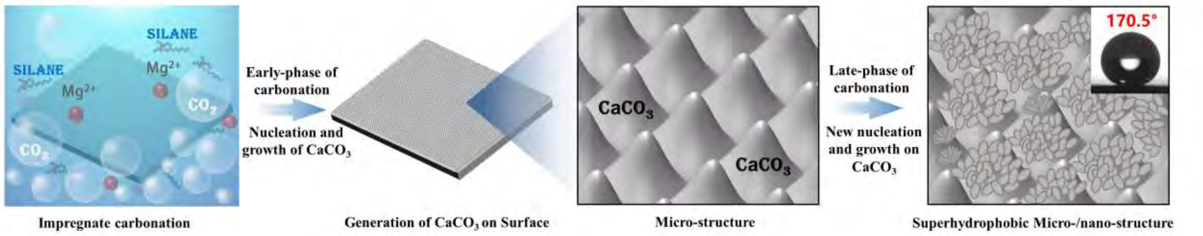

Keywords: Impregnate carbonation, In-situ self-generation of micro-/nano-structures, Manipulation of crystal morphology, low surface energy treatment, Low-carbon superhydrophobic concrete.

STUDY ON CHEMICAL METHOD TO STIMULATE THE CEMENTITIOUS PROPERTY OF STEEL SLAG

Wenzheng Li [a], Mingli Cao [a], Dan Wang [b]*, Jun Chang [a]*

[a] School of Civil Engineering, Dalian University of Technology, Dalian 116024, Liaoning, China
[b] Special Glass Key Lab of Hainan Province & State Key Laboratory of Marine Resource Utilization in South China Sea, Hainan University, Haikou 570228, China

SS exhibits a low utilization rate due to its low hydration activity and poor volume stability. In this study, the hydration activity and volume stability of SS were improved by the combined treatment of alkali and then carbonation (A_C for short). The crystal size of portlandite, the hydration product of A_SS, exhibits an initial increase followed by a subsequent decrease as the sodium silicate modulus increases, and the maximum grain size is observed at the modulus of 2.0. The impact of temperature on the carbonation of SS exhibits dual facets. A_C-SS is employed as supplementary cementitious material (SCM), and the optimal combined treatment method is A2.0_C100 according to the macroscopic compressive strength. Compared with untreated SS-OPC, the compressive strength increased by 27.09% and the expansion rate decreased by 21.53% at 28 days. The calcite generated by A2.0_C100-SS exhibits significant grain size and content, which can promote cement hydration. The QXRD results reveal that the $C_4A\check{C}H_{11}$ content in the Treated_SS-OPC system reaches 11.55 wt.%, imparting exceptional strength. The analysis of the pore structure reveals that the addition of A2.0_C100-SS to cement effectively reduces the porosity of the SS-OPC system, resulting in a denser internal structure and improved strength. Compared with untreated SS, the embodied CO_2 index (*CI*) in A2.0_C100-SS-OPC system was found to be the lowest at 9.867, indicating that the method of the A_C is more sustainable and environmentally friendly.

Keywords: Steel slag; Carbonation; Alkali-activated; Volume stability; Temperature

FRACTAL HYDRATION EVOLUTION OF A SUSTAINABLE LOW WATER/BINDER CEMENTITIOUS COMPOSITE: EXPERIMENTS AND SIMULATION

Liu, Kangning[a,b,c], Wang, Zhiyu[a,b], Yin, Tianyi[a,b], Feng, Yuan[a,b], Fan, Dingqiang[c],
Kang, Juntao[d], Yu, Rui[a,b,e]

[a] State Key Laboratory of Silicate Materials for Architectures, Wuhan University of Technology, Wuhan, 430070, China
[b] International School of Materials Science and Engineering, Wuhan University of Technology, Wuhan, 430070, China
[c] Department of Civil and Environmental Engineering, The Hong Kong Polytechnic University, Hong Kong, China
[d] School of Civil Engineering and Architecture, Wuhan University of Technology, Wuhan 430070, China
[e] Wuhan University of Technology Advanced Engineering Technology Research Institute of Zhongshan City, Xiangxing Road 6, 528400, Zhongshan, Guangdong, China
Email: r.yu@whut.edu.cn

This study investigates the feasibility of utilizing unique marine resources, seawater and coral powder, in the preparation of cementitious materials. Specifically, low-field nuclear magnetic resonance and hydration calorimetry are employed to examine the specific effects of seawater and coral powder on cement hydration and micro-structure evolution. The molecular dynamic simulation is employed to investigate the react mechanism of different $CaCO_3$ to the CSH. Finally, X-ray diffraction, scanning electron microscopy, and thermogravimetric analysis are conducted to analyze the influence of seawater and coral powder on cement hydration products. The results indicate that seawater can accelerate the nucleation and growth stage of cement hydration, but will hinder the diffusion stage, leading to the slow formation of gel pore structure. Compared to limestone powder, coral powder has a lower affinity with the C-S-H, as a result, coral powder cement paste has a lower degree of hydration and a slower formation of microstructure. This study explores the potential application of seawater and coral powder, providing a scientific basis for the development and utilization of sustainable seawater and sand-based building materials.

Keywords: Coral powder; Seawater; Fractal analysis; Hydration mechanism

RAPID CO_2 CATALYTIC ACTIVATION OF BINARY CEMENTING SYSTEM OF CSA AND PORTLAND CEMENT

Yang Liu, Shipeng Zhang*, and Chi Sun Poon

Department of Civil and Environmental Engineering, The Hong Kong Polytechnic University
*E-mail: shipeng.zhang@polyu.edu.hk

This study presents a novel approach for activating a binary cementing system of calcium sulfoaluminate (CSA) cement and ordinary Portland cement (OPC) using an instant CO_2 catalysis. The activation led to significant and rapid strength enhancement, with the binary cement achieving a strength of 15.42 MPa immediately after activation, all within one minute. The rapid CO_2 activation catalyzed a notable heat release, accelerating the hydration of ye'elimite to form ettringite, which is a crucial component capable of bridging gaps and imparting high initial strength. Simultaneously, the CO_2 activation catalyzed the increase in sulfur concentration, which in turn, also facilitated the formation of ettringite at an early age. Afterwards, the subsequent strength development was attributed to belite hydration. Apart from the rapid strength gain, employing CO_2 activation facilitated control over the pH value of the pore solution, thus archiving manipulation of ettringite's crystal morphology to strategically enhance the microstructure. Samples with lower pH values exhibited needle-like ettringite formations, whereas samples with higher pH values yielded rod-like and column-like ettringite crystal structures. The present study provides a new perspective on the potential application of CSA-based cement, such as precast concrete element, instant concrete product delivery, and urgent reconstruction.

Keywords: calcium sulfoaluminate cement; ordinary Portland cement; carbonation; rapid activation; diluted suspension

PREPARATION OF REACTIVE SEEDINGS BY IN SITU PRECARBONATION UNDER POWER ULTRASOUND-ASSISTED MIXING: ENHANCING THE HYDRATION AND MECHANICAL PROPERTIES OF OPC

Guangqi Xiong[1,2], Shuangshuang Liu[2], Keke Sun[2], Guangzhao Yang[2], Shipeng Zhang[2,*],
Chong Wang[2], Chi-sun Poon[2]

[1]College of Materials Science and Engineering, Chongqing University, Chongqing, 400045, China
[2] Department of Civil and Environmental Engineering & Research Centre for Resources Engineering toward Carbon Neutrality, The Hong Kong Polytechnic University, Hong Kong, 999077, China
E-mail: shipeng.zhang@polyu.edu.hk

In this study, a precarbonation process was developed using power ultrasound-assisted mixing to prepare a highly reactive seeding slurry. This prepared slurry was then added to the remaining cement paste for secondary mixing to enhance the carbon dioxide (CO_2) absorption efficiency and early hydration of ordinary Portland cement (OPC). The study investigated the effect of ultrasound time on the precarbonation mechanism of OPC. The results revealed that power ultrasound greatly facilitated the release of ions into the pore solution, promoting the formation of calcium carbonate, aluminum hydroxide, and C-S-H gels during the precarbonation stage. Following ultrasound treatment for 20 minutes, a substantial quantity of finer calcium carbonate seeds was observed, capturing an additional 7.09% CO_2 per dry mix. Subsequently, the seeding slurry prepared using power ultrasound-assisted mixing as highly active carbonated seeds acted as independent nucleation sites to enhance the formation of hydration products. This shortened the hydration induction period and ultimately resulted in improved microstructural densification of the hardened cement paste.

Keywords: in situ precarbonation; power ultrasound; seeding sizes; hydration; ordinary Portland cement

Poster Sessions

USE OF VOLCANIC ASH FROM TAJOGAITE (LA PALMA, CANARY ISLANDS) AS ALKALI-ACTIVATED BINDER PRECURSOR

Mañosa, J.[1], Maldonado-Alameda, A.[1,2], Aulinas, M.[3], **Chimenos, J.M.**[1]

[1] Departament de Ciència de Materials i Química Física, Universitat de Barcelona, C/Martí i Franquès, 1-11, 08028, Barcelona, Spain.
[2] Fundación Centro Tecnológico de Investigación Multisectorial (CETIM); Parque empresarial de Alvedro, Rúa H, 20, 15180 Culleredo, A Coruña, Spain.
[3] Departament de Mineralogia, Petrologia i Geologia Aplicada, Universitat de Barcelona, Martí i Franquès s/n, 08028, Barcelona, Spain
chimenos@ub.edu

The volcanic eruption of Tajogaite in La Palma (Canary Islands, Spain) produced approximately 200 Mm^3 of fine lapilli and ash. The valorization of the volcanic ash (VA) from this eruption promotes the circular economy on an island where the availability of natural resources is scarce. With this objective, the suitability of VA from La Palma to produce alkali-activated binders (AABs) was studied. The composition and physicochemical properties of the VA were thoroughly studied, and its potential reactivity was assessed through alkaline attacks. AABs were formulated using VA as the sole precursor and using different NaOH molarities. The samples were cured at 60 ºC for 3 days and afterward at room temperature until testing. The AABs were then analyzed with complementary techniques.

The results demonstrated that N-A-S-H and (C,N)-A-S-H gels were formed through alkaline activation of VA. Most of the crystalline phases of VA were very poorly reactive, hence, the microstructure of the AABs comprised a binder matrix with unreacted VA particles, which increase the mechanical properties of the material. The highest compressive strength of AABs (16 MPa) was obtained using a 6 M NaOH activator. The environmental assessment through a leaching test revealed that, although some metals and metalloids are activated through alkaline activation (higher values than in raw VA), the AABs could be considered non-hazardous materials at the end of their life cycle.

Keywords: Alkali-activated binders, Circular economy, Waste valorisation, Sustainable cement, Volcanic ash

EVALUATION AND COMPARISON OF THE ENVIRONMENTAL FOOTPRINT OF TWO REPAIR MORTARS THROUGH A LIFE CYCLE ASSESSMENT

Alfocea-Roig, A., Pompido-Pujol, G., **Formosa, J.***, and Giro-Paloma, J.

Departament de Ciència de Materials i Química Física, Universitat de Barcelona
joanformosa@ub.edu (*corresponding author)

The exponential growth of the global population and economy has led to a concerning increase in energy consumption, resource extraction, and subsequent acceleration of global warming. In light of these sustainability challenges, industries are proactively investigating environmentally friendly alternatives to mitigate adverse impacts on the environment, society, and economy throughout the entire product life cycle.

The main objective of this study is to conduct a comparative analysis of the environmental impacts of two types of mortars intended for the same application. One of the mortars, MPC-TUN, is a laboratory-scale alternative that utilizes a waste product from the steel industry known as Tundish deskulling waste (TUN) as a source of magnesium oxide for developing magnesium phosphate cements (MPC). The other mortar is a conventional epoxy-based one. To assess and compare the two mortars, the study employs the Life Cycle Assessment (LCA) methodology. Indeed, this comprehensive approach offers valuable insights into the overall sustainability performance of each mortar variant.

The results of these analyses suggest that the MPC-TUN mortar exhibits greater potential as a sustainable solution in comparison to the conventional epoxy-based mortar, particularly for quick repair applications. With continued research and development, the MPC-TUN mortar has the possibility of becoming a viable alternative in the construction industry, aligning with regulatory requirements and supporting sustainable environmental and social commitments. This finding emphasizes the importance of exploring eco-friendly alternatives in construction materials to minimize environmental impacts and promote socially responsible practices in the industry.

Keywords: Tundish deskulling waste; Life Cycle Assessment; Valorisation; Alternative mortar; Circular economy

ENVIRONMENTAL IMPLICATIONS OF WASTE-DERIVED POLYHYDROXYALKANOATE COMPOSITES AS CONSTRUCTION MATERIALS

Myung, Jaewook

Civil and Environmental Engineering, KAIST
jjaimyung@kaist.ac.kr

The construction industry is a significant contributor to global environmental degradation, particularly through the generation of waste and the consumption of non-renewable resources. As sustainability becomes an increasingly important aspect of construction practices, the search for eco-friendly alternatives has gained momentum. Polyhydroxyalkanoates (PHAs), a class of biopolymers produced by microbial fermentation of waste materials, offer promising potential as an eco-friendly alternative to traditional construction materials. PHA composites, developed by blending PHA with various waste-derived reinforcements, exhibit desirable mechanical properties and have the potential to replace non-renewable and energy-intensive construction materials. The environmental implications of using waste-derived PHA composites in construction materials are examined through a life cycle assessment (LCA) framework. The LCA encompasses the entire life cycle of PHA composites, from raw material acquisition and production to manufacturing, usage, and end-of-life scenarios. Key findings suggest that the production of PHA composites requires significantly lower energy and produces fewer greenhouse gas emissions compared to conventional construction materials. Furthermore, the incorporation of waste-derived reinforcements in PHA composites diverts waste from landfills, reducing their environmental impact. This research abstract provides valuable insights into the environmental implications of waste-derived PHA composites as construction materials.

Keywords: Polyhydroxyalkanoates, PHA composites, Waste-derived, Biopolymer, Sustainability

INFLUENCE OF ALKALI METAL CATIONS ON THE ATOMIC STRUCTURE AND MECHANICAL PROPERTIES OF GEOPOLYMER GEL PHASE: INSIGHTS FROM MOLECULAR SIMULATIONS

Tsvetkov, S[1], Fedotov, A[1,2], Kasprzhitskii, A[1,2], and Lazorenko, G[1,2]

[1]Novosibirsk State University, Pirogov Street, 2, Novosibirsk, 630090, Russia
[2]Rostov State Transport University, Narodnogo Opolcheniya Sq., Rostov-on-Don, 344038, Russia
E-mail: s.tsvetkov@g.nsu.ru

In this work, the effects caused by the kinds of alkali-activated ions (Li^+, Na^+, K^+, Cs^+ and Rb^+) on the structure and mechanical properties of geopolymeric (alkali aluminosilicate) gel were evaluated by molecular dynamics (MD) simulation. The bulk density, bond length, angle, radial distribution function (RDF), mean square displacement (MSD), elastic modulus, and bulk modulus, are calculated. In addition, the distribution pattern of H_2O molecules in the amorphous aluminosilicate gel phase and the preferred sorption sites were also investigated. The simulation results are in good agreement with the experimental results in terms of structural and mechanical properties. The MD simulation results have provided useful information on the behavior of alkali metal cations and water confined in geopolymeric gel phase, which is difficult to observe experimentally, contributing to a better understanding of the structure and mechanics in alkali-activated materials.

This work was supported by the Russian Science Foundation (Grant No. 19-79-10266, https://rscf.ru/project/19-79-10266/). The authors acknowledged the support from project № FSUS-2023-0001 «Creating a geoinformation system for studying landscape biocomplexes based on Earth remote sensing data using machine learning methods.

Keywords: Alkali-activated materials; Geopolymers; Alkali metal ions; Mechanical properties; Molecular Dynamics

Gold Sponsor:

新輝(建築管理)有限公司
Sanfield (Management) Ltd.

Silver Sponsors:

In alphabetical order of company name

青檬艾柯 LIMECHO

fortum
Powering a thriving world

NAMI

SCORETECH